BIOCHEMICAL DETERMINANTS OF NITRIC OXIDE SYNTHESIS IN SEVERE MALARIA

Matthew S. Alkaitis

Balliol College

University of Oxford

A dissertation submitted to the Faculty of the University of Oxford, Division of Medical Sciences for the degree of *Doctor of Philosophy (DPhil) in Biomedical Sciences*

Hilary Term, 2014

Abstract

Inhibition of nitric oxide (NO) signalling may contribute to the pathogenesis of severe malaria. This thesis examines the impact of *Plasmodium* infection on three key determinants of nitric oxide synthase (NOS) biochemistry: substrate availability, substrate/inhibitor homeostasis and cofactor availability. Arginine, the NOS substrate, is depleted in human patients with severe *Plasmodium falciparum* malaria and mice infected with *P. berghei* ANKA. Using heavy isotope tracer infusions to quantify arginine metabolism in infected mice, we found no evidence of increased catabolism by the enzyme arginase, widely assumed to be responsible for arginine depletion. Genetic knock-out of parasite arginase had no effect on arginine depletion in mice. Instead, our findings link arginine depletion to decreased rates of arginine and citrulline appearance in the plasma of infected mice. Asymmetric dimethylarginine (ADMA) competes with arginine for binding to the NOS catalytic site. We observed elevation of the ADMA/arginine ratio in Gambian children with severe malaria, favouring NOS inhibition. In mice infected with *P. berghei* ANKA, we found evidence of degradation of dimethylarginine dimethylaminohydrolase 1 (DDAH1), the enzyme primarily responsible for ADMA metabolism. We also observed reduced DDAH activity and accumulation of intracellular ADMA in hepatic tissue of infected mice, suggesting that DDAH dysfunction could contribute to disruption of ADMA/arginine homeostasis. Tetrahydrobiopterin (BH4) is an essential NOS cofactor. In *P. berghei* ANKA-infected mice, BH4 concentrations were decreased in plasma, erythrocytes and brain tissue, which could inhibit NO synthesis and promote NOS-dependent superoxide production. To reverse deficiencies of NOS substrate and cofactor availability, we infused *P. berghei* ANKA-infected mice with citrulline, an arginine precursor, and sepiapterin, a BH4 precursor. Restoration of systemic arginine and BH4 availability in infected mice improved whole blood nitrite concentrations, a biomarker of NO synthesis, but did not prevent onset of disease symptoms. These studies have identified biochemical disturbances that may contribute to severe malaria pathogenesis by inhibiting NO synthesis.

Supervisors

Supervisor, University of Oxford:

David J. Roberts

Nuffield Division of Clinical Laboratory Sciences, Radcliffe Department of Medicine,
University of Oxford, Oxford, United Kingdom

Supervisor, National Institutes of Health:

Hans C. Ackerman

Laboratory of Malaria and Vector Research, Division of Intramural Research,
National Institute of Allergy and Infectious Diseases, National Institutes of Health,
Rockville, Maryland, United States of America

Contributors and Collaborators

Direct Contributors:
(Made a concrete contribution to sample collection or analysis)

Jessica H. Chertow[1], Honghui Wang[2], Glenn Nardone[3], Michael Walther[4,5], David Conway[5,6], Joseph Okebe[6], Augustine Ebonyi[6], Madi Njie[6], Simon Correa[6], Shamanthi Jayasooriya[6], Allison Ikeda[1]

[1]Laboratory of Malaria and Vector Research, Division of Intramural Research, National Institute of Allergy and Infectious Diseases, National Institutes of Health, Rockville, MD, USA [2]Critical Care Medicine Department, National Institutes of Health, Bethesda, MD, USA [3]Research Technology Branch, National Institute of Allergy and Infectious Diseases, National Institutes of Health, Rockville, MD, USA [4]Laboratory of Malaria Immunology and Vaccinology, National Institute of Allergy and Infectious Diseases, National Institutes of Health, Bethesda, MD, USA [5]MRC Unit, Fajara, The Gambia, [6]London School of Hygiene and Tropical Medicine, London, UK

Collaborators:
(Provided lab space and equipment)

Keith Channon[1], Oliver Billker[2] and Anthony F. Suffredini[3]

[1]Division of Cardiovascular Medicine, Radcliffe Department of Clinical Medicine,
University of Oxford, Oxford, UK, [2]Wellcome Trust Sanger Institute, Hinxton Cambridge, UK,
[3]Critical Care Medicine Department, National Institutes of Health, Bethesda, MD, USA

Acknowledgements

First and foremost, I would like to thank my supervisors, David Roberts and Hans Ackerman, who have been extraordinarily supportive of my research as well as my broader career goals. I have truly appreciated their guidance as well as their encouragement of independent thought and inquiry. Keith Channon (Oxford), Oliver Billker (Sanger Institute) and Anthony Suffredini (CCMD/NIH) deserve special recognition for their provision of laboratory space and technical expertise in support of my work. I would like to thank Ashley Hale and Mark Crabtree (Oxford) for HPLC training, Malika Ahras and Stanley Barkhuysen (Sanger Institute) for training in animal procedures and Laurel Mendelsohn (NHLBI/NIH) for training in the measurement of nitrite. I am indebted to Akhil Vaidya (Drexel University College of Medicine) for kindly providing arginase knock-out *P. berghei* ANKA parasites. I would like to thank Jessica Chertow, Honghui Wang, Glenn Nardone, Michael Walther, David Conway, Joseph Okebe, Augustine Ebonyi, Madi Njie, Simon Correa, Shamanthi Jayasooriya and Allison Ikeda for their direct contributions to this work (detailed in Declaration below). Jessica Chertow deserves special appreciation for her contributions to sample collection and processing as well as many useful discussions about pathophysiology and experimental design. I would also like to especially thank Glenn Nardone for his advice on HPLC assay development and Honghui Wang for his help operating the Q-TOF LC/MS instrument. I am grateful to Thomas E. Wellems for his support and mentorship. Lastly, I would like to thank the National Institutes of Health Division of Intramural Research, the Wellcome Trust, the European Virtual Institute of Malaria Research (EVIMalaR), the Henry Griffith Keasbey and Anna Griffith Keasbey Memorial Foundation, and the National Institutes of Health Oxford-Cambridge Scholars Program for providing programmatic and financial support of this work.

Declaration

The work described in this thesis was conducted at the University of Oxford, the Wellcome Trust Sanger Institute and the United States National Institutes of Health from 2009-2014. Honghui Wang (CCMD/NIH) assisted with operation of the Q-TOF LC/MS instrument. Michael Walther (NIAID/NIH) and David Conway (London School of Hygiene and Tropical Medicine) organized the clinical study of Gambian children with severe malaria in collaboration with the MRC Unit, The Gambia (Joseph Okebe, Augustine Ebonyi, Madi Njie, Simon Correa and Shamanthi Jayasooriya contributed). Glenn Nardone (NIAID/NIH) performed HPLC analysis of arginine and ADMA in plasma samples from Gambian children. Allison Ikeda performed ELISA for sVCAM. Jessica Chertow (NIAID/NIH) performed DDAH1 western blot, performed qRT-PCR, assisted with blood and tissue collection for selected experiments, assisted with the DDAH activity assay and assisted with solid-phase extraction of mouse plasma and tissue samples for ADMA analysis. With these exceptions, I hereby declare that the experimental design, implementation, data collection, statistical analyses and interpretations presented in this thesis are my own work.

No part of this thesis has already been submitted, accepted, or is concurrently being accepted for any degree, diploma, certificate or other qualification in this University or elsewhere.



Matthew S. Alkaitis

October, 2014

Contents

Abstract ***i***

Supervisors ***ii***

Contributors and Collaborators ***ii***

Acknowledgements ***iii***

Declaration ***iv***

Contents ***v***

List of Figures ***xi***

List of Tables ***xv***

Abbreviations ***xvii***

1 Background **1**

1.1 Malaria Epidemiology **1**

1.2 *Plasmodium* spp. Biology and Transmission **2**

1.3 Clinical Features of Severe Malaria **5**

Diagnosis *5*

Severe Malaria Susceptibility *5*

Complications of Severe Malaria *5*

1.4 Clinical Management of Severe Malaria **11**

Anti-Malarial Chemotherapies *11*

Mortality *12*

Additional Management Strategies *14*

1.5 The Vascular Endothelium in Severe Malaria Pathogenesis **15**

Cytoadherence of Parasitized Erythrocytes *15*

Dysregulation of Inflammatory Signalling *16*

Effects of NO inhibition on Cytoadhesion and Inflammatory Mechanisms *17*

Loss of Endothelial Barrier Integrity *18*

Impaired Blood Flow *21*

1.6 Evidence and Implications of Impaired Nitric Oxide Synthesis in Severe Malaria **23**

1.7 Nitric Oxide Synthesis **26**

Nitric Oxide Synthase Expression and Regulation *26*

Structure of Thesis *28*

2 Arginine Depletion 29

2.1 Introduction 29

2.2 Arginine Availability in *P. berghei* ANKA-Infected Mice 32

2.3 Evaluation of Parasite Arginase as a Possible Cause of Arginine Depletion 35

Rationale for the Study of Parasite Arginase 35

Effect of Parasite Arginase Knock-Out on Disease Severity 37

Effect of Parasite Arginase Knock-Out on in Vivo Arginine Depletion 41

2.4 Evaluation of Reduced Dietary Intake as a Possible Cause of Arginine Depletion 42

2.5 Quantitative Assessment of Metabolic Rates in Plasma 46

Overview of Tracer Methodology 46

Rates of Appearance in Plasma 47

Rates of Inter-conversion among Arginine, Ornithine and Citrulline 50

Rate of Conversion of Arginine to Citrulline by NOS 62

2.6 Discussion 65

2.7 Conclusion 69

2.8 Materials and Methods 70

General Animal Model Procedures 70

HPLC Analysis of Amino Acids 73

Evans Blue Assessment of Blood-Brain Barrier Integrity 74

Metabolic Tracer Experiments 75

LC/MS Analysis of Metabolic Tracer Enrichment 77

Calculations of Flux using Stable Isotope Tracers 80

Statistical Analyses 84

Acknowledgements 85

3 Disruption of ADMA/Arginine Homeostasis 86

3.1 Introduction 86

3.2 ADMA/Arginine Homeostasis in Gambian Children with Severe Malaria 88

Plasma Concentrations of ADMA and Arginine 88

Mortality 93

Assessment of ADMA and Arginine in Defined Severe Malaria Syndromes 94

Relationship between the ADMA/Arginine Ratio, Lactate and sVCAM 97

Relationship between Hypoargininaemia and the ADMA/Arginine Ratio 101

3.3 ADMA/Arginine Homeostasis in *P. berghei* ANKA-Infected Mice 103

3.4 Hepatic DDAH Dysfunction 104

Rationale for the Study of Hepatic DDAH 104
Hepatic DDAH1 Protein and Gene Expression 105
Hepatic DDAH1 Enzyme Activity and Intracellular ADMA Accumulation 106

3.5 Assessment of DDAH Function in a Mouse Model of Haemolysis **108**
Chemical Induction of Haemolysis 108
Hepatic DDAH Function 110
Plasma ADMA/Arginine Ratios 111

3.6 Discussion **113**

3.7 Conclusion **116**

3.8 Materials and Methods **117**
Clinical Study Procedures 117
Animal Model Procedures 118
Biochemical and Molecular Assays 120
Statistical Analyses 126

Acknowledgements **126**

4 Tetrahydrobiopterin Depletion **128**

4.1 Introduction **128**

4.2 BH4 Availability in *P. berghei* ANKA-Infected Mice **131**

4.3 BH4 Supplementation by Intermittent Injection of Sepiapterin **139**

4.4 Discussion **146**

4.5 Conclusion **148**

4.6 Materials and Methods **149**
Animal Procedures 149
Biochemical Analysis 151
Statistical Analyses 154

Acknowledgements **155**

5 Arginine and Tetrahydrobiopterin Co-Supplementation **156**

5.1 Introduction **156**

5.2 Initial Investigations of Citrulline Pharmacology **158**
Rationale for Administration of Citrulline 158
Intermittent Injection of Citrulline 159

5.3 Simultaneous Infusion of Citrulline and Sepiapterin **161**

5.4 Physiological Effects of Simultaneous Citrulline and Sepiapterin Infusion **173**

Disease severity 173
Dietary Intake, Fluid Intake and Weight Loss 175

5.5 Effects of Citrulline and Sepiapterin Infusion on NOS Uncoupling **177**
Whole Blood Nitrite 177
Limitations of Whole Blood Nitrite as a Biomarker of NO Synthesis 179
Nitrotyrosine 182

5.6 Effect of Citrulline and Sepiapterin Infusion on Hepatic DDAH Function **184**

5.7 Effect of Citrulline and Sepiapterin Infusion on Phenylalanine Metabolism **186**

5.8 Discussion **191**

5.9 Conclusion **194**

5.10 Materials and Methods **195**
Animal Procedures 195
Biochemical Analysis 198
Statistical Analyses 206

Acknowledgements **206**

6 General Discussion **207**

6.1 Principal Findings **207**

6.2 Critical Evaluation of Findings **210**
Potential Therapeutic Efficacy of Arginine and BH4 Co-Supplementation 210
Candidate Approaches to Restoring NO Signalling Independent of NOS 211
Validity of Mouse Model for the Study of NO Synthesis 212
Differences between BH4 Availability in Mice and Humans 213
Other Limitations of Mouse Models in Severe Malaria Research 215

6.3 Ongoing and Future Investigations **216**
Clinical Studies 216
Autopsy Studies 217
Mechanistic Studies of Hepatic DDAH Function 218
Relating DDAH Genotype to Plasma ADMA 220

6.4 Previous Trials of Adjunctive Therapies **221**
Limitations of Previous Clinical Trials 228

6.5 Adjunctive Therapies Currently in Development **229**

6.6 Central Goals for Reducing the Global Malaria Burden **232**
Combating Parasite and Vector Resistance 232
Vaccine Development 232
Improved Clinical Management of Severe Malaria Research 233

APPENDICES 234

A HPLC Determination of Arginine, Citrulline and Ornithine 235

A.1 Introduction 235

A.2 Materials and Instrumentation 236

A.3 Assay Optimization 240

A.4 Assay Validation 247

A.5 Conclusion 255

Acknowledgements 255

B Quantitative Assessment of Urea Cycle Flux 256

B.1 Introduction 256

B.2 Glossary 258

B.3 Basic Calculation of Metabolic Kinetics 259

Definition of the Tracer-Tracee Ratio 259

Single Metabolite Rate of Appearance 260

Calculation of Substrate-Product Flux 263

B.4 Labelling Strategy 265

B.5 Calculation of Metabolic Kinetics in a Cyclical System 267

Definitions of Recycled, Non-Recycled and Total Rates of Appearance 267

Tracer-Specific Calculation of Appearance Rates 268

Calculation of Urea Cycle Recycling 272

Substrate-Product Flux between Urea Cycle Intermediates 279

B.6 Calculation of Arginine Metabolism by Nitric Oxide Synthase 281

B.7 Summary of Key Equations 284

B.8 Conclusion 286

C HPLC Determination of ADMA 288

C.1 Introduction 288

C.2 Materials and Methods 289

C.3 Assay Optimization and Validation 295

C.4 Conclusion 309

Acknowledgements 311

D HPLC-Based Quantification of DDAH Activity 312

D.1 Introduction 312

D.2 Materials and Methods 312

D.3 Assay Validation 314

D.4 Conclusions 318

Acknowledgements 318

E HPLC Determination of Tetrahydrobiopterin and 7,8-Dihydrobiopterin 319

E.1 Introduction 319

E.2 Materials and Methods 320

E.3 Overview of Assay Chemistry 323

E.4 Assay Optimization 326

E.5 Assay Validation 339

E.6 Conclusions 344

Acknowledgements 344

References 345

Word Count 382

List of Figures

CHAPTER 1

Figure 1.1 | Global *Plasmodium falciparum* endemicity (2010 Estimates) 2
Figure 1.2 | Illustration of the *P. falciparum* life-cycle 4
Figure 1.3 | Mortality in African children with severe malaria 13
Figure 1.4 | Sequestration in cerebral malaria 16
Figure 1.5 | Loss of endothelial barrier integrity in cerebral malaria 19
Figure 1.6 | Inhibition of nitric oxide signalling in severe malaria 25
Figure 1.7 | Nitric oxide synthase requires arginine and BH4 and is inhibited by ADMA 27

CHAPTER 2

Figure 2.1 | Overview of arginine, ornithine and citrulline metabolism in mammals 31
Figure 2.2 | *P. berghei* ANKA infection in C57BL/6 mice 32
Figure 2.3 | Depletion of plasma arginine, citrulline and ornithine 34
Figure 2.4 | Maintenance of plasma arginine/ornithine ratios 34
Figure 2.5 | Verification of arginase knock-out in *P. berghei* ANKA 36
Figure 2.7 | Knock-out of parasite arginase does not improve survival in infected mice 38
Figure 2.8 | Knock-out of parasite arginase does not prevent blood-brain barrier breakdown 40
Figure 2.6 | *P. berghei* ANKA arginase is not required for arginine depletion 41
Figure 2.9 | Dietary intake and weight loss in C57BL/6 mice 43
Figure 2.10 | Plasma amino acids in uninfected mice subjected to dietary restriction 45
Figure 2.11 | Basic metabolic tracer theory 46
Figure 2.12 | Rates of appearance of plasma arginine, ornithine and citrulline 49
Figure 2.13 | Utilization of plasma citrulline for arginine synthesis 52
Figure 2.14 | Appearance of plasma arginine 53
Figure 2.15 | Utilization of plasma arginine for ornithine synthesis 55
Figure 2.16 | Appearance of plasma ornithine 57
Figure 2.17 | Utilization of plasma ornithine 59
Figure 2.18 | Appearance of plasma citrulline 61
Figure 2.19 | Conversion of arginine to citrulline by NOS 64
Figure 2.20 | Summary of whole-body urea cycle flux in *P. berghei* ANKA-infected mice 66

CHAPTER 3

Figure 3.1 | DDAH metabolizes ADMA 87
Figure 3.2 | Plasma ADMA and arginine in Gambian children with severe malaria 90
Figure 3.3 | Identification of severe malaria sub-groups 95
Figure 3.4 | Plasma ADMA/arginine ratios in sub-groups of severe malaria patients 96
Figure 3.5 | Elevation of lactate in severe malaria 98
Figure 3.6 | Elevation of sVCAM in severe malaria 100
Figure 3.7 | Plot of plasma ADMA/arginine ratios vs arginine in healthy controls, acute malaria and post-recovery 102
Figure 3.8 | ADMA/arginine homeostasis in *P. berghei* ANKA-infected mice 103
Figure 3.9 | Hepatic DDAH1 protein is decreased in *P. berghei* ANKA-infected mice 105
Figure 3.10 | *P. berghei* ANKA decreases hepatic DDAH activity and increases hepatic ADMA 106
Figure 3.11 | Phenylhydrazine exposure causes weight loss, lethargy and anaemia 109
Figure 3.12 | Phenylhydrazine decreases hepatic DDAH activity and increases hepatic ADMA 110
Figure 3.13 | Phenylhydrazine increases plasma ADMA and ADMA/arginine ratios 112

CHAPTER 4

Figure 4.1 | Tetrahydrobiopterin synthesis and recycling pathways 129
Figure 4.2 | BH4 and 7,8-BH2 concentrations in plasma and red blood cells of *P. berghei* ANKA-infected mice 134
Figure 4.3 | Tissue BH4 and 7,8-BH2 concentrations in *P. berghei* ANKA-infected mice 136
Figure 4.4 | Sepiapterin treatment supplements 7,8-BH2 and BH4 139
Figure 4.5 | Erythrocyte BH4 and 7,8-BH2 are restored by sepiapterin treatment 141
Figure 4.6 | Effect of sepiapterin treatment on tissue BH4 and 7,8-BH2 143
Figure 4.7 | Sepiapterin treatment does not prevent severe symptoms in infected mice 144
Figure 4.8 | Whole blood nitrite in response to infection and sepiapterin injection 145

CHAPTER 5

Figure 5.1 | Arginine, citrulline and ornithine are not restored by intermittent citrulline injection 160
Figure 5.2 | Whole blood nitrite is not restored by intermittent citrulline injection 160
Figure 5.3 | Supplementation of plasma arginine, citrulline and ornithine by continuous infusion of citrulline and sepiapterin 162
Figure 5.4 | Effect of citrulline and sepiapterin infusion on plasma ADMA/arginine ratios 164
Figure 5.5 | Supplementation of tissue arginine, citrulline and ornithine by continuous infusion of citrulline and sepiapterin 166

Figure 5.6 | Supplementation of plasma and erythrocyte BH4 by continuous infusion of citrulline and sepiapterin 170
Figure 5.7 | Supplementation of tissue BH4 by continuous infusion of citrulline and sepiapterin 172
Figure 5.8 | Effect of citrulline and sepiapterin infusion on behavioural scores 174
Figure 5.9 | Dietary intake and weight loss in *P. berghei* ANKA-infected mice infused with citrulline and sepiapterin 176
Figure 5.10 | Simultaneous infusion of citrulline and sepiapterin improves whole blood nitrite in *P. berghei* ANKA-infected mice 178
Figure 5.11 | Dietary restriction reduces whole blood nitrite in uninfected mice 179
Figure 5.12 | Analysis of nitrite in food and water provided to experimental mice 180
Figure 5.13 | Plasma, brain and liver nitrotyrosine in *P. berghei* ANKA-infected mice 183
Figure 5.14 | No effect of citrulline and sepiapterin infusion on hepatic DDAH function in *P. berghei* ANKA-infected mice 185
Figure 5.15 | Citrulline and sepiapterin infusion restores plasma phenylalanine/tyrosine ratios 187
Figure 5.16 | Citrulline and sepiapterin infusion restores phenylalanine/tyrosine ratios in tissue 189

CHAPTER 6

Figure 6.1 | Decreased hepatic DDAH activity and increased hepatic ADMA in a mouse model of sickle cell disease 219

APPENDIX A

Figure A.1 | OPA derivatization reaction 238
Figure A.2 | Determination of common amino acid retention times 240
Figure A.3 | Assessment of candidate internal standards 242
Figure A.4 | Comparison of protein precipitation strategies 243
Figure A.5 | Plot of solvent A concentration vs time for optimized (84µl/min) program 245
Figure A.6 | Run-time optimization 246
Figure A.7 | Plots of standard curves for arginine, citrulline and ornithine 248

APPENDIX B

Figure B.1 | Schematic representation of single-metabolite turnover 262
Figure B.2 | Schematic representation of substrate-product conversion 264
Figure B.3 | Labelling strategy 266
Figure B.4 | Rates of appearance in a cyclical system 267
Figure B.5 | Fates of heavy isotope-labelled urea cycle tracers 268

Figure B.6 | Hypothetical two-intermediate model of cyclical metabolism 273
Figure B.7 | Metabolism of arginine tracer by nitric oxide synthase (NOS) 282

APPENDIX C

Figure C.1 | Derivatization Reaction 292
Figure C.2 | Plot of solvent A concentration vs time 293
Figure C.3 | Identification of analyte retention times 296
Figure C.4 | Chromatographic resolution of analytes 298
Figure C.5 | Survey of human and mouse plasma for potential contaminants. 299
Figure C.6 | Chromatographic separation of contaminant contributed by SPE column 300
Figure C.7 | Plot of standard curves 301

APPENDIX D

Figure D.1 | Chromatographic resolution of analytes 315
Figure D.2 | Assessment of DDAH activity assay kinetics 316
Figure D.3 | DDAH activity is quantitatively dependent on protein concentration 317

APPENDIX E

Figure E.1 | Sequence of analytical events for detection of BH4 and 7,8-BH2 323
Figure E.2 | Electrochemical detection of BH4 324
Figure E.3 | Oxidation of 7,8-BH2 325
Figure E.4 | Identification of Retention times for BH4 and 7,8-BH2 standards 326
Figure E.5 | Analytical cell voltage optimization 327
Figure E.6 | Guard cell voltage optimization 328
Figure E.7 | Neutralization of plasma samples 329
Figure E.8 | Neutralization of erythrocyte samples 332
Figure E.9 | Neutralization of aorta samples 333
Figure E.10 | Neutralization of liver samples 335
Figure E.11 | Neutralization of brain samples 336

List of Tables

CHAPTERS

Table 1.1 | Blantyre coma score 7
Table 2.1 | PCR Genotype Assay for Arginase Knock-Out and Wild-Type Parasites 71
Table 2.2 | Scoring System for the Assessment of Disease Symptoms in Mice 72
Table 2.3 | Mobile phase solvent ratios and pump program 74
Table 2.4 | List of monitored metabolites 79
Table 3.1 | Clinical laboratory values in Gambian Children with uncomplicated or severe malaria 89
Table 3.2 | Clinical laboratory values in Gambian Children with severe malaria who died. 93
Table 4.1| Scoring System for the Assessment of Disease Symptoms in Mice 150
Table 4.2 | Chemical reactions for the measurement of nitrite (NO2-) 154
Table 5.1 | Scoring System for the Assessment of Disease Symptoms in Mice 197
Table 5.2 | Mobile phase solvent ratios and pump program 200
Table 5.3 | Chemical reactions for the measurement of nitrite (NO2-) 204
Table 6.1 | Immune Modulation Therapies 222
Table 6.2 | Iron Chelation and Anti-Oxidant Therapies 224
Table 6.3 | Fluids and Osmotic Argents 226
Table 6.4 | Seizure prophylaxis 227
Table 6.5 | Other Strategies 228

APPENDICES

Table A.1 | Run time optimization 245
Table A.2 | Linearity of standards assayed over a range of concentrations 248
Table A.3 | Inter-day precision 249
Table A.4 | Limit of detection (LOD) 250
Table A.5 | Assessment of analyte stability 252
Table A.6 | Recovery of amino acid standards spiked into plasma samples 253
Table A.7 | Analysis recovery of amino acid standards spiked into plasma samples 254
Table B.1 | List of monitored metabolites 265
Table B.2 | List of metabolites monitored for calculation of arginine utilization by NOS 281
Table C.1 | Mobile phase solvent ratios and pump program 293
Table C.2 | Absolute and relative recovery of analytes from solid phase extraction 295

Table C.3 | Linearity of standards assayed over a range of concentrations 301
Table C.4 | Limit of detection (LOD) 302
Table C.5 | Intra- and inter-day precision 304
Table C.6 | Autosampler stability 305
Table C.7 | Recovery of standards spiked into human plasma 307
Table C.8 | Recovery of standards spiked into mouse plasma 308
Table E.1 | Quantitative comparison of sample processing with or without NaOH neutralization 330
Table E.2 | Quantitative comparison of erythrocytes processed with or without NaOH neutralization 332
Table E.3 | Analyte stability 338
Table E.4 | Linearity of standards assayed over a range of concentrations 339
Table E.5 | Limit of detection (LOD) 340
Table E.6 | Inter-day precision 341
Table E.7 | Recovery of standards spiked into mouse plasma 342
Table E.8 | Recovery of standards spiked into mouse red blood cell samples 343

Abbreviations

ADMA	Asymmetric dimethylarginine (N^G,N^G-dimethyl-L-arginine)
Ang-1 / Ang-2	Angiopoietin-1 / Angiopoietin-2
ASL	Argininosuccinate lyase
ASS1	Argininosuccinate synthetase 1
7,8-BH2	7,8-Dihydrobiopterin
BH4	Tetrahydrobiopterin
CAT	Cationic amino acid transporter
DDAH	dimethylarginine dimethylaminohydrolase
eNOS	Endothelial nitric oxide synthase
GTPCH	GTP cyclohydrolase
HPLC	High-performance liquid chromatography
ICAM1	Intercellular adhesion molecule 1
L-NMMA	N^G-monomethyl-L-arginine
MEA	N^G-monoethyl-L-arginine
NO	Nitric oxide
NOS	Nitric oxide synthase
nNOS	Neuronal NOS (NOS1)
iNOS	Inducible NOS (NOS2)
eNOS	Endothelial NOS (NOS3)
OTC	Ornithine transcarbamylase
PfEMP1	P. falciparum erythrocyte membrane protein 1
PHZ	Phenylhydrazine
Q-TOF LC/MS	Quadrupole time-of-flight liquid chromatography/mass spectrometry
SDMA	Symmetric dimethylarginine (N^G,$N^{G'}$-dimethyl-L-arginine)
SPR	Sepiapterin reductase
TNF	Tumour necrosis factor
TTR	Tracer/tracee ratio, see APPENDIX B: Glossary, p. 257
VCAM / sVCAM	Vascular cell adhesion molecule / soluble VCAM
vWF	von Willebrand factor

CHAPTER 1.

Background

Current estimates of world-wide mortality due to malaria range from 627,000 to 1,238,000 deaths per year, mostly in African children. Prompt treatment with parenteral artesunate improves survival in children with severe malaria, but mortality remains high among patients presenting with complications such as acidosis or coma. Development of effective therapies for these patients will require improved understanding of the pathophysiology of severe malaria. This thesis examines the biology and biochemistry of nitric oxide synthesis as a potential target for the development of adjunctive therapies to accompany anti-parasite drugs.

1.1 Malaria Epidemiology

An estimated 3.3 billion people are at risk of malaria infection, resulting in an approximately 207 million clinical cases and mortality estimates ranging from 627,000 (World Health Organization, 2013) to 1,238,000 (Murray et al., 2012) deaths per year. Malaria is caused by mosquito-borne parasitic protozoans of the genus *Plasmodium* and its endemicity is determined largely by climate and the ecology of mosquito vectors. The long lifespan, high densities and strong human-biting habit of African *Anopheles* mosquitoes results in annual exposures of 10 to 1,000 infective bites in some areas of sub-Saharan Africa (Gething et al., 2011). As a result of high transmission rates, roughly 80% of clinical malaria cases and 90% of deaths due to malaria occur in Africa, primarily among children under 5 years old (World Health Organization, 2013; Murray et al., 2012).

The majority of the remaining disease burden is borne by South-East Asian countries where transmission is far less stable and individuals receive an average of one or fewer infective bites per year (World Health Organization, 2013; Gething et al., 2011). Malaria was successfully eliminated from Europe, Russia and the United States of America in the mid-20th

century following the discovery of chloroquine, an anti-malarial drug, in 1934 and the insecticide dichlorodiphenyltrichloroethane (DDT) in 1939. In the latter part of the 20th century, the spread of chloroquine resistance, inadequate funding and stalled public health initiatives led to a resurgence of malaria disease burdens in the developing world. Renewed sources of funding and improved strategic implementation of public health measures have resulted in steady reductions in global infection rates and mortality over the past decade (World Health Organization, 2013; Murray et al., 2012; Feachem et al., 2010).

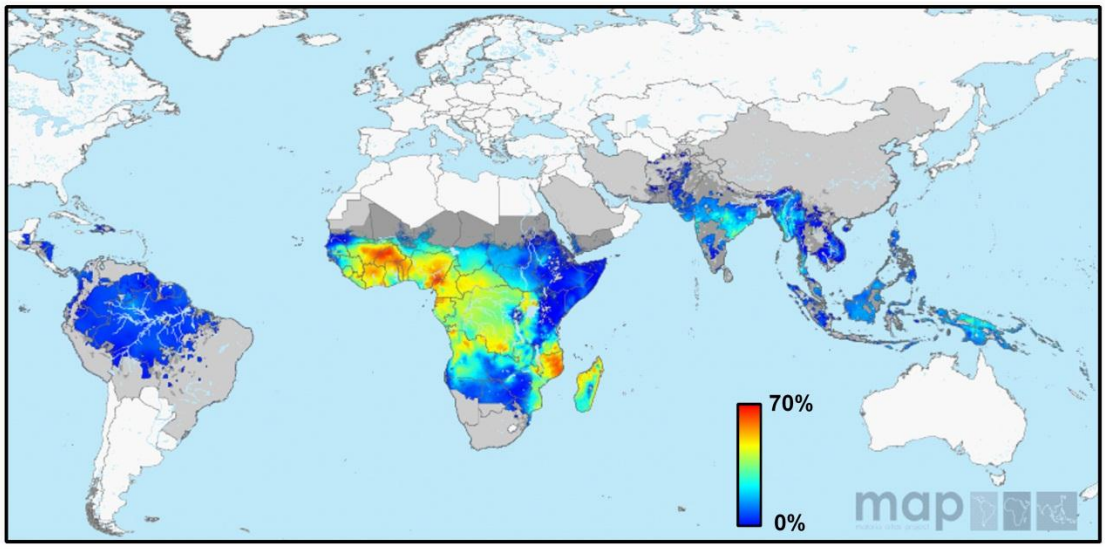


Figure 1.1 | Global *Plasmodium falciparum* endemicity (2010 Estimates). Colour gradient depicts estimated percentages of children (2-10 years old) infected with *P. falciparum* at any one time, averaged over the 12 months of 2010. Dark grey areas indicate unstable transmission (infection rate <0.1%). Light grey areas are malaria-free (white: not surveyed). Estimates are based on parasite rate surveys and environmental covariates. Reprinted with permission from the Malaria Atlas Project (Gething et al., 2011).

1.2 *Plasmodium* spp. Biology and Transmission

The periodic febrile symptoms of malaria were recognized long before the identification of a causative agent. The name "malaria" derives from Italian after the suggestion that the swamps and low-lying marshlands caused disease by exuding "bad air" (Smith and Sanford, 1985). Working in Algeria in 1880, Alphonse Laveran was the first to assert that malaria was caused by a parasite based on microscopic observation of infected blood samples. The biology

and transmission of *Plasmodium* spp. were steadily uncovered over the course of 1880's and 1890's, culminating with Ross' and Grassi's independent demonstrations of transmission by mosquito vectors among avian and human hosts, respectively (Ross, 1897; Grassi et al., 1899). Modern research on the pathophysiology of severe malaria can be traced back to Marchiafava and Bignami's 1892 monograph *On Summer-Autumn Malaria Fevers*, in which the Italian malariologists proposed that neurological symptoms associated with severe malaria were caused by physical obstruction of blood vessels by parasitized erythrocytes (Marchiafava and Bignami, 1892).

Malaria is transmitted by female mosquitoes of the genus *Anopheles*. Transmission begins when a mosquito vector ingests *Plasmodium* gametocytes while feeding on an infected host. Male and female gametocytes recombine to form a motile ookinete, which traverses the epithelial lining of the mosquito midgut and differentiates into an oocyst. The oocyst matures further and eventually releases sporozoites, which migrate to the mosquito's salivary glands via the mosquito's haemolymph. During a subsequent feeding, sporozoites are inoculated into the subcutaneous tissue of the new host, from which point they migrate to and penetrate blood vessels to enter circulation. Circulating sporozoites adhere to and invade hepatocytes in a process facilitated by circumsporozoite protein (CSP) expressed on the surface of the sporozoite. The human host remains asymptomatic for 1-2 weeks while liver-stage parasites replicate within hepatocytes. The blood stage begins when the hepatocyte ruptures and asexual merozoites forms (10,000-30,000/infected hepatocyte) are released into the blood stream and invade erythrocytes. Maturation of blood-stage parasites is characterized by a succession of intraerythrocytic forms known as rings, trophozoites and schizonts. At approximately 48 hours post-invasion, the schizont ruptures the host erythrocyte, releasing daughter merozoites which continue on to infect additional erythrocytes. During blood-stage infection, infected individuals experience episodes of fever and flu-like symptoms (headache, fatigue, nausea) which may progress to life-threatening complications (severe malaria). If sufficient immunity is acquired, symptoms may be mild or even absent despite significant blood-stage parasitaemia. A minority

of asexual blood stage parasites will differentiate into gametocytes, which are taken up in the blood meal of a feeding mosquito, completing the life cycle (FIG 1.2).

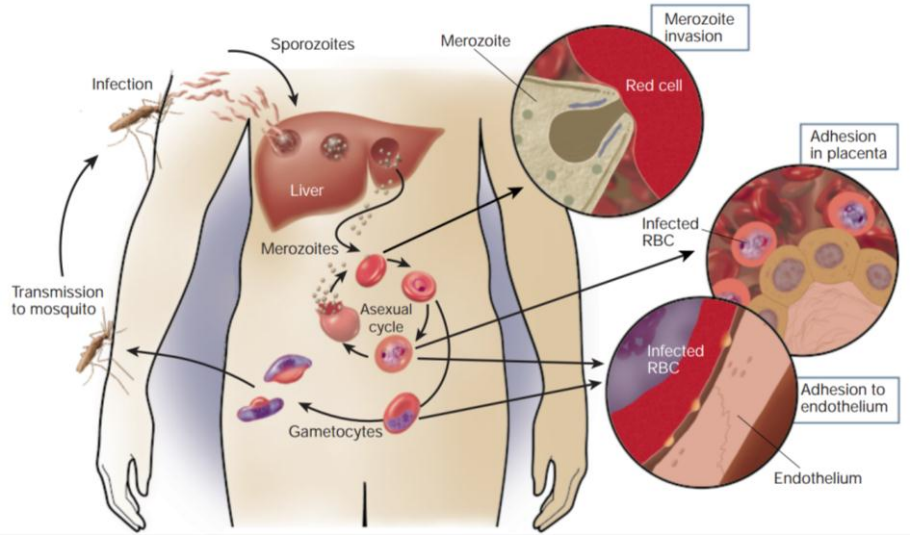


Figure 1.2 | Illustration of the *P. falciparum* life-cycle. Infection of the human host begins with the bite of infected mosquito. Inoculated sporozoites infect hepatocytes, replicate and release merozoites. The blood stage involves cyclical asexual replication within host erythrocytes, during which clinical features of malaria infection are apparent. The cycle is completed with differentiation of gametocytes which are taken up by a mosquito vector during feeding. Reprinted by permission from Macmillan Publishers Ltd: *Nature* (Miller et al., 2002), copyright 2002.

Malaria in humans is caused by *P. falciparum*, *P. vivax*, *P. ovale*, *P. malariae* and, according to recent reports, the primate malaria parasite *P. knowlesi* (Kantele and Jokiranta, 2011). Severe disease due to *P. vivax* and mixed infections has recently been recognized in South-East Asia (Barcus et al., 2007; Tjitra et al., 2008), but the vast majority of severe disease and malaria-associated mortality is due to *P. falciparum*, especially in Africa (World Health Organization, 2013). This thesis will focus on the pathophysiology of severe *P. falciparum* malaria in combination with observations of *P. berghei* ANKA infection in mice as an *in vivo* model.

1.3 Clinical Features of Severe Malaria

Diagnosis

Standard diagnosis of malaria infection is performed by microscopic observation of stained blood smears. Rapid diagnostic tests are now available for the detection of *P. falciparum* histidine rich protein 2 and lactate dehydrogenase. Increased sensitivity can be achieved by testing for parasite RNA or DNA using polymerase chain reaction (PCR), but this method does not provide quantitation of parasite load.

Severe Malaria Susceptibility

Immunity to malaria infection is acquired over years of repeated exposure. While acquired immunity does not provide complete protection from malaria infection, it substantially reduces the risk of severe complications. The highest burden of disease occurs in children between 1 and 5 years old living in malaria-endemic regions. These children have generally lost the protective effects of maternally-conferred antibodies (Reyburn et al., 2005), but have yet to acquire protective immunity and are therefore at high risk of severe complications from malaria infection. For example, children under 5 account 82% of all deaths due to malaria in Africa (World Health Organization, 2013). By adulthood, inhabitants of high transmission areas have generally acquired sufficient immunity, and additional infections produce mild symptoms or none at all. In areas with lower or irregular transmission rates, such as South-East Asia, acquired immunity is less common and all age groups are at risk of severe malaria during periods of increased transmission (Dondorp et al., 2008b).

Complications of Severe Malaria

The World Health Organization (WHO) definition of severe malaria includes a range of complications associated with increased risk of mortality: unarousable coma (Blantyre coma score of less than 3), acidosis (lactate > 5mmol/L, bicarbonate < 15 mmol/L, pH < 7.35), severe anaemia (haemoglobin < 5 g/dl or hematocrit < 15%), hypoglycaemia (glucose < 2.2 mmol/L or

< 40 mg/dL), prostration (inability to sit unsupported), renal impairment (urine output < 12 mL/kg/24hr or plasma creatinine above age-related normal range, persisting after rehydration) and respiratory distress (mild: sustained nasal flaring mild intercostal indrawing, severe: marked intercostal indrawing or deep acidotic breathing) (World Health Organization, Communicable Diseases Cluster, 2000). Hyperparasitaemia is also associated with increased risk of mortality but the threshold of increased risk varies according to local malaria endemicity (>2% of circulating erythrocytes or >100,000 parasites/µl in areas of low-intensity transmission and >5% of circulating erythrocytes or >250,000 parasites/µl in areas of high-intensity transmission) (World Health Organization, Communicable Diseases Cluster, 2000). Pulmonary oedema and jaundice are also indicators of severe malaria infection but are much more common in adults than in children. Multiple complications can occur in the same patient over the course of disease (Marsh et al., 1995).

Neurological Involvement

In a large cohort study, 47.6% of children under 14 years of age presented with some level of neurological involvement including seizures, psychosis, agitation, confusion, impaired consciousness and coma (Idro et al., 2007). The Blantyre coma score is the preferred metric used to assess neurological impairment as it can be applied to young children who have not yet learned to speak. This system utilizes assessments of ocular, motor and verbal responsiveness to score neurological competence on a scale of 0 (comatose) to 5 (normal) (Molyneux et al., 1989b) (TABLE 1.1). A Blantyre coma score of less than 3 indicates an unarousable coma and may be described by the term ‘cerebral malaria’ in the absence of other causes of coma, which are often difficult to rule out (World Health Organization, Communicable Diseases Cluster, 2000). A seminal autopsy study demonstrated that a significant minority (24%) of patients meeting the clinical criteria of cerebral malaria died of other causes (Taylor et al., 2004). Ophthalmoscopic assessment of malaria-induced retinal changes, including papilloedema, retinal whitening and haemorrhage, improves the accuracy of cerebral malaria diagnosis (Taylor

et al., 2004; Beare et al., 2004; Birbeck et al., 2010a). Lumbar puncture can also help exclude other potential causes of encephalopathy such as bacterial meningitis (Berkley et al., 1999).

Parameter	Score
Best Motor Response	
Localizes painful stimulus*	2
Withdraws limb from painful stimulus†	1
No response or inappropriate response	0
Best verbal response	
Cries appropriately with painful stimulus*	2
Moan or inappropriate cry	1
No response	0
Eye movement	
Directed (e.g. follows mother's face)	1
Not directed	0
Maximum total score (normal)	**5**
Minimum total score (comatose)	**0**

Table 1.1 | Blantyre coma score. Scoring system adapted by Molyneux et al. (see Molyneux et al., *QJM,* 1989) from the Glasgow coma score (Teasdale and Jennett, 1974). *Painful stimulus: apply pressure to patient's sternum with knuckles or blunt end of pencil † Painful stimulus: apply pressure on thumbnail bed with horizontal pencil.

Seizures are present in 80% of children with neurological involvement (Mohanty et al., 2003). Seizures may be repetitive, focal or prolonged (Waruiru et al., 1996). Onset of coma is typically rapid in children and often follows seizures. The onset of coma in affected adults is slower than in children and only occasionally associated with episodes of seizure, which occur in 15-20% of adult patients with neurological involvement (Mishra et al., 2007; Mishra and Newton, 2009). In adult and paediatric patients, seizures appear generalized, but focal origins can be identified by EEG (Crawley et al., 2001). Electrical discharges may be observed in the absence of overt clinical manifestations (Crawley et al., 1996, 2001). Roughly half of children with cerebral malaria exhibit increased brain volume as determined by MRI (Potchen et al.,

2012). Prior studies identified elevated opening lumbar CSF pressures (Newton et al., 1991; Waller et al., 1991) and elevated intracranial pressure in children with cerebral malaria (Newton et al., 1997). Abnormal posturing is more common in children than in adults and is typically associated with hypoglycaemia or raised intracranial pressure (Mishra and Newton, 2009). Disconjugate gaze, hemiparesis and cranial nerve involvement can also occur (World Health Organization, Communicable Diseases Cluster, 2000).

Impaired consciousness is associated with elevated risk of death from malaria infection (Marsh et al., 1995; von Seidlein et al., 2012). Children who survive cerebral malaria are also at risk of persistent neurological sequelae including epilepsy (Carter et al., 2004; Ngoungou et al., 2006) or persistent language, cognitive, motor and/or sensory disability (Idro et al., 2007; Brewster et al., 1990; van Hensbroek et al., 1997; Carter et al., 2005a; b; Boivin et al., 2007; Kihara et al., 2006). The incidence of epilepsy and other neurodisability was 26.5% in a recent study of strictly-defined retinopathy-positive children with cerebral malaria (Birbeck et al., 2010b). If behavioural problems, such as attention deficit hyperactivity disorder (ADHD), are also included, the rate of neurological sequelae rises further to 31.8% (Birbeck et al., 2010b). A separate 2 year follow up study of Ugandan children found 26% of paediatric cerebral malaria survivors demonstrated cognitive deficits, compared with only 8% of healthy controls (John et al., 2008). In adults, neurological sequelae are less common, ranging from 3-10%. In an Indian study, the most common sequelae in adults upon discharge were psychosis (4%), ataxia (3%) and extrapyramidal rigidity or hemiplegia (Bajiya and Kochar, 1996; Jain et al., 2008).

Acidosis

Lactic acidosis is consistently associated with increased risk of death from severe malaria across a range of studies in children (Taylor et al., 1993; Krishna et al., 1994; Waller et al., 1995; Planche et al., 2003) and adults (Day et al., 2000). Respiratory distress, a common clinical manifestation of acidosis, is also a prognostic indicator of poor outcome (Marsh et al., 1995; Hanson et al., 2010). Increased lactate production in brain tissue has been described in

animal models of malaria (Sanni et al., 2001; Penet et al., 2005). During anaerobic respiration, lactate is generated from pyruvate by lactate dehydrogenase in order to restore NAD^+ required for glycolysis. In a prospective study of Vietnamese adults, the lactate/pyruvate ratio was high in patients with severe malaria and was elevated further in those who died (Day et al., 2000). These finding suggest that increased blood acidity during malaria infection results from a shift from aerobic to anaerobic respiration due to insufficient tissue perfusion.

Sequestration and volume depletion have been investigated as potential mechanisms limiting tissue perfusion in severe malaria. Two independent intravital microscopy studies identified impaired microcirculation in patients with severe malaria and demonstrated that the prevalence of stagnant microcapillaries correlated with plasma lactate (Dondorp et al., 2008a; Hanson et al., 2012). In the second of these studies, hypovolaemia correlated poorly with lactate or quantitative scores of disease severity, suggesting that macrovascular dysfunction plays a lesser role than microvascular dysfunction in driving acidosis (Hanson et al., 2012). In agreement with this interpretation, children with severe malaria present with only mild volume-depletion, and no relationship was detected between hypovolaemia and acidosis in either of two studies (Planche et al., 2004; Jarvis et al., 2006). In addition, a large multi-centre randomized controlled trial recently demonstrated that intravenous fluid bolus is harmful in children with severe malaria (Maitland et al., 2011). Taken together, these results suggest that acidosis results from anaerobic respiration associated with microvascular dysfunction and impaired tissue perfusion. *P. falciparum* parasites express lactate dehydrogenase and may contribute to increased rates of lactate production during severe disease (Pfaller et al., 1982; Vander Jagt et al., 1981). Blood flow to the liver, a key site of lactate clearance, was found to be decreased Thai adults with severe malaria (Molyneux et al., 1989a), suggesting that impaired hepatic clearance could also exacerbate lactate accumulation.

Severe Anaemia

Malaria infection is a major cause of anaemia in the developing world (Kassebaum et al., 2014). Infected erythrocytes are lysed during blood stage replication of *Plasmodium* parasites, but it is estimated that for each infected erythrocyte, an additional 8.5 uninfected erythrocytes are destroyed or removed from circulation (Jakeman et al., 1999). Oxidative modification of bystander uninfected cells (Griffiths et al., 2001) and/or enhanced splenic function during malaria infection (Looareesuwan et al., 1987) may be responsible for this phenomenon. Inhibition of erythropoiesis during *P. falciparum* infection is also likely to contribute to severe malarial anaemia (Kurtzhals et al., 1997; Chang et al., 2004). It has been proposed that inflammatory signalling (Schofield and Grau, 2005) and the malarial pigment haemozoin (Casals-Pascual et al., 2006) are key upstream causes of impaired erythropoiesis. In the absence of co-morbid complications, malarial anaemia is associated with relatively low rates of mortality (1.3%), likely due in part to the availability of transfusion as a corrective measure in severe cases (Marsh et al., 1995).

Renal Impairment

Renal failure is common in Asian adults with severe malaria (Dondorp et al., 2008b; Trang et al., 1992), but has been described as rare in children (World Health Organization, Communicable Diseases Cluster, 2000). However, a recent analysis of clinical laboratory findings from a large, randomized trial comparing anti-malarial therapies in African children with severe malaria found elevated blood urea nitrogen to be one of the 5 best independent predictors of mortality (von Seidlein et al., 2012). This finding supports previous findings of higher blood urea nitrogen and higher creatinine in children who died from cerebral malaria compared with survivors (Waller et al., 1995). These observations suggest that renal insufficiency may contribute to the pathogenesis of severe malaria in children as well as adults, although elevated blood urea nitrogen could also arise from accelerated protein breakdown.

1.4 Clinical Management of Severe Malaria

Anti-Malarial Chemotherapies

In treating patients with severe malaria, rapid reduction of parasite burden with antimalarial drugs is a priority. Artemisinin derivatives, including artesunate, artemether and dihydroartemisinin, are currently the most effective class of antimalarial drugs. These compounds act on intraerythrocytic parasites as well as early-stage gametocytes, providing a wide therapeutic window for elimination of parasites and prevention of transmission (White, 2008). The presumptive mechanism of action of artemisinin derivatives involves the cleavage of a peroxide bridge by ferrous haem or free ferrous iron. The resulting radicals are highly reactive and have been proposed to kill parasites by inactivating parasite-expressed proteins, damaging the digestive vacuole or interfering with the ability of the parasite to detoxify haem by converting it to haemozoin (Kannan et al., 2002; Hartwig et al., 2009).

The current recommendation for treatment of severe malaria is artesunate (2.4 mg/kg) administered by intravenous or intramuscular injection at admission, 12hr, 24hr and once daily until the patient is able to tolerate oral medication (World Health Organization, 2010). If artesunate is unavailable, artemether may be used as an alternative (World Health Organization, 2010). Artemether should be administered by intramuscular injection at a dose of 3.2 mg/kg on admission and 1.2 mg/kg daily. If neither artesunate nor artemether are available, quinine dihydrochloride (20 mg salt/kg) may be infused over 4hr at admission followed by 10mg/kg infused over 2-8 hr every 8hr (World Health Organization, 2010). Quinine only kills late-stage intraerythrocytic parasites, providing a narrower therapeutic window than artemisinin derivatives. Quinine is also induces insulin secretion and can increase risk of hypoglycaemia. Large multi-centre randomized clinical trials have proven artesunate treatment to be superior to quinine treatment in African children <15 years old (Dondorp et al., 2010) and Asian patients of all ages (Dondorp et al., 2005). Artemether has also been shown to improve survival compared to quinine, but produced a smaller survival benefit than artesunate (van Hensbroek et al., 1996a; Tran et al., 1996). If resources for parenteral administration are not immediately available, pre-

referral administration of rectal artesunate (10 mg/kg) is recommended if the expected referral time is greater than 6 hours (Gomes et al., 2009; World Health Organization, 2010). Intramuscular artesunate, artemether or quinine may also be considered for pre-referral treatment. After a minimum 24hr of parenteral treatment, the patient should complete a full course of an effective combination therapy containing an artemisinin derivatives in combination with another longer-lasting anti-malarial (e.g. artesunate/amodiaquine, artemether/lumefantrine) (World Health Organization, 2010). Uncomplicated malaria should also be treated with a full course of an artemisinin combination therapy.

Mortality

In a large, multi-centre trial, parenteral artesunate reduced mortality rates in South-East Asian children and adults with severe malaria from 22% with quinine to 15% with artesunate (Dondorp et al., 2005). Compared to quinine, artesunate reduced mortality in patients presenting with cerebral malaria (37% with quinine vs 30% with artesunate) or acidosis (38% with quinine vs 26% with artesunate) (Dondorp et al., 2005). However, among artesunate-treated patients, mortality was lower in patients without coma (6%) or without acidosis (4%) (Dondorp et al., 2005). Parenteral artesunate also reduced mortality rates from 10.9% with quinine to 8.5% with artesunate in a study in African children with severe malaria (Dondorp et al., 2010). Among artesunate-treated individuals, mortality remained higher in those presenting with coma (18% with coma vs 4% without coma) or acidosis (15% with acidosis vs 4% without acidosis) (Dondorp et al., 2010). Across both groups in this study (quinine- and artesunate-treated), the following variables were independently associated with mortality: coma score, blood urea nitrogen, acidosis (measured by base excess), and convulsions (presence or absence of convulsions lasting longer than 30 min in duration or a frequency of 2 or more convulsions in the 24hr period prior to admission) (von Seidlein et al., 2012). The mortality rate was 42.6% in patients presenting with simultaneous elevation in blood urea nitrogen ($\geq$ 20 mg/dL), acidosis (base excess of less than -8 mmol/L), and impaired consciousness (Blantyre coma score of less

than 3 and/or convulsions) (FIG 1.3). In contrast, mortality was 0.9% in children presenting with none of these complications and no evidence of chronic disease (von Seidlein et al., 2012). Anti-parasite chemotherapies will remain a cornerstone of severe malaria treatment, but adjunctive therapies are needed to improve outcomes in patients with increased risk of mortality despite rapid parasite killing.

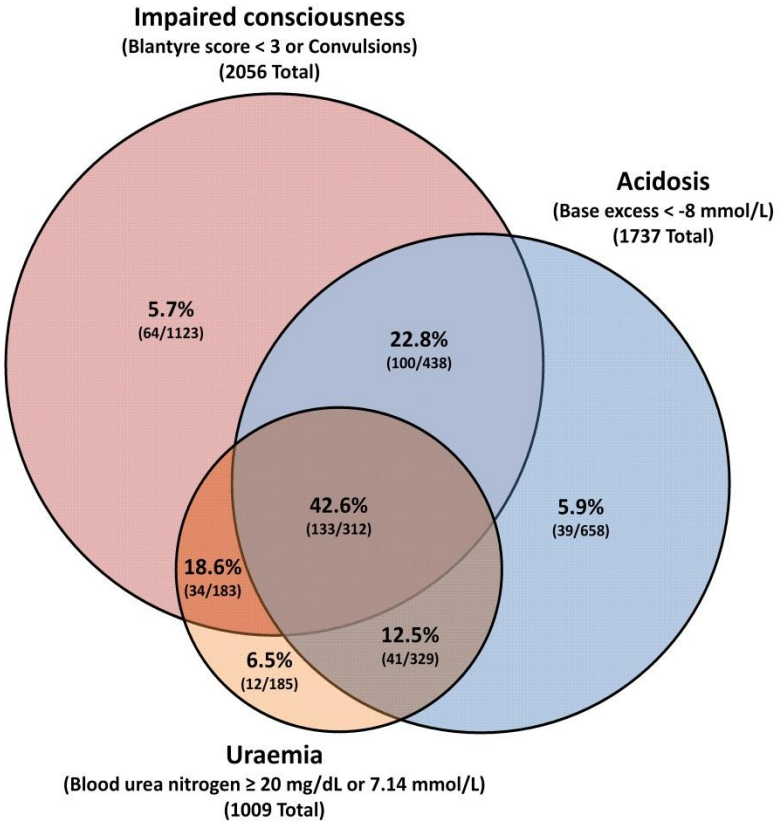


Figure 1.3 | Mortality in African children with severe malaria. Data are drawn from clinical assessments of 3,228 African children enrolled in prospective clinical trial of artesunate vs quinine (Dondorp et al., 2010). Mortality data are pooled from both treatment groups. Figure adapted from von Seidlein et al., *Clin. Infect. Dis.*, 2012.

Additional Management Strategies

Few approaches to treating severe malaria complications have proven effective. Haemofiltration resulted in rapid resolution of acidosis and significantly improved survival in Vietnamese adults with infection-associated renal failure (69% due to severe *falciparum* malaria) (Phu et al., 2002). Renal failure has long been presumed to be uncommon in children with severe malaria, but recent analyses have identified blood urea nitrogen as a strong independent predictor of mortality (von Seidlein et al., 2012). Elevated blood urea nitrogen may suggest that renal insufficiency is commonly overlooked in children with severe malaria, but could also reflect hypovolaemia or accelerated protein breakdown. Nevertheless, this finding suggests a rationale for further studies of haemofiltration in children presenting with elevated blood urea nitrogen and especially those also presenting with acidosis and/or coma who are at highest risk of death (von Seidlein et al., 2012).

Severe anaemia (haemoglobin < 5 g/dL) should be treated by transfusion where available (World Health Organization, 2010). Exchange transfusions have been suggested to reduce the risk of fluid overload, reduce circulating parasite load and remove harmful metabolites; however, comparative trials have not been completed and a meta-analysis of existing data showed no evidence of benefit (Riddle et al., 2002). Bacterial co-infections should be treated with antibiotics (Berkley et al., 1999; World Health Organization, 2010). Hypoglycaemia is associated with seizures, abnormal posturing, shock and coma in children (Mishra and Newton, 2009). Bolus glucose should be used to correct hypoglycaemia (glucose < 2.2 mmol/L). Pulmonary oedema is a potentially life-threatening complication that can occur in adults with severe malaria but is uncommon in children. Pulmonary oedema should be treated promptly by propping patient at a 45° angle, giving oxygen, administering a diuretic and halting intravenous fluids (World Health Organization, 2010). In severe cases, intubation and application of continuous positive airway pressure are recommended (World Health Organization, 2010). Large fluid bolus administration has been shown to be harmful in children (Maitland et al., 2011) and adults (Hanson et al., 2013) with severe malaria. Acute seizures may

be terminated with benzodiazepines (Ogutu et al., 2002; Mpimbaza et al., 2008; Muchohi et al., 2008). High-dose phenobarbital was shown to double mortality in Kenyan children with cerebral malaria, possibly due to respiratory depression (Crawley et al., 2000), highlighting the potential dangers of utilizing neuro-active agents with anaesthetic side-effects. Completed trials of experimental adjunctive therapies are reviewed in CHAPTER 6 (p. 220). Future development of effective therapies for patients at high risk of mortality or neurological sequelae requires a better understanding of severe malaria pathophysiology.

1.5 The Vascular Endothelium in Severe Malaria Pathogenesis

Cytoadherence of Parasitized Erythrocytes

Sequestration of late blood-stage *P. falciparum* parasites (trophozoites and schizonts) in the cerebral vasculature is a defining pathological finding in severe malaria with neurological complications (MacPherson et al., 1985; Pongponratn et al., 1991; Silamut et al., 1999; Taylor et al., 2004) (FIG 1.4). The brain typically displays the greatest density of cytoadherent infected red cells, followed by the heart, liver and skin (Turner, 1997). Among human malarias, cytoadherence is unique to *P. falciparum*, allowing *P. falciparum* to reach higher parasite densities and cause higher rates of severe disease than other *Plasmodium* species.

Cytoadherence of *P. falciparum*-infected red cells is mediated by a class of parasite-expressed protein ligands collectively referred to as *P. falciparum* erythrocyte membrane protein 1 (PfEMP1). PfEMP1 proteins are exported to the surface of the host erythrocyte between 18 and 24 hours post-invasion (trophozoite stage) where they form dense knob-like structures in the erythrocyte membrane (Leech et al., 1984; Magowan et al., 1988). PfEMP1 proteins are encoded by the highly variable *var* family of genes, only one of which is expressed at any point in time (Su et al., 1995; Baruch et al., 1995). Spontaneous changes in *var* expression provide a mechanism of immune evasion, but also determine alterations in binding phenotype (Roberts, 1992; Smith et al., 1995). PfEMP-1 proteins interact with a variety of endothelial cell ligands, including a CD36, chondroitin sulphate A, platelet/endothelial cell

adhesion molecule (PECAM) and intercellular adhesion molecule 1 (ICAM1) (Baruch et al., 1996; Gardner et al., 1996). Parasite isolates from patients with neurological complications were shown to exhibit increased ICAM1 binding tendency (Newbold et al., 1997) and endothelial expression of ICAM1 is elevated in the brains of patients who died of cerebral malaria (Turner et al., 1994). These findings implicate ICAM1-mediated cytoadherence in the pathogenesis of cerebral malaria. A recent report has also identified endothelial protein C receptor as a key ligand mediating cytoadherence in severe malaria (Turner et al., 2013).

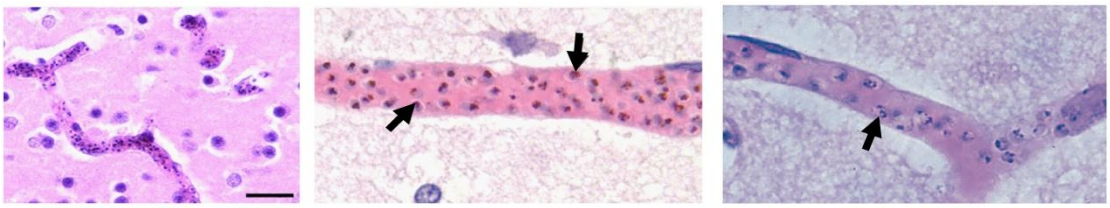


Figure 1.4 | Sequestration in cerebral malaria. Photomicrographs of *P. falciparum*-infected red blood cells sequestered in cerebral blood vessels (arrows). Scale bar in left panel = 25 µm. Middle and right panels obtained with 1000X magnification but scale bars not provided in original source articles. Left panel reprinted with permission from Elsevier: *American Journal of Pathology* (Dorovini-Zis et al., 2011), copyright 2011. Middle panel reprinted with permission from Annual Reviews, Inc: *Annual Review of Pathology: Mechanisms of Disease* (Haldar et al., 2007), copyright 2007. Right panel reprinted by permission from Macmillan Publishers Ltd: *Nature Medicine* (Taylor et al., 2004), copyright 2004.

Dysregulation of Inflammatory Signalling

Malaria infection leads to increased levels of both pro- and anti-inflammatory cytokines in mice (Rae et al., 2004) and in humans (Grau et al., 1989; Kwiatkowski et al., 1990; Brown et al., 1999a). Activation of toll-like receptors (TLRs), especially TLR2, by parasite-derived glycosylphosphatidylinositol (GPI) has been proposed as a central mechanism driving pro-inflammatory cytokine expression and release (Schofield and Hackett, 1993; Krishnegowda et al., 2005). In two landmark studies of African children, concentrations of the pro-inflammatory cytokine tumour necrosis factor (TNF) were higher in severe malaria than in uncomplicated malaria, and TNF was further elevated in fatal cases compared to survivors (Grau et al., 1989; Kwiatkowski et al., 1990). Subsequent investigations identified TNF promoter polymorphisms

that are associated with increased risk of developing cerebral malaria, neurological sequelae and death (Gimenez et al., 2003; Kwiatkowski, 2005).

These studies have resulted in assertions that over-production of TNF and other pro-inflammatory cytokines could promote severe malaria pathogenesis. This hypothesis is upheld by murine model experiments in which TNF receptor 2 (TNFR2) knock-out mice are demonstrate improved survival following *P. berghei* ANKA infection (Lucas et al., 1997). However, in a randomize clinical trial in Gambian children with cerebral malaria, anti-TNF antibody given as an adjunctive therapy had no effect on mortality and increased the incidence of neurological sequelae compared to placebo-treated controls (van Hensbroek et al., 1996b). Other clinical trials of anti-inflammatory interventions either showed evidence of harm (dexamethasone) or no improvement in survival (pentoxifylline) (See CHAPTER 6, p. 220). The results of these clinical trials highlight the discrepancy between immunopathological processes occurring in animal models and human patients, a subject of much debate (White et al., 2010).

Although of limited usefulness as a drug target, TNF may contribute to severe malaria pathogenesis by sensitizing the vascular endothelium and inducing upregulation of adhesion molecule expression (Fiedler et al., 2006). Interleukin-1α (IL-1α), another pro-inflammatory cytokine elevated in severe malaria (Kwiatkowski et al., 1990), also upregulates adhesion molecule expression in endothelial cells (De Caterina et al., 1995). The pro-inflammatory cytokine IL-6 and the anti-inflammatory cytokine IL-10 were highly correlated and found to be lower in Vietnamese adults with cerebral malaria compared to patients with other complications of severe malaria, but no neurological involvement (Day et al., 1999). Taken together, these observations suggest that excess cytokine signalling is associated with severe malaria, but not exclusively with cerebral pathology.

Effects of NO inhibition on Cytoadhesion and Inflammatory Mechanisms

Nitric oxide (NO) is a key regulator of cardiovascular and endothelial cell function with anti-inflammatory and anti-adherent effects. Binding of infected erythrocytes to endothelial

cells (Tripathi et al., 2006) and stimulation with *Plasmodium* glycosylphosphatidylinositol (GPI) toxin (Schofield et al., 1996) activate NF-κB signalling, which in turn promotes TNF secretion and upregulates ICAM1 expression. Nitric oxide down-regulates NF-κB signalling by direct S-nitrosylation of an NF-κB cysteine residue (Matthews et al., 1996) and by stabilization of IκBα, an endogenous NF-κB inhibitor (Peng et al., 1995). Down-regulation of NF-κB signalling may mediate the inhibitory effect of nitric oxide on TNF secretion (Iuvone et al., 1996) and adhesion molecule expression (De Caterina et al., 1995). These observations suggest that impaired NO synthesis could contribute to severe malaria pathogenesis by promoting inflammation and adhesion molecule expression. In support of this hypothesis, direct inhibition of nitric oxide synthesis has been shown to increase cytoadherence of parasitized red blood cells to vascular endothelial cells under flow conditions (Serirom et al., 2003).

Loss of Endothelial Barrier Integrity

In a majority of Malawian children dying from cerebral malaria, ring haemorrhages and extravascular fibrinogen leakage are associated with cytoadherent parasitized erythrocytes (Taylor et al., 2004; Dorovini-Zis et al., 2011) (FIG 1.5). Haemorrhage is also a common feature of retinopathy in children with cerebral malaria and is associated with increased mortality risk (Beare et al., 2004) (FIG 1.5). Haemorrhage and leakage of the blood-brain barrier could introduce plasma proteins, toxins or metabolites into the brain parenchyma which could subsequently contribute to adverse neurological complications. Supporting this possibility, oedema (Newton et al., 1994; Patankar et al., 2002) and downstream axonal injury (Medana et al., 2002, 2005; Dorovini-Zis et al., 2011) have been observed in some patients. In addition, loss of the endothelial barrier may promote activation of microglial cells and astrocytes which may further promote neuronal injury (Hunt and Grau, 2003). Microhaemorrhage and vascular leak are also observed in *P. berghei* ANKA-infected mice (Gramaglia et al., 2006; Serghides et al., 2011).

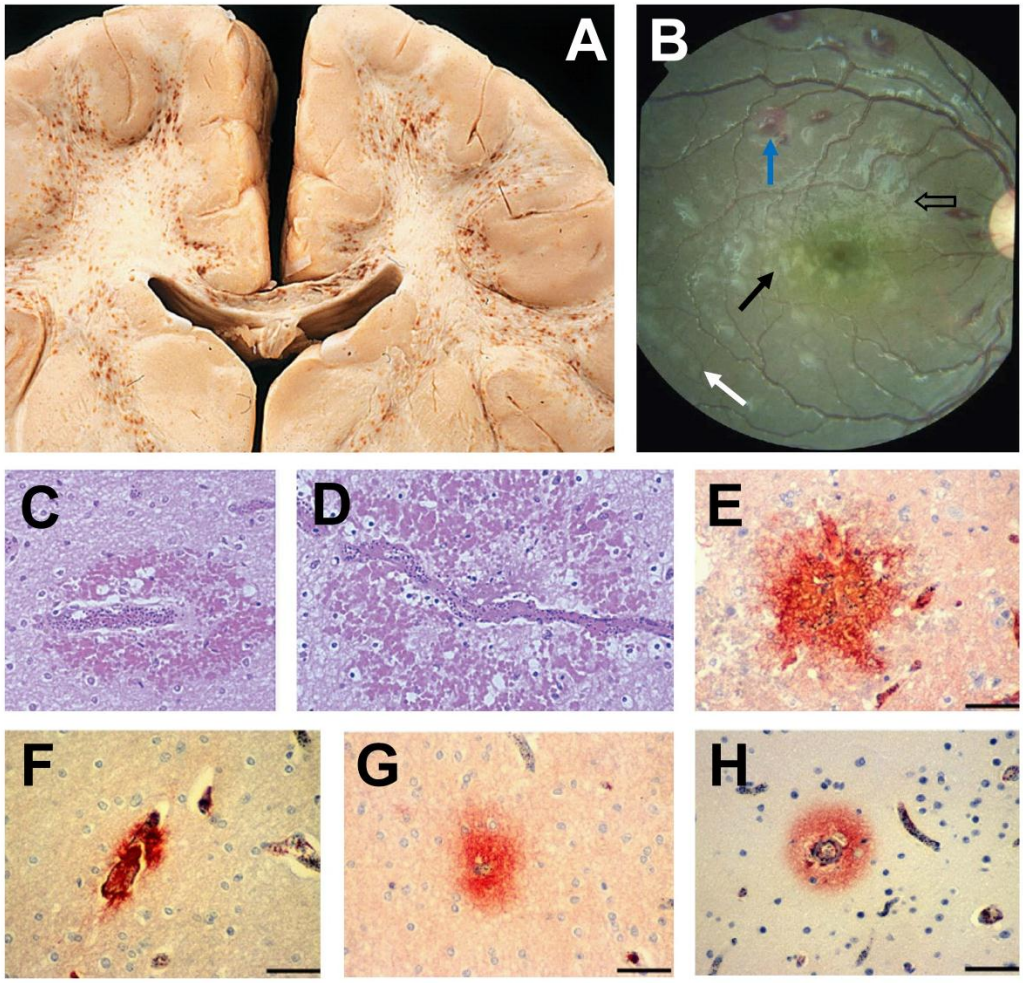


Figure 1.5 | Loss of endothelial barrier integrity in cerebral malaria. (**A**) Multiple petechial haemorrhages visible in a fixed coronal brain section from a Malawian child who died from cerebral malaria. (**B**) Observation of retinopathy including haemorrhage (blue arrow) and whitening around the fovea (black arrow) and in the periphery (white arrow). The open arrow indicates glare. (**C-D**) Microscopic photomicrographs (400X) of haemorrhages surrounding parasitized vessels. Scale bars not provided in original images. (**E-H**) Fibrinogen extravasation associated with a ring haemorrhage (**E**), thrombus occlusion (**F**) and parasitized red blood cells (**G-H**). Scale bars in panels E-H = 50µmM. Panels A, C & D reprinted by permission from Macmillan Publishers Ltd: *Nature Medicine* (Taylor et al., 2004), copyright 2004. Panel B republished with permission from The American Society of Tropical Medicine and Hygiene: *American Journal of Tropical Medicine and Hygiene* (Beare et al., 2006), copyright 2006; permission conveyed through Copyright Clearance Center, Inc. Panels E-H reprinted with permission from Elsevier: *American Journal of Pathology* (Dorovini-Zis et al., 2011), copyright 2011.

Endothelial barrier integrity is maintained by tight junctions between endothelial cells (Bazzoni and Dejana, 2004). Post-mortem pathological analysis of patients dying with cerebral malaria revealed disrupted expression patterns of the tight junction proteins zona occludens 1 (ZO-1), occludin and vinculin (Brown et al., 1999b; Pongponratn et al., 2003). In these studies,

aberrant expression of tight junction proteins was associated with the presence of cytoadherent parasitized red cells (Brown et al., 1999b; Pongponratn et al., 2003). Cytoadherence of *P. falciparum*-infected erythrocytes increase the permeability of endothelial cell layers *in vitro* (Tripathi et al., 2007; Taoufiq et al., 2008). Fausdil, a specific inhibitor of the GTPase RhoA, prevented loss of endothelial barrier integrity in this co-culture system, implicating RhoA activation as a mediator of cytoadherence-induced permeability (Taoufiq et al., 2008). RhoA is also regulated by the endothelial Tie2 receptor. Under normal conditions, constitutive activation of endothelial Tie2 by angiopoietin-1 (Ang-1) inhibits RhoA and maintains tight junction expression (Gamble et al., 2000; Mammoto et al., 2007). During severe malaria, the Ang-1/Tie2 antagonist angiopoietin 2 (Ang-2) is elevated and is associated with increased risk of mortality (Conroy et al., 2012; Yeo et al., 2008b; Weinberg et al., 2014). Ang-2 competes with Ang-1 for binding to Tie-2 but does not induce downstream signalling, resulting in vascular leak in addition to sensitization of the vascular endothelium to inflammatory signalling (Scharpfenecker et al., 2005; Roviezzo et al., 2005; Fiedler et al., 2006). Inhibition of constitutive NO synthesis increases exocytosis of Weibel-Palade bodies (Matsushita et al., 2003), in which Ang-2 is stored (Fiedler et al., 2004).

In contrast to RhoA, which down-regulates tight junction proteins and promotes cellular retraction, Rac1 is required for maintenance of endothelial barrier integrity (Wojciak-Stothard et al., 2009). Rac1 activation is dependent on constitutive NO signalling via cGMP-mediated activation of protein kinase G (PKG). In an *in vitro* system, treatment with the endogenous nitric oxide synthase inhibitor asymmetric dimethylarginine (ADMA) was sufficient to cause dispersion of tight junction proteins and increased permeability of the endothelial cell layer (Wojciak-Stothard et al., 2009). Taken together, these observations indicate that NO signalling contributes to endothelial barrier integrity by activating Rac1 in addition to suppressing Ang-2 release and promoting Tie2-mediated RhoA inhibition.

In *P. berghei* ANKA-infected mice, treatment with inhaled NO or administration of an NO donor therapy reduced cerebral haemorrhages and improved blood-brain barrier integrity

(Gramaglia et al., 2006; Serghides et al., 2011). These findings identify restoration of NO signalling as a potential approach to maintaining endothelial barrier integrity during severe malaria.

Impaired Blood Flow

Vasodilation

Nitric oxide synthesized by endothelial cells diffuses to smooth muscle cells and activates soluble guanlyate cyclase, causing vasodilation (Palmer et al., 1987; Rapoport et al., 1983). Vasodilation in response to hypoxia and shear stress were found to be impaired in Indonesian adults with severe malaria as determined by measuring changes in blood flow following 5 minute occlusion of the brachial artery (Yeo et al., 2007). In follow-up analyses, these quantitative measurements of vasodilation were found to be inversely correlated with plasma concentrations with ADMA, an endogenous nitric oxide synthase inhibitor (Yeo et al., 2010). In a separate study in Malian children with severe malaria, tricuspid regurgitation velocity was increased, pulmonary arterial systolic pressure was increased and nitrite, a break-down product of NO, was decreased (Janka et al., 2010). These studies indicate that inhibition of nitric oxide synthesis may impair vasodilation during severe malaria infection.

Intravascular Coagulation

Vascular flow may be further impaired by malaria-induced coagulation defects. Infected red cells have been shown to initiate platelet aggregation (Grau et al., 2003) and induce tissue factor display on endothelial cells, which initiates intravascular coagulation by activating thrombin (Francischetti et al., 2007). Nitric oxide inhibits platelet aggregation (Loscalzo, 2001; Villagra et al., 2007; Freedman and Loscalzo, 2003) and tissue factor display (Yang and Loscalzo, 2000). NO has also been shown to prevent platelet-dependent endothelial cell apoptosis (Grau et al., 2003).

Nitric oxide also plays a role in regulating release of the pro-coagulant von Willebrand factor (vWF), a pro-coagulant. vWF is released by exocytosis from Weibel-Palade bodies, a process that is inhibited by nitric oxide (Matsushita et al., 2003). Patients with severe malaria demonstrate increased concentrations of plasma vWF multimers and decreased concentrations of ADAMTS13, the protease responsible for inactivating vWF (Hollestelle et al., 2006; Mast et al., 2009). It has been proposed that vWF multimers mediate platelet-dependent binding of infected red cells to endothelial cells (Bridges et al., 2010), thereby contributing occlusion of the vascular lumen and impairing tissue perfusion. Fibrinogen may also serve as a bridge between endothelial cell adhesion molecules and parasite ligands (Gray and Craig, 2002)

Red Blood Cell Deformability

Erythrocyte deformability is compromised in severe malaria patients and serves as an prognostic indicator of poor outcome (Dondorp et al., 1997). Reduced deformability may prevent erythrocytes (average diameter ~7.5μm) from squeezing through microcapillaries with diameters ranging from 3-7 μm (Dondorp et al., 2000). The space available for passage may be further reduced during severe malaria infection due to cytoadherence of infected red cells, intravascular coagulation, rosetting of uninfected and infected red cells (Treutiger et al., 1992; Rowe et al., 1995) or platelet-mediated clumping of infected erythrocytes (Roberts et al., 2000; Pain et al., 2001; Chotivanich et al., 2004).

Decreased deformability could be due to insertion of parasite-derived proteins into the erythrocyte membrane or increased cytosolic viscosity due to the parasite itself (Glenister et al., 2002). Changes in patients with relatively low parasitaemia suggest that deformability is also decreased in uninfected bystander erythrocytes (Dondorp et al., 2000, 2004). Decreased deformability in uninfected red blood cells could be due to oxidant stress and associated changes in membrane chemistry (Dondorp et al., 2000). Inhibition of nitric oxide synthesis may also contribute to impaired red cell deformability. Nitric oxide has been shown to play a role in

maintaining red blood cell membrane plasticity (Bor-Kucukatay et al., 2003; Kleinbongard et al., 2006), although the mechanism has not been elucidated.

Impaired Microcirculation

Intravital microscopy was used to directly assess microcirculation in the rectal mucosa of Bangladeshi adults with severe malaria (Dondorp et al., 2008a). This study found slowing and stagnation of erythrocytes in the capillaries of patients with severe malaria compared with patients with uncomplicated malaria and healthy controls. The percentage of capillaries with stagnant erythrocytes was positively correlated with lactate and base deficit, suggesting that insufficient tissue perfusion caused a shift from aerobic to anaerobic respiration in these patients (Dondorp et al., 2008a). This finding is significant in light of other studies identifying hyperlactataemia as a highly accurate prognostic indicator of poor outcome (Day et al., 2000). In contrast to these findings in patients with severe malaria, patients with septicaemia exhibited greater percentage of blood vessels with rapidly-moving erythrocytes than healthy controls (Dondorp et al., 2008a). Impaired perfusion is also evident in the retina of a majority of Malawian children with cerebral malaria, as determined by fluorescein angiography (Beare et al., 2009). An intravital microscopy study in mice infected with *P. berghei* ANKA identified similar indications of impaired perfusion in pial arterioles and venules, including reduced red blood cell velocities and decreased vessel diameters (Cabrales et al., 2011, 2010). In this model, treatment with an exogenous NO donor improved blood flow and venule diameter in infected mice, suggesting that impaired NO signalling contributes to impaired microcirculation during malaria infection (Cabrales et al., 2011).

1.6 Evidence and Implications of Impaired Nitric Oxide Synthesis in Severe Malaria

Nitric oxide diffuses rapidly across cell membranes where it either initiates downstream signalling or is oxidized to nitrite (NO_2^-) or nitrate (NO_3^-). Early clinical studies of nitric oxide in patients with severe malaria assessed plasma and urinary nitrites and nitrates as biomarkers of

whole body nitric oxide synthesis. A small study of Cameroonian children with cerebral malaria reported higher plasma nitrites and nitrates in children who survived without sequelae compared with those who died and with those who experienced neurological sequelae (Cot et al., 1994). This study also used correlation analysis to show that low nitrites and nitrates were associated with longer duration of coma (Cot et al., 1994). In a separate study of Gabonese children, improved plasma nitrites and nitrates were observed after recovery from severe malaria (28 days after initial presentation) (Kremsner et al., 1996). A subsequent study of Tanzanian children with uncomplicated or severe malaria provided assessment of plasma and urinary nitrites and nitrates controlled for renal function by normalizing to creatinine (Anstey et al., 1996). This study reported decreased plasma and urinary nitrites and nitrates in children with uncomplicated malaria and further decreases in children with cerebral malaria (Anstey et al., 1996). In a more recent study of Indonesian adults, patients with severe malaria demonstrated lower exhaled NO and impaired vasodilation responses compared to patients with uncomplicated malaria and healthy controls (Yeo et al., 2007). It is unclear to what extent exhaled NO reflects NO synthesis in the vascular compartment, but the method of assessing vasodilation (reactive hyperaemia peripheral arterial tonometry following brachial artery occlusion) has been shown to be approximately 50% dependent on NO synthesis (Nohria et al., 2006).

Taken together, these studies provided a framework for the hypothesis that impaired nitric oxide synthesis contributes to the pathogenesis of severe malaria. Severe malaria pathogenesis is primarily driven by adverse changes in endothelial cell physiology and vascular haemodynamics, both of which are normally regulated by nitric oxide. Nitric oxide acts as a vasodilator, maintains the endothelial barrier, promotes erythrocyte deformability, inhibits inflammatory signalling, downregulates adhesion molecule expression, and inhibits exocytosis of angiopoietin-2 and von Willebrand Factor from Weibel-Palade bodies. Impaired NO production by nitric oxide synthase (NOS) may therefore contribute to vascular dysfunction associated with severe malaria (FIG 1.6).

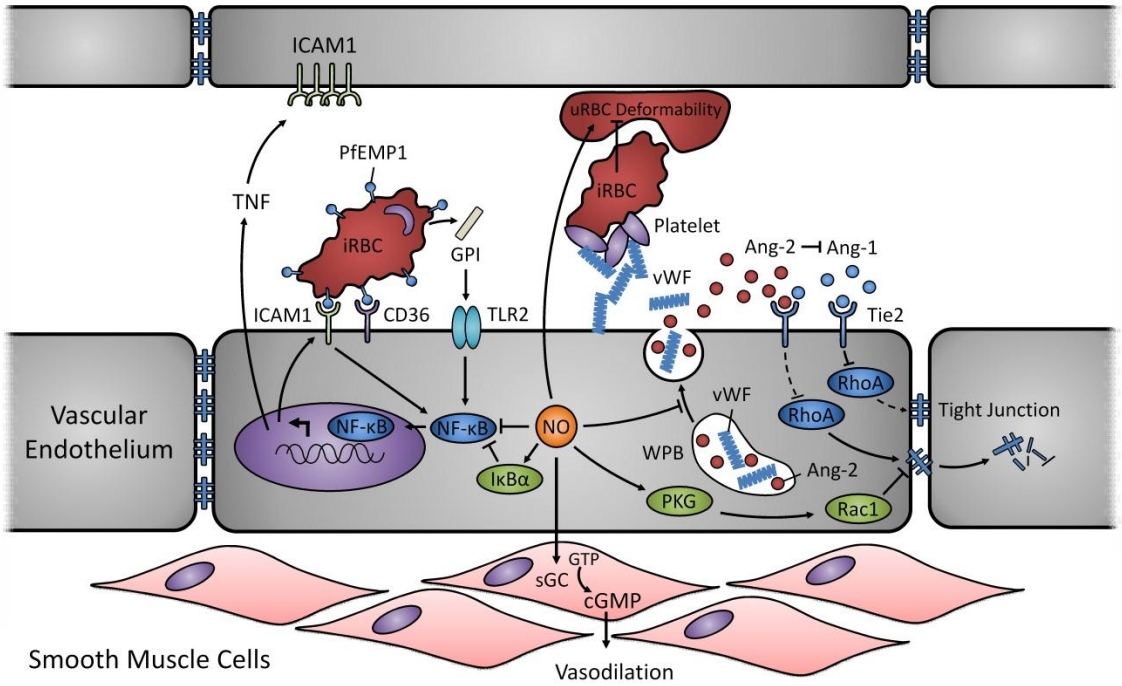


Figure 1.6 | Inhibition of nitric oxide signalling in severe malaria. Parasites export *P. falciparum* erythrocyte membrane protein 1 (PfEMP1) to the surface of the infected red blood cell (iRBC) where it facilitates adherence to the vascular endothelium by binding endothelial receptors such as CD36 and intercellular adhesion molecule 1 (ICAM1). ICAM1 binding and activation of toll-like receptor 2 (TLR2) by parasite glycosylphosphatidylinositol (GPI) both stimulate NF-κB translocation to the nucleus where it induces expression of adhesion molecules and inflammatory mediators such as tumor necrosis factor (TNF). Nitric oxide (NO) inhibits NF-κB by direct modification (S-nitrosylation) and by stabilization of IκBα, an inhibitor of NF-κB. NO acts as a vasodilator by activating soluble guanlyate cyclase (sGC) in smooth muscle cells, which synthesizes cyclic GMP (cGMP) and causes smooth muscle cells to relax. NO promotes deformability in uninfected red blood cells (uRBC), which is especially critical for passage through vessels partially occluded by adherent iRBC. NO also inhibits exocytosis of Weibel-Palade bodies (WPB), which contain von Willebrand factor (vWF) and angiopoietin-2 (Ang-2). vWF multimers can trigger thrombosis or facilitate platelet-mediated binding of iRBC to the vascular endothelium. Ang-1/Tie2 signalling inhibits RhoA and maintains integrity of the endothelial barrier. Ang-2 competes with Ang-1 for Tie2 binding, resulting in disinhibition of RhoA, which disperses tight junctions and increases permeability of the endothelial cell layer. NO stabilizes tight junction proteins by activating protein kinase G (PKG) and Rac1.

1.7 Nitric Oxide Synthesis

Nitric Oxide Synthase Expression and Regulation

Nitric oxide is synthesized by three nitric oxide synthase (NOS) isoforms: neuronal (nNOS or NOS1), inducible (iNOS or NOS2) and endothelial (eNOS or NOS3). Neuronal NOS is primarily expressed in central nervous system neurons, but has also been shown to be expressed in the myocardium (Xu et al., 1999; Ashley et al., 2002). Inducible NOS is induced by pro-inflammatory signalling (e.g. cytokine or LPS stimulation). Inducible NOS was discovered in macrophages but expression can be stimulated in a range of other cells as well, including smooth muscle cells and hepatocytes (Förstermann et al., 1994). Endothelial NOS is constitutively expressed in endothelial cells as well as cardiomyocytes (Balligand et al., 1995). The interpretations in this thesis will focus on the role of eNOS in maintaining vascular homeostasis, but the same substrates and cofactors are required for NO production by all three NOS isoforms.

All NOS isoforms utilize arginine as a substrate, and require molecular oxygen and reduced nicotinamide adenine dinucleotide phosphate (NADPH) as co-substrates (FIG 1.7). 6*R*-5,6,7,8-tetrahydro-L-biopterin (BH4), flavin adenine dinucleotide (FAD), flavin mononucleotide (FMN) and haem are essential NOS cofactors. Influx of Ca^{2+} causes calmodulin to bind all NOS isoforms, facilitating NO synthesis, but the Ca^{2+} threshold required for activation of iNOS is extremely low (< 40 nM) (Cho et al., 1992). Shear stress stimulates eNOS in a Ca^{2+}-independent manner via phosphorylation of key serine, threonine and tyrosine residues (Fulton et al., 1999; McCabe et al., 2000).

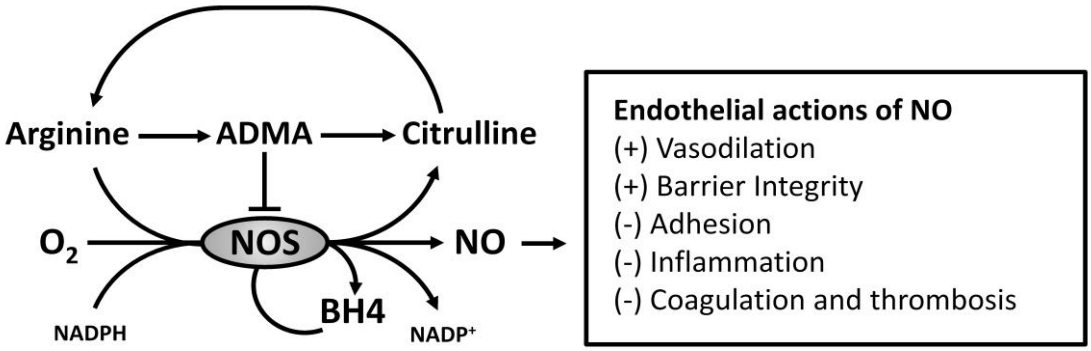


Figure 1.7 | Nitric oxide synthase requires arginine and BH4 and is inhibited by ADMA. Arginine oxygen and NADPH are co-substrates for the synthesis of nitric oxide (NO) by nitric oxide synthase (NOS). Tetrahydrobiopterin (BH4) is an essential NOS cofactor. Protein incorporated arginine may be methylated to form asymmetric dimethylarginine (ADMA) which is released during proteolysis and acts as a NOS inhibitor. ADMA is metabolized to citrulline by dimethylarginine dimethylaminohydrolase (DDAH) (not pictured). Citrulline is a product of NO synthesis and ADMA metabolism that may be converted to arginine by argininosuccinate synthetase 1 (ASS1) and argininosuccinate lyase (ASL) (not pictured).

During NO synthesis, electrons donated by NADPH at the carboxy-terminal reductase domain of NOS are transferred by FAD and FMN to the haem catalytic centre of the oxygenase domain, where oxygen is activated and arginine is subsequently oxidized to yield NO and citrulline (Stuehr et al., 1991). BH4 is required for these reactions; in its absence, electron flow to molecular oxygen becomes 'uncoupled' from arginine oxidation, resulting instead in production of superoxide (O_2^-) (Vasquez-Vivar et al., 1998; Xia et al., 1998; Pou et al., 1992; Vasquez-Vivar et al., 2002). The combination of increased oxidative stress and impaired NO signalling resulting from NOS uncoupling has been implicated in the pathogenesis of a wide range of disease states, including atherosclerosis (Hattori et al., 2007), hypertension (Landmesser et al., 2003; Du et al., 2008) and diabetes (Alp et al., 2003).

Nitric oxide synthesis is inhibited by accumulation of asymmetric N^G,N^G-dimethyl-L-arginine (ADMA), an endogenous NOS inhibitor (Cardounel et al., 2007) (FIG 1.7). Circulating ADMA is derived from protein-incorporated arginine residues that are methylated by protein arginine methyltransferase (PRMT) enzymes and subsequently released during proteolysis (Lee et al., 1977; Kakimoto and Akazawa, 1970). By inhibiting NOS, ADMA causes

vasoconstriction, increased blood pressure and decreased forearm blood flow (Vallance et al., 1992). Plasma ADMA is inversely correlated with endothelial function in hypercholesterolaemia (Böger et al., 1998) and hypertension (Perticone et al., 2005). Elevated plasma ADMA increases risk of complications and death in sickle-cell disease (Kato et al., 2009), coronary artery disease (Schnabel et al., 2005) and end-stage renal disease (Zoccali et al., 2001).

This thesis tests the hypothesis that dysregulation of arginine, BH4 and ADMA availability contributes to impaired nitric oxide synthesis in severe malaria.

Structure of Thesis

The results chapters of this thesis examine the effect of severe malaria infection on arginine availability (CHAPTER 2), homeostasis of arginine and ADMA (CHAPTER 3) and BH4 availability (CHAPTER 4). In CHAPTER 5 arginine and BH4 deficiencies are simultaneously restored in a mouse model of severe malaria in order to examine the effect on nitric oxide signalling. The main body of the thesis is concluded with a general discussion (CHAPTER 6) aimed at placing the conclusions drawn from this work into the broader context of severe malaria pathophysiology, development of therapeutic approaches and other research and policy priorities relevant to reducing the global burden of severe malaria.

Relevant materials and methods are included at the end of each results chapter, but full descriptions of the extensive assay development and validation required by this work are presented in APPENDICES A-E, following the main body of the thesis. This structure allows the reader to progress through biological questions, results and interpretations uninterrupted while still providing detailed descriptions of analytical aspects of this work.

CHAPTER 2.

Arginine Depletion

L-arginine is required as a substrate for the synthesis of nitric oxide (NO). Patients with severe malaria exhibit decreased plasma concentrations of arginine, which may contribute to impaired vasodilation and microcirculatory abnormalities by limiting NO synthesis. Previous studies have suggested that arginine depletion results from conversion of arginine to ornithine and urea by parasite- or host-expressed arginase. Using HPLC to analyze plasma from P. berghei ANKA-infected mice, we observed that plasma arginine, citrulline and ornithine are depleted to similar degrees, leaving the arginine/ornithine ratio unchanged. These findings cannot be explained solely by increased arginase activity. We also observed similar degrees of depletion of arginine, citrulline and ornithine in mice infected with arginase knock-out parasites, suggesting that parasite-expressed arginase is not required for arginine depletion in vivo. To control for suppression of feeding behaviour associated with P. berghei ANKA infection, we restricted the dietary intake in uninfected mice to match that of infected mice and observed moderate depletion of arginine and citrulline. However, depletion was greater in infected mice, implicating involvement of additional mechanisms such as impaired enteral absorption or synthesis. To further examine the effect of malaria infection on arginine metabolism, we infused heavy isotope-labelled metabolic tracers and quantitatively assessed appearance and interconversion of arginine, citrulline and ornithine in real-time. Malaria infection reduced the rates of appearance of plasma arginine, citrulline and ornithine but did not alter the rate of conversion of plasma arginine to ornithine. Utilization of arginine by NO synthase (NOS) was also reduced in infected mice. In summary, our findings implicate decreased rates of arginine and citrulline appearance in plasma, rather than arginase-mediated catabolism, as the primary mechanism of arginine depletion.

2.1 Introduction

L-arginine is required as a substrate for the synthesis of nitric oxide (NO). Patients with severe malaria exhibit decreased plasma concentrations of arginine (Lopansri et al., 2003; Yeo et al., 2007), which may contribute to impaired vasodilation (Yeo et al., 2007) and microcirculatory abnormalities (Dondorp et al., 2008a). Arginine bioavailability is dependent on dietary intake/absorption, protein turnover and inter-conversion with ornithine and citrulline (FIG 2.1). Studies of the human parasite *P. falciparum* and the murine parasite *P. berghei* ANKA in culture have suggested that arginine is consumed by parasite-expressed arginase, which

converts arginine to ornithine and urea (Olszewski et al., 2009). It has also been suggested that host arginase could contribute to arginine depletion. Cell-free haeme, which is released during haemolysis, has been shown to activate intracellular arginase in erythrocytes *in vitro* despite impaired arginine uptake (Omodeo-Sale et al., 2010). Haemolysis could also release host- or parasite-derived arginase directly into plasma. Consistent with this hypothesis, increased arginase activity has been observed in the plasma of Indonesian adults with severe malaria (Yeo et al., 2007) and found to correlate with cell-free haemoglobin (Yeo et al., 2009). Similarly, plasma arginase concentrations were elevated and correlated with cell-free haemoglobin in Malian children with severe malarial anaemia (Janka et al., 2010).

However, several observations suggest that arginase may not be primarily responsible for arginine depletion. In Indonesian adults with severe malaria, plasma arginase activity was normal in patients with moderately severe malaria (uncomplicated malaria with inability to tolerate oral medication), yet these patients exhibited arginine depletion similar to patients with severe malaria (Yeo et al., 2007). Furthermore, a recent study reported arginine depletion but no difference in plasma arginase activity among Tanzanian children with cerebral malaria or other forms of severe malaria compared to healthy controls (Weinberg et al., 2014). Plasma arginase activity also failed to correlate with cell-free haemoglobin in this study. Increased arginase activity has been implicated as the mechanism underlying plasma arginine depletion in patients with sickle cell disease, where plasma arginase activity is associated with decreased ratios of plasma arginine to ornithine (Morris et al., 2005). In contrast, patients with severe malaria demonstrate ornithine as well as arginine depletion (Lopansri et al., 2006; Yeo et al., 2007) and the ratio of arginine to ornithine does not differ significantly from healthy controls (Yeo et al., 2007). These findings cannot be explained solely by increased arginase activity. In this study, we use a mouse model of severe malaria to resolve the contribution of arginase to *in vivo* arginine depletion and explore the dynamics of whole-body arginine metabolism during malaria infection.

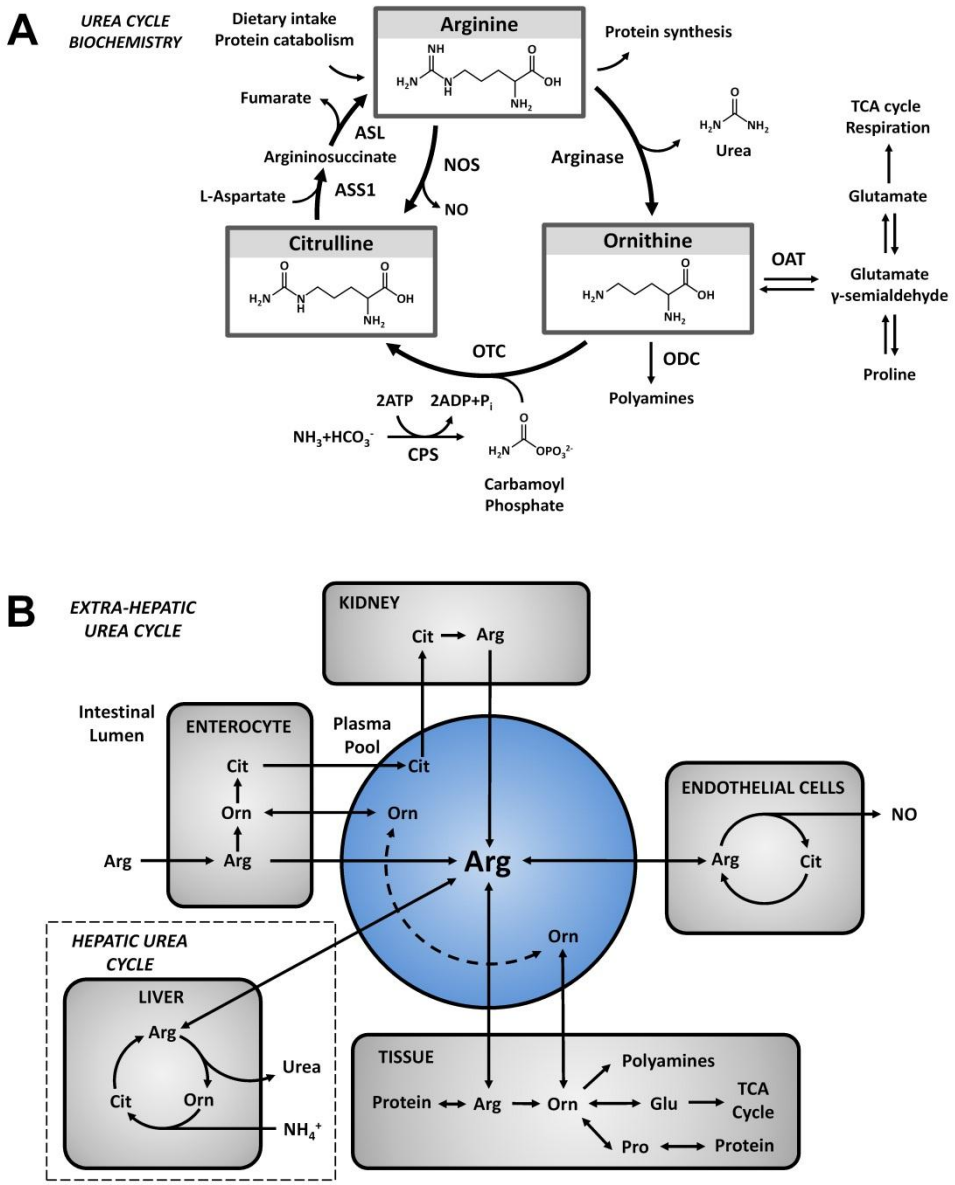


Figure 2.1 | Overview of arginine, ornithine and citrulline metabolism in mammals. (**A**) *Urea Cycle Biochemistry*: Plasma arginine is derived from enteral absorption, protein catabolism and synthesis from citrulline by argininosuccinate synthetase 1 (ASS1) and argininosuccinate lyase (ASL). Arginine is converted to citrulline during synthesis of nitric oxide (NO) by nitric oxide synthase (NOS). Arginase catabolizes arginine to ornithine and urea. Ornithine aminotransferase (OAT) converts ornithine to glutamate γ-semialdehyde, which is further metabolized to proline or to glutamate (which in turn may serve as a substrate for TCA cycle respiration). Alternatively, ornithine may be decarboxylated by ornithine decarboxylase (ODC) for polyamine synthesis. Ornithine transcarbamylase (OTC) catalyzes the conversion of ornithine and carbamoyl phosphate to citrulline. Carbamoyl phosphate is synthesized from ammonia and bicarbonate by carbamoyl phosphate synthetase (CPS). (**B**) *Extra-hepatic urea cycle:* Dietary arginine is either transferred to plasma pools directly or converted to ornithine and citrulline by enteral arginase and OTC, respectively. Citrulline is released into plasma pools where it is taken up into the kidney and utilized as a substrate for *de novo* arginine synthesis. Plasma arginine is the substrate for NO synthesis by endothelial or other NOS-expressing cells. Citrulline produced by NOS may be recycled back to arginine by local ASS1 and ASL. The primary metabolic fates of arginine are protein and ornithine synthesis. Ornithine may be further metabolized to proline, glutamate, polyamines or citrulline. *Hepatic urea cycle:* Arginine can be taken up by the liver to serve as a substrate for the hepatic urea cycle, which generates urea from ammonium (NH_4^+). Arginine, ornithine and citrulline intermediates in the hepatic urea cycle are tightly channeled to subsequent reactions, limiting exchange with plasma pools.

2.2 Arginine Availability in *P. berghei* ANKA-Infected Mice

Disease Progression in P. berghei ANKA-Infected Mice

Six days after inoculation with blood-stage *P. berghei* ANKA, C57BL/6 mice exhibited peripheral blood parasitaemia of 6.0% (IQR: 4.7-7.5%) and rapidly developed symptoms of severe disease, including lethargy, hunched posture and unresponsiveness (day 6 behavioural score: median [IQR]: 1 [0-4] out of 14, FIG 2.2). In a separate observation cohort, three quarters (75%) of infected mice died on day 6 post-inoculation, with the remainder succumbing by day 8 post-inoculation (FIG 2.2).

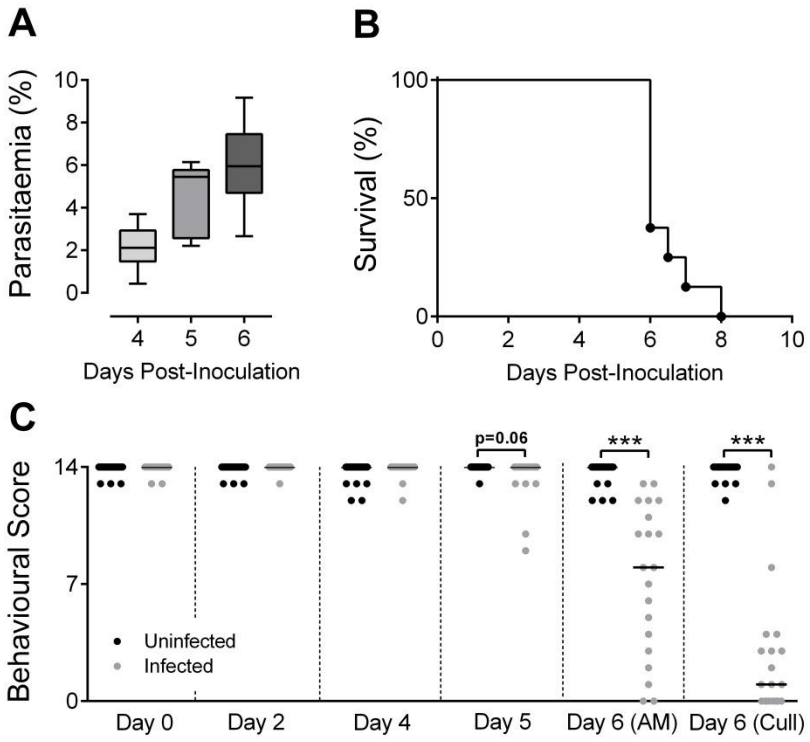


Figure 2.2 | *P. berghei* ANKA infection in C57BL/6 mice. (**A**) *P. berghei* ANKA-infected erythrocytes were microscopically counted and expressed as a percentage of total erythrocytes on days 4, 5 and 6 post-inoculation. Box-plots depict median, IQR, min and max values of data pooled from 3 independent experiments (total n=20). (**B**) *P. berghei* ANKA-infected mice were monitored for non-moribund survival. The humane endpoint for the study was established to be a behavioural score of 3 or less out of 14, at which point animals were euthanized. Data represent results from 2 independent experiments (total n=16). (**C**) Behaviour was assessed at baseline (BL) and 2, 4, 5 and 6 days post-inoculation with *P. berghei* ANKA (n=20). Uninfected littermates served as controls (n=24). Disease symptoms were assessed using seven indicators of neurological function each scored on a scale of 0 (moribund) to 2 (normal). D6 (AM) scores were assessed between 7-9AM in the morning; D6 (Cull) scores were assessed in the late morning or afternoon directly prior to tissue collection. Data are pooled from 3 independent experiments. Black lines indicate median values for each group. ***p<0.001 by Mann-Whitney test.

Plasma Arginine, Citrulline and Ornithine Concentrations

Patients with severe malaria exhibit similar degrees of arginine and ornithine depletion, leaving the ratio between them unchanged (Lopansri et al., 2006; Yeo et al., 2007). To determine whether severe disease is associated with depletion of arginine, ornithine and citrulline in *P. berghei* ANKA-infected mice, we developed a high performance liquid chromatography (HPLC) method of quantifying plasma amino acid concentrations (for assay development and validation, see APPENDIX A, p. 235). On days 4 and 6 post-inoculation, plasma arginine was decreased in infected mice compared to uninfected controls (uninfected median [IQR]: 84.7 [74.5-92.5] µmol/L, infected day 4: 62.2 [55.8-77.9] µmol/L, $p < 0.01$ vs uninfected, infected day 6: 53.2 [32.0-58.8] µmol/L, $p < 0.0001$ vs uninfected, FIG 2.3). Plasma citrulline was decreased on day 6 post-inoculation (uninfected: 57.9 [49.7-64.0] µmol/L vs infected day 6: 25.9 [22.3-30.7] µmol/L, $p < 0.0001$) but not day 4 (52.0 [40.2-56.7] µmol/L, $p = 0.37$ vs uninfected, FIG 2.3). Ornithine was also low on day 6 post-inoculation (uninfected: 46.3 [26.0-70.3] µmol/L vs infected day 6: 23.6 [14.3-36.8] µmol/L, $p < 0.01$) but not day 4 (34.1 [29.5-40.5] µmol/L, $p > 0.99$ vs uninfected, FIG 2.3). On day 6 post-inoculation, arginine and ornithine were depleted to similar degrees, and as a result the ratio of plasma arginine to ornithine did not fall in infected animals (uninfected: 1.7 [1.1-3.1] vs infected day 6: 2.4 [1.2-3.5], $p > 0.99$, FIG 2.4). Arginine depletion in *P. berghei* ANKA-infected mice cannot be explained solely by increased arginase activity, which would be expected to decrease the arginine/ornithine ratio by converting arginine to ornithine. Furthermore, increased arginase activity should increase plasma ornithine concentrations, but we observed lower ornithine concentrations in *P. berghei* ANKA-infected mice. Arginine depletion has been observed in a previous study of *P. berghei* ANKA-infected mice (Gramaglia et al., 2006), but our study is the first to identify ornithine and citrulline depletion in this mouse model. Plasma phenylalanine was elevated on day 6 post-inoculation (uninfected: 66.7 [47.5-75.1] µmol/L vs infected day 6: 102.3 [88.3-109.6] µmol/L, $p < 0.0001$, FIG 2.3), providing evidence against dilution of plasma amino acids as the cause of arginine, citrulline and ornithine depletion.

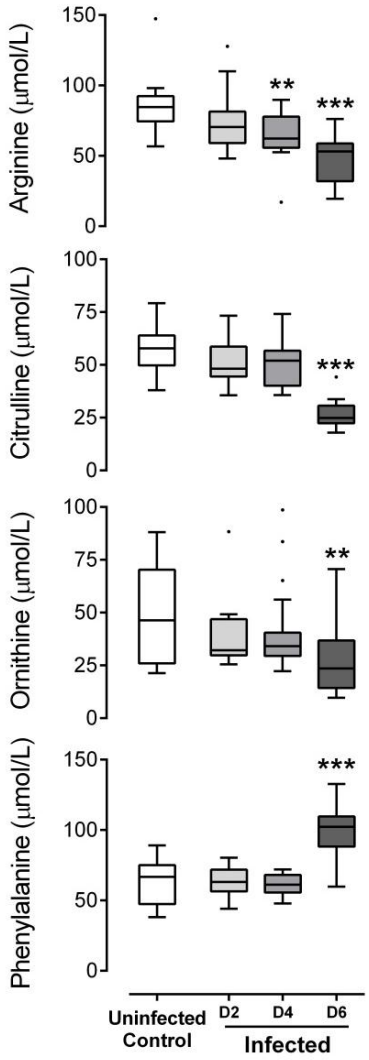


Figure 2.3 | Depletion of plasma arginine, citrulline and ornithine. Amino acids were measured by HPLC in plasma from mice culled on days 2, 4 or 6 (D2, D4, D6) post-inoculation with *P. berghei* ANKA. Uninfected littermates served as controls. Data represent results from 3 independent experiments (uninfected: n=24; infected day 2: n=20; infected day 4: n=21; infected day 6: n=20). Box-plots depict median and IQR. Whiskers extend to highest and lowest values within 1.5×IQR of the 75th and 25th percentiles and values outside this range were plotted as individual points (Tukey's method). **p<0.01, ***p<0.001 vs uninfected controls by Kruskal-Wallis test followed by Dunn's multiple comparisons test.

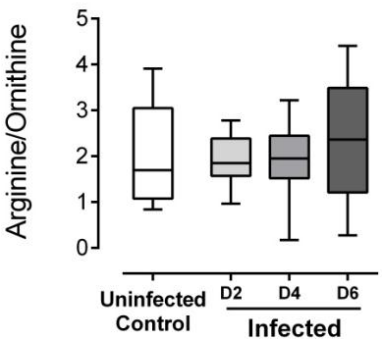


Figure 2.4 | Maintenance of plasma arginine/ornithine ratios. Amino acids were measured by HPLC in plasma from mice culled on days 2, 4 or 6 (D2, D4, D6) post-inoculation with *P. berghei* ANKA. Uninfected littermates served as controls. Data represent results from 3 independent experiments (uninfected: n=24; infected day 2: n=20; infected day 4: n=21; infected day 6: n=20). Box-plots depict median and IQR; whiskers depict range. Differences among groups were not found to be statistically significant (p>0.05) by Kruskal-Wallis test followed by Dunn's multiple comparisons test comparing each group to uninfected values.

2.3 Evaluation of Parasite Arginase as a Possible Cause of Arginine Depletion

Rationale for the Study of Parasite Arginase

It has been proposed that release (Yeo et al., 2007, 2009) or activation (Omodeo-Sale et al., 2010) of erythrocyte arginase contributes to arginine depletion. Unlike human erythrocytes, mouse red blood cells do not demonstrate significant arginase activity (Spector et al., 1985). As a result, depletion of arginine, citrulline and ornithine cannot be ascribed to release or activation of host erythrocyte arginase in mice infected with *P. berghei* ANKA. *P. falciparum* and *P. berghei* ANKA both express a functional arginase enzyme that was shown to be responsible for arginine consumption and ornithine production *in vitro* (Olszewski et al., 2009; Dowling et al., 2010). We therefore considered whether arginase expressed by *P. berghei* ANKA may contribute to arginine depletion *in vivo*.

Verification of Arginase Knock-Out in P. berghei ANKA Parasites

To determine whether parasite-expressed arginase is required for arginine depletion *in vivo*, we obtained a clonal population of *P. berghei* ANKA parasites lacking arginase and the wild-type background strain from Akhil Vaidya (Drexel Medical School, Philadelphia, PA, USA) (Olszewski et al., 2009). To confirm knock-out of parasite arginase, we developed a PCR-based genotype assay consisting of three primers (FIG 2.5). Primer A was designed to anneal to a sequence in the 3' flanking region of the arginase gene. This region was not altered during the double-crossover event used to knock out parasite arginase and replace it with a DHFR/TS selection factor (Olszewski et al., 2009). As a result, primer A was designed to anneal to both wild-type and knock-out DNA. Primers B and C were specific to the wild-type arginase sequence and DHFR/TS selection factor, respectively. The PCR products of primer A/B and A/C amplification were 402bp and 285bp, providing positive identification of wild-type and knock-out DNA, respectively (FIG 2.5). Using this assay on DNA extracted from the blood of infected mice, we verified that arginase was replaced with the DHFR/TS selection factor in arginase knock-out parasites (FIG 2.5). We found only one PCR product in the blood of carrier

mice used for parasite expansion and in C57BL/6 experimental mice assessed for arginine depletion on day 6 post-inoculation (FIG 2.5). Based on these findings, it is unlikely that the wild-type and knock-out parasite lines were cross-contaminated.

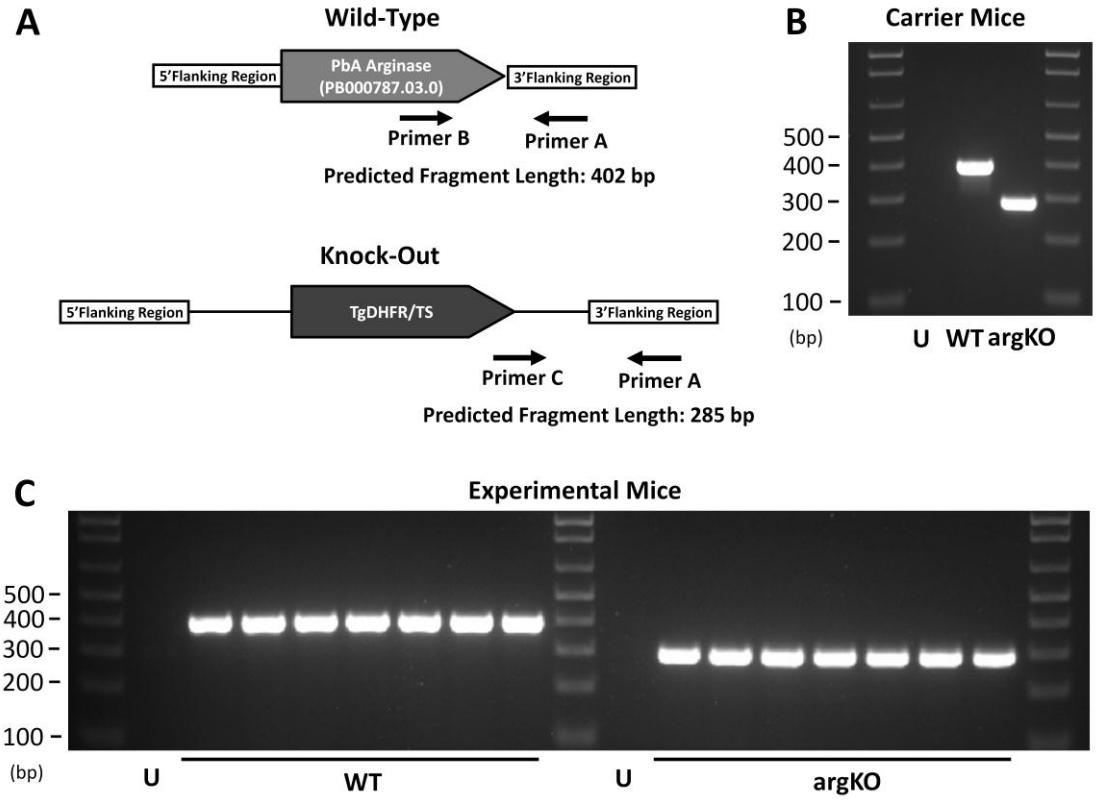


Figure 2.5 | Verification of arginase knock-out in *P. berghei* ANKA. (**A**) A three-primer system was designed to amplify fragments of different lengths in wild-type and knock-out parasites. DHFR/TS was used as a selection factor during creation of the knock-out strain. (**B**) PCR products separated by gel electrophoresis demonstrated purity of parasite lines in carrier mice. Lane 1 shows the absence of a PCR product from a blood sample of an uninfected carrier mouse (U). Lane 2 shows the PCR product from a carrier mouse infected with the wild-type *P. berghei* ANKA background strain (WT). Lane 3 shows the PCR product from a carrier mouse infected with arginase knock-out *P. berghei* ANKA (argKO). (**C**) PCR was performed on whole blood samples from experimental C57BL/6 mice on day 6 post-inoculation with wild-type (WT) or arginase knock-out (argKO) parasites. Whole blood from uninfected mice (U) was assayed as a negative control.

Effect of Parasite Arginase Knock-Out on Disease Severity

To determine the effect of parasite arginase knock-out on disease severity, cohorts of mice infected with wild-type (WT) and arginase knock-out *P. berghei* ANKA parasites (argKO) were assessed for parasite burden, behavioural symptoms and mortality. Six days after inoculation, parasitemia was significantly lower in mice infected with the argKO parasite (3.2% [2.7-4.0%]) compared to mice infected with the WT parasite (9.6% [6.6-11.4%], $p < 0.001$, FIG 2.6A). Rapid onset of symptoms, including hunched posture, lethargy and unresponsiveness, were observed both in mice infected with wild-type parasites and in mice infected with arginase knock-out parasites by day 6 post-inoculation. On day 6, quantitative scores of symptoms were not significantly different between groups in the morning (argKO-infected median behavioural score [IQR]: 7 [2-10] out of 14 vs WT-infected: 7 [5-7] out of 14, $p = 0.89$) or in the afternoon (argKO-infected: 1 [0-2] out of 14 vs WT-infected: 2 [1-3] out of 14, $p = 0.20$, FIG 2.6A). In groups of infected animals allowed to progress to a pre-defined humane mortality endpoint (behavioural score of 3 out of 14 or less), no difference in survival was observed between groups (log-rank $p = 0.53$, FIG 2.6B). These findings demonstrate that genetic deletion of parasite arginase impairs expansion but does not affect the virulence of *P. berghei* ANKA in C57BL/6 mice.

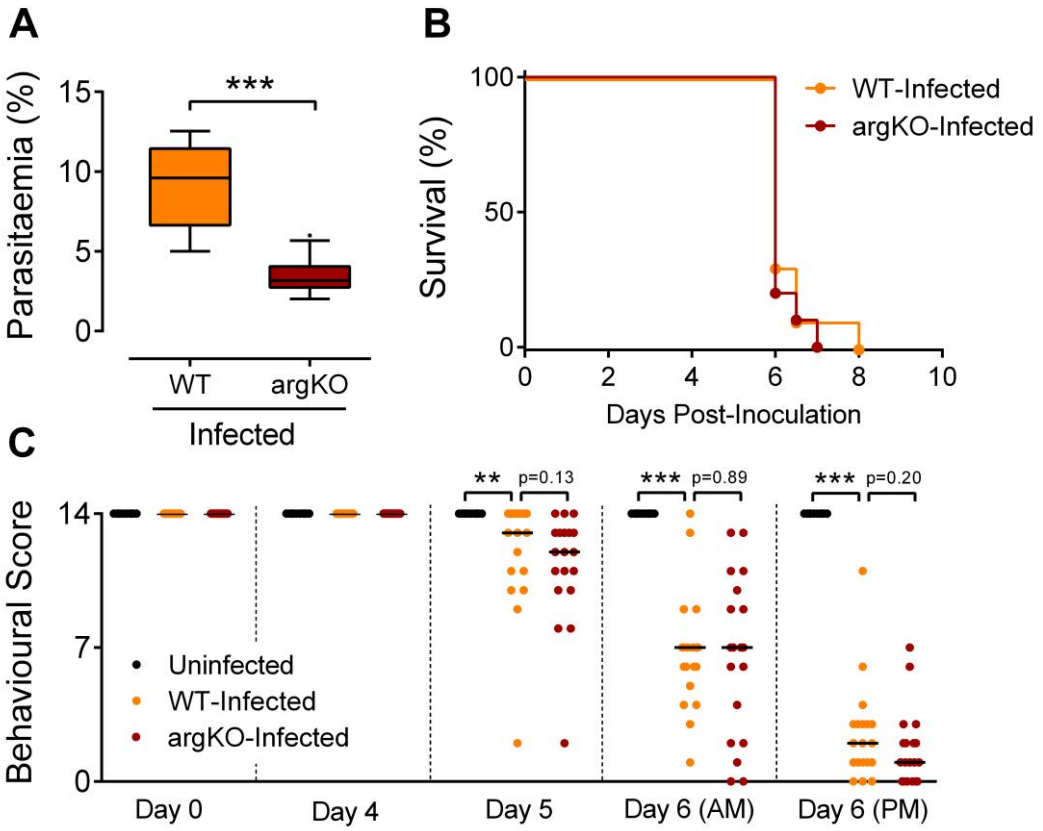


Figure 2.6 | Knock-out of parasite arginase does not improve survival in infected mice. (**A**) Mice infected with wild-type (WT) or arginase knock-out (argKO) *P. berghei* ANKA parasites were monitored for parasite burden by counting Giemsa-stained blood smears on day 6 post-inoculation. Box-plots depict median, IQR, min and max values of data pooled from 2 independent experiments (total n=19/group). (**B**) Groups of n=10 animals infected with arginase wild-type or arginase knock-out *P. berghei* ANKA parasites were assessed for non-moribund survival. The humane endpoint for the study was established *a priori* as a behavioural score of 3 out of 14 or less, at which point animals were euthanized. Survival was not different between groups as determined by log-rank test (p=0.53). (**C**) Mice infected with wild-type or arginase knock-out *P. berghei* ANKA parasites were monitored daily for disease symptoms. Symptoms were scored by assessing each of 7 parameters on a scale of 0 (moribund) to 2 (normal). D6 (AM) scores reflect assessments taken from 7AM-9AM in the morning for all animals and D6 (PM) scores reflect assessments taken in the afternoon. Results presented in panel C reflect n=19 mice infected with arginase wild-type parasites, n=19 mice infected with arginase knock-out parasites and n=10 uninfected controls. Black lines indicate median values for each group. $^{**}p < 0.01$, $^{***}p < 0.001$ by Mann-Whitney test.

Effect of Parasite Arginase Knock-Out on Blood-Brain Barrier Integrity

Disruption of the blood-brain barrier is observed in human (Taylor et al., 2004; Dorovini-Zis et al., 2011) and murine malaria (Gramaglia et al., 2006; Serghides et al., 2011). To assess integrity of the blood-brain barrier in mice infected with arginase knock-out or wild-type *P. berghei* ANKA parasites, infected mice and uninfected controls received intravenous injection of Evans blue dye on day 6 post-inoculation. After allowing dye to circulate for 1 hour, mice were euthanized and perfused with PBS to remove dye in the vascular compartment. Spectrophotometry was used to quantify the amount of dye that had leaked across the blood-brain barrier into the brain parenchyma.

Negligible Evans blue dye accumulation was observed in brain tissue from uninfected animals (mean ± SEM: 0.3 ± 0.2 µg Evans blue/mg brain tissue), indicating that minimal Evans blue is able to cross the blood-brain barrier under normal circumstances (FIG 2.7). By comparison, substantial dye accumulation was observed in the brains of mice infected with wild-type parasites (9.2 ± 1.8 µg Evans blue/mg brain tissue, $p < 0.05$ vs uninfected) and mice infected with arginase knock-out parasites (13.4 ± 1.8 µg Evans blue/mg brain tissue, $p < 0.01$ vs uninfected, FIG 2.7). These observations imply that disruption of the blood-brain barrier in infected animals enabled extravasation of Evans blue dye out of the vascular compartment. Mean dye extravasation was higher in the brains of mice infected with arginase knock-out parasites compared with wild-type parasites, but this difference was not statistically significant ($p = 0.41$, FIG 2.7). These results suggest that parasite arginase is not required to disrupt the blood-brain barrier in mice infected with *P. berghei* ANKA.

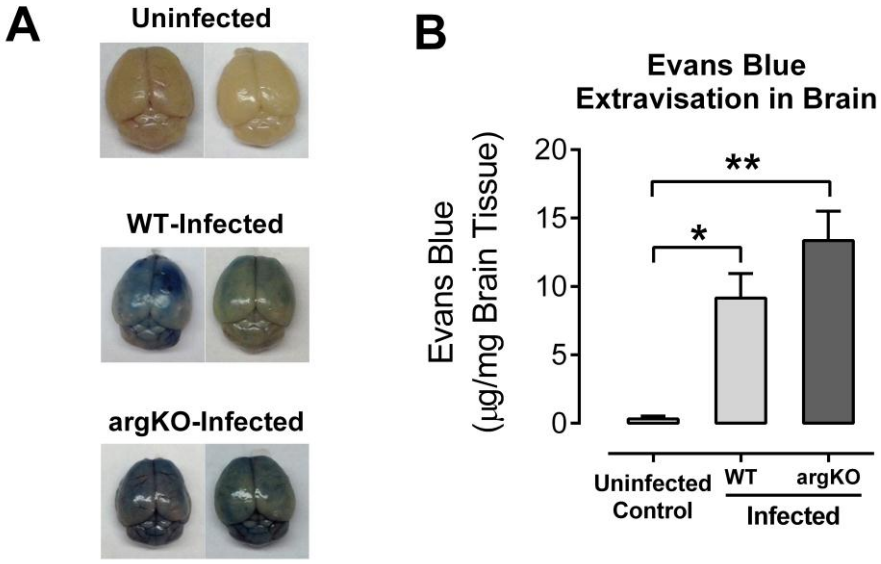


Figure 2.7 | Knock-out of parasite arginase does not prevent blood-brain barrier breakdown. (**A**) Photographs of brains from uninfected mice and mice infected with wild-type (WT) or arginase knock-out (argKO) *P. berghei* ANKA parasites following intravenous injection of Evans blue dye on day 6 post-inoculation. (**B**) Evans blue was extracted from brain tissue with *N,N*-dimethylformamide, quantified by measuring absorbance at 620nm with a spectrophotometer and normalizing to wet weight of the brain. Data are expressed as mean ± SEM for n=3 uninfected, n=3 WT-infected and n=4 argKO-infected mice. *p<0.05, **p<0.01 vs uninfected group by one-way ANOVA followed by Bonferroni post-test. The difference between the infected groups was not found to be statistically significant (p=0.41) by one-way ANOVA followed by Bonferroni post-test.

Effect of Parasite Arginase Knock-Out on in Vivo Arginine Depletion

On day 6 post-inoculation, plasma amino acids were assessed in mice infected with arginase knock-out (argKO) or wild-type (WT) parasites. Plasma arginine in mice infected with argKO parasites was depleted to the same degree as plasma arginine in mice infected with WT parasites (argKO-infected: 44.7 [40.3-49.5] µmol/L vs WT-infected: 48.9 [41.3-52.4] µmol/L, p = 0.33, FIG 2.8). Arginase knock-out parasites also caused a similar degree of ornithine depletion (argKO-infected: 16.4 [15.0-19.4] µmol/L vs WT-infected: 18.3 [16.9-21.4] µmol/L, p = 0.25, FIG 2.8) and a slightly greater degree of citrulline depletion (argKO-infected: 20.9 [19.3-25.2] µmol/L vs WT-infected: 24.3 [23.2-29.5] µmol/L, p < 0.05, FIG 2.8). These results demonstrate that parasite-expressed arginase is not required for depletion of arginine, citrulline or ornithine in experimentally-infected mice.

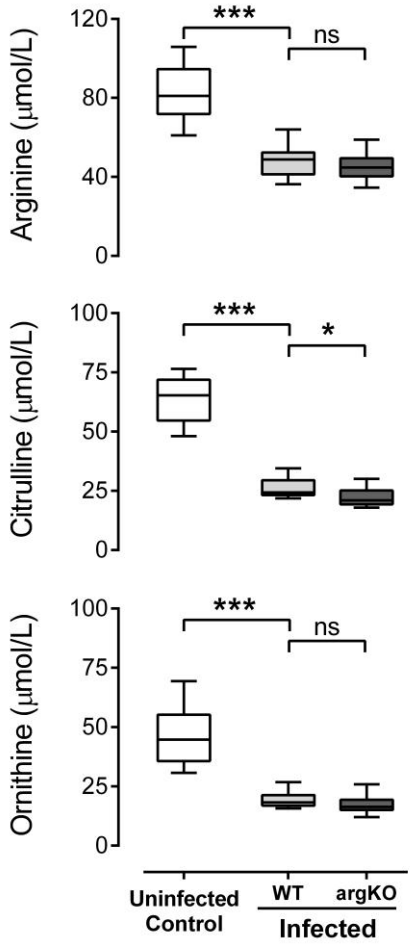


Figure 2.8 | *P. berghei* ANKA arginase is not required for arginine depletion. HPLC was used to quantify amino acids in plasma samples collected on day 6 post-inoculation from mice infected with wild-type (WT) or arginase knock-out (argKO) *P. berghei* ANKA parasites. Uninfected littermates served as controls. Data represent results from n=10 mice per group. Box-plots depict median, IQR, min and max values. *p<0.05, ***p<0.01 by Mann-Whitney test. ns (not significant): p > 0.05

2.4 Evaluation of Reduced Dietary Intake as a Possible Cause of Arginine Depletion

Dietary Intake and Weight Loss in C57BL/6 Mice

We considered whether dietary insufficiency could represent a previously unrecognized contributor to arginine depletion. *P. berghei* ANKA infection caused dietary intake to decrease on days 5 and 6 post-inoculation (uninfected day 5 mean ± SEM: 4.2 ± 0.2 g vs infected day 5: 2.7 ± 0.2 g, $p < 0.0001$; uninfected day 6: 4.5 ± 0.2 g vs infected day 6: 0.7 ± 0.2 $p < 0.0001$, FIG 2.9). To isolate the effect of decreased dietary intake from other infection-related changes in arginine metabolism, we limited dietary intake in an additional group of uninfected mice to match intake of *a priori* paired *P. berghei* ANKA-infected mice over 24 hour intervals.

Free access to water was provided for all animals. On day 6 post-inoculation, water consumption decreased in uninfected mice subjected to dietary restriction (uninfected + dietary restriction: 2.7 ± 0.2 mL vs *ad libitum*-fed uninfected 3.6 ± 0.2 mL, $p < 0.01$) and further decreased in infected mice (1.2 ± 0.2 mL, $p < 0.0001$ vs uninfected + dietary restriction, $p < 0.0001$ vs uninfected + *ad libitum* access to food, FIG 2.9). These results demonstrate that dietary restriction causes reduced water intake but that *P. berghei* ANKA infection causes further reductions in water intake.

Uninfected mice subjected to dietary restriction lost weight compared with controls with *ad libitum* access to food (uninfected + dietary restriction mean day 6 change in weight from initial ± SEM: -3.9 ± 0.2 g vs uninfected + *ad libitum* access to food: -0.3 ± 0.2 g, $p < 0.0001$, FIG 2.9). Infected mice experienced weight loss, but to a lesser degree than uninfected mice subjected to dietary restriction (infected day 6 change in weight from initial: -2.8 ± 0.2 g, $p < 0.0001$ vs uninfected + *ad libitum* access to food, $p < 0.0001$ vs uninfected + dietary restriction, FIG 2.9). Uninfected mice subjected to dietary restriction exhibit normal activity, including exploratory behaviour (day 6 median score [IQR]: 2 [2-2] out of 2) and body lift (2 [2-2] out of 2) while infected mice were largely immobile (exploratory behaviour score: 0 [0-0] out of 2, body lift score: 0 [0-0] out of 2) (see MATERIALS AND METHODS, p. 72 for details of scoring system). We speculate that additional weight loss in uninfected mice subjected to

dietary restriction may result from energy expenditure associated with greater levels of physical activity.

Across days 5 and 6 post-inoculation, change in weight correlated with food intake in both infected mice ($r_s = 0.66$, $p = 0.0001$) and uninfected mice subjected to dietary restriction ($r_s = 0.71$, $p < 0.0001$). These findings suggest that weight loss in mice infected with *P. berghei* ANKA was largely driven by reduced feeding behaviour.

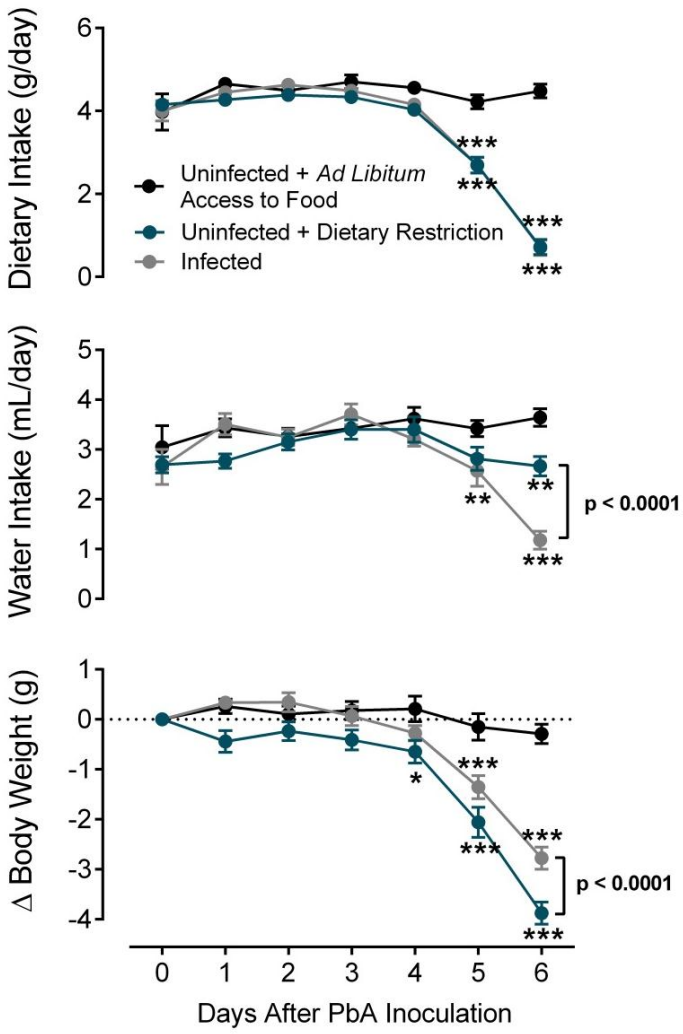


Figure 2.9 | Dietary intake and weight loss in C57BL/6 mice. Dietary intake and water intake were monitored by weight at 24hr intervals. Body weight is presented as change from initial weights taken directly before *P. berghei* ANKA inoculations. All mice were individually caged. Uninfected mice subjected to dietary restriction received only as much food as was consumed each day by an *a priori* paired mouse infected with *P. berghei* ANKA. Uninfected controls not subjected to dietary restriction were provided with *ad libitum* access to food. All groups were provided with free access to water. Data are expressed as mean ± SEM. Data are pooled from 6 independent experiments for a total of n=22 uninfected controls with *ad libitum* access to food and n=19 pairs of infected mice and uninfected mice subjected to dietary restriction. *p<0.05 **p<0.01, ***p<0.001 vs uninfected + *ad libitum* access to food by two-way ANOVA followed by Bonferroni post-test. p-values for uninfected + dietary restriction vs infected determined by two-way ANOVA followed by Bonferroni post-test.

Effect of Dietary Restriction on Plasma Arginine, Citrulline and Ornithine

As determined by HPLC analysis of plasma, dietary restriction in uninfected mice resulted in moderately reduced plasma arginine (median [IQR]: 77.3 [74.5-83.6] µmol/L) compared with uninfected controls with *ad libitum* access to food (91.3 [83.1-102.7] µmol/L, $p < 0.01$ vs uninfected + dietary restriction, FIG 2.10). Plasma arginine was further decreased in mice infected with *P. berghei* ANKA (53.5 [47.3-58.7] µmol/L, $p < 0.0001$ vs uninfected + dietary restriction, FIG 2.10). Plasma citrulline was also moderately decreased in uninfected mice subjected to dietary restriction (uninfected + dietary restriction: 34.3 [25.8-43.7] µmol/L vs uninfected + *ad libitum* access to food: 42.4 [32.0-55.5] µmol/L, $p < 0.05$) and further decreased in infected mice (17.9 [13.0-21.9] µmol/L, $p < 0.0001$ vs uninfected + dietary restriction, FIG 2.10). Plasma ornithine was not significantly reduced in uninfected mice subjected to dietary restriction compared with uninfected controls with *ad libitum* access to food (uninfected + dietary restriction: 41.0 [35.2-47.0] µmol/L vs uninfected + *ad libitum* access to food: 45.1 [38.2-57.5] µmol/L, $p = 0.17$, FIG 2.10). Plasma ornithine was reduced in *P. berghei* ANKA-infected mice (24.2 [18.4-32.0] µmol/L, $p < 0.001$ vs uninfected + dietary restriction, FIG 2.10).

These findings demonstrate that reduced feeding behaviour can induce moderate plasma arginine and citrulline depletion. However, *P. berghei* ANKA infection causes greater depletion of arginine, citrulline and ornithine than can be explained by reduced dietary intake alone. To further examine the effect of malaria infection on arginine metabolism, we used heavy isotope-labelled metabolic tracers to assess rates of appearance and interconversion of arginine, citrulline and ornithine in real-time.

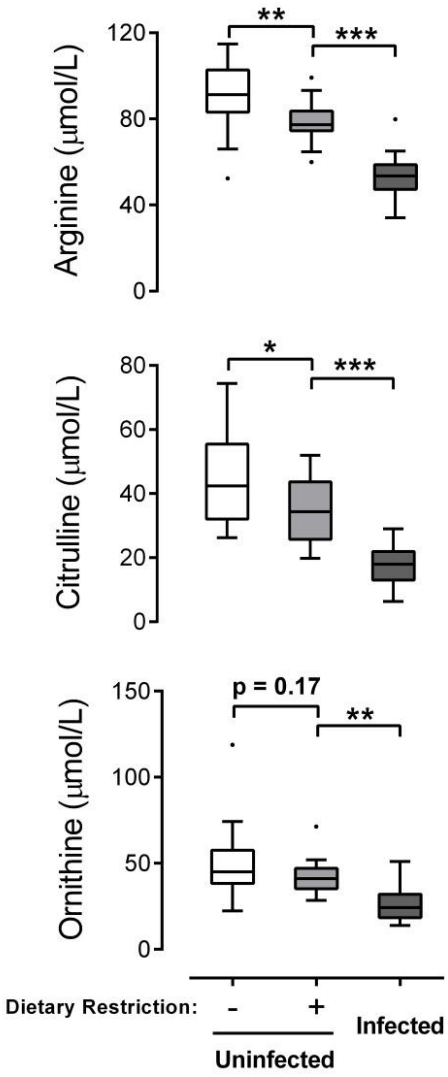


Figure 2.10 | Plasma amino acids in uninfected mice subjected to dietary restriction. HPLC was used to quantify amino acids in plasma samples from uninfected controls with or without dietary restriction and infected mice 6 days post-inoculation with *P. berghei* ANKA. Uninfected mice subjected to dietary restriction received only as much food as was consumed each day by an *a priori* paired mouse infected with *P. berghei* ANKA. Uninfected controls not subjected to dietary restriction were provided with *ad libitum* access to food. Data are pooled from 6 experiments for a total of n=22 uninfected controls with *ad libitum* access to food, n=19 pairs of infected mice and uninfected mice subjected to dietary restriction. Box-plots depict median and IQR. Whiskers extend to highest and lowest values within 1.5×IQR of the 75th and 25th percentiles, and values outside this range were plotted as individual points (Tukey's method). *p < 0.05, **p < 0.01. Uninfected mice with or without dietary restriction were compared by Mann-Whitney test; uninfected + dietary restriction values were compared to infected values by Wilcoxon matched-pairs signed rank test.

2.5 Quantitative Assessment of Metabolic Rates in Plasma

Overview of Tracer Methodology

To assess real-time arginine and ornithine metabolism *in vivo*, we continuously infused mice with arginine, citrulline and ornithine tracers labelled with ^{13}C and ^{15}N heavy isotopes. We selected arginine, citrulline and ornithine tracers that could be differentiated from each other following inter-conversion (see FIG B.3, p. 266) and developed a quadrupole-time of flight liquid chromatography/mass spectrometry (Q-TOF LC/MS) assay to determine plasma tracer enrichments in continuously-infused mice. The rate of appearance of endogenous arginine, ornithine and citrulline was calculated from the relative abundance of tracer during continuous infusion (FIG 2.11). Specific rates of conversion among arginine, ornithine and citrulline were calculated based on transfer of heavy isotope labels among metabolite pools. An in-depth description of tracer methodology and full derivations of relevant equations are available in MATERIALS AND METHODS (p. 77) and APPENDIX B (p.256).

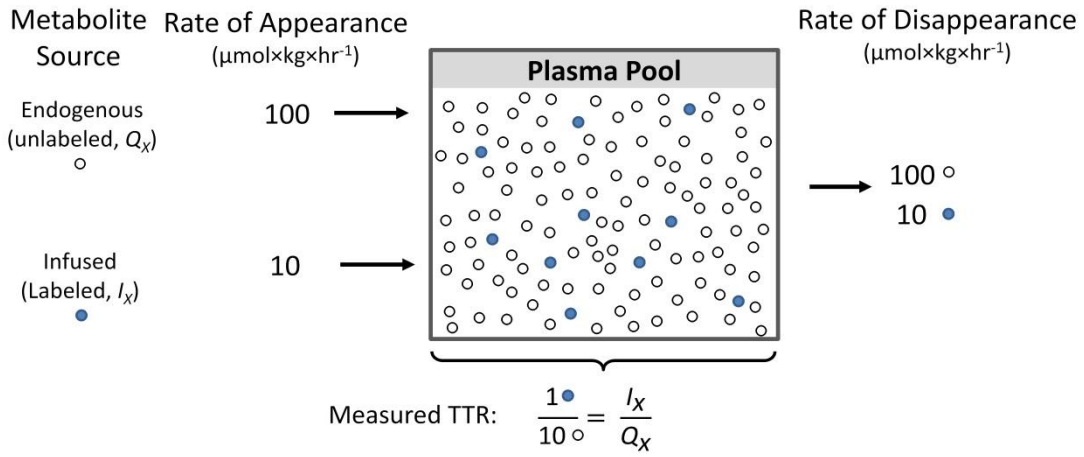


Figure 2.11 | Basic metabolic tracer theory. The rate of appearance of an endogenous metabolite (Q_X) can be determined by infusing a heavy isotope-labelled tracer at a rate of I_x. The presence of the heavy isotope tracer is assumed not to affect utilization (rate disappearance from the free plasma pool), which at steady-state will be equal to the rate of appearance. Enrichment of the tracer in the plasma pool (tracer-tracee ratio, or TTR) reflects the ratio of the rate of tracer infusion to the rate of endogenous metabolite appearance. The endogenous rate of appearance (Q_X) can be calculated by re-arranging this equation and substituting the known infusion rate and measured TTR value.

Rates of Appearance in Plasma

Arginine

The rate of appearance of plasma arginine was 503.3 [434.8-542.2] $\mu mol \times kg^{-1} \times hr^{-1}$ (median [IQR]) in uninfected controls with *ad libitum* access to food (FIG 2.12). The rate of appearance of arginine was decreased in uninfected mice subjected to dietary restriction (median [IQR]: 386.5 [330.4-440.0] $\mu mol \times kg^{-1} \times hr^{-1}$, $p < 0.01$ vs uninfected + *ad libitum* access to food, FIG 2.12). Arginine appearance was also reduced in infected mice (345.0 [217.8-436.1] $\mu mol \times kg^{-1} \times hr^{-1}$, $p < 0.05$ vs uninfected + *ad libitum* access to food, FIG 2.12). Decreased rates of appearance of plasma arginine may contribute to decreased plasma arginine concentrations observed in infected mice and uninfected mice subjected to dietary restriction (FIG 2.10). The rates of arginine appearance did not differ between infected mice and uninfected mice subjected to dietary restriction ($p = 0.49$) in contrast to the significant difference in plasma arginine concentrations observed in these groups (FIG 2.10). Taken together, our findings suggest that reduced rates of arginine appearance in plasma contribute to, but cannot fully explain arginine depletion in *P. berghei* ANKA-infected mice.

Ornithine

In uninfected mice with *ad libitum* access to food, the rate of appearance of plasma ornithine was 163.0 [149.5-187.8] $\mu mol \times kg^{-1} \times hr^{-1}$ (FIG 2.12). The median rate of ornithine appearance was decreased in uninfected mice subjected to dietary restriction (131.8 [105.3-162.3] $\mu mol \times kg^{-1} \times hr^{-1}$) compared to uninfected mice with *ad libitum* access to food, but this difference was of borderline statistical significance ($p = 0.05$ vs uninfected + *ad libitum* access to food, FIG 2.12). This finding is consistent with our previous observation that measured concentrations of ornithine were slightly, but not significantly lower in uninfected mice subjected to dietary restriction compared with uninfected mice with *ad libitum* access to food ($p = 0.17$, FIG 2.10). The rate of ornithine appearance was decreased in infected mice (116.3 [66.6-126.6] $\mu mol \times kg^{-1} \times hr^{-1}$) compared with uninfected controls subjected to dietary restriction ($p <$

0.05 vs uninfected + dietary restriction, FIG 2.12). This observation is consistent with the difference in plasma ornithine concentrations observed in these groups ($p < 0.01$, FIG 2.10). These findings suggest that decreased rates of ornithine appearance contribute to ornithine depletion in *P. berghei* ANKA-infected mice.

Citrulline

The rate of plasma citrulline appearance was 107.8 [90.6-125.6] $\mu mol \times kg^{-1} \times hr^{-1}$ in uninfected mice with *ad libitum* access to food (FIG 2.12). Citrulline appearance was decreased in uninfected mice subjected to dietary restriction (67.5 [60.5-73.0] $\mu mol \times kg^{-1} \times hr^{-1}$, $p < 0.001$ vs uninfected + *ad libitum* access to food) and further decreased in *P. berghei* ANKA-infected mice (44.2 [25.4-52.7] $\mu mol \times kg^{-1} \times hr^{-1}$, $p < 0.01$ vs uninfected + dietary restriction, FIG 2.12). These observations are consistent with our prior observation that plasma citrulline is decreased in uninfected mice subjected to dietary restriction ($p < 0.05$ vs uninfected + *ad libitum* access to food) and further decreased in in infected mice ($p < 0.0001$ vs uninfected + dietary restriction, FIG 2.10). Taken together, these findings suggest that reduced appearance of citrulline in plasma contributes to citrulline depletion in *P. berghei* ANKA-infected mice.

To further examine the metabolic dynamics associated with of reduced arginine, ornithine and citrulline appearance in plasma, we determined rates of interconversion among these metabolites.

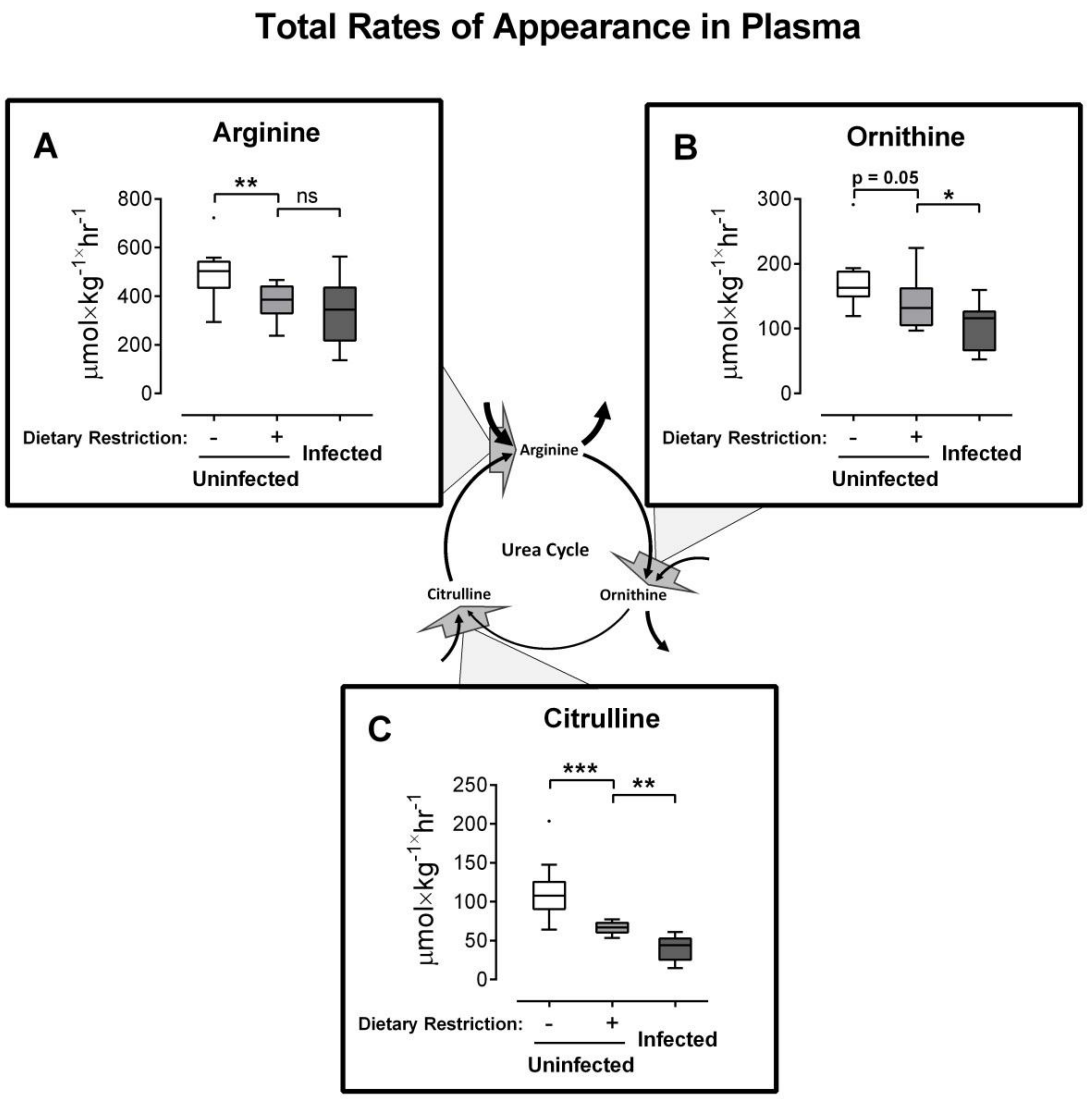


Figure 2.12 | Rates of appearance of plasma arginine, ornithine and citrulline. Rates of appearance of plasma arginine (**A**), ornithine (**B**) and citrulline (**C**) were calculated from plasma enrichment of continuously infused heavy isotope-labelled metabolic tracers, as measured by Q-TOF LC/MS. Uninfected mice subjected to dietary restriction received only as much food as was consumed each day by a paired mouse infected with *P. berghei* ANKA. Uninfected controls not subjected to dietary restriction were provided with *ad libitum* access to food. Data are pooled from 3 experiments for a total of n=10 uninfected controls with *ad libitum* access to food and n=10 pairs of infected mice and uninfected mice subjected to dietary restriction. Tracer infusions were performed on day 6 post-inoculation. Box-plots depict median and IQR. Whiskers extend to highest and lowest values within 1.5×IQR of the 75th and 25th percentiles with values outside this range plotted as individual points (Tukey's method). *p < 0.05, **p < 0.01, ***p < 0.001. Uninfected controls with or without dietary restriction were compared by Mann-Whitney test; uninfected controls + dietary restriction were compared to infected values by Wilcoxon matched-pairs signed rank test.

Rates of Inter-conversion among Arginine, Ornithine and Citrulline

Appearance of Arginine from Citrulline and Other Sources

Citrulline is an important precursor for the synthesis of arginine, so we quantitatively assessed the rate of conversion of citrulline to arginine. The rate of conversion of citrulline to arginine was decreased in uninfected mice subjected to dietary restriction (59.1 [39.2-71.3] $\mu mol \times kg^{-1} \times hr^{-1}$) compared with uninfected controls with *ad libitum* access to food (102.5 [76.5-137.6] $\mu mol \times kg^{-1} \times hr^{-1}$, $p < 0.01$ vs uninfected + dietary restriction, FIG 2.13). The median rate of citrulline-to-arginine conversion was further decreased in infected mice (40.3 [25.5-59.5] $\mu mol \times kg^{-1} \times hr^{-1}$), but this difference did not reach statistical significance compared with uninfected mice subjected to dietary restriction ($p = 0.06$ vs uninfected + dietary restriction, FIG 2.13). In all groups, a high percentage of plasma citrulline was utilized for arginine synthesis (uninfected + *ad libitum* access to food: 97.5% [74.6-109.5%], uninfected + dietary restriction: 94.6% [55.8-118.3%], $p = 0.89$ vs uninfected + *ad libitum* access to food, infected: 110.4% [91.0-119.7%] $p = 0.13$ vs uninfected + dietary restriction, FIG 2.13). Arginine synthesis from citrulline accounted for 19% [16.2-23.7%] of total arginine appearance in uninfected controls with *ad libitum* access to food (FIG 2.14). The percentage of arginine synthesized from plasma citrulline was decreased to 14.4% [13.2-19.1%] in uninfected mice subjected to dietary restriction ($p < 0.05$ vs uninfected + with *ad libitum* access to food) and further decreased in infected mice (12.6% [10.2-14.1%], $p < 0.01$ vs uninfected + dietary restriction, FIG 2.14).

In addition to synthesis from citrulline, plasma arginine is derived from enteral absorption and protein break-down (FIG 2.1, p. 31). The rates of arginine appearance from sources other than citrulline were calculated as the total rate of arginine appearance less the contribution of synthesis from citrulline. The rate of arginine appearance from enteral absorption, protein break-down or other sources was decreased in uninfected mice subjected to dietary restriction compared with uninfected mice with *ad libitum* access to food (uninfected + dietary restriction: 332.9 [273.6-368.3] $\mu mol \times kg^{-1} \times hr^{-1}$ uninfected + *ad libitum* access to food: 406.8 [316.3-433.5] $\mu mol \times kg^{-1} \times hr^{-1}$, $p < 0.05$) and was similarly reduced in infected mice

(304.1 [190.6-378.2] µmol×kg^{-1}×hr^{-1}, p = 0.56 vs uninfected + dietary restriction, FIG 2.14). Due to decreases in arginine synthesis from citrulline, arginine derived from other sources accounted for an increasing proportion of total arginine appearance (uninfected + *ad libitum* access to food: 80.9% [76.3-83.8%], uninfected + dietary restriction: 85.6% [80.9-86.9%], p < 0.05 vs uninfected + *ad libitum* access to food, infected: 87.4% [85.9-89.8%] p < 0.01 vs uninfected + dietary restriction, FIG 2.14).

In summary, although citrulline is almost exclusively utilized for arginine synthesis in all groups, the rate of citrulline conversion to arginine decreases due to dietary restriction and further decreases in *P. berghei* ANKA-infected mice. The proportion of arginine derived from citrulline also falls due to dietary restriction and decreases further during *P. berghei* ANKA infection. This observation implies that arginine synthesis from citrulline decreases faster than the decrease in appearance of arginine derived from other sources, such as protein break-down. Taken together, these findings indicate that decreased rates of synthesis from citrulline contribute to reduced rates of plasma arginine appearance.

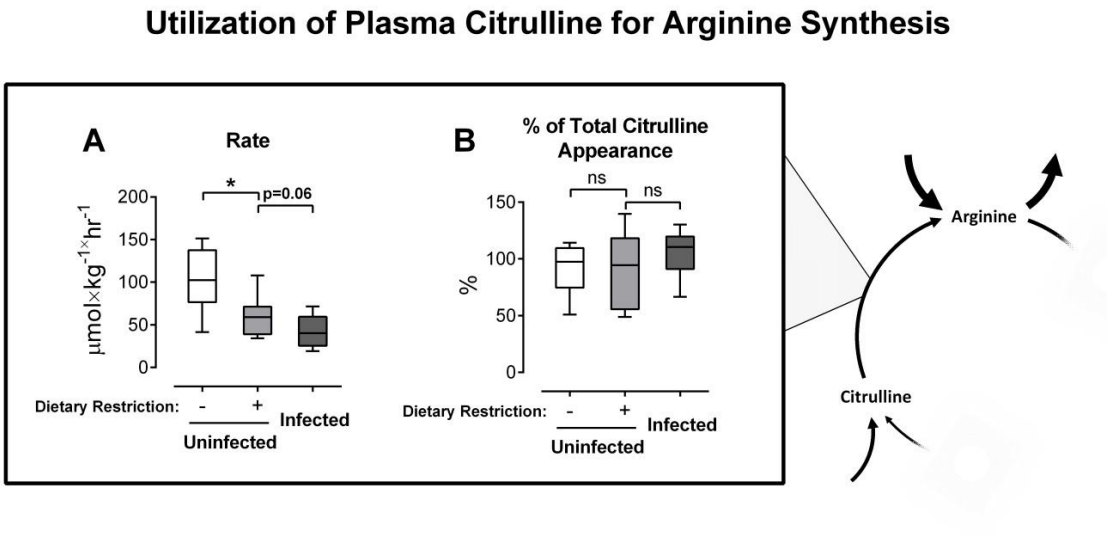


Figure 2.13 | Utilization of plasma citrulline for arginine synthesis. (**A**) The rate of conversion of citrulline to arginine was calculated from plasma enrichment of continuously infused heavy isotope-labelled metabolic tracers, as measured by Q-TOF LC/MS. (**B**) the rate of conversion of citrulline to arginine was calculated as a percent of the total rate of citrulline appearance. Uninfected mice subjected to dietary restriction received only as much food as was consumed each day by a paired mouse infected with *P. berghei* ANKA. Uninfected controls not subjected to dietary restriction were provided with *ad libitum* access to food. Data are pooled from 3 experiments for a total of n=10 uninfected controls with *ad libitum* access to food and n=10 pairs of infected mice and uninfected mice subjected to dietary restriction. Tracer infusions were performed on day 6 post-inoculation. Box-plots depict median, IQR, min and max. *$p < 0.05$, ns (not significant): $p > 0.05$. Uninfected controls with or without dietary restriction were compared by Mann-Whitney test; uninfected controls + dietary restriction were compared to infected values by Wilcoxon matched-pairs signed rank test.

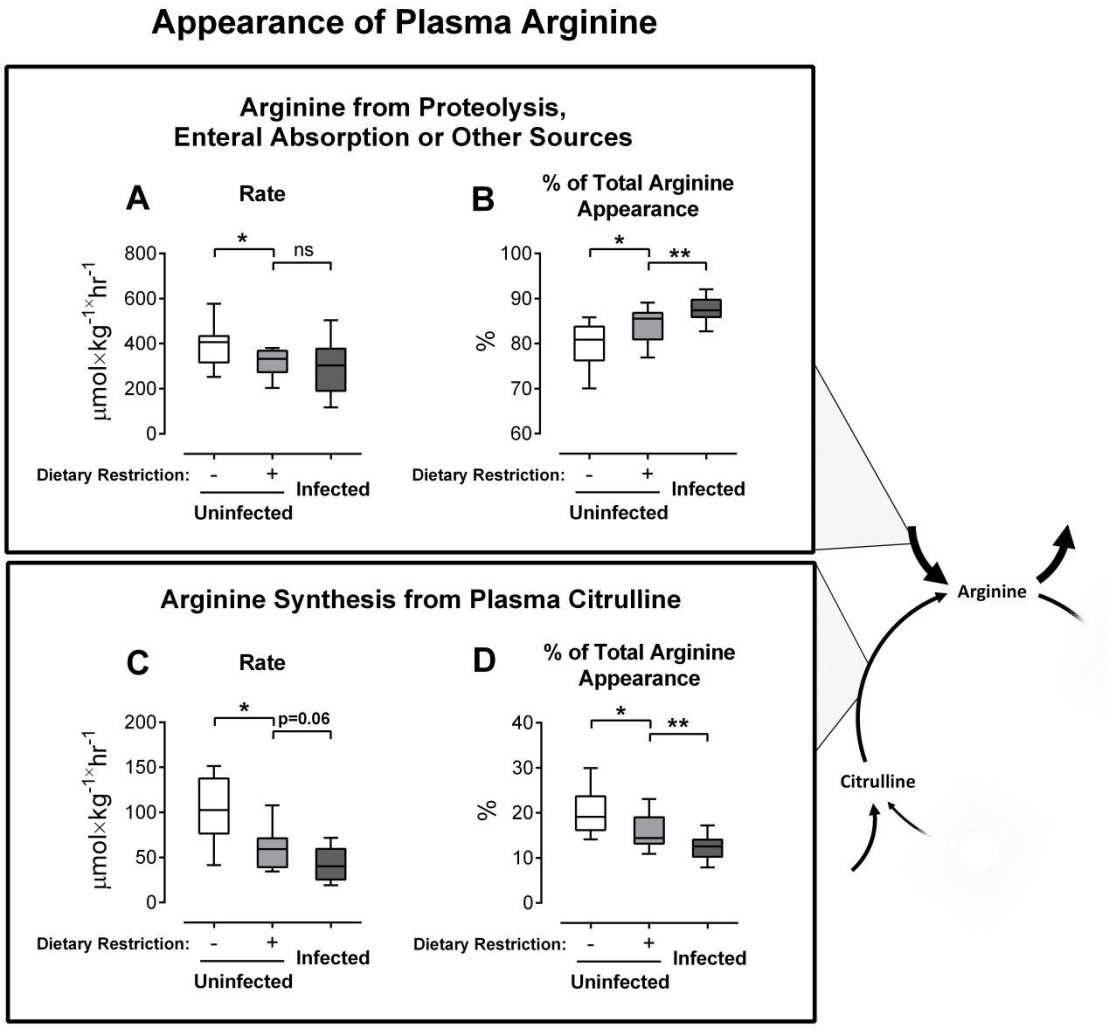


Figure 2.14 | Appearance of plasma arginine. (**A**) The rate of arginine appearance from sources other than citrulline was calculated as the difference between the total rate of arginine appearance and the rate of conversion of citrulline to arginine. (**B**) The rate of arginine appearance from sources other than citrulline was calculated as a percent of the total rate of arginine appearance (**C**) The rate of conversion of citrulline to arginine was calculated from plasma enrichment of continuously infused heavy isotope-labelled metabolic tracers, as measured by Q-TOF LC/MS. (**D**) The rate of arginine synthesis from citrulline was calculated as a percent of the total rate of arginine appearance. Uninfected mice subjected to dietary restriction received only as much food as was consumed each day by a paired mouse infected with *P. berghei* ANKA. Uninfected controls not subjected to dietary restriction were provided with *ad libitum* access to food. Data are pooled from 3 experiments for a total of n=10 uninfected controls with *ad libitum* access to food and n=10 pairs of infected mice and uninfected mice subjected to dietary restriction. Tracer infusions were performed on day 6 post-inoculation. Box-plots depict median, IQR, min and max. *$p < 0.05$, **$p < 0.01$, ns (not significant): $p > 0.05$. Uninfected controls with or without dietary restriction were compared by Mann-Whitney test; uninfected controls + dietary restriction were compared to infected values by Wilcoxon matched-pairs signed rank test.

Conversion of Arginine to Ornithine

Previous studies have implicated host and parasite arginase as the mechanism responsible for arginine depletion in severe malaria (Lopansri et al., 2003; Yeo et al., 2007; Olszewski et al., 2009; Omodeo-Sale et al., 2010). Arginase converts arginine to ornithine and urea, prompting us to assess the rate of conversion of arginine to ornithine in *P. berghei* ANKA-infected mice. The rate of arginine-to-ornithine conversion was not changed in uninfected mice subjected to dietary restriction or in *P. berghei* ANKA-infected mice (uninfected + *ad libitum* access to food: 106.4 [87.2-117.7] $\mu mol \times kg^{-1} \times hr^{-1}$, uninfected + dietary restriction: 115.2 [78.4-126.6] $\mu mol \times kg^{-1} \times hr^{-1}$, $p = 0.89$ vs uninfected + *ad libitum* access to food, infected: 107.4 [59.4-126.3] $\mu mol \times kg^{-1} \times hr^{-1}$, $p = 0.77$ vs uninfected + dietary restriction, FIG 2.15). In infected mice and uninfected mice subjected to dietary restriction, the rate of conversion of arginine to ornithine was maintained despite decreased rates of arginine appearance (FIG 2.12). As a result, arginine utilization for ornithine synthesis increased as a percentage of total arginine appearance in these groups (uninfected + dietary restriction: 26.1% [23.7-32.9%], infected: 29.2% [26.8-33.8%]) compared with uninfected mice with *ad libitum* access to food (21.1% [19.9-22.7%], $p < 0.01$ vs uninfected + dietary restriction, $p < 0.001$ vs infected, FIG 2.15).

In summary, we conclusively demonstrate that the rate of conversion of arginine to ornithine is not increased in mice infected with *P. berghei* ANKA. We cannot rule out the possibility that increased arginase activity may be required to maintain a constant rate of conversion of arginine to ornithine under conditions of limited arginine substrate. However, our findings indicate that increased arginase activity is not primarily responsible for arginine depletion in *P. berghei* ANKA-infected mice.

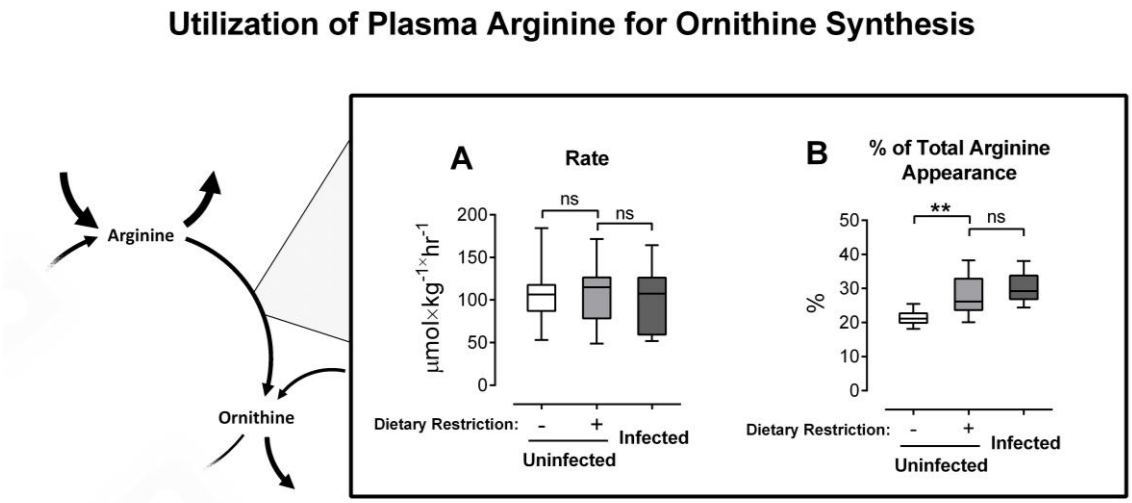


Figure 2.15 | Utilization of plasma arginine for ornithine synthesis. (**A**) The rate of conversion of arginine to ornithine was calculated from plasma enrichment of continuously infused heavy isotope-labelled metabolic tracers, as measured by Q-TOF LC/MS. (**B**) The rate of conversion of arginine to ornithine was calculated as a percentage of the total rate of arginine appearance. Uninfected mice subjected to dietary restriction received only as much food as was consumed each day by a paired mouse infected with *P. berghei* ANKA. Uninfected controls not subjected to dietary restriction were provided with *ad libitum* access to food. Data are pooled from 3 experiments for a total of n=10 uninfected controls with *ad libitum* access to food and n=10 pairs of infected mice and uninfected mice subjected to dietary restriction. Tracer infusions were performed on day 6 post-inoculation. Box-plots depict median, IQR, min and max. **p < 0.01, ns (not significant): p > 0.05. Uninfected controls with or without dietary restriction were compared by Mann-Whitney test; uninfected controls + dietary restriction were compared to infected values by Wilcoxon matched-pairs signed rank test.

Other Sources of Ornithine

Ornithine synthesis from sources other than arginine, such as glutamate or proline, was 63.1 [45.1-85.2] $\mu mol \times kg^{-1} \times hr^{-1}$ in uninfected mice with *ad libitum* access to food, but fell to 30.0 [20.6-45.2] $\mu mol \times kg^{-1} \times hr^{-1}$ in uninfected mice subjected to dietary restriction ($p < 0.01$ vs uninfected + *ad libitum* access to food, FIG 2.16). Ornithine synthesis from sources other than arginine fell even further in infected mice (5.6 [1.8-8.8] $\mu mol \times kg^{-1} \times hr^{-1}$, $p < 0.01$ vs uninfected + dietary restriction, FIG 2.16). In uninfected mice with *ad libitum* access to food, the rate of conversion of arginine to ornithine represented 65.2% [54.9-71.9%] of total ornithine synthesis (FIG 2.16). The rate of conversion of arginine to ornithine accounted for a greater percentage of total ornithine synthesis in uninfected mice subjected to dietary restriction (80.4% [70.9-83.3%], $p < 0.05$ vs uninfected + *ad libitum* access to food) and an even greater percentage in infected mice (94.1% [92.2-101.2%], $p < 0.01$ vs uninfected + dietary restriction, FIG 2.16).

These findings indicate that ornithine was almost entirely synthesized from arginine in infected mice with very little derived from other sources, such as proline or glutamate. This observation suggests that during infection proline and glutamate may be diverted to other metabolic uses, such as TCA cycle respiration. This process could be driven by changes in host metabolism and/or by direct metabolic competition with blood-stage parasites. In summary, ornithine depletion due to malaria infection can be attributed to impaired synthesis from substrates other than arginine.

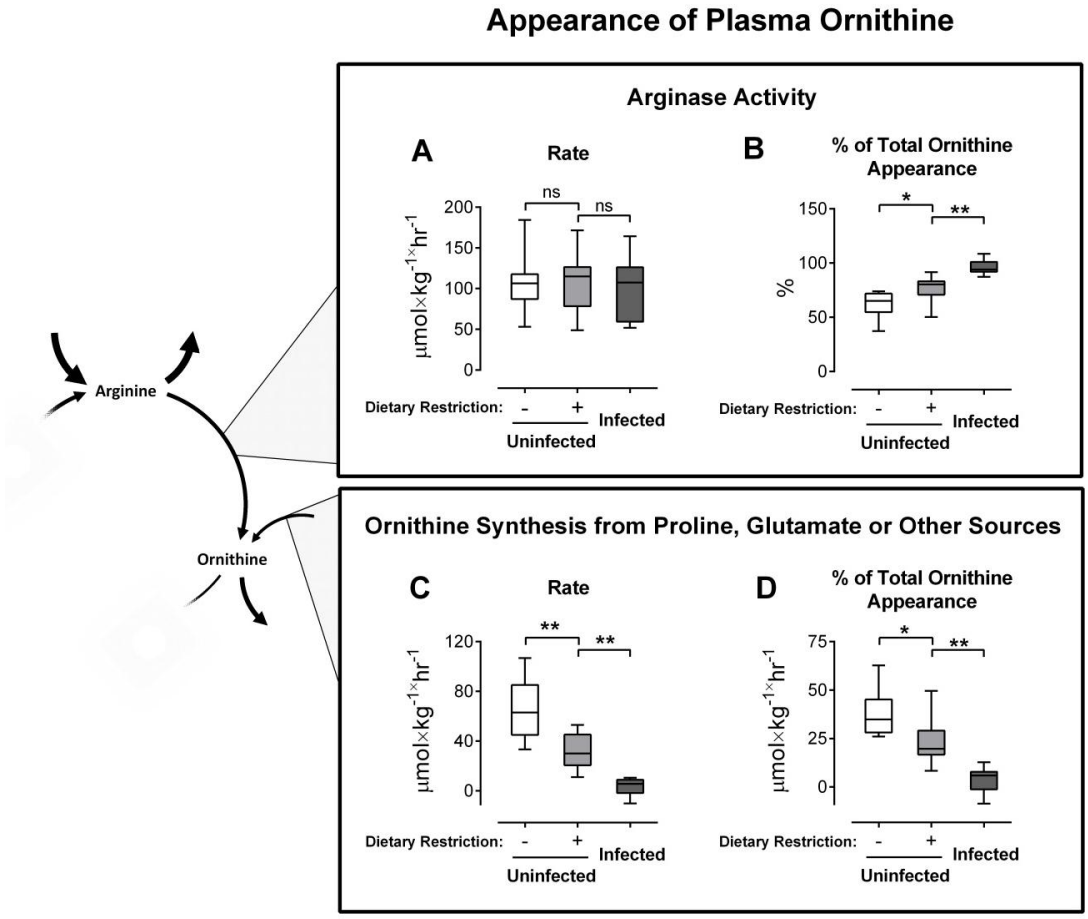


Figure 2.16 | Appearance of plasma ornithine. (**A**) The rate of conversion of arginine to ornithine was calculated from plasma enrichment of continuously infused heavy isotope-labelled metabolic tracers, as measured by Q-TOF LC/MS. (**B**) The rate of conversion of arginine to ornithine was calculated as a percentage of the total rate of ornithine appearance. (**C**) The rate of ornithine appearance from sources other than arginine was calculated as the difference between the total rate of ornithine appearance and the rate of conversion of arginine to ornithine. (**D**) The rate of ornithine appearance from sources other than arginine was calculated as a percent of the total rate of ornithine appearance. Uninfected mice subjected to dietary restriction received only as much food as was consumed each day by a paired mouse infected with *P. berghei* ANKA. Uninfected controls not subjected to dietary restriction were provided with *ad libitum* access to food. Data are pooled from 3 experiments for a total of n=10 uninfected controls with *ad libitum* access to food and n=10 pairs of infected mice and uninfected mice subjected to dietary restriction. Tracer infusions were performed on day 6 post-inoculation. Box-plots depict median, IQR, min and max. *$p < 0.05$ **$p < 0.01$, ns (not significant): $p > 0.05$. Uninfected controls with or without dietary restriction were compared by Mann-Whitney test; uninfected controls + dietary restriction were compared to infected values by Wilcoxon matched-pairs signed rank test.

Plasma Ornithine Utilization

The rate of conversion of plasma ornithine to citrulline was 22.9 [19.2-27.9] $\mu mol \times kg^{-1} \times hr^{-1}$ in uninfected mice with *ad libitum* access to food. The rate of conversion of ornithine to citrulline was decreased in uninfected mice subjected to dietary restriction (17.8 [13.2-21.3] $\mu mol \times kg^{-1} \times hr^{-1}$, $p < 0.05$ vs uninfected + *ad libitum* access to food) and further decreased in *P. berghei* ANKA-infected mice (15.7 [6.2-17.4] $\mu mol \times kg^{-1} \times hr^{-1}$, $p < 0.05$ vs uninfected mice + dietary restriction, FIG 2.17). The proportion of plasma ornithine utilized for citrulline synthesis did not change during dietary restriction (uninfected + dietary restriction: 13.5% [12.5-14.3%] vs uninfected + *ad libitum* access to food: 13.4% [11.8-17.1%], $p = 0.89$) but fell slightly in infected mice (11.9% [10.0-14.1%], $p < 0.05$ vs uninfected + dietary restriction, FIG 2.17). Accordingly, the rate of plasma ornithine utilization for non-urea cycle metabolism accounted for a slightly greater proportion of the total rate of ornithine appearance in infected mice (88.1% [85.9-90.0%]) compared with uninfected mice subjected to dietary restriction (86.5% [85.7-87.7%], $p < 0.05$ vs infected, FIG 2.17). These findings indicate a small but significant degree of diversion of plasma ornithine away from citrulline synthesis and toward non-urea cycle metabolism, such as glutamate synthesis or TCA cycle respiration. Reduced plasma ornithine appearance must also be considered a major cause of reduced citrulline synthesis from plasma ornithine.

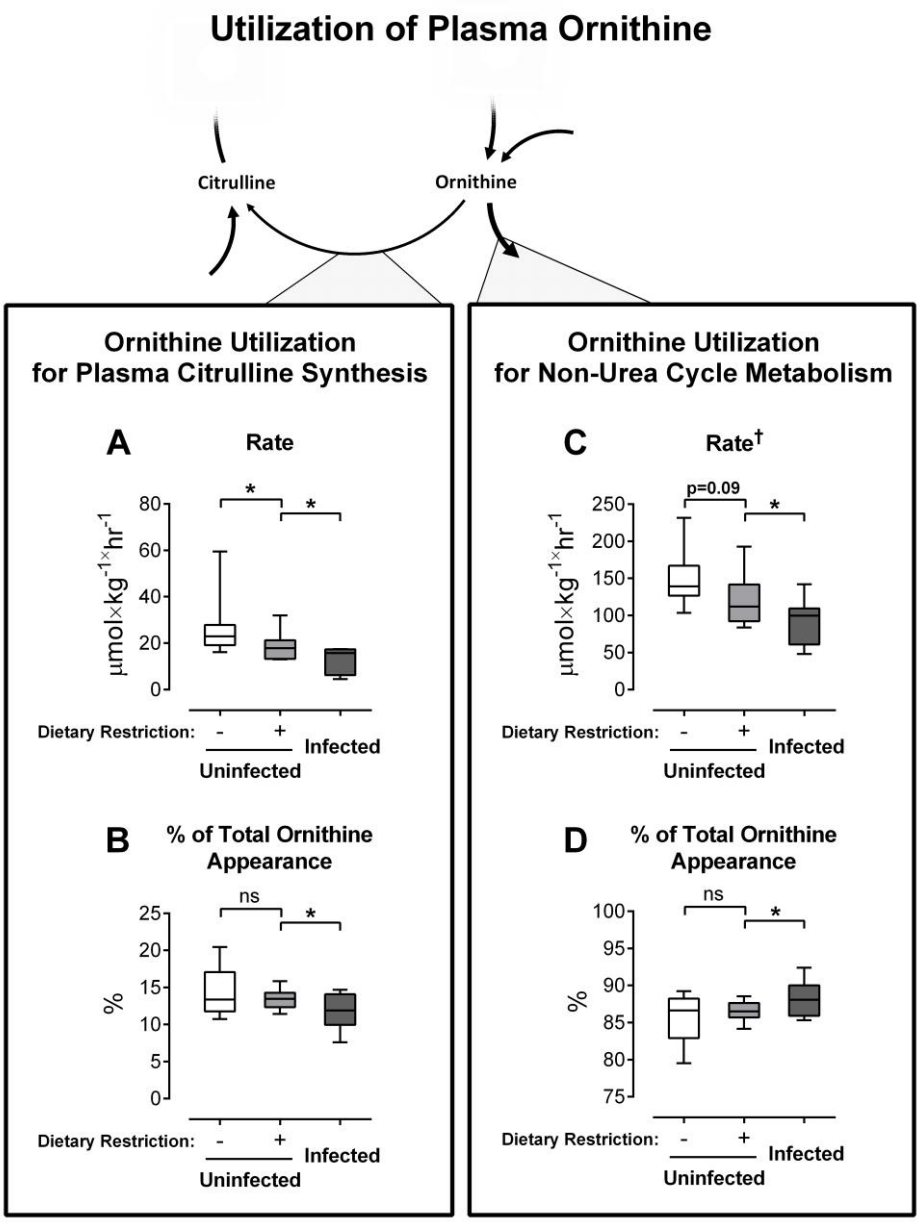


Figure 2.17 | Utilization of plasma ornithine. (**A**) The rate of conversion of ornithine to citrulline was calculated from plasma enrichment of continuously infused heavy isotope-labelled metabolic tracers, as measured by Q-TOF LC/MS. (**B**) The rate of conversion of ornithine to citrulline was calculated as a percentage of the total rate of ornithine appearance. (**C**) The rate of ornithine utilization for purposes other than citrulline synthesis was calculated as the difference between the total rate of ornithine appearance and the rate of conversion of ornithine to citrulline. (**D**) The rate of ornithine utilization for purposes other than citrulline synthesis was calculated as a percent of the total rate of ornithine appearance. Uninfected mice subjected to dietary restriction received only as much food as was consumed each day by a paired mouse infected with *P. berghei* ANKA. Uninfected controls not subjected to dietary restriction were provided with *ad libitum* access to food. Data are pooled from 3 experiments for a total of n=10 uninfected controls with *ad libitum* access to food and n=10 pairs of infected mice and uninfected mice subjected to dietary restriction. Tracer infusions were performed on day 6 post-inoculation. Box-plots depict median, IQR, min and max. *$p < 0.05$, ns (not significant): $p > 0.05$. Uninfected controls with or without dietary restriction were compared by Mann-Whitney test; uninfected controls + dietary restriction were compared to infected values by Wilcoxon matched-pairs signed rank test. †Rates not measured directly; calculated by inference from measured values based on the assumption that the rate of ornithine appearance equals the rate of ornithine disappearance (steady state flux).

Citrulline Synthesis

In addition to decreased rates of synthesis from plasma ornithine, the rate of citrulline appearance from other sources was decreased in uninfected mice subjected to dietary restriction (uninfected + dietary restriction: 47.0 [42.8-53.5] $\mu mol \times kg^{-1} \times hr^{-1}$ vs uninfected + *ad libitum* access to food: 83.2 [71.5-101.4], $p < 0.001$) and was further deceased in infected mice (29.3 [19.3-35.7] $\mu mol \times kg^{-1} \times hr^{-1}$, $p < 0.01$ vs uninfected + dietary restriction, FIG 2.18). Furthermore, the proportion of citrulline derived from sources other than plasma ornithine fell from 78.3% [75.4-79.5%] in uninfected mice with *ad libitum* access to food to 72.8% [68.0-77.0%] in uninfected mice subjected to dietary restriction ($p < 0.05$ vs uninfected + *ad libitum* access to food) and to 69.7% [65.3-72.6%] in infected mice ($p = 0.06$ vs uninfected + dietary restriction, FIG 2.18).

These findings indicate that the rate of citrulline synthesis from sources other than plasma ornithine fell faster than the rate of direct conversion from plasma ornithine. These findings may reflect reductions in enteral citrulline synthesis during dietary restriction and infection. Arginine absorbed in the gut may be converted to ornithine by arginase, which in turn serves as a substrate for enteral citrulline synthesis (FIG 2.1, p. 31). Dietary arginine has been identified as the major source of enteral citrulline synthesis, but ornithine absorbed directly from the intestinal lumen or synthesized from proline, glutamine or glutamate may also serve as substrates for enteral citrulline synthesis (Marini et al., 2010a; b). To the extent that enteral ornithine is partitioned from plasma ornithine pools, citrulline derived from enteral synthesis may not carry the heavy isotope label infused into plasma ornithine pools. If this is the case, enteral citrulline synthesis may account for a considerable proportion of citrulline appearance from sources other than plasma ornithine. Decreased enteral citrulline synthesis could arise from reduced dietary intake of arginine or impaired enteral absorption of arginine during infection.

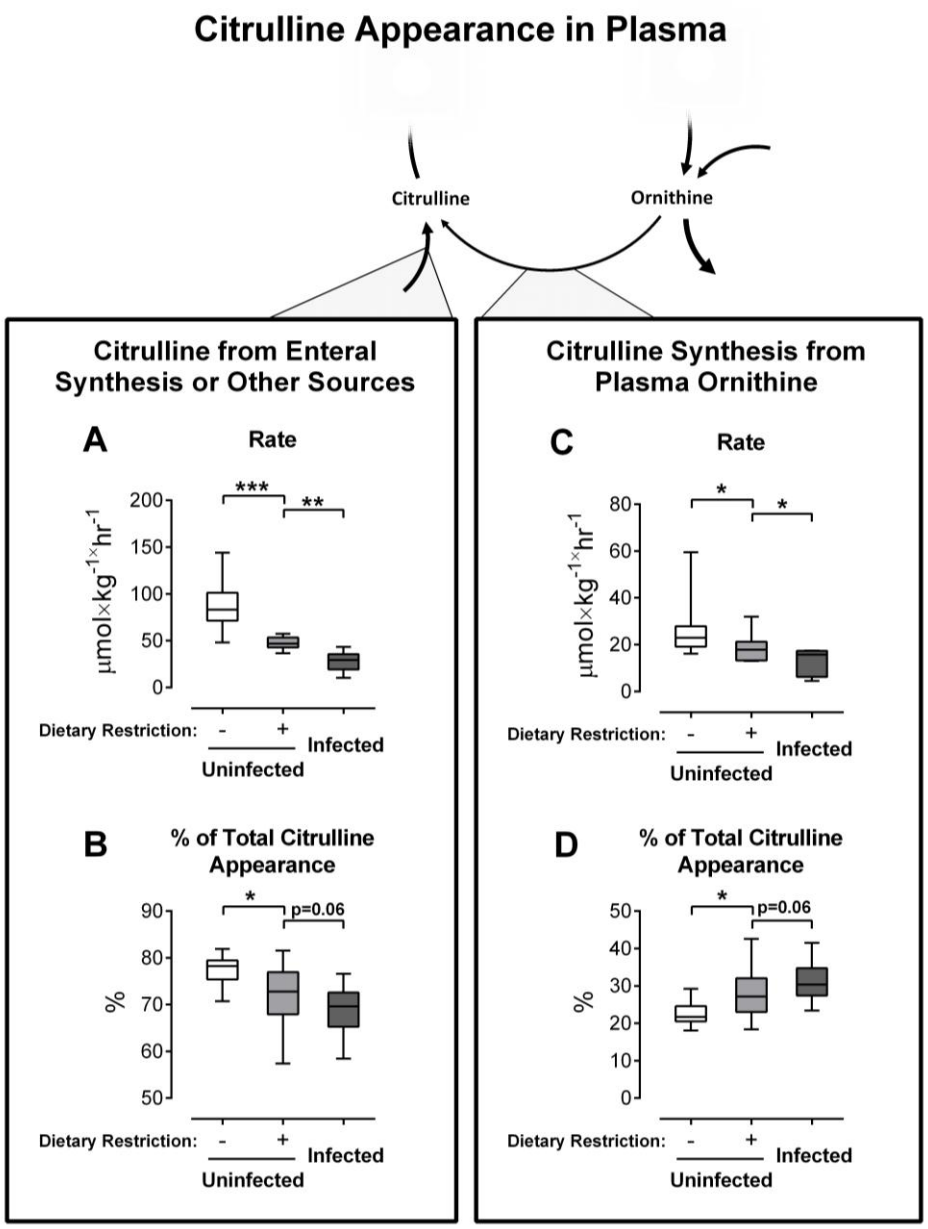


Figure 2.18 | Appearance of plasma citrulline. (**A**) The rate of citrulline appearance from sources other than plasma ornithine was calculated as the difference between the total rate of citrulline appearance and the rate of conversion of ornithine to citrulline. (**B**) The rate of citrulline appearance from sources other than plasma ornithine was calculated as a percent of the total rate of citrulline appearance. (**C**) The rate of conversion of ornithine to citrulline was calculated from plasma enrichment of continuously infused heavy isotope-labelled metabolic tracers, as measured by Q-TOF LC/MS. (**D**) The rate of conversion of ornithine to citrulline was calculated as a percentage of the total rate of citrulline appearance. Uninfected mice subjected to dietary restriction received only as much food as was consumed each day by a paired mouse infected with *P. berghei* ANKA. Uninfected controls not subjected to dietary restriction were provided with *ad libitum* access to food. Data are pooled from 3 experiments for a total of n=10 uninfected controls with *ad libitum* access to food and n=10 pairs of infected mice and uninfected mice subjected to dietary restriction. Tracer infusions were performed on day 6 post-inoculation. Box-plots depict median, IQR, min and max. *$p < 0.05$, **$p < 0.01$, ***$p < 0.001$, ns (not significant): $p > 0.05$. Uninfected controls with or without dietary restriction were compared by Mann-Whitney test; uninfected controls + dietary restriction were compared to infected values by Wilcoxon matched-pairs signed rank test.

Rate of Conversion of Arginine to Citrulline by NOS

Arginine is converted to citrulline during nitric oxide synthesis. To determine the rate of arginine utilization for NO synthesis, we assessed appearance of citrulline carrying the heavy isotope label from infused arginine tracer. In addition to direct conversion by NOS, arginine may be converted to citrulline indirectly via ornithine. Our tracer labelling strategy allowed us to distinguish between these two metabolic pathways (see APPENDIX B, p.281). The enzymes ASS1 and ASL are complexed with NOS to allow rapid recycling of citrulline back to arginine to sustain NO synthesis (Flam et al., 2001; Vukosavljevic et al., 2006; Erez et al., 2011). In order to calculate the total rate of plasma arginine utilization by NOS, we accounted for arginine substrates and citrulline products that had undergone one or more cycles of NO generation and recycling (see APPENDIX B, p.281).

The median rate of arginine utilization by NOS was 1.17 [0.83-2.03] $\mu mol \times kg^{-1} \times hr^{-1}$ in uninfected mice with *ad libitum* access to food, and this rate was unchanged in uninfected mice subjected to dietary restriction (1.13 [0.86-1.28] $\mu mol \times kg^{-1} \times hr^{-1}$, $p = 0.72$ vs uninfected + *ad libitum* access to food, FIG 2.19). The rate of arginine utilization for NO synthesis was decreased in mice infected with *P. berghei* ANKA (0.66 [0.49-0.82], $p < 0.01$ vs uninfected + dietary restriction, FIG 2.19). In uninfected mice with *ad libitum* access to food, arginine utilization by NOS accounted for 0.24% [0.16-0.37%] of the total rate of arginine appearance (FIG 2.19). A similar percentage of arginine was utilized by NOS in uninfected mice subjected to dietary restriction (0.28% [0.24-0.31%], $p = 0.39$ vs uninfected + *ad libitum* access to food) but a smaller percentage was observed in mice infected with *P. berghei* ANKA (0.16% [0.15-0.24%], $p < 0.01$ vs uninfected + dietary restriction, FIG 2.19).

Our method accounts for multiple cycles of NO synthesis and citrulline recycling to arginine, provided that metabolites are freely exchanged with plasma. However, rapid recycling of citrulline by the NOS-ASS1-ASL complex may enable multiple cycles of NO synthesis prior to exchange with plasma. In this case, the measured rate of conversion of plasma arginine to citrulline would underestimate the real molar rate of NO synthesis. Despite this limitation, our

findings strongly imply that the rate of NO synthesis from plasma arginine is lower in mice infected with *P. berghei* ANKA.

Our findings also illustrate that the proportion of plasma arginine utilized for NO synthesis is small relative to other metabolic uses of plasma arginine, such as protein synthesis. In humans, the rate of conversion of arginine to citrulline by NOS was determined to be 0.96 ± 0.1 $\mu mol \times kg^{-1} \times hr^{-1}$ (mean ± SD), averaged from equal periods of fed and fasted states (Castillo et al., 1996). This measured rate is similar to the rates we observed in uninfected mice with or without dietary restriction (uninfected + *ad libitum* access to food median [IQR]: 1.17 [0.83-2.03] $\mu mol \times kg^{-1} \times hr^{-1}$, uninfected + dietary restriction: 1.13 [0.86-1.28] $\mu mol \times kg^{-1} \times hr^{-1}$, FIG 2.19). The reported total rate of arginine appearance in humans was 82 ± 6.5 $\mu mol \times kg^{-1} \times hr^{-1}$ (mean ± SD) (Castillo et al., 1996), considerably lower than that observed in mice with *ad libitum* access to food (median [IQR]: 503.3 [434.8-542.2] $\mu mol \times kg^{-1} \times hr^{-1}$, FIG 2.12). As a result, the rate of conversion of arginine to citrulline by NOS accounted for 1.2 ± 0.13% (mean ± SD) of the total rate of arginine appearance in humans (Castillo et al., 1996), a greater proportion than in mice with *ad libitum* access to food (median [IQR]: 0.24% [0.16-0.37%], FIG 2.19). Thus, on a per-kilogram basis, the molar rate of arginine utilization by NOS is similar in humans and mice despite substantial differences in the total rate of arginine appearance.

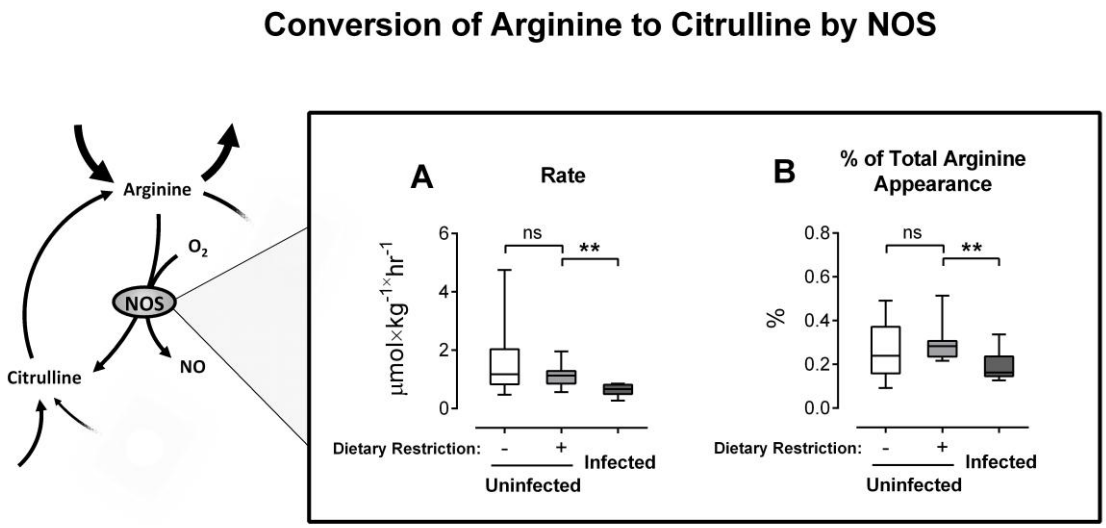


Figure 2.19 | Conversion of arginine to citrulline by NOS. (**A**) The rate of conversion of arginine to citrulline by NOS was calculated from plasma enrichment of continuously infused heavy isotope-labelled metabolic tracers, as measured by Q-TOF LC/MS. (**B**) The rate of conversion of arginine to citrulline by NOS was calculated as a percentage of the total rate of arginine appearance. Uninfected mice subjected to dietary restriction received only as much food as was consumed each day by a paired mouse infected with *P. berghei* ANKA. Uninfected controls not subjected to dietary restriction were provided with *ad libitum* access to food. Data are pooled from 3 experiments for a total of n=10 uninfected controls with *ad libitum* access to food and n=10 pairs of infected mice and uninfected mice subjected to dietary restriction. Tracer infusions were performed on day 6 post-inoculation. Box-plots depict median, IQR, min and max. **p < 0.01, ns (not significant): p > 0.05. Uninfected controls with or without dietary restriction were compared by Mann-Whitney test; uninfected controls + dietary restriction were compared to infected values by Wilcoxon matched-pairs signed rank test.

2.6 Discussion

Our findings challenge the hypothesis that arginine depletion is dependent on release/activation of host or parasite arginase during the parasite's life-cycle (Lopansri et al., 2003; Yeo et al., 2007; Olszewski et al., 2009; Omodeo-Sale et al., 2010). Arginine depletion has been observed in a previous study of *P. berghei* ANKA-infected mice (Gramaglia et al., 2006), but our study is the first to identify ornithine and citrulline depletion in this mouse model. In our experiments, we observed that arginine and ornithine are depleted to similar degrees, leaving the arginine/ornithine ratio unchanged. This finding is contrary to the hypothesis of increased arginase activity, which would be expected to decrease the arginine/ornithine ratio by converting arginine to ornithine. We also found that *P. berghei* ANKA-expressed arginase is not required to induce arginine depletion in infected mice. Using metabolic tracers to quantify whole body urea cycle metabolism, we observed that the rate of conversion of arginine to ornithine is unchanged during infection (FIG 2.20). Increased arginase activity may be required to maintain the rate of conversion of arginine to ornithine in the setting of low arginine, but our findings imply that reduced rates of arginine and citrulline appearance are primarily responsible for arginine depletion. One limitation of our study is that unlike human erythrocytes, mouse red blood cells do not demonstrate significant arginase activity (Spector et al., 1985). Our model does not, therefore, account for the possible contributions of release (Yeo et al., 2007, 2009) or activation (Omodeo-Sale et al., 2010) of erythrocyte arginase in human patients with severe malaria.

Our results indicate that a majority of citrulline is derived from sources other than plasma ornithine, such as enteral synthesis, and that more than 95% of citrulline is utilized for arginine synthesis. In *P. berghei* ANKA-infected mice, decreased rates of citrulline appearance from ornithine, enteral synthesis or other sources would therefore produce a direct decrease in the rate of *de novo* arginine synthesis. The rate of ornithine appearance is also reduced in *P. berghei* ANKA-infected mice, due to decreased rates of appearance from sources other than arginine, such as synthesis from proline or glutamate (FIG 2.20). Impaired ornithine synthesis

from proline or glutamate may reflect increased host or parasite utilization of these precursors for other metabolic purposes, such as protein synthesis or TCA cycle metabolism. Recycling of ornithine to citrulline is only a minor contributor to citrulline appearance (FIG 2.20), and, as a result, ornithine depletion would be expected to have a relatively small impact on the overall rate of arginine appearance.

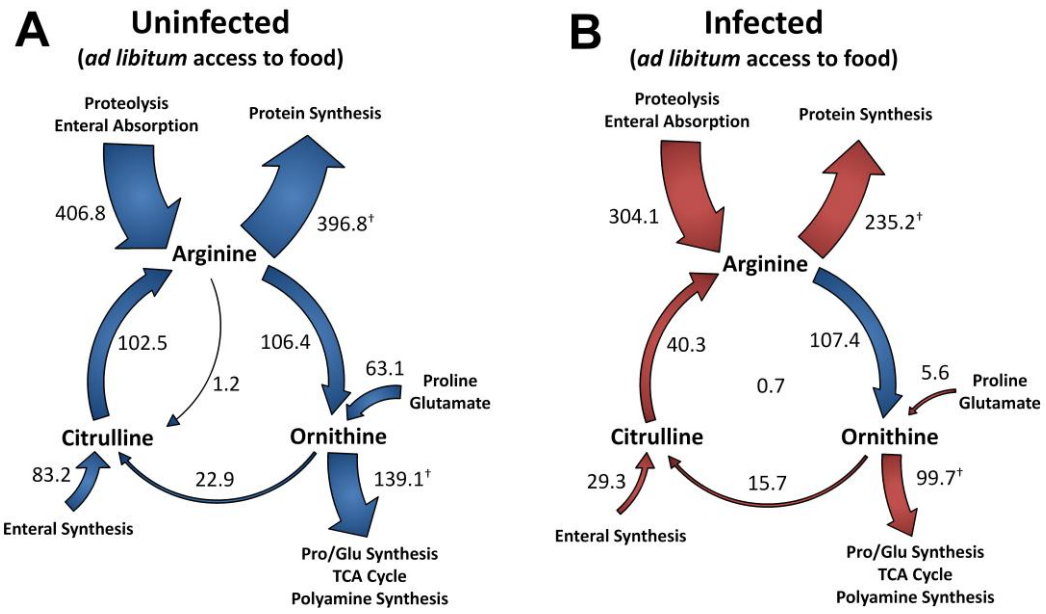


Figure 2.20 | Summary of whole-body urea cycle flux in *P. berghei* ANKA-infected mice. Median metabolic rates are shown in $\mu mol \times kg^{-1} \times hr^{-1}$ for uninfected controls with *ad libitum* access to food (**A**) and *P. berghei* ANKA-infected mice on day 6 post-inoculation (**B**). Arrows are sized in approximate proportion to the median metabolic rate represented. Blue arrows indicate normal values; red arrows indicate below-normal values. †Rates not measured directly; calculated by inference from measured values based on assumptions of steady-state flux in which rates of appearance equal rates of utilization.

Uninfected mice subjected to dietary restriction exhibited decreased rates of arginine, ornithine and citrulline appearance, demonstrating the central importance of nutrition as a determinant of arginine, ornithine and citrulline metabolism. In a study of Tanzanian children with cerebral malaria, reduced nutrient intake was considered as a possible contributor to arginine depletion but deemphasized on the grounds than mean fasting time of children with cerebral malaria was not significantly different from healthy controls (Lopansri et al., 2003).

However, this metric does not account for the quantity or content of recent dietary intake, nor alterations in gut physiology secondary to systemic infection. In addition, the authors interpreted similar plasma levels of histidine and glutamine between cases and controls as evidence of similar recent nutrition (Lopansri et al., 2003). These observations may not be sufficient to rule out dietary insufficiency as a contributor to arginine depletion. In our studies, plasma glutamine and histidine were not significantly different between infected and uninfected mice with *ad libitum* access to food, despite documented differences in dietary intake (infected plasma glutamate: 423.1 [405.2-543.4] μmol/L vs uninfected plasma glutamate: 498.3 [470.9-527.7] μmol/L, $p = 0.50$; infected plasma histidine: 83.4 [77.5-90.0] μmol/L vs uninfected plasma histidine: 82.5 [71.8-89.0] μmol/L, $p = 0.77$). These observations suggest that plasma glutamine and histidine concentrations may not represent effective biomarkers of dietary sufficiency during severe malaria infection.

Reduced dietary intake does not fully explain arginine depletion. Measured plasma concentrations of arginine, ornithine and citrulline were decreased in *P. berghei* ANKA-infected mice compared with uninfected mice subjected to dietary restriction. In addition, rates of appearance of ornithine and citrulline were lower in infected mice compared with uninfected mice subjected to dietary restriction. These observations suggest that *P. berghei* ANKA infection causes metabolic disturbances beyond suppression of feeding behaviour. Arginine absorbed in the enterocyte may be transported directly to the plasma or converted to citrulline by enteral arginase and ornithine transcarbamylase. Compounded with reduced dietary intake, impaired enteral absorption or impaired perfusion of the intestine could limit arginine and citrulline appearance in *P. berghei* ANKA infection. Autopsy studies in human patients have identified sequestration of infected erythrocytes in mucosal and villous capillaries which could interfere with normal gut physiology (Pongponratn et al., 1991; Seydel et al., 2006). Further studies are therefore required to investigate the effects of severe malaria infection on enteral absorption and perfusion. Dysregulation of transport systems such as the cationic amino acid

transporter (CAT) enzyme family during severe malaria could also result in retention of arginine and ornithine in the intracellular compartment of other organs and tissues.

We observed that the rate of conversion of arginine to citrulline by NOS was maintained during dietary restriction, but fell during *P. berghei* ANKA infection. Inadequate nitric oxide synthesis may contribute to pathology of the vascular endothelium during severe malaria, including impaired vasodilation (Yeo et al., 2007), dysregulation of tight junctions and loss of endothelial barrier integrity (Gramaglia et al., 2006; Wojciak-Stothard et al., 2009; Serghides et al., 2011; Dorovini-Zis et al., 2011), release of pro-coagulants (Matsushita et al., 2003; Hollestelle et al., 2006; Mast et al., 2009) and increased adhesion molecule expression, which facilitates cytoadherence of parasitized erythrocytes (De Caterina et al., 1995; Serirom et al., 2003; Taylor et al., 2004). In combination, these factors could result in microcirculatory occlusion and disruption of oxygen and nutrient delivery to the central nervous system and other vital organs (Dondorp et al., 2008a; Cabrales et al., 2010, 2011). Intravenous infusion of arginine is under investigation as an adjunctive therapy aimed at restoring endothelial function in patients with severe malaria (Yeo et al., 2007, 2008a; c, 2013). These studies assessed endothelial-dependent vasodilation by monitoring increased blood flow (reactive hyperaemia) in response to transient occlusion of the brachial artery. In a separate study, reactive hyperaemia was shown to be approximately 50% dependent on nitric oxide synthesis (Nohria et al., 2006). An initial investigation found that arginine infusion improved reactive hyperaemia in Indonesian adults with moderately severe malaria (*falciparum* parasitaemia, inability to tolerate oral medication and no WHO criteria for severe malaria) (Yeo et al., 2007). In a follow-up study in patients with severe malaria, intravenous arginine infusion did not improve reactive hyperaemic responses, but this study was underpowered for assessment of efficacy (6 patients received arginine and 2 patients received saline) (Yeo et al., 2013).

The absence of an observed effect in patients with severe malaria could be due to small sample sizes or to additional mechanisms limiting NOS enzyme activity. iNOS and eNOS protein levels are upregulated in brain tissue from *P. berghei* ANKA-infected mice (Ong et al.,

2013) and iNOS staining is increased in the brains of children who died of cerebral malaria (Clark et al., 2003). NOS expression in other organs must be studied as well, but these results suggest that NOS protein is not limiting in brain tissue. Increased NOS protein levels may be counter-balanced by decreased eNOS phosphorylation and increased eNOS and nNOS monomerization, as observed in brain tissue from *P. berghei* ANKA-infected mice (Ong et al., 2013). These observations suggest that a lower proportion of NOS protein is activated for NO synthesis during *P. berghei* ANKA infection. NOS activity could also be impaired by insufficient availability of the essential NOS cofactor tetrahydrobiopterin (BH4) and/or accumulation of the endogenous NOS inhibitor asymmetric dimethylarginine (ADMA). ADMA accumulation and BH4 availability are examined in CHAPTERS 3-5.

2.7 Conclusion

In summary, our findings implicate decreased rates of arginine and citrulline appearance in plasma, rather than arginase-mediated catabolism, as the primary mechanism of arginine depletion. These results suggest that arginase inhibition may be an ineffective approach to restoring arginine availability and could further decrease plasma ornithine concentrations. Our findings support arginine supplementation as an approach to correcting this deficit in arginine appearance, although our metabolic flux data suggests that very little would be converted to citrulline. Therefore, supplementation with citrulline may represent a more effective means of restoring NOS substrate pools (for further discussion, see CHAPTER 5, p. 156). However, additional mechanisms that could potentially limit NO synthesis must also be considered, including impaired uptake of arginine or citrulline into NOS-expressing cells, decreased NOS activation, ADMA accumulation or BH4 depletion.

2.8 Materials and Methods

General Animal Model Procedures

Animals, Housing and Diet

Animal experiments were performed at the National Institutes of Health (NIAID Comparative Medicine Branch) using protocols approved by the NIH ACUC under the identification ASP LMVR 18E. 10-week-old C57BL/6J male mice were obtained from the Jackson Laboratory (Bar Harbor, ME, USA) and 10-week-old Swiss Webster carriers for parasite expansion were obtained from Charles River Laboratories (Frederick, MD, USA). Time-course experiments (in which infected mice were culled on days 2, 4 and 6 post-inoculation) were replicated at the Wellcome Trust Sanger Institute under personal (PIL 80/12137) and project licenses (PPL 80/2158) issued by the UK Home Office in accordance with the Animals (Scientific Procedures) Act of 1986. Protocols reviewed by the Wellcome Trust Sanger Institute ethics committee. For these experiments, 10-week-old male C57BL/6J experimental mice and Tuck Ordinary outbred mice carriers for parasite expansion were obtained from Harlan Laboratories (London, UK).

Mice were maintained on acidified water and autoclaved rodent feed pellets (Teklad Global 18% Protein Extruded Rodent Diet, 2018SX, Harlan Laboratories). Pellets contained 18.6% crude protein, 6.2% fat, 44.2% carbohydrate, 14.7% fibre and 5.3% ash, with an energy density of 13.0 kJ/g (3.1 kcal/g). Pellets contained 1% L-arginine. For experiments involving dietary restriction in uninfected mice, including metabolic tracer experiments, mice were housed in individual cages (Instech Laboratories, Plymouth Meeting, PA, USA). Mice subjected to dietary restriction were staggered by one day from infected mice and fed in 24-hour intervals with only as much food as was consumed the previous 24 hours by a paired mouse infected with *P. berghei* ANKA. Such experiments also included *ad libitum*-fed uninfected controls provided with free access to food. All mice had free access to acidified water. For all other experiments, mice were housed in ventilated cages in groups of five with free access to food and water. Experimental groups were assigned in an alternating manner such that every experimental group

was represented in each cage of 5 littermates. All mice were maintained under a 12hr:12hr light:dark cycle and under temperature-controlled conditions.

Parasites and Inoculations

Arginase knock-out parasites and the wild-type parent line were a kind gift from Akhil Vaidya (Drexel Medical School, Philadelphia, PA, USA). Creation of the knock-out line has been previously described (Olszewski et al., 2009). For all other experiments *Plasmodium berghei* ANKA parasites were clone RMgm-29 (Janse et al., 2006). In all cases parasites were expanded from frozen stocks by intraperitoneal injection of carrier mice. After four days of parasite expansion, whole blood was obtained from the abdominal inferior vena cava under terminal anaesthesia. Cohorts of experimental mice were infected by intraperitoneal injection of 1×10^6 infected erythrocytes diluted in 200µl of 1×PBS (Lonza, Walkersville, MD, USA). This protocol results in blood-stage infection, bypassing the liver stage of the parasite's life-cycle. Blood-stage parasitaemia was monitored by examination of Giemsa-stained blood smears obtained by tail tip bleed.

Primer	Target Sequence	Primer Sequence (5'-3')
Primer A	Arginase 3'UTR	GAAAAATTTCGTTGTTTTAGTGTGTG
Primer B	Arginase coding region	AAAATCGATCCAAATAAAAATTCC
Primer C	DHFR/TS selection factor	CAATGATTCATAAATAGTTGGACTTG

Table 2.1 | PCR Genotype Assay for Arginase Knock-Out and Wild-Type Parasites. Three primers were designed to amplify fragments of different lengths using a common primer (Primer A) depending on whether the wild-type arginase gene was replaced by the selection factor (DHFR/TS) during homologous recombination. See FIG 2.5.

Parasite Genotyping

Plasmodium berghei ANKA arginase knock-out and wild-type parent genotypes were determined from DNA extracted from carrier mice whole blood with a DNeasy Kit (Qiagen, Manchester, UK) according to the manufacturer's instructions. DNA samples were amplified by PCR with primers targeting the arginase 3'UTR, arginase coding region and DHFR/TS selection

factor (TABLE 2.1 & FIG 2.5). PCR was performed with GoTaq Green master mix (Life Technologies, Paisley, UK) by performing 35 cycles of denaturation, annealing and elongation using temperatures of 95°C, 50°C and 68°C respectively. Amplified PCR products were run on a 1.5% agarose gel and visualized with ethidium bromide.

Behavioural Scoring and Quantification of Parasitaemia

Neurological symptoms were scored using a quantitative scoring scale adapted from the Rapid Murine Coma and Behaviour Scale (Carroll et al., 2010). Scores were assigned on a scale of 0 (moribund) to 2 (normal) for each of seven indicators: gait, balance, exploratory activity, body position, limb strength, touch escape and pinna reflex (TABLE 2.2). For survival experiments, the humane endpoint was established as a score of 3 or less. Parasitaemia was monitored by examination of Giemsa-stained blood smears obtained by tail tip bleed in live animals or from blood samples taken during tissue collection.

Category	Observation
Motor Performance	Gait
Activity	Body lift Exploratory Behaviour
Strength and Tone	Body Position Grasp of cage bars
Reflexes and Self-Preservation	Touch Escape Pinna Reflex

Table 2.2 | Scoring System for the Assessment of Disease Symptoms in Mice. System was adapted from the Rapid Murine Coma and Behaviour Scale (Carroll et al., 2010). Each observation was scored on a scale of 0 (moribund) to 2 (normal) yielding scores ranging from the minimum score of 0 (moribund mouse) to the maximum score of 14 (normal mouse).

Plasma Collection

Terminal anaesthesia was administered by intraperitoneal injection of 250mg/kg ketamine and 25mg/kg xylazine. The abdominal cavity was accessed and 700µl of blood was drawn from the abdominal inferior vena cava with a 25G×5/8” needle (BD, Franklin Lakes, NJ,

USA). To prevent coagulation, the syringe contained 60µl DPBS with K_3EDTA (final concentration of 1.6mg/ml K_3EDTA after 700 µl blood drawn). Plasma was separated from erythrocytes by centrifugation at 3,000*g* for 7 minutes at 4°C, snap-frozen on dry ice, and stored at -80°C until analysis.

HPLC Analysis of Amino Acids

Essential method details are presented below. For full assay optimization and validation, refer to APPENDIX A (p. 235). Plasma samples were deproteinated by mixing 12µl sample with 12µl 2M perchloric acid ($HClO_4$, Fisher Scientific, Pittsburgh, PA, USA) containing 50µM L-norvaline as an internal standard (Sigma-Aldrich, St. Louis, MO, USA). After centrifuging for 5 minutes at 16,100*g* and 4°C, supernatants were removed and neutralized by adding 10µl to 5µl of 1.5M potassium carbonate (Sigma-Aldrich, St. Louis, MO, USA) in a fresh tube. The resulting solution was diluted 1:2 in ultrapure water from a Milli-Q Synthesis system (EMD Millipore, Billerica, MA, USA) for a final dilution of 1:6. After centrifuging for 5 minutes at 16,100*g* and 4°C to remove potassium chlorate precipitate, samples were loaded into screw-cap polypropylene vials (Agilent Technologies, Santa Clara, CA, USA) for analysis. Amino acid standards (Sigma-Aldrich, St. Louis, MO, USA) were diluted to 50µM and processed in parallel to serve as an external standard for quantitation. HPLC was performed on a low-flow Agilent 1100 series instrument and Agilent Chemstation OpenLab CDS revision C.01.03 was used to control the instrument and acquire data. Samples were derivatized directly prior to analysis by programming the autosampler to draw 2µl of derivatization reagent, 2µl of sample, mix for 30s and inject. The derivatization reagent contained final concentrations of 1.5mg/ml (11.2 mM) ortho-phthaldialdehyde (Sigma-Aldrich, St. Louis, MO, USA) and 41.3mM 3-mercaptopropionic acid (Sigma-Aldrich, St. Louis, MO, USA) diluted in 200mM potassium tetraborate solution (pH 9.4). To prevent carry-over contamination, the needle was washed for 5 seconds between each programmed step using the autosampler's built-in flushport and a wash solution consisting of 10% HPLC-grade methanol (Fisher Scientific, Pittsburgh, PA,

USA) in ultrapure H_2O from a Milli-Q Synthesis system (EMD Millipore, Billerica, MA, USA). Analytes were separated with a 1.0mm×150mm Luna® C18(2) column with 5µm particles and 100Å pore size (Phenomenex, Torrance, CA, USA) protected with a 1.0mm×13mm ACE® C18 guard column with 3µm particles and 100Å pore size (MAC-MOD Analytical, Chadds Ford, PA, USA). Aqueous mobile phase (Solvent A) consisted of 0.1M sodium acetate (Fisher Scientific, Pittsburgh, PA, USA) in ultrapure H_2O from a Milli-Q Synthesis system (Millipore, Billerica, MA, USA) with 9% v/v methanol (Fisher Scientific, Pittsburgh, PA, USA) and 0.5% v/v tetrahydrofuran (Sigma-Aldrich, St. Louis, MO, USA) with pH adjusted to 8.3 with 3M NaOH (Sigma-Aldrich, St. Louis, MO, USA). Organic mobile phase (Solvent B) was HPLC-grade methanol (Fisher Scientific, Pittsburgh, PA, USA). Flow-rates and solvent ratios are summarized in TABLE 2.3. The column was maintained at 40°C for the duration of the run. Online fluorescence was measured at excitation and emission wavelengths of 340nm and 455nm, respectively. Chemstation OpenLab CDS software version C.01.03 was used for peak integration. Concentrations were calculated using both internal (L-norvaline) and external standards.

	Elapsed Time (min)											
	0	**10.87**	**16.3**	**21.73**	**27.17**	**28.8**	**35.32**	**40.75**	**43.5**	**48.5**	**48.6**	**65**
A (%):	96	86	86	70	60	53	50	30	0	0	96	96
B (%):	4	14	14	30	40	47	50	70	100	100	4	4

Table 2.3 | Mobile phase solvent ratios and pump program. The program was performed at a flow-rate of 84µl/min and a column temperature of 40°C. Sample was injected at 0 min.

Evans Blue Assessment of Blood-Brain Barrier Integrity

Evans blue (Sigma-Aldrich, St. Louis, MO, USA) was prepared at a concentration of 1% w/v in 1×PBS (Lonza, Walkersville, MD, USA) and sterile filtered with a 0.22µm syringe-tip filter prior to use. To assess blood-brain barrier integrity, 100µl of 1% Evans blue solution was injected into the lateral tail vein using a 30G needle (Becton Dickenson, Franklin Lakes,

NJ, USA). Mice were placed in a clean cage and the dye was allowed to circulate for 1 hour prior to administration of terminal anaesthesia by intraperitoneal injection of 250mg/kg ketamine and 25mg/kg xylazine. The thoracic cavity was accessed and a 21G butterfly needle was inserted into the left ventricle of the heart. The inferior vena cava was transected and the animal was perfused with 50mL 1×PBS delivered to the left ventricle at a rate of 5mL/min with a PHD2000 syringe pump (Harvard Apparatus, Holliston, MA, USA). After perfusion, the brain was dissected, photographed and placed in a pre-weighed tube containing 1mL *N*,*N*-dimethylformamide (Sigma-Aldrich, St. Louis, MO, USA). The final weight was recorded and the weight of brain tissue added was calculated. Evans blue dye was extracted from brain tissue by 48hr incubation in the dark. After incubation, tubes were centrifuged for 5min at 16,100*g* for 5 min to remove particulate debris. Supernatants were removed and absorbance at 620nm was determined spectrophotometrically and compared with a standard curve of Evans blue prepared at known concentrations (0-25µg/mL) in *N*,*N*-dimethylformamide. Final values were calculated as µg Evans blue/mg brain tissue.

Metabolic Tracer Experiments

Maintenance Infusions

For infusion experiments, 10-week-old male C57BL/6J mice were purchased with surgically-implanted silicone jugular vein catheters (2Fr at insertion point, 3Fr at access point) from the Jackson Laboratory (Bar Harbor, ME, USA). The day after arriving, mice were anaesthetized with inhaled isoflurane (4% induction, 2% maintenance) during set-up and connection of an infusion line. First, the catheter plug was removed and the locking solution was gently removed with a 1mL syringe fitted with a blunt luer stub adapter. The catheter was then attached to a saline infusion line supported by a specialized tether system with a spring-balanced arm and swivel (Instech Solomon, Plymouth Meeting, PA, USA) which allow free movement and rotation of the animal during continuous infusion. The catheter and infusion line

were joined with a 24-gauge hollow plug adapter and secured in place with a specialized harness (Instech Solomon, Plymouth Meeting, PA, USA).

Mice were housed in individual cages specialized to support free movement of the tether system for 1 day prior to inoculation and monitored for 6 days following inoculation. During this period, 0.9% sterile saline (Hospira, Lake Forest, IL, USA) was infused with a PHD2000 syringe pump (Harvard Apparatus, Holliston, MA, USA) at a rate of 25µl/hour to maintain catheter patency.

Tracer Infusions and Sampling

For metabolic tracer experiments, mice were simultaneously infused with the following tracers: L-[U-$^{13}C_6$;U-$^{15}N_4$]arginine (prime: 70µmol×kg^{-1}; continuous infusion: 70µmol×kg^{-1}×hr^{-1}), L-[ureido-^{13}C]citrulline (prime: 7µmol×kg^{-1}; continuous infusion: 7µmol×kg^{-1}×hr^{-1}) and L-[U-$^{13}C_5$]ornithine (prime: 15µmol×kg^{-1}; continuous infusion: 15µmol×kg^{-1}×hr^{-1}). This labelling strategy was chosen in order to allow calculation of rates of arginine, ornithine and citrulline appearance and interconversion (see APPENDIX B, FIG B.3, p. 266). Priming doses were administered over a period of 5 minutes and continuous infusions were delivered for a period of 4 hours. Plateau enrichment of arginine, citrulline and ornithine have previously been shown to occur by ~3 hours of infusion using comparable priming and maintenance doses (Marini et al., 2010a). Plasma sample collections were therefore performed after 4 hours of continuous infusion.

After the administration of the priming dose and 4 hours of continuous infusion, mice were briefly anaesthetized with inhaled isoflurane (1 minute exposure to 4%) and terminally anaesthetized by intraperitoneal injection of ketamine (250mg/kg) and xylazine (25mg/kg). One minute after administration of the ketamine/xylazine mixture, the mouse was rapidly disconnected from the infusion line and weighed for calculation of exact tracer infusion rate normalized to body weight (in units of µmol×kg^{-1}×hr^{-1}). Plasma samples were collected as described above.

LC/MS Analysis of Metabolic Tracer Enrichment

Underivatized plasma arginine, citrulline and ornithine and heavy isotope-labelled tracers were detected by quadrupole time-of-flight liquid chromatography/mass spectrometry (Q-TOF LC/MS) using an analytical approach adapted from published methods (Piraud et al., 2005; Armstrong et al., 2007).

Sample Preparation

For analysis of arginine and ornithine, plasma samples were deproteinated by diluting 50µl in 200µl pure HPLC-grade methanol (Fisher Scientific, Pittsburgh, PA, USA) for a 1:5 initial sample dilution. Methanol contained 12.5µM [D_7]asymmetric dimethyl-L-arginine (m+7) as an analytical internal standard. Precipitated samples were centrifuging at 16,100*g* for 5 minutes at 4°C and 150µl of supernatant was mixed with 150µl of 0.1mM tridecafluoroheptanoic acid (TDFHA, Sigma-Aldrich, St. Louis, MO, USA) dissolved in 18.2MΩ•cm ultrapure water (from Milli-Q Synthesis Ultrapure water system, Millipore, Billerica, MA, USA) for a final sample dilution of 1:10. A 'blank' sample was generated by processing a 50µl sample of ultrapure water in the same manner. To determine the chromatographic retention times and natural enrichment of arginine, citrulline, and ornithine, standard solutions containing 50µM of each unlabelled metabolite were prepared in the same manner. Due to interference of an unknown metabolite with the L-[ureido-^{13}C]citrulline peak (m/z 177.1069), each plasma sample was processed a second time by solid phase extraction for analysis of citrulline only. Frozen plasma was thawed and 55µl was added to a tube containing 55µl of 50µM [D_7]asymmetric dimethyl-L-arginine (m+7) as an analytical internal standard and 110µl of 200mM HCl diluted in ultrapure water. Oasis MCX 96-well µElution Plates (Waters Corporation, Milford, MA, USA) were conditioned with elution buffer prepared from ultrapure water, HPLC-grade methanol (Fisher Scientific, Pittsburgh, PA, USA) and 28% ammonium hydroxide (Sigma-Aldrich, St. Louis, MO, USA) in a ratio of 5:4:1 H_2O:MeOH:NH_4OH and

equilibrated with pure methanol. Acidified samples and internal standard (200µl) were loaded, washed with 0.1 N HCl followed by methanol, eluted with elution buffer and dried by vacuum centrifugation for 4.5hr at 45°C. Dried samples were reconstituted in 250µl 0.5mM TDFHA dissolved in a 50:50 mixture of ultrapure water and methanol for a final sample dilution of 1:5.

Chromatography

High-Performance Liquid Chromatography (HPLC) was used to separate underivatized amino acids for analysis by mass spectrometry. HPLC was carried out with an Agilent 1260 Infinity binary pump, Agilent 1100 series autosampler and Agilent 1200 series de-gasser and column temperature-control unit. Analytes were separated with a 2.1×50mm Zorbax Eclipse XDB-C18 column with 1.8µm particles and 100Å pore size (Agilent Technologies, Santa Clara, CA, USA). Agilent MassHunter Workstation Data Acquisition TOF/Q-TOF Software (revision B.04.00) was used to control the HPLC modules and acquire data from the mass spectrometer.

Solvent A consisted of 0.5mM tridecafluoroheptanoic acid (TDFHA) (Sigma-Aldrich, St. Louis, MO, USA) dissolved in 18.2MΩ•cm ultrapure water (from Milli-Q Synthesis Ultrapure water system, Millipore, Billerica, MA, USA). Solvent B consisted of pure HPLC-grade acetonitrile (Fisher Scientific, Pittsburgh, PA, USA). Prior to sample analysis the column was washed with 100% solvent B at a rate of 0.4 ml/min for 1hr. The column was then equilibrated with 100% solvent A at a rate of 0.4 ml/min for 20min and then 0.2ml/min for 5 minutes. A 'blank' ultrapure water sample subjected to the sample processing protocol described above was run prior to analysis of the first plasma sample. Samples were injected in a 40µl volume. Separation was accomplished with the following gradient program, beginning at a rate of 0.2 ml/min: 0%B for 2 min, 0% to 15%B from 2 to 3 min, 15%B held from 3 to 8 min, 15% to 25%B from 8 to 11min, 25%B held from 11 to 28min and reduced from 25% to 0%B from 28 to 29min. The column was then re-equilibrated by increasing the flow-rate to 0.4mL/min from 29.1min to 39min, then returning to 0.2mL/min from 39.1 to 45min in preparation for injection of the next sample.

Mass Spectrometry Instrumentation

Labelled and unlabelled amino acids were detected with an Agilent 6540 Ultra-High Definition Accurate-Mass Quadrupole Time-of-Flight (Q-TOF) mass spectrometer (Agilent Technologies, Santa Clara, CA, USA). A positive ESI source with Jetstream technology was used to ionize eluting compounds. A second Agilent 1100 series pump was used to continuously inject a reference mass solution (121.0587Da and 922.0098Da). The drying gas temperature was set to 350°C and a nebulizer pressure was set to 30psi. The capillary voltage was set to 3000V and the fragmentor voltage was set to 100V. The instrument was set to detect masses in the range of 50-1000m/z. The exact masses of ions monitored by Q-TOF LC/MS are listed in TABLE 2.4. Chromatograms for each ion were extracted from total ion current (TIC) data with an accuracy window of ±50 ppm and integrated using Agilent MassHunter Qualitative Analysis Software (revision B.05.00). The resulting integrated areas were used for calculations of tracer-tracee ratios (*TTR*) as described below.

Amino Acid	Identity of Monitored Metabolite	Mass shift (*m+x*)	Label	Molecular Formula of $[m+H]^+$ ion	Exact Mass (*m/z*)
Arginine	Unlabelled	m+0	-	$C_6H_{15}N_4O_2$	175.1195
	From citrulline tracer	m+1	^{13}C	$^{13}C_1C_5H_{15}N_4O_2$	176.1229
	Recycled from Ornithine	m+7	$^{13}C_5$, $^{15}N_2$	$^{13}C_5CH_{15}{}^{15}N_2N_2O_2$	182.1303
	Recycled from NOS (1 cycle)	m+8	$^{13}C_6$, $^{15}N_2$	$^{13}C_6H_{15}{}^{15}N_2N_2O_2$	183.13369
	Recycled from NOS (>1 cycle)	m+9	$^{13}C_6$, $^{15}N_3$	$^{13}C_6H_{15}{}^{15}N_3NO_2$	184.13072
	Infused arginine tracer	m+10	$^{13}C_6$, $^{15}N_4$	$^{13}C_6H_{15}{}^{15}N_4O_2$	185.1278
Citrulline	Unlabelled	m+0	-	$C_6H_{14}N_3O_3$	176.1035
	Infused citrulline tracer	m+1	^{13}C	$^{13}C_1C_5H_{14}N_3O_3$	177.1069
	From ornithine tracer	m+5	$^{13}C_5$	$^{13}C_5CH_{14}N_3O_3$	181.1203
	From arginine via NOS (1st cycle)	m+8	$^{13}C_6$, $^{15}N_2$	$^{13}C_6H_{14}{}^{15}N_2NO_3$	184.1177
	From arginine via NOS ($>1^{st}$ cycle)	m+9	$^{13}C_6$, $^{15}N_3$	$^{13}C_6H_{14}{}^{15}N_3O_3$	185.11474
Ornithine	Unlabelled	m+0	-	$C_5H_{13}N_2O_2$	133.0977
	Infused/recycled ornithine tracer	m+5	$^{13}C_5$	$^{13}C_5H_{13}N_2O_2$	138.1145
	From arginine tracer	m+7	$^{13}C_5$, $^{15}N_2$	$^{13}C_5H_{13}{}^{15}N_2O_2$	140.1085
ADMA	Analytical internal standard	m+7	D_7	$C_8H_{12}D_7N_4O_2$	210.19474

Table 2.4 | List of monitored metabolites. Heavy isotope labelled tracers were identified and quantified by Q-TOF LC/MS using the exact mass of the $[m+H]^+$ ion.

Calculations of Flux using Stable Isotope Tracers

Full derivation and discussion of equations are presented in APPENDIX B, p. 256. Key equations are reproduced below with page references to full derivations.

Tracer Tracee Ratio

A tracer-tracee ratio (*TTR*) describes the abundance of labelled tracer with mass *m+a* relative to the abundance of the target (tracee) metabolite with mass *m+0*. The heavy isotopes incorporated into tracers, such as ^{13}C and ^{15}N, occur in nature, although at much lower abundances than common ^{12}C and ^{14}N isotopes. As a result, the tracee metabolite pool contain some molecules with ^{13}C or ^{15}N at *a* positions such that the mass of these molecules resembles that of the tracer (*m+a*). In order to directly account for this background, a standard solution of non-enriched tracee metabolite is prepared in pure water and analyzed by mass spectrometry. This approach allows the calculation of a *TTR* value that describes the abundance of infused tracer with mass *m+a* accounting for any background contribution of naturally-occurring heavy isotopes in the tracee pool:

$$TTR_{X_{m+a}} = \frac{X_{m+a_{sample}}}{X_{m+0_{sample}}} - \frac{X_{m+a_{std}}}{X_{m+0_{std}}} \qquad Eq.\ 2.1$$

Where $TTR_{X_{m+a}}$ is the tracer-tracee ratio of metabolite *X* tracer with heavy isotopes incorporated at *a* positions measured in the sample, $X_{m+0_{sample}}$ is the abundance of unlabelled metabolite *X* trace with mass *m* and no incorporated heavy isotopes measured in the sample, $X_{m+a_{sample}}$ is the abundance of metabolite *X* tracer with heavy isotopes incorporated at *a* positions measured in the sample, and $X_{m+0_{std}}$ and $X_{m+a_{std}}$ are the abundances of tracee and tracer, respectively, measured in a pure non-enriched standard solution.

Single Metabolite Rate of Appearance

The rates of appearance of total arginine, recycled arginine and non-recycled arginine were calculated according to the following equations:

$$Q_{Arg_T} = \frac{I_{Arg_{m+10}} \times E_{IArg_{m+10}}}{TTR_{Arg_{m+10}}} \quad \textit{Eq.}\ 2.2$$

$$Q_{Arg_{NR}} = \frac{I_{Arg_{m+10}} \times E_{IArg_{m+10}}}{TTR_{Arg_{m+10}} + TTR_{Arg_{m+7}}} \quad \textit{Eq.}\ 2.3$$

$$Q_{Arg_R} = \left(\frac{I_{Arg_{m+10}} \times E_{IArg_{m+10}}}{TTR_{Arg_{m+10}}}\right) - \left(\frac{I_{Arg_{m+10}} \times E_{IArg_{m+10}}}{TTR_{Arg_{m+10}} + TTR_{Arg_{m+7}}}\right) \quad \textit{Eq.}\ 2.4$$

Where Q_{Arg_T} is the total rate of arginine appearance including recycling, $Q_{Arg_{NR}}$ is the rate of appearance of non-recycled arginine, Q_{Arg_R} is the rate of arginine recycling, $I_{Arg_{m+10}}$ is the rate at which labelled L-[U-$^{13}C_6$;U-$^{15}N_4$]arginine is infused, $E_{IArg_{m+10}}$ is the proportional enrichment of fully-labelled L-[U-$^{13}C_6$;U-$^{15}N_4$]arginine tracer in the infusion solution, $TTR_{Arg_{m+10}}$ is the tracer-tracee ratio of L-[U-$^{13}C_6$;U-$^{15}N_4$]arginine to unlabelled arginine, $TTR_{Arg_{m+7}}$ is the tracer-tracee ratio of L-[1,2,3,4,5-$^{13}C_5$;α,δ-$^{15}N_2$]arginine to unlabelled arginine. Refer to pp. 271-272 for full derivations.

The total rate ornithine appearance was calculated according to the following equation:

$$Q_{Orn_T} = \frac{I_{Orn_{m+5}} \times E_{IOrn_{m+5}}}{TTR_{Orn_{m+5}}} \times \left(1 + \frac{Q_{Arg_R}}{Q_{Arg_{NR}}}\right) \quad \textit{Eq.}\ 2.5$$

Where Q_{Orn_T} is the total rate of ornithine appearance including recycling, $I_{Orn_{m+5}}$ is the rate at which labelled L-[U-$^{13}C_5$]ornithine is infused, $E_{IOrn_{m+5}}$ is the proportional enrichment of fully-labelled L-[U-$^{13}C_5$]ornithine tracer in the infusion solution and $TTR_{Orn_{m+5}}$ is the tracer-tracee ratio of L-[U-$^{13}C_5$]ornithine to unlabelled ornithine. Q_{Arg_R} is the rate of arginine recycling calculated from *Eq.* 2.4, $Q_{Arg_{NR}}$ is the rate of appearance of non-recycled arginine calculated from *Eq.* 2.3. Refer to p. 270 and p. 277-278 for full derivations.

The total rate of citrulline appearance was calculated according to the following equation:

$$Q_{Cit_T} = \frac{I_{Cit_{m+1}} \times E_{ICit_{m+1}}}{TTR_{Cit_{m+1}}} - \left(I_{Cit_{m+1}} \times E_{ICit_{m+0}}\right) \qquad \textit{Eq.}\ 2.6$$

Where Q_{Cit_T} is the total rate of citrulline appearance including recycling, $I_{Cit_{m+1}}$ is the rate at which labelled L-[ureido-^{13}C]citrulline is infused, $E_{ICit_{m+1}}$ is the proportional enrichment of fully-labelled L-[ureido-^{13}C]citrulline tracer in the infusion solution, $TTR_{Cit_{m+1}}$ is the tracer-tracee ratio of L-[ureido-^{13}C]citrulline to unlabelled citrulline and $E_{ICit_{m+0}}$ is the proportional enrichment of fully-unlabelled citrulline in the infusion solution. Refer to p. 269 for full derivation.

Substrate-Product Flux

The rates of conversion between arginine, ornithine and citrulline were calculated according to the following equations:

$$Q_{Cit \rightarrow Arg} = \left(\frac{TTR_{Arg_{m+1}}}{TTR_{Cit_{m+1}}}\right) \times Q_{Arg_T} \times \left(\frac{Q_{Cit_T}}{Q_{Cit_T} + I_{Cit_{m+1}} \times E_{ICit_{m+0}}}\right) \qquad \textit{Eq.}\ 2.7$$

$$Q_{Arg\rightarrow Orn} = \left(\frac{TTR_{Orn_{m+7}}}{TTR_{Arg_{m+10}} + TTR_{Arg_{m+7}}}\right) \times Q_{Orn_T} \qquad \textit{Eq.}\ 2.8$$

$$Q_{Orn\rightarrow Cit} = \left(\frac{TTR_{Cit_{m+5}}}{TTR_{Orn_{m+5}}}\right) \times Q_{Cit_T} \qquad \textit{Eq.}\ 2.9$$

Where $Q_{Cit\rightarrow Arg}$ is the rate of conversion of citrulline to arginine, $Q_{Arg\rightarrow Orn}$ is the rate of conversion of arginine to ornithine, $Q_{Orn\rightarrow Cit}$ is the rate of conversion of ornithine to citrulline, $TTR_{Arg_{m+1}}$ is the tracer-tracee ratio of L-[guanidino-^{13}C]arginine (*m+1*) to unlabelled arginine, $TTR_{Cit(m+1)}$ is the tracer-tracee ratio of L-[ureido-^{13}C]citrulline (*m+1*) to unlabelled citrulline, Q_{Arg_T} is the total rate of arginine appearance including recycling calculated according to *Eq.* 2.2, Q_{Cit_T} is the total rate of citrulline appearance calculated according to *Eq.* 2.6, $I_{Cit_{m+1}}$ is the rate at which labelled L-[ureido-^{13}C]citrulline is infused, $E_{ICit_{m+0}}$ is the proportional enrichment of fully-unlabelled citrulline tracer in the infusion solution, $TTR_{Orn_{m+7}}$ is the tracer-tracee ratio of L-[U-$^{13}C_5$;U-$^{15}N_2$]ornithine (*m+7*) to unlabelled ornithine, $TTR_{Arg_{m+10}}$ is the tracer-tracee ratio of L-[U-$^{13}C_6$;U-$^{15}N_4$]arginine (*m+10*) to unlabelled arginine, $TTR_{Arg_{m+7}}$ is the tracer-tracee ratio of L-[1,2,3,4,5-$^{13}C_5$;α,δ-$^{15}N_2$]arginine (*m+7*) to unlabelled arginine, Q_{Orn_T} is the total rate of ornithine appearance including recycling calculated according to *Eq.* 2.5, $TTR_{Cit_{m+5}}$ is the tracer-tracee ratio of L-[1,2,3,4,5-$^{13}C_5$]citrulline (*m+5*) to unlabelled citrulline and $TTR_{Orn(m+5)}$ is the tracer-tracee ratio of L-[U-$^{13}C_5$]ornithine (*m+5*) to unlabelled ornithine. Refer to p. 279-280 for full derivations.

Conversion of Arginine to Citrulline by NOS

The rate of conversion of arginine to citrulline by NOS was calculated according to the following equation:

$$Q_{Arg\rightarrow Cit_{NOS}} = \left(\frac{TTR_{Cit_{m+9}} + TTR_{Cit_{m+8}}}{TTR_{Arg_{m+10}} + TTR_{Arg_{m+9}} + TTR_{Arg_{m+8}}}\right) \times Q_{Cit_T} \qquad Eq.\ 2.10$$

Where $Q_{Arg\rightarrow Orn_{NOS}}$ is the rate of conversion of arginine to citrulline by nitric oxide synthase, $TTR_{Cit_{m+9}}$ is the tracer-tracee ratio of L-[U-$^{13}C_6$; U-$^{15}N_3$]citrulline (*m+9*) to unlabelled citrulline, $TTR_{Cit_{m+8}}$ is the tracer-tracee ratio of L-[U-$^{13}C_6$;α,δ-$^{15}N_2$]citrulline (*m+8*) to unlabelled citrulline, $TTR_{Arg_{m+10}}$ is the tracer-tracee ratio of L-[U-$^{13}C_6$;U-$^{15}N_4$]arginine (*m+10*) to unlabelled arginine, $TTR_{Arg_{m+9}}$ is the tracer-tracee ratio of L-[U-$^{13}C_6$; α,δ,guanidino-$^{15}N_3$]arginine (*m+9*) to unlabelled arginine, $TTR_{Arg_{m+8}}$ is the tracer-tracee ratio of L-[U-$^{13}C_6$; α,δ-$^{15}N_2$]arginine (*m+8*) to unlabelled arginine and Q_{Cit_T} is the total rate of citrulline appearance calculated according to *Eq.* 2.6. In our experiments, the abundance of L-[U-$^{13}C_6$;α,δ-$^{15}N_2$]arginine (*m+8*) was indistinguishable from background noise, resulting in a $TTR_{Arg_{m+8}}$ value of 0. Refer to p. 283 for full derivation.

Statistical Analyses

With the exception of dietary intake, fluid intake, and change in bodyweight which are presented as mean ± SEM, data are presented as median and interquartile range (IQR). Statistical analyses were performed with GraphPad Prism 6 software and $p < 0.05$ was considered significant. Mann-Whitney test was used to compare behavioural scores between infected mice and uninfected controls. Kruskal-Wallis test followed by Dunn's multiple comparisons post-test was used to compare uninfected control plasma amino acid concentrations to values from mice infected with *P. berghei* ANKA on various days of infection. Mann-Whitney test was used to compare plasma amino acid concentrations and

behavioural scores in mice infected with wild-type *P. berghei* ANKA and mice infected with arginase knock-out *P. berghei* ANKA. Log-rank test was used to compare survival in mice infected with wild-type *P. berghei* ANKA and mice infected with arginase knock-out *P. berghei* ANKA. One-way ANOVA followed by Bonferroni post-test was used to compare Evan's blue dye extravasation between these groups and to uninfected controls. Two-way ANOVA followed by Bonferroni post-test was used to compare dietary intake, fluid intake and body weight between uninfected controls with *ad libitum* access to food, uninfected mice subjected to dietary restriction and infected mice. For plasma amino acid and flux values uninfected controls with or without dietary restriction were compared by Mann-Whitney test and uninfected controls subjected to dietary restriction were compared with infected mice by Wilcoxon matched-pairs signed rank test.

Acknowledgements

I would like to thank Akhil Vaidya for kindly providing arginase knock-out parasites and Honghui Wang for assistance in operating the Q-TOF LC/MS instrument. I am also grateful to Ivo Francischetti (NIAID/NIH) for making his infusion pump and tether systems available for these studies. This work was funded by the NIAID Division of Intramural Research, the European Virtual Institute of Malaria Research (EVIMalaR) and the Wellcome Trust (grant WT098051).

CHAPTER 3.

Disruption of ADMA/Arginine Homeostasis

Hepatic dimethylarginine dimethylaminohydrolase 1 (DDAH1) regulates the plasma ratio of arginine, the NOS substrate, and asymmetric dimethylarginine (ADMA), an endogenous NOS inhibitor. We used HPLC to assess arginine and ADMA in archived plasma samples from a previous case-control study of Gambian children with WHO-defined severe malaria or uncomplicated malaria. ADMA/arginine ratios were elevated in children with uncomplicated malaria and further elevated in children with severe malaria. ADMA/arginine ratios fell significantly in both groups upon recovery (assessed 28 days later). Among children with severe malaria ADMA/arginine ratios correlated with lactate, suggesting a possible contribution to impaired perfusion. We hypothesized that hepatic DDAH1 dysfunction could contribute to disruption of ADMA/arginine homeostasis in severe malaria. In a mouse model, Plasmodium berghei ANKA infection caused inactivation of hepatic DDAH1 as evidenced by decreased DDAH1 protein concentration, impaired enzyme activity, intracellular accumulation of ADMA in hepatic tissue, and elevation of the ADMA/arginine ratio in plasma. In uninfected mice, exposure to the haemolytic agent phenylhydrazine produced similar evidence of DDAH dysfunction, suggesting that haemolysis contributes to dysregulation of ADMA metabolism by inducing DDAH1 degradation. Loss of hepatic DDAH1 activity and disruption of ADMA/arginine homeostasis may contribute to severe malaria pathogenesis by inhibiting NO synthesis.

3.1 Introduction

Patients with severe malaria exhibit impaired endothelium-dependent vasodilation (Yeo et al., 2007) and reduced nitrite and nitrate concentrations in plasma and urine (Anstey et al., 1996), indicating decreased nitric oxide synthesis. Impaired NO signalling has been implicated in microcirculatory dysfunction (Dondorp et al., 2008a; Cabrales et al., 2011), loss of blood-brain barrier integrity (Gramaglia et al., 2006; Serghides et al., 2011; Dorovini-Zis et al., 2011) and cytoadherence of infected erythrocytes to the vascular endothelium (Serirom et al., 2003; Taylor et al., 2004). NO production by nitric oxide synthase (NOS) is dependent on the relative bioavailability of arginine, the NOS substrate, and asymmetric dimethylarginine (ADMA), an endogenous NOS inhibitor (Cardounel et al., 2007). ADMA is released during hydrolysis of

proteins that have been methylated by protein arginine methyltransferases (Kakimoto and Akazawa, 1970; Lee et al., 1977) (FIG 3.1). By inhibiting NOS, ADMA causes vasoconstriction, increased blood pressure, increased systemic vascular resistance and decreased forearm blood flow (Vallance et al., 1992; Achan et al., 2003; Kielstein et al., 2004).

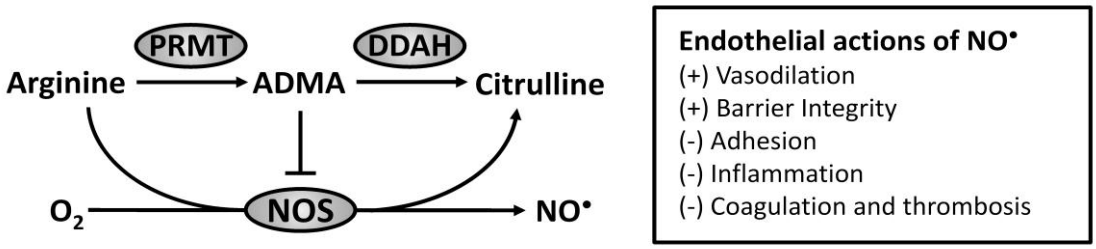


Figure 3.1 | DDAH metabolizes ADMA. Protein arginine methyltransferase (PRMT) methylates arginine residues in protein to form asymmetric dimethylarginine (ADMA). Free ADMA is released during proteolysis and acts as an endogenous inhibitor of nitric oxide (NO) production by NO synthase (NOS). Dimethylarginine dimethylaminohydrolase (DDAH) metabolizes free ADMA to citrulline.

Plasma arginine is depleted in Tanzanian children and Indonesian adults with severe malaria (Lopansri et al., 2003; Yeo et al., 2007; Weinberg et al., 2014). In Indonesian adults with severe malaria, plasma ADMA concentrations were elevated and inversely correlated with endothelium-dependent vasodilation (Yeo et al., 2010). In Tanzanian children with severe malaria, ADMA falls, but arginine falls to a greater degree, resulting in elevation of the ADMA/arginine ratio (equivalent to reducing the plasma arginine/ADMA ratio) (Weinberg et al., 2014). The mechanism responsible for dysregulation of ADMA relative to arginine in severe malaria is unknown.

Dimethylarginine dimethylaminohydrolase 1 (DDAH1) metabolizes ADMA at a rate inversely proportional to arginine concentration (Wang et al., 2006) and plays a central role in maintaining plasma ratios of ADMA to arginine (Hu et al., 2006; Wang et al., 2007). In Gambian children, an intronic *DDAH1* polymorphism is associated with susceptibility to severe malaria (Jallow et al., 2009), raising the possibility that DDAH1 might be functionally linked to disrupted ADMA/arginine homeostasis and impaired NO synthesis in severe malaria. In this

chapter, we identify dysregulation of ADMA/arginine homeostasis in a case-control study of Gambian children with severe malaria and hypothesize that ADMA clearance is impaired by hepatic DDAH1 inactivation. To test this hypothesis, we infect mice with *P. berghei* ANKA and assess changes in DDAH1 expression, protein levels and ADMA clearance in hepatic tissue, a major site of ADMA metabolism (Siroen et al., 2005; Nijveldt et al., 2003, 2004).

3.2 ADMA/Arginine Homeostasis in Gambian Children with Severe Malaria

Patients and Enrolment

We used HPLC to determine ADMA and arginine concentrations in archived plasma samples from a previous study of Gambian children with uncomplicated or severe malaria (Walther et al., 2009). In this study, 96 children with severe malaria and 102 children with uncomplicated malaria were enrolled at health centres in the peri-urban area around Fajara, The Gambia from 2005 to 2008. Blood was also drawn from 32 afebrile, aparasitaemic Gambian children who served as healthy controls. Archived plasma samples were available for 81/96 children with severe malaria, 75/102 children with uncomplicated malaria and 31/32 healthy controls (TABLE 3.1). Three children with severe malaria died, and follow-up assessments were completed 28 days after initial assessment on 85 patients with uncomplicated malaria and 72 patients with severe malaria. Archived plasma samples were available for 65/85 children with uncomplicated malaria and 47/72 children with severe malaria who completed follow-up visits (TABLE 3.1). Additional information about ethical approvals, enrolment practices and severe disease criteria are available in MATERIALS AND METHODS, p. 117.

Plasma Concentrations of ADMA and Arginine

We developed an HPLC-based method of determining ADMA and arginine concentrations in plasma samples (for complete description of assay development and validation, see APPENDIX C, p. 288). Plasma ADMA was low in children with uncomplicated malaria (median [IQR]: 0.40 [0.33-0.47] μmol/L) and severe malaria (0.40 [0.30-0.51] μmol/L)

compared with healthy controls (0.61 [0.56-0.69] μmol/L, $p < 0.0001$ vs uncomplicated, $p < 0.0001$ vs severe, FIG 3.2). ADMA did not differ between children with uncomplicated malaria and those with severe malaria ($p = 0.83$, FIG 3.2). ADMA remained low at the 28-day follow-up visit for patients recovered from malaria (FIG 3.2, TABLE 3.1). Plasma arginine was decreased in children with uncomplicated malaria compared with healthy controls and further decreased in children with severe malaria (healthy: 88.7 [79.3-102.5] μmol/L, uncomplicated malaria: 45.0 [35.4-55.7] μmol/L, $p < 0.0001$ vs healthy, severe malaria: 31.7 [23.0-40.6] μmol/L, $p < 0.0001$ vs uncomplicated, FIG 3.2). By the 28-day follow up visit, plasma arginine concentration increased to 56.7 [42.1-78.9] μmol/L among children who recovered from severe malaria and to 70.8 [58.6-85.1] μmol/L among children who recovered from uncomplicated malaria ($p < 0.0001$ vs acute in both groups), but remained lower than the arginine concentration observed in healthy Gambian children (88.7 [79.3-102.5] μmol/L; $p < 0.0001$ for either comparison, FIG 3.2).

	Healthy Controls	**Uncomplicated Malaria**		**Severe Malaria**	
		Acute	Recovery	Acute	Recovery
Enrolled	32	102	85	96	72
Plasma Samples Available	31	75	65	81	47
Age, years	7 [5.0-9.5]	7 [4.0-7.5]	-	4 [2.7-5.0] [a,d]	-
Weight, kg	18 [15-26.5]	19.3 [14.0-26.0]	-	14 .0 [11.0-16.0] [a,d]	-
Temperature, °C	36.8 [36.6-37.0]	38.0 [36.8-38.7] [b]	-	38.6 [38.1-39.4] [b,d]	-
Respiratory Rate, breaths/min	-	36 [28-48]	-	48 [38-60] [d]	-
Parasitaemia, %	-	2.9 [1.1-6.1]	-	9.2 [4.8-17.1] [d]	-
Glucose, mmol/L	-	6 [5.2-6.6]	-	6.8 [5.3-8.4] [c]	-
Haemoglobin, g/dL	-	11.3 [10.2-12.7]	12.0 [11.1-13.1] [e]	9.7 [7.0-10.8] [d]	11.9 [10.9-12.7]
ADMA, μmol/L	0.61 [0.56-0.69]	0.40 [0.33-0.47] [b]	0.40 [0.33-0.47]	0.40 [0.30-0.51] [b]	0.44 [0.37-0.50]
Arginine, μmol/L	88.7 [79.3-102.5]	45.0 [35.4-55.7] [b]	70.8 [58.6-85.1] [g]	31.7 [23.0-40.6] [b,d]	56.7 [42.1-78.9] [g]
ADMA/Arginine, $\times 10^{-3}$	6.7 [5.8-8.2]	8.8 [7.2-11.6] [b]	5.7 [4.8-6.8] [g]	13.5 [11.2-17.1] [b,d]	7.4 [5.9-10.1] [g]
Lactate, mmol/L	-	2.8 [2.2-4.0]	-	5.0 [3.2-6.9] [d]	-
sVCAM, ng/mL	905 [777-1073]	905 [726-1313]	695 [513-979] [f]	1266 [827-1806] [d]	841 [643-1154]

Table 3.1 | Clinical laboratory values in Gambian Children with uncomplicated or severe malaria
Values are presented as median [interquartile range]
[a] $p < 0.001$ [b] $p < 0.0001$ for acute severe or acute uncomplicated malaria vs healthy controls by Mann-Whitney test
[c] $p < 0.05$, [d] $p < 0.0001$ for acute severe malaria vs acute uncomplicated malaria by Mann-Whitney test
[e] $p < 0.05$, [f] $p < 0.001$, [g] $p < 0.0001$ for recovery vs acute by Wilcoxon matched-pairs signed-rank test

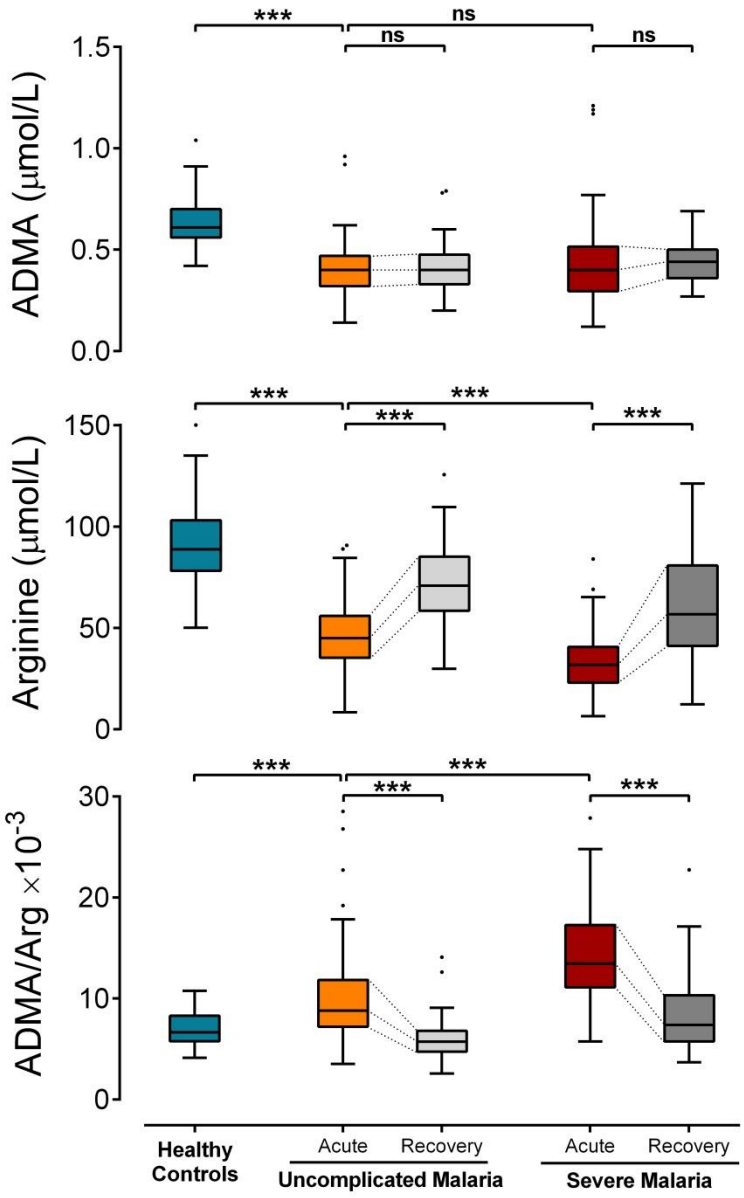


Figure 3.2 | Plasma ADMA and arginine in Gambian children with severe malaria. Concentrations of ADMA and arginine in plasma from Gambian children with acute uncomplicated malaria (n=75, orange box-plot) and acute severe malaria (n=81, red box-plot) were analyzed by HPLC. Samples from 31 healthy children served as controls (blue box-plot). At a follow-up visit 28 days after initial assessment, plasma ADMA and arginine were also determined in children who had recovered from uncomplicated malaria (n=65, light grey box-plot) or severe malaria (n= 47, dark grey box-plot). Box-plots depict median and IQR. Whiskers extend to highest and lowest values within 1.5×IQR of the 75th and 25th percentiles and values outside this range were plotted as individual points (Tukey's method). ***p < 0.0001, ns = p > 0.05. Mann-Whitney test was used for unpaired analyses among acute malaria and healthy control values. Wilcoxon matched pairs signed rank test was used to for pair-wise analyses of acute and recovery values.

Plasma ADMA/Arginine Homeostasis

In cultured endothelial cells, ADMA inhibition of NOS is blunted with the addition of exogenous arginine (Cardounel et al., 2007). These findings demonstrate that as a competitive inhibitor, the effect of ADMA on NOS activity is dependent on arginine substrate availability, prompting us to examine the ADMA/arginine ratio. The ratio of ADMA to arginine was elevated in children with severe malaria (13.5 [11.2-17.1] $\times 10^{-3}$) compared to children with uncomplicated malaria (8.8 [7.2-11.6] $\times 10^{-3}$, $p < 0.0001$ vs severe) and healthy controls (6.7 [5.8-8.2] $\times 10^{-3}$, $p < 0.0001$ vs severe, $p < 0.0001$ vs uncomplicated, FIG 3.2). At follow-up, 28 days after initial assessments, the ADMA/arginine ratio returned to normal in children who had recovered from uncomplicated malaria (5.7 [4.8-6.8] $\times 10^{-3}$, $p < 0.0001$ vs acute) and severe malaria (7.4 [5.9-10.1] $\times 10^{-3}$, $p < 0.0001$ vs acute, FIG 3.2). These observations suggest that elevation of the ADMA/arginine ratio is an acute metabolic disturbance associated with a symptomatic episode of malaria.

Previous Studies of ADMA and Arginine in Malaria

Our results agree closely with a recent study of ADMA and arginine in Tanzanian children with severe malaria (Weinberg et al., 2014). In the study conducted by Weinberg et al., cerebral malaria was defined as *P. falciparum* parasitaemia, Blantyre Coma Score ≤ 2 and absence of alternative cause for coma; non-cerebral severe malaria was defined as presence of at least 1 WHO criterion for severe malaria, but with Blantyre Coma Score > 2; and moderately severe malaria was defined as fever within the previous 48 hours, > 1000 parasites/µl, no WHO criteria for severe malaria and inability to tolerate oral medication (Weinberg et al., 2014). Weinberg et al. found similarly low plasma arginine concentrations in children with moderately severe malaria, cerebral malaria and non-cerebral severe malaria. Consistent with our findings, Weinberg et al. also observed decreased ADMA in moderately severe malaria and cerebral malaria, although ADMA values in children with non-cerebral severe malaria were not significantly different from healthy control values (Weinberg et al., 2014). As we observed in

our study, the degree of arginine depletion was greater than that of ADMA. Weinberg et al. described this disruption with the ratio of arginine to ADMA. Recalculating these values as ADMA/arginine ratios for comparison to our own data, Weinberg et al. observed ratios of 7.1 [5.8-9.0] $\times 10^{-3}$ (median [IQR]) in healthy controls, 12.6 [10.7-15.1] $\times 10^{-3}$ in moderately severe malaria, 12.3 [10.0-15.1] $\times 10^{-3}$ in non-cerebral severe malaria and 13.2 [11.1-16.4] $\times 10^{-3}$ in cerebral severe malaria (Weinberg et al., 2014). These values correspond well to the ADMA/arginine ratios observed in our study (TABLE 3.1 & FIG 3.2), with the exception that we found a significant difference between ADMA/arginine ratios in uncomplicated and severe malaria, whereas Weinberg et al. found no difference between moderately severe, severe and cerebral malaria (Weinberg et al., 2014). This discrepancy may be explained by the definition used by Weinberg et al. to define moderately severe malaria, which included inability to tolerate oral medication (Weinberg et al., 2014). This criterion may have selected children with greater dietary insufficiency (and potentially greater arginine depletion) than uncomplicated cases in our study which were not defined based on intolerance of oral medication. These are the first studies to examine ADMA/arginine homeostasis in African children with severe malaria, the patient population that bears the greatest burden of malaria-related mortality (World Health Organization, 2012; Murray et al., 2012).

Arginine depletion and disruption of ADMA/arginine homeostasis have also been observed in Indonesian adults with moderately severe and severe malaria (Yeo et al., 2010). Similar to African children, adults with moderately severe malaria demonstrated decreased ADMA and a greater degree of arginine depletion, leading to disruption of ADMA/arginine homeostasis (Yeo et al., 2010). In contrast to severe malaria in children and moderately severe malaria in adults, Indonesian adults with severe malaria demonstrated elevated ADMA (Yeo et al., 2010). The apparent discrepancy in plasma ADMA in children and adults with severe malaria may reflect differences in severe malaria pathophysiology observed in older versus younger patients (Idro et al., 2005).

Mortality

Only 3 out of 96 children (3.1%) enrolled with severe malaria in our study died. This rate is lower than mortality rates observed in a recent large multi-centre clinical trial in African children (8.5% in children treated with artesunate and 10.9% in children treated with quinine) (Dondorp et al., 2010). All three children who died in our study presented with hyperlactataemia (non-survivor 1: 16.2 mmol/L, non-survivor 2: 7.6 mmol/L, non-survivor 3: 12.8 mmol/L), and one patient also presented with neurological involvement (non-survivor 1 Blantyre coma score: 2, TABLE 3.2). ADMA/arginine ratios were significantly higher in non-survivors (non-survivor 1: 27.9 mmol/L, non-survivor 2: 18.9 mmol/L, non-survivor 3: 19.1 mmol/L) compared to children presenting with severe malaria who recovered (13.3 [11.1-16.8], p = 0.01 vs non-survivors). A larger, prospective study would be required to determine the prognostic significance of presentation with elevated plasma ADMA/arginine ratios.

	Non-Survivor 1	Non-Survivor 2	Non-Survivor 3
Age, years	4	12	4
Weight, kg	9	31	13
Temperature, °C	40.8	39.9	37.7
Respiratory Rate, breaths/min	60	46	70
Blantyre Coma Score	2	5	5
Parasitaemia, %	13	10.4	46
Glucose, mmol/L	3.5	7.8	1.5
ADMA, µmol/L	2.34	0.39	0.49
Arginine, µmol/L	83.9	20.6	25.6
ADMA/Arginine, $\times 10^{-3}$	27.9	18.9	19.1
Lactate, mmol/L	16.2	7.6	12.8

Table 3.2 | Clinical laboratory values in Gambian Children with severe malaria who died.

Assessment of ADMA and Arginine in Defined Severe Malaria Syndromes

Stratification of Severe Malaria Cohort by Disease Manifestation

To further investigate ADMA/arginine ratios associated with different disease manifestations, we stratified severe malaria patients into subgroups associated with higher or lower risk of mortality based on previous studies in African children. In our cohort of children with severe malaria, four major disease manifestation sub-groups were identified and ranked in the following order according to previously-observed mortality rates (Marsh et al., 1995): acidosis, cerebral malaria, prostration and severe anaemia (FIG 3.3). Patients presenting with these four manifestations alone or in combination accounted for 78/81 severe malaria admissions for whom archived plasma samples were available. Patients presenting with multiple disease manifestations carry the highest risk of mortality (Marsh et al., 1995), but the limited scope of our study prevented sufficient resolution of every relevant combination of co-morbidities. As a result, patients with multiple syndromes were included in the highest-risk sub-group and excluded from lower-risk sub-groups (FIG 3.3). For example, according to this system, the ‘cerebral malaria’ group includes patients presenting with both cerebral malaria and prostration but does not include patients presenting with both cerebral malaria and acidosis, who would instead be included in the ‘acidosis’ group (FIG 3.3).

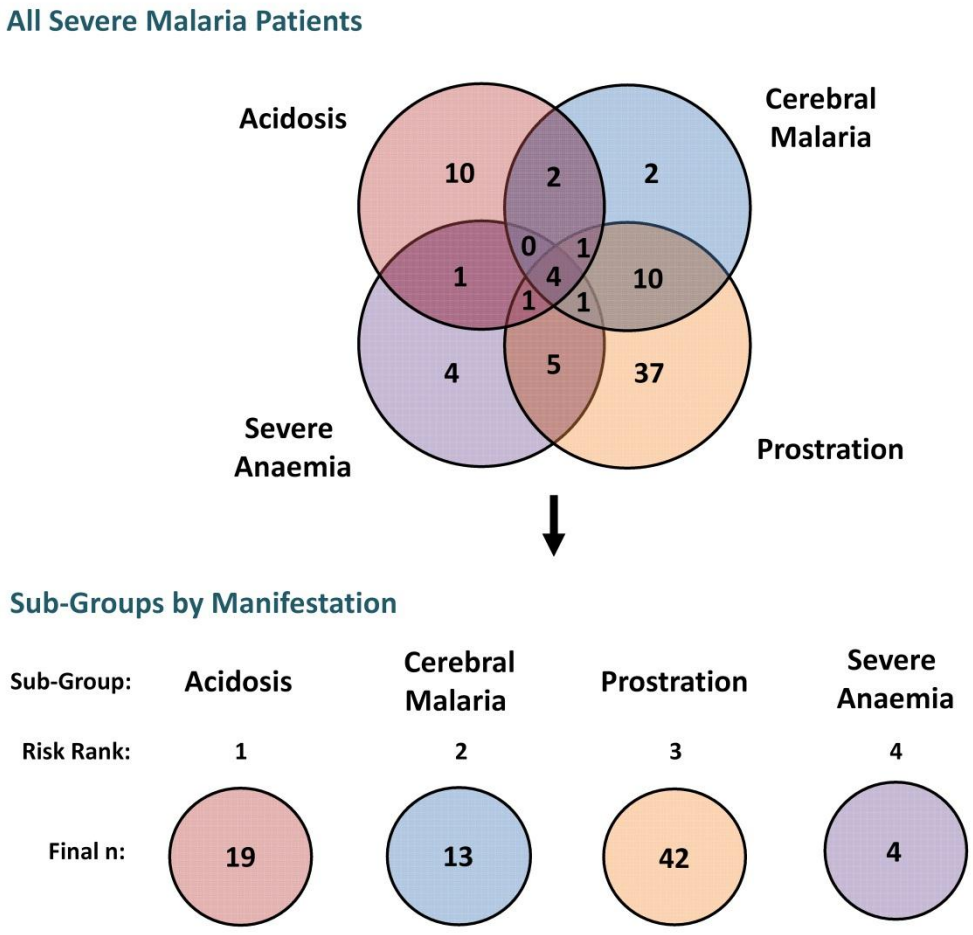


Figure 3.3 | Identification of severe malaria sub-groups. Cerebral malaria was defined as Blantyre coma score ≤2 in the absence of hypoglycaemia or hypovolaemia with the coma lasting for at least 2 hrs; acidosis was defined as serum lactate >7 mmol/L; severe anaemia was defined as Hb < 6g/dl; and prostration was defined as inability to sit unsupported (children >6 months old) or inability to suck (children <6 months old). Patients presenting with multiple syndromes were placed in the higher risk sub-group and excluded from lower-risk sub-groups. Numbers describe patients for whom ADMA and arginine laboratory values were available.

ADMA/Arginine Homeostasis According to Disease Manifestation

Children presenting with acidosis exhibited higher plasma ADMA/arginine ratios (17.5 [14.4-19.5] $\times 10^{-3}$) compared to those with cerebral malaria without acidosis (12.2 [10.0-18.1] $\times 10^{-3}$, $p < 0.05$ vs acidosis) or prostration without acidosis or cerebral malaria (12.8 [10.7-14.7], $p < 0.01$ vs acidosis, FIG 3.4). The median ADMA/arginine ratio was 18.0 in patients with severe anaemia and no other complications, but the small number of patients available for this group (n=4) limited effective comparison to other groups. All three deaths occurred in the sub-group with acidosis, although one of these patients also presented with cerebral malaria. A larger study is required to more effectively assess associations between ADMA/arginine ratios and specific combinations of severe malaria manifestations.

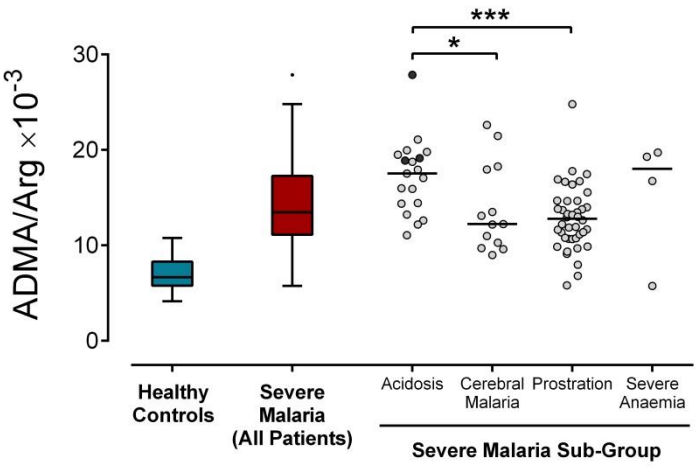
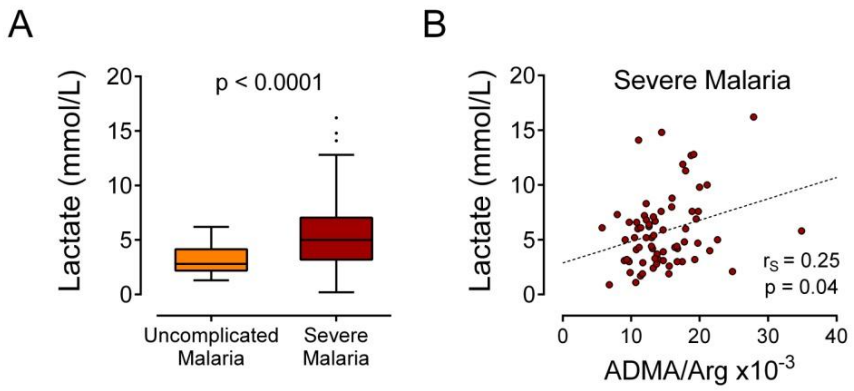


Figure 3.4 | Plasma ADMA/arginine ratios in sub-groups of severe malaria patients. Concentrations of ADMA and arginine were analyzed by HPLC in plasma from Gambian children with severe acidosis (n=19), cerebral malaria (n=13), prostration (n=42) or severe anaemia (n=4) and plotted as individual data points (grey). Patients who died are represented by filled circles (n=3). All severe malaria patients are also graphed as a single combined group for reference (red box-plot). Samples from 31 healthy children served as controls (blue box-plot). Box-plots depict median and IQR. Whiskers extend to highest and lowest values within 1.5×IQR of the 75th and 25th percentiles and values outside this range were plotted as individual points (Tukey's method). *$p < 0.05$, ***$p < 0.001$ by Mann-Whitney test.

Relationship between the ADMA/Arginine Ratio, Lactate and sVCAM

Lactate

Lactate is a biomarker of impaired tissue perfusion that is associated with increased risk of mortality from severe malaria in children (Taylor et al., 1993; Krishna et al., 1994; Waller et al., 1995; Planche et al., 2003). In our study, lactate was elevated in children with severe malaria (5.0 [3.2-6.9] mmol/L) compared to children with uncomplicated malaria (2.8 [2.2-4.0] mmol/L, $p < 0.0001$, FIG 3.5). Lactate was positively correlated with the ADMA/arginine ratio among children with severe malaria ($r_s = 0.25$, $p = 0.04$, FIG 3.5). Lactate was also positively correlated with ADMA in children with severe malaria ($r_s = 0.24$, $p = 0.04$) but not arginine ($r_s = 0.10$, $p = 0.43$, FIG 3.5). These observations suggest that failure to regulate ADMA and resulting elevation of ADMA/arginine ratios may have a greater impact on tissue perfusion than arginine depletion alone. Alternatively, the correlation between plasma ADMA and lactate could indicate that poor tissue perfusion contributes to elevation of plasma ADMA relative to arginine. Impaired perfusion of liver tissue has been observed in adults with severe malaria (Molyneux et al., 1989a), which could limit hepatic clearance of plasma ADMA (Siroen et al., 2005; Nijveldt et al., 2003, 2004; Hu et al., 2006).



C

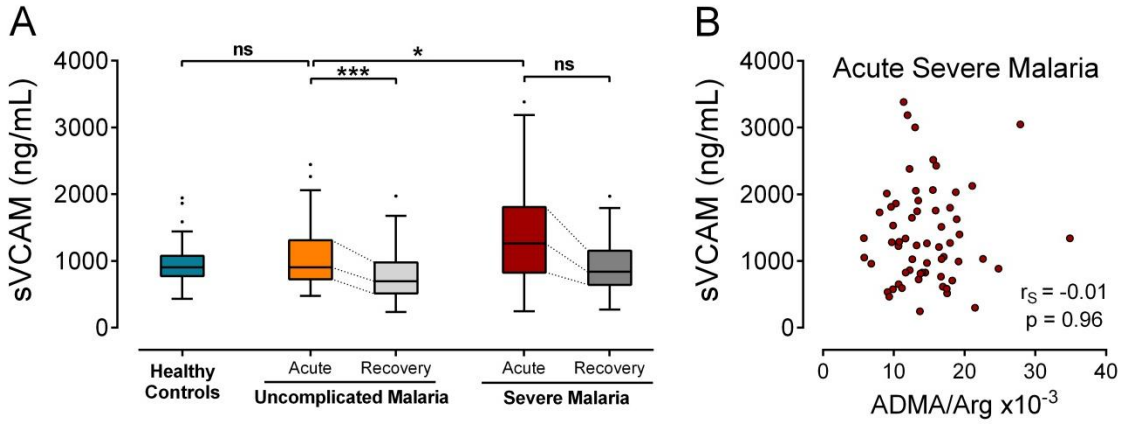
	Correlations with Lactate								
	Severe malaria			Uncomplicated Malaria			Severe + Uncomplicated Malaria		
	r_s	p	XY pairs	r_s	p	XY pairs	r_s	p	XY pairs
ADMA/Arg	0.25	0.04*	71	0.08	0.74	20	0.22	0.04*	91
ADMA	0.24	0.04*	71	0.09	0.71	20	0.30	0.004**	91
Arginine	0.10	0.43	71	-0.17	0.47	20	0.15	0.16	91

Figure 3.5 | Elevation of lactate in severe malaria. (A) Lactate was determined in children with acute uncomplicated malaria (n=28, orange box-plot) and acute severe malaria (n=85, red box-plot) with a hand-held Lactate Pro instrument. Box-plots depict median and IQR. Whiskers extend to highest and lowest values within 1.5×IQR of the 75th and 25th percentiles with values outside this range plotted as individual points (Tukey's method). (**B**) Graph of lactate vs ADMA/arginine ratios in children with acute severe malaria. r_s: spearman's rho. (**C**) Spearman's correlation was used to assess the relationship between lactate and ADMA, arginine and the ADMA/arginine ratio among severe and uncomplicated malaria patients. r_s: spearman's rho. *p < 0.05, **p < 0.01 by spearman's correlation.

Soluble VCAM

We measured soluble vascular cell adhesion molecule (sVCAM) as a biomarker of endothelial activation. Plasma sVCAM was elevated in children with severe malaria compared to healthy controls and children with uncomplicated malaria (acute severe: 1266 [827-1806] ng/mL, acute uncomplicated: 905 [726-1313] ng/mL, $p < 0.05$ vs acute severe, healthy control: 905 [777-1073] ng/mL, $p < 0.05$ vs acute severe, FIG. 3.6). Median sVCAM concentrations were decreased in children who recovered from severe malaria (841 [643-1154] ng/mL) but this difference did not reach statistical significance ($p = 0.09$ vs acute severe, FIG. 3.6). In contrast, plasma sVCAM in children with acute uncomplicated malaria was not significantly different from concentrations in healthy controls (acute uncomplicated: 905 [726-1313] ng/mL, $p = 0.84$ vs healthy controls) but decreased following recovery (recovered uncomplicated: 695 [513-979] ng/mL, $p < 0.001$ vs acute uncomplicated, FIG. 3.6).

Soluble VCAM was positively correlated with plasma ADMA in severe malaria patients ($r_s = 0.57$, $p < 0.0001$, FIG. 3.6). This observation suggests that ADMA, a NOS inhibitor, is associated with endothelial activation and release of sVCAM into circulation. However, sVCAM was also positively correlated with arginine ($r_s = 0.50$, $p < 0.0001$, FIG. 3.6), suggesting that increased availability of NOS substrate is also associated with increased release of sVCAM. Furthermore, sVCAM did not correlate with the ADMA/arginine ratio ($r_s = -0.01$, $p = 0.96$, FIG. 3.6), a key determinant of NOS activity (Cardounel et al., 2007). These findings are inconsistent with the hypothesis that NOS inhibition contributes to endothelial activation and sVCAM release. Haemolysis results in exposure of erythrocyte proteins to proteases, which leads to release of both arginine and ADMA (Davids et al., 2012a). Release of cell-free haemoglobin and subsequent release of free haem could induce endothelial stress and sVCAM release. Haemolysis may therefore explain the observed positive correlation between ADMA, arginine and sVCAM in children with severe malaria.



C

	Correlations with sVCAM								
	Severe malaria			Uncomplicated Malaria			Severe + Uncomplicated Malaria		
	r_s	p	XY pairs	r_s	p	XY pairs	r_s	p	XY pairs
ADMA/Arg	-0.01	0.96	61	-0.17	0.19	58	0.02	0.81	119
ADMA	0.57	<0.0001***	61	0.60	<0.0001***	58	0.60	< 0.0001***	119
Arginine	0.50	<0.0001***	61	0.42	0.001***	58	0.39	< 0.0001***	119

Figure 3.6 | Elevation of sVCAM in severe malaria. (**A**) sVCAM was determined in children with acute uncomplicated malaria (n=59, orange box-plot) and acute severe malaria (n=61, red box-plot) by ELISA. Samples from 31 healthy children served as controls (blue box-plot). At a follow-up visit 28 days after initial assessment, plasma sVCAM was also determined in children who had recovered from uncomplicated malaria (n=60, light grey box-plots) or severe malaria (n= 43, dark grey box-plots). Box-plots depict median and IQR. Whiskers extend to highest and lowest values within 1.5×IQR of the 75th and 25th percentiles with values outside this range plotted as individual points (Tukey's method). (**B**) Graph of sVCAM vs ADMA/arginine ratios in children with acute severe malaria. r_s: spearman's rho. (**C**) Spearman's correlation was used to assess the relationship between sVCAM and ADMA, arginine and the ADMA/arginine ratio among severe and uncomplicated malaria patients. r_s: spearman's rho. ***p < 0.001 by spearman's correlation.

Relationship between Hypoargininaemia and the ADMA/Arginine Ratio

In children with uncomplicated and severe malaria, ADMA is decreased but arginine is depleted to a greater degree, resulting in elevation of the ADMA/arginine ratio. To conceptualize the relationship between changes in plasma arginine and resulting changes in the ADMA/arginine ratio, we plotted ADMA/arginine values against arginine concentrations observed in healthy controls, severe malaria and uncomplicated malaria (FIG 3.7). In the absence of experimental induction of hypoargininaemia in healthy subjects, it is unclear to what extent ADMA/arginine ratios would be expected to rise as arginine falls in healthy individuals. Therefore, we represent two conceptual models for comparison with observed measurements: 'complete compensation', in which ADMA is down-regulated in response to arginine depletion such that normal ADMA/arginine ratios are preserved, and 'no compensation' in which ADMA concentrations remain unchanged in response to arginine depletion (FIG 3.7). In the latter model, the ADMA/arginine ratio is described by the reciprocal function ADMA/arginine = 0.61μM/[arginine], where the constant 0.61μM is the geometric mean ADMA concentration in healthy controls ('no compensation band,' FIG 3.7).

Children with acute severe malaria and acute uncomplicated malaria are to the left of healthy controls on the x-axis, indicating depletion of plasma arginine. ADMA/arginine ratios in children with acute malaria fall below the 'no compensation' model, but above the normal range ('complete compensation model') (FIG 3.7). Thus, during acute malaria, ADMA is down-regulated, but not to a sufficient degree to preserve normal ADMA/arginine ratios. After recovery from severe and uncomplicated malaria, plasma ADMA/arginine ratios decreased as a result of increasing plasma arginine concentrations while ADMA remained constant (FIG 3.7). It is unclear whether elevation of ADMA/arginine ratios in children with severe malaria can be entirely attributed to hypoargininaemia or whether excess ADMA release or insufficient ADMA clearance may also contribute. To investigate whether ADMA clearance is impaired in severe malaria, we identified ADMA/arginine dysregulation in a mouse model of severe malaria and

studied the function of dimethylarginine dimethylaminohydrolase 1 (DDAH1), the enzyme primarily responsible for clearance of circulating ADMA.

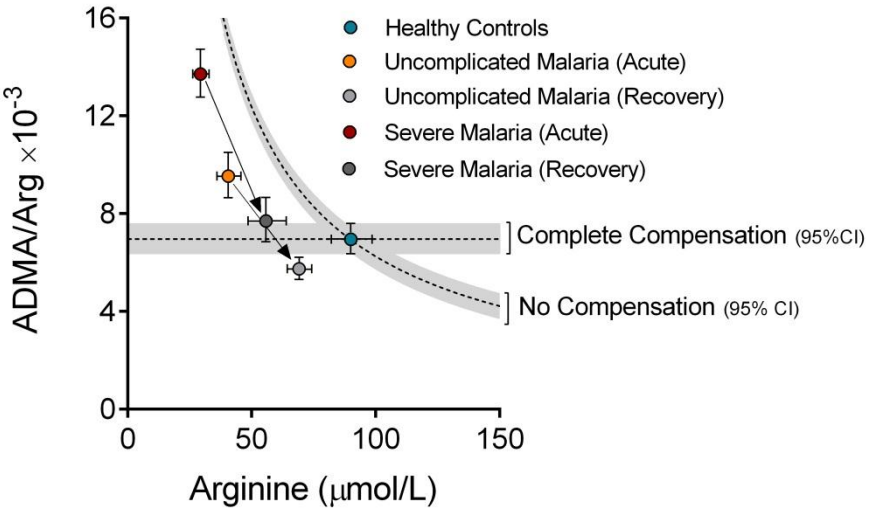


Figure 3.7 | Plot of plasma ADMA/arginine ratios vs arginine in healthy controls, acute malaria and post-recovery. Geometric means (circles) and 95% CIs (bars) were plotted for plasma arginine concentrations and ADMA/arginine ratios in healthy controls (n=32, blue), acute uncomplicated malaria (n=75, orange), recovered uncomplicated malaria (n=65, light grey), acute severe malaria (n=81, red) and recovered severe malaria (n=47, dark grey). Arrows indicate shift in plasma arginine concentrations and ADMA/arginine ratios from acute to recovery values. Compensatory down-regulation of plasma ADMA in proportion to decreased arginine concentrations would preserve normal ADMA/arginine ratios (complete compensation band). In the absence of ADMA regulation in response to decreased arginine concentrations (no compensation band), the ADMA/arginine ratio would increase according to a reciprocal function, holding ADMA constant at the healthy control geometric mean value of 0.61μM: ADMA/arginine = 0.61μM/[Arginine].

3.3 ADMA/Arginine Homeostasis in *P. berghei* ANKA-Infected Mice

We used HPLC to determine whether C57BL/6 mice infected with *P. berghei* ANKA effectively model the disruption of ADMA/arginine homeostasis observed in Gambian children. On day 6 post-inoculation, plasma arginine concentrations were lower in infected mice compared with uninfected controls (infected: 46.7 [39.2-53.3] µmol/L vs uninfected control: 78.1 [66.5-101.9] µmol/L, $p < 0.0001$, FIG 3.8). Plasma ADMA levels were also lower in infected mice (infected: 0.44 [0.40-0.49] µmol/L vs uninfected control: 0.59 [0.54-0.63] µmol/L, $p < 0.0001$, FIG 3.8). ADMA was decreased to a lesser degree than arginine, resulting in increased ratios of ADMA to arginine in infected mice (infected: 9.8 [8.7-12.5] $\times 10^{-3}$ vs uninfected control: 7.1 [5.9-8.8] $\times 10^{-3}$, $p < 0.0001$, FIG 3.8). These findings recapitulate observations from Gambian children with severe malaria, suggesting that this mouse model is appropriate for the study of ADMA/arginine homeostasis in the context of severe malaria.

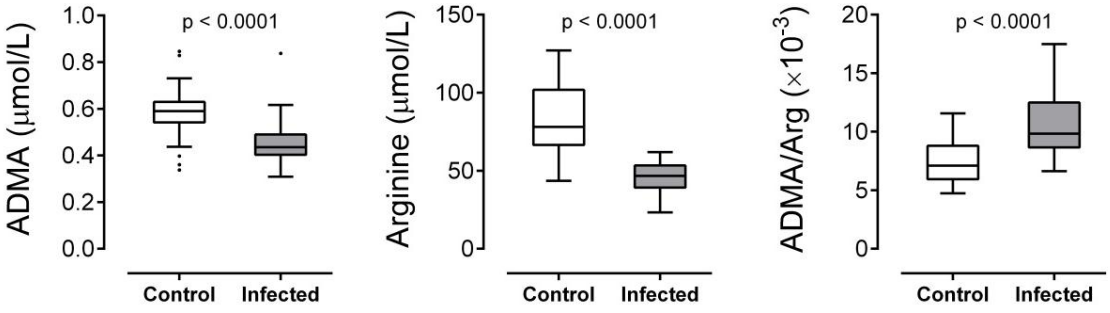


Figure 3.8 | ADMA/arginine homeostasis in *P. berghei* ANKA-infected mice. Concentrations of ADMA and arginine were determined by HPLC in plasma from *P. berghei* ANKA-infected mice 6 days post-inoculation (n=23) and uninfected controls (n=28). The ADMA/arginine ratio was calculated from measured values. Box-plots depict median and IQR. Whiskers extend to highest and lowest values within 1.5×IQR of the 75th and 25th percentiles with values outside this range plotted as individual points (Tukey's method). *$p < 0.0001$ by Mann-Whitney test.

3.4 Hepatic DDAH Dysfunction

Rationale for the Study of Hepatic DDAH

Hepatic DDAH1 is a key regulator of ADMA/arginine homeostasis. Heterozygous knock-out of DDAH1 in mice increased plasma ADMA, elevated blood pressure and decreased NO-dependent vasodilation in *ex vivo* aortic rings (Leiper et al., 2007). Conversely, transgenic over-expression of DDAH1 decreased plasma ADMA concentrations, increased urinary nitrites/nitrates and decreased blood pressure (Dayoub et al., 2003). A second DDAH isoform (DDAH2) has been identified (Leiper et al., 1999), but in contrast to *DDAH1*, suppression of *DDAH2* expression did not result in altered plasma ADMA concentrations (Wang et al., 2007). The liver expresses DDAH1 (Leiper et al., 1999) and metabolic tracer studies have identified the liver as a major site for clearance of circulating ADMA (Nijveldt et al., 2003). Induction of *DDAH1* expression in liver lowers plasma ADMA (Hu et al., 2006). Preoperative patients undergoing liver transplant demonstrated higher plasma levels of ADMA compared with healthy controls (Nijveldt et al., 2004; Siroen et al., 2004; Mookerjee et al., 2007), and a significant decrease in circulating ADMA was observed as early as 1 day after liver transplantation (Siroen et al., 2004). Conversely, patients with acute rejection of their liver graft had elevated ADMA compared to patients without episodes of rejection (Siroen et al., 2004). Taken together, these results from human patients and animal studies have identified hepatic DDAH1 to be a key regulator of circulating ADMA. Therefore we assessed changes in hepatic DDAH1 expression, protein levels and ADMA clearance in a mouse model of severe malaria.

Hepatic DDAH1 Protein and Gene Expression

To determine whether *P. berghei* ANKA infection inhibits hepatic DDAH1 function, we assessed *Ddah1* gene expression and protein levels in liver tissue from C57BL/6 mice 6 days after inoculation with *P. berghei* ANKA. Using quantitative RT-PCR to assess hepatic *Ddah1* mRNA transcripts relative to *Gapdh*, we found that *Ddah1* gene expression was not changed by *P. berghei* ANKA infection (median [IQR]: 1.1 [1.0-1.1]-fold of uninfected control, p = 0.40 vs uninfected control, FIG 3.9). In contrast, as determined by Western blot, DDAH1 protein levels in liver samples from *P. berghei*-infected mice were reduced to a median of 0.23-fold of control values (IQR: 0.05-0.46, p < 0.0001 vs uninfected control, FIG 3.9). These data demonstrate that *P. berghei* ANKA infection decreases DDAH1 protein by a post-transcriptional mechanism.

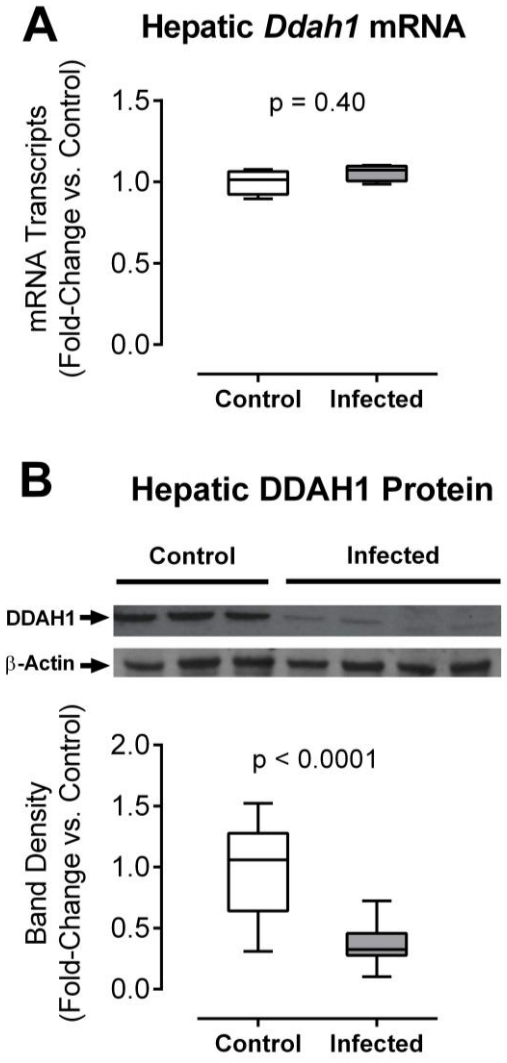


Figure 3.9 | Hepatic DDAH1 protein is decreased in *P. berghei* ANKA-infected mice. (**A**) Quantitative RT-PCR was performed to quantify hepatic *Ddah1* mRNA 6 days post-inoculation with P. berghei ANKA. Values were normalized to *Gapdh* mRNA and expressed as fold-change vs. control values. Liver samples were analyzed from n=12 control mice and n=12 infected mice (6 days post-inoculation) randomly selected from 2 independent experiments. (**B**) Western blot was used to detect hepatic DDAH1 protein (38 kDa) in liver samples from P. berghei ANKA-infected mice 6 days post-inoculation and uninfected controls. β-actin (42kDa) was assessed as a loading control Densitometry was used to quantify DDAH1 band density normalized to β-actin and expressed as fold-change vs. control values. Data are pooled from n=12 control mice and n=12 infected mice randomly selected from 3 independent experiments. Boxplots represent median, IQR and range. Mann-Whitney test was used to compare groups.

Hepatic DDAH1 Enzyme Activity and Intracellular ADMA Accumulation

To determine the functional effect of hepatic DDAH1 degradation, we quantified DDAH activity in liver homogenates by measuring the rate of citrulline production in the presence of saturating concentrations of ADMA substrate (2.5 mM). To confirm that this assay specifically quantifies DDAH activity, we demonstrated that liver homogenates only produce citrulline after the addition of exogenous ADMA substrate (for complete description of assay validation, see APPENDIX D, p. 312). Hepatic DDAH activity was lower in mice infected with *P. berghei* ANKA compared with uninfected controls (infected: 3.83 [3.22-4.19] nmol citrulline × mg protein^{-1}×hr^{-1} vs uninfected control: 6.48 [5.23-7.49] nmol citrulline × mg protein^{-1}×hr^{-1}, $p < 0.0001$, FIG 3.10). To assess the effect of decreased hepatic DDAH activity on hepatic ADMA accumulation, we determined intracellular ADMA concentrations in PBS-perfused liver samples from infected and uninfected control mice. Hepatic ADMA was increased in infected mice compared with uninfected controls (infected: 126.5 [88.9-198.2] pmol/mg protein vs uninfected control: 49.7 [35.3-77.8] pmol/mg protein, $p < 0.0001$, FIG 3.10). These results suggest that loss of hepatic DDAH1 protein and activity result in intracellular ADMA accumulation in the liver tissue of *P. berghei* ANKA-infected mice.

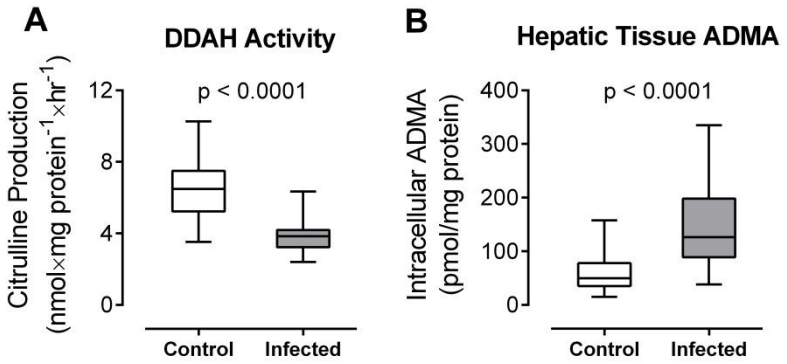


Figure 3.10 | *P. berghei* ANKA decreases hepatic DDAH activity and increases hepatic ADMA. (**A**) DDAH activity was assessed by quantification of citrulline production by liver homogenates in the presence of saturating concentrations of ADMA substrate (2.5 mM). Citrulline production was calculated on a per-hour basis and normalized to protein content. (**B**) Intracellular hepatic ADMA was assessed by HPLC in perfused liver samples and normalized to protein content. Liver samples were collected from uninfected controls (n=28) and *P. berghei* ANKA-infected mice on day 6 post-inoculation (n=25). Results were pooled from 3 independent experiments. Boxplots represent median, IQR and range. Mann-Whitney test was used to compare groups.

Potential Role of Oxidative Stress in DDAH Degradation

P. berghei ANKA infection did not alter *DDAH1* transcription but lowered DDAH1 protein levels, implying increased degradation of DDAH1 protein during infection. Previous *in vitro* studies of cultured smooth muscle cells have identified oxidative stress as a potential upstream cause of DDAH degradation. In these experiments, overexpression of the $p22^{phox}$ subunit of NADPH oxidase increased generation of reactive oxygen species, decreased DDAH protein levels, impaired DDAH activity and caused accumulation of both intracellular and extracellular ADMA in smooth muscle cell cultures (Luo et al., 2010). Treatment of $p22^{phox}$-transfected smooth muscle cells with the proteasome inhibitor epoxomicin raised DDAH protein concentrations and reduced intracellular ADMA (Luo et al., 2010). This finding raises the possibility that oxidative modification of DDAH protein may target it for proteasomal degradation. Reactive oxygen species are increased in the livers of *P. yoelii*-infected mice (Dey et al., 2012), suggesting that oxidative stress may contribute to DDAH degradation during malaria infection.

Free haem is one potential contributor to oxidative stress during malaria infection. Ferrous free haem catalyzes the Fenton reaction, in which hydrogen peroxide (H_2O_2) is broken down to form hydroxide anions (OH^-) and hydroxyl radicals ($HO^\bullet$) (Dixon and Stockwell, 2014). Hydroxyl radicals are highly-reactive non-specific oxidants that can participate in secondary reactions such as lipid oxidation, protein oxidation and DNA damage. Cell-free haemoglobin (with the haem iron in the Fe^{2+} state) released during haemolysis may be oxidized to methaemoglobin (with the haem iron in the Fe^{3+} state), which spontaneously releases the haem prosthetic group. Malaria infection causes haemolysis via schizont rupture of infected erythrocytes as well as induced lysis of uninfected bystander erythrocytes. As a result, free haem is increased in the plasma of *P. berghei* ANKA-infected mice (Pamplona et al., 2007) and in the livers of *P. yoelii*-infected mice (Dey et al., 2012). We hypothesized that malaria-associated haemolysis contributes to degradation of DDAH1 protein by release of free haem and induction of oxidative stress in liver tissue.

3.5 Assessment of DDAH Function in a Mouse Model of Haemolysis

Chemical Induction of Haemolysis

To isolate the effect of haemolysis on hepatic DDAH function in the absence of malaria infection, we assessed DDAH protein levels and activity in uninfected mice exposed to the haemolytic agent phenylhydrazine (PHZ) for 3 or 5 consecutive days (40 mg/kg/d, FIG 3.11A). Phenylhydrazine-exposed mice demonstrated weight-loss beginning 24hr after the second injection (PHZ-exposed day 3 change in body weight from baseline, mean ± SEM: -1.4 ± 0.1 g vs saline control: -0.2 ± 0.2 g, $p < 0.01$) and continuing through the final measurement 24 hr after the fifth injection (PHZ-exposed day 6: -4.5 ± 0.4 g vs saline control: -1.0 ± 0.3 g, $p < 0.01$, FIG 3.11B). Phenylhydrazine-exposed mice also exhibited abnormal behaviour, including lethargy and non-responsiveness, starting 24hr after the third injection (PHZ-exposed day 3 behavioural score, mean ± SEM: 11.3 ± 0.8 vs saline control: 14.0 ± 0.0, $p < 0.001$, FIG 3.11C).

Mice exposed to phenylhydrazine for 3 days developed anaemia compared to controls injected with saline (PHZ-exposed Hb, median [IQR]: 6.3 [6.1-6.6] g/dL vs saline control Hb: 12.8 [12.5-14.1] g/dL, $p < 0.0001$, PHZ-exposed RBC count: 2.1 [1.9-2.4] × 10^9 cells/mL vs saline control RBC count: 7.6 [7.3-7.9] × 10^9 cells/mL, $p < 0.0001$, FIG 3.11D-E). After 5 days of phenylhydrazine exposure, haemoglobin was further decreased (3.2 [2.4-4.1] g/dL, $p < 0.001$ vs 3 days of PHZ exposure), but red blood cell counts were not significantly different from values in mice subjected to only 3 days of exposure (1.5 [1.0-2.2] × 10^9 cells/mL, $p = 0.13$ vs 3 days of PHZ exposure, FIG 3.11D).

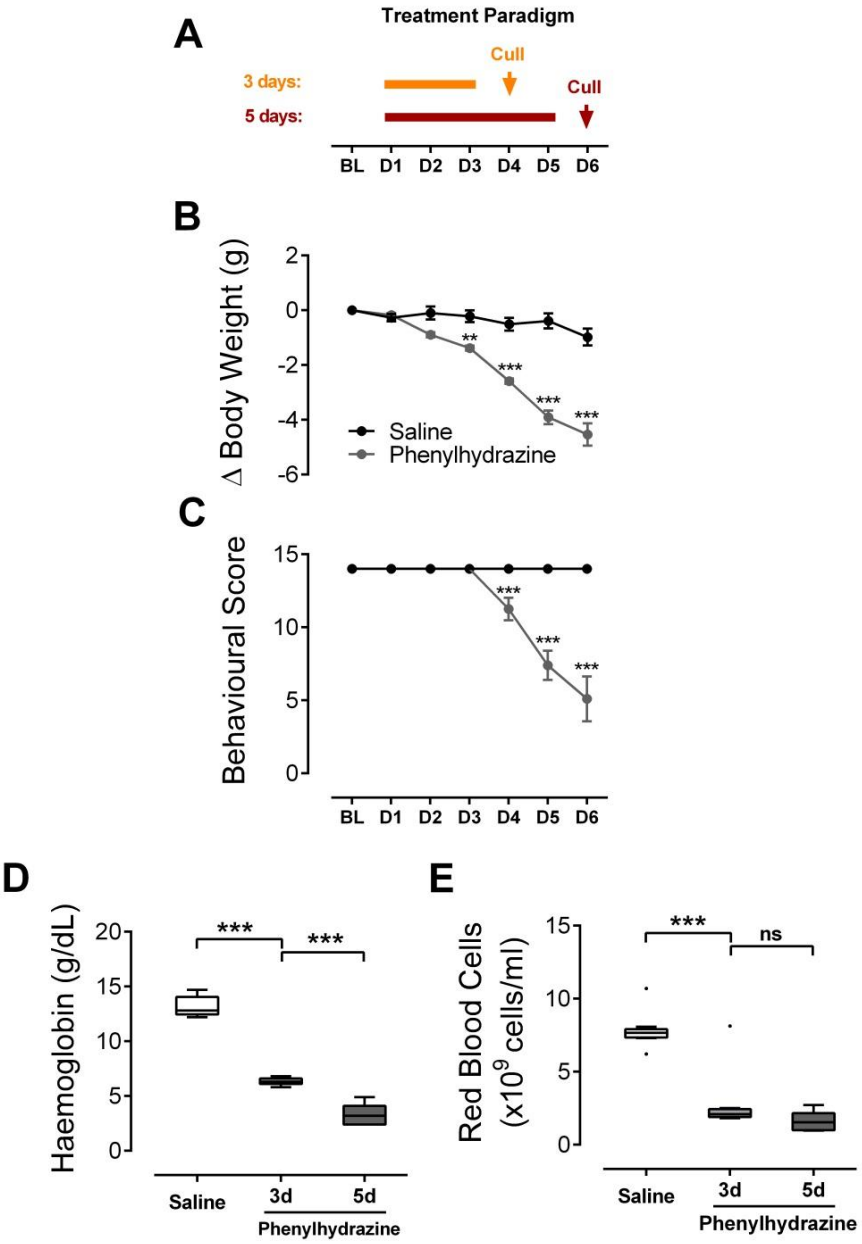


Figure 3.11 | Phenylhydrazine exposure causes weight loss, lethargy and anaemia. (**A**) Mice were exposed to phenylhydrazine (40mg/kg/d) by once daily intraperitoneal injection for 3 (n=10) or 5 days (n=10). Mice injected with saline vehicle served as controls (n=10). Mice were culled 24hr after the final injection for collection of blood and tissue samples. 2 mice from the 5-day treatment group died between the final injection and tissue collection the following day. (**B-C**) Behaviour and bodyweight were assessed at baseline (BL) and daily during administration of saline or phenylhydrazine. Data are presented as mean ± SEM. ***p<0.01, ***p<0.001 by two-way ANOVA followed by Bonferroni post-test. (**D-E**) Whole blood haemoglobin was assessed with a HemoCue instrument and red blood cells were counted with a Nexcelom Cellometer in blood from saline-treated controls (n=9) and mice exposed to phenylhydrazine for 3 (n=9) or 5 days (n=7). Box-plots depict median and IQR. Whiskers extend to highest and lowest values within 1.5×IQR of the 75th and 25th percentiles and values outside this range were plotted as individual points (Tukey's method). ***p<0.001 by Mann-Whitney test. ns (not significant): p > 0.05

Hepatic DDAH Function

To determine the effect of phenylhydrazine exposure on DDAH activity, we quantified the rate of citrulline production in the presence of saturating concentrations of ADMA substrate (for assay validation, see APPENDIX D, p. 312). DDAH activity was decreased in liver tissue of mice exposed to phenylhydrazine for 3 days (PHZ-3d, median [IQR]: 6.2 [5.9-7.0] nmol citrulline×mg protein^{-1}×hr^{-1} vs saline control: 7.5 [7.0-8.1] nmol citrulline × mg protein^{-1}×hr^{-1}, $p < 0.05$) and further decreased in mice treated exposed to phenylhydrazine for 5 days (PHZ-5d: 4.9 [4.5-5.3] nmol citrulline×mg protein^{-1}×hr^{-1}, $p < 0.0001$ vs saline, $p < 0.05$ vs PHZ-d3, FIG 3.12). Impaired DDAH activity corresponded to increased intracellular ADMA concentrations in the livers of mice exposed to phenylhydrazine for 3 or 5 days (saline: 131.7 [101.8-148.7] pmol/mg protein, PHZ-3d: 292.5 [260.2-342.6], $p < 0.0001$ vs saline, PHZ-d5: 592.5 [476.2-633.5], $p < 0.0001$ vs PHZ-3d, $p < 0.0001$ vs saline, FIG 3.12). These results demonstrate that phenylhydrazine-induced haemolysis is sufficient to cause hepatic DDAH1 dysfunction and local ADMA accumulation in liver tissue. Direct assessment of hepatic DDAH1 protein by Western blot is required to determine if loss of activity is associated with decreased protein levels, as observed in *P. berghei* ANKA-infected mice.

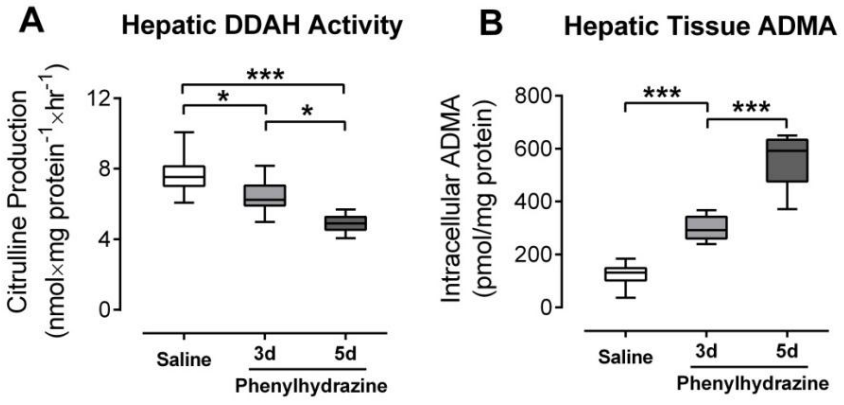


Figure 3.12 | Phenylhydrazine decreases hepatic DDAH activity and increases hepatic ADMA. (**A**) DDAH activity was assessed in liver samples collected from mice exposed to phenylhydrazine (40mg/kg) for 3 (n=9) or 5 days (n=7). Saline-treated mice (n=9) served as controls. DDAH activity was determined by quantification of citrulline production in liver homogenates spiked with saturating concentrations of ADMA substrate (2.5 mM). Citrulline production was calculated on a per-hour basis and normalized to protein content. (**B**) Intracellular hepatic ADMA was assessed by HPLC in perfused liver samples and normalized to protein content. Boxplots depict median, IQR and range. *p<0.05 ***p<0.001 by one-way ANOVA followed by Bonferroni post-test.

Plasma ADMA/Arginine Ratios

To assess whether phenylhydrazine exposure affected circulating ADMA/arginine homeostasis, we used HPLC to determine ADMA and arginine concentrations in the plasma of phenylhydrazine-treated mice. ADMA was increased after 3 days or 5 days of phenylhydrazine exposure (PHZ-3d: 0.90 [0.88-1.02] µmol/L, PHZ-5d (1.28 [1.21-1.46] µmol/L, $p < 0.001$ vs PHZ-3d) compared with saline-treated controls (0.59 [0.57-0.66] µmol/L $p < 0.0001$ vs PHZ-3d, $p < 0.0001$ vs PHZ-5d, FIG 3.13). Arginine was elevated in mice exposed to phenylhydrazine for 5 days (157.4 [109.9-191.2] µmol/L vs saline control: 98.2 [89.9-107.1] µmol/L, $p < 0.010$) but was not significantly different from control values in mice exposed to phenylhydrazine for 3 days (122.4 [103.4 -127.0], $p = 0.11$ vs saline control, FIG 3.13). Plasma ADMA/arginine ratios rose in mice receiving 3 or 5 days of phenylhydrazine exposure (PHZ-3d: 8.2 [7.2-9.0] $\times 10^{-3}$, PHZ-d5: 8.9 [7.7-11.4] $\times 10^{-3}$, saline control: 6.3 [5.6-7.3] $\times 10^{-3}$, $p < 0.05$ vs PHZ-d3, $p < 0.001$ vs PHZ-d5, FIG 3.13). These results demonstrate that phenylhydrazine exposure causes elevation of plasma ADMA concentrations to greater degree than arginine, resulting in increased ADMA/arginine ratios. Elevated ADMA/arginine ratios may be due to disproportionate release of ADMA and arginine from lysed red blood cells or impaired ADMA clearance by hepatic DDAH.

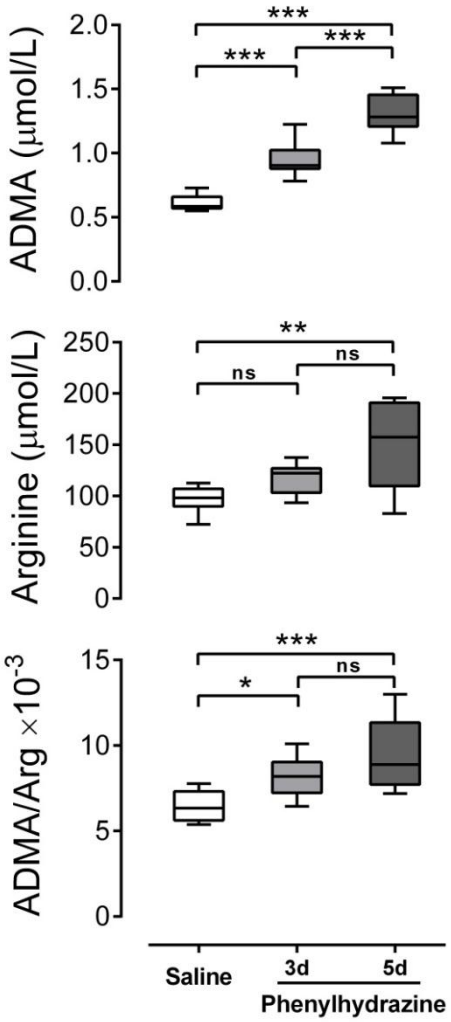


Figure 3.13 | Phenylhydrazine increases plasma ADMA and ADMA/arginine ratios. HPLC was used to determine arginine and ADMA concentrations in plasma samples from saline-treated controls (n=9) and mice exposed to phenylhydrazine for 3 (n=9) or 5 days (n=7). Box-plots depict median, IQR and range. *p < 0.05, **p < 0.01, ***p < 0.001, by one-way ANOVA followed by Bonferroni post-test. ns (not significant): p > 0.05.

3.6 Discussion

Plasma ratios of ADMA to arginine are increased in Gambian children with severe malaria and correlate with lactate, a biomarker of impaired tissue perfusion associated with increased risk of mortality from severe malaria in children (Taylor et al., 1993; Krishna et al., 1994; Waller et al., 1995; Planche et al., 2003). In a mouse model of severe malaria, we found that hepatic DDAH1 protein and enzyme activity are decreased, resulting in accumulation of intracellular ADMA in liver tissue and elevated ratios of ADMA to arginine in plasma. In uninfected mice, exposure to the haemolytic agent phenylhydrazine produced similar evidence of DDAH dysfunction, suggesting that acute malaria infection may induce DDAH1 degradation via haemolysis. These findings implicate impaired ADMA clearance by hepatic DDAH1 as one potential mechanism exacerbating disruption of ADMA/arginine homeostasis in severe malaria.

Elevation of the ADMA/arginine ratio could also result from disproportionate release of ADMA and arginine from protein break-down. Human erythrocytes contain total (free plus protein-incorporated) ADMA concentrations in the range of 47.85 ± 1.68 µmol/L, extrapolated from a concentration of 15.95 ± 0.56 µmol/L reported for hydrolysates of erythrocyte samples diluted 1:3 in water (Davids et al., 2012a). Rat erythrocytes contain a similar concentration of total ADMA, estimated to be 40.6 ± 7.2 µmol/L (Billecke, 2006). Extrapolating from a total amino acid content of 13.56 mol/L in human erythrocytes and approximately 2.5-3.0% arginine content (exact figure not given), the ratio of total ADMA to total arginine in erythrocytes, including protein-incorporated residues, is on the order of 1.0-1.5 $\times 10^{-4}$ (Davids et al., 2012a). This value is more than an order of magnitude below the ADMA/arginine ratios we observed in the plasma of healthy Gambian children (6.7 [5.8-8.2] $\times 10^{-3}$) and uninfected mice (7.1 [5.9-8.8] $\times 10^{-3}$). Following haemolysis, erythrocyte proteins are exposed to proteolysis. If arginine and ADMA were released in proportion to the total amounts incorporated in erythrocyte proteins, then haemolysis and associated protein break-down would be expected to introduce less ADMA relative to arginine than is already present in plasma, driving plasma ADMA/arginine ratios down.

However, incubation of human erythrocyte lysates *ex vivo* has been shown to release a much greater percentage of total ADMA content (27.4 ± 1.0%) compared to arginine (~0.003%, exact figure not provided) (Davids et al., 2012a). The magnitude of this discrepancy in release rates suggest that the ratio of ADMA to arginine released from break-down of erythrocyte proteins could in fact be as high as 1:1, although these experiments must be repeated to specifically quantify this ratio. These results suggest that break-down of erythrocyte proteins following haemolysis would contribute disproportionately high amounts of ADMA relative to arginine and could contribute to elevation of the ADMA/arginine ratio. In phenylhydrazine-exposed mice, we found elevation of both ADMA and arginine, with a disproportionate rise in ADMA contributing to elevation of the ADMA/arginine ratio. This finding may be explained by preferential degradation of methylated protein residues following haemolysis. We also observed impaired hepatic DDAH activity and accumulation of intracellular hepatic ADMA in phenylhydrazine-exposed mice, suggesting that haemolysis could simultaneously increase ADMA release from erythrocyte proteins and inhibit ADMA clearance by hepatic DDAH.

Further studies are necessary to determine the relative importance of hepatic DDAH dysfunction and direct release of ADMA from breakdown of erythrocyte proteins released during haemolysis. ADMA/arginine ratios should be explicitly assessed in intact erythrocytes and following incubation of lysates. Conversely, if oxidative stress causes DDAH1 degradation, the role of DDAH dysfunction could be isolated using models of oxidative stress that do not induce haemolysis. Hepatic DDAH1 is largely expressed in endothelial cells (Hu et al., 2009), leading us to hypothesize that over-expression of the NADPH oxidase subunit Nox2 in endothelial cells (Bendall et al., 2007) would result in degradation of hepatic DDAH1 protein and impaired ADMA clearance in a mouse model. If this hypothesis is correct, this system would allow us to examine the effect of oxidative stress-induced hepatic DDAH dysfunction on plasma ADMA/arginine ratios in the absence of haemolysis. The relevance of DDAH dysfunction to circulating ADMA/arginine ratios could also be explored with the use of interventional approaches that successfully protect DDAH1 protein during malaria infection or

phenylhydrazine exposure. A recent study in rats showed that sustained treatment with the farnesoid X receptor agonist GW4064 resulted in induction of hepatic DDAH1 transcription, decreased plasma ADMA concentrations and increased plasma arginine concentrations (Hu et al., 2006). Farnesoid X receptor activation and transgenic DDAH1 over-expression should be considered as potential approaches to improving DDAH function during haemolytic insult. In addition to hepatic DDAH1 dysfunction and haemolysis-associated protein breakdown, renal insufficiency (Vallance et al., 1992) or increased methylation of protein-bound arginine residues by *Plasmodium* parasites (Fan et al., 2009) must also be considered as potential contributors to elevated ADMA/arginine ratios.

Elevation of ADMA relative to arginine favours NOS inhibition because ADMA competes with arginine for the NOS active site (Cardounel et al., 2007). ADMA also competes with arginine for cellular uptake, which could limit arginine availability for NO synthesis (Closs et al., 1997). Inhibition of NO by ADMA could contribute to impaired vasoregulation during severe malaria. In Indonesian adults with severe malaria, plasma ADMA concentrations correlated inversely with reactive hyperaemia responses following brachial artery occlusion (Yeo et al., 2007). Plasma ADMA has also been shown to correlate inversely with endothelial function in hypercholesterolaemia (Böger et al., 1998) and hypertension (Perticone et al., 2005). Direct infusion of ADMA in healthy volunteers decreases plasma cGMP, increases mean arterial blood pressure and increases systemic vascular resistance (Vallance et al., 1992; Achan et al., 2003; Kielstein et al., 2004). Plasma cGMP was decreased by infusion of ADMA at a dose of 0.5 mg/kg over a 40-minute infusion, which raised plasma ADMA from 1.02 ± 0.26 µmol/L to 4.17 ± 0.99 µmol/L (Kielstein et al., 2004). A 6-fold higher dose (resulting in plasma concentrations of 15.66 ± 4.29 µmol/L) was required to increase mean arterial blood pressure, increase systemic vascular resistance and decrease renal plasma flow (Vallance et al., 1992; Achan et al., 2003; Kielstein et al., 2004). However, heterozygous knock-out of DDAH1 only raised plasma and tissue ADMA by approximately 20% in mice, yet resulted in elevation of mean arterial blood pressure and impaired relaxation of *ex vivo* aortic rings (Leiper et al., 2007).

These results indicate a direct role of DDAH in regulating endothelial NO synthesis, possibly independent of plasma ADMA concentrations.

Elevation of ADMA/arginine ratios could also promote loss of endothelial barrier integrity during severe malaria infection. In porcine aortic endothelial cell cultures, ADMA increased permeability of the endothelial cell layer by limiting NO-mediated activation of protein kinase G (PKG) and the GTPase Rac1, which promotes stability of endothelial tight junctions (Wojciak-Stothard et al., 2009). Inhibition of NO also increases exocytosis of angiopoietin-2 (Ang-2), which sensitizes the endothelium to inflammatory cytokines and destabilizes the endothelial barrier by antagonizing angiopoietin-1/Tie2 signalling (Matsushita et al., 2003; Fiedler et al., 2006; Mammoto et al., 2007). Angiopoietin-2 is elevated in Indonesian adults (Yeo et al., 2008b) and Tanzanian children with severe malaria (Weinberg et al., 2014). In Tanzanian children with severe malaria, plasma angiopoietin-2 was inversely correlated with plasma arginine/ADMA ratios (equivalent to a positive correlation with ADMA/arginine ratios) (Weinberg et al., 2014). This observation suggests that NOS inhibition due to disrupted ADMA/arginine homeostasis may promote Ang-2 exocytosis. Activation of Rac1 and inhibition of Ang-2 exocytosis by exogenous NO may have contributed to improved blood-brain barrier integrity previously observed in *P. berghei* ANKA-infected mice treated with an NO-donor (Gramaglia et al., 2006; Cabrales et al., 2011) or inhaled NO (Serghides et al., 2011). By inhibiting NO synthesis, ADMA accumulation relative to arginine could also promote adhesion molecule expression (De Caterina et al., 1995), cytoadherence of parasitized red blood cells (Serirom et al., 2003) and pro-inflammatory cytokine signalling (Iuvone et al., 1996).

3.7 Conclusion

Taken together, these findings suggest that disruption of ADMA/arginine homeostasis could contribute to severe malaria pathogenesis by inhibiting NO synthesis. We have identified hepatic DDAH1 dysfunction as a potential mechanism contributing to elevation of plasma

ADMA/arginine ratios in severe malaria. Therapies that increase *DDAH1* expression or protect DDAH1 protein from degradation may be beneficial for the treatment of severe malaria or other disease states characterized by ADMA accumulation.

3.8 Materials and Methods

Clinical Study Procedures

Human Subjects, Enrolment and Sample Collection

Patient enrolment and sample collection were previously conducted following ethical review and approval by the Gambian Government/MRC Joint Ethics Committee and the Ethics Committee of the London School of Hygiene & Tropical Medicine (SCC 670, SCC 1002, SCC 1003, SCC 1077 & SCC 1113 [healthy controls]) (Walther et al., 2009). Analysis of plasma samples and clinical data at the National Institutes of Health was exempted from further ethical review by the NIH Office of Subjects Research (Exemption #5161). Children with severe malaria or uncomplicated malaria were enrolled at health centres in a peri-urban area around Fajara, The Gambia. Enrolment sites included the Royal Victoria Teaching Hospital, the Brikama Health Centre, the MRC Fajara Gate Clinic and the Jammeh Foundation for Peace Hospital in Serekunda. Written consent was obtained from the parents or guardians for all children enrolled in this study and standard medical care was provided to patients that chose not to enrol in the study.

Acute uncomplicated malaria was defined as asexual *P. falciparum* parasitaemia of >5000 parasites/μl detected by slide microscopy with an episode of fever (temperature >37.5°C) within the previous 48 hrs and the absence of severe criteria. Acute severe malaria was defined as parasitaemia of >5000 parasites/μl, a history of fever and one or more of the following: severe anaemia (Hb < 6g/dl, which is the threshold set by the Gambian government where a child should receive blood transfusion), severe acidosis (serum lactate >7 mmol/L), cerebral malaria (Blantyre coma score ≤2 persisting after correction of hypoglycaemia or hypovolaemia with the coma lasting at least for 2 hrs), and/or severe prostration (inability to sit unsupported in

children > 6 months or inability to suck in children < 6 months). Patients with severe malaria were admitted and treated with quinine, and uncomplicated malaria was treated with chloroquine plus sulfadoxine-pyrimethamine according to Gambian Government Treatment Guidelines (Guidelines for the Management of Malaria, 2005).

Ninety-six children with severe malaria and 102 children with uncomplicated malaria were enrolled during the 2005-2008 malaria seasons. Approximately 4 ml of blood was collected in heparinized vacutainers (Becton Dickenson, Franklin Lakes, NJ, USA) at the time of initial presentation and at a follow-up visit 28 days after initial assessment,). Among severe malaria patients, there were 3 deaths and 65 completed follow-up visits, of which 47 archived plasma samples were available for analysis. Follow-up assessments were completed on 85 patients with uncomplicated malaria, of which 65 archived plasma samples were available for analysis. Blood was also drawn from 31 afebrile, aparasitaemic Gambian children of similar age who served as healthy controls.

Clinical Laboratory Analysis

P. falciparum parasitaemia was determined by bright-field microscopy of Giemsa-stained blood smears. 50 fields were counted at high power. Full blood counts were obtained with a Medonic^{TM} instrument (Clinical Diagnostics solutions, Inc., Fort Lauderdale, FL, USA). Lactate was measured with a handheld Lactate Pro device (Arkray, Edina, MN, USA). Soluble VCAM (sVCAM) was determined in plasma by ELISA (R&D Systems, Minneapolis, MN, USA) according to the manufacturer's instructions. Laboratory staff members were unaware of clinical status of the subjects.

Animal Model Procedures

Animals, Housing and Diet

Animal experiments were performed at the National Institutes of Health (NIAID Comparative Medicine Branch) using protocols approved by the NIH ACUC under the

identification ASP LMVR 18E. 10-week-old C57BL/6J male mice were obtained from the Jackson Laboratory (Bar Harbor, ME, USA) and 10-week-old Swiss Webster carriers for parasite expansion were obtained from Charles River Laboratories (Frederick, MD, USA). Mouse model experiments were replicated at the Wellcome Trust Sanger Institute under personal (PIL 80/12137) and project licenses (PPL 80/2158) issued by the UK Home Office in accordance with the Animals (Scientific Procedures) Act of 1986. Protocols reviewed by the Wellcome Trust Sanger Institute ethics committee. For this experiment, 10-week-old male C57BL/6J experimental mice and Tuck Ordinary outbred mice carriers for parasite expansion were obtained from Harlan Laboratories (London, UK). Mice were housed in temperature-controlled cages maintained at 20-22ºC with a 12hr/12hr light-dark cycle and free access to water and autoclaved rodent feed pellets (Teklad Global 18% Protein Extruded Rodent Diet, 2018SX, Harlan Laboratories). Experimental groups were assigned in an alternating manner such that every experimental group was represented in each cage of communally-housed littermates.

Parasites, Inoculations and Parasitaemia Assessment

P. berghei ANKA parasites, clone RMgm-29 (Janse et al., 2006), were expanded from frozen stocks by intraperitoneal injection of carrier mice. After four days of parasite expansion, whole blood was obtained from the abdominal inferior vena cava under terminal anaesthesia. Cohorts of experimental mice were infected by intraperitoneal injection of 1×10^6 infected erythrocytes diluted in 200 µl of PBS (Lonza, Walkersville, MD, USA). This protocol results in blood-stage infection, bypassing the liver stage of the parasite's life-cycle. Blood-stage parasitaemia was monitored by examination of Giemsa-stained blood smears obtained by tail tip bleed. Six days after i.p. inoculation with blood-stage *P. berghei* ANKA, C57BL/6 mice exhibited peripheral blood parasitaemia of 7.41% (IQR: 5.23-9.68).

Phenylhydrazine Administration and Assessment of Anaemia

Male, 10-week-old C57BL/6J mice were exposed to phenylhydrazine (40mg/kg/d) by once-daily intraperitoneal injections for 3 or 5 days. Treated mice were culled 24 hr after the final injection for collection of blood and tissue samples. Phenylhydrazine HCl (Sigma-Aldrich, St. Louis, MO, USA) was diluted in sterile 0.9% saline solution (Hospira, Lake Forest, IL, USA) and neutralized to pH 7.4 with 3M NaOH (Sigma-Aldrich, St. Louis, MO, USA). Phenylhydrazine solution was sterilized with a 0.22µm syringe-tip filtration, aliquoted in sterile cryovials and stored at -80°C until use. Haemoglobin was measured with an Hb201+ analyzer (HemoCue, Brea, CA, USA) and red blood cells were counted with a Cellometer AutoT4 counter (Nexcelom, Lawrence, MA, USA).

Blood and Tissue Sample Collection

On day 6 post-inoculation, terminal anaesthesia was administered by intraperitoneal injection of 250mg/kg ketamine and 25mg/kg xylazine. The abdominal cavity was accessed and 700µl of blood was drawn from the abdominal inferior vena cava with a 25G×5/8" needle (BD, Franklin Lakes, NJ, USA). To prevent coagulation, the syringe contained 60 µl DPBS with K_3EDTA (final concentration of 1.6mg/ml K_3EDTA after mixed with 700 µl of blood). Plasma was separated from erythrocytes by immediate centrifugation at 3,000*g* for 7 minutes at 4°C, snap-frozen on dry ice, and stored at -80°C until analysis. Remaining blood was removed from the vascular compartment by transcardial perfusion with 20 ml 1×PBS. Lung, liver, kidney, spleen, aorta, heart and whole brain were dissected, removed, snap-frozen on dry ice and stored at -80ºC until analysis.

Biochemical and Molecular Assays

Solid Phase Extraction of Plasma Samples for ADMA Analysis

Plasma was thawed and 10µl was diluted in 35µl 1×PBS (Lonza, Walkersville, MD, USA) containing N^G-monoethyl-L-arginine (MEA) (Enzo Life Sciences, Farmingdale, NY,

USA) as an internal standard. Oasis MCX 96-well µElution Plates (Waters Corporation, Milford, MA, USA) were conditioned with elution buffer prepared from ultrapure water (Milli-Q Synthesis system, Millipore Corporation, Billerica, MA, USA), HPLC-grade methanol (Fisher Scientific, Pittsburgh, PA, USA) and 28% ammonium hydroxide (Sigma-Aldrich, St. Louis, MO, USA) in a ratio of 5:4:1 H_2O:MeOH:NH_4OH and equilibrated with methanol. Samples were loaded, washed with 0.1 N HCl (Sigma-Aldrich, St. Louis, MO, USA) followed by methanol, eluted with elution buffer, dried by vacuum centrifugation at 45°C and reconstituted in 10µl ultrapure water.

Determination of Arginine and ADMA in Human Plasma

Human samples were extracted as described above and mixed 1:1 with a derivatization reagent containing 7.46 mM ortho-phthaldialdehyde (Sigma-Aldrich, St. Louis, MO, USA) and 27.5 mM 3-mercaptopropionic acid (Sigma-Aldrich, St. Louis, MO, USA) in 200 mM potassium tetraborate (Sigma-Aldrich, St. Louis, MO, USA), pH 9.4, and 3 µl was injected onto a 2×100 mm C18(2) column with 100 Å pores and 5 µm particles (Phenomenex, Torrance, CA, USA). Chromatography was performed isocratically at a flow-rate of 0.3 ml/min. The mobile phase consisted of 25 mM ammonium phosphate (Sigma-Aldrich, St. Louis, MO, USA) and 9% acetonitrile (Fisher Scientific, Pittsburgh, PA, USA) in ultrapure water from a Milli-Q Synthesis system (EMD Millipore, Billerica, MA, USA). Derivatized analytes were detected by on-line fluorescence detection using excitation and emission wavelengths of 340 nm and 455nm respectively. Following elution of arginine, sensitivity was increased 32-fold for the detection of ADMA by increasing the gain on the fluorescence detector. Following elution of ADMA, sensitivity was returned to normal and a second solvent containing 50 % acetonitrile and 50 % ultrapure water was introduced at 12 % to accelerate elution of the MEA internal standard. The column was then washed with 100 % solvent B for 5 minutes and re-equilibrated prior to injection of the following sample. Chemstation revision B was used for data acquisition and analysis. Analyte peaks were integrated and quantified by comparison to the internal standard.

This assay, used only for analysis of plasma from Gambian children, is an early iteration of the HPLC assay described in APPENDIX C, p. 288. Inter- and inter-day variation was < 5% for repeat analysis of human samples using this assay.

Determination of Arginine and ADMA in Mouse Plasma

Mouse plasma samples were extracted as described above and analyzed using the fully validated HPLC assay described in APPENDIX C, p. 288. These analyses were performed on a low-flow Agilent 1100 series HPLC instrument and Agilent Chemstation OpenLab CDS revision C.01.03 was used to control the instrument and acquire data. The autosampler was programmed to draw 1.7µl of ortho-phthaldialdehyde (OPA) derivatization solution and 1.7µl of the current sample in the sequence, mix the contents in the needle for 30s and inject the derivatized sample onto the column. OPA derivatization reagent contained 7.46 mM ortho-phthaldialdehyde (Sigma-Aldrich, St. Louis, MO, USA) and 27.5 mM 3-mercaptopropionic acid (Sigma-Aldrich, St. Louis, MO, USA) in 200 mM potassium tetraborate (Sigma-Aldrich, St. Louis, MO, USA), pH 9.4. Chromatography was performed on a 1×100 mm C18(2) column with 3 µm particles and 100 Å pore size (Phenomenex, Torrance, CA, USA) at a flow-rate of 90 µl/min. Solvent A consisted of 25 mM sodium phosphate and 5% acetonitrile in ultrapure water and solvent B consisted of 50% acetonitrile in ultrapure water. Separations were accomplished by 20 min of isocratic conditions followed by a gradient from 0%B at 20 min to 18%B at 42 min. The column was then washed with 100 % solvent B for 5 minutes and re-equilibrated for 13 minutes prior to injection of the following sample. The column was maintained at 35°C for all runs. Online fluorescence was measured at excitation and emission wavelengths of 340nm and 455nm, respectively. The fluorescence detector's photomultiplier tube (PMT) gain was set to 11 for initial normal-sensitivity analysis. At 20min, PMT gain was switched to 16 for the detection of low-concentration analytes (L-NMMA, ADMA, and SDMA). At 37 minutes PMT gain was switched back to 11 for detection of the MEA internal standard with normal

sensitivity. Chemstation OpenLab CDS software version C.01.03 was used for peak integration. Analyte peaks were quantified by comparison to the internal standard (MEA).

Quantitative RT-PCR

RNA was extracted from Trizol preserved liver tissue using Qiagen RNeasy kit (Qiagen, Valencia, CA, USA). RNA was reverse transcribed in the presence or absence of reverse transcriptase using Invitrogen Superscript® VILO™ MasterMix (Life Technologies, Carlsbad, CA, USA), followed by quantitative PCR using SensiMix SYBR® Green PCR Mix (Bioline, Taunton, MA, USA). Primer pairs 5'-CATGTCTTGCTGCACCGAAC-3' and 5'-GACCTTTGCGCTTTCTGG-3' were used to amplify DDAH1. Mouse GAPDH was simultaneously amplified as an internal control, using primer sequences: GAPDH: sense, 5′-CATCACCATCTTCCAGGAGCG-3′; antisense, 5′-GAGGGGCCATCCACAGTCTTC-3′ (Bivalacqua et al., 2007).

Western Blot

Liver samples were thawed and homogenized in 1X PBS containing protease inhibitor cocktail (Roche Applied Sciences, Indianapolis, IN) using a Lab Gen 7 series hand held homogenizer (Cole Parmer, Vernon Hills, IL, USA). Homogenates were centrifuged for 5 min at 16,100*g* and 4°C and supernatants were removed and placed on ice. Protein concentrations were determined with a Pierce BCA Protein Assay Kit (Thermo Scientific, Sunnyvale, CA, USA) according to the manufacturer's instructions. Protein homogenates (50 μg) were mixed 1:1 with 2X SDS sample buffer (Life Technologies, Carlsbad, CA, USA) and heated at 95° C for 10 min. Proteins were separated on a 4-12 % SDS-polyacrylamide gel (Life Technologies, Carlsbad, CA, USA) at a constant voltage (90-100 V) and transferred to nitrocellulose membrane with an iBlot transfer apparatus (20V for 8min) (Life Technologies, Carlsbad, CA, USA). The membrane was incubated for 1h in a blocking buffer consisting of 5% nonfat dry

milk and 0.1 % Tween 20 in 1×PBS (Lonza, Walkersville, MD, USA). The membrane was then incubated overnight in blocking buffer containing 1:3000 anti- DDAH1 (Sigma-Aldrich, St. Louis, MO, USA) at 4° C with constant rocking. After washing with PBS containing 0.1 % Tween-20, the membrane was incubated for 1h in blocking buffer containing 1:10,000 anti-rabbit-HRP secondary antibody (GE Healthcare UK Ltd.). The membrane was then washed with 1×PBS, treated with West Femto substrate (Pierce) and visualized with CL-Xposure blue X-ray film (Thermo Scientific, Sunnyvale, CA, USA). Membranes were stripped and re-probed with an anti-ß actin-HRP (Abcam, Cambridge, MA, USA) antibody as a control.

DDAH Enzyme Activity Assay

Frozen liver samples were homogenized in 8 µl 1×PBS (Lonza, Walkersville, MD, USA) per mg wet weight of tissue with a Lab Gen 7 series hand held homogenizer (Cole Parmer, Vernon Hills, IL, USA). Homogenized samples were centrifuged for 5 min at 16,100*g* and 4°C to remove insoluble material. Supernatants were diluted 1:5 in 1×PBS spiked with ADMA (Cayman Chemical, Ann Arbor, MI, USA) for a final concentration of 2.5 mM ADMA. Spiked homogenates were mixed and sampled immediately (0 hr time point) and after 2 hr at 37°C. At each time point, citrulline was quantified by mixing 15 µl of homogenate with 15µl of 2M perchloric acid containing 25 µmol/L MEA as an internal standard. Samples were centrifuged for 5min at 16,100*g* and 4°C to remove precipitate, and 10 µl of the supernatant was neutralized with 5µl 1.5M potassium carbonate (Sigma-Aldrich, St. Louis, MO, USA) in a fresh tube. Neutralized samples were further diluted 1:2 in ultrapure water and centrifuged to remove potassium perchlorate precipitate. HPLC was performed on a low-flow Agilent 1100 series instrument and Agilent Chemstation OpenLab CDS revision C.01.03 was used to control the instrument and acquire data. Samples were derivatized directly prior to analysis by programming the autosampler to draw 2µl of derivatization reagent, 2µl of sample, mix for 30s and inject. The derivatization reagent contained final concentrations of 1.5mg/ml (11.2 mM)

ortho-phthaldialdehyde (Sigma-Aldrich, St. Louis, MO, USA) and 41.3mM 3-mercaptopropionic acid (Sigma-Aldrich, St. Louis, MO, USA) diluted in 200mM potassium tetraborate solution (pH 9.4). Citrulline and the MEA internal standard were separated with a 1×100 mm C18(2) column with 3 μm particles and 100Å pore size (Phenomenex, Torrance, CA, USA). Solvent A was composed of 0.1M sodium acetate (Fisher Scientific, Pittsburgh, PA, USA), 9 % v/v methanol (Fisher Scientific, Pittsburgh, PA, USA) and 0.5 % v/v tetrahydrofuran (Sigma-Aldrich, St. Louis, MO, USA) in ultrapure water (Milli-Q Synthesis system, Millipore Corporation, Billerica, MA, USA) with pH adjusted to 8.3 with 3M NaOH (Sigma-Aldrich, St. Louis, MO, USA). Organic mobile phase (Solvent B) was HPLC-grade methanol (Fisher Scientific, Pittsburgh, PA, USA) and separation of analytes was accomplished with a gradient from 0% solvent B to 25 % solvent B over 20min at a flow-rate of 70 μl/min. The column was then washed with 100 solvent B for 5 min and re-equilibrated with 100% Solvent A for 20 minutes. The column was maintained at 40°C for the duration of the run. Citrulline and the MEA internal standard were quantified by fluorescence detection using excitation and emission wavelengths of 340 nm and 455 nm respectively. Citrulline production was calculated by taking the difference of starting (0 hr) and ending (2 hr) concentrations, dividing by the 2 hr time interval and normalizing to protein content as quantified by BCA colourimetric assay (Thermo Scientific, Sunnyvale, CA, USA) according to the manufacturer's instructions.

Determination of Tissue ADMA

Frozen liver samples were homogenized in 8 μl 1×PBS per mg wet weight of tissue with a Lab Gen 7 series hand held homogenizer (Cole Parmer, Vernon Hills, IL, USA). Homogenized samples were centrifuged for 5 min at 16,100 × G and 4°C to remove insoluble material. An aliquot of supernatant was stored for protein quantification and a second was precipitated by mixing 1:1 with 2M perchloric acid (Fisher Scientific, Pittsburgh, PA, USA) containing N^G-monoethyl-L-arginine (MEA) (Enzo Life Sciences, Farmingdale, NY, USA) as

an internal standard. Precipitated samples were centrifuged for 5 min at 16,100*g* and 4°C and the resulting supernatant was removed and neutralized with 4 volumes of 0.5M Na_2HPO_4 (Acros Organics, Geel, Belgium). Neutralized samples were extracted with Oasis MCX 96-well μElution Plates (Waters Corporation, Milford, MA, USA) and analyzed with HPLC conditions as described above for determination of concentrations of arginine and ADMA in mouse plasma. Measured ADMA concentrations were normalized to soluble protein as quantified by BCA colourimetric assay (Thermo Scientific, Sunnyvale, CA, USA) according to the manufacturer's instructions.

Statistical Analyses

Data are expressed as median and inter-quartile range (IQR). Statistical analyses were performed with GraphPad Prism 6.02 software and $p < 0.05$ was considered significant. Mann-Whitney test was used to compare median values between healthy controls and children with uncomplicated or severe malaria. Wilcoxon matched-pairs signed rank test was used to compare median acute and recovery values in children with uncomplicated or severe malaria. Spearman correlations were used to determine associations between clinical laboratory values. Mann-Whitney test was used to compare values between infected mice and uninfected controls.

Acknowledgements

I am indebted to the patients and families who participated in this study. I would like to acknowledge the logistical support and patient care provided by the nurses, field workers, laboratory assistants, drivers and administrative staff of The MRC Unit, The Gambia, the Royal Victoria Teaching Hospital, the Brikama Health Centre, the MRC Fajara Gate Clinic and the Jammeh Foundation for Peace Hospital in Serekunda. I am grateful to Lamin Manneh who supervised data collection. Michael Walther (NIAID/NIH) and David Conway (London School of Hygiene and Tropical Medicine) organized the clinical study of Gambian children with

severe malaria in collaboration with the MRC Unit, The Gambia (Joseph Okebe, Augustine Ebonyi, Madi Njie, Simon Correa and Shamanthi Jayasooriya contributed). Glenn Nardone (NIAID/NIH) performed HPLC analysis of arginine and ADMA in plasma samples from Gambian children. Allison Ikeda performed ELISA for sVCAM. Jessica Chertow (NIAID/NIH) performed DDAH1 western blot, performed qRT-PCR, assisted with blood and tissue collection for selected experiments, assisted with the DDAH activity assay and assisted with solid-phase extraction of mouse plasma and tissue samples for ADMA analysis. Funding to support patient enrolment and sample collection was provided by the MRC Unit, The Gambia. Biochemical analyses of clinical samples and animal model experiments were funded by the NIAID Division of Intramural Research and the Wellcome Trust (grant WT098051).

CHAPTER 4.

Tetrahydrobiopterin Depletion

We hypothesized that malaria infection leads to depletion of tetrahydrobiopterin (BH4), an essential cofactor required for NO production by nitric oxide synthase (NOS). As determined by HPLC, BH4 was increased in aorta and liver tissue, but low in plasma, red blood cells and brain tissue of C57BL/6 mice 6 days post-inoculation with Plasmodium berghei ANKA. 7,8-dihydrobiopterin (7,8-BH2) is the major product of BH4 oxidation. The ratio of BH4 to 7,8-BH2 was decreased in plasma, erythrocytes and brain tissue, suggesting that oxidation may contribute to BH4 depletion. Since BH4 does not easily cross the plasma membrane, we administered sepiapterin, which is taken up and sequentially converted to 7,8-BH2 and BH4 by sepiapterin reductase (SR) and dihydrofolate reductase (DHFR), respectively. Intermittent intraperitoneal injection of sepiapterin improved BH4 concentrations in the red blood cells, brain and aorta of infected mice, indicating that BH4 recycling pathways in these tissues remain active despite P. berghei ANKA infection. Increased BH4 availability in sepiapterin treated mice did not improve whole blood nitrite, a biomarker of NO synthesis. Low arginine may have been limiting. In summary, we have shown that sepiapterin treatment improves BH4 availability in erythrocyte, brain and aorta in P. berghei ANKA-infected mice.

4.1 Introduction

(*6R*)-5,6,7,8-Tetrahydrobiopterin (BH4) is required for synthesis of NO by nitric oxide synthase (NOS) (Kwon et al., 1989; Tayeh and Marletta, 1989). BH4 is synthesized from guanosine-5'-triphosphate (GTP) by GTP cyclohydrolase (GTPCH), 6-pyruvoyl tetrahydrobiopterin synthase (PTPS) and sepiapterin reductase (SR) (Thony et al., 2000) (FIG 4.1). In mammalian cells, GTPCH-regulated conversion of GTP to 7,8-dihydroneopterin triphosphate is the rate-limiting step in this pathway (Tatham et al., 2009). As a NOS cofactor, BH4 performs both structural and biochemical functions. Structurally, BH4 stabilizes the active NOS homodimer (Baek et al., 1993; Klatt et al., 1995) and induces conformational changes in NOS that promote catalytic activity (Crane et al., 1998). Biochemically, the donation of an electron by BH4 to produce a transient $BH4^{\bullet +}$ radical is required for the oxidation of arginine to citrulline (Hurshman et al., 1999; Wei et al., 2001, 2003) and formation of a ferrous iron-NO

complex at the NOS haem catalytic centre (Stuehr et al., 1991; Daff, 2010). In the final step of NO synthesis, $BH4^{\bullet+}$ recaptures an electron from this ferrous iron-NO complex, restoring BH4 to its fully-reduced state and releasing NO (Wei et al., 2003, 2008).

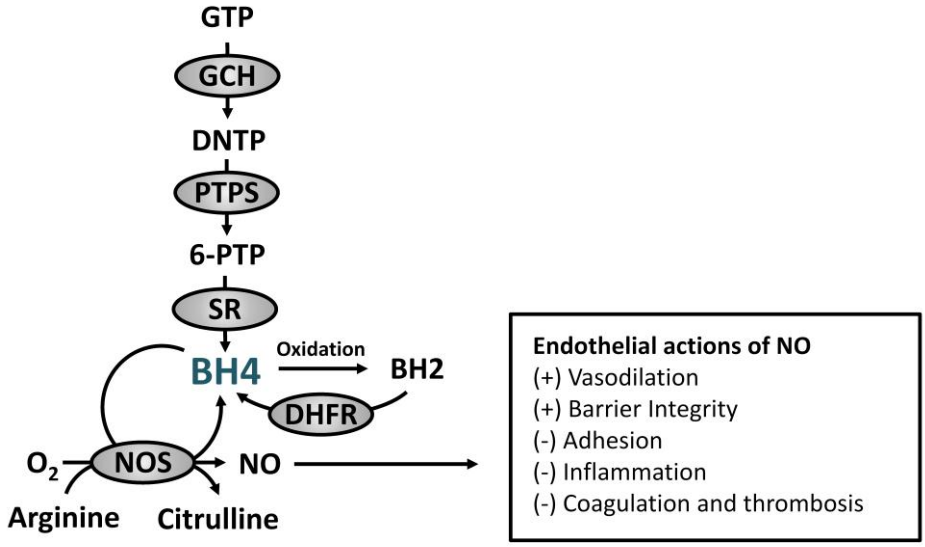


Figure 4.1 | Tetrahydrobiopterin synthesis and recycling pathways. GTP: Guanosine triphosphate, GTPCH: GTP cyclohydrolase, DNTP: dihydroneopterin triphosphate, PTPS: pyruvoyl tetrahydropterin synthase, 6-PTP: 6-pyruvoyl-tetrahydropterin, SR: sepiapterin reductase, BH4: tetrahydrobiopterin, 7,8-BH2: 7,8-dihydrobiopterin, DHFR: dihydrofolate reductase, NOS: nitric oxide synthase, NO: nitric oxide

When BH4 is depleted, NOS is unable to oxidize arginine to produce NO and instead releases activated oxygen directly as superoxide (O_2^-) (Pou et al., 1992; Vasquez-Vivar et al., 1998; Xia et al., 1998; Vasquez-Vivar et al., 2002). This state of impaired NO synthesis and increased superoxide production is termed NOS uncoupling. The most abundant product of BH4 oxidation at physiological pH is 7,8-dihydrobiopterin (7,8-BH2), which competes with BH4 for the NOS binding site (Crabtree et al., 2008). 7,8-BH2 is catalytically-inactive and displacement of BH4 by 7,8-BH2 results in NOS uncoupling (Vasquez-Vivar et al., 2002). Dihydrofolate reductase (DHFR) is the enzyme responsible for recycling 7,8-BH2 back to catalytically-active BH4 (Curtius et al., 1985) (FIG 4.1). DHFR inhibition with methotrexate or by siRNA knock-down induces NOS uncoupling by decreasing the ratio of BH4 to 7,8-BH2 without affecting

total biopterin concentrations (Crabtree et al., 2009a; Sugiyama et al., 2009). In comparison, GTPCH knock-down induces NOS uncoupling by decreasing cellular concentrations of both BH4 and 7,8-BH2 without altering the ratio between them (Crabtree et al., 2009a; b). These findings imply that NOS uncoupling is determined by BH4 stoichiometry relative to both 7,8-BH2 and NOS protein. This interpretation is supported by the observation that concomitant knock-down of DHFR and GTPCH induces greater superoxide production than knock-down of either gene alone (Crabtree et al., 2009a). Furthermore, in a study of patients with coronary artery disease, both tissue BH4 concentrations and BH4 to 7,8-BH2 ratios were correlated with acetylcholine-mediated vasodilation and were inversely correlated with and superoxide production (Antoniades et al., 2007).

In addition to these effects on NOS biochemistry, DHFR-mediated recycling of 7,8-BH2 to BH4 may also play a key role in BH4 transport. In a series of studies in mice, tissue uptake of BH4 was shown to be sensitive to DHFR inhibition and injection of mice with the 6S enantiomer of BH4 results in tissue accumulation of primarily 6R-BH4 (Sawabe et al., 2004). These findings suggest that the primary mechanism of BH4 transport across the plasma membrane is via oxidation to 7,8-BH2, an achiral compound, and subsequent reduction to bioactive 6R-BH4 within the cell.

In a recent intravital microscopy study, vasodilation of pial vessels following acetylcholine or NMDA stimulation was found to be impaired in *P. berghei* ANKA-infected mice (Ong et al., 2013). In this model, superfusion of BH4 improved acetylcholine- and NMDA-induced pial vasodilation in infected mice (Ong et al., 2013). This finding implies that BH4 depletion limits NO synthesis in the cerebral vasculature during malaria infection. However, BH4 bioavailability has not been adequately characterized by direct quantification in the context of severe malaria. We hypothesized that severe malaria infection would result in BH4 depletion in mice infected with *P. berghei* ANKA. We also hypothesized that BH4 bioavailability could be restored by administration of the BH4 precursor sepiapterin.

4.2 BH4 Availability in *P. berghei* ANKA-Infected Mice

Plasma

To determine whether *P. berghei* ANKA infection causes BH4 depletion in the blood compartment, we used HPLC to quantify BH4 in plasma and erythrocyte samples collected on days 2, 4 and 6 post-inoculation. A complete description of HPLC method development and validation is available in APPENDIX E, p. 319. Plasma BH4 was decreased on day 6 post-inoculation with *P. berghei* ANKA compared to uninfected controls (infected day 6 median [IQR]: 0.03 [0.02-0.05] µmol/L vs uninfected control: 0.14 [0.08-0.19] µmol/L, $p < 0.01$, FIG 4.2). Our HPLC method also allows quantitation of 7,8-dihydrobiopterin (7,8-BH2), the primary product of BH4 oxidation. 7,8-BH2 was also decreased in plasma on day 6 post-inoculation with *P. berghei* ANKA (infected day 6: 0.06 [0.05-0.08] µmol/L vs uninfected control: 0.09 [0.08-0.10] µmol/L, $p < 0.05$, FIG 4.2). BH4 was decreased to a greater degree than 7,8-BH2, resulting in a lower ratio of BH4 to 7,8-BH2 one day 6 post-inoculation (infected day 6: 0.4 [0.4-0.9] vs uninfected control: 1.4 [0.7-2.0], $p < 0.05$, FIG 4.2). This finding implies that *P. berghei* ANKA infection increases oxidation of BH4 to 7,8-BH2 in plasma.

The physiological relevance of plasma BH4 availability is not fully understood. *In vitro* (Sawabe et al., 2005a) and animal studies (Sawabe et al., 2005b, 2004) have demonstrated that cellular uptake of BH4 likely involves oxidation of BH4 to 7,8-BH2 followed by recycling of 7,8-BH2 back to BH4 in the cell. In a separate set of experiments, monolayers of rat aortic endothelial cells were shown to take up greater quantities of sepiapterin and 7,8-BH2 from the apical surface of the cell layer compared with the basolateral surface (Ohashi et al., 2011). BH4 was not tested in this experimental system, but these results suggest that plasma may provide a reservoir of BH4 and 7,8-BH2 available for cellular uptake to complement *de novo* synthesis.

In a cohort of patients with coronary artery disease undergoing bypass graft surgery, high plasma BH4 concentrations were associated with impaired acetylcholine-induced vasorelaxation in saphenous vein rings, whereas high tissue BH4 concentrations were associated with greater relaxation (Antoniades et al., 2007). These findings suggest an inverse relationship

between plasma BH4 and vascular function, but these effects may be independently driven by inflammation as opposed to functionally related (Antoniades et al., 2007). Considering this study was conducted entirely in patients with coronary artery disease, it is also unclear whether the same relationship would be found in healthy individuals or in other disease states.

Erythrocytes

BH4 in packed red blood cells was decreased on day 4 and day 6 post-inoculation with *P. berghei* ANKA) compared to uninfected controls (infected day 4: 0.11 [0.08-0.14] µmol/L, infected day 6: 0.07 [0.05-0.08] µmol/L, uninfected control: 0.22 [0.17-0.24] µmol/L, $p < 0.01$ vs infected day 4, $p < 0.0001$ vs infected day 6, FIG 4.2). 7,8-BH2 was also decreased on day 4 and day 6 post-inoculation compared to uninfected controls (infected day 4: 0.09 [0.08-0.10] µmol/L, infected day 6: 0.06 [0.05-0.07] µmol/L, uninfected control: 0.12 [0.11-.16] µmol/L, $p < 0.05$ vs day 4 infected, $p < 0.0001$ vs day 6 infected, FIG 4.2). Decreases in both BH4 and 7,8-BH2 resulted in decreased total biopterin concentrations (BH4 + 7,8-BH2) on days 4 and 6 post-inoculation (infected day 4: 0.20 [0.18-0.25] µmol/L, infected day 6: 0.13 [0.09-0.16] µmol/L, uninfected control: 0.36 [0.32-0.45] µmol/L, $p < 0.01$ vs infected day 4, $p < 0.0001$ vs infected day 6). This observation suggests that *de novo* BH4 synthesis may be impaired in erythrocytes during in *P. berghei* ANKA infection. BH4 was depleted to a greater degree than 7,8-BH2, resulting in reduced ratios of BH4 to 7,8-BH2 in erythrocytes on day 6 post-inoculation (infected day 6: 1.1 [0.9-1.2] vs uninfected control: 1.5 [1.3-1.8], $p < 0.01$, FIG 4.2). This finding implies that oxidative stress induced by *P. berghei* ANKA infection may also contribute to erythrocyte BH4 depletion by oxidizing BH4 to 7,8-BH2.

Rodent erythrocytes express GTPCH during development, though activity is much lower in fully mature erythrocytes (Tanaka et al., 1989; Kerler et al., 1990). *P. berghei* ANKA parasites preferentially infects young erythrocytes and reticulocytes (Cromer et al., 2006) and may specifically disrupt BH4 synthesis in the cell population with the highest GTPCH activity. An atypical pyruvoyl tetrahydropterin synthase enzyme is expressed by *P. falciparum* that is

capable of utilizing the BH4 biosynthesis intermediate dihydroneopterin triphosphate for folate synthesis (Dittrich et al., 2008). If *P. berghei* ANKA parasites express a similar enzyme, utilization of dihydroneopterin triphosphate for folate synthesis instead of BH4 synthesis may contribute to BH4 depletion (Dittrich et al., 2008).

It has been recently suggested that erythrocytes contain functional eNOS (Kleinbongard et al., 2006; Cortese-Krott et al., 2012; Wood et al., 2013), although others have found no evidence of erythrocyte eNOS activity (Bohmer et al., 2012). A variety of NOS inhibitors have been also been shown to reduce red blood cell deformability (Bor-Kucukatay et al., 2003; Kleinbongard et al., 2006), although the mechanism by which NO may maintain deformability has yet to be determined. Decreased deformability of both infected and uninfected red blood cells is recognized as a key feature of severe malaria pathophysiology and may contribute to impaired microvascular perfusion, insufficient oxygen delivery and acidosis in patients with severe disease (Dondorp et al., 1997; Day et al., 2000). In infected red blood cells, reduced plasma membrane deformability may be explained by insertion of parasite-derived proteins into the plasma membrane, but apparent reductions in the deformability of uninfected bystander erythrocytes have not been sufficiently explained. It is possible that impaired erythrocyte eNOS activity due to BH4 depletion may play a role. Reduced alpha-tocopherol concentrations in the plasma membrane of erythrocytes have provided evidence that blood-stage malaria parasites induce significant oxidative stress (Griffiths et al., 2001). Our observation of decreased BH4/7,8-BH2 ratios suggests that oxidation contributes to depletion of erythrocyte BH4.

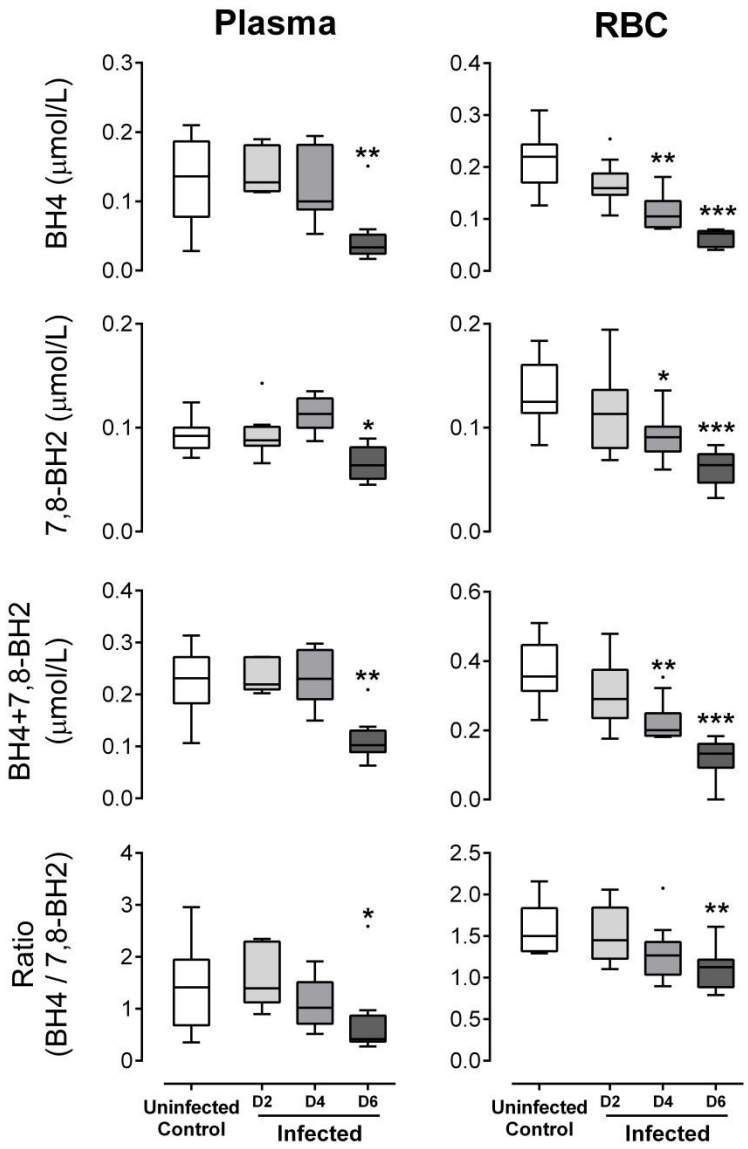


Figure 4.2 | BH4 and 7,8-BH2 concentrations in plasma and red blood cells of *P. berghei* ANKA-infected mice. Tetrahydrobiopterin (BH4) and 7,8-dihydrobiopterin (7,8-BH2) were quantified by HPLC analysis in plasma and red blood cells from P. berghei ANKA-infected mice and controls. Samples were collected from infected mice on days 2 (n=8), 4 (n=11) and 6 (n=9) post-inoculation and from uninfected controls (n=13). Box-plots depict median and IQR. Whiskers extend to highest and lowest values within 1.5×IQR of the 75th and 25th percentiles and values outside this range were plotted as individual points (Tukey's method). *p<0.05, **p<0.01, ***p<0.001 vs uninfected controls by Kruskal-Wallis test followed by Dunn's multiple comparisons test.

Aortic and Hepatic BH4

To determine the effect of *P. berghei* ANKA infection on tissue BH4 availability, we quantified BH4 in aorta and liver samples collected from *P. berghei* ANKA-infected mice 6 post-inoculation. Aortic BH4 was increased in infected mice compared with uninfected controls (infected: 49.0 [33.7-52.8] pmol/mg protein vs uninfected control: 32.5 [24.9-41.4] pmol/mg protein, $p < 0.05$ vs infected, FIG 4.3). Median aortic 7,8-BH2 concentrations were raised in infected mice, but this difference did not reach statistical significance (infected: 7.9 [6.1-10.7] pmol/mg protein vs uninfected control: 6.6 [5.1-8.1] pmol/mg protein, $p = 0.07$). The ratio of BH4 to 7,8-BH2 in aorta tissue was not changed in infected mice (infected: 5.3 [4.1-7.5] vs uninfected control: 5.1 [4.2-6.0], $p = 0.55$, FIG 4.3). *P. berghei* ANKA infection increased hepatic BH4 (infected: 80.1 [72.3-89.9] pmol/mg protein vs uninfected control: 60.2 [57.8-69.8] pmol/mg protein, $p < 0.05$) and hepatic 7,8-BH2 (infected: 6.2 [5.3-6.6] pmol/mg protein vs uninfected control: 4.8 [3.7-5.5] pmol/mg protein, $p < 0.01$), but did not alter the BH4/7,8-BH2 ratio (infected: 13.5 [11.8-15.3] vs uninfected control: 15.1 [10.9-16.5], $p = 0.54$, FIG 4.3). Pro-inflammatory signalling results in upregulation of GTP cyclohydrolase transcription and BH4 synthesis in endothelial cells (Katusic et al., 1998) and may contribute to elevated BH4 observed in aorta and liver tissue. Phenylalanine also induces of BH4 synthesis (Harada et al., 1993), suggesting that elevation of phenylalanine in *P. berghei* ANKA-infected mice could also contribute to increased BH4 in aorta and liver tissue (see FIG 2.3, p. 34).

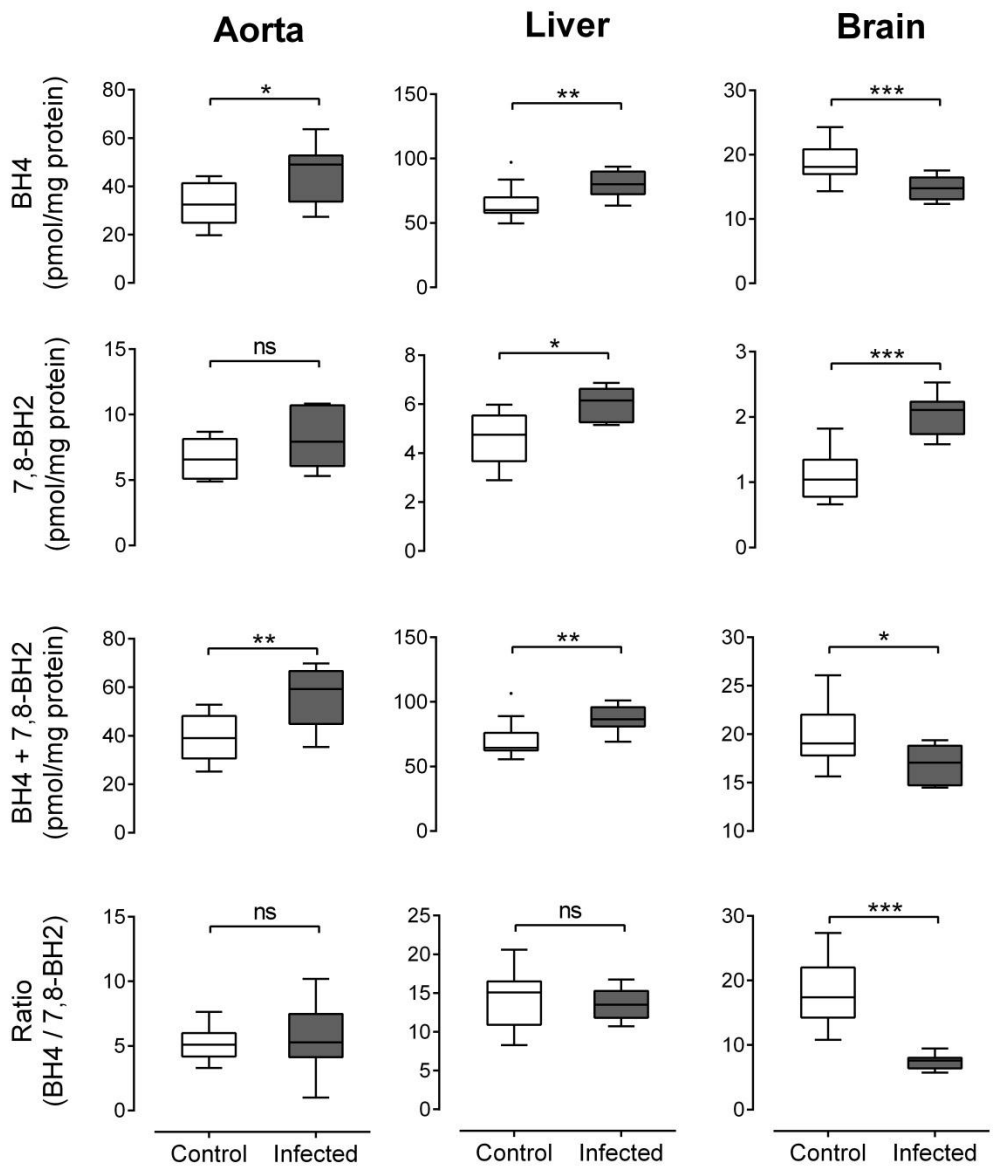


Figure 4.3 | Tissue BH4 and 7,8-BH2 concentrations in *P. berghei* ANKA-infected mice. Tetrahydrobiopterin (BH4) and 7,8-dihydrobiopterin (7,8-BH2) were quantified by HPLC analysis and normalized to soluble protein in aorta, liver and brain tissue from *P. berghei* ANKA-infected mice 6 days post-inoculation (n=9) and uninfected controls (n=13). Box-plots depict median and IQR. Whiskers extend to highest and lowest values within 1.5×IQR of the 75th and 25th percentiles and values outside this range were plotted as individual points (Tukey's method). *p<0.05, **p<0.01, ***p<0.001 vs uninfected controls by Mann-Whitney test. ns (not significant): p>0.05

BH4 in Brain Tissue

In contrast to aorta and liver tissue, BH4 was decreased in the brains of infected mice (infected: 14.8 [13.1-16.5] pmol/mg protein vs uninfected control: 18.1 [17.0-20.8] pmol/mg protein, $p < 0.001$, FIG 4.3). Brain 7,8-BH2 was increased in *P. berghei* ANKA-infected mice (infected: 2.1 [1.7-2.2] pmol/mg protein vs uninfected control: 1.0 [0.8-1.3] pmol/mg protein, $p < 0.0001$), resulting in decreased BH4/7,8-BH2 ratios (infected: 7.6 [6.4-8.0] vs uninfected control: 17.4 [14.3-22.0], $p < 0.0001$, FIG 4.3). This observed decrease in brain BH4/7,8-BH2 ratios suggest that infection may have induced a pro-oxidative environment in brain tissue but not in other tissues studied, or may reflect different biological responses to inflammatory signalling. A recent intravital microscopy study demonstrated that BH4 superfusion improves vasodilation in response to acetylcholine or NMDA stimulation of pial vessels in *P. berghei* ANKA-infected mice (Ong et al., 2013). This finding suggests that low BH4 availability limits NO synthesis in cerebral endothelial cells during in *P. berghei* ANKA infection, although BH4 could have also been depleted in neurons, astroglia or other cell-types in brain tissue.

It has recently been shown that iNOS and eNOS are both upregulated in the brains of *P. berghei* ANKA-infected mice (Ong et al., 2013). Immunohistochemical studies in brain tissue from children who died of severe malaria have also demonstrated increased inducible nitric oxide synthase (iNOS) staining (Clark et al., 2003; Maneerat et al., 2000). Elevated NOS expression in the presence of diminished BH4 promotes NOS uncoupling, as observed following knock-down of GTPCH in a high eNOS-expressing cell system (Crabtree et al., 2009b). The authors of this study suggest that absolute cellular BH4 concentrations influence NOS coupling insofar as they reflect the stoichiometry of BH4 to NOS protein. The importance of BH4:NOS stoichiometry has also been illustrated *in vivo* with the observation that transgenic over-expression of eNOS (which reduces the BH4:eNOS ratio) increases aortic and cardiac superoxide production in mice (Bendall et al., 2005). Concomitant over-expression of transgenic *GCH1*, the gene encoding GTPCH, restores BH4:NOS stoichiometry and attenuates superoxide production (Bendall et al., 2005). These findings imply that the combination of increased NOS

expression, decreased absolute concentrations of BH4 and decreased ratios of BH4 to 7,8-BH2 would promote NOS uncoupling in the brains of *P. berghei* ANKA-infected mice.

Two previous studies have been conducted on cerebrospinal fluid (CSF) from African children with cerebral malaria (Dobbie et al., 2000; Weiss et al., 1998). One study employed an analytical technique that did not allow separate analyses of BH4 and 7,8-BH2 but instead quantified concentrations of total biopterins, including BH4, 7,8-BH2 and biopterin (a product of 7,8-BH2 oxidation). This study found decreased concentrations of total biopterins in the CSF of children with deeper coma (Blantyre coma score of 0-1) compared to those with less severe impairment (Blantyre score of 4), although total CSF biopterin concentrations were not significantly different between those patients who died and those who survived (Weiss et al., 1998). A second study distinguished BH4 and 7,8-BH2 concentrations in the CSF children with cerebral malaria, but this study did not include a control group, limiting any inferences about whether cerebral malaria causes general derangements in CSF biopterin concentrations (Dobbie et al., 2000). Among children with severe malaria, this study found similar CSF BH4 concentrations in children who survived with no neurological sequelae, those who survived with sequelae and those who died (Dobbie et al., 2000). 7,8-BH2 concentrations were elevated in the CSF of children who died, which would favour NOS uncoupling (Dobbie et al., 2000). It is unclear to what degree concentrations of BH4 and 7,8-BH2 in the CSF reflect tissue levels available to cerebral eNOS and nNOS.

4.3 BH4 Supplementation by Intermittent Injection of Sepiapterin

Treatment Paradigm

To supplement BH4, we treated *P. berghei* ANKA-infected mice with sepiapterin, a compound that is converted to 7,8-BH2 by sepiapterin reductase and subsequently recycled to BH4 by dihydrofolate reductase (FIG 4.4). Sepiapterin was administered by intraperitoneal injection every 8 hours at a dose of 5mg/kg (15mg/kg total per day) starting on the day of inoculation with *P. berghei* ANKA. Mice were culled for tissue collection 8-14 hours after the final injection (administered at midnight on day 5 post-inoculation).

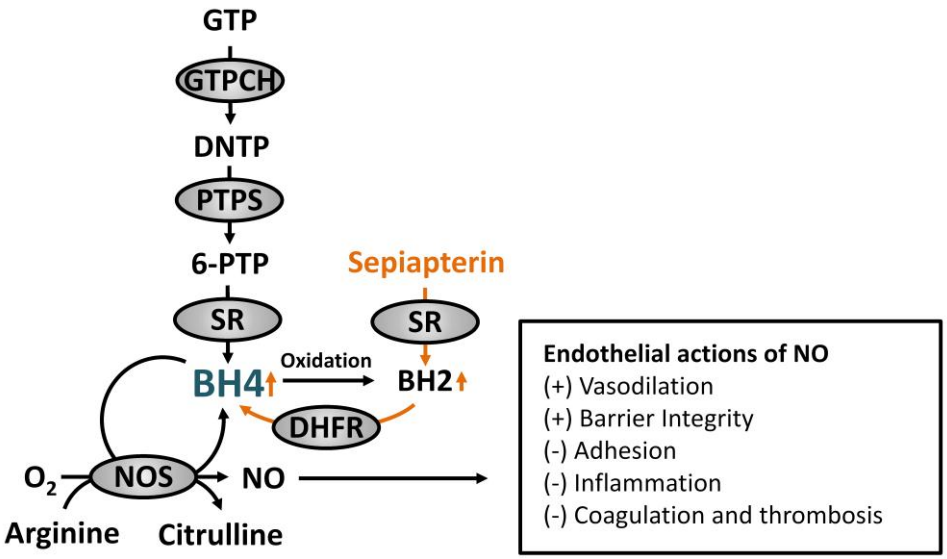


Figure 4.4 | Sepiapterin treatment supplements 7,8-BH2 and BH4. GTP: Guanosine triphosphate, GTPCH: GTP cyclohydrolase, DNTP: dihydroneopterin triphosphate, PTPS: pyruvoyl tetrahydropterin synthase, 6-PTP: 6-pyruvoyl-tetrahydropterin, SR: sepiapterin reductase, BH4: tetrahydrobiopterin, 7,8-BH2: 7,8-dihydrobiopterin, DHFR: dihydrofolate reductase, NOS: nitric oxide synthase, NO: nitric oxide

Effect of Sepiapterin Supplementation on Plasma and Red Blood Cell BH4

In *P. berghei* ANKA-infected mice, intermittent sepiapterin injection had no effect on plasma BH4 concentrations (infected + sepiapterin: 0.06 [0.05-0.07] µmol/L vs infected + saline: 0.06 [0.04-0.08] µmol/L, $p > 0.99$) or plasma 7,8-BH2 concentrations (infected + sepiapterin: 0.08 [0.06-0.09] µmol/L vs infected + saline: 0.06 [0.05-0.09] µmol/L, $p = 0.62$, FIG 4.5). The BH4/7,8-BH2 ratio was also unaffected by intermittent sepiapterin injection (infected + sepiapterin: 0.9 [0.6-1.1] vs infected + saline: 0.9 [0.8-1.0], $p = 0.84$, FIG 4.5). In red blood cells, intermittent sepiapterin treatment improved BH4 concentrations (infected + sepiapterin: 0.50 [0.37-0.80] µmol/L vs infected + saline: 0.16 [0.15-0.18] µmol/L, $p < 0.0001$, FIG 4.5). Red blood cell BH4 concentrations in *P. berghei* ANKA-infected mice treated with sepiapterin were not different from baseline values in uninfected mice ($p = 0.95$, FIG 4.5). Intermittent sepiapterin treatment similarly restored erythrocyte 7,8-BH2 to baseline values (infected + sepiapterin: 0.31 [0.26-0.54] µmol/L vs infected + saline: 0.11 [0.10-0.14] µmol/L, $p < 0.0001$, FIG 4.5). Due to similar effects on both BH4 and 7,8-BH2, the ratio of BH4 to 7,8-BH2 in red blood cells was not affected by intermittent sepiapterin treatment (infected + sepiapterin: 1.4 [1.4-1.6] vs infected + saline: 1.5 [1.2-1.7], $p = 0.95$, FIG 4.5). These findings suggest that sepiapterin reductase and dihydrofolate reductase remain active in erythrocytes during *P. berghei* ANKA infection. Our results cannot rule out an effect of sepiapterin treatment on plasma levels, but suggest that any effect would have subsided in the 8-14 hour interval between the final sepiapterin injection and sample collection.

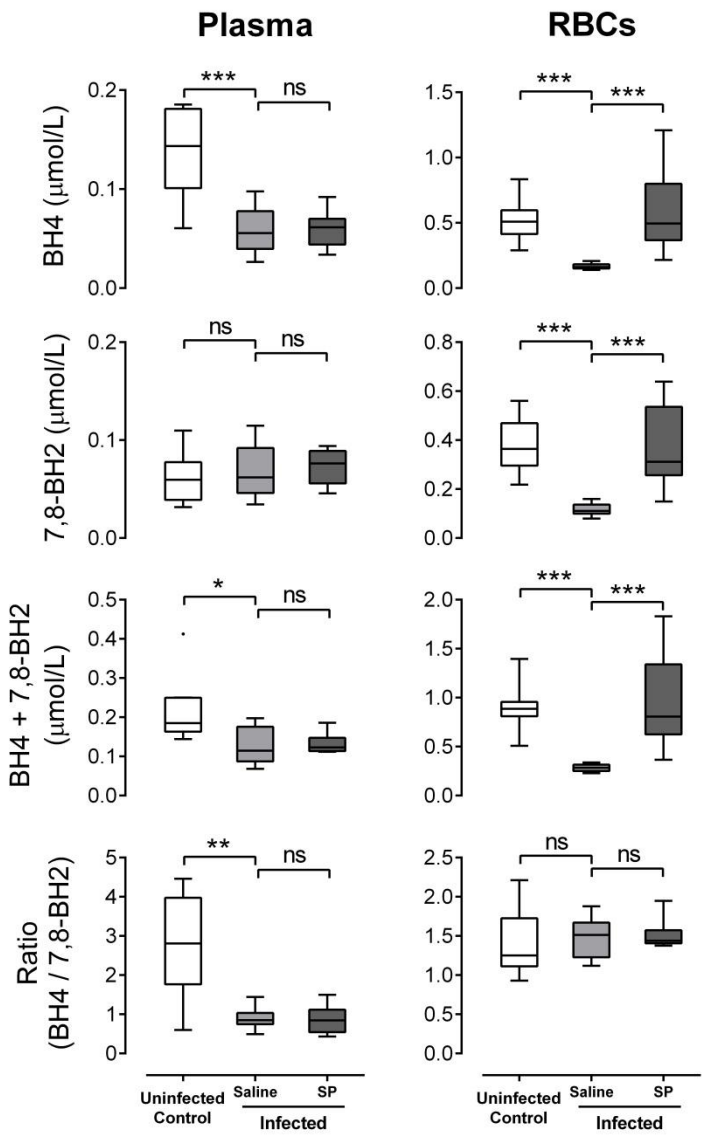


Figure 4.5 | Erythrocyte BH4 and 7,8-BH2 are restored by sepiapterin treatment. Tetrahydrobiopterin (BH4) and 7,8-dihydrobiopterin (7,8-BH2) were quantified by HPLC analysis in plasma and red blood cells from *P. berghei* ANKA-infected mice treated with saline (n=10) or sepiapterin (5mg/kg q8h starting on the day of inoculation, n=10). Samples were collected on day 6 post-inoculation. Uninfected mice treated with saline (n=10) served as controls. Box-plots depict median and IQR. Whiskers extend to highest and lowest values within 1.5×IQR of the 75th and 25th percentiles and values outside this range were plotted as individual points (Tukey's method). *p<0.05, **p<0.01, ***p<0.001 by Mann-Whitney test. ns (not significant): p>0.05

Effect of Sepiapterin Supplementation on Tissue BH4

Intermittent sepiapterin administration in *P. berghei* ANKA-infected mice increased aortic BH4 (infected + sepiapterin: 48.7 [34.0-74.2] pmol/mg protein vs infected + saline: 15.1 [13.7-17.3] pmol/mg protein, $p < 0.0001$) and 7,8-BH2 (infected + sepiapterin: 6.7 [4.7-8.4] pmol/mg protein vs infected + saline: 2.3 [1.8-2.8] pmol/mg protein, $p < 0.0001$, FIG 4.6). Sepiapterin treatment had no effect on the ratio of BH4 to 7,8-BH2 in aorta tissue (infected + sepiapterin: 7.6 [5.3-12.4] vs infected + saline: 6.8 [5.0-9.2], $p = 0.35$, FIG 4.6). Intermittent sepiapterin treatment had no effect on hepatic BH4 (infected + sepiapterin: 64.0 [54.4-74.8] pmol/mg protein vs infected + saline: 56.8 [52.8-64.1] pmol/mg protein, $p = 0.19$), 7,8-BH2 (infected + sepiapterin: 46.4 [39.5-52.1] pmol/mg protein vs infected + saline: 46.0 [22.6-53.0] pmol/mg protein, $p = 0.84$) or the ratio of BH4 to 7,8-BH2 (infected + sepiapterin: 1.4 [1.2-2.1] vs infected + saline: 1.5 [1.2-2.4], $p = 0.89$, FIG 4.6). In brain tissue, intermittent sepiapterin administration increased BH4 (infected + sepiapterin: 15.4 [11.1-21.6] pmol/mg protein vs infected + saline: 9.4 [8.4-10.6] pmol/mg protein, $p < 0.01$) and 7,8-BH2 (infected + sepiapterin: 5.4 [4.3-5.8] pmol/mg protein vs infected + saline: 3.5 [3.2-4.6] pmol/mg protein, $p < 0.01$), but had no effect on the ratio of BH4 to 7,8-BH2 (infected + sepiapterin: 2.6 [2.5-3.0] vs infected + saline: 2.4 [2.0-2.9], $p = 0.18$, FIG 4.6).

These results demonstrate that aorta and brain tissue retain sufficient sepiapterin reductase and dihydrofolate reductase activity during *P. berghei* ANKA infection to convert sepiapterin to 7,8-BH2 and BH4, respectively. The absence of increased BH4 or 7,8-BH2 in liver tissue following sepiapterin administration may result from failure of liver tissue to take up sepiapterin and/or convert it to 7,8-BH2 and BH4 or failure to detect transient increases in BH4 and 7,8-BH2 with sample collection occurring 8-14 hours after the final injection.

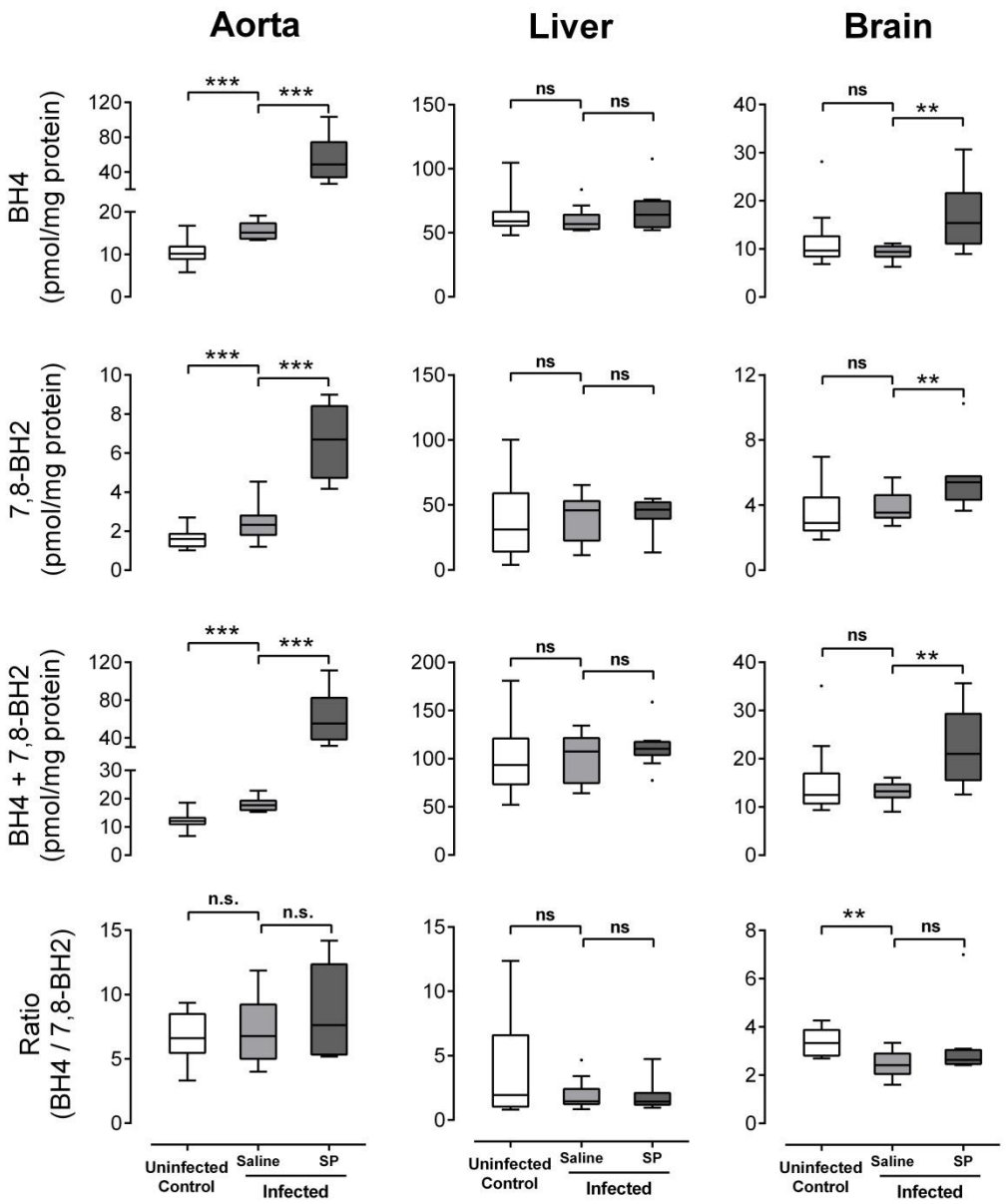


Figure 4.6 | Effect of sepiapterin treatment on tissue BH4 and 7,8-BH2. Tetrahydrobiopterin (BH4) and 7,8-dihydrobiopterin (7,8-BH2) were quantified by HPLC analysis in aorta, liver and brain tissue from *P. berghei* ANKA-infected mice treated with saline (n=10) or sepiapterin (5mg/kg q8h starting on the day of inoculation, n=10). Tissue samples were collected on day 6 post-inoculation. Uninfected mice treated with saline (n=10) also served as controls. Box-plots depict median and IQR. Whiskers extend to highest and lowest values within 1.5×IQR of the 75th and 25th percentiles and values outside this range were plotted as individual points (Tukey's method). *p<0.05, **p<0.01, ***p<0.001 by Mann-Whitney test. ns (not significant): p>0.05

Disease Phenotype

To determine the effect of intermittent sepiapterin administration on progression of *P. berghei* ANKA infection, we quantified behavioural symptoms in cohorts of *P. berghei* ANKA-infected mice treated with sepiapterin or saline (control). On day 6 post-inoculation, rapid onset of symptoms, including hunched posture, lethargy and unresponsiveness, were observed in both sepiapterin-treated mice and in saline-treated controls infected with *P. berghei* ANKA. Quantitative scores of symptoms were not significantly different between groups on the morning of day 6 (infected + sepiapterin: 9 [3-12] out of 14 vs infected + saline: 7 [1-10] out of 14, p = 0.27) and directly prior to tissue collection (infected + sepiapterin: 2 [0-4] out of 14 vs infected + saline: 1 [0.0-2] out of 14, p = 0.31, FIG 4.7). Parasitaemia on day 6 post-inoculation was not affected by sepiapterin treatment (infected + sepiapterin: 6.3% [4.8-7.4%] vs infected + saline: 6.3% [5.0-7.5%], p = 0.91).

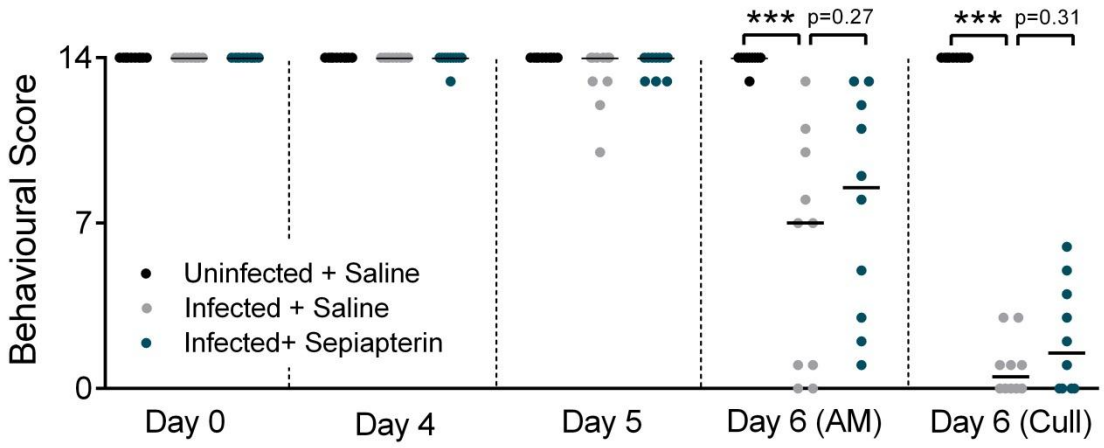


Figure 4.7 | Sepiapterin treatment does not prevent severe symptoms in infected mice. Mice infected with *P. berghei* ANKA parasites were treated with saline (n=10) or sepiapterin (5mg/kg q8h starting on the day of inoculation, n=10) and monitored daily for disease symptoms. Uninfected mice treated with saline served as controls (n=10). Symptoms were scored by assessing each of 7 parameters on a scale of 0 (moribund) to 2 (normal). D6 (AM) scores reflect assessments taken from 7AM-9AM in the morning for all animals and D6 (Cull) scores reflect assessments taken directly prior to tissue collection. Black lines indicate median values for each group. ***p < 0.001 by Mann-Whitney test.

Nitrite

Whole blood nitrite is reflective of eNOS activity (Kleinbongard et al., 2003). In a previous clinical study of Malian children with severe malarial anaemia, whole blood nitrite concentrations were decreased at admission but recovered after treatment with antimalarial therapy and transfusion (Janka et al., 2010). We used chemical reduction and a nitric oxide analyzer to determine nitrite concentrations in whole blood samples from *P. berghei* ANKA-infected mice and uninfected controls. Whole blood nitrite was decreased in infected mice 6 days post-inoculation (0.33 [0.26-0.47] µmol/L) compared with uninfected controls (0.49 [0.44-0.65] µmol/L, $p < 0.05$ vs infected day 6, FIG 4.8A), implying decreased systemic NO production. We also assessed whole blood nitrite in mice infected with *P. berghei* ANKA and treated with sepiapterin. Intermittent sepiapterin injection moderately increase in the median whole blood nitrite concentration in *P. berghei* ANKA-infected mice (0.49 [0.37-1.40] µmol/L) compared to infected mice treated with saline (0.39 [0.21-0.67] µmol/L), but this difference did not reach statistical significance ($p = 0.15$, FIG 4.8B).

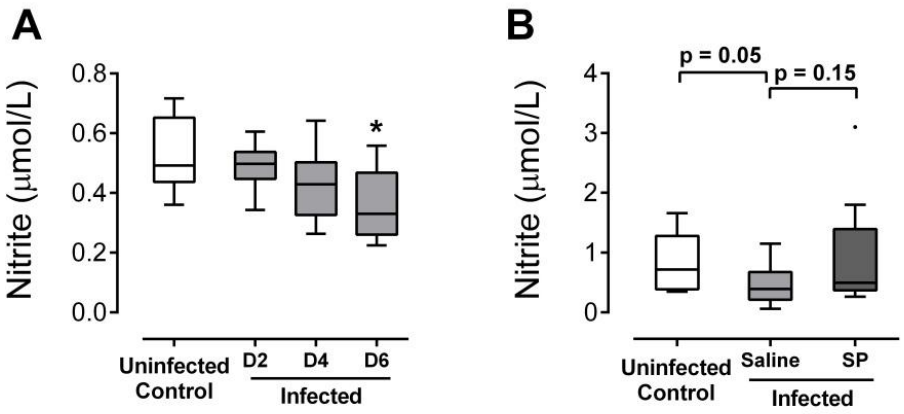


Figure 4.8 | Whole blood nitrite in response to infection and sepiapterin injection. (**A**) Whole blood was collected at days 2 (n=9), 4 (n=10) and 6 (n=11) post-inoculation with *P. berghei* ANKA (PbA) and nitrite was assessed by chemical reduction to NO and detection with a nitric oxide analyzer. Uninfected animals (n=10) served as controls. *p<.05 vs uninfected control group by Kruskal-Wallis test followed by Dunnett's multiple-comparisons post-hoc test. (**B**) Whole blood nitrite was assessed mice infected with *P. berghei* ANKA and treated with saline (n=10) or sepiapterin (n=10). Sepiapterin was administered on days 0-5 post-inoculation by intraperitoneal injection 3 timed daily for a total dose of 15mg/kg/d. Whole blood samples were collected on day 6 post-inoculation. Uninfected mice treated with saline served as controls (n=10). p-values were determined by Mann-Whitney test.

4.4 Discussion

This study is the first to directly quantify blood and tissue BH4 availability during malaria infection. In the blood compartment, we have demonstrated that BH4 bioavailability was decreased in the red blood cells of wild-type mice following experimental malaria infection. The ratio of BH4 to 7,8-BH2 was decreased in both plasma and erythrocytes, suggesting that oxidation contributes to BH4 depletion in both contexts. BH4 was increased in the aorta and liver of *P. berghei* ANKA-infected mice, which may result from pro-inflammatory signalling (Katusic et al., 1998) or induction of GTP cyclohydrolase by phenylalanine (Harada et al., 1993). In contrast, BH4 was decreased in the brains of *P. berghei* ANKA-infected mice. We also observed elevated 7,8-BH2 and decreased BH4/7,8-BH2 ratios in brain tissue, implicating oxidation as an important contributor to depletion BH4 in brain tissue during *P. berghei* ANKA infection. Low BH4 availability and decreased BH4/7,8-BH2 ratios may limit NO synthesis and contribute to impaired vasodilation of pial vessels in response to acetylcholine or NMDA stimulation (Ong et al., 2013). This hypothesis is further supported by the observation that BH4 superfusion improves pial vasodilation in response to acetylcholine or NMDA (Ong et al., 2013).

We demonstrated that intermittent intraperitoneal administration of sepiapterin results in restoration of erythrocyte BH4 and elevation of BH4 concentrations in brain and aorta tissue. BH4 supplementation as a therapeutic approach promises the possibility of improving endothelial dysfunction while reducing the risk of hypotension associated with therapies aimed at downstream NO signalling targets, but the efficacy of direct BH4 administration has had mixed results in human patients with cardiovascular disease. Early physiological experiments demonstrated improved eNOS-dependent vasodilation following direct BH4 infusion in individuals with hypertension (Higashi et al., 2002), hypercholesterolaemia (Stroes et al., 1997), diabetes (Heitzer et al., 2000), and a history of smoking (Heitzer et al., 2000). Early small trials also demonstrated that oral BH4 therapy improved forearm blood flow in hypercholesterolaemic patients (Cosentino et al., 2008) and reduced blood pressure in patients with poorly-controlled

hypertension (Porkert et al., 2008). These studies were limited in scope, largely due to the instability of oral BH4 preparations. In 2007, the US Food and Drug Administration approved use of sapropterin, a thermo- and photo-stable, orally available preparation of synthetic 6R-BH4 (trade-name: Kuvan, manufactured by BioMarin Pharmaceutical, Inc., Novato, CA, USA) for the treatment of phenylketonuria (PKU). PKU is a metabolic disorder resulting from a loss-of-function mutation in the BH4-dependent enzyme phenylalanine hydroxylase that is characterized by accumulation of plasma phenylalanine and potentially severe neurological complications. Large phase III trials demonstrated that sapropterin significantly reduced plasma phenylalanine levels by 1 week of treatment and that sapropterin was well-tolerated (Levy et al., 2007; Trefz et al., 2009). The efficacy and safety profiles demonstrated in these trials resulted in high interest in the potential to treat cardiovascular disease characterized by endothelial dysfunction. However, in preliminary Phase II trials, no benefit was demonstrated in patients with systemic hypertension (NCT00325962), or peripheral artery disease (NCT00403494) (BioMarin Pharmaceutical Inc., 2009, 2007). Initial results suggesting an improvement in vasoreactivity in sickle cell patients treated with sapropterin (BioMarin Pharmaceutical Inc., 2008) have yet to be followed up or published.

A recently published report on sapropterin treatment in patients with coronary artery disease provides some mechanistic insight into limitations of oral BH4 supplementation as a therapeutic approach to treating cardiovascular disease (Cunnington et al., 2012). In this study, oral sapropterin treatment failed to improve brachial flow-mediated vasodilation, aortic or carotid distensibility or acetylcholine-induced vasodilation in *ex vivo* saphenous vein rings (Cunnington et al., 2012). Plasma and saphenous vein tissue BH4 concentrations were higher in patients receiving sapropterin treatment compared with placebo-treated controls, but a concomitant increase in 7,8-BH2 concentrations yielded no improvement in the ratio of BH4 to oxidized biopterin species (Cunnington et al., 2012). Failure to improve BH4/7,8-BH2 ratios may explain the lack of effect on conversion of arginine to citrulline or superoxide production in *ex vivo* saphenous vein samples (Cunnington et al., 2012). Furthermore, exogenous BH4 added

to whole blood was rapidly oxidized and incubation of *ex vivo* saphenous vein rings with exogenous BH4 paradoxically reduced the ratio of BH4 to oxidized biopterins due to accumulation of 7,8-BH2 (Cunnington et al., 2012). The ability of BH4 to recouple NOS may therefore be limited by BH4 oxidation, 7,8-BH2 accumulation and the resulting failure to improve BH4/7,8-BH2 ratios.

4.5 Conclusion

In our experiments, sepiapterin treatment elevated BH4 in erythrocytes, aorta and brain, but did not alter the ratio of BH4 to 7,8-BH2. Failure to improve BH4/7,8-BH2 ratios may explain why whole blood nitrite, a biomarker of NO synthesis, was not improved in sepiapterin-treated mice. Arginine depletion and elevation of the ADMA/arginine ratio may have also limited the ability of BH4 supplementation to improve NO synthesis. In CHAPTER 5, we explore the effects of simultaneous supplementation of arginine and BH4 in *P. berghei* ANKA-infected mice.

4.6 Materials and Methods

Animal Procedures

Experimental Animals

Animal experiments were performed at the National Institutes of Health (NIAID Comparative Medicine Branch) using protocols approved by the NIH ACUC under the identification ASP LMVR 18E. 10-week-old C57BL/6J male mice were obtained from the Jackson Laboratory (Bar Harbor, ME, USA) and 10-week-old Swiss Webster carriers for parasite expansion were obtained from Charles River Laboratories (Frederick, MD, USA). Mice were housed in temperature-controlled cages maintained at 20-22ºC with a 12hr/12hr light-dark cycle and free access to water and autoclaved rodent feed pellets (Teklad Global 18% Protein Extruded Rodent Diet, 2018SX, Harlan Laboratories, Frederick, MD, USA).

Time-course experiments (in which infected mice were culled on days 2, 4 and 6 post-inoculation) were replicated at the Wellcome Trust Sanger Institute under personal (PIL 80/12137) and project licenses (PPL 80/2158) issued by the UK Home Office in accordance with the Animals (Scientific Procedures) Act of 1986. Protocols reviewed by the Wellcome Trust Sanger Institute ethics committee. For this experiment, 10-week-old male C57BL/6J experimental mice and Tuck Ordinary outbred mice carriers for parasite expansion were obtained from Harlan Laboratories (London, UK).

Experimental groups were assigned in an alternating manner such that every experimental group was represented in each cage of communally-housed littermates.

Infections

P. berghei ANKA parasites, clone RMgm-29 (Janse et al., 2006), were expanded from frozen stocks by intraperitoneal injection of carrier mice. After four days of parasite expansion, whole blood was obtained from the abdominal inferior vena cava under terminal anaesthesia. Cohorts of experimental mice were infected by intraperitoneal injection of 1×10^6 infected erythrocytes diluted in 200 µl of PBS (Lonza, Walkersville, MD, USA). This protocol results in

blood-stage infection, bypassing the liver stage of the parasite's life-cycle. For sepiapterin treatment experiments, inoculations were alternated between saline-treated infected controls and sepiapterin-treated infected mice.

Behavioural Scoring and Quantification of Parasitaemia

Neurological symptoms were scored using a quantitative scoring scale adapted from the Rapid Murine Coma and Behaviour Scale (Carroll et al., 2010). Scores were assigned on a scale of 0 (moribund) to 2 (normal) for each of seven indicators: gait, balance, exploratory activity, body position, limb strength, touch escape and pinna reflex (TABLE 4.1). Parasitaemia was monitored by examination of Giemsa-stained blood smears obtained by tail tip bleed in live animals or from blood samples taken during tissue collection.

Category	Observation
Motor Performance	Gait
Activity	Body lift Exploratory Behaviour
Strength and Tone	Body Position Grasp of cage bars
Reflexes and Self-Preservation	Touch Escape Pinna Reflex

Table 4.1| Scoring System for the Assessment of Disease Symptoms in Mice. System was adapted from the Rapid Murine Coma and Behaviour Scale (Carroll et al., 2010). Each observation was scored on a scale of 0 (moribund) to 2 (normal) yielding scores ranging from the minimum score of 0 (moribund mouse) to the maximum score of 14 (normal mouse).

Sepiapterin Administration

Sepiapterin (Schirck's Laboratories, Jona, Switzerland) was dissolved in sterile 0.9% saline (Hospira, Lake Forest, IL, USA), sterilized with a 0.22µm syringe-tip filter, aliquoted and stored at -80°C until use. Sepiapterin (5mg/kg) was administered by intraperitoneal injection in a volume of 200µl three times a day starting on the day of inoculation (day 0). Uninfected and

infected controls were injected with equivalent volumes of sterile 0.9% saline (Hospira, Lake Forest, IL, USA). Mice were euthanized for tissue collection 8-14 hours after the final injection (administered at midnight on day 5 post-inoculation).

Blood and Tissue Collection

Terminal anaesthesia was administered by intraperitoneal injection of 250mg/kg ketamine and 25mg/kg xylazine. The abdominal cavity was accessed and 700µl of blood was drawn from the abdominal inferior vena cava with a 25G×5/8" needle (BD, Franklin Lakes, NJ, USA). To prevent coagulation, the syringe contained 60µl DPBS with K_3EDTA (final concentration of 1.6mg/ml K_3EDTA after 700 µl blood drawn). Plasma was separated from erythrocytes by centrifugation at 3,000*g* for 7 minutes at 4°C and snap-frozen on dry ice. The buffy coat was removed and discarded to ensure the purity of red blood cell samples. Mice were transcardially perfused with 20 ml PBS and lung, liver, kidney, spleen, aorta, heart and whole brain were dissected, removed, and snap-frozen on dry ice. All samples were stored at -80°C until analysis.

Biochemical Analysis

HPLC Determination of BH4 and 7,8-BH2

BH4 and 7,8-BH2 concentrations in tissue, plasma and red blood samples were determined by high-performance liquid chromatography (HPLC) with sequential electrochemical and fluorescence detection. A complete description of method development and validation is available in APPENDIX E, p. 319.

Tissue samples (~30mg) were homogenized in 15µl ice-cold resuspension buffer per mg (~450µl) using a hand-held homogenizer (Cole Parmer, Vernon Hills, IL, USA). Resuspension buffer consisted of 1mM dithioerythritol (Acros Organics, Geel, Belgium) and 0.5µM EDTA (Sigma-Aldrich, St. Louis, MO, USA) diluted in 1×DPBS (Lonza, Walkersville, MD, USA). Homogenized samples were centrifuged for 5 min at 16,100*g* and 4 °C to remove insoluble

protein. To precipitate proteins, supernatants were then mixed 9:1 with ice-cold precipitation acid consisting of 1M phosphoric acid (Fisher Scientific, Pittsburgh, PA, USA), 2M trichloroacetic acid (Fisher Scientific, Pittsburgh, PA, USA) and 1mM dithioerythritol (DTE) (Acros Organics, Geel, Belgium) diluted in 1×DPBS (Lonza, Walkersville, MD, USA). Instead of homogenization, whole aortas were subjected to three freeze–thaw cycles on dry ice in 200µl resuspension buffer prior to mixing with precipitation acid as above. Red blood cells and plasma samples were diluted 1:10 in resuspension buffer prior to mixing with precipitation acid as above. Following precipitation, all samples were centrifuged for 5 min at 16,100*g* and 4 °C. Supernatants were loaded into 250µl capacity polypropylene vials (Agilent Technologies, Santa Clara, CA, USA) and loaded into the autosampler. All samples were maintained on ice during processing.

Samples were injected (100µl injection volume) onto an isocratic HPLC system consisting of an 1100 series degasser and isocratic pump and a 1260 Infinity series autosampler, temperature-control unit and fluorescence detector with a 8µl flow cell, all obtained from Agilent Technologies (Santa Clara, CA, USA). A CouloChem III electrochemical detector (Thermo Scientific, Sunnyvale, CA, USA) was installed after the column and before the fluorescence detector. Chromatography was performed on a 4.6mm×250mm ACE® C18 column with 5µm particles and 100Å pore size (MAC-MOD Analytical, Chadds Ford, PA, USA) with a 4.6mm×13mm ACE® C18 guard column with 5µm particles and 100Å pore size (MAC-MOD Analytical, Chadds Ford, PA, USA). Analytes were separated isocratically with a mobile phase comprised of 50mM HPLC-grade sodium acetate (Fisher Scientific, Pittsburgh, PA, USA), 5mM citric acid (Fisher Scientific, Pittsburgh, PA, USA), 48µM EDTA (Sigma-Aldrich, St. Louis, MO, USA), and 160µmol/L dithioerythritol (DTE) (Acros Organics, Geel, Belgium) prepared in ultrapure water (Milli-Q Synthesis system, Millipore Corporation, Billerica, MA, USA). The flow rate was 1.3 ml/min with a 19-minute rune-time between sample injections. For detection of BH4, the electrochemical detector's analytical cell was set to a voltage of +75mV for electrode 1 and -400mV for electrode 2. The guard cell voltage was set to

+900mV to oxidize 7,8-BH2 to biopterin, which is fluorescent. Oxidized 7,8-BH2 was quantified using fluorescence detector excitation and emission wavelengths of 350 and 450 nm, respectively, and a photomultiplier tube gain of 18.

Agilent Chemstation OpenLab CDS revision C.01.03 (Agilent Technologies, Santa Clara, CA, USA) was used to control the instrument, acquire data and integrate peaks. A 35900E analog-to-digital converter (Agilent Technologies, Santa Clara, CA, USA) was used to facilitate communication between the electrochemical detector and Chemstation OpenLab. BH4 and 7,8-BH2 were quantified by comparison of integrated peak areas to external standard solutions of BH4 and 7,8-BH2 (Schircks Laboratories, Jona, Switzerland) diluted to known concentrations (0.1 nmol/L-50 nmol/L). For tissue analysis, measured concentrations were and normalized to soluble protein content, which was separately assayed with a Pierce BCA Protein Assay Kit (Thermo Scientific, Sunnyvale, CA, USA) according to the manufacturer's instructions.

Whole Blood Nitrite

Immediately after collection, 100µl of whole blood was mixed with 25µl of a solution containing potassium hexacyanoferrate(III) (800mM) (Sigma-Aldrich, St. Louis, MO, USA) to oxidize ferrous haem, *N*-ethylmaleimide (100mM) (Sigma-Aldrich, St. Louis, MO, USA) to block thiols and 10% v/v Nonidet-40 substitute (Fisher Scientific, Pittsburgh, PA, USA) to solubilize cell membranes. Samples were promptly snap-frozen on dry ice and stored at -80°C until analysis. For analysis, whole blood samples were thawed and deproteinated by mixing 1:1 with methanol (EMD Millipore, Billerica, MA, USA) and centrifuging for 5min at 16,100*g* and 4°C. Supernatants were injected into a reaction chamber containing potassium iodide (66.9mM) and iodine (28.5mM) (Sigma-Aldrich, St. Louis, MO, USA) diluted in a 2:7 mixture of ultrapure water (Milli-Q Synthesis System, Millipore Corporation, Billerica, MA, USA) and acetic acid, glacial (Fisher Scientific, Pittsburgh, PA, USA). NO produced by reduction of nitrite in plasma samples was detected with a Nitric Oxide Analyzer 280i (GE Healthcare,

Pittsburgh, PA, USA) and compared with standards of known concentration prepared from sodium nitrite (Sigma-Aldrich, St. Louis, MO, USA). The chemistry of relevant reactions is presented in TABLE 4.2. Data processing and peak integrations were performed with OriginPro 8 software.

Nitrite Assay Chemistry
A. Generation of NO from NO_2^- $I^- + NO_2^- + 2H^+ \rightarrow NO + ½\ I_2 + H_2O$
B. Generation of Chemilluminescence $NO + O_3 \rightarrow NO_2^{\bullet} + O_2$ $NO_2^{\bullet} \rightarrow NO_2 + hv$

Table 4.2 | Chemical reactions for the measurement of nitrite (NO2-). (**A**) Nitrite is chemically reduced to nitric oxide in a solution of iodine and acetic acid. (**B**) NO generated from NO2- reduction is detected by chemilluminescence using a nitric oxide analyzer.

Statistical Analyses

Data are presented as median and inter-quartile range (IQR). Statistical analyses were performed with GraphPad Prism 6 software and $p < 0.05$ was considered significant. In the time-course experiment, Kruskal-Wallis test followed by Dunn's multiple comparisons post-test was used to compare plasma and erythrocyte BH4 and 7,8-BH2 concentrations in uninfected controls to values from mice infected with *P. berghei* ANKA for 2, 4 or 6 days. In sepiapterin treatment experiments, Mann-Whitney test was used to compare biochemical values and behavioural scores between uninfected and saline-treated infected controls and between saline-treated infected controls and sepiapterin-treated infected mice.

Acknowledgements

Oliver Billker (Wellcome Trust Sanger Institute) provided animal facility access, animals, laboratory space and supplies for time-course experiments. Keith Channon (Department of Cardiovascular Medicine, University of Oxford) provided laboratory space, supplies and HPLC equipment for analysis of sepiapterin experiment samples. I would like to thank Ashley Hale and Mark Crabtree (Oxford) for HPLC training, Malika Ahras and Stanley Barkhuysen (Sanger Institute) for training in animal procedures and Laurel Mendelsohn (NHLBI/NIH) for training in the measurement of nitrite. This work was funded by the NIAID Division of Intramural Research, the European Virtual Institute of Malaria Research (EVIMalaR) and the Wellcome Trust (grant WT098051).

CHAPTER 5.

Arginine and Tetrahydrobiopterin Co-Supplementation

P. berghei ANKA infection causes depletion of arginine, the NOS substrate, and BH4, the NOS cofactor. Supplementation of BH4 alone failed to improve whole blood nitrite (a biomarker of NO synthesis). In this chapter, we test the hypothesis that co-supplementation of arginine and BH4 is required to restore NO synthesis in P. berghei ANKA-infected mice. To reverse arginine and BH4 deficiencies, we infused infected mice intravenously with citrulline, an arginine precursor, and sepiapterin, a BH4 precursor. Restoration of systemic arginine and BH4 availability in infected mice produced only minor improvement in whole blood nitrite concentrations, a biomarker of NO synthesis, and failed to prevent onset of severe disease symptoms. Reversal of severe malaria pathogenesis may require therapeutic interventions that improve NO signalling by a NOS-independent mechanism. We observed that infusion of citrulline and sepiapterin reduced the ratio of phenylalanine to tyrosine in plasma, liver tissue and brain tissue, suggesting that BH4 supplementation improved activity of phenylalanine hydroxylase. The biochemistry and clinical relevance of impaired phenylalanine metabolism in severe malaria require further study.

5.1 Introduction

Production of nitric oxide (NO) by nitric oxide synthase (NOS) requires arginine as a substrate and tetrahydrobiopterin (BH4) as a cofactor. In previous chapters, we have shown that both arginine and BH4 are depleted in the blood compartment of *P. berghei* ANKA-infected mice. Administration of sepiapterin improved BH4 availability in plasma, erythrocytes, brain and aorta, but limited availability of arginine substrate may have prevented restoration of NO synthesis.

BH4 depletion causes NOS uncoupling, a state in which NO synthesis is inhibited and superoxide (O_2^-) production is increased (Pou et al., 1992; Vasquez-Vivar et al., 1998; Xia et al., 1998). Superoxide rapidly reacts with NO, interfering with NO signalling and producing the highly reactive peroxynitrite anion ($ONOO^-$) (Milstien and Katusic, 1999). Peroxynitrite causes significant cellular damage by nitrating lipids, DNA and thiol and hydroxyl groups on protein,

thereby disrupting enzymatic function (Ridnour et al., 2004). Peroxynitrite also rapidly oxidizes BH4 to 7,8-BH2, exacerbating NOS uncoupling (Beckman et al., 1990; Kuzkaya et al., 2003).

In the absence of BH4, increasing concentrations of arginine accelerate NADPH consumption and increase superoxide production by uncoupled eNOS (Druhan et al., 2008). These results suggest that under conditions of BH4 depletion, the introduction of arginine may induce conformational changes in eNOS that promote electron flow and increase superoxide production if BH4 is not available to couple oxygen activation to arginine oxidation. These observations suggest that restoration of arginine without correcting BH4 deficiency may be ineffective or even harmful. In this chapter, we identify a method of simultaneous BH4 and arginine supplementation and examine downstream biomarkers of NO synthesis and NOS uncoupling in *P. berghei* ANKA-infected mice.

5.2 Initial Investigations of Citrulline Pharmacology

Rationale for Administration of Citrulline

During NOS-mediated nitric oxide synthesis, arginine is oxidized to citrulline. Argininosuccinate synthetase 1 (ASS1) and argininosuccinate lyase (ASL) enzymes are complexed with NOS, allowing rapid recycling of citrulline back to arginine in order to support sustained NO synthesis (Flam et al., 2001; Vukosavljevic et al., 2006; Erez et al., 2011). The identification of this mechanism raises the possibility that citrulline serves as a secondary substrate pool from which arginine can be generated in close proximity to NOS. Because *P. berghei* ANKA infection depletes both arginine and citrulline, effective restoration of NOS substrate pools may require supplementation of both arginine and citrulline.

In a recent study in a mouse model of endotoxaemia, intravenous infusion with citrulline was shown to improve arginine availability and intestinal perfusion to a greater degree than direct infusion of an equivalent quantity of arginine (Wijnands et al., 2012). This study also demonstrated that arginine infusion had no significant effect on plasma citrulline concentrations, whereas citrulline infusion supplemented both citrulline and arginine in plasma. In CHAPTER 2, we used heavy isotope-labelled metabolic tracers to show that even during *P. berghei* ANKA infection, nearly all plasma citrulline is utilized for arginine synthesis (FIG 2.13, p. 52). This observation explains why citrulline infusion effectively supplemented arginine availability in the endotoxaemia study (Wijnands et al., 2012).

In contrast, our flux analysis demonstrated that only 21.1% of plasma arginine was utilized for ornithine synthesis in uninfected mice with *ad libitum* access to food, and 39.2% in *P. berghei* ANKA-infected mice (FIG 2.15, p. 55). Furthermore, the percentages of ornithine utilized for citrulline synthesis were 13.5% and 11.9% in uninfected mice with *ad libitum* access to food and *P. berghei* ANKA-infected mice, respectively (FIG 2.17, p. 59). These figures indicate that the percentage of arginine ultimately converted to citrulline via ornithine is 2.8% in uninfected mice and 4.7% in *P. berghei* ANKA-infected mice. These observations demonstrate that only a small minority of arginine is converted to citrulline via ornithine and may explain

why arginine infusion had no effect on plasma citrulline concentrations in the experiments of Wijnands and colleagues (Wijnands et al., 2012). Based on this evidence, we assessed the ability of citrulline administration to reverse depletion of both citrulline and arginine in *P. berghei* ANKA-infected mice.

Intermittent Injection of Citrulline

We first evaluated the effects of intermittent intraperitoneal citrulline administration at a dose of 200mg/kg every 8 hours (600mg/kg total per day), with injections beginning the day of inoculation with *P. berghei* ANKA (6 days total). Mice were culled for blood and tissue sample collection 8-14 hours after the final injection, which was administered at midnight on day 5 post-inoculation. Intermittent administration of citrulline by intraperitoneal injection did not significantly improve plasma citrulline (infected + citrulline: 22.7 [17.4-29.9] µmol/L vs infected + saline: 23.8 [19.4-29.2] µmol/L, p = 0.81), arginine (infected + citrulline: 60.8 [54.8-70.01] µmol/L vs infected + saline: 55.3 [50.7-63.2] µmol/L, p = 0.36) or ornithine (infected + citrulline: 27.7 [24.8-31.2] µmol/L vs infected + saline: 31.9 [28.8-32.6] µmol/L, p = 0.14) in *P. berghei* ANKA-infected mice (FIG 5.1). Intraperitoneal administration of citrulline also had no effect on whole blood nitrite, a biomarker of NO synthesis (infected + citrulline: 0.36 [0.31-0.40] µmol/L vs infected + saline: 0.33 [0.28-0.51] µmol/L p = 0.95, FIG 5.2). These findings suggest that the half-life of intraperitoneal citrulline injection would require >8hr frequency of injections to raise trough plasma citrulline concentrations. We therefore used continuous infusion of citrulline in subsequent experiments.

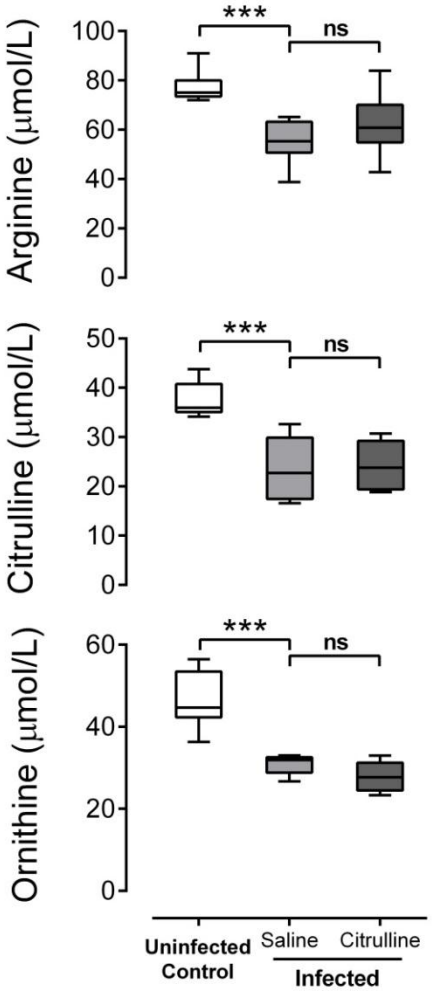


Figure 5.1 | Arginine, citrulline and ornithine are not restored by intermittent citrulline injection. Plasma amino acids were quantified by HPLC. *P. berghei* ANKA-infected mice received intermittent intraperitoneal injections of citrulline (200mg/kg q8h, n=10) or saline (n=10). Plasma samples were collected on day 6 post-inoculation. Uninfected mice treated with saline served as controls (n=10). Boxplots depict median, IQR and range. ***p<0.001 by Mann-Whitney test. ns (not significant): p>0.05.

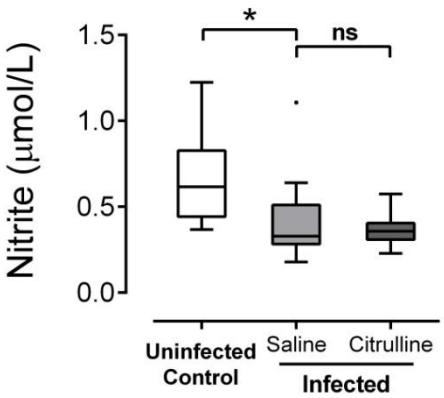


Figure 5.2 | Whole blood nitrite is not restored by intermittent citrulline injection. Whole blood nitrite was quantified by chemical reduction and detection with a nitric oxide analyzer. *P. berghei* ANKA-infected mice received intermittent intraperitoneal injections of citrulline (200mg/kg q8h, n=10) or saline (n=10). Whole blood samples were collected on day 6 post-inoculation. Uninfected mice treated with saline served as controls (n=10). Boxplots depict median, IQR and range. ***p<0.001 by Mann-Whitney test. ns (not significant): p>0.05.

5.3 Simultaneous Infusion of Citrulline and Sepiapterin

A previous study demonstrated supplementation of both citrulline and arginine following continuous intravenous administration of 1.25 g/kg citrulline over 6 hours (equating to 5 $g \times kg^{-1} \times d^{-1}$ if administered at the same rate for a full 24hr) (Wijnands et al., 2012). We hypothesized that continuous infusion of citrulline at a dose of 2.4 $g \times kg^{-1} \times d^{-1}$ would effectively restore plasma citrulline and arginine availability in *P. berghei* ANKA-infected mice. We have previously shown that intermittent injection of sepiapterin at a dose of 5mg/kg every 8 hours ($15mg \times kg^{-1} \times d^{-1}$ total) restored BH4 in erythrocytes and elevated BH4 in brain and aorta tissue (see FIG 4.5, p. 141 and FIG 4.6 p. 143). We therefore infused sepiapterin ($15mg \times kg^{-1} \times d^{-1}$) alongside citrulline to determine if this intervention could simultaneously supplement BH4 and arginine. Citrulline and sepiapterin were diluted in sterile saline (0.9%) and infused at a volumetric rate of 25µl/hr. Infusions were started the day before inoculation with *P. berghei* ANKA and continued for the duration of the infection. Saline-infused infected and uninfected mice served as controls.

Effect of Citrulline and Sepiapterin Infusion on Plasma Arginine, Citrulline and Ornithine

Compared to infected controls infused with saline, *P. berghei* ANKA-infected mice infused with citrulline and sepiapterin exhibited elevated plasma citrulline (infected + citrulline/sepiapterin: 404.5 [313.9-535.1] µmol/L vs infected + saline: 28.1 [20.9-37.2] µmol/L, $p < 0.0001$), arginine (infected + citrulline/sepiapterin: 200.5 [195.7-216.2] µmol/L vs infected + saline: 64.4 [52.0-81.2] µmol/L, $p < 0.0001$) and ornithine (infected + citrulline/sepiapterin: 99.8 [93.2-130.7] µmol/L vs infected + saline: 32.7 [22.5-35.8] µmol/L, $p < 0.0001$) on day 6 post-inoculation with *P. berghei* ANKA (FIG 5.3). These observations of increased plasma arginine and ornithine following infusion of citrulline and sepiapterin demonstrate that ASS1, ASSL and arginase remain functional during *P. berghei* ANKA infection.

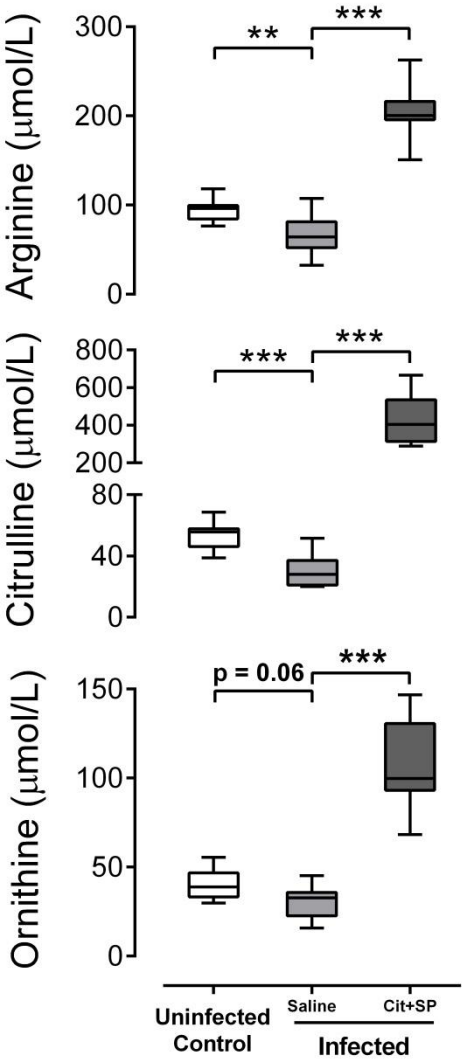


Figure 5.3 | Supplementation of plasma arginine, citrulline and ornithine by continuous infusion of citrulline and sepiapterin. Plasma arginine, citrulline and ornithine were determined by HPLC on day 6 post-inoculation with *P. berghei* ANKA. *P. berghei* ANKA-infected mice received continuous intravenous infusion of saline (n=9) or 2.4g×kg^{-1}×d^{-1} citrulline + 15mg×kg^{-1}×d^{-1} sepiapterin (n=11). Saline-infused uninfected mice (n=12) served as controls. Data are pooled from 3 independent experiments. Box-plots depict median and IQR. Whiskers extend to highest and lowest values within 1.5×IQR of the 75th and 25th percentiles, and values outside this range were plotted as individual points (Tukey's method). *p<0.05, **p<0.01, ***p<0.001 by Mann-Whitney test. ns (not significant): p>0.05.

Effect of Citrulline and Sepiapterin Infusion on Plasma ADMA/Arginine Ratios

Previous *in vitro* studies have demonstrated that metabolism of ADMA by dimethylarginine dimethylaminohydrolase 1 (DDAH1) is inhibited by exogenous arginine (Wang et al., 2006). This finding implies that arginine acts as a DDAH inhibitor in order to maintain the ratio of ADMA to arginine. In the presence of rising arginine concentrations, DDAH would be inhibited and ADMA would also rise. Conversely, falling concentrations of arginine would dis-inhibit DDAH, which would increase the rate of ADMA clearance. We have shown that continuous infusion of citrulline and sepiapterin elevates plasma arginine, so we investigated the effect of this intervention on plasma ADMA concentrations. We found that median plasma ADMA concentrations were marginally but not significantly raised in *P. berghei* ANKA-infected mice infused with citrulline and sepiapterin (0.60 [0.49-0.71] µmol/L) compared to controls infused with saline (0.51 [0.42-0.63] µmol/L, $p = 0.20$ vs infected + sepiapterin, FIG 5.4). Thus, plasma ADMA was not substantially changed despite the fact that citrulline and sepiapterin infusion raised plasma arginine concentrations 4.2-fold compared to saline-infused infected controls (infected + citrulline/sepiapterin: 193.6 [154.6-229.2] µmol/L vs infected + saline: 53.9 [36.4-67.3] µmol/L, $p < 0.0001$, FIG 5.4). In *P. berghei* ANKA-infected mice infused with citrulline and sepiapterin, plasma ADMA concentrations were not different from values in uninfected controls (infected + citrulline/sepiapterin: 0.60 [0.49-0.71] µmol/L vs uninfected + saline: 0.60 [0.59-0.67] µmol/L, $p = 0.64$) despite the fact that citrulline and sepiapterin infusion raised plasma arginine concentrations 2.3-fold compared to uninfected controls (infected + citrulline/sepiapterin: 193.6 [154.6-229.2] µmol/L vs uninfected + saline: 94.0 [80.2-103.2] µmol/L, $p < 0.0001$, FIG 5.4). These findings directly contradict the hypothesis that plasma arginine concentrations influence plasma ADMA concentrations by inhibiting DDAH. With plasma ADMA concentrations remaining relatively constant, supplementation of arginine reduced the ADMA/arginine ratio in citrulline and sepiapterin-infused mice (infected + citrulline/sepiapterin: 3.3 [3.0-3.6] $\times 10^{-3}$ vs infected + saline: 10.0 [8.3-12.1] $\times 10^{-3}$, $p < 0.0001$, FIG 5.4). These results demonstrate that the plasma ADMA/arginine ratio can be corrected in *P.*

berghei ANKA-infected mice by supplementation of arginine without correction of underlying DDAH dysfunction (see, FIG 5.14, p. 185).

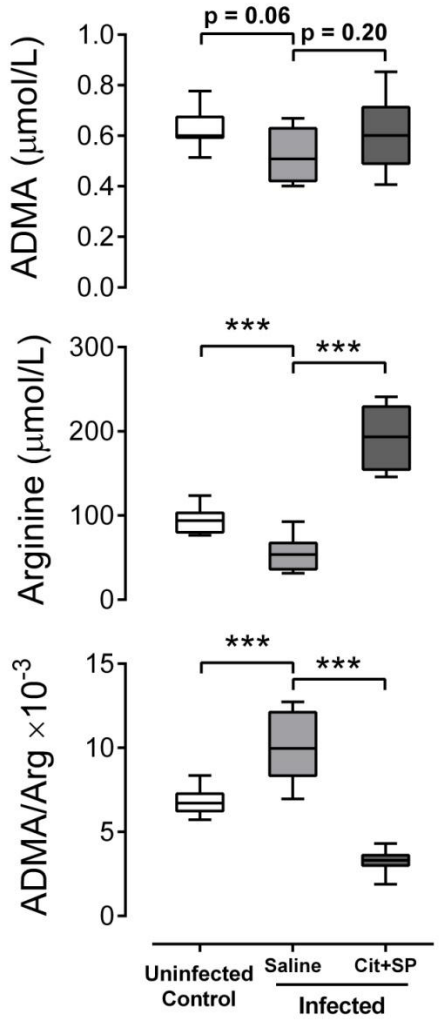


Figure 5.4 | Effect of citrulline and sepiapterin infusion on plasma ADMA/arginine ratios. Plasma ADMA and arginine were determined by HPLC on day 6 post-inoculation with *P. berghei* ANKA. *P. berghei* ANKA-infected mice received continuous intravenous infusion of saline (n=9) or 2.4g×kg^{-1}×d^{-1} citrulline + 15mg×kg^{-1}×d^{-1} sepiapterin (n=11). Saline-infused uninfected mice (n=12) served as controls. Data are pooled from 3 independent experiments. Box-plots depict median and IQR. Whiskers extend to highest and lowest values within 1.5×IQR of the 75th and 25th percentiles, and values outside this range were plotted as individual points (Tukey's method). *p<0.05, **p<0.01, ***p<0.001 by Mann-Whitney test.

Effect of Citrulline and Sepiapterin Infusion on Tissue Arginine, Citrulline and Ornithine

We used HPLC to determine the effects of *P. berghei* ANKA infection and citrulline/sepiapterin co-infusion on tissue concentrations of arginine, citrulline and ornithine. In aorta tissue, *P. berghei* ANKA infection did not significantly alter arginine (infected + saline: 4.7 [4.2-5.5] nmol/mg protein vs uninfected + saline: 4.3 [3.7-4.6] nmol/mg protein, $p = 0.08$) or ornithine (infected + saline: 0.6 [0.4-1.0] nmol/mg protein vs uninfected + saline: 0.5 [0.4-0.6] nmol/mg protein, $p = 0.34$), but depleted aortic citrulline (infected + saline: 1.2 [1.1-1.3] nmol/mg protein vs uninfected + saline: 2.7 [2.0-3.5] nmol/mg protein, $p < 0.0001$, FIG 5.5). Compared to saline-infused infected controls, infected mice infused with citrulline and sepiapterin demonstrated increased arginine (7.3 [5.9-8.4] nmol/mg protein, $p < 0.01$ vs infected + saline), citrulline (18.0 [16.7-28.7] nmol/mg protein, $p < 0.0001$ vs infected + saline) and ornithine (1.2 [0.7-1.9] nmol/mg protein, $p < 0.05$ vs infected + saline, FIG 5.5).

In liver tissue, *P. berghei* ANKA infection elevated arginine (infected + saline: 0.20 [0.16-0.24] nmol/mg protein vs uninfected + saline: 0.10 [0.12-0.13] nmol/mg protein, $p < 0.01$) and ornithine (infected + saline: 2.9 [2.3-3.5] nmol/mg protein vs uninfected + saline: 2.1 [1.8-2.3] nmol/mg protein, $p < 0.01$), but had no effect on citrulline (infected + saline: 1.4 [1.1-1.5] nmol/mg protein vs uninfected + saline: 1.2 [1.1-1.4] nmol/mg protein, $p = 0.19$, FIG 5.5). Infusion of citrulline and sepiapterin had no effect on liver arginine in infected mice (0.17 [0.15-0.21] nmol/mg protein, $p = 0.38$ vs infected + saline) but increased concentrations of citrulline (2.5 [2.3-3.8] nmol/mg protein, $p < 0.0001$ vs infected + saline) and ornithine (5.2 [4.2-6.6] nmol/mg protein, $p < 0.001$ vs infected + saline, FIG 5.5).

Compared to uninfected controls, *P. berghei* ANKA-infected mice demonstrated higher arginine concentrations in brain tissue (infected + saline: 6.4 [4.7-6.8] nmol/mg protein vs uninfected + saline: 3.3 [3.1-3.5] nmol/mg protein, $p < 0.0001$, FIG 5.5), but ornithine was unchanged (infected + saline: 0.5 [0.5-0.6] nmol/mg protein vs uninfected + saline: 0.5 [0.5-0.7] nmol/mg protein, $p = 0.64$, FIG 5.5). Citrulline in brain tissue was not determined because the peak was too small and poorly resolved from a closely-eluting unidentified peak for reliable

quantification. Compared to infected controls infused with saline, infected mice infused with citrulline and sepiapterin demonstrated increased brain arginine (23.2 [11-28.6] nmol/mg protein, $p < 0.0001$ vs infected + saline) and ornithine (1.7 [0.8-2.0] nmol/mg protein, $p < 0.01$ vs infected + saline, FIG 5.5).

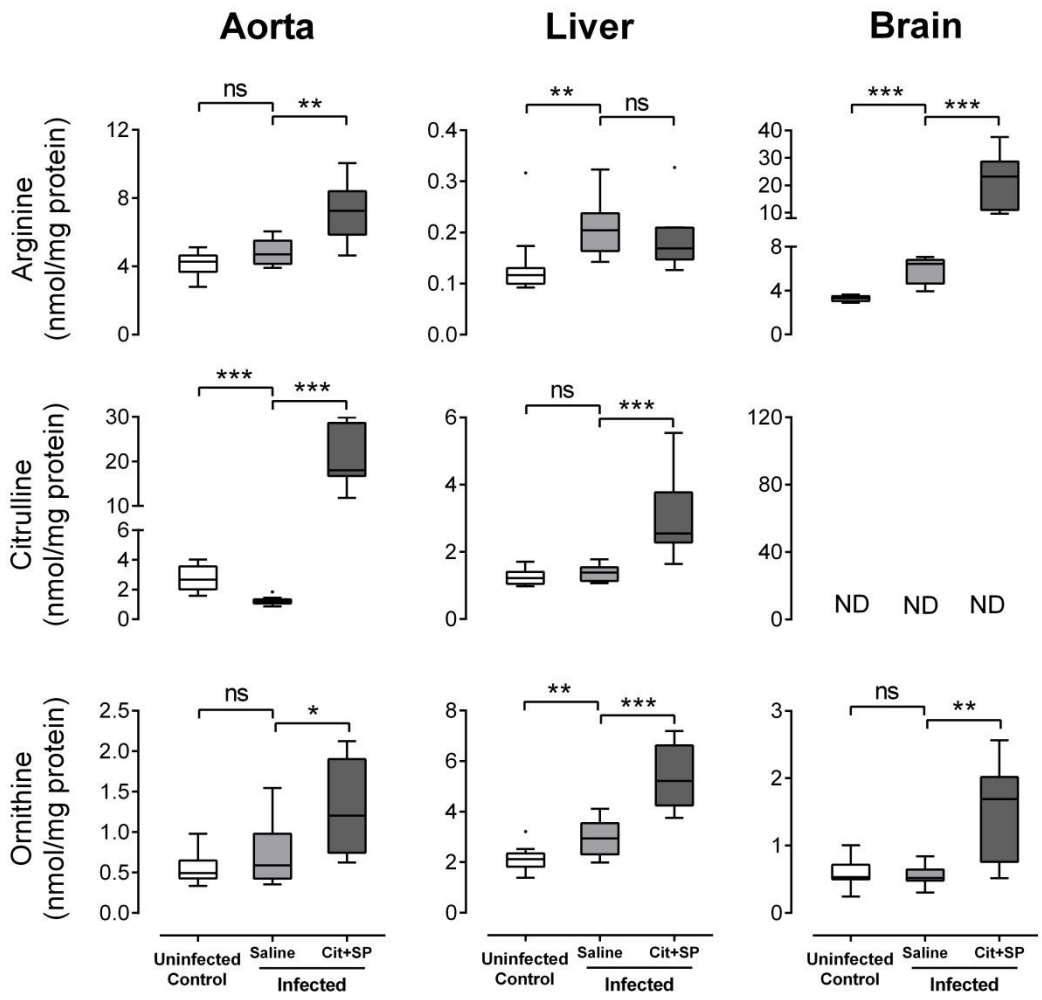


Figure 5.5 | Supplementation of tissue arginine, citrulline and ornithine by continuous infusion of citrulline and sepiapterin. Tissue concentrations of arginine, citrulline and ornithine were determined by HPLC and normalized to soluble protein. *P. berghei* ANKA-infected mice received continuous intravenous infusion of saline (n=9) or 2.4g×kg^{-1}×d^{-1} citrulline + 15mg×kg^{-1}×d^{-1} sepiapterin (n=11). Tissue samples were collected on day 6 post-inoculation. Saline-infused uninfected mice (n=12) served as controls. Data are pooled from 3 independent experiments. Citrulline in brain tissue was not determined (ND) because the peak was too small and poorly resolved from a closely-eluting unidentified peak for reliable quantification. Box-plots depict median and IQR. Whiskers extend to highest and lowest values within 1.5×IQR of the 75th and 25th percentiles, and values outside this range were plotted as individual points (Tukey's method). *p<0.05, **p<0.01, ***p<0.001 by Mann-Whitney test. ns (not significant): p>0.05.

Despite significant depletion of plasma arginine pools, these findings demonstrate that *P. berghei* ANKA infection does not compromise intracellular availability of arginine in aorta and increases arginine concentrations in liver and brain. Arginine could have accumulated from increased uptake of plasma arginine, increased rates of intracellular proteolysis or reduced efflux of arginine derived from protein break-down. Reported intra-endothelial cell arginine concentrations based on estimated cell volumes range from 107 ± 9 µmol/L (Mitchell et al., 1990) to 840µmol/L ± 90 (Baydoun et al., 1990) in bovine aortic endothelial cells. Calibrated preparation of tissue slices of known thickness and measurement of surface area should be considered a more accurate method of determining the volume of tissue for the determination of intracellular concentrations on a per volume basis[1]. A study based on this approach determined that rat brain tissue contains arginine concentrations of 94.0 ± 7.8 µmol/L (mean ± SEM) (Cardounel and Zweier, 2002) compared to rat plasma arginine concentrations of 62 ± 18 µmol/L (mean ± SD) measured in a different study by the same group (Cardounel et al., 2007). These results suggest that tissue and plasma concentrations of arginine are somewhat, though not completely equilibrated. However, it is unclear to what extent intracellular arginine pools are utilized for NO synthesis. Cationic amino acid transporter-1 (CAT1) is localized to the cellular membrane in close proximity with caveolar NOS, raising the possibility that NO synthesis may depend in part or entirely on direct uptake of extracellular arginine (McDonald et al., 1997).

Citrulline is rapidly recycled to arginine by ASS1 and ASL enzymes in complex with NOS (Flam et al., 2001; Erez et al., 2011), suggesting that citrulline may also serve as a secondary NOS substrate pool. This proposition is supported by the observation that extracellular citrulline increases NO synthesis (Flam et al., 2001). In our study, we found that *P. berghei* ANKA infection resulted in depletion of both extracellular citrulline in plasma and intracellular citrulline in aorta tissue, which may limit substrate availability for NO synthesis. In

[1] Note: In this thesis, we present intracellular amino acid concentrations as nanomolar amounts per milligram of soluble protein. This approach allows values to be normalized to the quantity of tissue analyzed without requiring preparation of precise tissue sections.

contrast, citrulline was not decreased in liver tissue. Due to urea cycle metabolism, liver citrulline availability may be more dependent on local synthesis from ornithine than on uptake from plasma pools.

We demonstrate that continuous infusion of citrulline increases NOS substrate availability in tissue. Citrulline availability was improved in aorta and liver, and arginine availability was improved in aorta and brain tissue. Compared to infected controls infused with saline, infected mice receiving citrulline and sepiapterin infusion had similar liver arginine concentrations but greater ornithine concentrations, suggesting that excess arginine may have been converted to ornithine by arginase, which is highly expressed in liver tissue. Ornithine was also increased in aorta and brain tissue, suggesting the presence of intrinsic arginase activity or increased rates of uptake due to supplementation of plasma ornithine pools.

Effect of Citrulline and Sepiapterin Infusion on Plasma and Erythrocyte BH4 and 7,8-BH2

Compared to infected controls infused with saline, mice infused with citrulline and sepiapterin exhibited elevated plasma BH4 (infected + citrulline/sepiapterin: 0.76 [0.61-1.28] µmol/L vs infected + saline: 0.09 [0.07-0.16] µmol/L, $p < 0.0001$) and 7,8-BH2 (infected + citrulline/sepiapterin: 0.58 [0.53-0.89] µmol/L vs infected + saline: 0.08 [0.06-0.09] µmol/L, $p < 0.0001$) on day 6 post-inoculation with *P. berghei* ANKA (FIG 5.6). BH4 and 7,8-BH2 were supplemented to similar degrees in plasma, resulting in no effect on BH4/7,8-BH2 ratios (infected + citrulline/sepiapterin: 1.2 [0.8-1.6] µmol/L vs infected + saline: 1.2 [1.2-1.8] µmol/L, $p = 0.15$, FIG 5.6).

P. berghei ANKA-infected mice infused with citrulline and sepiapterin exhibited elevated red blood cell BH4 (infected + citrulline/sepiapterin: 3.12 [2.75-6.45] µmol/L vs infected + saline: 0.22 [0.20-0.27] µmol/L, $p < 0.0001$) and 7,8-BH2 (infected + citrulline/sepiapterin: 0.91 [0.77-1.63] µmol/L vs infected + saline: 0.09 [0.08-0.11] µmol/L, $p < 0.0001$, FIG 5.6). Continuous infusion with citrulline and sepiapterin elevated erythrocyte BH4

to a greater degree than 7,8-BH2, resulting in improvement of the BH4/7,8-BH2 ratio (infected + citrulline/sepiapterin: 3.9 [3.5-4.0] vs infected + saline: 2.7 [2.1-3.0], $p < 0.001$, FIG 5.6).

Sepiapterin infusion raised BH4 and 7,8-BH2 to supraphysiological concentrations in both plasma and red blood cells in *P. berghei* ANKA-infected mice. These observations indicate that sepiapterin reductase (SR) and dihydrofolate reductase (DHFR) remain functional during infection and effectively convert sepiapterin to 7,8-BH2 and recycle 7,8-BH2 to BH4. These findings are in contrast to intermittent injection of sepiapterin which had no effect on plasma BH4 or 7,8-BH2 concentrations when assessed 8-14 hours after the final injection (see FIG 4.5, p. 141). In addition, intermittent sepiapterin injections restored BH4 and 7,8-BH2 to normal concentrations in the red blood cells of *P. berghei* ANKA-infected mice, as assessed 8-14 hours after the final injection (see FIG 4.5, p. 141), whereas continuous sepiapterin infusion raised BH4 and 7,8-BH2 well above physiological concentrations. Taken together, these findings suggest that sepiapterin is converted to BH4 in erythrocytes and other tissues and a portion of this newly-generated BH4 is exported to plasma, as evident during continuous infusion. We hypothesize that excess BH4 produced from injected sepiapterin would have been cleared during the interval between the final sepiapterin injection and sample collection in our previous experiment.

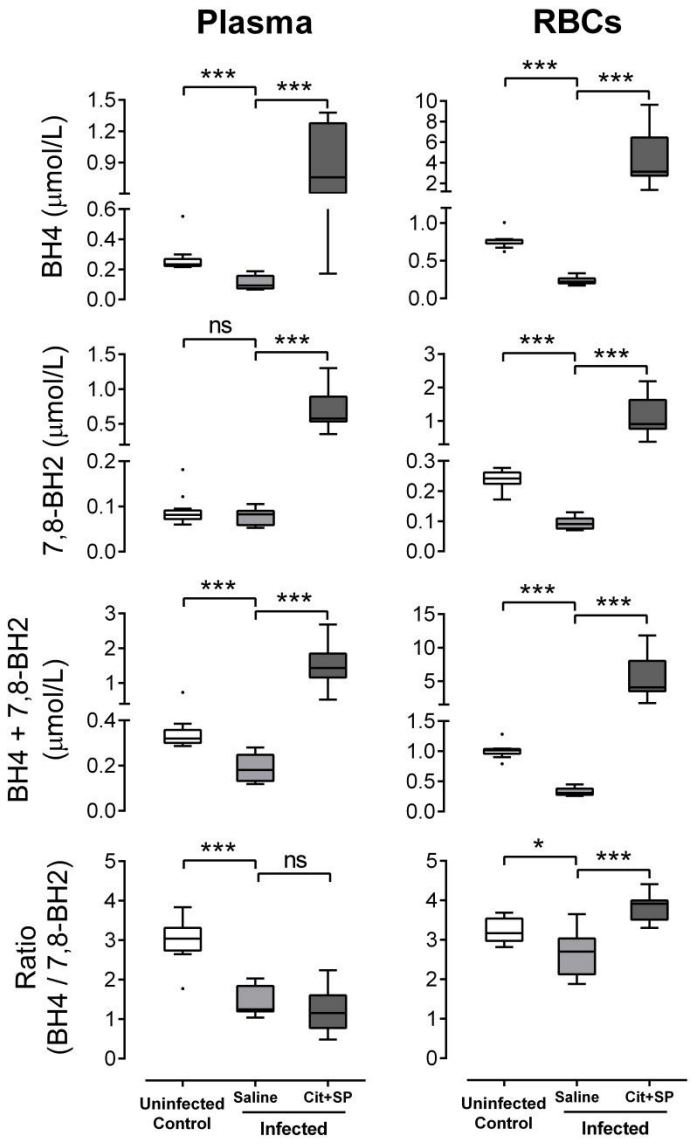


Figure 5.6 | Supplementation of plasma and erythrocyte BH4 by continuous infusion of citrulline and sepiapterin. Plasma and erythrocyte BH4 and 7,8-BH2 were determined by HPLC on day 6 post-inoculation. *P. berghei* ANKA-infected mice received continuous intravenous infusion of saline (n=9) or 2.4g×kg^{-1}×d^{-1} citrulline + 15mg×kg^{-1}×d^{-1} sepiapterin (n=11). Saline-infused uninfected mice (n=12) served as controls. Data are pooled from 3 independent experiments. Box-plots depict median and IQR. Whiskers extend to highest and lowest values within 1.5×IQR of the 75th and 25th percentiles, and values outside this range were plotted as individual points (Tukey's method). *p<0.05, **p<0.01, ***p<0.001 by Mann-Whitney test. ns (not significant): p>0.05.

Effect of Citrulline and Sepiapterin Infusion on Tissue BH4 and 7,8-BH2

We used HPLC to determine the effects of simultaneous citrulline and sepiapterin infusion on tissue concentrations of BH4 and 7,8-BH2. Compared to infected controls infused with saline, *P. berghei* ANKA-infected mice infused with citrulline and sepiapterin exhibited elevated BH4 concentrations in aorta tissue, (infected + citrulline/sepiapterin: 341.9 [318.8-470.6] pmol/mg protein vs infected + saline: 49.0 [33.7-52.8] pmol/mg protein, $p < 0.0001$) liver tissue (infected + citrulline/sepiapterin: 249.5 [164.4-409.6] pmol/mg protein vs infected + saline: 80.1 [72.4-89.9] pmol/mg protein, $p < 0.0001$) and brain tissue (infected + citrulline/sepiapterin: 39.9 [26.1-64.7] pmol/mg protein vs infected + saline: 14.8 [13.1-16.5] pmol/mg protein, $p < 0.0001$, FIG 5.7). Citrulline and sepiapterin infusion also increased tissue 7,8-BH2 concentrations in aortic tissue, (infected + citrulline/sepiapterin: 84.3 [63.6-98.4] pmol/mg protein vs infected + saline: 7.9 [6.1-10.7] pmol/mg protein, $p < 0.0001$) liver tissue (infected + citrulline/sepiapterin: 19.2 [11.6-33.4] pmol/mg protein vs infected + saline: 6.2 [5.3-6.6] pmol/mg protein, $p < 0.0001$) and brain tissue (infected + citrulline/sepiapterin: 8.4 [2.3-15.4] pmol/mg protein vs infected + saline: 2.1 [1.7-2.2] pmol/mg protein, $p < 0.0001$) of *P. berghei* ANKA-infected mice (FIG 5.7). Infusion of citrulline and sepiapterin had no effect on BH4/7,8-BH2 ratios in aorta tissue, (infected + citrulline/sepiapterin: 4.7 [3.4-5.6] vs infected + saline: 5.3 [4.1-7.5], $p = 0.23$), liver tissue (infected + citrulline/sepiapterin: 13.4 [11.3-18.0] vs infected + saline: 13.5 [11.8-15.3], $p = 0.84$) or brain tissue (infected + citrulline/sepiapterin: 6.0 [4.4-10.9] vs infected + saline: 7.6 [6.4-8.0], $p = 0.23$, FIG 5.7).

We previously found that intermittent injection of sepiapterin elevated BH4 and 7,8-BH2 concentrations in aorta and brain tissue but had no effect on BH4 or 7,8-BH2 in liver tissue (FIG 4.6 p. 143). The current experiment demonstrates that continuous infusion of sepiapterin elevates BH4 and 7,8-BH2 in liver tissue in addition to aorta and brain. These findings suggest that excess BH4 is cleared more rapidly from liver tissue as compared to aorta and brain. Thus in previous experiments, accumulated BH4 was evident in aorta and brain but may have been cleared from liver tissue in the 8-14hr interval between the final injection and tissue collection.

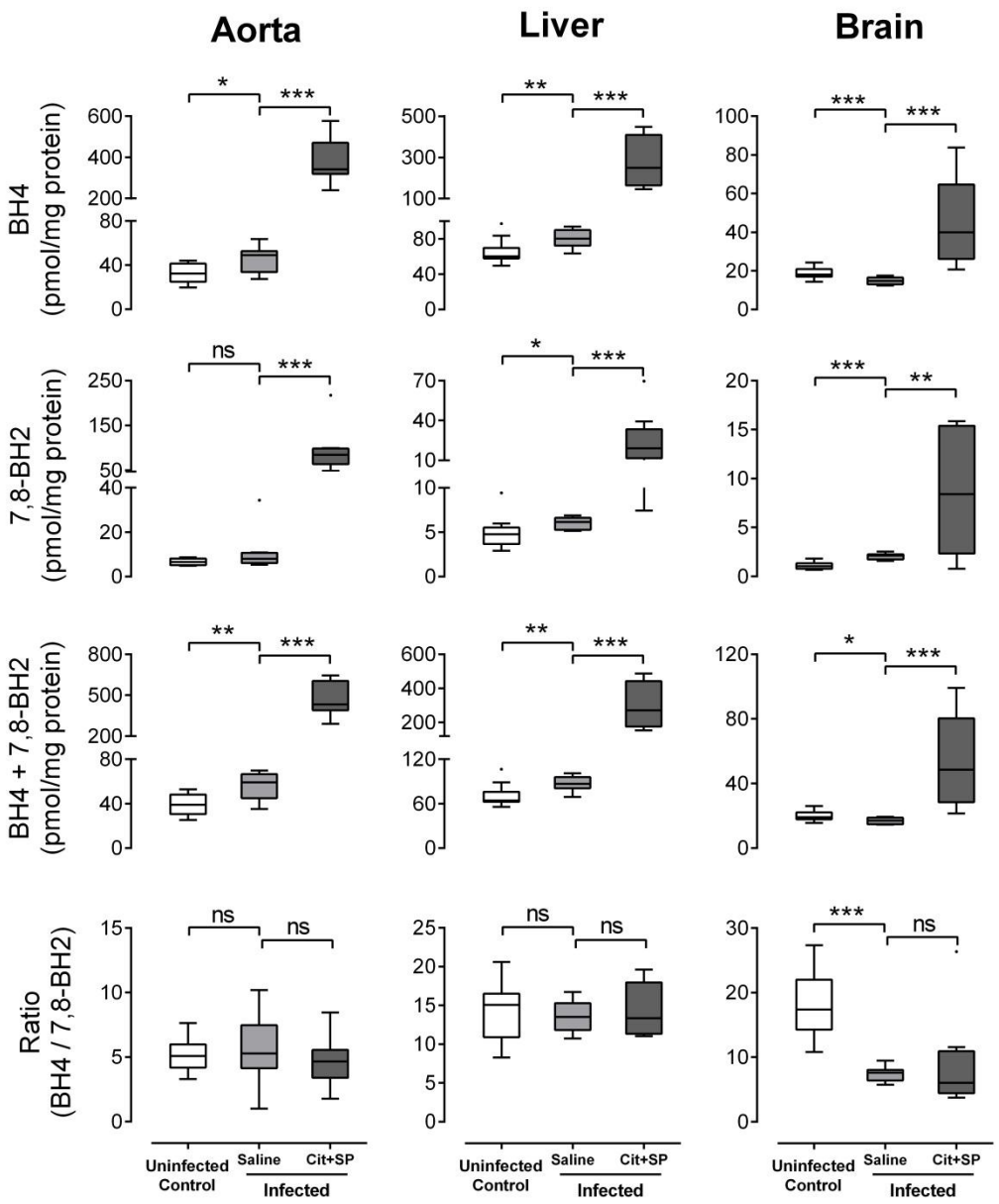


Figure 5.7 | Supplementation of tissue BH4 by continuous infusion of citrulline and sepiapterin. Tissue BH4 and 7,8-BH2 were determined by HPLC and normalized to soluble protein. *P. berghei* ANKA-infected mice received continuous intravenous infusion of saline (n=9) or 2.4g×kg^{-1}×d^{-1} citrulline + 15mg×kg^{-1}×d^{-1} sepiapterin (n=11). Tissue samples were collected on day 6 post-inoculation. Saline-infused uninfected mice (n=12) served as controls. Data are pooled from 3 independent experiments. Box-plots depict median and IQR. Whiskers extend to highest and lowest values within 1.5×IQR of the 75th and 25th percentiles, and values outside this range were plotted as individual points (Tukey's method). *p<0.05, **p<0.01, ***p<0.001 by Mann-Whitney test. ns (not significant): p>0.05.

5.4 Physiological Effects of Simultaneous Citrulline and Sepiapterin Infusion

Disease severity

To determine the effect of BH4 and arginine co-supplementation on disease progression, we quantified behavioural symptoms in cohorts of *P. berghei* ANKA-infected mice infused with saline or citrulline and sepiapterin. On day 6 post-inoculation, rapid onset of symptoms, including hunched posture, lethargy and unresponsiveness, were observed in saline-infused infected controls in the morning (infected + saline behavioural score: 2 [0-7] out of 14 vs uninfected + saline: 14 [14-14], $p < 0.0001$) and directly before tissue collection (infected + saline behavioural score: 1 [0-3] out of 14 vs uninfected + saline: 14 [14-14], $p < 0.0001$, FIG 5.8). *P. berghei* ANKA-infected mice infused with citrulline and sepiapterin demonstrated higher median behavioural scores than infected controls infused with saline on the morning of day 6 post-inoculation (6 [0-13], $p = 0.37$ vs infected + saline) and directly before tissue collection (1.5 [1-12], $p = 0.10$ vs infected + saline), but these differences did not reach statistical significance (FIG 5.8). From these observations, we conclude that simultaneous supplementation of arginine and BH4 does not provide mice with substantial protection from severe symptoms associated with *P. berghei* ANKA infection. In contrast, survival is improved in *P. berghei* ANKA-infected mice treated with inhaled nitric oxide (Serghides et al., 2011) or with intermittent injection of the nitric oxide donor DPTA-NONOate (Gramaglia et al., 2006; Cabrales et al., 2011).

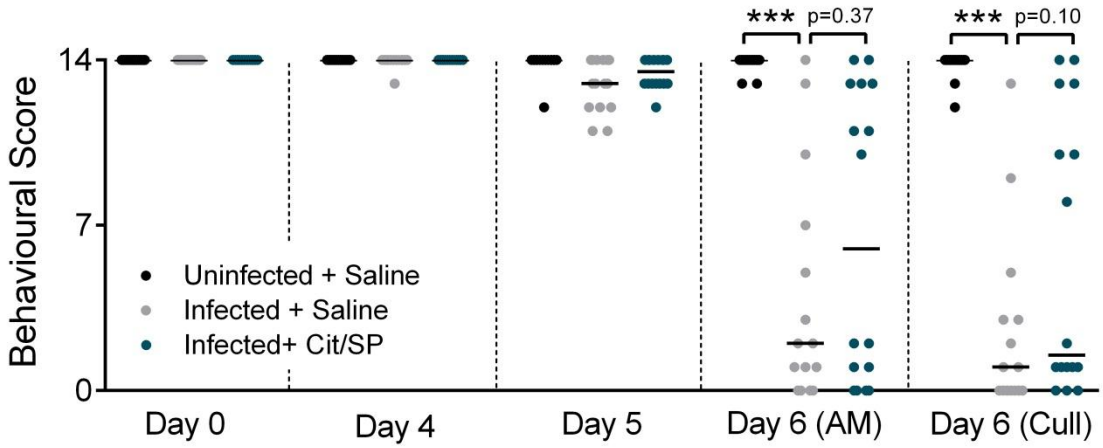


Figure 5.8 | Effect of citrulline and sepiapterin infusion on behavioural scores. *P. berghei* ANKA-infected mice received continuous intravenous infusion of saline (n=15) or 2.4g×kg^{-1}×d^{-1} citrulline + 15mg×kg^{-1}×d^{-1} sepiapterin (n=16). Saline-infused uninfected mice (n=15) served as controls. Symptoms were scored by assessing each of 7 parameters on a scale of 0 (moribund) to 2 (normal). D6 (AM) scores reflect assessments taken from 7AM-9AM in the morning for all animals and D6 (Cull) scores reflect assessments taken directly before each animal was culled for tissue collection. Pooled data from 4 independent experiments are plotted as individual points with medians indicated by black lines. ***p<0.001 by Mann-Whitney test.

Dietary Intake, Fluid Intake and Weight Loss

We measured the effect of citrulline + sepiapterin infusion on dietary intake, fluid intake and body weight. On day 5 post-inoculation, dietary intake was decreased in *P. berghei* ANKA-infected mice infused with saline (2.6 ± 0.1 g) compared with uninfected controls (4.3 ± 0.2 g, $p < 0.0001$, FIG 5.9). Infusion of citrulline and sepiapterin had no effect on dietary intake in infected mice on day 5 post-inoculation (2.7 ± 0.2 g, $p > 0.99$ vs infected + saline, FIG 5.9). On day 6 post-inoculation, dietary intake was further decreased in infected mice infused with saline (infected + saline: 0.2 ± 0.1 vs uninfected: 4.0 ± 0.4 g, $p < 0.0001$, FIG 2.9). Infected mice infused with citrulline and sepiapterin consumed more food than infected controls infused with saline (infected + citrulline/sepiapterin: 1.3 ± 0.4 g vs infected + saline: 0.2 ± 0.1, $p < 0.01$) but still significantly less than uninfected mice ($p < 0.0001$, FIG 5.9). On day 6 post-inoculation water intake was reduced to similar degrees in infected mice treated with saline (1.3 ± 0.2 g) and infected mice infused with citrulline and sepiapterin (1.8 ± 0.3, $p = 0.42$ vs infected + saline) compared to uninfected controls (4.1 ± 0.5 g, $p < 0.0001$ vs infected + citrulline/sepiapterin, $p < 0.0001$ vs infected + saline, FIG 5.9). Similar degrees of weight loss were also observed in infected controls treated with saline (-3.1 ± 0.3 g from day 0) and in infected mice infused with citrulline and sepiapterin (-3.3 ± 0.3 g from day 0, $p > 0.99$ vs infected + saline). For comparison, uninfected mice only lost 0.5 ± 0.2 g from day 0 ($p < 0.0001$ vs infected + citrulline/sepiapterin, $p < 0.0001$ vs infected + saline, FIG 5.9). These results demonstrate that simultaneous infusion of citrulline and sepiapterin results in marginally increased dietary intake in *P. berghei* ANKA-infected mice but had no effect on water intake or weight-loss.

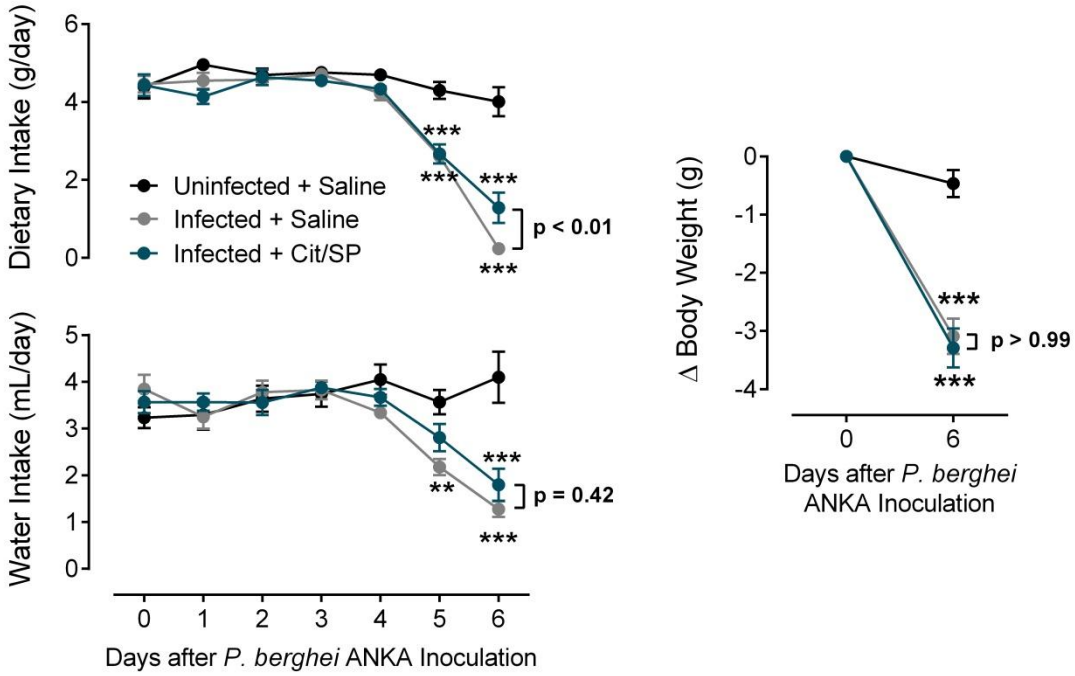


Figure 5.9 | Dietary intake and weight loss in *P. berghei* ANKA-infected mice infused with citrulline and sepiapterin. All mice were individually caged and provided with ad libitum-access to water and formulated diet. Daily intake and body mass were monitored daily by weight. Data are expressed as mean ± SEM for a total of n=15 uninfected mice infused with saline, n=15 *P. berghei* ANKA-infected mice infused with saline and n=16 infected mice infused with 2.4g×kg^{-1}×d^{-1} citrulline + 15mg×kg^{-1}×d^{-1} sepiapterin. Data are pooled from 4 independent experiments. **p<0.01, ***p<0.001 vs uninfected control group by two-way ANOVA followed by Bonferroni post-test.

5.5 Effects of Citrulline and Sepiapterin Infusion on NOS Uncoupling

NOS uncoupling results in decreased production of nitric oxide and increased production of superoxide. We hypothesized that by supplementing both arginine and BH4, simultaneous infusion of sepiapterin and citrulline would improve NO synthesis and re-couple NOS. To test this hypothesis, we assessed whole blood nitrite as a biomarker of systemic NO synthesis and tissue nitrotyrosine as a biomarker of superoxide generation.

Whole Blood Nitrite

Median whole blood nitrite concentrations were lower in *P. berghei* ANKA-infected mice infused with saline (0.28 [0.25-0.34] µmol/L) than uninfected mice infused with saline (0.33 [0.27-0.43] µmol/L). This difference was not found to be statistically significant ($p = 0.34$) in contrast to previous analyses in which whole blood nitrite concentrations were decreased in infected mice compared to uninfected controls (see FIG 4.8, p. 145, FIG 5.2, p. 160 and FIG 5.11, p. 179). Simultaneous infusion of citrulline and sepiapterin improved whole blood nitrite in *P. berghei* ANKA-infected mice (0.35 [0.32-0.40] µmol/L) compared with saline-infused controls (0.28 [0.25-0.34] µmol/L, $p < 0.05$, FIG 5.10). These results suggest that simultaneous infusion of citrulline and sepiapterin restores NO synthesis in *P. berghei* ANKA-infected mice. However, infected mice infused with citrulline and sepiapterin consumed more food than infected controls infused with saline, prompting us to consider whether dietary nitrite intake could have contributed to improved whole blood nitrite.

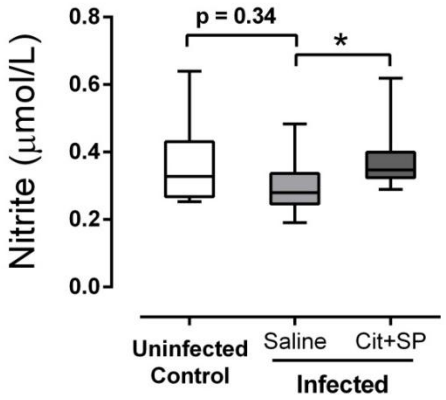


Figure 5.10 | Simultaneous infusion of citrulline and sepiapterin improves whole blood nitrite in *P. berghei* ANKA-infected mice. Whole blood nitrite concentrations were determined by chemical reduction and chemilluminescent detection with a nitric oxide analyzer. *P. berghei* ANKA-infected mice received continuous intravenous infusion of saline (n=9) or 2.4g×kg^{-1}×d^{-1} citrulline + 15mg×kg^{-1}×d^{-1} sepiapterin (n=11). Whole blood samples were collected on day 6 post-inoculation. Saline-infused uninfected mice (n=12) served as controls. Data are pooled from 3 independent experiments. Boxplots depict median, IQR and range. *p<0.05 by Mann-Whitney test.

Limitations of Whole Blood Nitrite as a Biomarker of NO Synthesis

Effect of Dietary Restriction on Whole Blood Nitrite

To determine the effects of dietary intake on whole blood nitrite, we analyzed whole blood samples from the dietary restriction experiments described in CHAPTER 2 (p. 42). In uninfected mice subjected to dietary restriction, whole blood nitrite was reduced (0.37 [0.35-0.39] µmol/L) compared with uninfected mice with *ad libitum* access to food (0.44 [0.39-0.64] µmol/L, $p < 0.01$, FIG 5.11). Whole blood nitrite did not vary significantly between uninfected mice subjected to dietary restriction and *P. berghei* ANKA-infected mice (infected: 0.39 [0.32-0.41] µmol/L, $p = 0.74$ vs uninfected + dietary restriction, FIG 5.11). These findings suggest that sustained dietary intake plays a central role in the maintenance of whole blood nitrite concentrations, either via intake of amino acid substrates for NO synthesis or by direct ingestion of dietary nitrite.

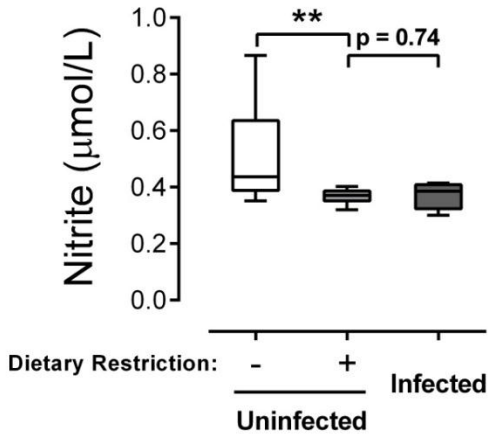


Figure 5.11 | Dietary restriction reduces whole blood nitrite in uninfected mice. Whole blood nitrite concentrations were determined by chemical reduction and chemilluminescent detection with a nitric oxide analyzer. Whole blood samples were collected from uninfected mice with *ad libitum* access to food (n=10), uninfected subjected to dietary restriction (n=9) and *P. berghei* ANKA-infected mice 6 days post-inoculation (n=9). Uninfected mice subjected to dietary restriction received only as much food as was consumed each day by a paired mouse infected with *P. berghei* ANKA. Data are pooled from 3 independent experiments. Box-plots depict median, IQR and range. Uninfected controls with or without dietary restriction were compared by Mann-Whitney test, **$p < 0.01$; uninfected + dietary restriction values were compared to infected values by Wilcoxon matched-pairs signed rank test.

Assessment of Nitrite in Food and Water Provided to Experimental Mice

We used chemical reduction and a nitric oxide analyzer to determine if formulated rodent diet pellets contained nitrite that could potentially be absorbed directly into circulation. Prior to analysis, we pulverized sample pellets with a mortar and pestle and added 10µl of ultrapure de-ionized water (Milli-Q Synthesis System from Millipore Corporation, Billerica MA, USA) for each milligram of dry food. The resulting slurry was vortexed vigorously for 5 minutes and centrifuged for 5 minutes at 16,100 × G and 4°C. Nitrite concentrations in the extracted aqueous supernatant were analyzed and compared to sodium nitrite ($NaNO_2$) standards of known concentrations (FIG 5.12). The concentration of nitrite in extracted aqueous supernatant was determined be 0.21 µmol/L (FIG 5.12). We also considered whether acidified water provided to experimental mice might contain nitrite. Acidified water provided was analyzed directly by chemical reduction of nitrite and detection with a nitric oxide analyzer. Nitrite concentrations in acidified water were not distinguishable from the background noise of the assay (FIG 5.12).

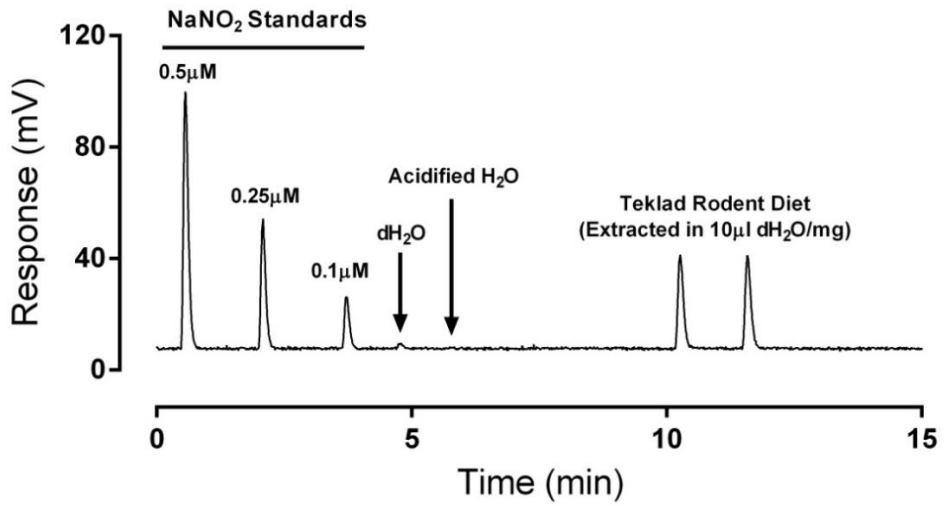


Figure 5.12 | Analysis of nitrite in food and water provided to experimental mice. Nitrite concentrations were determined by chemical reduction and chemilluminescent detection with a nitric oxide analyzer. Sodium nitrite ($NaNO_2$) was dissolved in ultrapure water and dilutions of 0.5 µM, 0.25 µM and 0.1µM were as calibration standards (first 3 peaks from left). Ultrapure distilled water (dH_2O) was injected as a blank (4th peak). Acidified water provided to mice did not produce a peak distinguishable from background noise. Teklad rodent diet was extracted in 10µl ultrapure distilled water per mg dry weight (final 2 peaks). Nitrite concentrations were quantified by interpolating areas against a standard curve constructed from the areas produced by known concentrations of sodium nitrite.

The concentration of nitrite in extracted aqueous supernatant (0.21 µmol/L) was used to calculate the molar amount of nitrite contained in dry food (by mass):

$$0.21\ \mu\text{M}\ \text{NO}_2 \times \frac{10\ \mu\text{l}\ \text{H}_2\text{O}}{\text{mg dry food}} = 2.1\ \text{nmol}\ \text{NO}_2/\text{g dry food} \qquad \textit{Eq 5.1}$$

We then used this value to calculate the theoretical increase in whole blood nitrite concentration for each mouse on day 6 post-inoculation if all dietary nitrites were absorbed completely and distributed throughout the circulating blood volume. For this calculation, we used the measured dietary intake and bodyweight of each mouse and estimated the circulating blood volume to be 72 mL/kg (Diehl et al., 2001). A sample calculation is shown based on a dietary intake of 4.5g and a bodyweight of 25.6g:

$$\frac{2.1\ \text{nmol}\ \text{NO}_2}{\text{g dry food}} \times 4.5\ \text{g dry food intake} = 9.7\ \text{nmol}\ \text{NO}_2 \qquad \textit{Eq 5.2}$$

$$9.7\ \text{nmol}\ \text{NO}_2 \times \frac{1}{25.6\ \text{g body weight}} \times \frac{\text{kg body weight}}{72\ \text{mL blood}} = 5.2\ \mu\text{mol/L}\ \text{NO}_2 \qquad \textit{Eq 5.3}$$

Applying this calculation to the citrulline/sepiapterin co-infusion experiment, we found that uninfected mice consumed dietary nitrite on day 6 equivalent to 5.0 µmol/L (IQR: 4.5-5.8 µmol/L) if completely absorbed into circulation. This figure is more than one order of magnitude higher than the measured whole blood nitrite concentration in this group (0.33 [0.27-0.43] µmol/L), suggesting incomplete absorption and/or continual clearance. *P. berghei* ANKA-infected mice infused with saline consumed the equivalent of 0.0 µmol/L (IQR: 0.0-0.68 µmol/L) nitrite on day 6 post-inoculation, whereas infected mice infused with citrulline and sepiapterin consumed the equivalent of 0.52 µmol/L (IQR: 0.0-2.55 µmol/L, $p = 0.12$ vs infected + saline, $p < 0.0001$ vs uninfected).

Taken together these results indicate that whole blood nitrite is influenced by nitrite intake in the diet and that dietary intake of nitrite could have contributed to increased whole blood nitrite in infected mice infused with citrulline and sepiapterin compared to infected controls infused with saline. This observation does not preclude the possibility that whole blood nitrite could also be increased by improved NO synthesis in *P. berghei* ANKA-infected mice treated with citrulline and sepiapterin.

Nitrotyrosine

Nitrotyrosine is formed by the nitration of tyrosine residues by peroxynitrite. We used ELISA to investigate plasma, liver and brain nitrotyrosine as a biomarker of uncoupled NOS activity. Neither *P. berghei* ANKA infection nor co-supplementation of citrulline and sepiapterin altered plasma nitrotyrosine concentrations (uninfected: 226 [195-279] ng nitro-BSA equivalents/mL, infected + saline: 252 [172-282] ng nitro-BSA equivalents/mL, $p = 0.60$ vs uninfected, infected + citrulline/sepiapterin: 0.261 [205-380] ng nitro-BSA equivalents/mL, $p = 0.52$ vs infected + saline, FIG 5.13). Nitrotyrosine was assessed in uninfected and infected brain samples from another experiment. *P. berghei* ANKA infection had no effect on brain nitrotyrosine (infected: 74 [59-106] ng nitro-BSA equivalents/mg protein vs uninfected: 94 [58-136] ng nitro-BSA equivalents/mg, $p = 0.67$, FIG 5.13). Because infection alone produced no effect on brain nitrotyrosine, the effect of citrulline and sepiapterin infusion was not studied. *P. berghei* ANKA infection decreased nitrotyrosine in liver tissue (infected + saline: 147 [122-167] ng nitro-BSA equivalents/mg protein vs uninfected: 204 [165-221] ng nitro-BSA equivalents/mg protein, $p < 0.01$, FIG 5.13). Citrulline and sepiapterin treatment partially reversed this decrease in liver nitrotyrosine (171 [143-199] ng nitro-BSA equivalents/mg protein), but this difference was not statistically significant compared to infected controls infused with saline ($p = 0.24$, FIG 5.13).

Contradicting our hypothesis, these results suggest that *P. berghei* ANKA infection decreases the rate of peroxynitrite formation. Determining the mechanism of decreased

peroxynitrite formation requires further investigation. Reduced nitrotyrosine could result from inhibition of superoxide generation or from inhibition of nitric oxide synthesis, since both are required to produce peroxynitrite. The observation that the decrease in nitrotyrosine was partially, though not significantly, reversed by citrulline and sepiapterin supplementation suggests that nitrotyrosine may be more reflective of NO synthesis than of superoxide generation by uncoupled NOS. This interpretation would have to be confirmed with alternate read-outs of local NO synthesis, such as tissue concentrations of cyclic GMP, a secondary messenger generated by NO activation of soluble guanlyate cyclase. Specific assays for generation of superoxide anions with and without addition of a NOS-specific inhibitor (e.g. L-N^G-nitroarginine methyl ester or L-NAME) would be required to more closely investigate NOS-specific superoxide generation (Crabtree et al., 2009b; a).

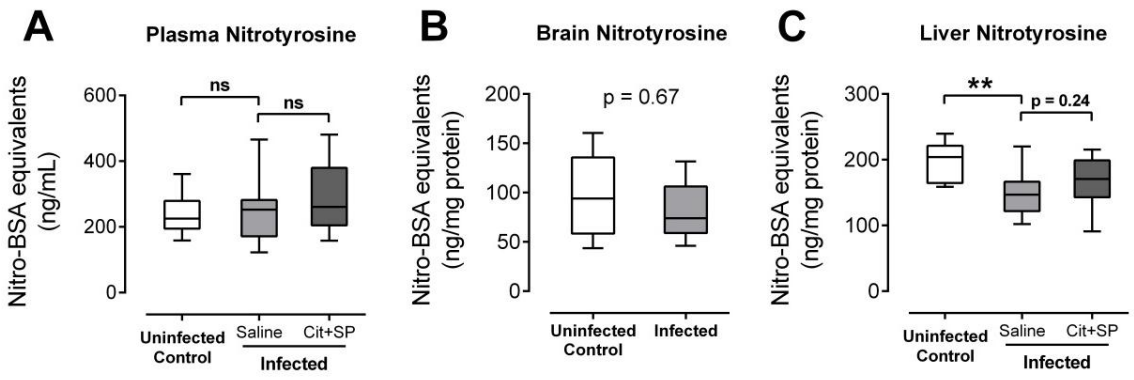


Figure 5.13 | Plasma, brain and liver nitrotyrosine in *P. berghei* ANKA-infected mice. Nitrotyrosine was assayed by ELISA in plasma (**A**), homogenized brain (**B**) and homogenized liver samples (**C**). Nitrotyrosine concentrations were normalized to soluble protein in tissue homogenates. Samples in panels A and C were collected from uninfected mice infused with saline (n=12), *P. berghei* ANKA-infected mice infused with saline (n=9) and infected mice infused with 2.4g×kg^{-1}×d^{-1} citrulline + 15mg×kg^{-1}×d^{-1} sepiapterin (n=11). Samples were collected 6 days post-inoculation. Samples in panel B were collected from a separate cohort of *P. berghei* ANKA-infected mice 6 days post-inoculation (n=5) and uninfected (n=5) controls. **p < 0.01 by Mann-Whitney test. ns (not significant): p > 0.05.

5.6 Effect of Citrulline and Sepiapterin Infusion on Hepatic DDAH Function

Hepatic dimethylarginine dimethylaminohydrolase-1 (DDAH1) plays a major role in regulating plasma asymmetric dimethylarginine (ADMA), an endogenous NOS inhibitor (Hu et al., 2006; Wang et al., 2007). *P. berghei* ANKA infection causes loss of hepatic DDAH1 protein and impaired DDAH activity (see CHAPTER 3, FIGS 3.10 & 3.9, p. 105-106). In cultured smooth muscle cells, increased oxidative stress due to overexpression of the $p22^{phox}$ subunit of NADPH oxidase caused proteasome-mediated degradation of DDAH protein and loss of ADMA clearance activity (Luo et al., 2010). Based on this evidence, we hypothesized that NOS uncoupling could promote oxidative modification and degradation of hepatic DDAH during *P. berghei* ANKA infection. To indirectly assess whether NOS uncoupling contributes to hepatic DDAH degradation, we investigated the effects of citrulline and sepiapterin infusion on hepatic DDAH activity and accumulation of intracellular hepatic ADMA. In *P. berghei* ANKA-infected mice, we found that increased hepatic BH4 concentrations following infusion of citrulline and sepiapterin had no effect on hepatic DDAH activity (infected + citrulline/sepiapterin: 5.1 [3.7-5.8] nmol citrulline × mg $protein^{-1}$ × hr^{-1} vs infected + saline: 4.8 [4.3-5.3] nmol citrulline × mg $protein^{-1}$ × hr^{-1}, p = 0.80) or intracellular ADMA (infected + citrulline/sepiapterin: 200 [153-268] pmol/mg protein vs infected + saline: 235 [180-265] pmol/mg protein, p = 0.47, FIG 5.14). These results demonstrate that restoration of plasma BH4 and arginine is not sufficient to improve hepatic DDAH activity in *P. berghei* ANKA-infected mice. Additional experiments are required to evaluate the role of oxidative stress in hepatic DDAH dysfunction (see CHAPTER 6, p. 219), but our current experiments indicate that NOS uncoupling may not represent a central source of oxidative stress. Despite ongoing hepatic DDAH dysfunction, supplementation of plasma arginine successfully corrected plasma ADMA/arginine ratios (FIG 5.4, p. 164).

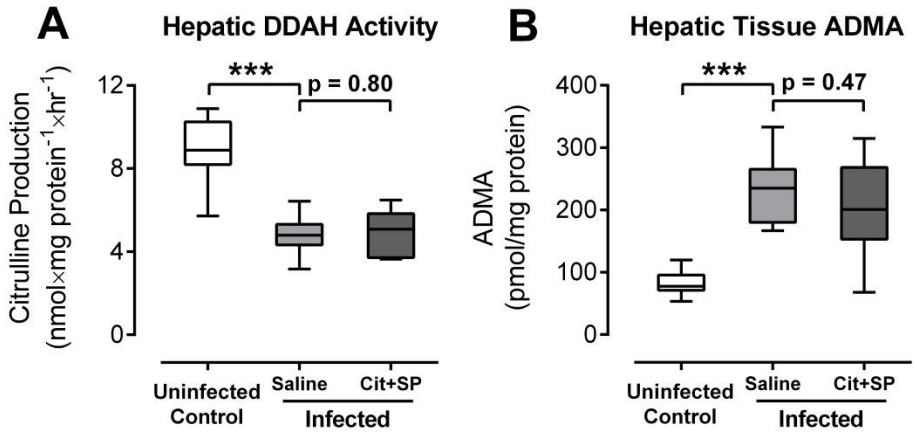


Figure 5.14 | No effect of citrulline and sepiapterin infusion on hepatic DDAH function in *P. berghei* ANKA-infected mice. (**A**) DDAH activity was assessed by quantification of citrulline production in liver homogenates spiked with saturating concentrations of ADMA substrate (2.5 mM). Citrulline production was calculated on a per-hour basis and normalized to protein content. (**B**) Intracellular hepatic ADMA was assessed by HPLC in perfused liver samples and normalized to protein content. Liver samples were collected 6 says post-inoculation in *P. berghei* ANKA-infected mice infused with saline (n=9) and infected mice infused with 2.4g×kg^{-1}×d^{-1} citrulline + 15mg×kg^{-1}×d^{-1} sepiapterin (n=11). Liver samples from uninfected mice infused with saline (n=13) served as controls. Data are pooled from 3 independent experiments. Boxplots represent median, IQR and range. ***p<0.001 by Mann-Whitney test. ns (not significant): p > 0.05.

5.7 Effect of Citrulline and Sepiapterin Infusion on Phenylalanine Metabolism

Phenylalanine is elevated in children with cerebral malaria (Enwonwu et al., 1999, 2000; Lopansri et al., 2006) as well as *P. berghei* ANKA-infected mice (see CHAPTER 2, FIG 2.3, p. 34). The enzyme phenylalanine hydroxylase (PAH) regulates circulating phenylalanine concentrations by hydroxylating phenylalanine to form tyrosine. Phenylalanine hydroxylase requires BH4 as a cofactor for this reaction, raising the possibility that insufficient BH4 availability may contribute to elevated plasma phenylalanine. We have demonstrated that infusion of citrulline and sepiapterin effectively supplements BH4 in the blood compartment and in tissue, including the liver, which is the primary site of phenylalanine hydroxylase expression. To determine if BH4 supplementation improved phenylalanine metabolism, we investigated phenylalanine and tyrosine concentrations in mice infused with citrulline and sepiapterin.

Effect of Citrulline and Sepiapterin Infusion on Plasma Phenylalanine and Tyrosine

Confirming our previous findings (see CHAPTER 2, FIG 2.3, p. 34), *P. berghei* ANKA-infected mice demonstrated elevated plasma phenylalanine concentrations (infected + saline: 112.6 [105.0-116.1] µmol/L vs uninfected + saline: 70.4 [57.5-80.3] µmol/L, $p < 0.0001$, FIG 5.15). We also found that tyrosine was decreased in infected mice (infected + saline: 58.1 [44.8-67.4] µmol/L vs uninfected + saline: 77.4 [67.7-94.6] µmol/L, $p < 0.0001$), resulting in elevation of the phenylalanine/tyrosine ratio (infected + saline: 2.0 [1.8-2.4] vs uninfected + saline: 0.9 [0.8-1.0], $p < 0.0001$, FIG 5.15). Compared to infected controls infused with saline, infected mice infused with citrulline and sepiapterin demonstrated reduced phenylalanine (98.9 [83.3-109.0] µmol/L, $p < 0.05$ vs uninfected + saline), elevated tyrosine (68.0 [64.5-76.6] µmol/L, $p < 0.05$ vs uninfected + saline) and an associated reduction in the phenylalanine/tyrosine ratio (1.3 [1.2-1.7], $p < 0.0001$ vs uninfected + saline, FIG 5.15).

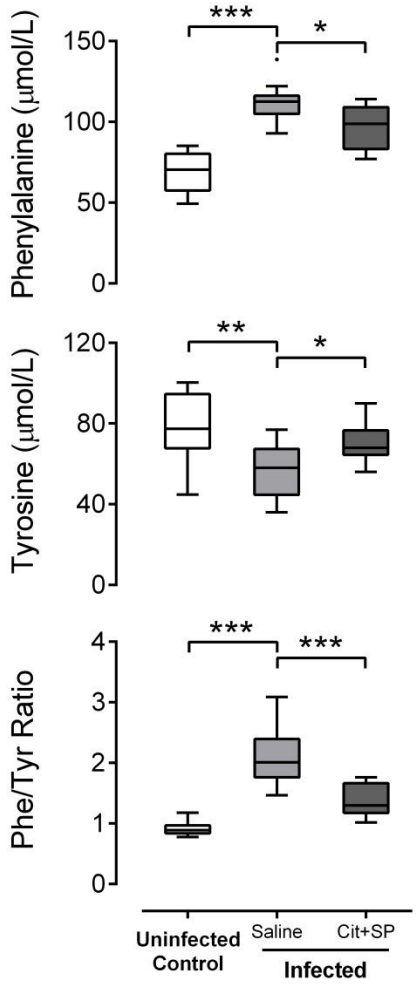


Figure 5.15 | Citrulline and sepiapterin infusion restores plasma phenylalanine/tyrosine ratios. Plasma phenylalanine and tyrosine were determined by HPLC 6 days post-inoculation with *P. berghei* ANKA. *P. berghei* ANKA-infected mice received continuous intravenous infusion of saline (n=9) or 2.4g×kg^{-1}×d^{-1} citrulline + 15mg×kg^{-1}×d^{-1} sepiapterin (n=11). Saline-infused uninfected mice (n=12) served as controls. Data are pooled from 3 independent experiments. Box-plots depict median, IQR, min and max. Whiskers extend to highest and lowest values within 1.5×IQR of the 75th and 25th percentiles, and values outside this range were plotted as individual points (Tukey's method). *p<0.05, **p<0.01, ***p<0.001 by Mann-Whitney test. ns (not significant): p>0.05.

Effect of Citrulline and Sepiapterin Infusion on Tissue Phenylalanine and Tyrosine

Phenylalanine is converted to tyrosine primarily by phenylalanine hydroxylase (PAH) expressed in the liver. Tyrosine is released into circulation and taken up by the brain as a substrate for dopamine, epinephrine and norepinephrine synthesis. In the livers of *P. berghei* ANKA-infected mice, phenylalanine was elevated (infected + saline: 1.05 [0.96-1.18] nmol/mg protein vs uninfected + saline: 0.73 [0.59-0.76] nmol/mg protein, $p < 0.0001$) as was tyrosine (infected + saline: 0.74 [0.73-0.86] nmol/mg protein vs uninfected + saline: 0.68 [0.56-0.74] nmol/mg protein, $p < 0.05$, FIG 5.16). Phenylalanine was raised to a greater degree than tyrosine, resulting in elevation of the phenylalanine/tyrosine ratio in the livers of infected mice (infected + saline: 1.4 [1.3-1.5] vs uninfected + saline: 1.1 [1.0-1.1], $p < 0.0001$, FIG 5.16). Infusion of citrulline and sepiapterin had no effect on liver phenylalanine (1.01 [0.95-1.17] nmol/mg protein, $p = 0.59$ vs infected + saline) or tyrosine (0.82 [0.73-0.86] nmol/mg protein, $p = 0.43$ vs infected + saline, FIG 5.16). However, compared to saline-infused infected controls, phenylalanine/tyrosine ratios were decreased in infected mice infused with citrulline and sepiapterin (1.3 [1.2-1.4], $p < 0.05$ vs infected + saline, FIG 5.16). These observations suggest that co-supplementation of sepiapterin and citrulline improves phenylalanine hydroxylase activity in the liver tissue of *P. berghei* ANKA-infected mice.

Compared to uninfected controls, *P. berghei* ANKA-infected mice demonstrated higher phenylalanine concentrations in brain tissue (infected + saline: 4.79 [4.00-5.66] nmol/mg protein vs uninfected + saline: 1.94 [1.83-2.12] nmol/mg protein, $p < 0.0001$, FIG 5.16). In contrast, tyrosine was not altered by infection (infected + saline: 2.66 [1.99-2.85] nmol/mg protein vs uninfected + saline: 2.19 [1.78-2.52] nmol/mg protein, $p = 0.17$, FIG 5.16). As a result of increased phenylalanine paired with unaltered tyrosine, the phenylalanine/tyrosine ratio was elevated in the brain tissue of infected mice (infected + saline: 1.8 [1.7-2.1] vs uninfected + saline: 0.9 [0.8-1.0], $p < 0.0001$, FIG 5.16). Infusion of citrulline and sepiapterin had no effect on brain phenylalanine (3.34 [2.21-6.17] nmol/mg protein, $p = 0.45$ vs infected + saline) or tyrosine (2.25 [1.77-3.83] nmol/mg protein, $p = 0.98$ vs infected + saline, FIG 5.16). However, compared

to saline-infused infected controls, phenylalanine/tyrosine ratios were decreased in infected mice infused with citrulline and sepiapterin (1.4 [1.2-1.6], $p < 0.001$ vs infected + saline, FIG 5.16).

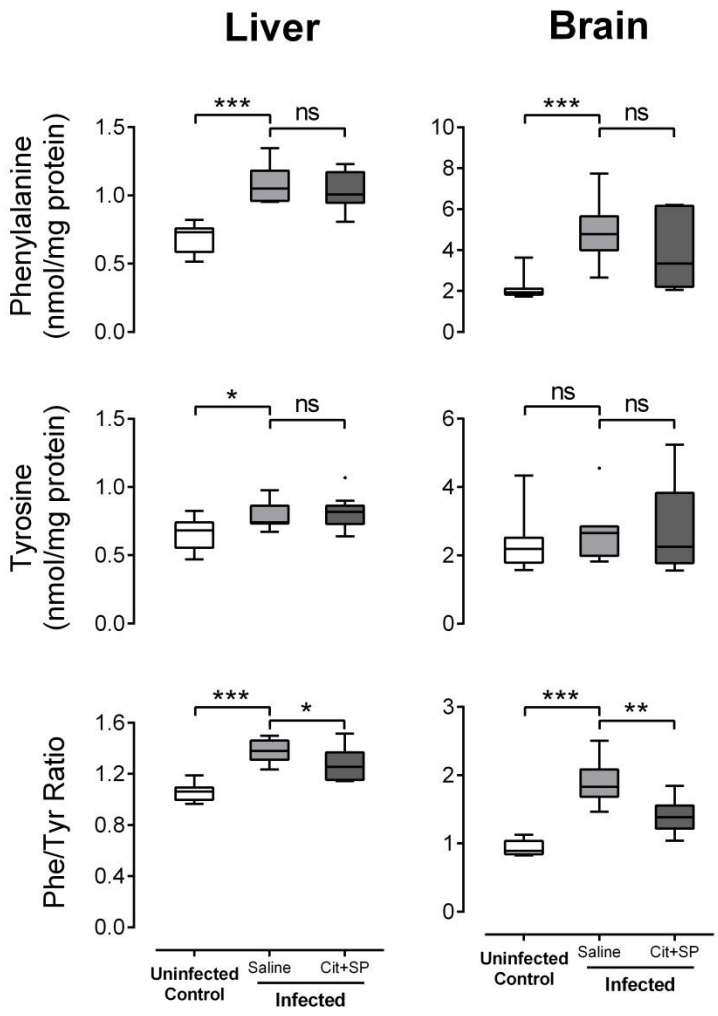


Figure 5.16 | Citrulline and sepiapterin infusion restores phenylalanine/tyrosine ratios in tissue. Tissue phenylalanine and tyrosine concentrations were determined by HPLC 6 days post-inoculation with *P. berghei* ANKA. *P. berghei* ANKA-infected mice received continuous intravenous infusion of saline (n=9) or 2.4g×kg^{-1}×d^{-1} citrulline + 15mg×kg^{-1}×d^{-1} sepiapterin (n=11). Saline-infused uninfected mice (n=12) served as controls. Data are pooled from 3 independent experiments. Box-plots depict median and IQR. Whiskers extend to highest and lowest values within 1.5×IQR of the 75th and 25th percentiles, and values outside this range were plotted as individual points (Tukey's method). *p<0.05, **p<0.01, ***p<0.001 by Mann-Whitney test. ns (not significant):

Implications of Improved Phenylalanine/Tyrosine Ratios

We considered whether supplementation of arginine, citrulline and ornithine could have reduced the rate of endogenous protein-breakdown and decreased phenylalanine release. Reduced rates of protein break-down would be expected to lower free tyrosine, but we observed increased plasma tyrosine and decreased phenylalanine/tyrosine ratios in mice infused with citrulline and sepiapterin. These observations strongly suggest that BH4 supplementation improved phenylalanine hydroxylase activity in infected mice.

In patients phenylketonuria, inborn loss-of-function mutation of the phenylalanine hydroxylase gene causes hyperphenylalaninaemia and severe neurological complications, including mental retardation, attention deficit disorder and neuromotor impairment (Scriver and Clow, 1980b; a). Hyperphenylalaninaemia and neurological disease also occur in individuals with loss-of-function mutations in the gene encoding GTP cyclohydrolase (GTPCH), which is required for *de novo* BH4 biosynthesis. The neurological symptoms observed in patients with highly elevated plasma phenylalanine may be explained either by direct neurotoxicity of high circulating phenylalanine concentrations (Kaufman, 1989) or by the essential role of phenylalanine hydroxylation in the synthesis of the neurotransmitters dopamine, epinephrine and norepinephrine. In a prior study of Tanzanian children, plasma phenylalanine was elevated from 61 ± 13 μmol/L (mean ± SD) in healthy controls to 177 ± 81 μmol/L in children with cerebral malaria and plasma phenylalanine/tyrosine ratios were elevated from 1.3 ± 0.3 in healthy controls to 2.2 ± 0.9 in children with cerebral malaria. Plasma phenylalanine can reach much higher concentrations (>1,000 μmol/L) in phenylketonuric patients, but varies widely over time based on dietary intake of phenylalanine (Krause et al., 1985). Based on available data, it is difficult to definitively compare plasma phenylalanine between phenylketonuric patients and cerebral malaria patients, who are likely in a state of dietary insufficiency due to impaired consciousness and other symptoms which may have occurred earlier in the course of disease. We speculate that it is unlikely that severe malaria confers the same risk of extreme phenylalanine accumulation observed in phenylketonuria, but the effects of impaired

phenylalanine metabolism on neurotransmitter synthesis could be relevant to severe malaria pathogenesis. The relationship between BH4 bioavailability and phenylalanine metabolism should be studied further in children with severe malaria and especially those with neurological involvement.

5.8 Discussion

In this chapter we demonstrate that simultaneous infusion of citrulline and sepiapterin results in effective supplementation of BH4 and arginine in plasma, erythrocytes, brain tissue, aorta tissue and liver tissue in *P. berghei* ANKA-infected mice. Despite meeting this pharmacological endpoint, whole blood nitrite, a biomarker of NO synthesis was only marginally improved and infused mice were not substantially protected from symptoms of severe disease.

From a pharmacological standpoint, citrulline infusion was highly effective in improving NOS substrate availability. In infused mice, plasma levels of citrulline and arginine were increased, the plasma ratio of ADMA to arginine was decreased, arginine was increased in aorta and brain tissue and citrulline was increased in aorta and liver tissue. We also supplemented BH4 in consideration of studies in humans that have shown lack of efficacy or even harm when arginine was supplemented in disease states associated with BH4 depletion. For example, 3g of arginine per day delivered orally for 6 months resulted in reduced flow-mediated vasodilation, vascular compliance and plasma and urinary nitrites and nitrates in a cohort study of patients with peripheral arterial disease (Wilson et al., 2007). In addition, patients receiving arginine also scored lower on treadmill assessments of exercise capacity compared with placebo-treated controls. Similarly, treatment with 3g of arginine three times daily for 6 months failed to produce a significant effect on ejection fraction or vascular stiffness in a study of patients who suffered myocardial infarction (Schulman et al., 2006). The group receiving arginine treatment exhibited a higher death rate than the control group leading to closure of enrolment due to safety concerns (Schulman et al., 2006). Can the general lack of

efficacy of arginine supplementation be ascribed to the failure to also replete BH4? Based on available biochemical data (Cardounel et al., 2005; Druhan et al., 2008), supplementation of arginine under conditions of BH4 depletion is not only insufficient to recouple NOS, but in fact exacerbates NOS uncoupling. Arginine supplementation is currently under investigation as an adjunctive therapy for the treatment of severe malaria (Yeo et al., 2007, 2008a; c, 2013). These demonstrations of the potentially harmful effects of arginine supplementation highlight the need for BH4 to be rigorously characterized in humans with severe malaria and supplemented alongside arginine if deficiencies are observed.

In our studies, continuous infusion of sepiapterin improved absolute concentrations of BH4 and improved the ratio of BH4 to 7,8-BH2 in erythrocytes, but failed to correct the BH4/7,8-BH2 ratio in plasma or brain tissue, where it is reduced by infection. Continuous sepiapterin infusion did not improve the BH4/7,8-BH2 ratio in aorta or liver tissue, although infection alone also had no effect in these tissues. NOS uncoupling is influenced by the stoichiometry of BH4 to NOS protein and by the ratio of BH4 to 7,8-BH2 (Crabtree et al., 2009a; a; Vasquez-Vivar et al., 2002). *P. berghei* ANKA infection raises brain eNOS and iNOS protein concentrations to ~1.8-fold and ~1.5fold, respectively (exact figures not provided) (Ong et al., 2013). In our studies, continuous infusion of sepiapterin and citrulline improved BH4 to 2.2-fold of baseline in brain tissue, which should restore BH4:NOS stoichiometry. However, continuous sepiapterin infusion did not improve ratios of BH4 to 7,8-BH2 in brain tissue, which were reduced in the brains of *P. berghei* ANKA-infected mice. In BH4-replete eNOS, increasing concentrations of 7,8-BH2 displace bound BH4, resulting in reduced NO synthesis and increased superoxide production (Crabtree et al., 2008; Vasquez-Vivar et al., 2002). Failure to correct the BH4/7,8-BH2 ratio may have limited restoration of NO synthesis in mice infused with citrulline and sepiapterin.

In contrast to NOS, which binds 7,8-BH2 with equivalent affinity to BH4 (Vasquez-Vivar et al., 2002), phenylalanine hydroxylase (PAH) binds 7,8-BH2 with less than one tenth of the observed affinity for BH4 (Shiman et al., 1994). Compared to NOS enzyme kinetics, PAH

activity may be determined to a greater degree by BH4:PAH stoichiometry and to a lesser degree by BH4:7,8-BH2 stoichiometry. In *P. berghei* ANKA-infected mice, citrulline and sepiapterin infusion proportionally supplemented both BH4 and 7,8-BH2 in plasma, aorta, liver and brain and decreased phenylalanine/tyrosine ratios in plasma, liver and brain. These observations suggest that improvement in BH4:PAH stoichiometry increased PAH activity despite the failure of citrulline and sepiapterin infusion increase the BH4/7,8-BH2 ratio. The biochemistry and clinical relevance of impaired phenylalanine metabolism in severe malaria require further study.

In a previous study, mice received twice-daily intraperitoneal injection of arginine, BH4, nor-N^G-hydroxy-L-arginine (nor-NOHA, an arginase inhibitor), or combinations of these treatments (Martins et al., 2012). None of these treatments produced a significant effect on behavioural symptoms or survival, but all treatments increased plasma nitrite concentrations (Martins et al., 2012). The combination of BH4, arginine and nor-NOHA increased plasma nitrite in excess of 4-5μM (exact figure not provided), a greater response than that achieved with continuous administration of arginine alone by osmotic pump in the same study (Martins et al., 2012) and much greater than we were able to achieve with continuously-infused citrulline and sepiapterin. Although plasma arginine levels were not measured in the mice treated with a combination of arginine, BH4 and nor-NOHA, it is unlikely that intermittent administration would achieve superior pharmacokinetics to continuously infused citrulline, which we have shown increased both citrulline and arginine well above baseline in plasma and tissue (with the exception of liver arginine). The dramatic nitrite response in the experiment of Martins et al. might be due to administration of fully-reduced BH4, which may have improved the BH4/7,8-BH2 ratio to a greater degree than we achieved sepiapterin. However, in a recent study, oral BH4 administration in human patients with coronary artery disease showed no improvement in the ratio of BH4 to oxidized biopterin species, conversion of arginine to citrulline or superoxide production in *ex vivo* vascular tissue (Cunnington et al., 2012). These observations suggest that failure to improve BH4/7,8-BH2 ratios may also limit the efficacy of direct BH4 administration.

5.9 Conclusion

In summary, despite successful supplementation of both arginine and BH4, simultaneous infusion of citrulline and sepiapterin achieved only minor improvement in whole blood nitrite in *P. berghei* ANKA-infected mice. NO synthesis may have been limited by reduced NOS phosphorylation, as has been observed in the brains of *P. berghei* ANKA-infected mice (Ong et al., 2013). Citrulline and sepiapterin infusion also failed to significantly improvement behavioural scores in contrast to the dramatic improvement in behavioural symptoms and survival in mice treated with nitric oxide donor therapies (Gramaglia et al., 2006; Cabrales et al., 2011). Historically, improved survival in *P. berghei* ANKA-infected mice correlates poorly with clinical outcomes in human patients with severe malaria (White et al., 2010). However, the contrast between the strong protective effect of NO donor therapies in prior experiments and the lack of a similar effect in citrulline and sepiapterin-infused mice in our experiments raises the possibility that reversal of severe malaria pathogenesis may require therapeutic interventions that bypass NOS altogether. Candidate NOS-independent approaches to therapeutically improving NO signalling are discussed in CHAPTER 6, p. 211.

5.10 Materials and Methods

Animal Procedures

Experimental Animals

Animal experiments were performed at the National Institutes of Health (NIAID Comparative Medicine Branch) using protocols approved by the NIH ACUC under the identification ASP LMVR 18E. For experiments conducted at the NIH, 10-week-old C57BL/6J male mice were obtained from the Jackson Laboratory (Bar Harbor, ME, USA) and 10-week-old Swiss Webster carriers for parasite expansion were obtained from Charles River Laboratories (Germantown, MD, USA). Mice were housed in temperature-controlled conditions with a 12hr/12hr light-dark cycle and free access to water and autoclaved rodent feed pellets (Teklad Global 18% Protein Extruded Rodent Diet, 2018SX, Harlan Laboratories, Frederick, MD, USA). For infusion experiments, mice pre-catheterized mice were purchased from the Jackson Laboratory (Bar Harbor, ME, USA) and housed in specialized cages as described below.

Intermittent Citrulline Administration

Citrulline (Sigma-Aldrich, St. Louis, MO, USA) was dissolved in sterile 0.9% saline (Hospira, Lake Forest, IL, USA), sterile-filtered with a 0.22µm syringe-tip filter and stored at -80°C until use. Citrulline (200mg/kg) was administered by intraperitoneal injection in a volume of 200µl three times a day starting on the day of inoculation (day 0). Uninfected and infected controls were injected with equivalent volumes of sterile 0.9% saline (Hospira, Lake Forest, IL, USA). Mice were euthanized for tissue collection 8-14 hours after the final injection (administered at midnight on day 5 post-inoculation).

Infusion of Citrulline and Sepiapterin

Ten-week-old male C57BL/6J mice were purchased with surgically-implanted silicone jugular vein catheters (2Fr at insertion point, 3Fr at access point) from the Jackson Laboratory

(Bar Harbor, ME, USA). The day after arriving, mice were anaesthetized with inhaled isoflurane (4% induction, 2% maintenance) during set-up and connection of an infusion line. First, the catheter plug was removed and the locking solution was gently removed with a 1mL syringe fitted with a blunt luer stub adapter. The catheter was then attached to an infusion line supported by a specialized tether system with a spring-balanced arm and swivel (Instech Solomon, Plymouth Meeting, PA, USA) which allow free movement and rotation of the animal during continuous infusion. The catheter and infusion line were joined with a 24-gauge hollow plug adapter and secured in place with a specialized harness (Instech Solomon, Plymouth Meeting, PA, USA). Mice were housed in individual cages specialized to support free movement of the tether system. Individual cages were fitted with removable water bottles and food hoppers.

Citrulline (Sigma-Aldrich, St. Louis, MO, USA) and sepiapterin (Schirck's Laboratories, Jona, Switzerland) were prepared by dissolving in 0.9% sterile saline (Hospira, Lake Forest, IL, USA), sterilized with a 0.22µm syringe-tip filter, aliquoted and stored at -80°C until use. Concentrations of citrulline and sepiapterin were selected to provide doses of $2.4g \times kg^{-1} \times d^{-1}$ and $15mg \times kg^{-1} \times d^{-1}$, respectively, when delivered at a rate 25µl/hour. Uninfected and infected control mice were infused with 0.9% sterile saline (Hospira, Lake Forest, IL, USA). All infusions were delivered with a PHD2000 syringe pump (Harvard Apparatus, Holliston, MA, USA). Infusions were started the day before inoculation and continued throughout the duration of the experiment. On a daily basis, citrulline/sepiapterin syringes were replaced with new syringes containing freshly-thawed infusate. Saline syringes were also replaced on a daily basis. Replacement of syringes was conducted in a biosafety cabinet to maintain sterility of infusate and care was taken to avoid introduction of air bubbles into the infusion line.

Infections

P. berghei ANKA parasites, clone RMgm-29 (Janse et al., 2006), were expanded from frozen stocks by intraperitoneal injection of carrier mice. After four days of parasite expansion,

whole blood was obtained from the abdominal inferior vena cava under terminal anaesthesia. Cohorts of experimental mice were infected by intraperitoneal injection of 1×10^6 infected erythrocytes diluted in 200 µl of PBS (Lonza, Walkersville, MD, USA). This protocol results in blood-stage infection, bypassing the liver stage of the parasite's life-cycle. Inoculations were alternated between saline-treated infected controls and experimentally-treated infected mice.

Behavioural Scoring and Quantification of Parasitaemia

Neurological symptoms were scored using a quantitative scoring scale adapted from the Rapid Murine Coma and Behaviour Scale (Carroll et al., 2010). Scores were assigned on a scale of 0 (moribund) to 2 (normal) for each of seven indicators: gait, balance, exploratory activity, body position, limb strength, touch escape and pinna reflex (TABLE 5.1). Parasitaemia was monitored by examination of Giemsa-stained blood smears obtained by tail tip bleed in live animals or from blood samples taken during tissue collection.

Category	Observation
Motor Performance	Gait
Activity	Body lift Exploratory Behaviour
Strength and Tone	Body Position Grasp of cage bars
Reflexes and Self-Preservation	Touch Escape Pinna Reflex

Table 5.1 | Scoring System for the Assessment of Disease Symptoms in Mice. System was adapted from the Rapid Murine Coma and Behaviour Scale (Carroll et al., 2010). Each observation was scored on a scale of 0 (moribund) to 2 (normal) yielding scores ranging from the minimum score of 0 (moribund mouse) to the maximum score of 14 (normal mouse).

Blood and Tissue Collection

Terminal anaesthesia was administered by intraperitoneal injection of 250mg/kg ketamine and 25mg/kg xylazine. The abdominal cavity was accessed and 700µl of blood was drawn from the abdominal inferior vena cava with a 25G×5/8" needle (BD, Franklin Lakes, NJ,

USA). To prevent coagulation, the syringe contained 60µl DPBS with K_3EDTA (final concentration of 1.6mg/ml K_3EDTA after 700 µl blood drawn). Plasma was separated from erythrocytes by centrifugation at 3,000*g* for 7 minutes at 4°C and snap-frozen on dry ice. The buffy coat was removed and discarded to ensure the purity of red blood cell samples. Mice were transcardially perfused with 20 ml PBS and lung, liver, kidney, spleen, aorta, heart and whole brain were dissected, removed, and snap-frozen on dry ice. All samples were stored at -80°C until analysis.

Biochemical Analysis

HPLC Analysis of Amino Acids in Plasma and Tissue

Essential method details are presented below. For full assay optimization and validation, refer to APPENDIX A (p. 235). Plasma samples were deproteinated by mixing 12µl sample with 12µl 2M perchloric acid ($HClO_4$, Fisher Scientific, Pittsburgh, PA, USA) containing 50µM L-norvaline as an internal standard (Sigma-Aldrich, St. Louis, MO, USA). After centrifuging for 5 minutes at 16,100*g* and 4°C, supernatants were removed and neutralized by adding 10µl to 5µl of 1.5M potassium carbonate (Sigma-Aldrich, St. Louis, MO, USA) in a fresh tube. The resulting solution was diluted 1:2 in ultrapure water from a Milli-Q Synthesis system (EMD Millipore, Billerica, MA, USA) for a final dilution of 1:6. After centrifuging for 5 minutes at 16,100*g* and 4°C to remove potassium chlorate precipitate, samples were loaded into screw-cap polypropylene vials (Agilent Technologies, Santa Clara, CA, USA) for analysis. Amino acid standards (Sigma-Aldrich, St. Louis, MO, USA) were diluted to 50µM and processed in parallel to serve as an external standard for quantitation. HPLC was performed on a low-flow Agilent 1100 series instrument and Agilent Chemstation OpenLab CDS revision C.01.03 was used to control the instrument and acquire data. Samples were derivatized directly prior to analysis by programming the autosampler to draw 2µl of derivatization reagent, 2µl of sample, mix for 30s and inject. The derivatization reagent contained final concentrations of 1.5mg/ml (11.2 mM) ortho-phthaldialdehyde (Sigma-Aldrich, St. Louis, MO, USA) and

41.3mM 3-mercaptopropionic acid (Sigma-Aldrich, St. Louis, MO, USA) diluted in 200mM potassium tetraborate solution (pH 9.4). To prevent carry-over contamination, the needle was washed for 5 seconds between each programmed step using the autosampler's built-in flushport and a wash solution consisting of 10% HPLC-grade methanol (Fisher Scientific, Pittsburgh, PA, USA) in ultrapure H_2O from a Milli-Q Synthesis system (EMD Millipore, Billerica, MA, USA). Analytes were separated with a 1.0mm×150mm Luna® C18(2) column with 5µm particles and 100Å pore size (Phenomenex, Torrance, CA, USA) protected with a 1.0mm×13mm ACE® C18 guard column with 3µm particles and 100Å pore size (MAC-MOD Analytical, Chadds Ford, PA, USA). Aqueous mobile phase (Solvent A) consisted of 0.1M sodium acetate (Fisher Scientific, Pittsburgh, PA, USA) in ultrapure H_2O from a Milli-Q Synthesis system (Millipore, Billerica, MA, USA) with 9% v/v methanol (Fisher Scientific, Pittsburgh, PA, USA) and 0.5% v/v tetrahydrofuran (Sigma-Aldrich, St. Louis, MO, USA) with pH adjusted to 8.3 with 3M NaOH (Sigma-Aldrich, St. Louis, MO, USA). Organic mobile phase (Solvent B) was HPLC-grade methanol (Fisher Scientific, Pittsburgh, PA, USA). Flow-rates and solvent ratios are summarized in TABLE 5.2. The column was maintained at 40°C for the duration of the run. Online fluorescence was measured at excitation and emission wavelengths of 340nm and 455nm, respectively. Chemstation OpenLab CDS software version C.01.03 was used for peak integration. Concentrations were calculated using both internal (L-norvaline) and external standards. Tissue samples (~30mg) were homogenized in 1×PBS (Lonza, Walkersville, MD, USA) using a hand-held homogenizer (Cole Parmer, Vernon Hills, IL, USA), centrifuged for 5 minutes at 16,100*g* and 4°C to remove insoluble protein, and processed as described above. Tissue amino acid concentrations were normalized to soluble protein content as determined by the Pierce BCA Protein Assay (Thermo Scientific, Sunnyvale, CA, USA) according to the manufacturer's instructions.

	Elapsed Time (min)											
	0	**10.87**	**16.3**	**21.73**	**27.17**	**28.8**	**35.32**	**40.75**	**43.5**	**48.5**	**48.6**	**65**
A (%):	96	86	86	70	60	53	50	30	0	0	96	96
B (%):	4	14	14	30	40	47	50	70	100	100	4	4

Table 5.2 | Mobile phase solvent ratios and pump program. The program was performed at a flow-rate of 84µl/min and a column temperature of 40°C. Sample was injected at 0 min.

Determination of ADMA in Plasma and Tissue

Essential method details are presented below. For full assay optimization and validation, refer to APPENDIX C (p. 288). Plasma was thawed and 10µl was diluted in 35µl 1×PBS (Lonza, Walkersville, MD, USA) containing N^G-monoethyl-L-arginine (MEA) (Enzo Life Sciences, Farmingdale, NY, USA) as an internal standard. Oasis MCX 96-well µElution Plates (Waters Corporation, Milford, MA, USA) were conditioned with elution buffer prepared from ultrapure water (Milli-Q Synthesis system, Millipore Corporation, Billerica, MA, USA), HPLC-grade methanol (Fisher Scientific, Pittsburgh, PA, USA) and 28% ammonium hydroxide (Sigma-Aldrich, St. Louis, MO, USA) in a ratio of 5:4:1 H_2O:MeOH:NH_4OH and equilibrated with methanol. Samples were loaded, washed with 0.1 N HCl (Sigma-Aldrich, St. Louis, MO, USA) followed by methanol, eluted with elution buffer, dried by vacuum centrifugation at 45°C and reconstituted in 10µl ultrapure water. Reconstituted samples were loaded into screw-cap polypropylene vials (Agilent Technologies, Santa Clara CA, USA) for analysis. HPLC was performed on a low-flow Agilent 1100 series instrument and Agilent Chemstation OpenLab CDS revision C.01.03 was used to control the instrument and acquire data. The autosampler was programmed to draw 1.7µl of ortho-phthaldialdehyde (OPA) derivatization solution and 1.7µl of the current sample in the sequence, mix the contents in the needle for 30s and inject the derivatized sample onto the column. OPA derivatization reagent contained 7.46 mM ortho-phthaldialdehyde (Sigma-Aldrich, St. Louis, MO, USA) and 27.5 mM 3-mercaptopropionic acid (Sigma-Aldrich, St. Louis, MO, USA) in 200 mM potassium tetraborate (Sigma-Aldrich, St.

Louis, MO, USA), pH 9.4. Chromatography was performed on a 1×100 mm C18(2) column with 3 μm particles and 100 Å pore size (Phenomenex, Torrance, CA, USA) at a flow-rate of 90 μl/min. Solvent A consisted of 25 mM sodium phosphate and 5% acetonitrile in ultrapure water and solvent B consisted of 50% acetonitrile in ultrapure water. Separations were accomplished by 20 min of isocratic conditions followed by a gradient from 0%B at 20 min to 18%B at 42 min. The column was then washed with 100 % solvent B for 5 minutes and re-equilibrated for 13 minutes prior to injection of the following sample. The column was maintained at 35°C for all runs. Online fluorescence was measured at excitation and emission wavelengths of 340nm and 455nm, respectively. The fluorescence detector's photomultiplier tube (PMT) gain was set to 11 for initial normal-sensitivity analysis. At 20min, PMT gain was switched to 16 for the detection of low-concentration analytes (L-NMMA, ADMA, and SDMA). At 37 minutes PMT gain was switched back to 11 for detection of the MEA internal standard with normal sensitivity. Chemstation OpenLab CDS software version C.01.03 was used for peak integration. Analyte peaks were quantified by comparison to the internal standard (MEA).

Frozen liver samples were homogenized in 8 μl 1×PBS per mg wet weight of tissue with a Lab Gen 7 series hand held homogenizer (Cole Parmer, Vernon Hills, IL, USA). Homogenized samples were centrifuged for 5 min at 16,100 × G and 4°C to remove insoluble material. An aliquot of supernatant was stored for protein quantification and a second was precipitated by mixing 1:1 with 2M perchloric acid (Fisher Scientific, Pittsburgh, PA, USA) containing N^G-monoethyl-L-arginine (MEA) (Enzo Life Sciences, Farmingdale, NY, USA) as an internal standard. Precipitated samples were centrifuged for 5 min at 16,100*g* and 4°C and the resulting supernatant was removed and neutralized with 4 volumes of 0.5M Na_2HPO_4 (Acros Organics, Geel, Belgium). 400μl of the neutralized sample was loaded onto an Oasis MCX 96-well μElution Plate (Waters Corporation, Milford, MA, USA), extracted and analyzed by HPLC as described determination of concentrations of plasma ADMA. Measured ADMA

concentrations were normalized to soluble protein as quantified by BCA colourimetric assay (Thermo Scientific, Sunnyvale, CA, USA) according to the manufacturer's instructions.

HPLC Determination of BH4 and 7,8-BH2

BH4 and 7,8-BH2 concentrations in tissue, plasma and red blood samples were determined by high-performance liquid chromatography (HPLC) with sequential electrochemical and fluorescence detection. A complete description of method development and validation is available in APPENDIX E, p. 319. Tissue samples (~30mg) were homogenized in 15µl ice-cold resuspension buffer per mg (~450µl) using a hand-held homogenizer (Cole Parmer, Vernon Hills, IL, USA). Resuspension buffer consisted of 1mM dithioerythritol (Acros Organics, Geel, Belgium) and 0.5µM EDTA (Sigma-Aldrich, St. Louis, MO, USA) diluted in 1×DPBS (Lonza, Walkersville, MD, USA). Homogenized samples were centrifuged for 5 min at 16,100*g* and 4 °C to remove insoluble protein. To precipitate proteins, supernatants were then mixed 9:1 with ice-cold precipitation acid consisting of 1M phosphoric acid (Fisher Scientific, Pittsburgh, PA, USA), 2M trichloroacetic acid (Fisher Scientific, Pittsburgh, PA, USA) and 1mM dithioerythritol (DTE) (Acros Organics, Geel, Belgium) diluted in 1×DPBS (Lonza, Walkersville, MD, USA). Instead of homogenization, whole aortas were subjected to three freeze–thaw cycles on dry ice in 200µl resuspension buffer prior to mixing with precipitation acid as above. Red blood cells and plasma samples were diluted 1:10 in resuspension buffer prior to mixing with precipitation acid as above. Following precipitation, all samples were centrifuged for 5 min at 16,100*g* and 4 °C. Supernatants were loaded into 250µl capacity polypropylene vials (Agilent Technologies, Santa Clara, CA, USA) and loaded into the autosampler. All samples were maintained on ice during processing.

Samples were injected (100µl injection volume) onto an isocratic HPLC system consisting of an 1100 series degasser and isocratic pump and a 1260 Infinity series autosampler, temperature-control unit and fluorescence detector with a 8µl flow cell, all obtained from Agilent Technologies (Santa Clara, CA, USA). A CouloChem III electrochemical detector

(Thermo Scientific, Sunnyvale, CA, USA) was installed after the column and before the fluorescence detector. Chromatography was performed on a 4.6mm×250mm ACE® C18 column with 5µm particles and 100Å pore size (MAC-MOD Analytical, Chadds Ford, PA, USA) with a 4.6mm×13mm ACE® C18 guard column with 5µm particles and 100Å pore size (MAC-MOD Analytical, Chadds Ford, PA, USA). Analytes were separated isocratically with a mobile phase comprised of 50mM HPLC-grade sodium acetate (Fisher Scientific, Pittsburgh, PA, USA), 5mM citric acid (Fisher Scientific, Pittsburgh, PA, USA), 48µM EDTA (Sigma-Aldrich, St. Louis, MO, USA), and 160µmol/L dithioerythritol (DTE) (Acros Organics, Geel, Belgium) prepared in ultrapure water (Milli-Q Synthesis system, Millipore Corporation, Billerica, MA, USA). The flow rate was 1.3 ml/min with a 19-minute rune-time between sample injections. For detection of BH4, the electrochemical detector's analytical cell was set to a voltage of +75mV for electrode 1 and -400mV for electrode 2. The guard cell voltage was set to +900mV to oxidize 7,8-BH2 to biopterin, which is fluorescent. Oxidized 7,8-BH2 was quantified using fluorescence detector excitation and emission wavelengths of 350 and 450 nm, respectively, and a photomultiplier tube gain of 18.

Agilent Chemstation OpenLab CDS revision C.01.03 (Agilent Technologies, Santa Clara, CA, USA) was used to control the instrument, acquire data and integrate peaks. A 35900E analog-to-digital converter (Agilent Technologies, Santa Clara, CA, USA) was used to facilitate communication between the electrochemical detector and Chemstation OpenLab. BH4 and 7,8-BH2 were quantified by comparison of integrated peak areas to external standard solutions of BH4 and 7,8-BH2 (Schircks Laboratories, Jona, Switzerland) diluted to known concentrations (0.1 nmol/L-50 nmol/L). For tissue analysis, measured concentrations were and normalized to soluble protein content, which was separately assayed with a Pierce BCA Protein Assay Kit (Thermo Scientific, Sunnyvale, CA, USA) according to the manufacturer's instructions.

Whole Blood Nitrite

Immediately after collection, 100µl of whole blood was mixed with 25µl of a solution containing potassium hexacyanoferrate(III) (800mM) (Sigma-Aldrich, St. Louis, MO, USA) to oxidize ferrous haem, *N*-ethylmaleimide (100mM) (Sigma-Aldrich, St. Louis, MO, USA) to block thiols and 10% v/v Nonidet-40 substitute (Fisher Scientific, Pittsburgh, PA, USA) to solubilize cell membranes. Samples were promptly snap-frozen on dry ice and stored at -80°C until analysis. For analysis, whole blood samples were thawed and deproteinated by mixing 1:1 with methanol (EMD Millipore, Billerica, MA, USA) and centrifuging for 5min at 16,100*g* and 4°C. Supernatants were injected into a reaction chamber containing potassium iodide (66.9mM) and iodine (28.5mM) (Sigma-Aldrich, St. Louis, MO, USA) diluted in a 2:7 mixture of ultrapure water (Milli-Q Synthesis System, Millipore Corporation, Billerica, MA, USA) and acetic acid, glacial (Fisher Scientific, Pittsburgh, PA, USA). NO produced by reduction of nitrite in plasma samples was detected with a Nitric Oxide Analyzer 280i (GE Healthcare, Pittsburgh, PA, USA) and compared with standards of known concentration prepared from sodium nitrite (Sigma-Aldrich, St. Louis, MO, USA). The chemistry of relevant reactions is presented in TABLE 5.3. Data processing and peak integrations were performed with OriginPro 8 software.

Nitrite Assay Chemistry
A. Generation of NO from NO_2^- $I^- + NO_2^- + 2H^+ \rightarrow NO + ½\ I_2 + H_2O$
B. Generation of Chemilluminescence $NO + O_3 \rightarrow NO_2^{\bullet} + O_2$ $NO_2^{\bullet} \rightarrow NO_2 + hv$

Table 5.3 | Chemical reactions for the measurement of nitrite (NO2-). (**A**) Nitrite is chemically reduced to nitric oxide in a solution of iodine and acetic acid. (**B**) NO generated from NO2- reduction is detected by chemilluminescence using a nitric oxide analyzer.

Nitrotyrosine

Nitrotyrosine concentrations were determined by ELISA and compared to a standard curve of nitrated bovine serum albumin (BSA) according to the manufacturer's instructions (Millipore Corporation, Billerica, MA, USA). Nitrotyrosine concentrations in tissue samples were normalized to soluble protein content.

DDAH Enzyme Activity Assay

Frozen liver samples were homogenized in 8 µl 1×PBS (Lonza, Walkersville, MD, USA) per mg wet weight of tissue with a Lab Gen 7 series hand held homogenizer (Cole Parmer, Vernon Hills, IL, USA). Homogenized samples were centrifuged for 5 min at 16,100*g* and 4°C to remove insoluble material. Supernatants were diluted 1:5 in 1×PBS spiked with ADMA (Cayman Chemical, Ann Arbor, MI, USA) for a final concentration of 2.5 mM ADMA. Spiked homogenates were mixed and sampled immediately (0 hr time point) and after 2 hr at 37°C. At each time point, citrulline was quantified by mixing 15 µl of homogenate with 15µl of 2M perchloric acid containing 25 µmol/L N^G-monoethyl-L-arginine (MEA) as an internal standard. Samples were centrifuged for 5min at 16,100*g* and 4°C to remove precipitate, and 10 µl of the supernatant was neutralized with 5µl 1.5M potassium carbonate (Sigma-Aldrich, St. Louis, MO, USA) in a fresh tube. Neutralized samples were further diluted 1:2 in ultrapure water and centrifuged to remove potassium perchlorate precipitate. HPLC was performed using the same method as described above for measurement of plasma amino acids, with the following exceptions: 1) analytes were separated with a 1×100 mm C18(2) column with 3 µm particles and 100Å pore size (Phenomenex, Torrance, CA, USA) and 2) separation of analytes was accomplished with a gradient from 0% solvent B to 25 % solvent B over 20min at a flow-rate of 70 µl/min. The column was then washed with 100 solvent B for 5 min and re-equilibrated with 100% Solvent A for 20 minutes. Citrulline production was calculated by taking the difference of starting (0 hr) and ending (2 hr) concentrations, dividing by the 2 hr

time interval and normalizing to protein content as quantified by BCA colourimetric assay (Thermo Scientific, Sunnyvale, CA, USA) according to the manufacturer's instructions.

Statistical Analyses

With the exception of dietary intake, water intake and change in weight, which are presented as mean ± SEM, data are presented as median and inter-quartile range (IQR). Statistical analyses were performed with GraphPad Prism 6 software and $p < 0.05$ was considered significant. In intermittent citrulline injection and citrulline/sepiapterin infusion experiments, Mann-Whitney test was used to compare values between uninfected and saline-treated infected controls and between saline-treated infected controls and infected mice treated with citrulline or citrulline and sepiapterin co-infusion. Two-way ANOVA followed by Bonferroni post-test was used to compare dietary intake, water intake and change in weight across groups.

Acknowledgements

I am grateful to Ivo Francischetti (NIAID/NIH) for making his infusion pump and tether systems available for these studies. Jessica Chertow (NIAID/NIH) assisted with sample preparation for analysis of hepatic DDAH activity and analysis of ADMA in plasma and liver tissue. This work was funded by the NIAID Division of Intramural Research.

CHAPTER 6.

General Discussion

In this chapter, principal findings are summarized and evaluated. Ongoing studies and opportunities for future investigations are outlined. To conclude, past and current candidates for adjunctive therapies are reviewed and the importance of severe malaria research is contextualized alongside other priorities for global malaria-control efforts.

6.1 Principal Findings

Inhibition of nitric oxide (NO) production by nitric oxide synthase (NOS) may contribute to the pathogenesis of severe malaria. In this thesis, analytical biochemical techniques were developed to examine the effect of severe malaria infection on availability of arginine, the NOS substrate, tetrahydrobiopterin, an essential NOS cofactor, and asymmetric dimethylarginine (ADMA), an endogenous NOS inhibitor.

We showed that *P. berghei* ANKA infection in mice causes arginine depletion consistent with previous reports in human patients with severe *falciparum* malaria (Lopansri et al., 2003; Yeo et al., 2007; Weinberg et al., 2014). Previous studies have implicated parasite- and host-derived arginase as the mechanism of arginine depletion (Yeo et al., 2007; Olszewski et al., 2009; Omodeo-Sale et al., 2010). In *P. berghei* ANKA-infected mice, we observed depletion of citrulline and ornithine as well as arginine, leaving arginine/ornithine ratios unchanged. These findings recapitulate observations in Indonesian adults with severe malaria (Yeo et al., 2007) and cannot be explained solely by increased arginase activity. To further explore the role of parasite-expressed arginase, we obtained *P. berghei* ANKA parasites in which the arginase gene had been knocked out. These arginase knock-out parasites caused depletion of arginine, citrulline and ornithine indistinguishable from wild-type parasites, indicating that parasite-expressed arginase is not required for *in vivo* arginine depletion. We

found that dietary restriction in uninfected mice caused moderate arginine and citrulline depletion. These findings suggest that nutritional status may be an under-recognized contributor to arginine depletion during severe malaria infection. We further explored arginine metabolism in *P. berghei* ANKA-infected mice by infusing heavy isotope-labelled metabolic tracers. This analysis demonstrated that the rate of conversion of arginine to ornithine remained constant in *P. berghei* ANKA-infected mice. Although increased arginase activity may be required to maintain this rate of conversion under conditions of reduced arginine availability, these results imply that arginase is not primarily responsible for arginine depletion. Instead, our data implicate reduced rates of arginine appearance in plasma. Our findings suggest that reduced appearance of arginine is due in part to dietary insufficiency and reduced synthesis from citrulline, but impaired enteral absorption or transport could also contribute. The rate of citrulline appearance was also decreased, likely due to impaired enteral synthesis associated with dietary insufficiency and/or impaired enteral absorption of precursors. The rate of ornithine appearance was decreased due to almost complete inhibition of ornithine synthesis from sources other than arginine, such as glutamate or proline. Our metabolic tracer analysis also showed that the rate of conversion of arginine to citrulline by NOS was decreased in infected mice. Taken together, our findings do not support the hypothesis that release and/or activation of arginase is the primary mechanism of arginine depletion, as has been previously suggested.

Synthesis of NO by NOS is determined by the abundance of arginine relative to the endogenous inhibitor ADMA. We studied ADMA availability in Gambian children and found that the ratio of ADMA to arginine was elevated in children with severe malaria but returned to normal following recovery. The ADMA/arginine ratio was positively correlated with plasma lactate, suggesting that elevation of the ADMA/arginine ratio was associated with impaired tissue perfusion and anaerobic respiration. Elevation of the ADMA/arginine ratio could result from arginine depletion, increased ADMA release or impaired ADMA clearance. To begin resolving these potential contributors, we used a mouse model to investigate the effect of malaria infection on dimethylarginine dimethylaminohydrolase (DDAH), the enzyme

responsible for metabolic clearance of ADMA. In *P. berghei* ANKA-infected mice, we observed degradation of DDAH protein, loss of ADMA-clearance activity and elevation of intracellular ADMA in the liver, a key site for removal of circulating ADMA. Exposure to the haemolytic agent phenylhydrazine produced similar hepatic DDAH dysfunction and elevation of the plasma ADMA/arginine ratio in mice. These observations suggest that cell-free haemoglobin and haem released during haemolysis increase oxidative stress in the liver and contribute to DDAH dysfunction. Taken together, our findings implicate degradation of hepatic DDAH as a potential mechanism of ADMA accumulation relative to arginine in severe malaria.

Tetrahydrobiopterin (BH4) is an essential NOS co-factor. We quantified BH4 in *P. berghei* ANKA-infected mice and found BH4 to be depleted in plasma, erythrocytes and brain tissue. In all three cases, we found decreased ratios of BH4 to 7,8-BH2, a product of BH4 oxidation, indicating that infection-associated oxidative stress may contribute to BH4 depletion. Intermittent injection of sepiapterin, which is converted to 7,8-BH2 and subsequently to BH4, restored erythrocyte BH4 and increased BH4 in brain tissue but did not increase whole blood nitrite, a biomarker of NO synthesis. We therefore hypothesized that effective re-coupling of NOS would require co-supplementation of both arginine and BH4.

We administered citrulline to *P. berghei* ANKA-infected mice by intermittent intraperitoneal injection, but found no effect on plasma citrulline or arginine concentrations. Continuous co-infusion of citrulline and sepiapterin successfully improved plasma levels of citrulline, arginine, ornithine and BH4 in *P. berghei* ANKA-infected mice. Simultaneous infusion of citrulline and sepiapterin also increased citrulline, arginine, ornithine and BH4 in aorta, brain and liver tissue, but had no effect on BH4/7,8-BH2 ratios in these tissues. Infected mice infused with citrulline and sepiapterin were not substantively protected from onset of severe disease symptoms. We observed a marginal but significant increase in whole blood nitrite in mice infused with citrulline and sepiapterin, indicating that restoration of arginine and BH4 bioavailability improves NO synthesis. However, we identified dietary intake of nitrite as a potential confounder. We also assessed nitrotyrosine as a marker of peroxynitrite formation

from uncoupled NOS, but found no change in plasma or brain nitrotyrosine and decreased nitrotyrosine in liver tissue, which may reflect impaired NO synthesis. Simultaneous infusion of citrulline and sepiapterin reduced phenylalanine/tyrosine ratios in plasma, brain and liver of *P. berghei* ANKA-infected mice. This finding suggests that restoration of BH4 availability improved activity of phenylalanine hydroxylase, which converts phenylalanine to tyrosine.

6.2 Critical Evaluation of Findings

Potential Therapeutic Efficacy of Arginine and BH4 Co-Supplementation

Our findings provide novel support for citrulline infusion as a viable approach to restoring NOS substrate availability in severe malaria. In our studies, citrulline infusion supplemented plasma pools of both citrulline and arginine. Although arginine is required as a substrate for NO synthesis, recent work has demonstrated that citrulline also contributes to overall substrate availability due to rapid recycling to arginine by ASS1 and ASL enzymes in complex with NOS (Flam et al., 2001; Vukosavljevic et al., 2006; Erez et al., 2011). Citrulline was not studied in recent assessments of arginine infusion in patients with uncomplicated or severe malaria (Yeo et al., 2007, 2008a; c, 2013), but our metabolic tracer analysis suggests that the rate of conversion of arginine to citrulline (via ornithine) amounts to only 2.8% of total arginine metabolism in uninfected mice and 4.7% in *P. berghei* ANKA-infected mice. In contrast, >95% of citrulline is utilized for arginine synthesis. The limited ability of exogenous arginine to supplement circulating citrulline pools may explain why arginine infusion was inferior to citrulline in improving intestinal perfusion in a mouse model of endotoxaemia (Wijnands et al., 2012).

We observed decreased BH4, elevated 7,8-BH2 and decreased BH4/7,8-BH2 ratios in brain tissue from *P. berghei* ANKA-infected mice. Others have observed upregulation of eNOS and iNOS protein in this model (Ong et al., 2013). This combination of conditions would decrease BH4:NOS stoichiometry and BH4:7,8-BH2 stoichiometry, favouring NOS uncoupling. Infusion of citrulline and sepiapterin improved BH4 in brain tissue, but failed to correct

BH4/7,8-BH2 ratios. Further investigation is required to determine effective methods of correcting BH4/7,8-BH2 ratios. One possible approach is direct administration of BH4 and co-administration of an anti-oxidant to prevent oxidation of BH4 to 7,8-BH2. Effective pharmacological strategies identified in mouse model experiments could also be studied in humans using non-invasive methods of quantifying blood flow and oxygenation.

Cell-free oxygenated haemoglobin (oxyhaemoglobin) released during haemolysis scavenges and inactivates nitric oxide by oxidizing it to nitrate (NO_3^-) (Reiter et al., 2002; Minneci, 2005). Severe malaria is characterized by increased cell-free haemoglobin in both mice (Gramaglia et al., 2006) and human patients (Janka et al., 2010; Yeo et al., 2009). In Malian children with severe malarial anaemia, cell-free haemoglobin correlated with the ability of plasma to scavenge NO (Janka et al., 2010). In Indonesian adults, cell-free haemoglobin was inversely correlated with reactive hyperaemic responses following transient occlusion of the brachial artery (Yeo et al., 2009). These findings suggest that cell-free haemoglobin scavenges NO and functionally limits NO signalling in severe malaria. It is conceivable that restoration of NOS substrate and cofactor availability may not be sufficient to overcome the NO-scavenging effects of cell-free haemoglobin. A recent study identified reduced phosphorylation of eNOS in brain tissue (Ong et al., 2013), which may also limit the ability of substrate and cofactor supplementation to restore NO synthesis. If enhancement of endogenous NO synthesis is insufficient to restore NO signalling during severe malaria, strategies that restore NO signalling by a NOS-independent mechanism may be required.

Candidate Approaches to Restoring NO Signalling Independent of NOS

Inhaled nitric oxide reduces blood-brain barrier leakage and the incidence of cerebral haemorrhage in *P. berghei* ANKA-infected mice (Serghides et al., 2011). Two trials of inhaled nitric oxide (NCT01255215, NCT01388842) are currently underway, both in Ugandan children with severe malaria. Inhaled nitric oxide induces vasodilation in the pulmonary vasculature (Benzing and Geiger, 1994). In patients with sickle cell disease, inhaled nitric oxide increased

conversion of cell-free oxyhaemoglobin to methaemoglobin, which does not scavenge NO (Reiter et al., 2002). This finding indicates that inhaled NO therapy may reduce systemic NO scavenging by cell-free oxyhaemoglobin. Inhaled NO may also react with blood components to form compounds that could release NO at a distant site, such as iron-nitrosyl compounds (Reiter et al., 2002) or S-nitrosohaemoglobin (Jia et al., 1996), but this mechanism of action has yet to be definitively proven in inhaled NO therapy.

Nitrite is utilized as a pool for NOS-independent NO production, and should be considered as an alternative approach to restoring NO signalling. Reduction of nitrite to nitric oxide by deoxyhaemoglobin has been implicated in hypoxic vasodilation (Cosby et al., 2003; Huang et al., 2005) and may improve vascular reactivity in severe malaria. Administration of exogenous nitrite has been shown to be safe in healthy volunteers (Cosby et al., 2003) and sickle cell patients (Mack et al., 2008). As a therapeutic intervention, nitrite has demonstrated beneficial effects on NO-dependent physiological read-outs in animal models of haemolysis (Minneci et al., 2008), ischaemia/reperfusion (Duranski et al., 2005), LPS-induced shock (Cauwels et al., 2009), ASL deficiency (Erez et al., 2011) and *P. berghei* ANKA infection (Serghides et al., 2011). The stability and low cost of nitrite make it suitable for use in resource-poor settings.

Validity of Mouse Model for the Study of NO Synthesis

The results presented in this thesis demonstrate that mice infected with *P. berghei* ANKA represent an appropriate model for the study of nitric oxide synthesis in the context of severe malaria. Specifically, we have shown that 1) arginine and ornithine depletion in *P. berghei* ANKA-infected mice (FIG 2.3, p. 34) accurately reproduces previous observations in human patients (Lopansri et al., 2003; Yeo et al., 2007); 2) elevation of ADMA/arginine ratios in *P. berghei* ANKA-infected mice (FIG 3.8, p. 103) accurately reproduce findings in Gambian children with severe malaria (TABLE 3.1, p. 89 and FIG 3.2, p. 90) and 3) decreased whole blood

nitrite in in *P. berghei* ANKA-infected mice (FIG 4.8, p. 145) accurately reproduces previous observations in human patients (Janka et al., 2010).

NO scavenging by cell-free haemoglobin has been identified in both human malaria (Yeo et al., 2009; Janka et al., 2010) and *P. berghei* ANKA-infected mice (Gramaglia et al., 2006). Down-stream mechanisms of disease influenced by NO synthesis also show similarities in *P. berghei* ANKA-infected mice and humans with severe malaria. Impaired microcirculation and occluded vessels are observed in the cerebral vasculature of *P. berghei* ANKA-infected mice (Cabrales et al., 2010), similar to findings in human patients (Dondorp et al., 2008a). Microhaemorrhage and leakage of the blood-brain barrier are also observed in both *P. berghei* ANKA-infected mice (Gramaglia et al., 2006; Serghides et al., 2011) and humans with severe malaria (Brown et al., 1999b; Taylor et al., 2004; Dorovini-Zis et al., 2011).

Differences between BH4 Availability in Mice and Humans

In contrast, our investigation of BH4 availability in mice is not likely to accurately reflect BH4 availability in humans with severe malaria. Pooling data from all available mouse experiments described in this thesis, we determined that plasma from healthy, uninfected mice contains BH4 concentrations of 215.8 [138.5-299.8] nmol/L (median [IQR]) and 7,8-BH2 concentrations of 85.96 [71.83-122.5] nmol/L. These values contrast sharply with available human data. In a study of patients with coronary artery disease, plasma BH4 concentrations were 21.3 [11.5-42.1] nmol/L (median [IQR]) and plasma 7,8-BH2 concentrations were 15.1 [11.6-19.2] nmol/L (Antoniades et al., 2007). This comparison indicates that plasma BH4 concentrations are approximately 10-fold higher and 7,8-BH2 concentrations are more than 5-fold higher in mouse plasma than in human plasma. The study of coronary artery disease patients did not include healthy controls, so the effect of coronary artery disease cannot be ruled out.

During development of the BH4 assay (see APPENDIX E, p. 319), we determined BH4 and 7,8-BH2 concentrations in the plasma of 3 healthy human controls. Measured BH4

concentrations were 7.4, 8.7, and 9.2 nmol/L and 7,8-BH2 concentrations were 3.1, 5.5 and 7.5 nmol/L in each subject, respectively. These data suggest that BH4 and 7,8-BH2 may be even lower in healthy humans.

Available measurements in vascular tissue also suggest that intracellular BH4 is much more abundant in mice than in humans. In the same study of patients with coronary artery disease, BH4 was quantified in pmol per gram tissue in the saphenous vein (lower tertile: 8.9 [5.6-17.2] pmol/g tissue, middle tertile: 8.5 [4.6-12.2] pmol/g tissue, upper tertile: 9.1 [5.3–15.1] pmol/g tissue) and internal mammary artery (lower tertile: 10.9 (6.02–18.9] pmol/g tissue, middle tertile: 6.4 [3.2–13.5] pmol/g tissue upper tertile: 5.7 [2.7–14.6] pmol/g tissue), with tertiles determined by total plasma biopterins (whole-cohort data not provided) (Antoniades et al., 2007). Although mouse aorta would be an appropriate comparator, we did not weigh aorta tissue before analysis and instead normalized to milligrams of soluble protein. Weights were available for brain tissue. If calculated on the basis of pmol/g tissue for comparison to human tissue, mouse brain contained a 462.0 [442.7-528.2] pmol/g tissue, in the range of 40-80 times the concentration of BH4 observed in human vascular tissue. On a pmol per milligram soluble protein basis, mouse brain contained slightly more than half of the BH4 concentrations measured in mouse aorta tissue (brain: 18.1 [17.0-20.8] pmol/mg soluble protein, aorta: 32.5 [24.9-41.4] pmol/mg soluble protein), suggesting that mouse aorta would also contain much higher levels of biopterins than human vascular tissue. Patients with coronary artery disease may experience increased oxidation of tissue BH4 to 7,8-BH2, but BH4 concentrations in mouse tissue were still higher than total biopterin concentrations in the human saphenous vein (lower tertile: 71.5 [39.1-239.2] pmol/g tissue, middle tertile: 35.0 [20.2–58.3] pmol/g tissue, upper tertile: 32.7 [22.2-52.4] pmol/g tissue) and internal mammary artery (lower tertile: 10.9 (6.02–18.9] pmol/g tissue, middle tertile: 6.4 [3.2–13.5] pmol/g tissue upper tertile: 5.7 [2.7–14.6] pmol/g tissue) (Antoniades et al., 2007).

BH4 concentrations are not routinely measured in human erythrocytes. One study measured BH4 concentrations of 14.5 ± 8.4 nmol/L (mean ± SD) in children and 12.5 ± 7.1

nmol/L in (mean ± SD) in adults. These values are on the order of 30 times less than we measured in mouse erythrocytes (433 [243-660] nmol/L, pooled from uninfected mice in all available experiments). Taken together, these comparisons demonstrate that mice exhibit higher levels of BH4 in plasma, erythrocytes and tissue. As a result, it is unclear whether our observations of BH4 availability in *P. berghei* ANKA-infected mice are relevant to severe malaria in humans.

Other Limitations of Mouse Models in Severe Malaria Research

Mice infected with *P. berghei* ANKA might not be an appropriate model for the study of direct cell-cell interactions between infected erythrocytes and endothelial cells. Parasitized erythrocytes are the predominant adherent cell type observed in the cerebral vasculature of human patients dying of cerebral malaria (Brown et al., 1999b; Taylor et al., 2004; Dorovini-Zis et al., 2011). In contrast, leukocytes are the predominant adherent cell type observed in the cerebral microvasculature of *P. berghei* ANKA-infected mice, although parasitized erythrocytes may be trapped in vessels occluded by adherent leukocytes (Cabrales et al., 2010). Adherent monocytes and leukocytes are also evident in the brains of human patients who died from cerebral malaria (Patnaik et al., 1994). Irrespective of the type of adherent cell, cytoadherence in the cerebral vasculature promotes vascular occlusion, insufficient perfusion and acidosis (Dondorp et al., 2008a; Cabrales et al., 2011). However, specific signal transduction events in endothelial cells likely differ according to the adherent cell type, binding ligand and receptor.

P. berghei ANKA-infected mice have not historically served as an effective pre-clinical model for predicting the efficacy of novel adjunctive therapies in human severe malaria patients. Notable examples include dexamethasone and anti-TNF antibody, which both proved to be protective in *P. berghei* ANKA-infected mice (Neill and Hunt, 1995; Grau et al., 1987) but caused increased incidence of complications and neurological sequelae in humans (Warrell et al., 1982; van Hensbroek et al., 1996b). In animal model experiments, experimental and environmental conditions are strictly controlled, and animal test subjects and infective agents

tend to be genetically homogenous in contrast to the genetic and environmental diversity encountered in human disease. In addition, experimental interventions in murine malaria are often delivered before the onset of symptoms, whereas in a clinical setting, disease symptoms are typically well-established before treatment can be started. In a clinical setting, candidate interventions would not be administered alone, as is typical in mouse model experiments, but rather in combination with anti-malarial therapies. Based on a combination of these factors and the underlying differences in the pathogenesis of murine and human malaria, it appears that a survival benefit in *P. berghei* ANKA-infected mice is a poor predictor of efficacy in human severe malaria. However, the use of interventions in mouse model studies should be considered an important tool for the investigation of specific molecular and biochemical disease mechanisms that correlate well with observations in human patients.

6.3 Ongoing and Future Investigations

Clinical Studies

We are currently collecting blood samples from Malawian children with severe malaria for analyses of BH4 availability and amino acid profiles, including arginine, citrulline, ornithine, phenylalanine and tyrosine. These studies will allow us to confirm prior observations of ornithine depletion (Lopansri et al., 2006; Yeo et al., 2007). We have observed citrulline depletion in *P. berghei* ANKA-infected mice, but to our knowledge, citrulline depletion has not been previously described in patients with severe malaria. Analysis of these samples will allow us to determine if plasma and erythrocyte BH4 is depleted, as we observed in *P. berghei* ANKA-infected mice.

Our group has also developed methods for quantifying vascular reactivity and oxygen consumption in human patients by using laser Doppler, laser speckle and oximetry modalities to monitor blood flow and blood oxygenation before, during and after transient arterial occlusion (Rowley et al., 2014). A study is in progress to apply these methods to determine vasoreactivity and oxygen consumption in Malawian children with severe malaria. We plan to further explore

the relevance of impaired NO in the pathogenesis of severe malaria by investigating relationships between biochemical determinants of NO synthesis and physiological read-outs from these blood flow studies. In the future, blood flow studies could be used to monitor the physiological effects of interventions such as infusion of citrulline and sepiapterin or BH4. The methods we have developed for the quantification of rates of arginine, ornithine and citrulline metabolism could also be applied to humans with severe malaria, although appropriate quantities of metabolic tracers would prove costly.

Autopsy Studies

Through collaboration with the Blantyre Malaria Project (Malawi), we are arranging to apply our analytic techniques to a series of archived tissue samples collected at autopsy from children dying from severe malaria. We have proposed to measure DDAH activity and intracellular ADMA accumulation in liver tissue and to determine the relationship between these read-outs of hepatic DDAH function and elevation of the ADMA/arginine ratio in plasma. These assessments would allow us to evaluate the hypothesis that hepatic DDAH dysfunction contributes to elevation of the ADMA/arginine ratio in humans with severe malaria. We have also proposed to analyze BH4 availability in liver and brain samples. A major confounding factor in these analyses could be the interval between time of death and sample collection. Documentation and case records will be thoroughly examined to control for this variable to the extent possible.

Mechanistic Studies of Hepatic DDAH Function

Studies are underway to further investigate the mechanism of hepatic DDAH dysfunction in *P. berghei* ANKA-infected mice. In studies of chemically-induced haemolysis, we observed impaired hepatic DDAH activity, accumulation of intracellular hepatic ADMA and elevation of the plasma ADMA/arginine ratio (FIG 3.12, p. 110, FIG 3.13, p. 112). These findings suggest that haemolysis plays a central role in promoting hepatic DDAH degradation.

Sickle cell disease is caused by a mutation in the β chain of haemoglobin yielding haemoglobin S (HbS). Under low oxygen tensions, haemoglobin S polymerizes and causes sickling of the erythrocyte. As a result of sickling and reduced stability of circulating erythrocytes, individuals with sickle cell disease are exposed to chronic haemolysis. In preliminary experiments, we have assessed hepatic DDAH function in transgenic mice expressing human haemoglobin S (C57BL/6J $Hba^{tm1(HBA)Tow}Hbb^{tm2(HBG1,HBB*)Tow}$). We found that mice with transgenic haemoglobin S (HbS) exhibited decreased DDAH activity (5.99 [4.49-6.92] nmol citrulline×mg^{-1}×hr^{-1}) compared to wild-type controls (8.52 [7.58-9.32] nmol citrulline×mg^{-1}×hr^{-1}, $p < 0.01$, FIG 6.1A). Intracellular ADMA was elevated in the livers of mice with transgenic HbS (176.1 [135.2-224.4] pmol/mg protein) compared to wild-type controls (73.4 [61.3-99.9] pmol/mg protein, $p < 0.01$), consistent with loss of DDAH-mediated clearance of ADMA (FIG 6.1B). In combination with our previous observations of impaired hepatic DDAH activity in *P. berghei* ANKA-infected mice and mice exposed to phenylhydrazine (see CHAPTER 3, FIG 3.10, p.106 & FIG 3.12, p. 110), these findings suggest that DDAH dysfunction may be a common pathophysiological mechanism across range of haemolytic disease states.

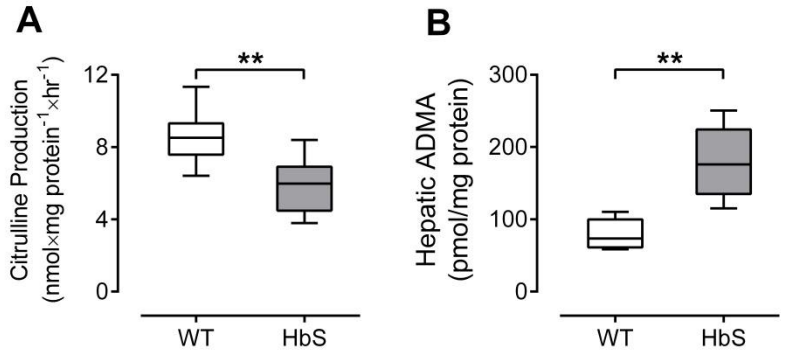


Figure 6.1 | Decreased hepatic DDAH activity and increased hepatic ADMA in a mouse model of sickle cell disease. (**A**) DDAH activity was assessed in liver samples from mice expressing human haemoglobin S (HbS, n=7) or wild-type controls (n=8) by quantifying citrulline production in the presence of saturating concentrations of ADMA substrate (2.5 mM). Citrulline production was calculated on a per-hour basis and normalized to protein content. (**B**) Intracellular hepatic ADMA was assessed by HPLC in perfused liver samples and normalized to protein content. Data are pooled from two independent experiments. Boxplots depict median, IQR and range. **p<0.01 by Mann-Whitney test.

To distinguish the effects of red cell destruction versus anaemia on hepatic DDAH function, we plan to assess hepatic DDAH activity and accumulation of ADMA in the liver and plasma following direct haem injection or phlebotomy. Direct injection of haem will allow us to determine whether free haem released during haemolysis is a mediator of hepatic DDAH dysfunction. Repeated phlebotomy in mice will provide a model of anaemia without red cell destruction.

We have hypothesized that degradation of DDAH protein is due to oxidative stress. This hypothesis is based on previous *in vitro* studies that demonstrated proteasome-dependent DDAH degradation in smooth muscle cells transfected with a subunit of NADPH oxidase (Luo et al., 2010). To further explore the role of oxidative stress in DDAH degradation *in vivo* we have proposed to investigate DDAH function in transgenic mice that over-express Nox2, a subunit of an endothelial NADPH oxidase homolog (Bendall et al., 2007). If oxidative stress is a key mechanism driving DDAH degradation, we hypothesize that Nox2-transgenic mice will exhibit decreased hepatic DDAH activity, accumulation of intracellular ADMA and elevation of the plasma ADMA/arginine ratio. Conversely, we are considering whether DDAH degradation

might be averted during *P. berghei* ANKA infection or artificial haemolysis in transgenic mice expressing high levels of extracellular superoxide dismutase. We are also considering whether DDAH activity could be preserved in mice that over-express transgenic DDAH (Dayoub et al., 2003; Jacobi et al., 2005). Increased rates of DDAH transcription and translation may not be able to restore DDAH function if any additional protein produced is rapidly degraded. Identifying a successful method of preserving DDAH function will be essential to investigating the relationship between hepatic DDAH and circulating ADMA.

Relating DDAH Genotype to Plasma ADMA

We also plan to investigate the relationship between DDAH and plasma ADMA by pairing genetic data with biochemical analysis of approximately 700 plasma samples from children with severe malaria from the MalariaGEN Gambian case-control study (Jallow et al., 2009). Biochemical analysis of plasma ADMA and arginine is currently underway. A genome-wide association analysis of this study population identified a polymorphism in the *DDAH1* gene that was associated with increased risk of severe malaria (Jallow et al., 2009). We have proposed to stratify patients with severe malaria by DDAH genotype to determine whether elevated plasma ADMA concentrations or ADMA/arginine ratios are associated with the risk-associated allele. It is unlikely that the identified single nucleotide polymorphism (SNP) is responsible for functional changes in DDAH expression and/or regulation. The more likely scenario is that the identified SNP is in linkage disequilibrium with one or more additional polymorphisms that are responsible for functional effects. Functional polymorphisms could be identified by sequencing the *DDAH1* gene in this sample set and identifying polymorphisms with the strongest associations with the ADMA/arginine ratio.

6.4 Previous Trials of Adjunctive Therapies

A range of adjunctive therapies have been tested in clinical trials in an effort to improve outcomes achieved with standard approaches to the treatment of severe malaria (see CHAPTER 1, p. 11). Below we identify and briefly review 22 randomized controlled trials of 13 candidate adjunctive therapies. Only comparative trials in patients with severe malaria are presented; dose-finding, pharmacokinetic and uncomplicated malaria studies are not discussed.

Immune Modulation Therapies

Dexamethasone, a corticosteroid, was the first adjunctive therapy to be tested in a randomized controlled trial (Warrell et al., 1982) (TABLE 6.1). In this study, no difference in mortality was observed, but dexamethasone was shown to both lengthen the duration of coma and increased the rate of complications such as pneumonia and late gastrointestinal bleeding (Warrell et al., 1982). Anti-TNF antibody also proved to be harmful, as the incidence of neurological sequelae was much higher in the treatment group compared to placebo-treated controls (van Hensbroek et al., 1996b). A trial of intravenous hyperimmune immunoglobulin had to be halted due to higher rates of mortality in the treatment group early in the study, which made it highly unlikely that the intervention would prove superior to standard care (Taylor et al., 1992). This result may have been driven in part by the higher incidence of deep coma and acidosis at baseline in patients randomized to the treatment arm (Taylor et al., 1992). Pentoxifylline, a non-selective phosphodiesterase inhibitor that suppresses inflammatory signalling, reduced the duration of coma in 2 out of 3 published trials but showed no definitive effect on mortality due to small study sizes (Di Perri et al., 1995; Looareesuwan et al., 1998; Das et al., 2003). Taken together, the results of these trials call into question the importance of the host immune response, especially TNF signalling, as a central mechanism in the pathogenesis of severe malaria.

Table 6.1 | Immune Modulation Therapies

Therapy	Dose	Patients	Outcome	Reference
Dexamethasone	1.5-2.0 mg/kg iv over 48hr	100 Thai children and adults with cerebral malaria	No difference in mortality, but dexamethasone increased duration of coma (63hr) vs placebo (47hr) and increased rate of complications from 22% to 52%	(Warrell et al., 1982)
Dexamethasone	11.4 mg/kg iv over 48hr	38 Indonesian children and adults with impaired consciousness	No difference in mortality, duration of coma or parasite clearance	(Hoffman et al., 1988)
Hyperimmune immunoglobulin	400mg/kg iv over 3hr	31 Malawian children with cerebral malaria	5/16 in treatment group died vs 1/15 in placebo; trial stopped due to non-superiority of treatment; no difference in duration of coma or duration of fever	(Taylor et al., 1992)
anti-TNF monoclonal antibody (B-C7)	5 mg/kg iv over 15 min	610 Gambian children with cerebral malaria	No difference in mortality, but anti-TNF antibody increased incidence of neurological sequelae (6.8%) vs placebo (2.2%)	(van Hensbroek et al., 1996b)
Curdlan sulfate	4 mg/kg q8h for 4 days	50 Thai adults with severe malaria; 30 Thai adults with severe/cerebral malaria (2 trials)	Shorter duration of fever in 1 out of 2 trials; no effect on parasite clearance or mortality	(Havlik et al., 2005)
Pentoxifylline	10 mg/kg/d iv for 3 days	56 Burundian children with cerebral malaria	Pentoxifylline shortened duration of coma (6hr) vs placebo (46hr); trend towards reduced mortality in treatment group	(Di Perri et al., 1995)
Pentoxifylline	0.83 mg/kg/h vs 1.67 mg/kg/h iv for 3 days	45 Thai adults with severe malaria	No difference in duration of coma or mortality	(Looareesuwan et al., 1998)
Pentoxifylline	10 mg/kg/d iv for 3 days	52 Indian adults with cerebral malaria	Pentoxifylline reduced TNF and shortened duration of coma (22hr) vs placebo (64hr); trend towards reduced mortality in pentoxifylline group	(Das et al., 2003)

Iron Chelation and Anti-Oxidant Therapies

Iron is an essential nutrient for *P. falciparum* parasites and participates in oxidation-reduction reactions that generate reactive oxygen species. Iron chelation has been explored as a possible method of accelerating parasite clearance and limiting oxidative damage to host tissue (TABLE 6.2). An initial trial of the iron chelator deferoxamine demonstrated reduced duration of coma and accelerated parasite clearance (Gordeuk et al., 1992). However, a follow-up trial in a larger sample size was stopped early when mortality was found to be increased to 18% in deferoxamine-treated children compared to 10.5% mortality in placebo-treated controls (Thuma et al., 1998). A harmful side-effect of iron chelation may be reduced iron availability for erythropoiesis in already-anaemic patients, although this hypothesis has not specifically been investigated. Deferiprone, an alternative iron chelator, reduced duration of coma but this trial was far too small to detect any effect on mortality (Mohanty et al., 2002). Iron chelators may also be particularly unsuited for co-administration with artesunate, which relies on iron for its mechanism of action (Meshnick et al., 1993).

The anti-oxidant *N*-acetylcysteine has been tested as an approach to limiting oxidative damage in patients with severe malaria. An initial trial in only 30 patients showed accelerated normalization of blood lactate (Watt et al., 2002), but this effect was not reproduced in a larger follow-up study (Charunwatthana et al., 2009). Parasite clearance times were slightly lengthened in patients treated with *N*-acetylcysteine in this second trial, raising concerns of interference with the mechanism of action of artesunate, which involves generation of reactive oxygen species to kill asexual *P. falciparum* parasites.

Table 6.2 | Iron Chelation and Anti-Oxidant Therapies

Therapy	Dose	Patients	Outcome	Reference
Deferoxamine	100 mg/kg/d iv for 3 days	83 Zambian children with cerebral malaria	Deferoxamine shortened duration of coma (20hr) vs placebo (43hr) and accelerated parasite clearance; no significant effect on mortality	(Gordeuk et al., 1992)
Deferoxamine	100 mg/kg/d iv for 3 days	352 Zambian children with cerebral malaria	Deferoxamine increased mortality (18%) vs placebo (10.5%, p=0.07); trial stopped early	(Thuma et al., 1998)
Deferiprone	75 mg/kg/d oral or via nasogastric tube if comatose	45 Indian adults with uncomplicated or severe malaria	Deferiprone shortened duration of coma (29hr) vs placebo (56hr) and accelerated parasite clearance; no significant effect on mortality	(Mohanty et al., 2002)
N-acetylcysteine	300 mg/kg iv over 20hr	30 Thai men with severe malaria	*N*-acetylcysteine accelerated lactate normalization (21hr) vs placebo (42hr); non-significant trend toward earlier tolerance of oral medication	(Watt et al., 2002)
N-acetylcysteine	300 mg/kg iv over 20hr	108 Thai and Bangladeshi adults with severe malaria	No difference in mortality, lactate normalization or duration of coma. N-acetylcysteine prolonged parasite clearance by 6 hours	(Charunwatthana et al., 2009)

Fluids and Osmotic Agents

Volume expansion has been explored as an approach to correcting acidosis and hypovolaemia associated with severe malaria (TABLE 6.3). Children with cerebral malaria also demonstrate increased intracranial pressure, leading to the suggestion that infusion of human albumin in saline would allow for volume expansion while simultaneously increasing colloidal osmotic pressure and attenuate risk of oedema. In a small study of Kenyan children, volume expansion with saline containing 4.5% albumin was shown to reduce mortality compared with administration of saline alone (Maitland et al., 2005). Fluids were given as a bolus of 20ml/kg in patients with moderate acidosis (base deficit 8-15mmol/L) or 40ml/kg in patients with severe acidosis (base deficit >15mmol/L) (Maitland et al., 2005). Additional 20ml/kg boluses were given to patients who developed severe hypotension, oliguria or worsening acidosis (Maitland et al., 2005). This study only included a control group treated with maintenance fluids in the moderate acidosis arm, although mortality assessments were performed on pooled data from the moderate acidosis and severe acidosis arms (Maitland et al., 2005). As a result, this study was not sufficiently powered to evaluate the impact of rapid volume expansion compared to maintenance fluids only (Maitland et al., 2005). A second study found no difference in mortality with volume expansion with 4.5% albumin in saline compared with volume expansion with gelofusine, a synthetic colloid (Akech et al., 2006). This study did not include a control group that was treated with only maintenance fluids (Akech et al., 2006). The effect of aggressive volume expansion (20-60mL/kg) on mortality was subsequently assessed in a large randomized controlled trial in 6 health centres in Uganda, Kenya and Tanzania (Maitland et al., 2011). Aggressive fluid expansion increased mortality from 7.3% (no bolus) to 10.5% with saline bolus and 10.6% with albumin bolus in all enrolled children with severe febrile illness (Maitland et al., 2011). Sub-group analysis of children with severe malaria, who comprised 57% of the total study, showed that mortality was increased from 5.8% with no fluid bolus to 9.2% with albumin or saline bolus (Maitland et al., 2011). Based on these results, rapid fluid expansion cannot be recommended for routine treatment of severe malaria in children. Concerns have also been

raised about increased risk of pulmonary oedema in adults treated with fluid resuscitation (Hanson et al., 2013), although no comparative trials have been conducted to date in adults.

Raised intracranial pressure (Newton et al., 1997) and elevated opening lumbar CSF pressures (Newton et al., 1991; Waller et al., 1991) are observed in children with cerebral malaria. The osmotic agent mannitol can temporarily decrease intracranial pressure by increasing solute concentration in the blood compartment and drawing fluid from the brain parenchyma. In a randomized trial in Ugandan children, mannitol administration had no effect on duration of coma or mortality (Namutangula et al., 2007), but a second study in Indian adults observed increased duration of coma and a non-significant increase in mortality in mannitol-treated patients (Mohanty et al., 2011). These results suggest that mannitol does not provide significant benefit and may even be harmful in adults.

Table 6.3 | Fluids and Osmotic Argents

Therapy	Dose	Patients	Outcome	Reference
Albumin (4.5% in saline)	20mL/kg (moderate acidosis) 40ml/kg (severe acidosis)	150 Kenyan children with severe malaria complicated by acidosis	Albumin reduced mortality (4%) vs saline (18%) but had no significant effect on resolution of acidosis	(Maitland et al., 2005)
Albumin (4.5%) vs. Gelofusine (4%) in saline	20mL/kg or 40ml/kg (if in shock)	80 Kenyan children with severe malaria complicated by acidosis	No significant effect on mortality or resolution of acidosis	(Akech et al., 2006)
Fluid bolus (with or without 5% albumin)	20mL/kg-60ml/kg	3141 Ugandan, Kenyan and Tanzanian children with febrile illness and impaired perfusion	Sub-group analysis of children with malaria showed fluid bolus (with or without albumin) increased mortality (9.2%) vs no bolus (5.8%)	(Maitland et al., 2011)
Mannitol	1g/kg iv	156 Ugandan children with cerebral malaria	No difference in duration of coma or mortality	(Namutangula et al., 2007)
Mannitol	1.5g/kg followed by 0.5g/kg q8h iv	61 Indian adults with severe malaria and brain swelling	Mannitol increased duration of coma (90hr) vs placebo (32hr) and non-significantly increased mortality (30%) vs placebo (13%)	(Mohanty et al., 2011)

Seizure prophylaxis

Phenobarbital has been used to terminate prolonged seizures in children with cerebral malaria, prompting comparative trials of prophylactic phenobarbital administration. Low-dose prophylactic phenobarbital (3.5mg/kg) reduced the incidence of seizures in a small study of Thai adults and children with severe malaria, but this trial was not powered to detect a survival benefit (White et al., 1988). A subsequent trial of higher dose phenobarbital (20mg/kg) similarly showed a reduction in incidence of seizures, but significantly increased mortality (18%) compared to placebo-treated controls (8%) (Crawley et al., 2000). Respiratory arrest was more common in children treated with phenobarbital, suggesting one possible mechanism by which phenobarbital may have increased mortality (Crawley et al., 2000).

Table 6.4 | Seizure prophylaxis

Therapy	Dose	Patients	Outcome	Reference
Phenobarbital	3.5mg/kg intramuscular	48 Thai children and adults with cerebral malaria	Phenobarbital reduced incidence of seizure (12.5%) vs placebo (54%)	(White et al., 1988)
Phenobarbital	20mg/kg intramuscular	340 Kenyan children with cerebral malaria	Phenobarbital significantly increased mortality (18%) vs placebo (8%); reduced incidence of >3 seizures from 27% to 11%	(Crawley et al., 2000)

Levamisole

Cytoadherence of parasitized red blood cells in the cerebral vasculature is a defining pathological observation in patients with cerebral malaria. Levamisole is an alkaline phosphatase inhibitor that decreases binding of parasitized red blood cells to endothelial cells *in vitro* by modulating phosphorylation of CD36, a key receptor involved in cytoadherence (Ho et al., 2005). In a preliminary trial in patients with uncomplicated *falciparum* malaria, levamisole increased circulating late stage parasites, suggesting that it had inhibited sequestration of parasitized erythrocytes (Dondorp et al., 2007). However, a randomized controlled trial in

Bangladeshi adults with severe malaria failed to reproduce these results and furthermore showed no effect on microvascular flow or resolution of hyperlactataemia (Maude et al., 2014).

Dichloroacetate

Dichloroacetate activates pyruvate dehydrogenase, diverting pyruvate that would otherwise be utilized in lactic acid fermentation. In a small preliminary study dichloroacetate reduced plasma lactate to a greater degree than placebo (Krishna et al., 1996), but these results have not been confirmed nor has mortality been assessed in additional studies. In an immortalized human endothelial cell line, parasitized red blood cells increased endothelial barrier permeability in a contact-independent manner that the authors linked to reduction of pH (Zougbede et al., 2011). These findings suggest that correction of lactate could be beneficial, but treatment of the underlying causes of lactate accumulation may be more effective. Blood lactate correlates with microvascular obstruction (Dondorp et al., 2008a), suggesting that impaired tissue perfusion is responsible for hyperlactataemia.

Table 6.5 | Other Strategies

Therapy	Dose	Patients	Outcome	Reference
Levamisole HCl	150mg oral or via nasogastric tube if comatose	56 Bangladeshi adults with severe malaria	No effect on parasite clearance, sequestration estimates, microvascular flow or normalization of plasma lactate	(Maude et al., 2014)
Dichloroacetate	46mg/kg iv, 2 doses 12hr apart	20 Thai adults with severe malaria	Dichloroacetate reduced lactate to a greater degree (42%) than placebo (16%) at 8hr after the first dose	(Krishna et al., 1996)

Limitations of Previous Clinical Trials

A majority of these comparative trials were not sufficiently powered to detect realistic changes in mortality. A majority of these trials also used quinine as the standard-of-care anti-malarial drug. Artesunate has proven to be more efficacious than quinine (Dondorp et al., 2005,

2010). As artesunate becomes more frequently used in standard severe malaria management, even greater power may be required in order to prove a benefit of novel adjunctive therapies over standard care. Another limitation is the heterogeneous nature of severe malaria complications. Future clinical trials should utilize preliminary pathophysiology studies and carefully-designed enrolment criteria to target patient populations that are most likely to benefit.

6.5 Adjunctive Therapies Currently in Development

NO-Restoration Therapies

Intravenous arginine infusion is currently under investigation as a method of restoring endogenous NO synthesis in severe malaria. An initial investigation demonstrated improved reactive hyperaemia and exhaled NO following arginine infusion in Indonesian adults with moderately severe malaria (*falciparum* parasitaemia, inability to tolerate oral medication and no WHO criteria for severe malaria) (Yeo et al., 2007). An additional safety study was also conducted in patients with moderately severe malaria (Yeo et al., 2008a). An initial study in patients with severe malaria showed no effect on lactate or vascular function, but was powered more as a pharmacokinetic study than an efficacy study (6 treatment, 2 controls) (Yeo et al., 2013). In severe malaria patients receiving infusions, plasma arginine responses were 40% lower than predicted from a previous pharmacokinetic study in moderately severe malaria (Yeo et al., 2008c), suggesting that additional dose-finding studies and/or investigation of citrulline infusion may be required prior to commencement of larger randomized controlled trials. As an alternative NOS-independent approach to restoring NO signalling, inhaled nitric oxide is currently under investigation in two clinical trials (NCT01255215, NCT01388842). The biochemistry and physiology of inhaled nitric oxide are discussed above (see p. 211).

Erythropoietin

Erythropoietin (Epo) is a hormone produced primarily in renal tubules in response to hypoxia. Epo promotes the survival of erythroid precursor cells in the bone marrow by activating homodimeric Epo receptor (EpoR) and stimulating anti-apoptotic pathways. EpoR has also been identified in in neurons (Masuda et al., 1993; Sakanaka et al., 1998), glial cells (Nagai et al., 2001) and endothelial cells (Anagnostou et al., 1990, 1994; Beleslin-Cokic et al., 2004), indicating extrahematopoietic functions. Stimulation of heterodimeric receptors comprised of EpoR and the common beta chain receptor subunit (CD131) in the central nervous system promotes neuroprotection in animal models of spinal cord injury and cerebral ischaemia (Brines et al., 2004; Siren et al., 2001). Treatment with recombinant erythropoietin improves survival in *P. berghei* ANKA-infected mice by tempering cytokine and cellular immune responses, preventing neuronal apoptosis and maintaining endothelial barrier integrity (Kaiser et al., 2006; Wiese et al., 2008; Wei et al., 2014).

In a retrospective observational study of Kenyan children with cerebral malaria, plasma erythropoietin of greater than 200U/L was associated with lower risk of neurological sequelae (Casals-Pascual et al., 2008). This finding supports the hypothesis that endogenous erythropoietin produces a neuroprotective effect that could be enhanced with exogenous administration. This study reported an age-dependent effect in which younger children had higher plasma concentrations of erythropoietin and lower risk of neurological sequelae (Casals-Pascual et al., 2008). In a pathology study of adults, erythropoietin receptor expression was found to be upregulated in severe malaria, but endogenous erythropoietin expression was not altered (Medana et al., 2009). These observations may indicate age-related differences in the importance of erythropoietin signalling as an endogenous neuroprotective mechanism. A small safety trial in Malian children observed no adverse effects in response to high doses erythropoietin (1,500 U/kg/d for 3 days) (Picot et al., 2009). This study was not comparative, and thus provides no additional information on the potential use of exogenous erythropoietin as an adjunctive therapy.

Rosiglitazone

Rosiglitazone is a peroxisome proliferator-activated receptor-γ (PPARγ) agonist that reduces parasitaemia, inhibits pro-inflammatory signalling and improves survival in *P. berghei* ANKA-infected mice (Serghides et al., 2009). A randomized trial of rosiglitazone was conducted in Thai adults with uncomplicated malaria to test safety and preliminary efficacy (Boggild et al., 2009). Parasite clearance times were shorter and plasma concentrations of the pro-inflammatory cytokines interleukin-6 and monocyte chemoattractant protein-1 were lower in rosiglitazone-treated patients (Boggild et al., 2009). Rosiglitazone increases insulin sensitivity, which may exacerbate hypoglycaemia and limit its potential use as an adjunctive therapy in patients with severe malaria.

Activated Charcoal

Oral activated charcoal improves survival in *P. berghei* ANKA-infected mice (de Souza et al., 2010). The authors observed reduced cytokine expression in splenic T cells and hypothesized that activated charcoal adsorbs pro-inflammatory cytokines, thus reducing immune activation (de Souza et al., 2010). Oral activated charcoal was administered in combination with artesunate in healthy adults and had no effect on artesunate pharmacokinetics (de Souza et al., 2010). However, potential interference with the anti-parasite efficacy of artesunate would have to be ruled out prior to trials in patients with severe malaria.

6.6 Central Goals for Reducing the Global Malaria Burden

Combating Parasite and Vector Resistance

Emerging resistance to pyrethroid insecticides in *Anopheles* vectors and emerging resistance to artemisinin derivatives in *P. falciparum* parasites threaten to reduce the efficacy of the two most important approaches to reducing malaria-associated mortality—transmission control and rapid reduction of parasite load in infected individuals. Insecticide-treated mosquito nets and indoor residual spraying are cornerstones of vector control (Phillips-Howard et al., 2003), but rely on the continued efficacy of pyrethroids and DDT, the most efficacious and cost-effective insecticides available. Few alternatives currently exist, and even fewer are in development (Enayati and Hemingway, 2010; Barnes et al., 2005; Pluess et al., 1996).

Effective malaria control and prevention of mortality also relies on the ability to treat symptomatic infections. Parasite resistance to artemisinin derivatives is emerging in Western Cambodia and the border between Thailand and Myanmar (Dondorp et al., 2009; Noedl et al., 2010; Amaratunga et al., 2012; Phyo et al., 2012), the same sites where resistance to chloroquine and sulfadoxine-pyrimethamine previously emerged. No viable alternative therapies currently exist. Strategies to contain and eliminate resistant parasites are needed if artemisinin derivatives are to retain their current utility in treating uncomplicated and severe malaria.

Vaccine Development

Development of an effective vaccine is a central goal in ongoing malaria research, and would likely be required for malaria eradication to be feasible. Vaccine development is aimed at a wide range of stages in the parasite life-cycle, from preventing initial infection by sporozoites to limiting asexual expansion during the blood stage to blocking transmission by targeting gametocytes. Only one vaccine, RTS,S/AS01E, has been tested in large phase III trials. RTS,S/AS01E is a pre-erythrocytic vaccine that targets the circumsporozoite protein in order to inactivate inoculated sporozoites and prevent initial liver infection. In phase III trials, 6-12

week-old infants were immunized once per month for 3 months (The RTS,S Clinical Trials Partnership, 2012). The vaccine was shown to be safe but only moderately effective as it conferred 30% protection against clinical malaria and 26% protection against severe malaria in the 12 months after final dose (The RTS,S Clinical Trials Partnership, 2012). More effective vaccines are required.

Improved Clinical Management of Severe Malaria Research

Significant progress has been made in the last decade to sharply reduce global malaria transmission, and mortality has decreased accordingly (World Health Organization, 2013). However, even under ideal circumstances, malaria elimination is still a distant prospect in many areas of the world, especially in sub-Saharan Africa. In the meantime, substantial numbers of lives stand to be saved by improved clinical treatment of severe malaria. Paradoxically, improved transmission control may result in diminished immunity, leaving large populations at risk of severe disease if an outbreak were to occur (Snow et al., 1997). Improved strategies for the clinical management of severe malaria are immediately required to reduce current morbidity and mortality burdens and will continue to be needed until malaria is ultimately eradicated.

This thesis explores the biology and biochemistry of nitric oxide synthesis as a potential target for adjunctive therapies to improve outcomes in severe malaria. This work has emphasized the importance of quantitative method development in order to obtain a holistic view of nitric oxide biochemistry in the context of severe malaria. It is hoped that further refinement of the methods and biological insights described in this thesis may ultimately produce interventional strategies with proven clinical benefit in the treatment of severe malaria.

APPENDICES

Method Development and Validation

APPENDIX A.

HPLC Determination of Arginine, Citrulline and Ornithine

Arginine, the nitric oxide synthase substrate, is synthesized from citrulline and degraded by arginase to form ornithine. A high performance liquid chromatography (HPLC) assay was developed to measure arginine, ornithine and citrulline in a single analytical run.

A.1 Introduction

Arginine, the NOS substrate, is depleted in the plasma of patients with severe *P. falciparum* malaria (Lopansri et al., 2003; Yeo et al., 2007; Weinberg et al., 2014). Although arginine is converted to citrulline during nitric oxide synthesis, citrulline can be rapidly recycled to arginine by local argininosuccinate synthetase (ASS1) and argininosuccinate lyase (ASL) enzymes (Flam et al., 2001; Vukosavljevic et al., 2006; Erez et al., 2011). Ornithine acts as a precursor for citrulline synthesis as well as a product of arginine degradation by arginase. Blood stage malaria infection has been associated with release/activation of parasite- and host-derived arginase enzymes (Yeo et al., 2007; Olszewski et al., 2009; Omodeo-Sale et al., 2010). The thorough assessment of arginine metabolism in the context of severe malaria requires accurate determination of arginine as well as its precursor (citrulline) and major degradation product (ornithine). This analytical capacity was developed using high-performance liquid chromatography (HPLC) techniques to measure arginine, citrulline, and ornithine in a single analytical run.

A.2 Materials and Instrumentation

Equipment

All HPLC instrument modules were manufactured by Agilent Technologies. The instrument consisted of a G1379A microdegasser, a G1376A capillary flow binary pump with a zero-volume union used to bypass the micro-flow meter, a G1377 low-flow, high-precision autosampler with a G1330B sample plate temperature-control unit, a G1316A column temperature-control unit and a G1321B fluorescence detector with a 4µl flow cell. Agilent Chemstation OpenLab CDS revision C.01.03 was used to control the instrument and acquire data. A 1.0mm×150mm Luna® C18(2) column with 3µm particles and 100Å pore size (Phenomenex, Torrance, CA, USA) was installed for initial assay development. Due to high back-pressure, the final assay was optimized and validated on an equivalent column with 5µm particles (Phenomenex, Torrance, CA, USA). A 1.0mm×13mm ACE® C18 guard column with 3µm particles and 100Å pore size (MAC-MOD Analytical, Chadds Ford, PA, USA) was installed to protect the primary column.

Reagents

Aqueous mobile phase (Solvent A) consisted of 0.1M sodium acetate (Fisher Scientific, Pittsburgh, PA, USA) in ultrapure H_2O from a Milli-Q Synthesis system (EMD Millipore, Billerica, MA, USA) with 9% v/v methanol (Fisher Scientific, Pittsburgh, PA, USA) and 0.5% v/v tetrahydrofuran (Sigma-Aldrich, St. Louis, MO, USA) with pH adjusted to 8.3 with 3M NaOH (Sigma-Aldrich, St. Louis, MO, USA). Organic mobile phase (Solvent B) was HPLC-grade methanol (Fisher Scientific, Pittsburgh, PA, USA). The derivatization reagent was prepared from ortho-phthaldialdehyde (Sigma-Aldrich, St. Louis, MO, USA) dissolved in HPLC-grade methanol to a concentration of 50mg/ml (372.8mM), 3-mercaptopropionic acid (Sigma-Aldrich, St. Louis, MO, USA) and 200mM potassium tetraborate, pH 9.4 (Sigma-Aldrich, St. Louis, MO, USA). A concentrated solution was prepared by adding 50µl of 50mg/ml OPA in methanol and 6µl 3-mercaptopropionic acid to 444µl of 200mM potassium

tetraborate. Prior to use in analysis, this concentrated solution was diluted 3:10 in 200mM potassium tetraborate, yielding a working solution of 1.5mg/mL (11.2mM) OPA and 41.3mM 3-mercaptopropionic acid in 200mM potassium tetraborate. Deproteination and neutralization were accomplished with 2M perchloric acid (Fisher Scientific, Pittsburgh, PA, USA) and 1.5M potassium carbonate (Sigma-Aldrich, St. Louis, MO, USA). Ultrapure H_2O from a Milli-Q Synthesis system (EMD Millipore, Billerica, MA, USA) was used for sample dilution. All amino acid standards were from Sigma-Aldrich (St. Louis, MO, USA). High-concentration stock standards were dissolved in ultrapure water at a concentration of 125mM, except for L-tyrosine, which was dissolved in 1M HCl due to low solubility in pure water, L-glutamate and L-tryptophan which were prepared at a concentration of 62.5 mM and L-aspartate, which was prepared at a concentration of 31.25mM. Standards were diluted into a combined amino acid standard at a concentration of 2.5mM, aliquoted and stored at -80°C until use.

Sample and Standard Preparation

Plasma samples were obtained from experimental and control mice terminally anaesthetized by intraperitoneal injection of 250mg/kg ketamine and 25mg/kg xylazine. The abdominal cavity was accessed and 700µl of blood was drawn from the abdominal inferior vena cava with a 25G×5/8" needle (BD, Franklin Lakes, NJ, USA). To prevent coagulation, the syringe contained 60µl DPBS with K_3EDTA (final concentration of 1.6mg/ml K_3EDTA after 700 µl blood drawn). Plasma was separated from erythrocytes by centrifugation at 3,000*g* for 7 minutes at 4°C, snap-frozen on dry ice, and stored at -80°C until analysis. On the day of analysis, thawed plasma samples were deproteinated by mixing 12µl sample with 12µl 2M perchloric acid containing 50µM L-norvaline as an internal standard. After centrifuging for 5 minutes at 16,100*g* and 4°C, 10µl of supernatants were removed and neutralized by adding to 5µl of 1.5M potassium carbonate in a fresh tube. The resulting solution was diluted 1:2 in ultrapure water for a final dilution of 1:6. After centrifuging for 5 minutes at 16,100*g* and 4°C to remove potassium chlorate precipitate, samples were loaded into screw-cap polypropylene vials

(Agilent Technologies, Santa Clara CA) for analysis. Amino acid standards were diluted to 50µM and processed in parallel to serve as an external standard for quantitation.

Derivatization, Sample Injection and Data Acquisition

Ortho-phthaldialdehyde (OPA) derivatization (FIG A.1) is the most common method of amino acid derivatization for HPLC analysis (Molnar-Perl, 2001). The autosampler was programmed to draw 2µl of OPA solution and 2µl of the current sample in the sequence, mix the contents in the needle for 30s and inject the derivatized sample onto the column. To prevent carry-over contamination, the needle was washed for 5 seconds between each programmed step using the autosampler's built-in flushport and a wash solution consisting of 10% HPLC-grade methanol (Fisher Scientific, Pittsburgh, PA, USA) in ultrapure H_2O from a Milli-Q Synthesis system (EMD Millipore, Billerica, MA, USA). The column was maintained at 40°C for all runs. Online fluorescence was measured at excitation and emission wavelengths of 340nm and 455nm, respectively. Fluorescence detector photomultiplier tube (PMT) gain was set to 11. Chemstation OpenLab CDS software version C.01.03 was used for peak integration.

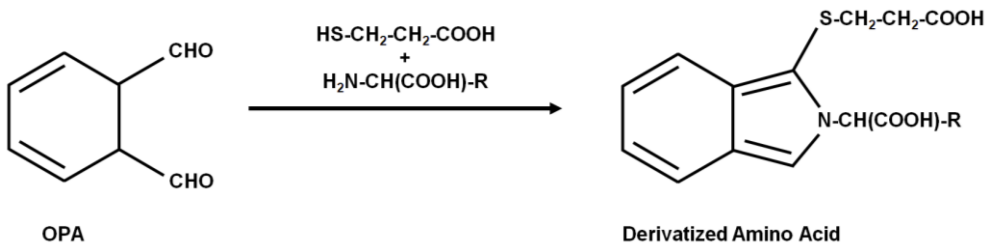


Figure A.1 | OPA derivatization reaction. Ortho-phthaldialdehyde (OPA) reacts with mercaptopropionic acid (HS-CH2-CH2-COOH) and the primary amine of an amino acid (H2H-CH(COOH)-R) to form a fluorescent product. Unbound OPA is not fluorescent at the analytical excitation and emission wavelengths.

Quantification of Analytes

Internal and external standards were used for quantification of analytes. A combined external standard of 22 common amino acids was diluted to a known concentration of 50μM, processed and analyzed alongside samples. A response factor (RF) was calculated for each amino acid in the external standard:

$$\mathrm{RF} = \frac{\text{Analyte Peak Area}_{External\ Std}}{50\mu\mathrm{M}} \qquad \textit{Eq A.1}$$

L-norvaline (50μM) was used as an internal standard. Concentrations of amino acid analytes in the sample were calculated from this external standard response factor and normalized to recovery of the internal standard (IS):

$$[\text{Analyte}]_{Sample} = \frac{\text{Analyte Peak Area}_{Sample}}{\mathrm{RF}} \times \frac{\text{IS Peak Area}_{Standard}}{\text{IS Peak Area}_{Sample}} \qquad \textit{Eq A.2}$$

A.3 Assay Optimization

Peak identification

Peaks identities and retention times were determined by separate analysis of individual standard solutions of 22 common amino acids. Twenty of the twenty-two amino acids were successfully identified as peaks with unique retention times (FIG B.2A). Cysteine and Proline were not detectable with this assay (FIG B.2B).

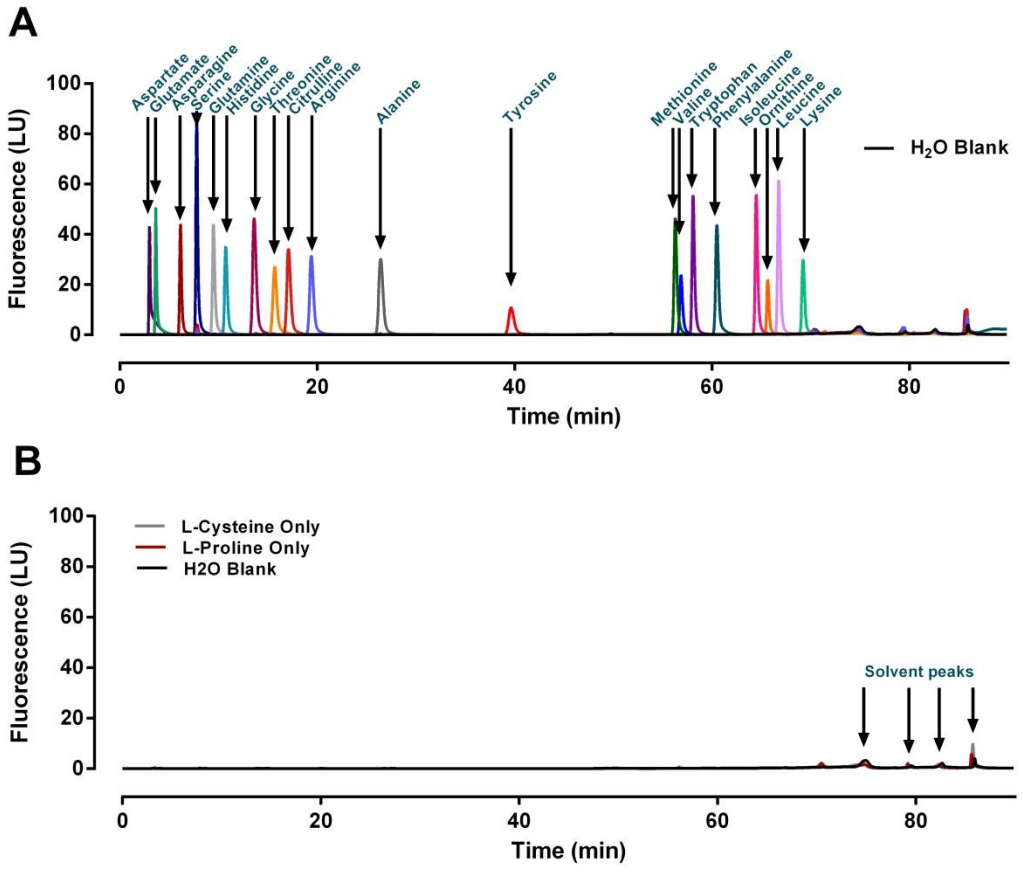


Figure A.2 | Determination of common amino acid retention times. (**A**) Standard solutions of 20 common amino acids were run independently to identify retention times of each peak. (**D**) Cysteine and proline standards were not detectable with this assay.

Selection of Internal Standard

Further studies were conducted to compare the applicability of L-norvaline and L-norleucine for use as an internal standard to control quantification for differences in sample processing and derivatization. To accomplish this aim, L-norvaline and L-norleucine were assessed alone and in combination with the full combined amino acid standard. L-norleucine was found to co-elute with leucine while L-norvaline was well separated from all common amino acids represented in the standard. L-norvaline was therefore selected as an appropriate internal standard for further assay development (FIG A.3).

Sample Processing Optimization

After initial determination of chromatography and data acquisition parameters, two potential strategies for sample deproteination were assessed: precipitation with 10% w/v 5-sulfosalicylic acid (SSA) and precipitation with 2M perchloric acid ($HClO_4$), followed by neutralization with an equal volume of 1.5M potassium carbonate (K_2CO_3). Perchloric acid + potassium carbonate neutralization was selected for further assay development based on the absence of major artifact peaks and improved peak size compared with 5-sulfosalicylic acid-treated samples (FIG A.4).

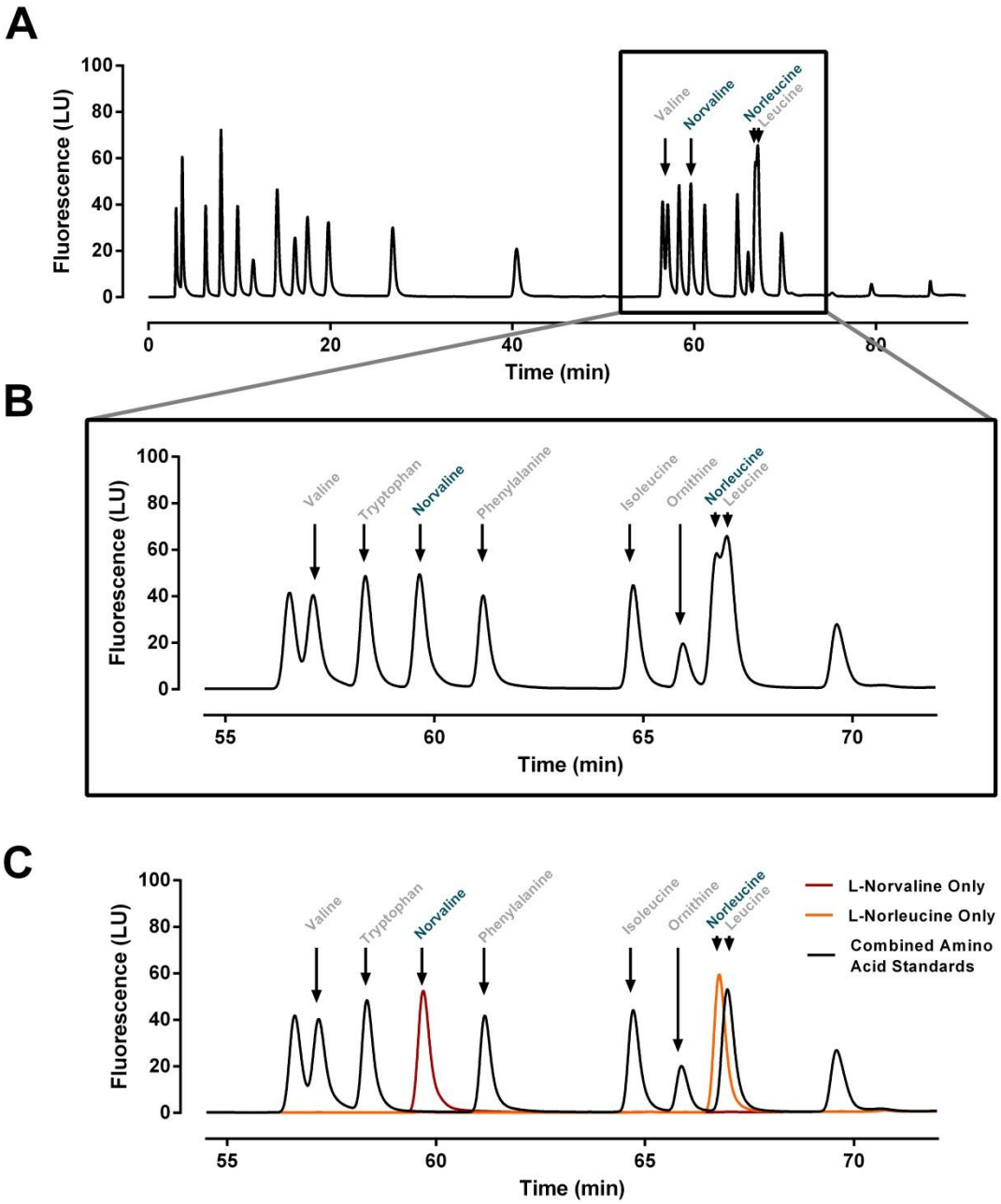


Figure A.3 | Assessment of candidate internal standards. (**A**) A combined amino acid standard was spiked with L-norvaline (50µM) and L-norleucine (50µM) to assess separation from target analytes. (**B**) Magnified segment of chromatogram from panel A showing overlap of norleucine and leucine peaks. L-norvaline eluted as a unique, distinguishable peak. (**C**) Norvaline (red trace) and norleucine (orange trace) were identified by analyzing standard solutions independently.

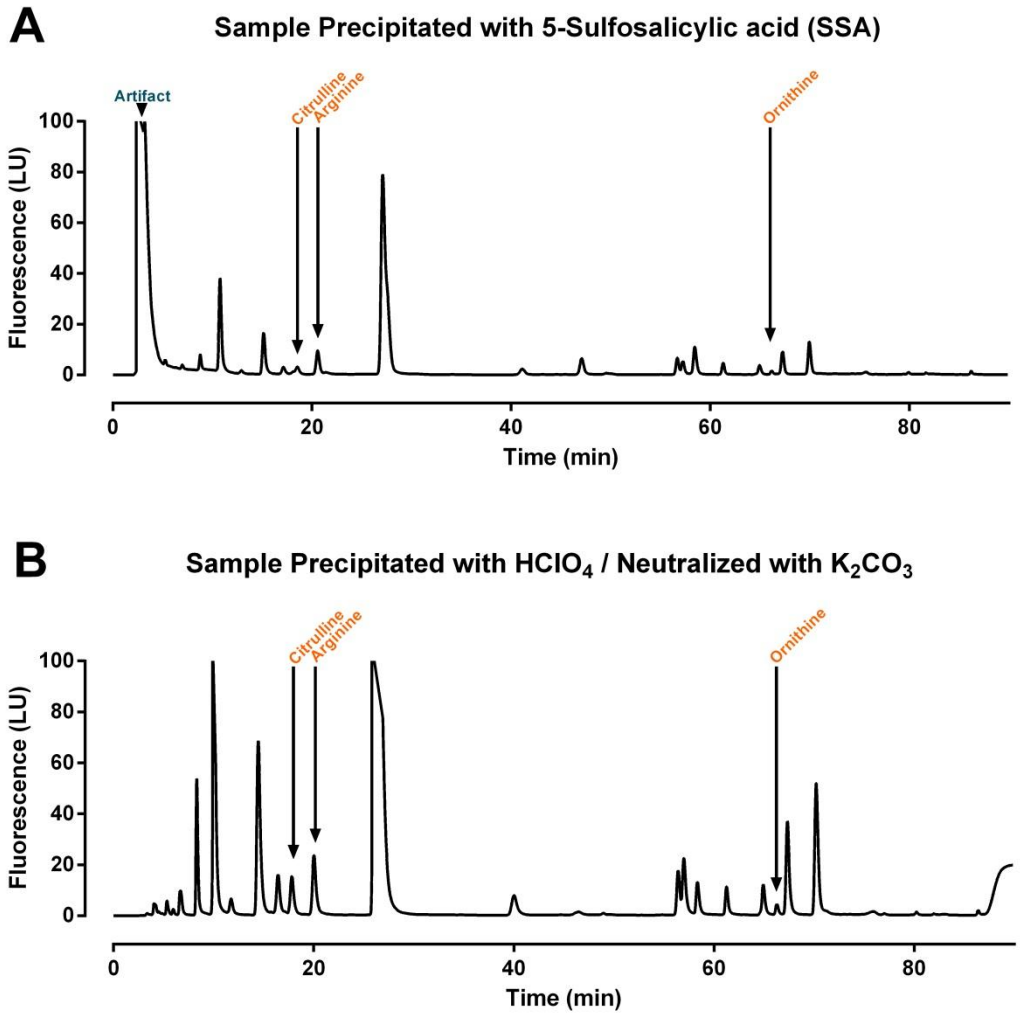


Figure A.4 | Comparison of protein precipitation strategies. (**A**) Plasma samples were precipitated with 10% w/v 5-sulfosalicylic acid. The first off-scale peak is an artifact of unknown identity. (**B**) Alternatively, plasma samples were precipitated with 2M perchloric acid ($HClO_4$) and neutralized with an equal volume of 1.5M K_2CO_3.

Run-Time Optimization

At a flow-rate of 42µl/min, the transition from aqueous solvent A to organic solvent B yielded peak back-pressures of ~190bar on the 1.0mm×150mm Luna® C18(2) column with 3µm particles. Because the column was designated with a maximum 245 pressure rating, flow-rates could not be effectively increased without risking damage to the column matrix. In order to reduce back-pressure and achieve shorter run-times, an equivalent column with 5µm particles was installed. In addition, a 1.0mm×13mm ACE® C18 guard column with 3µm particles was installed to protect the primary column. The original pump program was modified proportionally to account for the change in flow rate and the increase in the effective column length provided by the guard column installation (TABLE A.1, FIG A.5 & FIG A.6).

Flow Rate (µl/min)	Mobile Phase	Elapsed Time (min) 0	20	30	40	50	53	65	75	80	85	85	100	Total time
42	A (%):	96	86	86	70	60	53	50	30	0	0	96	96	**1hr 40min**
	B (%):	4	14	14	30	40	47	50	70	100	100	4	4	

Flow Rate (µl/min)	Mobile Phase	Elapsed Time (min) 0	11	16	22	27	29	35	41	44	49	49	65	Total time
84	A (%):	96	86	86	70	60	53	50	30	0	0	96	96	**1hr 5min**
	B (%):	4	14	14	30	40	47	50	70	100	100	4	4	

Table A.1 | Run time optimization. The original pump program (42µl/min, top program) was re-calibrated to account for the change in flow rate and the increase in effective column length due to the installation of a guard column (84µl/min, bottom program).

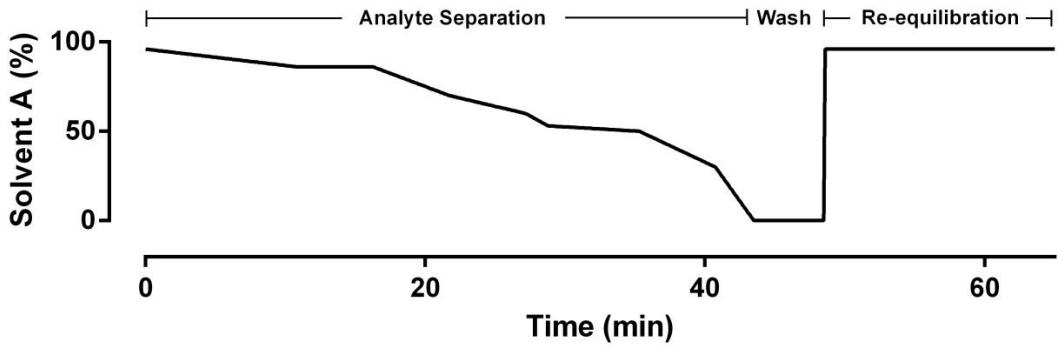


Figure A.5 | Plot of solvent A concentration vs time for optimized (84µl/min) program. Sample was injected at 0 min. Chromatographic separation of analytes was achieved in the first 41 minutes of the program. The column was then washed for 5 minutes with 100% solvent B and re-equilibrated for 16 minutes prior to injection of the next sample.

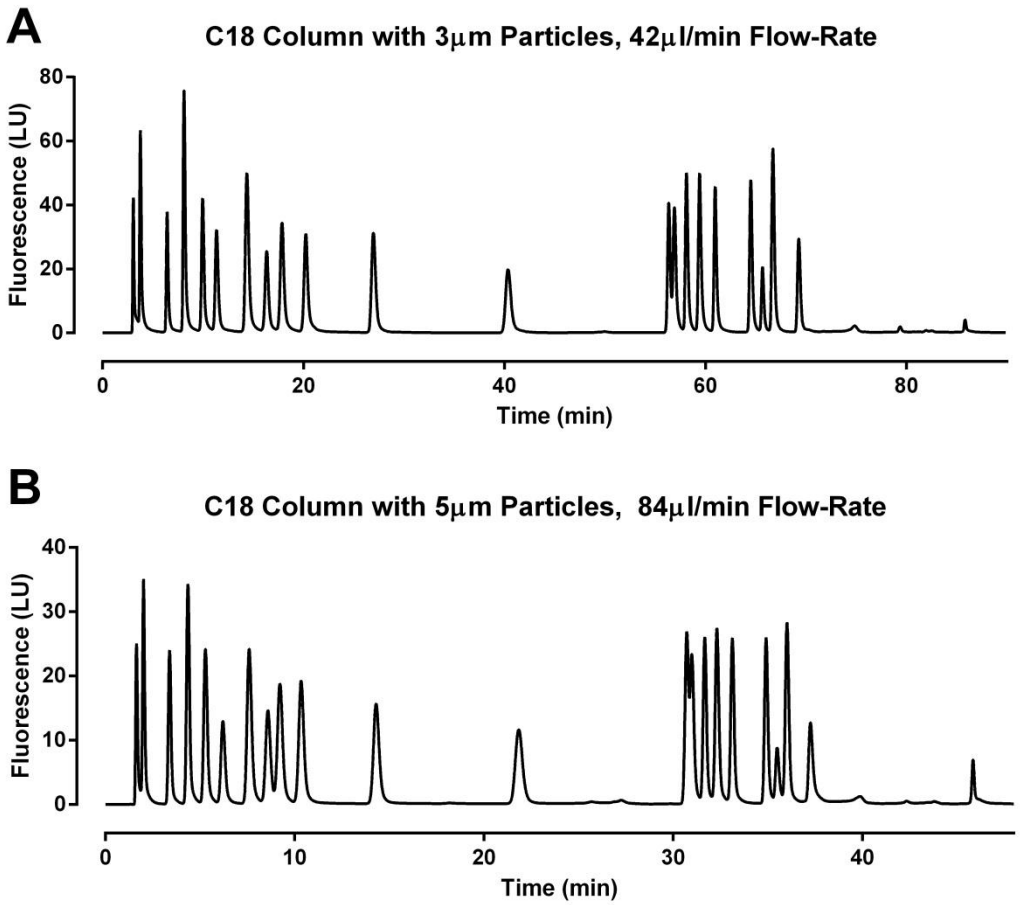


Figure A.6 | Run-time optimization. (**A**) Sample chromatogram of combined amino acid standards run on a 1.0mm×150mm Luna® C18(2) column with 3µm particles at a flow-rate of 42µl/min. (**B**) Sample chromatogram of combined amino acid standards run on an equivalent column with 5µm particles at a flow-rate of 84µl/min.

A.4 Assay Validation

Standard Curve Linearity

To assess linearity, the combined standard solution was diluted to yield a 9-point standard curve. Standard curves for each analyte were highly linear with R^2 values greater than 0.9994 (TABLE A.2) with the exception of aspartate (R^2=0.9981). Standard curves for arginine, citrulline and ornithine are illustrated in FIG A.7. Throughout the range of concentrations tested, the ornithine fluorescent signal was found to be roughly one third that of arginine and citrulline. Previously published assays also demonstrate ornithine peaks with a relatively lower fluorescent signal (Zhang and Kaye, 2004). Under standard analysis conditions, arginine, citrulline, ornithine were quantifiable at concentrations of up to 200μM, which was the highest standard concentration tested (TABLE A.2).

Amino Acid	Concentration of Standards (µM)									R^2
	200	150	100	50	25	10	5	2.5	1	
Asp	-	476	342	167	87.2	35.7	19.5	10.4	5.5	0.9981
Glu	-	-	522	265	134	54.6	28.3	14.1	6.4	1
Asn	946	725	495	258	130	51.7	26.1	13.2	5.6	0.9994
Ser	-	1202	831	415	211	82.2	42.2	24.5	21.8	0.9995
Gln	1322	1005	677	349	175	68.7	34.8	16.8	6.9	0.9998
His	906	661	442	222	110	43.5	22	10.4	5.1	0.9997
Gly	1842	1363	912	457	226	88.3	45.4	24	18.8	0.9999
Thr	1057	779	532	267	133	52.5	26.7	13.4	7.1	0.9999
Cit	1542	1136	768	387	194	76.8	39.2	19.3	8.4	0.9999
Arg	1584	1157	771	393	194	76.2	38.1	18.8	7.9	0.9997
Ala	1414	1036	708	348	176	69.1	36.1	19.1	11.7	0.9998
Tyr	1205	903	612	308	156	62.4	32.1	15.9	7.4	0.9999
Met	1392	1069	722	375	190	77.1	39.6	20	7.8	0.9995
Val	1297	973	673	341	176	71.4	37.7	19.1	9.5	0.9997
Trp	-	1082	726	371	187	74.7	37.9	18.7	7.8	0.9999
Phe	1354	1023	697	361	186	77	41.8	22.9	11.9	0.9998
Ile	1194	898	620	313	161	65.2	34.1	17.2	7.9	0.9997
Orn	470	346	227	110	53.6	20.3	9.9	4.8	2.5	0.9996
Leu	-	1088	745	378	194	77.5	40.1	20.1	9.6	0.9997
Lys	943	705	469	235	118	41.2	20.9	10.2	4.1	1.0000

Table A.2 | Linearity of standards assayed over a range of concentrations. Values expressed as mean integrated areas (relative light units × s) averaged from n=3 independent standard curves. Peaks that exceeded the upper threshold of detection (flooded signal) are noted with a dash. Linearity was assessed by calculating the R^2 value of the line of best fit for each analyte standard curve.

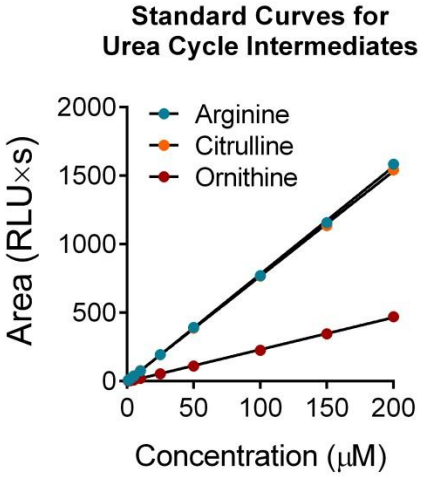


Figure A.7 | Plots of standard curves for arginine, citrulline and ornithine. Nine-point dilutions of a combined external standard of 22 common amino acids was prepared and assayed in triplicate Standard curves are shown for arginine, citrulline and ornithine.

Inter-day Precision

Inter-day precision was calculated from 5 repeat analyses of the same human and mouse plasma samples. The coefficient of variation (CV) was calculated and expressed as a percent (%CV):

$$\%\mathrm{CV} = \frac{s}{\bar{x}} \times 100\% \qquad \textit{Eq A.3}$$

Where s is the standard deviation and $\bar{x}$ is the mean of repeated measurements. %CV values were <5% for arginine, citrulline and ornithine in both mouse and human plasma (TABLE A.3).

	Human plasma				Mouse plasma			
Analyte	**Concentration (µM)**			**%CV**	**Concentration (µM)**			**%CV**
Asp	5.3	±	1.1	20.1	7.1	±	0.6	8.6
Glu	64.3	±	3.2	5.0	29.3	±	1.2	4.1
Asn	59.3	±	3.5	5.9	47.7	±	0.9	1.8
Ser	113.4	±	6.6	5.8	95.7	±	2.6	2.7
Gln	-	±	-	-	-	±	-	-
His	83.9	±	5.3	6.4	86.9	±	3.4	3.9
Gly	203.5	±	8.8	4.3	180.6	±	2.8	1.5
Thr	194.0	±	9.4	4.8	118.4	±	3.7	3.2
Cit	20.8	±	0.9	4.3	61.2	±	1.4	2.3
Arg	80.2	±	3.9	4.8	74.7	±	1.0	1.3
Tyr	110.0	±	4.9	4.5	91.0	±	2.2	2.4
Trp	49.4	±	1.8	3.7	49.2	±	1.5	3.0
Met	-	±	-	-	-	±	-	-
Val	-	±	-	-	-	±	-	-
Phe	74.9	±	3.2	4.3	65.0	±	1.3	2.0
Ile	121.2	±	2.9	2.4	52.5	±	1.3	2.5
Orn	86.3	±	3.6	4.1	49.5	±	0.8	1.5
Leu	218.9	±	7.8	3.6	115.7	±	3.5	3.0
Lys	260.2	±	9.3	3.6	185.3	±	5.4	2.9

Table A.3 | Inter-day precision. Human mouse and plasma samples were repeatedly analyzed on 5 different days. Measured concentrations are reported as mean ± SD for repeated analyses and precision was assessed by calculating the coefficient of variation as a percent (%CV).

Limit of Detection

The limit of detection (LOD) is the lowest concentration that can be reliably distinguished from baseline noise. The LOD was determined by assaying 3 independent water blank samples and 3 independent combined standards diluted to a concentration of 1.0µM for each analyte (TABLE A.4). The lower limit of detection was calculated from these values according to the equation described in (Armbruster and Pry, 2008):

$$\mathrm{LOD} = \mathrm{Mean}_{Blank} + 1.645 \times \mathrm{SD}_{Blank} + 1.645 \times \mathrm{SD}_{Low\ Standard} \qquad Eq\ A.4$$

Analyte	LOD (µM)
Asp	0.44
Glu	0.16
Asn	0.20
Ser	0.77
Gln	0.22
His	0.18
Gly	1.00
Thr	0.22
Cit	0.12
Arg	0.34
Ala	0.43
Tyr	0.10
Met	0.18
Val	0.26
Trp	0.35
Phe	0.51
Ile	0.29
Orn	0.31
Leu	0.45
Lys	0.66

Table A.4 | Limit of detection (LOD). Values determined from ultrapure water blank samples (n=3) and low-concentration combined amino acid standards diluted to 1µM (n=3).

Stability of Dissolved Analytes

This method utilizes automated derivatization of samples directly prior to injection onto the column. This approach is preferable to manual batch derivatization because it provides a consistent, fixed time interval between derivatization and analysis. In our method, samples and derivatization reagent were mixed in the autosampler needle, allowing for re-analysis of the remaining underivatized sample. We analyzed the stability of dissolved analytes maintained at 4°C in the autosampler over a 24 hour period by comparing repeat analyses of 3 combined amino acid standards at 0 and 24 hour intervals (TABLE A.5). Measurements of all analytes at 24hr were ≥99.0% of initial (0hr), demonstrating that analytes and OPA solution are stable at 4°C for 24 hours (TABLE A.5).

Sample Matrix Effects

Sample matrix effects were assessed by spiking known concentrations of standards into human and plasma mouse samples (TABLE A.6 & TABLE A.7). Recovery was calculated as an absolute concentration and as a percentage of the known concentration of the standard used to spike samples:

$$\%\, Recovery = \left(\frac{[Analyte]_{Sample+Spike} - [Analyte]_{Sample\ Alone}}{50\mu M}\right) \times 100 \qquad Eq\ A.5$$

Recovery of arginine, citrulline and ornithine were >94.0% in human and mouse plasma, confirming the absence of interfering matrix effects (TABLE A.6 & TABLE A.7).

Analyte Stability (% of 0hr)				
Analyte	**0hr**	**24hr**		
Asp	100	105.0	±	4.6
Glu	100	99.3	±	2.6
Asn	100	99.1	±	1.1
Ser	100	100.8	±	1.4
Gln	100	97.7	±	1.1
His	100	99.3	±	2.5
Gly	100	99.4	±	2.1
Thr	100	101.3	±	1.3
Cit	100	100.1	±	1.1
Arg	100	99.0	±	1.7
Ala	100	102.6	±	1.7
Tyr	100	100.8	±	1.1
Met	100	101.8	±	1.3
Val	100	102.7	±	1.2
Trp	100	100.2	±	1.8
Nval	100	101.1	±	1.1
Phe	100	100.2	±	1.0
Ile	100	102.2	±	1.3
Orn	100	104.7	±	8.0
Leu	100	101.8	±	1.3
Lys	100	104.4	±	5.0

Table A.5 | Assessment of analyte stability. Data were determined from repeat assessments of three combined amino acid standards (50µM) at 0 and 24hr. Values are expressed as mean % of initial at 0hr ±SD.

Human Plasma												
	Measured Concentration (µM)						Recovery					
Analyte	Plasma Only			Plasma + Spike (50µM)			Concentration (µM)			Percent of initial (%)		
Asp	4.4	±	0.2	50.4	±	1.1	46.0	±	1.3	92.0	±	2.5
Glu	90.1	±	2.9	128.9	±	1.3	38.8	±	3.2	77.5	±	6.3
Asn	58.0	±	1.2	103.7	±	1.7	45.7	±	1.1	91.3	±	2.1
Ser	116.4	±	2.3	-	±	-	-	±	-	-	±	-
Gln	-	±	-	-	±	-	-	±	-	-	±	-
His	83.4	±	1.1	134.6	±	2.1	51.2	±	1.1	102.4	±	2.1
Gly	212.6	±	3.5	-	±	-	-	±	-	-	±	-
Thr	199.4	±	3.3	239.4	±	5.0	40.0	±	2.5	80.0	±	5.1
Cit	19.3	±	0.3	67.9	±	0.7	48.6	±	0.6	97.1	±	1.3
Arg	81.6	±	1.2	128.7	±	2.2	47.2	±	1.2	94.3	±	2.3
Ala	-	±	-	-	±	-	-	±	-	-	±	-
Tyr	114.7	±	1.7	160.8	±	3.4	46.1	±	1.9	92.2	±	3.7
Trp	50.4	±	0.8	99.2	±	1.6	48.8	±	0.9	97.6	±	1.8
Met	-	±	-	-	±	-	-	±	-	-	±	-
Val	-	±	-	-	±	-	-	±	-	-	±	-
Phe	78.1	±	1.0	124.0	±	2.5	45.9	±	1.6	91.8	±	3.1
Ile	125.6	±	3.2	166.3	±	3.6	40.6	±	2.7	81.3	±	5.5
Orn	91.2	±	0.7	142.6	±	3.5	51.4	±	2.9	102.7	±	5.8
Leu	230.7	±	5.4	-	±	-	-	±	-	-	±	-
Lys	291.4	±	3.2	339.5	±	9.5	48.1	±	6.3	96.1	±	12.7

Table A.6 | Recovery of amino acid standards spiked into plasma samples. Recovery was calculated by quantifying plasma samples with or without addition of amino acid standards at a final concentration of 50µM. Results are from spike-recovery analyses of three aliquots of the same plasma assayed on three different days. Recovery was calculated as a percentage of the known concentration of the added standards (50µM). All values are mean ± SD.

Mouse Plasma

Analyte	Measured Concentration (µM)		Recovery	
	Plasma Only	Plasma + Spike (50µM)	Concentration (µM)	Percent of initial (%)
Asp	11.7 ± 0.6	64.8 ± 2.2	53.1 ± 1.8	106.2 ± 3.5
Glu	80.7 ± 2.7	141.3 ± 1.8	60.6 ± 3.8	121.1 ± 7.6
Asn	49.5 ± 3.3	90.6 ± 1.1	41.2 ± 2.5	82.3 ± 5.1
Ser	102.9 ± 3.9	- ± -	- ± -	- ± -
Gln	- ± -	- ± -	- ± -	- ± -
His	63.2 ± 3.3	112.3 ± 0.6	49.2 ± 2.9	98.3 ± 5.7
Gly	234.3 ± 15.7	- ± -	- ± -	- ± -
Thr	118.8 ± 4.8	161.3 ± 0.6	42.5 ± 4.8	84.9 ± 9.5
Cit	37.0 ± 1.3	84.3 ± 0.6	47.3 ± 1.3	94.6 ± 2.5
Arg	74.4 ± 0.9	122.0 ± 0.9	47.6 ± 1.4	95.1 ± 2.8
Ala	- ± -	- ± -	- ± -	- ± -
Tyr	61.9 ± 2.9	108.0 ± 0.9	46.1 ± 2.6	92.3 ± 5.3
Trp	49.3 ± 2.9	95.4 ± 1.2	46.1 ± 2.3	92.2 ± 4.6
Met	- ± -	- ± -	- ± -	- ± -
Val	- ± -	- ± -	- ± -	- ± -
Phe	44.4 ± 2.2	90.0 ± 0.9	45.6 ± 1.7	91.2 ± 3.4
Ile	57.0 ± 1.6	104.1 ± 0.2	47.1 ± 1.8	94.1 ± 3.6
Orn	34.3 ± 1.7	85.9 ± 0.5	51.6 ± 1.7	103.1 ± 3.4
Leu	124.7 ± 3.9	170.5 ± 0.4	45.7 ± 5.9	91.3 ± 11.7
Lys	189.3 ± 9.3	238.1 ± 3.1	48.8 ± 7.9	97.6 ± 15.8

Table A.7 | Analysis recovery of amino acid standards spiked into plasma samples. Recovery was calculated by quantifying plasma samples with or without addition of amino acid standards at a final concentration of 50µM. Results are from spike-recovery analyses of three aliquots of the same plasma assayed on three different days. Recovery was calculated as a percentage of the known concentration of the added standards (50µM). All values are mean ± SD.

A.5 Conclusion

The key urea cycle intermediates citrulline and ornithine are rarely adequately identified, separated and quantified in published studies, although some studies have provided preliminary assay qualification (Zhang and Kaye, 2004; Wu and Meininger, 2008). Building on these published methods, our assay provides reliable quantitation based on both external and internal standards.

Acknowledgements

I am grateful to Glenn Nardone (NIAID/NIH) for his helpful advice on assay development. This work was funded by the NIAID Division of Intramural Research.

APPENDIX B

Quantitative Assessment of Urea Cycle Flux

Infusion of heavy isotope-labelled metabolic tracers allows direct quantitation of urea cycle metabolic rates, or flux. Common equations used in published studies of urea cycle metabolism were derived from a model of linear metabolism that assumes substrate cannot be recycled from product pools. This assumption does not apply to many common urea cycle tracers. This appendix describes development of a heavy isotope labelling strategy and computational approach to quantify urea cycle metabolism taking recycling into account.

B.1 Introduction

Impaired nitric oxide production due to disturbances in plasma availability of arginine, citrulline and ornithine may contribute to the pathophysiology of a wide variety of disease states, including severe malaria (Lopansri et al., 2003; Yeo et al., 2007), persistent neonatal hypertension (Pearson et al., 2001), sickle cell disease (Schnog et al., 2004; Morris et al., 2005) and coronary artery disease (Tang et al., 2009). Conclusions in these studies are largely drawn from static assessment of plasma arginine, citrulline and ornithine concentrations in patient groups and controls. Measurements made at a single point in time provide limited information about the dynamic metabolic changes that may be responsible for alterations in plasma metabolite concentrations.

Further investigation of disease states involving altered or disrupted urea cycle metabolism requires direct quantification of *in vivo* metabolic rates. Metabolic flux may be quantified as a function of time by assessing accumulation of continuously infused metabolic tracers enriched with heavy isotopes such as ^{13}C and/or ^{15}N. Based on the known rate of infusion and resulting abundance of the tracer in plasma pools, the *in vivo* rate of appearance of

the endogenous metabolite may be quantified. A similar computational approach may be used to quantify the rate at which one metabolite is converted to another. Heavy isotope-labelled tracers have previously been utilized to investigate the dietary sources of urea cycle intermediates (Marini et al., 2010a; Marini, 2012; Marini et al., 2012), the metabolic impact of mutations in key urea cycle enzymes (Marini et al., 2007; Erez et al., 2011), and the dynamic response of whole-body urea cycle metabolism to dietary restriction (Castillo et al., 1993, 1994; Beaumier et al., 1995; Castillo et al., 1995).

The computational methodologies utilized in published urea cycle tracer studies are based on preceding studies of whole-body phenylalanine appearance and enzymatic conversion to tyrosine (Clarke and Bier, 1982; Thompson et al., 1989). These analyses of phenylalanine metabolism are based on the fundamental assumption that labelled tyrosine could not be recycled to phenylalanine pools and that heavy isotope enrichment of the phenylalanine pool could therefore be considered to arise only from direct infusion of heavy isotope-labelled phenylalanine (Clarke and Bier, 1982; Thompson et al., 1989). Such assumptions of linear metabolism are appropriate for the study of phenylalanine, which does not participate in cyclical metabolic pathways. However, similar assumptions of a linear system cannot be applied to the urea cycle, in which arginine, ornithine and citrulline can each be recycled. In this appendix, we derive a set of equations that may be used to calculate urea cycle flux taking the rate of recycling into account.

B.2 Glossary

Term	Definition
X_{m+0}	Abundance of unlabelled metabolite *X* of mass *m* with no incorporated heavy isotopes (arbitrary units)
X_{m+a}	Abundance of metabolite *X* with mass *m* and heavy isotopes (^{13}C, ^{15}N or ^{2}H) incorporated at *a* positions (arbitrary units)
$TTR_{X_{m+a}}$	Tracer-tracee ratio, the ratio of metabolite *X* tracer with mass *m+a* to unlabelled metabolite *X* tracee with mass *m+0*
I	The rate at which a heavy isotope-labelled tracer is infused ($\mu mol \times kg^{-1} \times hr^{-1}$)
Q_{X_T}	The total rate of appearance of metabolite *X* ($\mu mol \times kg^{-1} \times hr^{-1}$), including recycling by a cyclical metabolic pathway
Q_{X_R}	The rate of metabolite *X* recycling ($\mu mol \times kg^{-1} \times hr^{-1}$)
$Q_{X_{NR}}$	The rate of appearance of metabolite *X* from sources other than recycling (NR: non-recycled) ($\mu mol \times kg^{-1} \times hr^{-1}$)
$Q_{X \rightarrow Y}$	The rate at which metabolite *X* is converted to metabolite *Y* ($\mu mol \times kg^{-1} \times hr^{-1}$)
$E_{IX_{m+a}}$	The enrichment of fully-labelled metabolite *X* tracer (*m+a*) as the proportion of all fully-labelled, partially labelled and unlabelled metabolite *X* present in the tracer preparation.
$E_{IX_{m+0}}$	The enrichment of fully-unlabelled metabolite *X* tracer (*m+0*) as the proportion of all fully-labelled, partially labelled and unlabelled metabolite *X* present in the tracer preparation.

B.3 Basic Calculation of Metabolic Kinetics

Assumptions

Heavy isotope-labelled metabolic tracers are assumed to be evenly and freely distributed throughout free pools of the target metabolite. Metabolism of heavy isotope-labelled tracers is assumed to be indistinguishable from unlabelled tracer. Finally, it is assumed that the addition of exogenous tracer to the system has negligible effects on the underlying rates of metabolism.

Definition of the Tracer-Tracee Ratio

The tracer-tracee ratio (*TTR*) describes the abundance of labelled tracer with mass *m+a* relative to the abundance of the target (tracee) metabolite with mass *m+0*. The heavy isotopes incorporated into tracers, such as ^{13}C and ^{15}N, occur in nature, although at much lower abundances than common ^{12}C and ^{14}N isotopes. As a result, the tracee metabolite pool contains some molecules with ^{13}C or ^{15}N at *a* positions such that the mass of these molecules resembles that of the tracer (*m+a*). In order to directly account for this background, a standard solution of non-enriched tracee metabolite is prepared in pure water and analyzed by mass spectrometry. This approach allows the calculation of a *TTR* value that describes the abundance of infused tracer with mass *m+a* accounting for any background contribution of naturally-occurring heavy isotopes in the tracee pool:

$$TTR_{X_{m+a}} = \frac{X_{m+a_{sample}}}{X_{m+0_{sample}}} - \frac{X_{m+a_{std}}}{X_{m+0_{std}}} \qquad Eq\ B.1$$

Where $TTR_{X_{m+a}}$ is the tracer-tracee ratio of metabolite *X* tracer with heavy isotopes incorporated at *a* positions measured in the sample, $X_{m+0_{sample}}$ is the abundance of unlabelled metabolite *X* trace with mass *m* and no incorporated heavy isotopes measured in the sample, $X_{m+a_{sample}}$ is the abundance of metabolite *X* tracer with heavy isotopes incorporated at *a* positions measured in

the sample, and $X_{m+0_{std}}$ and $X_{m+a_{std}}$ are the abundances of tracee and tracer, respectively, measured in a pure non-enriched standard solution.

Single Metabolite Rate of Appearance

The rate of appearance of metabolite *X* can be described by the term Q_X. The enrichment of a continuously-infused tracer (expressed as a *TTR*) reflects the ratio between the rate of tracer infusion (I_X) and the rate of tracee appearance (Q_X) according to the following equation (see FIG B.1 for schematic representation):

$$TTR_{X_{m+a}} = \frac{I_{X_{m+a}}}{Q_X} \qquad \textit{Eq B.2}$$

Where $TTR_{X_{m+a}}$ is the tracer-tracee ratio of labelled metabolite *X* tracer with mass *m+a* to unlabelled metabolite *X* with mass *m+0* calculated from *Eq B.1*, $I_{X\ m+a}$ is the rate at which labelled metabolite *X* tracer with mass *m+a* is infused (expressed in μmol×kg^{-1}×hr^{-1}), and Q_X is the rate of appearance of metabolite *X* (expressed in μmol×kg^{-1}×hr^{-1}).

Labelled tracers are typically enriched to 98% or 99% with heavy isotopes at each labelled position. Therefore, for a 99% enriched tracer with *a* labelled positions, the proportional enrichment of metabolite *X* tracer containing a label at every position ($E_{IX_{m+a}}$) is approximately $(0.99)^a$ of the known molar amount of metabolite *X* tracer. As a result, *Eq B.2* must be corrected so that the molar rate of tracer infusion (I_X, expressed in μmol×kg^{-1}×hr^{-1}) reflects the proportion of fully-labelled metabolite *X* tracer present in the infusion. The amount of endogenous metabolite appearing in plasma must also be corrected for the proportion of tracer infusion that may be unlabelled ($E_{IX_{m+0}}$) due to incomplete label enrichment:

$$TTR_{X_{m+a}} = \frac{I_{X_{m+a}} \times E_{IX_{m+a}}}{Q_X + \left(I_{X_{m+a}} \times E_{IX_{m+0}}\right)} \qquad \textit{Eq B.3}$$

Where $E_{IX_{m+a}}$ is the proportional enrichment of fully-labelled metabolite *X* tracer in the infusion solution, $E_{IX_{m+0}}$ is the proportional enrichment of fully-unlabelled metabolite *X* tracer in the infusion solution, and all other terms are as they appear in *Eq B.2.*

In contrast to *TTR* values, E_I infusion enrichment values are calculated as a proportion of the total abundance of all detected metabolites in the infusion solution. For example, a solution of 99% enriched L-[U-$^{13}C_6$;U-$^{15}N_4$]arginine (*m+10*) would theoretically contain a proportion of $(0.99)^{10}$ or 0.904 of fully-labelled tracer and a proportion of only $(0.01)^{10}$ or 0.1×10^{-20} unlabelled arginine. This demonstrates that for tracers labelled at multiple positions, $E_{IX_{m+0}} \approx 0$. The majority of the remaining metabolites in the tracer infusion would be lacking C^{13} or N^{15} at only one (m+9) or two positions (m+8). The exact values of $E_{IX_{m+a}}$ and $E_{IX_{m+0}}$ may be observed directly by analyzing the infusion solution by mass spectrometry and calculating the abundance of fully-labelled and full-unlabelled metabolite *X* tracer as a proportion of the sum total of all fully-labelled, partially-labelled and unlabelled metabolite *X* present in the tracer infusion.

Rearranging *Eq B.3*, the rate of appearance of metabolite *X* (Q_X) may be calculated based on the known molar rate of tracer infusion ($I_{X_{m+a}}$), the proportion of fully-labelled and fully-unlabelled metabolites in the tracer infusion ($E_{IX_{m+a}}$ and $E_{IX_{m+0}}$) and the experimentally-determined plasma tracer abundance ($TTR_{X_{m+a}}$) at plateau:

$$Q_X = \frac{I_{X_{m+a}} \times E_{IX_{m+a}}}{TTR_{X_{m+a}}} - \left(I_{X_{m+a}} \times E_{IX_{m+0}}\right) \qquad \textit{Eq B.4}$$

Where all terms are as they appear in *Eq B.2* and *Eq B.3*. For tracers labelled at multiple positions, $E_{IX_{m+0}} \approx 0$; therefore the term $I_{X_{m+a}} \times E_{IX_{m+0}} \approx 0$.

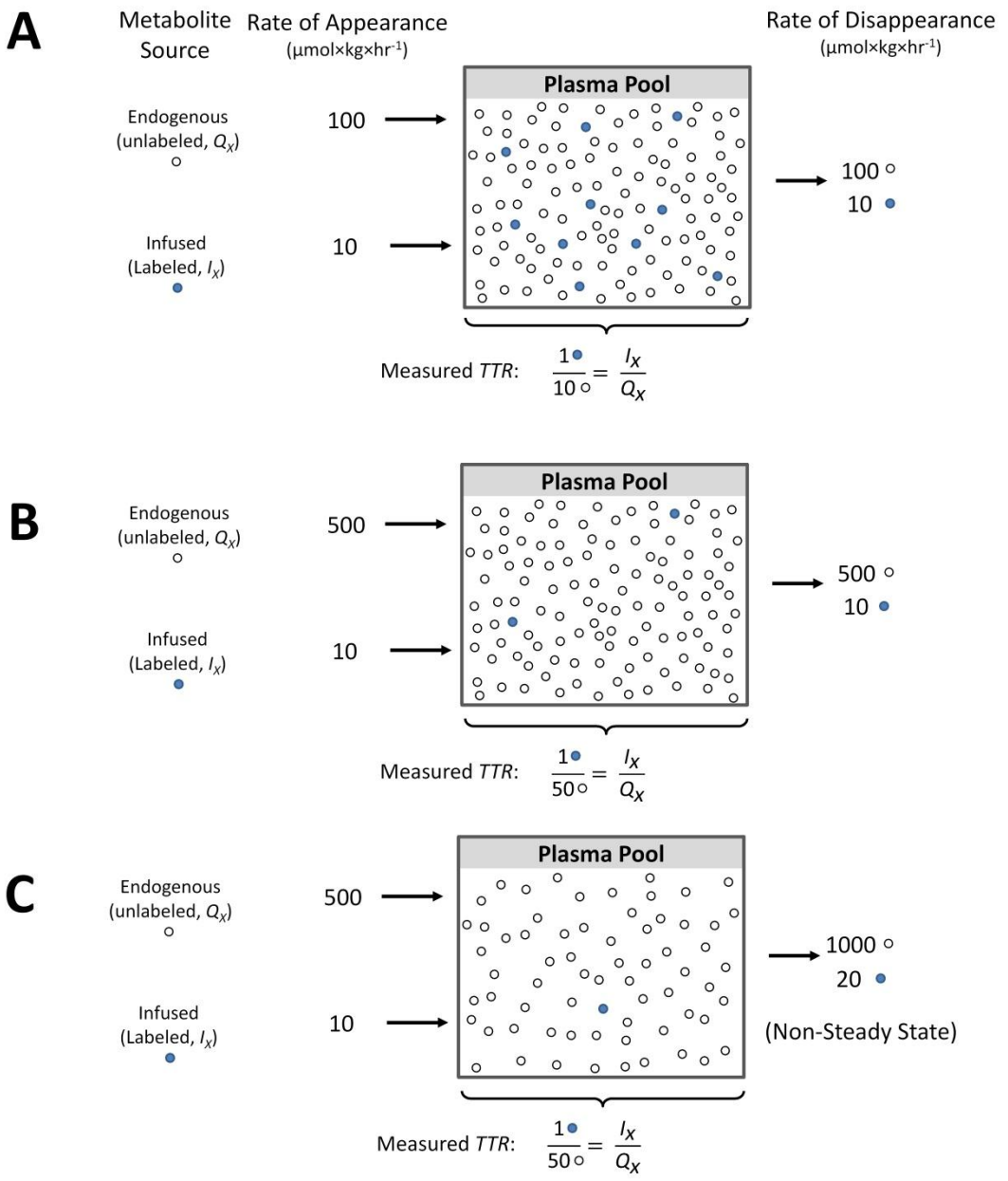


Figure B.1 | Schematic representation of single-metabolite turnover. (**A**) The rate of appearance of an endogenous metabolite (Q_X) can be determined by infusing a heavy isotope-labelled tracer at a rate of I_X. The presence of the heavy isotope tracer is assumed not to affect utilization (rate disappearance from the free plasma pool), which at steady-state will be equal to the rate of appearance. Enrichment of the tracer in the plasma pool (tracer-tracee ratio, or TTR) reflects the ratio of the rate of tracer infusion to the rate of endogenous metabolite appearance. (**B**) A second hypothetical scenario in which the tracer is infused at the same rate (10µmol×kg^{-1}×hr^{-1}) into a system with a five-fold higher rate of appearance of the endogenous metabolite compared to panel A. The measured tracer-tracee ratio (TTR) decreases proportionally to the ratio of tracer infusion to endogenous rate of appearance. (**C**) A third hypothetical scenario in which the assumption of steady-state kinetics has been broken and the rate of disappearance increases compared to panel B, but the rate of appearance remains the same. Removal from the plasma pool does not differentiate between tracer and endogenous metabolite, resulting in no change in the measured TTR.

Calculation of Substrate-Product Flux

In order to calculate the specific rate of conversion from substrate *X* to product *Y*, two tracers must be infused: 1) a labelled substrate *X* tracer with mass *m+a* and 2) a labelled product *Y* tracer with mass *m+b*. In order to perform both infusions simultaneously in the same subject, the *m+a* heavy isotope label must be distinguishable from the *m+b* label after conversion from substrate *X* to product *Y*.

The tracer-tracee ratio $TTR_{Y_{m+a}}$ describes the relative abundance of product *Y* carrying *m+a* label derived from substrate *X* tracer with mass *m+a* and can be described based on the same fundamental assumptions and principle described in *Eq B.2*. In this case, the entry of *m+a* labelled tracer is determined not by direct infusion, but by the rate of observed substrate-to-product flux ($Q_{X\rightarrow Y_{Obs}}$) multiplied by the proportion of substrate that carries the label ($TTR_{X_{m+a}}$). Thus, to calculate $TTR_{Y_{m+a}}$, *Eq B.2* is adapted by describing *I* with the term $TTR_{X_{m+a}} \times Q_{X\rightarrow Y_{Obs}}$ (see FIG B.2 for schematic representation):

$$TTR_{Y\,m+a} = \frac{TTR_{X\,m+a} \times Q_{X\rightarrow Y\,Obs}}{Q_Y} \qquad Eq\ B.5$$

Where $TTR_{Y_{m+a}}$ is the tracer-tracee ratio of product *Y* carrying *m+a* label derived from substrate *X*, $TTR_{X_{m+a}}$ is the tracer-tracee ratio of substrate *X* carrying the *m+a* label, $Q_{X\rightarrow Y_{Obs}}$ is the observed rate of substrate-to-product flux, and Q_Y is the rate of product *Y* appearance, calculated from *Eq B.4* based on $I_{Y_{m+b}}$ and $TTR_{Y_{m+b}}$.

In this calculation, the observed value $Q_{X\rightarrow Y_{Obs}}$ could in fact include a contribution from fully-unlabelled metabolite *X* that may be present in the tracer infusion. To account for this possibility, the observed value $Q_{X\rightarrow Y_{Obs}}$ may be calculated as the real value $Q_{X\rightarrow Y}$ multiplied by a factor of $(Q_x + I_{X_{m+a}} \times E_{IX_{m+0}})/Q_x$. Making this substitution in *Eq B.5* and re-arranging:

$$Q_{X\to Y} = \left(\frac{TTR_{Y_{m+a}}}{TTR_{X_{m+a}}}\right) \times Q_Y \times \left(\frac{Q_X}{Q_X + I_{X_{m+a}} \times E_{IX_{m+0}}}\right) \qquad Eq\ B.6$$

Where $Q_{X\to Y}$ is the real rate of substrate-to-product flux, Q_X is the rate of metabolite *X* appearance, calculated from *Eq B.4*, $I_{X_{m+a}}$ is the rate at which labelled metabolite *X* tracer with mass *m+a* is infused, $E_{IX_{m+0}}$ is the proportional enrichment of fully-unlabelled metabolite *X* tracer in the infusion solution, and all remaining terms are as they appear in *Eq B.5*. For tracers labelled at multiple positions, $E_{IX_{m+0}} \approx 0$; therefore the term $Q_x/(Q_x + I_{X_{m+a}} \times E_{IX_{m+0}}) \approx 1$.

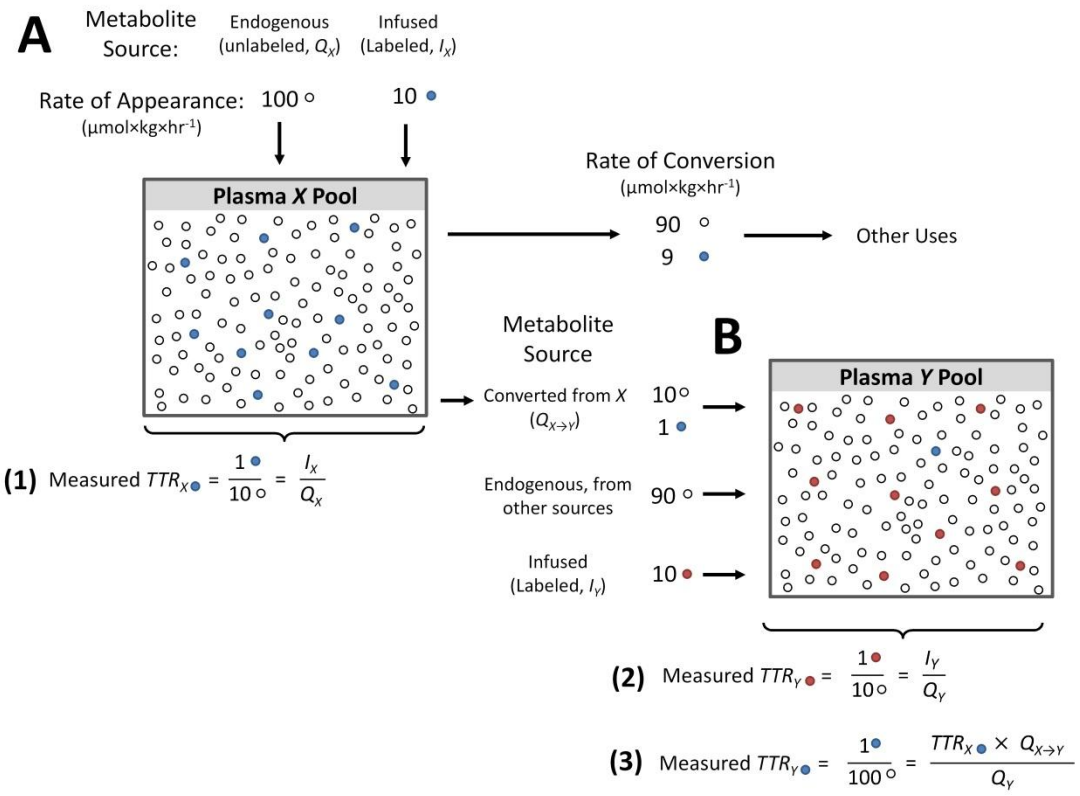


Figure B.2 | Schematic representation of substrate-product conversion. (**A**) Enrichment of the metabolite *X* tracer (blue spot) is dependent on the ratio of metabolite *X* tracer infusion rate (I_X) to the rate of endogenous metabolite *X* appearance (Q_X), as described in equation (1). Metabolite *X* that serves as a substrate for product *Y* synthesis will carry metabolite *X* tracer proportional to the enrichment of tracer in the metabolite *X* pool. (**B**) The total endogenous rate of metabolite *Y* appearance is determined from the enrichment of metabolite *Y* tracer (red spot), as described in equation (2). The enrichment of metabolite *X* tracer (blue spot) appearing in plasma pools is related to the rate of conversion of substrate *X* to product *Y* as described in equation (3).

B.4 Labelling Strategy

To assess real-time urea cycle kinetics, we selected three heavy isotope-labelled tracers: L-[U-$^{13}C_6$;U-$^{15}N_4$]arginine, L-[U-$^{13}C_5$]ornithine and L-[ureido-^{13}C]citrulline. This labelling strategy avoids overlap between the masses of heavy isotope labels of tracers and their associated urea cycle products (TABLE B.1 & FIG B.3). Performance of this tracer strategy for the measurement of nitric oxide synthase is discussed in Section B.6 Calculation of Arginine Metabolism by Nitric Oxide Synthase , p. 281.

Amino Acid	Identity of Monitored Metabolite	Mass shift (*m+x*)	Label	Molecular Formula of $[m+H]^+$ ion	Exact Mass Monitored
Arginine	Unlabelled	m+0	-	$C_6H_{15}N_4O_2$	175.1195
	From citrulline tracer	m+1	^{13}C	$^{13}C_1C_5H_{15}N_4O_2$	176.1229
	Recycled arginine tracer	m+7	$^{13}C_5$, $^{15}N_2$	$^{13}C_5CH_{15}{}^{15}N_2N_2O_2$	182.1303
	Infused arginine tracer	m+10	$^{13}C_6$, $^{15}N_4$	$^{13}C_6H_{15}{}^{15}N_4O_2$	185.1278
Citrulline	Unlabelled	m+0	-	$C_6H_{14}N_3O_3$	176.1035
	Infused citrulline tracer	m+1	^{13}C	$^{13}C_1C_5H_{14}N_3O_3$	177.1069
	From ornithine tracer	m+5	$^{13}C_5$	$^{13}C_5CH_{14}N_3O_3$	181.1203
Ornithine	Unlabelled	m+0	-	$C_5H_{13}N_2O_2$	133.0977
	Infused/recycled ornithine tracer	m+5	$^{13}C_5$	$^{13}C_5H_{13}N_2O_2$	138.1145
	From arginine tracer	m+7	$^{13}C_5$, $^{15}N_2$	$^{13}C_5H_{13}{}^{15}N_2O_2$	140.1085

Table B.1 | List of monitored metabolites. Detailed are mass shift, heavy isotope label, and the molecular formula and exact mass of the $[m+H]^+$ ion monitored by Q-TOF LC/MS.

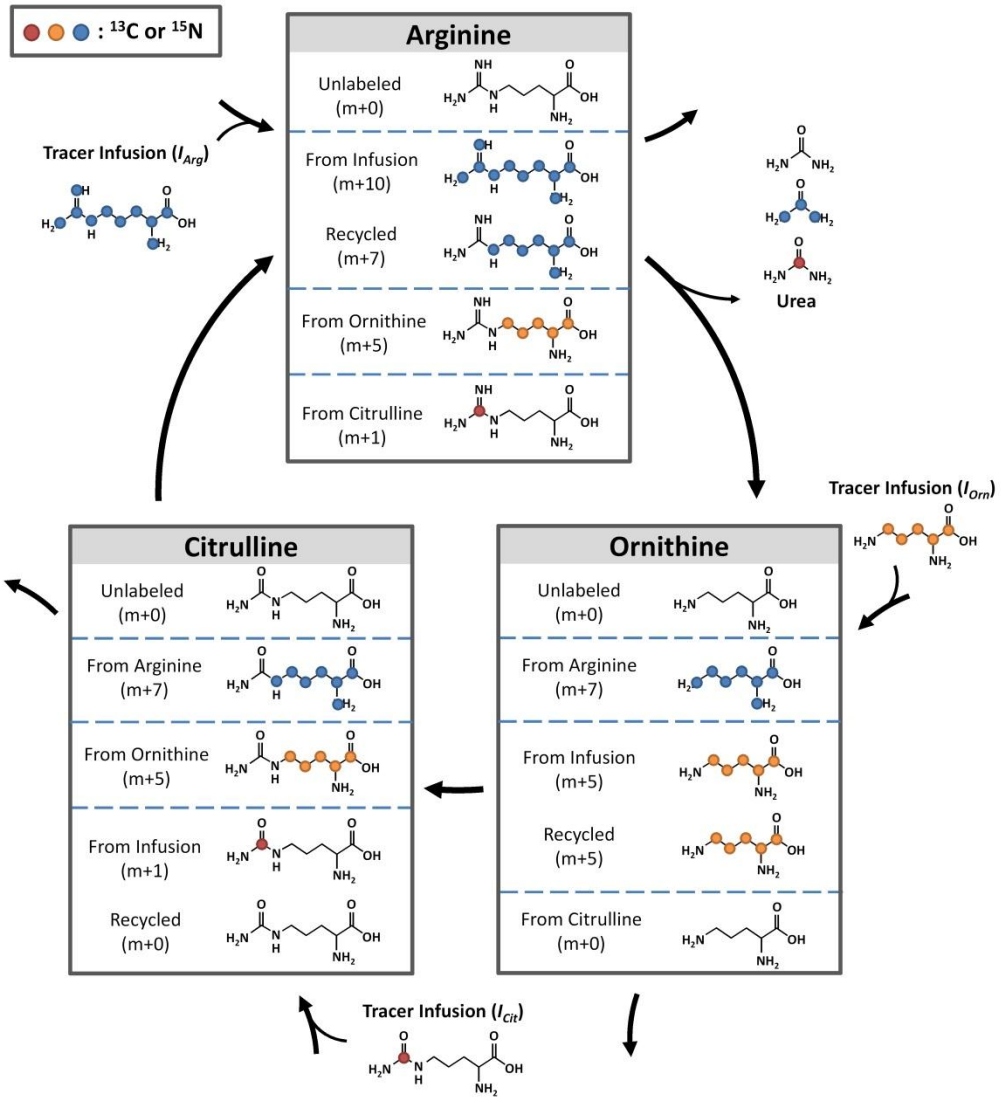


Figure B.3 | Labelling strategy. Infused tracers include L-[U-$^{13}C_6$;U-$^{15}N_4$]arginine (m+10), L-[U-$^{13}C_5$]ornithine (m+5) and L-[ureido-^{13}C]citrulline (m+1). Recycled arginine tracer will appear as L-[1,2,3,4,5-C_5;α,δ-$^{15}N_2$]arginine (m+7) due to loss of one ^{13}C and two ^{15}N atoms during conversion to ornithine. Recycled L-[ureido-^{13}C]citrulline tracer will appear as unlabelled citrulline (m+0) due to loss of the ^{13}C label during the degradation of L-[guanidino-^{13}C]arginine to ornithine. Recycled L-[U-$^{13}C_5$]ornithine tracer cannot be differentiated from freshly-infused ornithine tracer.

B.5 Calculation of Metabolic Kinetics in a Cyclical System

Definitions of Recycled, Non-Recycled and Total Rates of Appearance

For a generic intermediate (metabolite *X*) participating in a metabolic cycle, we defined Q_{X_R} as the rate at which metabolite *X* is recycled and $Q_{X_{NR}}$ as the rate at which metabolite *X* appears from sources other than recycling. $Q_{X_{NR}}$ thus includes direct inputs into metabolite *X* pools from sources outside of the cycle as well as indirect metabolic inputs that first enter the cycle as another intermediate (FIG B.4). We also defined Q_{X_T} to describe the total rate of appearance of metabolite *X* from all sources including recycling:

$$Q_{X_T} = Q_{X_{NR}} + Q_{X_R} \qquad Eq\ B.7$$

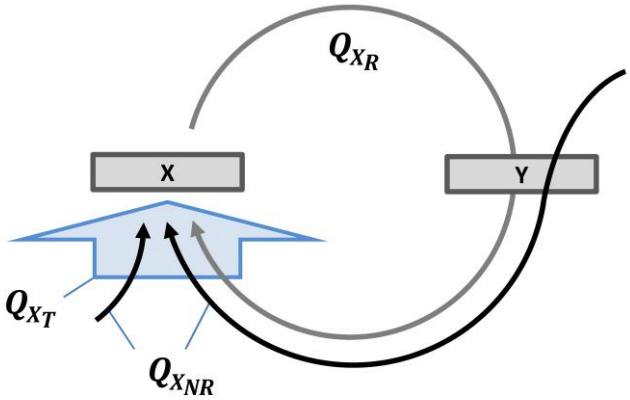


Figure B.4 | Rates of appearance in a cyclical system. Q_{X_T} (filled blue arrow) is the total rate of appearance of metabolite *X*. Q_{X_R} (grey arrow) is the rate at which metabolite *X* is recycled by a cyclical metabolic system. $Q_{X_{NR}}$ (black arrows) is the rate of appearance of non-recycled metabolite *X*, including both direct metabolic inputs and indirect inputs that enter the cycle as another intermediate in the system.

Tracer-Specific Calculation of Appearance Rates

Heavy isotope-labelled metabolic tracers may be recycled in one of the following manners: 1) with all labelled positions replaced with naturally-occurring isotopes, 2) with all labelled positions remaining unmodified or 3) with a portion of the labelled positions replaced with naturally-occurring isotopes and the remainder recycled without modification (FIG B.5).

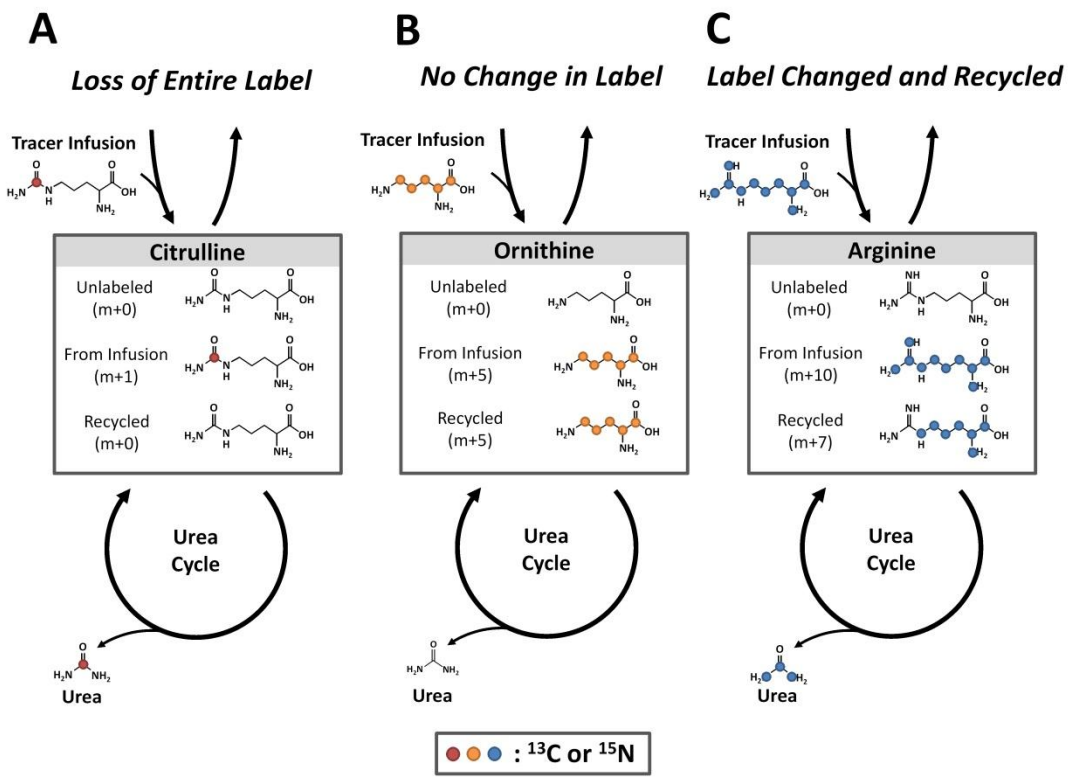


Figure B.5 | Fates of heavy isotope-labelled urea cycle tracers. (**A**) Infused L-[uriedo-^{13}C]citrulline will be recycled as unlabelled citrulline after the ^{13}C is removed in the form of urea during arginine-to-ornithine conversion. (**B**) The heavy isotope label of infused L-[U-$^{13}C_5$]ornithine is not modified or eliminated during recycling (**C**) L-[U-$^{13}C_6$;U-$^{15}N_5$]arginine contains heavy isotopes in both the guanidino group and the carbon skeleton of arginine. During recycling, the labelled 5-carbon backbone and two labelled nitrogen positions are recycled, but one ^{13}C and two ^{15}N are removed with urea during arginine-to-ornithine conversion.

Turnover of ureido-labelled citrulline tracer

During recycling, the entire heavy isotope label is eliminated from citrulline tracers that carry a ^{13}C or ^{15}N label incorporated into the ureido group (FIG B.5A). During conversion of citrulline to arginine, ^{13}C or ^{15}N labels incorporated into the ureido group are left intact as the ureido group is converted to the guanidino group of arginine. During the degradation of arginine by arginase, however, the guanidino group containing the heavy isotope label is removed with the formation of urea. Any citrulline recycled from the ornithine pool will not carry a heavy isotope label in the ureido group. Because the label is not recycled, the enrichment of ureido-labelled citrulline can be used to calculate the total rate of citrulline appearance by applying *Eq B.4*:

$$Q_{Cit_T} = \frac{I_{Cit_{m+1}} \times E_{ICit_{m+1}}}{TTR_{Cit_{m+1}}} - \left(I_{Cit_{m+1}} \times E_{ICit_{m+0}}\right) \qquad Eq\ B.8$$

Where Q_{Cit_T} is the total rate of citrulline appearance including recycling, $I_{Cit_{m+1}}$ is the rate at which labelled L-[ureido-^{13}C]citrulline is infused, $E_{ICit_{m+1}}$ is the proportional enrichment of fully-labelled L-[ureido-^{13}C]citrulline tracer in the infusion solution, $TTR_{Cit_{m+1}}$ is the tracer-tracee ratio of L-[ureido-^{13}C]citrulline to unlabelled citrulline and $E_{ICit_{m+0}}$ is the proportional enrichment of fully-unlabelled tracer in the infusion solution.

Turnover of labelled ornithine tracer

In contrast, heavy isotope-labelled ornithine tracers will not be modified by recycling. During full-turn urea cycle metabolism, the original carbon, nitrogen and oxygen components of ornithine are preserved. In addition, the original seven hydrogens bound to the carbon skeleton are also retained. As a result, freshly infused tracer cannot be distinguished from tracer that has been recycled (FIG B.5B). The apparent enrichment of ornithine tracer can only therefore be used to calculate the appearance of ornithine from sources other than recycling:

$$Q_{Orn_{NR}} = \frac{I_{Orn_{m+5}} \times E_{IOrn_{m+5}}}{TTR_{Orn_{m+5}}} \qquad Eq\ B.9$$

Where $Q_{Orn_{NR}}$ is the rate of appearance of non-recycled ornithine, $I_{Orn_{m+5}}$ is the rate at which labelled L-[U-$^{13}C_5$]ornithine is infused, $E_{IOrn_{m+5}}$ is the proportional enrichment of fully-labelled L-[U-$^{13}C_5$]ornithine tracer in the infusion solution and $TTR_{Orn_{m+5}}$ is the tracer-tracee ratio of L-[U-$^{13}C_5$]ornithine to unlabelled ornithine. In the heavy isotope-labelled tracer infusion, fully-unlabelled ornithine was undetectable. Therefore, $E_{IOrn_{m+0}} \approx 0$ and the *Eq B.4* term $I_{X_{m+a}} \times E_{IX_{m+0}} \approx 0$.

Turnover of guanidino- and carbon skeleton-labelled arginine tracer

During recycling, the guanidino group of arginine will be removed as urea, but the carbon skeleton will remain unchanged. As a result, L-[U-$^{13}C_6$;U-$^{15}N_4$]arginine (*m+10*) will be recycled as L-[1,2,3,4,5-$^{13}C_5$;α,δ-$^{15}N_2$]arginine with mass *m+7* (FIG B.5C). As a result, accumulation of fully-labelled with mass *m+10* is derived entirely from the infusion (as opposed to recycling) and can be used to calculate the total rate of arginine appearance:

$$Q_{Arg_T} = \frac{I_{Arg_{m+10}} \times E_{IArg_{m+10}}}{TTR_{Arg_{m+10}}} \qquad Eq\ B.10$$

Where Q_{Arg_T} is the total rate of arginine appearance including recycling, $I_{Arg_{m+10}}$ is the rate at which labelled L-[U-$^{13}C_6$;U-$^{15}N_4$]arginine is infused, $E_{IArg_{m+10}}$ is the proportional enrichment of fully-labelled L-[U-$^{13}C_6$;U-$^{15}N_4$]arginine tracer in the infusion solution and $TTR_{Arg_{m+10}}$ is the tracer-tracee ratio of L-[U-$^{13}C_6$;U-$^{15}N_4$]arginine to unlabelled arginine. In the heavy isotope-labelled tracer infusion, fully-unlabelled arginine was undetectable; therefore $E_{IArg_{m+0}} \approx 0$ and the *Eq B.4* term $I_{X_{m+a}} \times E_{IX_{m+0}} \approx 0$.

The pooled enrichment of L-[U-$^{13}C_6$;U-$^{15}N_4$]arginine (*m+10*) and L-[1,2,3,4,5-$^{13}C_5$;α,δ-$^{15}N_2$]arginine (*m+7*) is diluted only by the appearance of arginine from sources other than recycling. An increased rate of recycling would result in a greater proportion of arginine (*m+7*) relative to arginine (*m+10*), but would not change the pooled enrichment. Similar to the calculation of non-recycled ornithine appearance in *Eq B.9*, the pooled enrichment of L-[U-$^{13}C_6$;U-$^{15}N_4$]arginine (*m+10*) and L-[1,2,3,4,5-$^{13}C_5$;α,δ-$^{15}N_2$]arginine (*m+7*) can therefore be used to calculate the appearance of non-recycled arginine:

$$Q_{Arg_{NR}} = \frac{I_{Arg_{m+10}} \times E_{IArg_{m+10}}}{TTR_{Arg_{m+10}} + TTR_{Arg_{m+7}}} \qquad Eq\ B.11$$

Where $Q_{Arg_{NR}}$ is rate of appearance of non-recycled arginine, $TTR_{Arg_{m+7}}$ is the tracer-tracee ratio of L-[1,2,3,4,5-$^{13}C_5$;α,δ-$^{15}N_2$]arginine to unlabelled arginine and remaining terms are as they appear in *Eq B.10*.

Calculation of Urea Cycle Recycling

Arginine Recycling

The presence of guanidino and carbon skeleton labels allows calculation of both the total rate of arginine appearance and the rate of appearance of non-recycled arginine (*Eq B.10* and *Eq B.11*). The rate of arginine recycling can be calculated by rearranging *Eq B.7* and substituting *Eq B.10* and *Eq B.11*:

$$Q_{Arg_R} = Q_{Arg_T} - Q_{Arg_{NR}} \qquad \textit{Eq B.12}$$

$$Q_{Arg_R} = \left(\frac{I_{Arg_{m+10}} \times E_{IArg_{m+10}}}{TTR_{Arg_{m+10}}}\right) - \left(\frac{I_{Arg_{m+10}} \times E_{IArg_{m+10}}}{TTR_{Arg_{m+10}} + TTR_{Arg_{m+7}}}\right) \qquad \textit{Eq B.13}$$

Where Q_{Arg_R} is the rate of arginine recycling, Q_{Arg_T} is total rate of arginine appearnce, $Q_{Arg_{NR}}$ is the rate of appearance of non-recycled arginine, $I_{Arg_{m+10}}$ is the rate at which labelled L-[U-$^{13}C_6$;U-$^{15}N_4$]arginine is infused, $E_{IArg_{m+10}}$ is the proportional enrichment of fully-labelled L-[U-$^{13}C_6$;U-$^{15}N_4$]arginine tracer in the infusion solution and $TTR_{Arg_{m+10}}$ is the tracer-tracee ratio of L-[U-$^{13}C_6$;U-$^{15}N_4$]arginine to unlabelled arginine and $TTR_{Arg_{m+7}}$ is the tracer-tracee ratio of L-[1,2,3,4,5-$^{13}C_5$;α,δ-$^{15}N_2$]arginine to unlabelled arginine.

Metabolism of labelled L-[U-$^{13}C_6$;U-$^{15}N_4$]arginine by nitric oxide synthase is discussed in Section B.6 Calculation of Arginine Metabolism by Nitric Oxide Synthase , p. 281.

Relationship between Recycling of Intermediates in the Urea Cycle

The rate of arginine recycling may be determined as the difference between the rate of turnover of the guanidino group and the rate of turnover of the carbon skeleton (*Eq B.13*). However, this approach cannot be used to determine the rate of recycling of ornithine or ureido-labelled citrulline tracers, which are either unaffected by recycling (all ornithine tracers) or indistinguishable from endogenous metabolite following recycling (ureido-labelled citrulline tracer). In order to determine the mathematical relationship between the rates of recycling of two intermediates in the same cyclical metabolic pathway, we first considered a simple hypothetical cycle consisting of two intermediates, metabolite *X* and metabolite *Y* (FIG B.6).

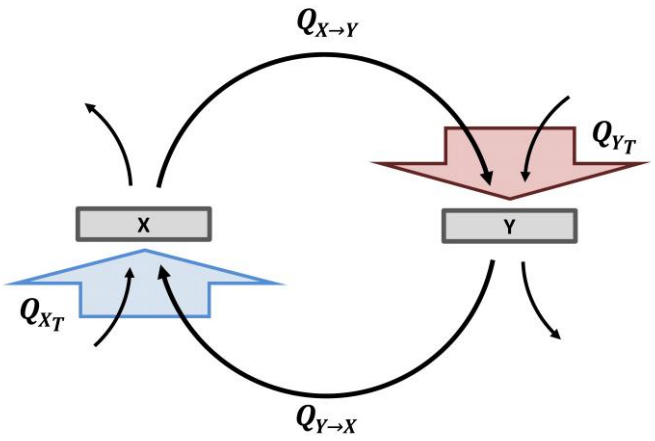


Figure B.6 | Hypothetical two-intermediate model of cyclical metabolism. Q_{X_T} is the total rate of appearance of metabolite *X* (blue arrow). Q_{Y_T} is the total rate of appearance of metabolite *Y* (red arrow). Metabolite *X* is converted *Y* at a rate of $Q_{X\to Y}$ and metabolite *Y* is converted to metabolite *X* at a rate of $Q_{Y\to X}$.

Considering this hypothetical system, Q_{X_R} is the rate at which metabolite *X* is converted to *Y* and recycled back to *X*. Therefore, Q_{X_R} can be calculated as a proportion of the rate of conversion of *Y* to *X* ($Q_{Y\rightarrow X}$) corresponding to proportion of *Y* originally derived from *X*:

$$Q_{X_R} = \left(\frac{Q_{X\rightarrow Y}}{Q_{Y_T}}\right) \times Q_{Y\rightarrow X} \qquad \textit{Eq B.14}$$

Where Q_{X_R} is the rate of metabolite *X* recycling, $Q_{X\rightarrow Y}$ is the rate at which metabolite *X* is converted to metabolite *Y*, Q_{Y_T} is the total rate of metabolite *Y* appearance, and $Q_{Y\rightarrow X}$ is the rate at which metabolite *Y* is converted to metabolite *X*.

The same calculation may be performed to determine the rate of metabolite *Y* recycling:

$$Q_{Y_R} = \left(\frac{Q_{Y\rightarrow X}}{Q_{X_T}}\right) \times Q_{X\rightarrow Y} \qquad \textit{Eq B.15}$$

Where Q_{Y_R} is the rate of metabolite *Y* recycling, Q_{X_T} is the total rate of metabolite *X* appearance, and remaining terms are as they appear in *Eq B.14*.

Eq B.14 and *Eq B.15* may be solved for the term $Q_{X\rightarrow Y} \times Q_{Y\rightarrow X}$ and combined by the transitive property:

$$Q_{X_R} \times Q_{Y_T} = Q_{Y_R} \times Q_{X_T} \qquad \textit{Eq B.16}$$

$$\therefore \frac{Q_{X_R}}{Q_{X_T}} = \frac{Q_{Y_R}}{Q_{Y_T}} \qquad \textit{Eq B.17}$$

Where Q_{X_R} is the rate of metabolite *X* recycling, Q_{X_T} is the total rate of metabolite *X* appearance, Q_{Y_R} is the rate of metabolite *Y* recycling and Q_{Y_T} is the total rate of metabolite *Y* appearance.

The outcome of the above derivation is the same whether the conversion of metabolite *X* to metabolite *Y* occurs in a single step or via a third metabolite *Z*. Furthermore, the same derivation could be applied to compare the rate of recycling of metabolite *X* and metabolite *Z* where metabolite *Y* is an intermediate in the conversion of *X* to *Z* or of *Z* to *X*. Therefore:

$$\frac{Q_{X_R}}{Q_{X_T}} = \frac{Q_{Y_R}}{Q_{Y_T}} = \frac{Q_{Z_R}}{Q_{Z_T}} \qquad \textit{Eq B.18}$$

Where Q_{Z_R} is the rate of metabolite *Z* recycling, Q_{Z_T} is the total rate of metabolite *Z* appearance and remaining terms are as they appear in *Eq B.17*.

Applying *Eq B.18* to the urea cycle :

$$\frac{Q_{Arg_R}}{Q_{Arg_T}} = \frac{Q_{Cit_R}}{Q_{Cit_T}} = \frac{Q_{Orn_R}}{Q_{Orn_T}} \qquad \textit{Eq B.19}$$

Where Q_{Arg_R} is the rate of arginine recycling, Q_{Arg_T} is the total rate of arginine appearance, Q_{Cit_R} is the rate of citrulline recycling, Q_{Cit_T} is the total rate of citrulline appearance, Q_{Orn_R} is the rate of ornithine recycling and Q_{Orn_T} is the total rate of ornithine appearance.

Citrulline Recycling

Eq B.19 can be re-arranged to calculate the rate of citrulline recycling from experimentally-determined rates of arginine recycling, total arginine appearance and total citrulline appearance:

$$Q_{Cit_R} = \left(\frac{Q_{Arg_R}}{Q_{Arg_T}}\right) \times Q_{Cit_T} \qquad \textit{Eq B.20}$$

Substituting for Q_{Cit_T} according to *Eq B.8*:

$$Q_{Cit_R} = \left(\frac{Q_{Arg_R}}{Q_{Arg_T}}\right) \times \left(\frac{I_{Cit_{m+1}} \times E_{CitTracer_{m+1}}}{TTR_{Cit_{m+1}}} - I_{Cit_{m+1}} \times E_{ICit_{m+0}}\right) \qquad \textit{Eq B.21}$$

Where Q_{Cit_R} is the rate of citrulline recycling, Q_{Arg_R} is the rate of arginine recycling calculated from *Eq B.13*, Q_{Arg_T} is the total rate of arginine appearance including recycling calculated from *Eq B.10*, Q_{Cit_T} is the total rate of citrulline appearance including recycling calculated from *Eq B.8*, $I_{Cit_{m+1}}$ is the rate at which labelled L-[ureido-^{13}C]citrulline is infused, $E_{ICit_{m+1}}$ is the proportional enrichment of fully-labelled L-[ureido-^{13}C]citrulline tracer in the infusion solution $TTR_{Cit_{m+1}}$ is the tracer-tracee ratio of L-[ureido-^{13}C]citrulline to unlabelled citrulline and $E_{ICit_{m+0}}$ is the proportional enrichment of fully-unlabelled citrulline in the infusion solution.

Ornithine Recycling

In order to obtain the rate of ornithine recycling from a known rate of arginine recycling using *Eq B.19*, Q_{Orn_T} the term must be substituted according to *Eq B.7*:

$$\frac{Q_{Arg_R}}{Q_{Arg_T}} = \frac{Q_{Orn_R}}{Q_{Orn_{NR}} + Q_{Orn_R}} \qquad \textit{Eq B.22}$$

Solving for Q_{Orn_R} and substituting $Q_{Arg_{NR}}$ for $Q_{Arg_T} - Q_{Arg_R}$ according to *Eq B.7*:

$$Q_{Orn_R} = \left(\frac{Q_{Arg_R}}{Q_{Arg_{NR}}}\right) \times Q_{Orn_{NR}} \qquad \textit{Eq B.23}$$

Substituting for $Q_{Orn_{NR}}$ according to *Eq B.9*:

$$Q_{Orn_R} = \left(\frac{Q_{Arg_R}}{Q_{Arg_{NR}}}\right) \times \left(\frac{I_{Orn_{m+5}} \times E_{IOrn_{m+5}}}{TTR_{Orn_{m+5}}}\right) \qquad \textit{Eq B.24}$$

Where Q_{Orn_R} is the rate of ornithine recycling, Q_{Arg_R} is the rate of arginine recycling calculated from *Eq B.13*, $Q_{Arg_{NR}}$ is the rate of appearance of non-recycled arginine calculated from *Eq B.11*, $I_{Orn_{m+5}}$ is the rate at which labelled L-[U-$^{13}C_5$]ornithine is infused, $E_{IOrn_{m+5}}$ is the proportional enrichment of fully-labelled L-[U-$^{13}C_5$]ornithine tracer in the infusion solution and $TTR_{Orn_{m+5}}$ is the tracer-tracee ratio of L-[U-$^{13}C_5$]ornithine to unlabelled ornithine.

Total Rate of Ornithine Appearance

Having derived a calculation for the rate of ornithine recycling, the total rate of ornithine appearance can be calculated by substituting *Eq B.9* and *Eq B.24* into *Eq B.7* and simplifying:

$$Q_{Orn_T} = Q_{Orn_{NR}} + Q_{Orn_R} \qquad \textit{Eq B.25}$$

$$Q_{Orn_T} = \frac{I_{Orn_{m+5}} \times E_{IOrn_{m+5}}}{TTR_{Orn_{m+5}}} + \left(\frac{Q_{Arg_R}}{Q_{Arg_{NR}}} \times \frac{I_{Orn_{m+5}} \times E_{IOrn_{m+5}}}{TTR_{Orn_{m+5}}} \right) \qquad \textit{Eq B.26}$$

$$Q_{Orn_T} = \frac{I_{Orn_{m+5}} \times E_{IOrn_{m+5}}}{TTR_{Orn_{m+5}}} \times \left(1 + \frac{Q_{Arg_R}}{Q_{Arg_{NR}}} \right) \qquad \textit{Eq B.27}$$

Where Q_{Orn_T} is the total rate of ornithine appearance including recycling, $I_{Orn_{m+5}}$ is the rate at which labelled L-[U-$^{13}C_5$]ornithine is infused, $E_{IOrn_{m+5}}$ is the proportional enrichment of fully-labelled L-[U-$^{13}C_5$]ornithine tracer in the infusion solution and $TTR_{Orn_{m+5}}$ is the tracer-tracee ratio of L-[U-$^{13}C_5$]ornithine to unlabelled ornithine. Q_{Arg_R} is the rate of arginine recycling calculated from *Eq B.13*, $Q_{Arg_{NR}}$ is the rate of appearance of non-recycled arginine calculated from *Eq B.11*.

Substrate-Product Flux between Urea Cycle Intermediates

Conversion of Citrulline to Arginine

Conversion of L-[ureido-^{13}C]citrulline to L-[guanidino-^{13}C]arginine was used to determine the rate conversion of citrulline to arginine according to *Eq B.6*:

$$Q_{Cit\rightarrow Arg} = \left(\frac{TTR_{Arg_{m+1}}}{TTR_{Cit_{m+1}}}\right) \times Q_{Arg_T} \times \left(\frac{Q_{Cit_T}}{Q_{Cit_T} + I_{Cit_{m+1}} \times E_{ICit_{m+0}}}\right) \qquad \textit{Eq B.28}$$

Where $Q_{Cit\rightarrow Arg}$ is the rate of conversion of citrulline to arginine, $TTR_{Arg_{m+1}}$ is the tracer-tracee ratio of L-[guanidino-^{13}C]arginine (*m+1*) to unlabelled arginine, $TTR_{Cit(m+1)}$ is the tracer-tracee ratio of L-[ureido-^{13}C]citrulline (*m+1*) to unlabelled citrulline, Q_{Arg_T} is the total rate of arginine appearance including recycling calculated according to *Eq B.10*, Q_{Cit_T} is the total rate of citrulline appearance including recycling calculated according to *Eq B.8*, $I_{Cit_{m+1}}$ is the rate at which labelled L-[ureido-^{13}C]citrulline is infused and $E_{ICit_{m+0}}$ is the proportional enrichment of fully-unlabelled tracer in the infusion solution.

Conversion of Arginine to Ornithine

Synthesis of L-[U-$^{13}C_5$;U-$^{15}N_2$]ornithine (*m+7*) from labelled arginine was used to determine the rate of conversion of arginine to citrulline. Both freshly-infused L-[U-$^{13}C_6$;U-$^{15}N_4$]arginine (*m+10*) and recycled L-[1,2,3,4,5-$^{13}C_5$;α,δ-$^{15}N_2$]arginine (*m+7*) serve as substrates for the production of L-[U-$^{13}C_5$;U-$^{15}N_2$]ornithine (*m+7*). Therefore the combined enrichment of m+7 and m+10 was substituted into *Eq B.6*:

$$Q_{Arg\rightarrow Orn} = \left(\frac{TTR_{Orn_{m+7}}}{TTR_{Arg_{m+10}} + TTR_{Arg_{m+7}}}\right) \times Q_{Orn_T} \qquad \textit{Eq B.29}$$

Where $Q_{Arg\rightarrow Orn}$ is the rate of conversion of arginine to ornithine, $TTR_{Orn_{m+7}}$ is the tracer-tracee ratio of L-[U-$^{13}C_5$;U-$^{15}N_2$]ornithine (*m+7*) to unlabelled ornithine, $TTR_{Arg_{m+10}}$ is the tracer-tracee ratio of L-[U-$^{13}C_6$;U-$^{15}N_4$]arginine (*m+10*) to unlabelled arginine, $TTR_{Arg_{m+7}}$ is the tracer-tracee ratio of L-[1,2,3,4,5-$^{13}C_5$;α,δ-$^{15}N_2$]arginine (*m+7*) to unlabelled arginine, and Q_{Orn_T} is the total rate of ornithine appearance including recycling calculated according to *Eq B.27*. In the heavy isotope-labelled tracer infusion, fully-unlabelled arginine was undetectable; therefore $E_{IArg_{m+0}} \approx 0$ and the *Eq B.6* term $Q_x/(Q_x + I_{X_{m+a}} \times E_{IX_{m+0}}) \approx 1$.

Conversion of Ornithine to Citrulline

Conversion of L-[U-$^{13}C_5$]ornithine (*m+5*) to L-[1,2,3,4,5-$^{13}C_5$]citrulline (*m+5*) was used to determine the rate conversion of ornithine to citrulline according to *Eq B.6*:

$$Q_{Orn\rightarrow Cit} = \left(\frac{TTR_{Cit_{m+5}}}{TTR_{Orn_{m+5}}}\right) \times Q_{Cit_T} \qquad \textit{Eq B.30}$$

Where $Q_{Orn\rightarrow Cit}$ is the rate of conversion of ornithine to citrulline, $TTR_{Cit_{m+5}}$ is the tracer-tracee ratio of L-[1,2,3,4,5-$^{13}C_5$]citrulline (*m+5*) to unlabelled citrulline, $TTR_{Orn(m+5)}$ is the tracer-tracee ratio of L-[U-$^{13}C_5$]ornithine (*m+5*) to unlabelled ornithine and Q_{Cit_T} is the total rate of citrulline appearance including recycling calculated according to *Eq B.8*. In the heavy isotope-labelled tracer infusion, fully-unlabelled arginine was undetectable; therefore $E_{IOrn_{m+0}} \approx 0$ and the *Eq B.6* term $Q_x/(Q_x + I_{X_{m+a}} \times E_{IX_{m+0}}) \approx 1$.

B.6 Calculation of Arginine Metabolism by Nitric Oxide Synthase

Metabolism of Arginine Tracer by NOS

To calculate the rate of arginine utilization by nitric oxide synthase, we considered the products that would result from NO production using the arginine tracer as a substrate. We identified L-[U-$^{13}C_6$; U-$^{15}N_3$]citrulline (*m+9*) as the by-product of generating one molar equivalent of nitric oxide from the labelled L-[U-$^{13}C_6$;U-$^{15}N_4$]arginine (*m+10*) substrate (FIG B.7). ASS and ASL exist in complex with NOS (Erez et al., 2011), facilitating recycling of citrulline generated as a by-product of NO synthesis. Such recycling would result in L-[U-$^{13}C_6$; α,δ,guanidino-$^{15}N_3$]arginine (*m+9*), which could also serve as a substrate for NO synthesis, yielding L-[U-$^{13}C_6$;α,δ-$^{15}N_2$]citrulline (*m+8*) as a by-product (FIG B.7). Further recycling would generate L-[U-$^{13}C_6$;α,δ-$^{15}N_2$]arginine (*m+8*). Citrulline synthesized directly from labelled arginine by NOS would be distinguishable from citrulline synthesized from arginine indirectly (via ornithine), which would appear as L-[1,2,3,4,5-$^{13}C_5$;α,δ-$^{15}N_2$]citrulline (*m+7*). Likewise, arginine recycled from NOS would be distinct from L-[1,2,3,4,5-$^{13}C_5$;α,δ-$^{15}N_2$]arginine (*m+7*) generated by recycling via ornithine (FIG B.7). Identities and exact masses monitored by Q-TOF LC/MS are listed in TABLE B.2.

Amino Acid	Identity of Monitored Metabolite	Mass shift (*m+x*)	Label	Molecular Formula of $[m+H]^+$ ion	Exact Mass Monitored
Arginine	Unlabelled	m+0	-	$C_6H_{15}N_4O_2$	175.1195
	Recycled from NOS (1 cycle)	m+8	$^{13}C_6$, $^{15}N_2$	$^{13}C_6H_{15}{}^{15}N_2N_2O_2$	183.13369
	Recycled from NOS (>1 cycle)	m+9	$^{13}C_6$, $^{15}N_3$	$^{13}C_6H_{15}{}^{15}N_3NO_2$	184.13072
	Infused arginine tracer	m+10	$^{13}C_6$, $^{15}N_4$	$^{13}C_6H_{15}{}^{15}N_4O_2$	185.1278
Citrulline	Unlabelled	m+0	-	$C_6H_{14}N_3O_3$	176.1035
	From arginine via NOS (1st cycle)	m+8	$^{13}C_6$, $^{15}N_2$	$^{13}C_6H_{14}{}^{15}N_2NO_3$	184.1177
	From arginine via NOS (>1st cycle)	m+9	$^{13}C_6$, $^{15}N_3$	$^{13}C_6H_{14}{}^{15}N_3O_3$	185.11474

Table B.2 | List of metabolites monitored for calculation of arginine utilization by NOS. Detailed are mass shift, heavy isotope label, and the molecular formula and exact mass of the $[m+H]^+$ ion monitored by Q-TOF LC/MS.

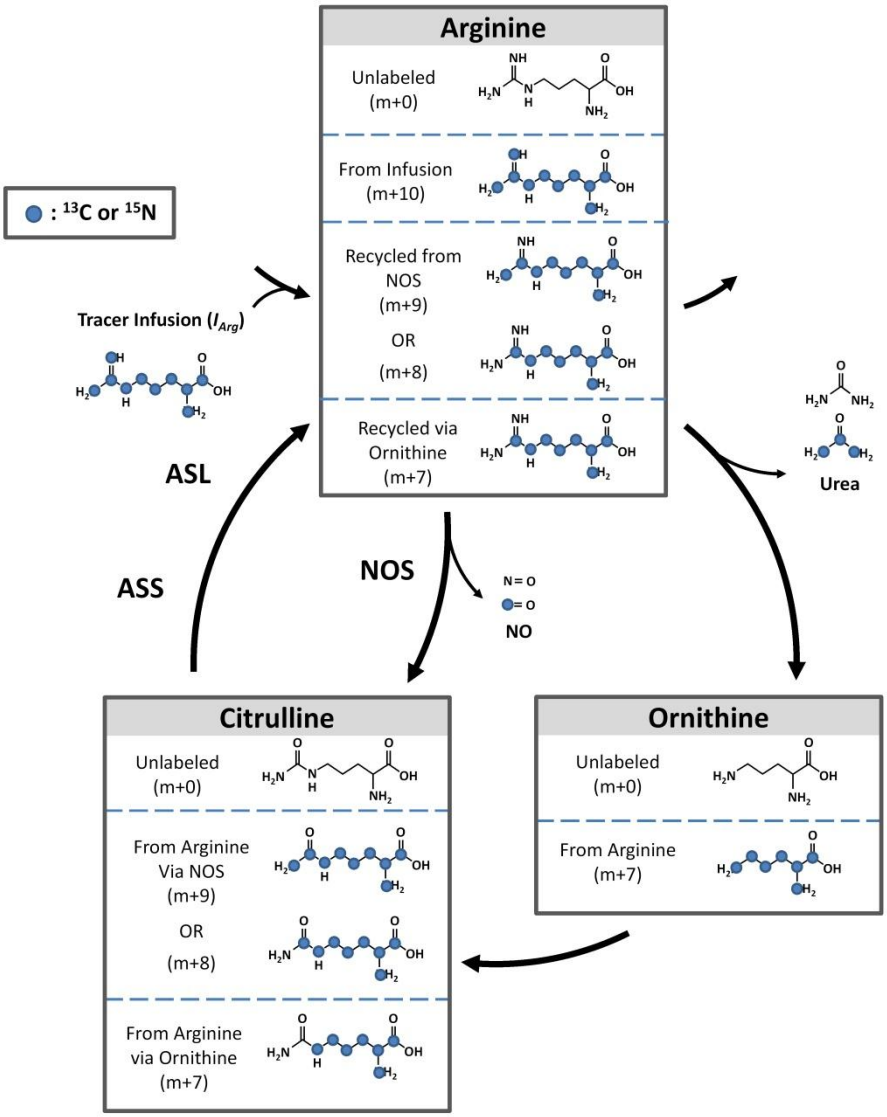


Figure B.7 | Metabolism of arginine tracer by nitric oxide synthase (NOS). Labelled L-[U-$^{13}C_6$;U-$^{15}N_4$]arginine (m+10), was infused. Labelled arginine tracer converted to ornithine will yield L-[1,2,3,4,5-C_5;α,δ-$^{15}N_2$]citrulline (m+7) and L-[1,2,3,4,5-C_5;α,δ-$^{15}N_2$]arginine (m+7). Labelled arginine converted directly to citrulline by nitric oxide synthase (NOS) will appear as L-[U-$^{13}C_6$; U-$^{15}N_3$]citrulline (*m+9*) which may be recycled to arginine pools as L-[U-$^{13}C_6$; α,δ,guanidino-$^{15}N_3$]arginine (*m+9*). Further cycles of NOS utilization would yield L-[U-$^{13}C_6$;α,δ-$^{15}N_2$]citrulline (*m+8*), and L-[U-$^{13}C_6$;α,δ-$^{15}N_2$]arginine (*m+8*).

Quantitation of Conversion of Arginine to Citrulline by NOS

Synthesis of L-[U-$^{13}C_6$; U-$^{15}N_3$]citrulline (*m+9*) and L-[U-$^{13}C_6$;α,δ-$^{15}N_2$]citrulline (*m+8*) from labelled arginine was used to determine the rate of conversion of arginine to citrulline by NOS. These products can arise from freshly-infused L-[U-$^{13}C_6$;U-$^{15}N_4$]arginine (*m+10*) or labelled arginine used for one (L-[U-$^{13}C_6$; α,δ,guanidino-$^{15}N_3$]arginine, *m+9*) or multiple (L-[U-$^{13}C_6$; α,δ-$^{15}N_2$]arginine, *m+8*) cycles of utilization by NOS followed by recycling to arginine pools. Therefore the combined enrichments of citrulline with *m+8* and *m+9* labels were considered as products and the combined enrichments of arginine with *m+8*, *m+9* and *m+10* labels were considered as substrates for substitution into *Eq B.6*:

$$Q_{Arg\rightarrow Cit_{NOS}} = \left(\frac{TTR_{Cit_{m+9}} + TTR_{Cit_{m+8}}}{TTR_{Arg_{m+10}} + TTR_{Arg_{m+9}} + TTR_{Arg_{m+8}}}\right) \times Q_{Cit_T} \qquad Eq\ B.31$$

Where $Q_{Arg\rightarrow Orn_{NOS}}$ is the rate of conversion of arginine to citrulline by nitric oxide synthase, $TTR_{Cit_{m+9}}$ is the tracer-tracee ratio of L-[U-$^{13}C_6$; U-$^{15}N_3$]citrulline (*m+9*) to unlabelled citrulline, $TTR_{Cit_{m+8}}$ is the tracer-tracee ratio of L-[U-$^{13}C_6$;α,δ-$^{15}N_2$]citrulline (*m+8*) to unlabelled citrulline, $TTR_{Arg_{m+10}}$ is the tracer-tracee ratio of L-[U-$^{13}C_6$;U-$^{15}N_4$]arginine (*m+10*) to unlabelled arginine, $TTR_{Arg_{m+9}}$ is the tracer-tracee ratio of L-[U-$^{13}C_6$; α,δ,guanidino-$^{15}N_3$]arginine (*m+9*) to unlabelled arginine, $TTR_{Arg_{m+8}}$ is the tracer-tracee ratio of L-[U-$^{13}C_6$; α,δ-$^{15}N_2$]arginine (*m+8*) to unlabelled arginine and Q_{Cit_T} is the total rate of citrulline appearance calculated according to *Eq B.8*. In our experiments, the abundance of L-[U-$^{13}C_6$;α,δ-$^{15}N_2$]arginine (*m+8*) was indistinguishable from background noise, resulting in a $TTR_{Arg_{m+8}}$ value of 0. In the heavy isotope-labelled tracer infusion, fully-unlabelled arginine was undetectable; therefore $E_{IArg_{m+0}} \approx 0$ and the *Eq B.6* term $Q_x/(Q_x + I_{X_{m+a}} \times E_{IX_{m+0}}) \approx 1$.

B.7 Summary of Key Equations

Single metabolite kinetics

Arginine

$$Q_{Arg_T} = \frac{I_{Arg_{m+10}} \times E_{IArg_{m+10}}}{TTR_{Arg_{m+10}}}$$ *Eq B.10, p. 271*

$$Q_{Arg_{NR}} = \frac{I_{Arg_{m+10}} \times E_{IArg_{m+10}}}{TTR_{Arg_{m+10}} + TTR_{Arg_{m+7}}}$$ *Eq B.11, p. 271*

$$Q_{Arg_R} = \left(\frac{I_{Arg_{m+10}} \times E_{IArg_{m+10}}}{TTR_{Arg_{m+10}}}\right) - \left(\frac{I_{Arg_{m+10}} \times E_{IArg_{m+10}}}{TTR_{Arg_{m+10}} + TTR_{Arg_{m+7}}}\right)$$ *Eq B.13, p. 272*

Ornithine

$$Q_{Orn_T} = \frac{I_{Orn_{m+5}} \times E_{IOrn_{m+5}}}{TTR_{Orn_{m+5}}} \times \left(1 + \frac{Q_{Arg_R}}{Q_{Arg_{NR}}}\right)$$ *Eq B.27,* p. 278

$$Q_{Orn_{NR}} = \frac{I_{Orn_{m+5}} \times E_{IOrn_{m+5}}}{TTR_{Orn_{m+5}}}$$ *Eq B.9, p. 270*

$$Q_{Orn_R} = \left(\frac{Q_{Arg_R}}{Q_{Arg_{NR}}}\right) \times \left(\frac{I_{Orn_{m+5}} \times E_{IOrn_{m+5}}}{TTR_{Orn_{m+5}}}\right)$$ *Eq B.24, 277*

***Citrulline*[2]**

$$Q_{Cit_T} = \frac{I_{Cit_{m+1}} \times E_{ICit_{m+1}}}{TTR_{Cit_{m+1}}} - \left(I_{Cit_{m+1}} \times E_{ICit_{m+0}}\right) \qquad \textit{Eq B.8, 269}$$

$$Q_{Cit_R} = \left(\frac{Q_{Arg_R}}{Q_{Arg_T}}\right) \times \left(\frac{I_{Cit_{m+1}} \times E_{CitTracer_{m+1}}}{TTR_{Cit_{m+1}}} - I_{Cit_{m+1}} \times E_{ICit_{m+0}}\right) \qquad \textit{Eq B.21, 276}$$

Substrate-Product Flux

Conversion of Citrulline to Arginine

$$Q_{Cit \rightarrow Arg} = \left(\frac{TTR_{Arg_{m+1}}}{TTR_{Cit_{m+1}}}\right) \times Q_{Arg_T} \times \left(\frac{Q_{Cit_T}}{Q_{Cit_T} + I_{Cit_{m+1}} \times E_{ICit_{m+0}}}\right) \qquad \textit{Eq B.28, 279}$$

Conversion of Arginine to Ornithine

$$Q_{Arg \rightarrow Orn} = \left(\frac{TTR_{Orn_{m+7}}}{TTR_{Arg_{m+10}} + TTR_{Arg_{m+7}}}\right) \times Q_{Orn_T} \qquad \textit{Eq B.29, 279}$$

Conversion of Ornithine to Citrulline

$$Q_{Orn \rightarrow Cit} = \left(\frac{TTR_{Cit_{m+5}}}{TTR_{Orn_{m+5}}}\right) \times Q_{Cit_T} \qquad \textit{Eq B.30, 280}$$

Conversion of Arginine to Citrulline by NOS

$$Q_{Arg \rightarrow Cit_{NOS}} = \left(\frac{TTR_{Cit_{m+9}} + TTR_{Cit_{m+8}}}{TTR_{Arg_{m+10}} + TTR_{Arg_{m+9}} + TTR_{Arg_{m+8}}}\right) \times Q_{Cit_T} \qquad \textit{Eq B.31, 283}$$

[2] Non-recycled citrulline flux ($Q_{Cit_{NR}}$) was not required, but can be derived by substituting *Eq B.8* and *Eq B.21* into *Eq B.7*

B.8 Conclusion

In a linear metabolic pathway such as the conversion of phenylalanine to tyrosine, recycling of labelled product back to substrate pools is negligible. As a result, observed enrichment of a heavy isotope-labelled substrate may be assumed to arise directly from infusion of labelled tracer (Clarke and Bier, 1982; Thompson et al., 1989). If similar assumptions of linear metabolism are applied to a cyclical metabolic pathway such as the urea cycle, heavy isotope tracer that is fully recycled will be considered equivalent to tracer that experiences no metabolic transitions and remains static in the free substrate pool. Therefore, underlying assumptions of linear metabolism cannot be applied to the quantification of flux between specific urea cycle intermediates if the relevant tracers may be fully recycled without elimination or modification of the heavy isotope label.

The quantitative relevance of this phenomenon was demonstrated in a study of human patients infused with either L-[5,5-$^{2}H_2$]citrulline or L-[ureido-^{13}C]citrulline (Castillo et al., 1993). The authors found that rate of citrulline appearance was significantly lower ($p < 0.05$) when calculated based on enrichment of L-[5,5-$^{2}H_2$]citrulline as compared with the same calculation based on enrichment of L-[ureido-^{13}C]citrulline (Castillo et al., 1993). This discrepancy arises because the L-[ureido-^{13}C]citrulline tracer is diluted by appearance of endogenous citrulline from any source, whereas the L-[5,5-$^{2}H_2$]citrulline tracer is only diluted by the appearance of non-recycled citrulline (any recycled citrulline will also contain tracer and provides no dilution effect). The difference between these two measured rates of appearance will be equivalent to the rate of full-turn citrulline recycling. These findings thus illustrate that linear assumptions cannot be effectively applied to the kinetic analysis of non-ureido-labelled citrulline tracers. Similar limitations would apply to the use of non-guanidino-labelled arginine tracers such as L-[1,2-$^{13}C_2$]arginine.

Tracers that violate the assumptions of linear metabolic models may still be used if the rate of recycling can be calculated for at least one metabolite. The rate of recycling can only be determined by observation of a metabolic tracer that may be recycled with a detectable heavy

isotope label that is distinguishable from the original label. This concept has been previously developed in a study of methionine metabolism (Storch et al., 1988). In this study, the authors determined that the rate of methionine remethylation could be calculated as the difference between the rate of elimination of the methionine carbon skeleton (carrying a ^{13}C label) and the rate of elimination of the methyl group (carrying a $^{2}H_3$ label) (Storch et al., 1988). To our knowledge, this computational approach has not previously been applied to L-arginine recycling by the urea cycle, where the rate of arginine recycling may be conceptualized as the difference between the rate of elimination of the guanidino group and the rate of elimination of the arginine carbon skeleton. In summary, our analytical approach provides a novel means to quantify the contribution of recycling to urea cycle metabolism, which cannot be accomplished with existing mathematical methodologies.

APPENDIX C.

HPLC Determination of ADMA

Nitric oxide synthesis by NOS is dependent on the relative availability of arginine, the NOS substrate, and asymmetric dimethylarginine (ADMA), an endogenous NOS inhibitor. A high performance liquid chromatography (HPLC) assay was developed to measure arginine ADMA and related methylarginine compounds in a single analytical run. This assay provides unique advantages of small sample volume requirements, excellent separation of target metabolites from potential contaminants and validation for both human and mouse plasma samples.

C.1 Introduction

Protein-incorporated arginine residues may be methylated post-translationally by protein arginine methyltransferases (PRMTs) (Kakimoto and Akazawa, 1970; Lee et al., 1977). Subsequent hydrolytic break-down of methylated proteins results in the release of three methylarginine derivatives: N^G,N^G-dimethyl-L-arginine (asymmetric dimethylarginine, ADMA), N^G-monomethyl-L-arginine (L-NMMA) and N^G,$N^{G'}$-dimethyl-L-arginine (symmetric dimethylarginine, SDMA). ADMA is metabolized to dimethylamine and citrulline by dimethylarginine dimethylaminohydrolase (DDAH) (Achan et al., 2003) or cleared by renal excretion (Vallance et al., 1992). L-NMMA and SDMA are also excreted by the kidney, but are not degraded by DDAH (Vallance et al., 1992).

Nitric oxide (NO) production by nitric oxide synthase (NOS) requires L-arginine as a substrate and is inhibited by ADMA and L-NMMA (Cardounel et al., 2007). SDMA does not inhibit NO synthesis, but all three methylarginine derivatives inhibit cellular uptake of arginine, which could limit NOS substrate availability (Closs et al., 1997). In humans, ADMA infusion decreases forearm blood flow, decreases plasma cGMP, increases mean arterial blood pressure and increases systemic vascular resistance (Vallance et al., 1992; Achan et al., 2003; Kielstein et al., 2004). Plasma ADMA is inversely correlated with endothelial function in

hypercholesterolaemia (Böger et al., 1998) and hypertension (Perticone et al., 2005). Elevated plasma ADMA increases risk of complications and death in sickle-cell disease (Kato et al., 2009), coronary artery disease (Schnabel et al., 2005), stroke (Worthmann et al., 2011) and end-stage renal disease (Zoccali et al., 2001). To support further investigation of methylarginine accumulation in severe malaria, we developed a high performance liquid chromatography (HPLC) assay to quantify arginine, ADMA, L-NMMA and SDMA in a single analytical run.

While several validated HPLC methods have been published (Heresztyn et al., 2004; Zhang and Kaye, 2004; Marra et al., 2003; Blackwell et al., 2009; Teerlink et al., 2002; Jones et al., 2010), we have addressed five key analytical goals that have not previously been met in a single assay. First, existing assays typically require 100-200µl of plasma sample for extraction and analysis, a prohibitive requirement for studies utilizing archived plasma samples, mouse models of disease or other limitations on sample volume. Second, we have achieved chromatographic separation of highly abundant interfering amino acids from target metabolites. This measure aims to improve assay reliability if solid phase extraction fails to completely remove highly abundant contaminants. Third, we have validated our method for analysis of mouse as well as human plasma, expanding the application of this assay to basic animal model research in addition to clinical studies. Fourth, we utilized the non-endogenous compound monoethyl-L-arginine (MEA) as an internal standard following a previously published approach (Blackwell et al., 2009). Fifth, we have utilized automated derivatization and validated reproducibility of results over a 24-hour period, allowing a daily workflow cycle to support continuous throughput of sample analysis.

C.2 Materials and Methods

Instrumentation

All HPLC instrument modules were manufactured by Agilent Technologies (Santa Clara, CA, USA). The instrument consisted of a G1379A microdegasser, a G1376A capillary flow binary pump with a zero-volume union used to bypass the micro-flow meter, a G1377 low-

flow, high-precision autosampler with a G1330B sample plate temperature-control unit, a G1316A column temperature-control unit and a G1321B fluorescence detector with a 4µl flow cell. Agilent Chemstation OpenLab CDS revision C.01.03 was used to control the instrument and acquire data. Analytes were separated on a 1.0mm×100mm Luna® C18(2) column with 3µm particles and 100Å pore size (Phenomenex, Torrance, CA, USA). A 1.0mm×13mm ACE® C18 guard column with 3µm particles and 100Å pore size (MAC-MOD Analytical, Chadds Ford, PA, USA) was installed to protect the primary column.

Reagents

Ultrapure water (18.2MΩ•cm resistivity at 25°C) was obtained from a Milli-Q Synthesis system (EMD Millipore, Billerica, MA, USA). HPLC-grade acetonitrile and methanol were obtained from Fisher Scientific (Pittsburgh, PA, USA). For solid phase extraction, 0.1N HCl was prepared in ultrapure water from 37% HCl (Sigma-Aldrich, St. Louis, MO, USA), and elution buffer was prepared from ultrapure water, HPLC-grade methanol and 28-30% ammonium hydroxide (Sigma-Aldrich, St. Louis, MO, USA) in a ratio of 5:4:1 H_2O:MeOH:NH_4OH. For chromatography, aqueous mobile phase (Solvent A) consisted of 25mM sodium phosphate, pH 6.8 prepared from sodium phosphate dibasic (Acros Organics, Geel, Belgium) and sodium phosphate monobasic (Acros Organics, Geel, Belgium) and 5% v/v HPLC-grade acetonitrile (Fisher Scientific, Pittsburgh, PA, USA) in ultrapure water. Solvent B was 50% ultrapure water and 50% HPLC-grade acetonitrile. The derivatization reagent was prepared from ortho-phthaldialdehyde (Sigma-Aldrich, St. Louis, MO, USA) dissolved in HPLC-grade methanol to a concentration of 50mg/ml (372.8mM), 3-mercaptopropionic acid (Sigma-Aldrich, St. Louis, MO, USA) and 200mM potassium tetraborate, pH 9.4 (Sigma-Aldrich, St. Louis, MO, USA). A five-fold concentrated solution was prepared by adding 50µl of 50mg/ml OPA in methanol and 6µl 3-mercaptopropionic acid to 444µl of 200mM potassium tetraborate. Prior to use in analysis, this five-fold concentrated solution was diluted 1:5 in potassium tetraborate, yielding a working solution of 7.46mM OPA and 27.54mM 3-

mercaptopropionic acid. For make-up of standards of known concentrations, L-arginine was from Sigma-Aldrich (St. Louis, MO, USA), L-NMMA, ADMA and SDMA were from Calbiochem (EMD Millipore, Billerica, MA, USA) and N^G-monoethyl-L-arginine (MEA) was from Enzo Life Sciences (Farmingdale, NY, USA). L-arginine, L-NMMA, ADMA, SDMA and MEA were weighed, dissolved in ultrapure water and stored at -80°C until use.

Solid Phase Extraction

Solid phase extraction (SPE) was performed with a Waters Oasis MCX 96-well µElution Plate, 2 mg sorbent per well, 30 µm particle size (Waters Corporation, Milford, MA, USA). Vacuum was applied with an extraction plate manifold (Waters Corporation, Milford, MA, USA). Wells were conditioned with 250µl elution buffer and equilibrated with 300µl ultrapure water. Plasma samples were thawed, centrifuged at 16,100*g* for 5 min at 4°C and 12µl was added to 42µl of 1X PBS without Mg^{2+} or Ca^{2+} (Lonza, Walkersville, MD, USA) containing 11.43µM MEA (for a final concentration of 40µM after extraction, drying and reconstituting). 45µl was loaded into the SPE well and applied to the sorbent under low vacuum (-50 to -100 mmHg). Each well was subsequently washed with 250µl 0.1N HCl and 300µl methanol. Analytes were then eluted with 250µl elution buffer and dried at 45°C under vacuum for 3.5-4hr. Dried samples were then reconstituted in 10µl ultrapure water and loaded into screw-capped polypropylene sample vials (Agilent Technologies, Santa Clara, CA, USA) for analysis.

Deproteination

For chromatographic investigation, some plasma samples were deproteinated by mixing 1:1 with 2M perchloric acid ($HClO_4$, Fisher Scientific, Pittsburgh, PA, USA), centrifuging for 5 minutes at 16,100*g* to remove protein precipitate and neutralizing with 1.5M potassium carbonate (Sigma-Aldrich, St. Louis, MO, USA).

On-Line Derivatization

The autosampler was programmed to draw 1.7µl of ortho-phthaldialdehyde derivatization solution and 1.7µl of the current sample in the sequence, mix the contents in the needle for 30s and inject the derivatized sample onto the column (see FIG C.1 for derivatization reaction). Before and after each of these steps, the needle was washed for 5 seconds with 10% HPLC-grade methanol diluted in ultrapure water using the built-in autosampler flushport to prevent carry-over contamination.

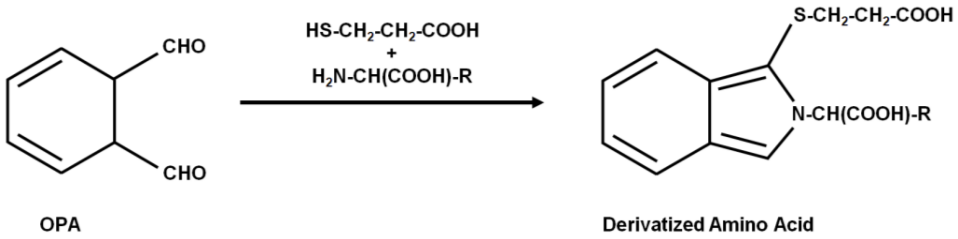


Figure C.1 | Derivatization Reaction. Ortho-phthaldialdehyde (OPA) reacts with mercaptopropionic acid (HS-CH2-CH2-COOH) and the primary amine of an amino acid (H2H-CH(COOH)-R) to form a highly fluorescent product. Unbound OPA is not fluorescent at the analytical excitation and emission wavelengths.

Chromatography and Fluorescence Detection

Chromatographic separation was performed isocratically for 20 minutes followed by a gradient from 0%B at 20 min to 18%B at 42 min. The column was then washed with 100 % solvent B for 5 minutes and re-equilibrated with 0%B for 13 minutes prior to injection of the following sample (TABLE C.1 & FIG C.2). The column was maintained at 35°C for all runs. Online fluorescence was measured at excitation and emission wavelengths of 340nm and 455nm, respectively. The fluorescence detector's photomultiplier tube (PMT) gain was set to 11 for initial normal-sensitivity analysis. At 20min, PMT gain was switched to 16 for the detection of low-concentration analytes (L-NMMA, ADMA, and SDMA). At 37 minutes PMT gain was

switched back to 11 for detection of MEA with normal sensitivity. Chemstation OpenLab CDS software version C.01.03 was used for peak integration.

	Elapsed Time (min)						
	0	20	42	42.1	47	47.1	60
A (%):	100	100	82	0	0	100	100
B (%):	0	0	18	100	100	0	0

Table C.1 | Mobile phase solvent ratios and pump program. The program was performed at a flow-rate of 90µl/min and a column temperature of 35°C. Sample was injected at 0 min.

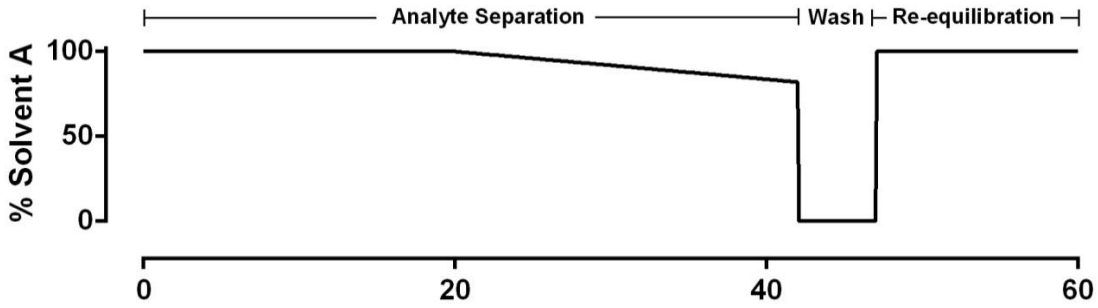


Figure C.2 | Plot of solvent A concentration vs time. Sample was injected at 0 min. Chromatographic separation of analytes was achieved in the first 42 minutes of the program. The column was then washed for 5 minutes with 100% solvent B and re-equilibrated for 13 minutes prior to injection of the next sample.

Quantification of Sample Analytes

Internal and external standards were used for quantification of analytes. A combined standard of 50μM arginine, 0.5μM L-NMMA, 0.5μM ADMA and 0.5μM SDMA was spiked with the internal standard MEA, extracted, dried, reconstituted and analyzed in parallel with each set of samples. Based on the peak areas of this combined standard, a response factor (RF) was calculated for each amino acid in the external standard:

$$\mathrm{RF} = \frac{\text{Analyte Peak Area}_{External\ Std}}{[\text{External Std}]} \qquad \textit{Eq C.1}$$

Where [External Std] is 50μM for arginine and 0.5μM for L-NMMA, ADMA and SDMA.

MEA (40μM) was used as an internal standard. Concentrations of amino acid analytes in the sample were calculated from the external standard response factor and normalized to recovery of MEA:

$$[\text{Analyte}]_{Sample} = \frac{\text{Analyte Peak Area}_{Sample}}{\mathrm{RF}} \times \frac{\text{MEA Peak Area}_{Standard}}{\text{MEA Peak Area}_{Sample}} \qquad \textit{Eq C.2}$$

C.3 Assay Optimization and Validation

Solid Phase Extraction Recovery

ADMA, L-NMMA and SDMA were present in sub-micromolar concentrations in the plasma of healthy individuals. To assess the recovery of our sample preparation protocol, we analyzed standards prepared with or without solid phase extraction. Absolute recoveries for all metabolites (including MEA) ranged from 95.8-103.0% and relative recoveries (normalized to MEA) ranged from 93.9-101.0 (TABLE C.2). These results indicated sufficient recovery to proceed with assay development.

Analyte	Absolute Recovery (%)	Relative Recovery (%)
Arg	98.3 ± 2.8	96.4 ± 2.1
L-NMMA	95.8 ± 2.8	93.9 ± 1.7
ADMA	103.0 ± 2.5	101.0 ± 1.9
SDMA	100.8 ± 3.3	98.8 ± 2.6
MEA	102.0 ± 2.0	100.0

Table C.2 | Absolute and relative recovery of analytes from solid phase extraction. Standards (n=12) containing 50µM arginine, 0.5µM L-NMMA, 0.5µM ADMA, 0.5µM SDMA and 50µM MEA were extracted with mixed-mode cation exchange columns. Absolute recovery values reflect integrated areas expressed as a percentage of standards analyzed without solid phase extraction (mean ±SD). Relative recovery values were normalized to the internal standard MEA.

Peak Identification

Peak identities and retention times were determined by separate analysis of individual arginine, L-NMMA, homoarginine, ADMA, SDMA and MEA standards (FIG C.3).

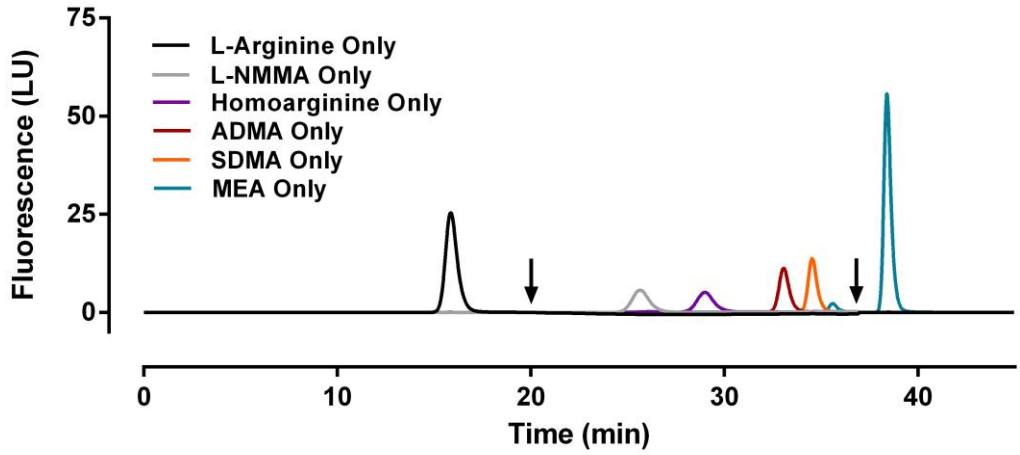


Figure C.3 | Identification of analyte retention times. Arginine (50µM), L-NMMA (0.5µM), homoarginine (0.5µM), ADMA (0.5µM), SDMA (0.5µM) and MEA (50µM) were analyzed individually to determine retention times. Arrows at 20 minutes and 37 minutes indicate switch to increased sensitivity (PMT gain 16) and back to normal sensitivity (PMT gain 11), respectively.

Chromatography

Chromatographic conditions were designed to achieve baseline separation of arginine, L-NMMA, ADMA, SDMA and MEA (internal standard) in both human and mouse plasma samples (FIG C.4). The homoarginine peak exhibited evidence of minor contamination in the form of irregular and asymmetric peak shape in human and mouse plasma samples (FIG C.4). For this reason, homoarginine was excluded from further consideration in assay validation.

We screened for high-concentration plasma metabolites that contain primary amines which react with the OPA derivatization reagent. Without effective separation, even small amounts of such contaminants inadvertently retained during solid phase extraction could significantly distort quantification of sub-micromolar methylarginine concentrations in human and mouse plasma. To screen for such compounds, we processed human and mouse plasma samples in parallel by 1) solid phase extraction or 2) perchloric acid acidification and potassium carbonate neutralization to deproteinate samples for full amino acid analysis. Using this approach, we identified alanine and taurine as two high-concentration amine-containing compounds present in human and mouse plasma (FIG C.5). The chromatographic conditions of our assay ensure that both alanine and taurine were effectively separated from all target metabolites (FIG C.5).

We also observed that the solid phase extraction (SPE) resin contributed a contaminant of unknown identity whether a standard, plasma or water sample was extracted by SPE (FIG C.6). We optimized the chromatographic conditions to ensure separation of L-NMMA from this unknown SPE contaminant (FIG C.6).

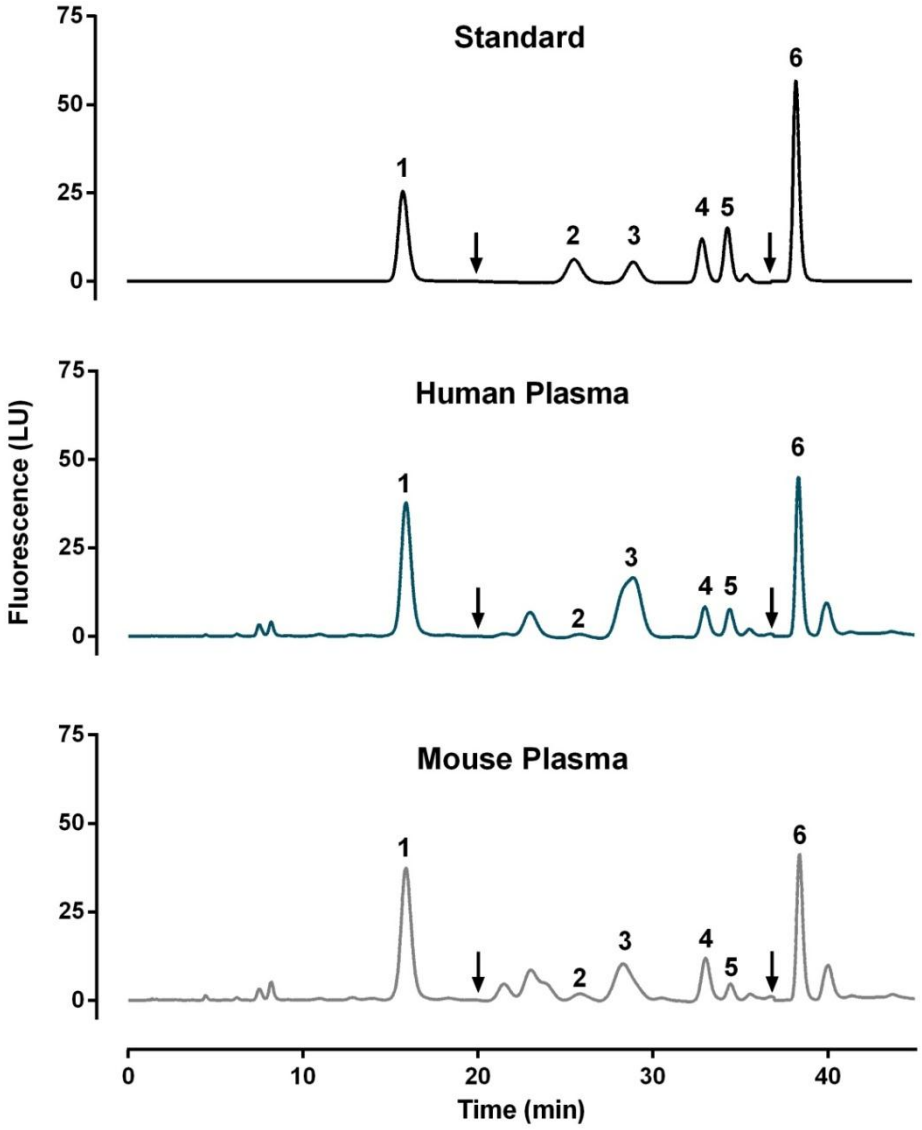


Figure C.4 | Chromatographic resolution of analytes. Peak identities are 1. arginine, 2. L-NMMA, 3. homoarginine, 4. ADMA, 5. SDMA and 6. MEA. Concentrations in the standard (top panel) were 50µM arginine, 0.5µM L-NMMA, 0.5µM homoarginine, 0.5µM ADMA, 0.5µM SDMA, 50µM MEA. Concentrations in human plasma (middle panel) were 89.7µM arginine, 0.09µM L-NMMA, 0.35µM ADMA, 0.28µM SDMA. Concentrations in mouse plasma (bottom panel) were 83.7µM arginine, 0.14µM L-NMMA, 0.51µM ADMA, 0.13µM SDMA. Arrows at 20 minutes and 37 minutes indicate switch to increased sensitivity (PMT gain 16) and back to normal sensitivity (PMT gain 11), respectively.

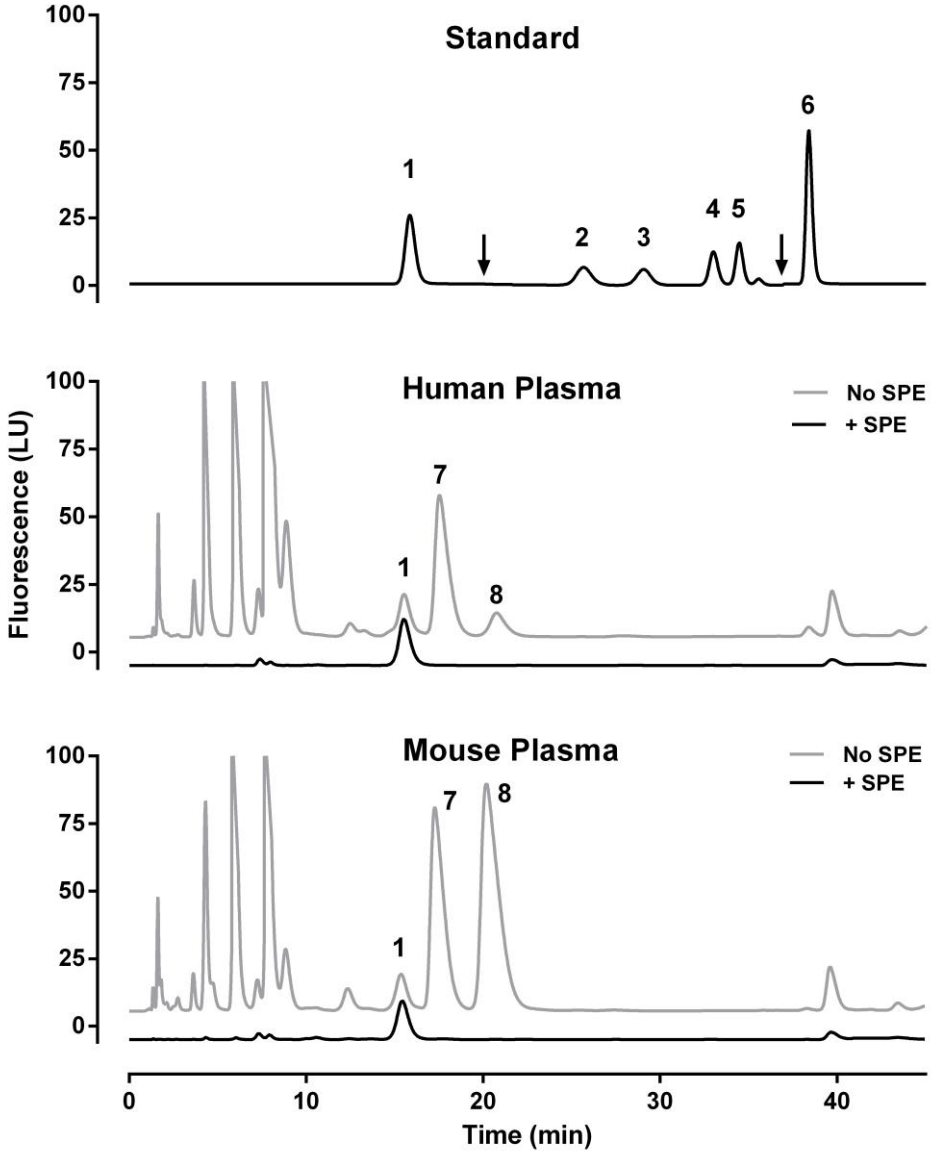


Figure C.5 | Survey of human and mouse plasma for potential contaminants. Human and mouse plasma were processed with protein precipitation (no SPE) or with solid phase extraction using mixed-mode cation exchange columns (+SPE). For these analyses, plasma samples were not spiked with MEA (internal standard) and PMT gain remained constant (11) for the duration of the run. Plasma samples were compared to a combined standard (top panel) to identify potential contaminants that may co-elute with target analytes if not fully eliminated by SPE. Arrows at 20 minutes and 37 minutes indicate switch to increased sensitivity (PMT gain 16) and back to normal sensitivity (PMT gain 11), respectively. Sensitivity was not increased in the bottom 2 panels and traces were artificially shifted up (No SPE) and down (+SPE) to aid visualization. Peak identities are 1. arginine, 2. L-NMMA, 3. homoarginine, 4. ADMA, 5. SDMA, 6. MEA, 7. alanine and 8. taurine.

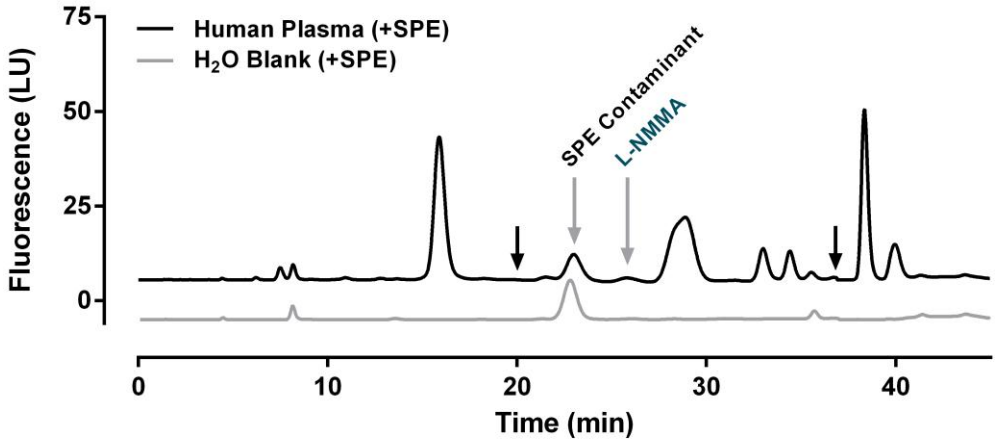


Figure C.6 | Chromatographic separation of contaminant contributed by SPE column. Under the selected chromatographic conditions (isocratic separation with 5% acetonitrile for first 20min), an unknown contaminant contributed by the solid phase extraction column was well-separated from L-NMMA. The H_2O blank was generated by performing solid phase extraction on an aliquot of ultrapure water. Traces are artificially shifted up (human plasma) or down (H_2O blank) to aid visualization.

Standard Curve Linearity

To assess linearity, a combined standard solution containing arginine, L-NMMA, ADMA, SDMA and MEA was serially diluted to yield a nine-point standard curve. At each point, L-NMMA, ADMA and SDMA were 1/100th of the concentration of arginine and MEA, consistent with the difference in order of magnitudes observed in plasma. Standard curves for all analytes were highly linear with R^2 values of greater than 0.9995 for all metabolites (TABLE C.3). Standard curves for analytes measured at high and low sensitivities are illustrated in FIG C.7. With the selected chromatographic and fluorescent detection conditions, arginine was off-scale above 150µM and MEA was off-scale above 100µM. However, MEA was spiked to provide a final concentration of 40µM for routine use as an internal standard and quantification at higher concentrations would not be required.

	Standard Concentration (μM)									
Analyte	**250**	**150**	**100**	**50**	**25**	**10**	**5**	**2.5**	**1**	**R^2**
Arg	-	3275.8	2210.8	1131.9	559.8	217.0	105.3	51.5	19.8	0.9998
MEA	-	-	3266.0	1583.5	795.0	310.2	153.2	75.0	28.8	0.9998

	Standard Concentration (μM)									
Analyte	**2.5**	**1.5**	**1.0**	**0.5**	**0.25**	**0.1**	**0.05**	**0.025**	**0.01**	**R^2**
L-NMMA	2079.0	1291.0	864.4	440.9	219.6	87.8	43.6	22.7	10.4	0.9995
ADMA	2163.3	1341.1	896.0	454.8	226.8	88.4	44.1	21.6	8.6	0.9996
SDMA	2283.0	1417.0	947.4	481.7	239.8	93.7	46.4	22.8	8.9	0.9995

Table C.3 | Linearity of standards assayed over a range of concentrations. Values expressed as mean integrated areas (relative light units × s) averaged from n=3 independent standard curves. Peaks that exceeded the upper threshold of detection (flooded signal) are noted with a dash. Linearity was assessed by calculating the R^2 value of the line of best fit for each analyte standard curve.

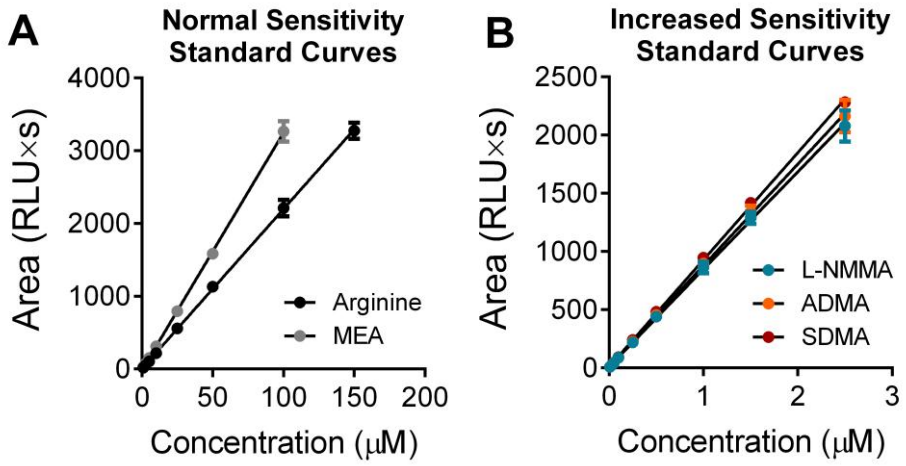


Figure C.7 | Plot of standard curves. 9-point dilutions of a combined external standard was prepared and assayed in triplicate. Combined standards contained arginine, L-NMMA, ADMA, SDMA and MEA (internal standard). The fluorescence detector photomultiplier tube gain was set to 11 for peaks detected at normal sensitivity curves (**A**) and to 16 for peaks detected with increased sensitivity (**B**). In each dilution, arginine and MEA were 100× more concentrated than L-NMMA, ADMA and SDMA.

Limit of Detection

The limit of detection (LOD) describes the lowest concentration that can be distinguished from baseline noise with a degree of confidence, generally set at 95%. The LOD was determined by assaying n=3 independently-prepared water blank samples and n=3 independently-prepared combined standards containing 1.0µM arginine, 0.01µM L-NMMA, 0.01µM ADMA and 0.01µM SDMA (TABLE C.4). The limit of detection was calculated according to the following equation (Armbruster and Pry, 2008):

$$\mathrm{LOD} = \mathrm{Mean}_{Blank} + 1.645 \times \mathrm{SD}_{Blank} + 1.645 \times \mathrm{SD}_{Low\ Standard} \qquad Eq\ C.3$$

Analyte	LOD (µM)
Arginine	0.21
L-NMMA	0.025
ADMA	0.007
SDMA	0.005

Table C.4 | Limit of detection (LOD). Values determined from ultrapure water blank samples (n=3) and low-concentration combined amino acid standards (n=3) diluted to 1µM for arginine and 0.01µM for L-NMMA, ADMA and SDMA.

Intra- and Inter-day Precision

Precision was calculated from 5 parallel analyses of human and mouse plasma samples analyzed on the same (intra-day precision) or different days (inter-day precision). The coefficient of variation (CV) was calculated and expressed as a percent (%CV):

$$\%\mathrm{CV} = \frac{s}{\bar{x}} \times 100\% \qquad \textit{Eq C.4}$$

Where s is the standard deviation and $\bar{x}$ is the mean of repeated measurements.

Intra-day %CV values were <5% for all analytes in both human and mouse plasma (TABLE C.5). Inter-day %CV values were ≤5% for arginine, ADMA and SDMA in human plasma and for arginine and ADMA in mouse plasma (TABLE C.5). Despite standard deviations comparable to ADMA, the inter-day %CV values for SDMA and L-NMMA in mouse plasma were higher (5.7% and 15.8%, respectively) because their mean concentrations were substantially lower than ADMA (0.12 µmol/L for SDMA and 0.15 µmol/L for L-NMMA vs 0.53 µmol/L for ADMA, TABLE C.5). Similarly, the inter-day %CV of L-NMMA was 10.4% in human plasma in association with a mean concentration of 0.17 µmol/L (compared to 0.50 µmol/L for ADMA, TABLE C.5).

Intra-day Precision

Analyte	Human plasma				Mouse plasma			
	Concentration (µmol/L)			%CV	Concentration (µmol/L)			%CV
Arg	90.9	±	1.8	1.9	90.3	±	1.3	1.4
L-NMMA	0.13	±	0.00	2.0	0.16	±	0.01	4.0
ADMA	0.42	±	0.01	2.2	0.53	±	0.01	1.9
SDMA	0.41	±	0.01	2.9	0.12	±	0.00	2.4

Inter-day Precision

Analyte	Human plasma				Mouse plasma			
	Concentration (µmol/L)			%CV	Concentration (µmol/L)			%CV
Arg	98.0	±	4.4	4.5	87.9	±	2.9	3.3
L-NMMA	0.17	±	0.02	10.4	0.15	±	0.02	15.8
ADMA	0.50	±	0.02	3.8	0.53	±	0.02	3.1
SDMA	0.47	±	0.02	5.0	0.12	±	0.01	5.7

Table C.5 | Intra- and inter-day precision. Human mouse and plasma samples were repeatedly analyzed 5 times on the same day (intra-day measurements) on 5 different days (inter-day measurements). Measured concentrations are reported as mean ± SD for repeated analyses and precision was assessed by calculating the coefficient of variation as a percent (%CV).

Stability of Dissolved Analytes

We employed automated derivatization of samples directly prior to injection onto the column. This approach is preferable to manual batch derivatization (Teerlink et al., 2002) because it provides a consistent, fixed time interval between derivatization and analysis. This approach avoids the possibility that different decay rates among batch-derivatized target analytes and internal standards could return inconsistent results in later samples.

We analyzed the stability of dissolved analytes maintained at 4°C in the autosampler over a 24 hour period by comparing repeat analyses of n=3 combined amino acid standards at 0, 12 and 24 hour intervals. At the 24hr time point, measurements of all analytes were >97% of initial (0hr), demonstrating that analytes and OPA derivatization solution are stable at 4°C for 24 hours (TABLE C.6).

Analyte stability (% of Initial at 0hr)

Analyte	12hr			24hr		
Arg	99.83	±	0.66	99.66	±	1.11
L-NMMA	100.08	±	0.72	99.33	±	0.69
ADMA	99.41	±	0.30	98.58	±	0.11
SDMA	99.04	±	0.18	97.89	±	0.49
MEA	100.11	±	0.52	100.05	±	0.72

Table C.6 | Autosampler stability. Values are expressed as mean % of initial at 0hr ±SD. Data were determined from repeat assessments of three independent standards consisting of 50µM arginine, 0.5µM L-NMMA, 0.5µM ADMA, 0.5µM SDMA and 50µM MEA.

Sample Matrix Effects

Sample matrix effects were assessed by spiking known concentrations of standards into human and plasma mouse samples. Recovery was calculated as an absolute concentration and as a percentage of the known concentration of the standard used to spike samples:

$$\%\ Recovery\ = \left(\frac{[Analyte]_{Sample+Spike} - [Analyte]_{Sample\ Alone}}{[Spike]}\right) \times 100\% \qquad Eq\ C.5$$

Recovery values were tabulated for human plasma samples in TABLE C.7 and for mouse plasma samples in TABLE C.8. Across two concentrations of spiked standards, recovery of Arginine was within ±5% for arginine, L-NMMA, ADMA and SDMA in human plasma (TABLE C.7) and for ADMA in mouse plasma (TABLE C.8). Recoveries were within ±10% for arginine, L-NMMA and SDMA in mouse plasma (TABLE C.8).

Human Plasma				
Analyte	Spike Added (µM)	Measured Concentration (µM)	Recovery	
			Concentration (µM)	Percent of initial (%)
Arginine	-	90.0 ± 1.1	-	-
	50.0	141.2 ± 2.5	51.1 ± 2.5	102.3 ± 5.0
	100.0	186.8 ± 3.8	96.8 ± 3.8	96.8 ± 3.8
L-NMMA	-	0.13 ± 0.00		
	0.5	0.62 ± 0.00	0.49 ± 0.00	97.1 ± 0.8
	1.0	1.09 ± 0.02	0.96 ± 0.02	95.7 ± 2.1
ADMA	-	0.43 ± 0.01		
	0.5	0.92 ± 0.01	0.50 ± 0.01	99.4 ± 1.3
	1.0	1.38 ± 0.02	0.95 ± 0.02	95.4 ± 2.3
SDMA	-	0.40 ± 0.01		
	0.5	0.92 ± 0.01	0.52 ± 0.01	104.5 ± 1.4
	1.0	1.41 ± 0.02	1.01 ± 0.02	101.4 ± 2.1

Table C.7 | Recovery of standards spiked into human plasma. Recovery was calculated by quantifying plasma samples with or without addition of amino acid standards at the indicated concentrations. Spikes were performed in three aliquots of the same plasma samples per condition. Recovery was calculated as a percentage of the known concentration of the added standards. All values are mean ± SD.

Mouse Plasma				
Analyte	Spike Added (µM)	Measured Concentration (µM)	Recovery	
			Concentration (µM)	Percent of initial (%)
Arginine	-	87.7 ± 3.0	-	-
	50.0	140.8 ± 3.0	53.1 ± 3.0	106.3 ± 6.0
	100.0	189.0 ± 9.4	101.3 ± 9.4	101.3 ± 9.4
L-NMMA	-	0.16 ± 0.00		
	0.5	0.61 ± 0.08	0.45 ± 0.08	90.7 ± 15.2
	1.0	1.09 ± 0.05	0.93 ± 0.05	93.5 ± 4.7
ADMA	-	0.54 ± 0.01		
	0.5	1.06 ± 0.02	0.51 ± 0.02	102.9 ± 3.2
	1.0	1.56 ± 0.06	1.01 ± 0.06	101.4 ± 6.1
SDMA	-	0.13 ± 0.01		
	0.5	0.68 ± 0.03	0.55 ± 0.03	109.2 ± 5.1
	1.0	1.18 ± 0.07	1.05 ± 0.07	104.6 ± 7.2

Table C.8 | Recovery of standards spiked into mouse plasma. Recovery was calculated by quantifying plasma samples with or without addition of amino acid standards at the indicated concentrations. Spikes were performed in three aliquots of the same plasma samples per condition. Recovery was calculated as a percentage of the known concentration of the added standards. All values are mean ± SD.

C.4 Conclusion

We have described an HPLC method capable of quantifying arginine, ADMA, L-NMMA and SDMA in a single analytical run. ADMA accumulation has been identified as a biomarker and potential mediator of endothelial dysfunction and cardiovascular disease (Zoccali et al., 2001; Schnabel et al., 2005; Kato et al., 2009; Worthmann et al., 2011), leading to the suggestion that routine measurement of ADMA could provide clinically-useful information (Kielstein and Cooke, 2007). However, as a competitive inhibitor, the effect of ADMA accumulation on NOS activity is also determined by relative arginine concentrations (Cardounel et al., 2007). It is therefore necessary to simultaneously quantify arginine and ADMA, which cannot be accomplished by ELISA-based quantification of ADMA. Like ADMA, L-NMMA inhibits NOS and arginine transport (Closs et al., 1997; Cardounel et al., 2007). SDMA does not inhibit NOS, but inhibits cellular arginine uptake (Closs et al., 1997) and serves as a biomarker of renal dysfunction (Kielstein et al., 2006; Bode-Böger et al., 2006). These findings emphasize the importance of simultaneously assessing arginine, ADMA, L-NMMA and SDMA.

ADMA, L-NMMA and SDMA are present in human and mouse plasma in sub-micromolar concentrations. We addressed this challenge by using mixed-mode cation exchange solid phase extraction (SPE) to isolate basic plasma metabolites, including ADMA, L-NMMA, and SDMA. Using this approach, we achieved >95% and >93% absolute and relative recoveries, respectively, indicating near-complete retention and elution of target metabolites during SPE. Previous published methods reported absolute recoveries in the range of 85% using solid phase extraction columns from the same manufacturer and similar loading, washing and elution conditions (Teerlink et al., 2002). We speculate that we were able to achieve improved recoveries primarily by applying low vacuum during sample loading and washing. This approach increases the duration of column saturation by samples and solvents, ensuring that binding and elution reactions proceed to completion. Our method also achieved improved lower limit of detection and standard curve linearity.

The primary advantage of our method is the use of minimal sample volume (12µl). Published methods require sample volumes ranging from 100µl (Jones et al., 2010) to 200µl (Teerlink et al., 2002; Marra et al., 2003; Blackwell et al., 2009), and in some cases 500µl (Heresztyn et al., 2004). Such sample requirements can be prohibitive for research applications where sample volume is limited, such as analysis of archived clinical samples or plasma from mouse model studies. A second advantage of our approach is the use of the non-endogenous arginine derivative monoethyl-L-arginine (MEA) as an internal standard, following the approach of Blackwell and colleagues (Blackwell et al., 2009). Use of MEA as an internal standard provides several key advantages over use of endogenous metabolites such as L-NMMA (Teerlink et al., 2002). Of principal importance, use of L-NMMA as an internal standard precludes quantification of endogenous L-NMMA concentrations. In contrast, use of a well-separated non-endogenous internal standard enables further investigation into the potential roles of L-NMMA in physiology and disease pathogenesis. In addition, physiological or pathophysiological variation in plasma L-NMMA concentrations would produce error in arginine, ADMA and SDMA values normalized to the L-NMMA internal standard, although this error could be minimized by addition of high L-NMMA concentrations.

The primary disadvantages of our method are the significant sample processing requirements and relatively long chromatographic run-time (55 min). The extended run-time was required to effectively separate L-NMMA from the unknown SPE contaminant and from arginine and taurine that may not be completely removed during sample clean-up. Use of low-flow conditions also required a relatively long re-equilibration period (13 min). To accommodate the relatively long run-time, we verified the stability of target metabolites and the OPA/3-mercaptopropionic derivatization reagent over 24 hours. This data supports use of a 24-hour work-flow where samples may be processed daily and analyzed overnight. A number of mass spectrometry-based assays for methylarginine derivatives have been published in recent years (Kirchherr and Kühn-Velten, 2005; Martens-Lobenhoffer and Bode-Böger, 2003; Schwedhelm et al., 2007; Bishop et al., 2007; El-Khoury et al., 2012; Gervasoni et al., 2011;

Servillo et al., 2013). Compared to HPLC-based methods, mass spectrometry-based analysis typically requires less intensive sample processing and allows for shorter run-times. Despite these advantages, mass spectrometry requires greater investment in instrumentation and maintenance, highlighting the importance of guidelines for thorough HPLC method development and validation, as we have described here.

In summary, we have developed and validated a chromatographic method for extracting, separating and quantifying arginine, L-NMMA, ADMA and SDMA with the unique advantages of small sample volume requirements, excellent separation of target metabolites from potential contaminants and validation for both human and mouse plasma samples.

Acknowledgements

I am grateful to Glenn Nardone (NIAID/NIH) for his initial work on this assay and helpful advice on further development described here. This work was funded by the NIAID Division of Intramural Research.

APPENDIX D.

HPLC-Based Quantification of DDAH Activity

Dimethylarginine dimethylaminohydrolase (DDAH) is responsible for metabolism of the endogenous NOS inhibitor asymmetric dimethylarginine (ADMA) to citrulline. We developed an HPLC-based assay to assess DDAH activity in liver tissue.

D.1 Introduction

Dimethylarginine dimethylaminohydrolase (DDAH) catalyzes the conversion of asymmetric dimethylarginine (ADMA) to citrulline and dimethylamine. DDAH is highly expressed in hepatic tissue and the liver serves as a major site of uptake of circulating ADMA (Siroen et al., 2005; Nijveldt et al., 2003, 2004). To complement molecular studies of hepatic DDAH expression and protein levels, we developed an assay to determine DDAH activity in *ex vivo* liver tissue.

D.2 Materials and Methods

Tissue Preparation, Spike and Incubation

Frozen liver samples were homogenized in 8 µl 1×PBS (Lonza, Walkersville, MD, USA) per mg wet weight of tissue with a Lab Gen 7 series hand held homogenizer (Cole Parmer, Vernon Hills, IL, USA). Homogenized samples were centrifuged for 5 min at 16,100*g* and 4°C to remove insoluble proteins. Supernatants were diluted 1:5 in 1×PBS spiked with ADMA (Cayman Chemical, Ann Arbor, MI, USA) for a final concentration of 2.5 mM ADMA. Spiked homogenates were vortex and sampled immediately (0hr time point) and after a 2 hr incubation at 37°C. At each time point, proteins were precipitated by mixing 15 µl of homogenate with 15µl of 2M perchloric acid containing 25 µmol/L N^G-monoethyl-L-arginine

(MEA) (Enzo Life Sciences, Farmingdale, NY, USA) as an internal standard. Precipitated samples were centrifuged for 5min at 16,100*g* and 4°C to and supernatants (10 µl) were neutralized by removing to a new tube containing 5µl 1.5M potassium carbonate (Sigma Aldrich, St. Louis, MO, USA). Neutralized samples were further diluted 1:2 in ultrapure water and centrifuged to remove potassium perchlorate precipitate.

HPLC Quantification of Citrulline

The derivatization reagent was prepared from ortho-phthaldialdehyde (Sigma-Aldrich, St. Louis, MO, USA) dissolved in HPLC-grade methanol to a concentration of 50mg/ml (372.8mM), 3-mercaptopropionic acid (Sigma-Aldrich, St. Louis, MO, USA) and 200mM potassium tetraborate, pH 9.4 (Sigma-Aldrich, St. Louis, MO, USA). A concentrated solution was prepared by adding 50µl of 50mg/ml OPA in methanol and 6µl 3-mercaptopropionic acid to 444µl of 200mM potassium tetraborate. Prior to use in analysis, this concentrated solution was diluted 3:10 in potassium tetraborate, yielding a working solution of 1.5mg/mL (11.2mM) OPA and 41.3mM 3-mercaptopropionic acid. Deproteination and neutralization were accomplished with 2M perchloric acid (Fisher Scientific, Pittsburgh, PA, USA) and 1.5M potassium carbonate (Sigma-Aldrich, St. Louis, MO, USA). Samples were derivatized by programming the autosampler to mix 2µl of sample with 2µl of working derivatization reagent.

Citrulline was separated by HPLC using a 1×100 mm C18(2) column with 3 µm particles and 100Å pore size (Phenomenex, Torrance, CA, USA). Solvent A was composed of 0.1M sodium acetate (Fisher Scientific, Pittsburgh, PA, USA) in ultrapure water from a Milli-Q Synthesis system (EMD Millipore, Billerica, MA, USA) with 9 % v/v methanol (Fisher Scientific, Pittsburgh, PA, USA) and 0.5 % v/v tetrahydrofuran (Sigma-Aldrich, St. Louis, MO, USA) with pH adjusted to 8.3 with 1M NaOH (Sigma-Aldrich, St. Louis, MO, USA). Organic mobile phase (Solvent B) was HPLC-grade methanol (Fisher Scientific, Pittsburgh, PA, USA) and separation of analytes was accomplished with a gradient from 0% solvent B to 25 % solvent

B over 20min at a flow-rate of 70 µl/min. The column was then washed with 100% methanol (solvent B) for 5 minutes and re-equilibrated with 100% solvent A for 20 minutes.

Citrulline was quantified by fluorescence detection using excitation and emission wavelengths of 340 nm and 455 nm respectively and normalized to the recovery of the MEA internal standard. Photomultiplier tube (PMT) gain was set to 12 for detection of citrulline. At 15.5 minutes, PMT gain was lowered to 8 so that the ADMA peak would not be off-scale. At 19.5 minutes, PMT gain was returned to 12 for detection of MEA (FIG D.1).

Quantification of DDAH Activity

DDAH activity was calculated by taking the difference of starting (0 hr) and ending (2 hr) citrulline concentrations, dividing by 2 hr and normalizing to protein content as quantified by BCA colourimetric assay (Thermo Scientific, Waltham, MA, USA) according to the manufacturer's instructions.

D.3 Assay Validation

Chromatography

Citrulline, ADMA and MEA (internal standard) were well-separated under the selected chromatographic conditions (FIG D.1). ADMA concentrations were two orders of magnitude higher than citrulline and MEA. We reduced the sensitivity of the fluorescence detector mid-way through the HPLC program in order prevent the ADMA peak from appearing as a flooded signal (FIG D.1).

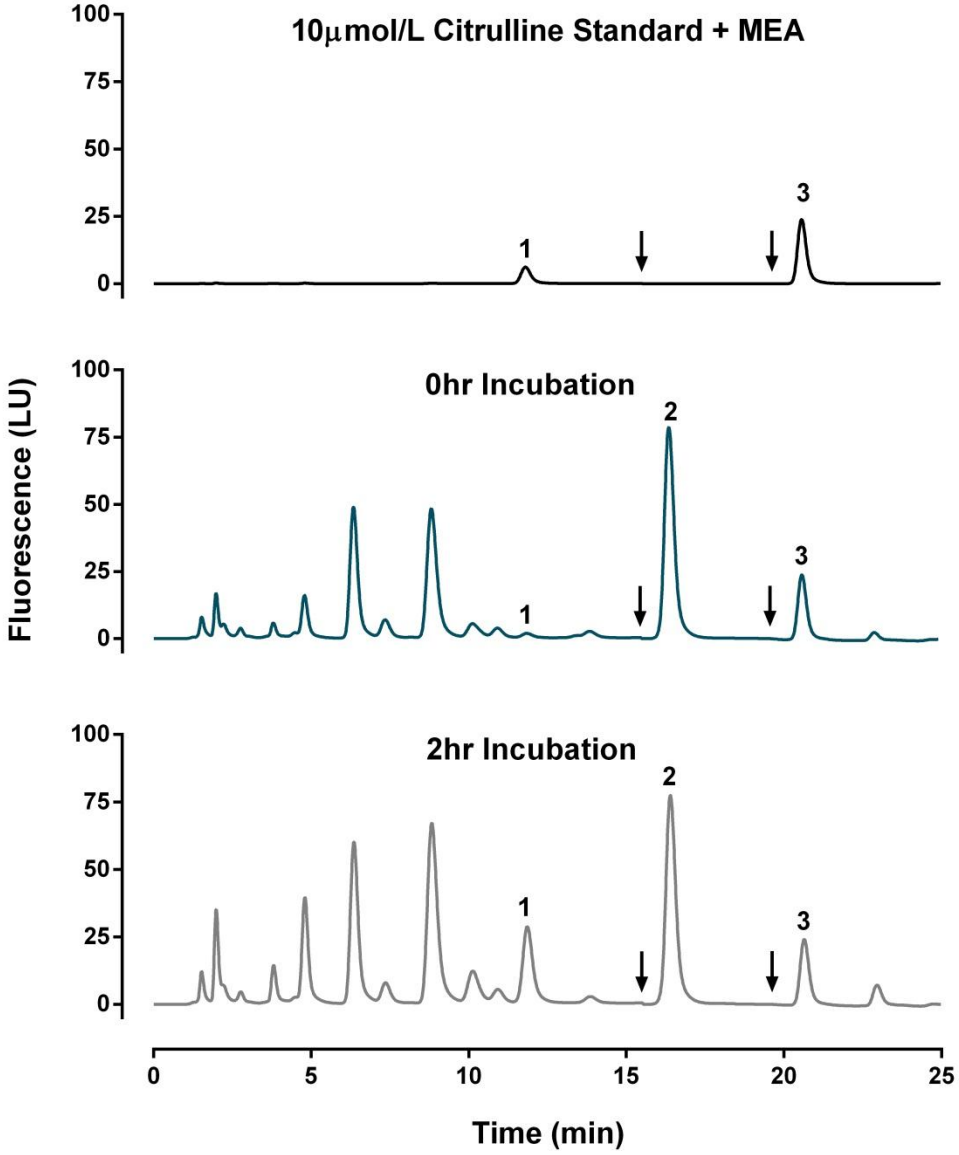


Figure D.1 | Chromatographic resolution of analytes. Peak identities are 1. Citrulline (DDAH product), 2. ADMA (DDAH substrate, spiked at 2.5 mol/L) and 3. MEA(internal standard, spiked at 25μmol/L). A standard solution of citrulline (10 μmol/L) was processed alongside samples and used for quantification of citrulline (top panel). Liver homogenates were sampled immediately after addition of 2.5 mol/L ADMA (middle panel). Liver homogenates were incubated at 37°C for 2 hours and sampled again to determine the rate of citrulline production by DDAH in the presence of excess ADMA substrate (bottom panel). Arrows at 15.5 minutes and 19.5 minutes indicate switch to decreased sensitivity (PMT gain 8) and back to normal sensitivity (PMT gain 12), respectively.

Verification of Citrulline as a Stable, Specific Read-Out

DDAH activity in liver homogenates was assessed by quantifying citrulline production in the presence of saturating concentrations of ADMA substrate (2.5mM). To validate this assay, we first demonstrated that exogenous citrulline (25 µM) was stable in the liver homogenate matrix after a 2hr incubation at 37°C (0hr: 26.3 ± 1.6 µM, 2hr: 25.3 ± 3.0 µM, $p > 0.05$). These data demonstrate that citrulline produced by DDAH is not degraded or further metabolized by other enzyme systems. We also demonstrated that citrulline production was negligible in the absence of exogenous ADMA (0 hr: 0.52 ± 0.19 µM, 2hr: 0.39 ± 0.07 µM, $p > 0.05$, FIG D.2). These data confirm that citrulline is only produced by liver homogenates in the presence of exogenous ADMA and may therefore be considered DDAH-specific.

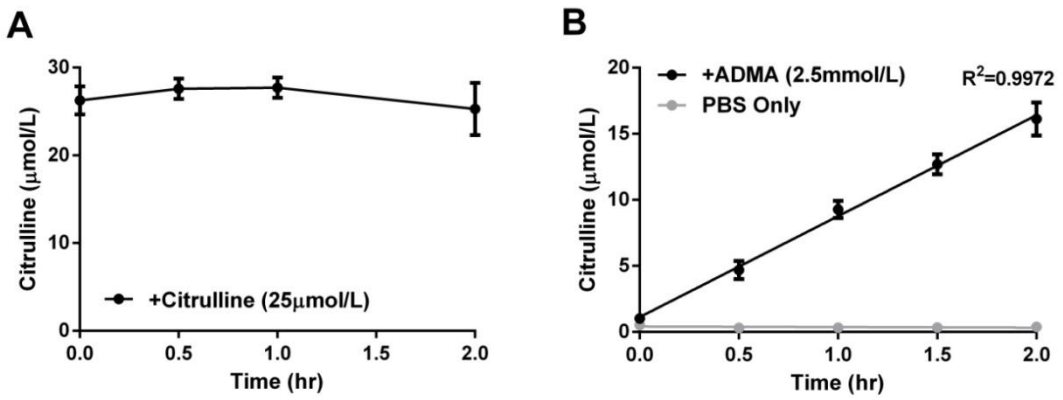


Figure D.2 | Assessment of DDAH activity assay kinetics. (**A**) Citrulline (25 µmol/L) was spiked into 3 replicates of liver homogenate from a healthy mouse. Citrulline concentrations measured by HPLC in 3 replicate spiked homogenates did not vary significantly at any time point tested ($p > 0.05$ vs 0hr by Wilcoxon matched-pairs signed rank test). (**B**) ADMA (2.5 mmol/L) was spiked into 3 replicates of liver homogenate from a healthy mouse. Citrulline concentrations were measured by HPLC in each replicate after 0, 0.5, 1, 1.5 and 2 hrs of incubation. R^2 = 0.9972 for line of best fit of mean citrulline concentrations at each time point. In the absence of exogenous ADMA (PBS only), Citrulline concentrations in 3 replicates of the same liver homogenate were not increased after 2 hr at 37°C (0hr: 0.52 ± 0.19 µmol/L, 2hr: 0.39 ± 0.07 µmol/L, $p>0.05$ by Wilcoxon matched-pairs signed rank test).

Verification of Approximate V_{max} Kinetics

In liver homogenates spiked with 2.5 mM ADMA, a constant rate of citrulline production was observed over 2 hr (R^2 = 0.9972), confirming that DDAH-mediated citrulline production is constant over 2 hr at this saturating concentration of ADMA substrate (FIG D.2).

Verification of Quantitative Relationship with Homogenate Concentration

We assayed a range of dilutions of the same liver homogenate and demonstrated a quantitative relationship between the measured change in citrulline concentration per hour and liver homogenate concentration (R^2 = 0.9995) (FIG D.3). These results demonstrate that the rate of citrulline production in ADMA-spiked liver homogenates is quantitatively proportional to the amount of DDAH enzyme present.

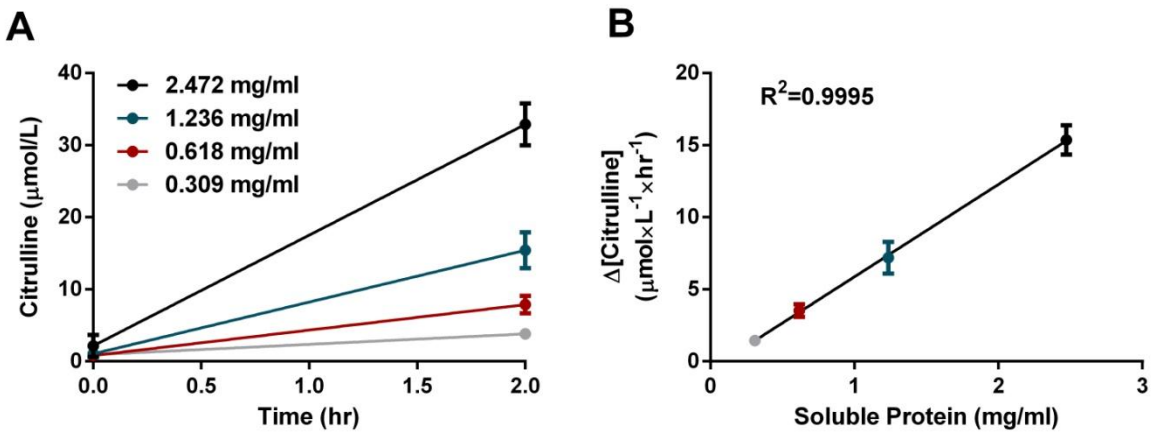


Figure D.3 | DDAH activity is quantitatively dependent on protein concentration. (**A**) Varying concentrations of liver homogenate (0.309, 0.618, 1.236 and 2.472 mg/ml soluble protein) were spiked with 2.5 mmol/L ADMA. Citrulline was measured at 0hr and 2hr. (**B**) DDAH activity for each spiked liver homogenate dilution was assessed by calculating the change in citrulline concentration per hour. R^2 = 0.9995 for line of best fit of mean change in citrulline concentration per hour for 3 replicates of each liver homogenate dilution.

D.4 Conclusions

Assessment of citrulline production as a read-out has previously been used to determine DDAH activity in ex vivo tissue samples by either HPLC (Davids et al., 2012b) or colourimetric methods (Tain and Baylis, 2007). We have validated an HPLC-based assay by demonstrating that citrulline is both a stable and specific read-out of DDAH activity in homogenized liver matrix. We have also demonstrated that our assay conditions approximate V_{max} enzyme kinetics and that measured DDAH activity is quantitatively related to the concentration of liver homogenate, and by implication, to the amount of DDAH protein in the sample.

Acknowledgements

I would like to thank to Glenn Nardone (NIAID/NIH) for his helpful advice on assay development and Jessica Chertow (NIAID/NIH) and Carlos Carhaus for their assistance in sample processing. This work was funded by the NIAID Division of Intramural Research.

APPENDIX E.

HPLC Determination of Tetrahydrobiopterin and 7,8-Dihydrobiopterin

(6R)-5,6,7,8-tetrahydro-L-biopterin (BH4) is an essential nitric oxide synthase cofactor. 7,8-dihydro-L-biopterin is the primary product of BH4 oxidation. This appendix describes optimization and validation of an HPLC-based method for the measurement of BH4 and 7,8-BH2 using paired electrochemical and fluorescence detection.

E.1 Introduction

Nitric oxide synthase (NOS) requires (6R)-5,6,7,8-tetrahydro-L-biopterin (BH4) arginine as a substrate for the synthesis of nitric oxide (NO). In the absence of BH4, NOS becomes uncoupled, producing superoxide (O_2^-) instead of NO. 7,8-dihydrobiopterin (7,8-BH2) is the primary product of BH4 oxidation and competes with BH4 for binding to NOS. Continuing study of BH4 and 7,8-BH2 as key determinants of NO synthesis and NOS uncoupling requires accurate determination of both metabolites in biological samples including plasma, erythrocytes and tissue samples. Here we describe the development and validation of a reverse-phase high performance liquid chromatography (HPLC) method with paired electrochemical and fluorescence detection for this purpose.

Historically, BH4 and 7,8-BH2 were quantified by analyzing a sample twice by high-performance liquid chromatography (HPLC): once following oxidation under acidic conditions and once following oxidation under alkaline conditions (Fukushima and Nixon, 1980). BH4 is oxidized to biopterin (a naturally fluorescent metabolite) under acidic conditions, but not alkaline conditions, whereas 7,8-BH2 is oxidized to biopterin under both conditions. According to this method, the concentration of BH4 was determined as the difference between the biopterin response produced by each pre-column chemical treatment (Fukushima and Nixon,

1980). This approach introduces significant limitations in quantifying both BH4 and 7,8-BH2. With regard to BH4, the analytical error associated with quantification would be compounded due the dependence of the final value on two separate measurements, each contributing error. As a result, determination of BH4 with this method is limited for analysis of relatively small amounts of BH4, especially in a sample that also contained large amounts of 7,8-BH2. With regard to 7,8-BH2, this analytical method does not differentiate between endogenous 7,8-BH2 and biopterin. As a result, combined 7,8-BH2 and biopterin values must be reported despite the fact that little is known about the effect of biopterin on NOS activity.

To work around these limitation, Hyland developed an HPLC assay with paired electrochemical and fluorescent detection modalities to determine BH4, 7,8-BH2 and biopterin concentrations in a single analytical run (Hyland, 1985). In this appendix, we describe the establishment of a modified version of this assay in our lab and optimization sample processing methods for analysis of mouse plasma, erythrocyte, aorta, liver and brain samples.

E.2 Materials and Methods

Instrumentation

The instrument consisted of a G1322A degasser (Agilent Technologies, Santa Clara, CA, USA), a G1310A isocratic pump (Agilent Technologies, Santa Clara, CA, USA), a G1329B autosampler with a G1330B sample plate temperature-control unit (Agilent Technologies, Santa Clara, CA, USA), a CouloChem III electrochemical detector (Thermo Scientific, Sunnyvale, CA, USA) and a G1321B fluorescence detector with a 8µl flow cell (Agilent Technologies, Santa Clara, CA, USA). Agilent Chemstation OpenLab CDS revision C.01.03 (Agilent Technologies, Santa Clara, CA, USA) was used to control the instrument and acquire data. A 35900E analog-to-digital converter (Agilent Technologies, Santa Clara, CA, USA) was used to facilitate communication between the electrochemical detector and Chemstation OpenLab. Analytes were separated on a 4.6mm×250mm ACE® C18 column with 5µm particles and 100Å pore size (MAC-MOD Analytical, Chadds Ford, PA, USA). A

4.6mm×13mm ACE® C18 guard column with 5µm particles and 100Å pore size (MAC-MOD Analytical, Chadds Ford, PA, USA) was installed to protect the primary column.

Reagents

The mobile phase consisted of 50mM HPLC-grade sodium acetate (Fisher Scientific, Pittsburgh, PA, USA), 5mM citric acid (Fisher Scientific, Pittsburgh, PA, USA), 48µM EDTA (Sigma-Aldrich, St. Louis, MO, USA), and 160µmol/L dithioerythritol (DTE) (Acros Organics, Geel, Belgium) prepared in ultrapure water (Milli-Q Synthesis system, Millipore Corporation, Billerica, MA, USA). Samples were diluted or homogenized in resuspension buffer containing 1mM dithioerythritol (Acros Organics, Geel, Belgium) and 0.5µM EDTA (Sigma-Aldrich, St. Louis, MO, USA) diluted in 1×DPBS (Lonza, Walkersville, MD, USA). Precipitation acid consisted of 1M phosphoric acid (Fisher Scientific, Pittsburgh, PA, USA), 2M trichloroacetic acid (Fisher Scientific, Pittsburgh, PA, USA) and 1mM dithioerythritol (DTE) (Acros Organics, Geel, Belgium) diluted in 1×DPBS (Lonza, Walkersville, MD, USA). BH4, 7,8-BH2 and biopterin standards were obtained from Schircks Laboratories (Jona, Switzerland).

Sample Processing

Tissue samples (~30mg) were homogenized in 15µl ice-cold resuspension buffer per mg using a hand-held homogenizer (Cole Parmer, Vernon Hills, IL, USA). Homogenized samples were centrifuged for 5 min at 16,100*g* and 4 °C to remove insoluble protein. Supernatants were then mixed 9:1 with ice-cold precipitation acid to precipitate proteins. Instead of homogenization, whole aortas were subjected to three freeze–thaw cycles on dry ice in 200µl resuspension buffer prior to mixing with precipitation acid as above. Red blood cells and plasma samples were diluted 1:10 in resuspension buffer prior to mixing with precipitation acid as above. Following precipitation, all samples were centrifuged for 5 min at 16,100*g* and 4 °C. Supernatants were loaded into 250µl capacity polypropylene vials (Agilent Technologies, Santa

Clara, CA, USA) and loaded into the autosampler. All samples were maintained on ice during processing.

Chromatography, Electrochemistry and Fluorescence Detection

Samples were injected in a volume of 100µl. Chromatographic separation was performed isocratically with a flow rate of 1.3 ml/min and a 19-minute rune-time between sample injections. The voltage of electrode 1 was set to +75mV, the voltage of electrode 2 was set to -400mV and the guard voltage was set to +900mV. The fluorescence detector excitation and emission wavelengths were set to 350 and 450 nm, respectively, and the photomultiplier tube gain was set of 18.

Quantification of Sample Analytes

Chemstation OpenLab CDS software version C.01.03 was used for peak integration External standards were used for quantification of analytes. A combined standard of BH4 and 7,8-BH2 was prepared and diluted to 50, 10, 5, 1, 0.5, 0.25 and 0.1 nmol/L in resuspension buffer. This standard curve was analyzed and peak areas were used to determine BH4 and 7,8-BH2 concentrations in experimental samples by interpolation. For tissue analysis, measured concentrations were and normalized to soluble protein content, which was separately assayed with a Pierce BCA Protein Assay Kit (Thermo Scientific, Sunnyvale, CA, USA) according to the manufacturer's instructions.

E.3 Overview of Assay Chemistry

This assay utilizes sequential electrochemical and fluorescence detection to quantify BH4 and 7,8-BH2 without interference from endogenous biopterin (FIGURE E.1). Samples are prepared for analysis without pre-column oxidation. With BH4 and 7,8-BH2 in their native oxidation states, each analyte migrates across the column matrix at a rate different from the other and different from biopterin.

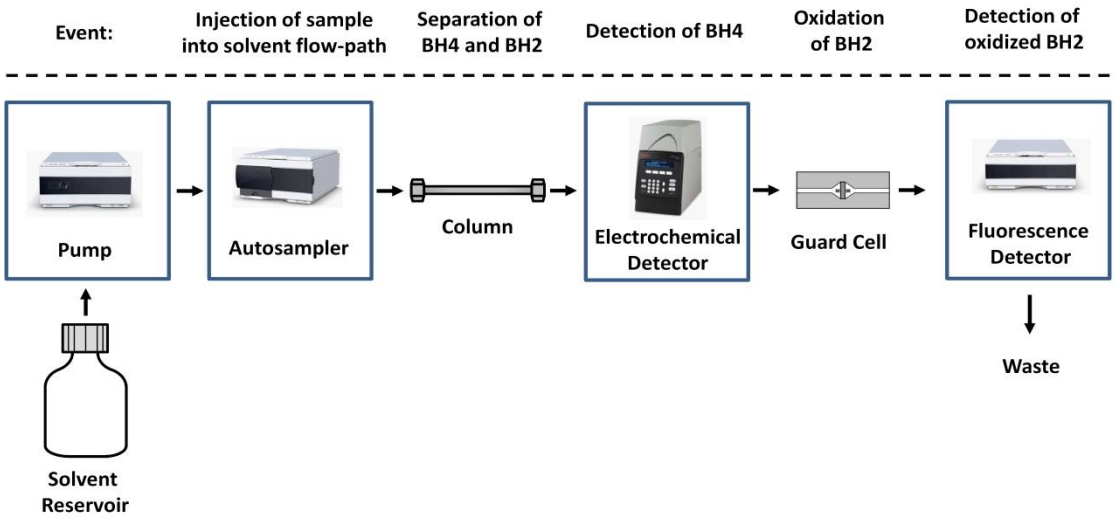


Figure E.1 | Sequence of analytical events for detection of BH4 and 7,8-BH2. Arrows indicate solvent flow-path. Solvent flow is maintained by an isocratic pump. Samples are injected by the autosampler and chromatographically separated by a C18 column. The analytical cell of the electrochemical detector is used to detect BH4. Prior to detection by the fluorescence detector, the guard cell oxidizes 7,8-BH2, which is not fluorescent, to biopterin, which is fluorescent. Photographs of individual modules courtesy of http://www.esainc.com/products (electrochemical detector) and http://www.chem.agilent.com/en-US/products-services/Instruments-Systems/Liquid-Chromatography (all other modules).

Electrochemical Detection of BH4

After eluting from the column, separated analytes are passed through the analytical cell of the electrochemical detector, where BH4 is detected. The analytical cell contains two porous electrodes that apply a voltage to dissolved analytes as they flow though the electrode matrix. The first electrode is set to a positive voltage that oxidizes to BH4 to quinoid dihydrobiopterin (q-BH2, distinct from 7,8-BH2). Newly-formed q-BH2 is rapidly reduced back to BH4 by the second electrode, which applies a negative voltage. The change in current generated by the reduction of q-BH2 to BH4 is used to quantify the amount of BH4 the sample. 7,8-BH2 is unaffected by the voltages applied by the analytical cell.

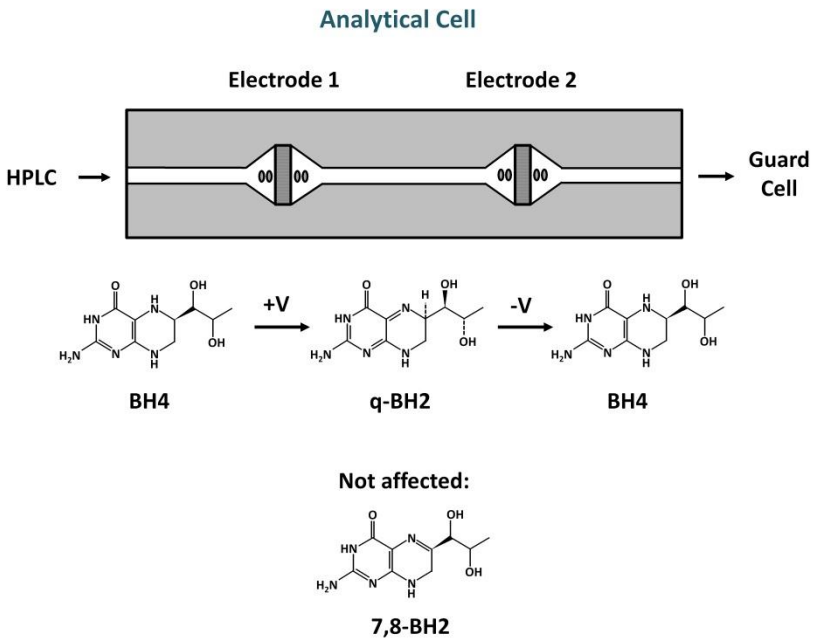


Figure E.2 | Electrochemical detection of BH4. BH4 eluting from the HPLC column is passed to the analytical cell of the electrochemical detector. The first electrode applies a positive voltage (+V) that oxidizes BH4 to quinoid BH2 (q-BH2). The second electrode applies a negative voltage (-V) that reduces q-BH2 back to BH4, generating a current that is used to quantify the amount of BH4 in the original sample.

Oxidation and detection of BH4

The guard cell is placed after the analytical cell and set to a high voltage in order to oxidize 7,8-BH2, which is not fluorescent, to biopterin, which is fluorescent, prior to detection by the fluorescence detector (FIG E.3). In contrast to pre-column chemical oxidation, the electrochemical oxidation step in this assay occurs after chromatographic separation of 7,8-BH2 and biopterin in their native states. Therefore, 7,8-BH2 is converted to biopterin for detection, but only after it has already been separated from endogenous biopterin, allowing identification of each analyte based on unique retention times.

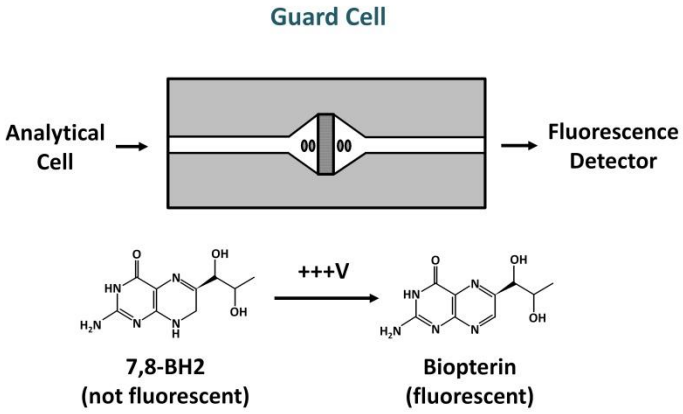


Figure E.3 | Oxidation of 7,8-BH2. The guard cell applies a large positive voltage (+++V) to oxidize 7,8-BH2 to biopterin, which is fluorescent. Oxidized 7,8-BH2 is then passed to the fluorescence detector for quantification.

E.4 Assay Optimization

Peak Identification

Retention times were determined by separate analysis of individual BH4, 7,8-BH2 and biopterin standards dissolved in buffer (FIG E.4). 7,8-BH2 was distinguishable from biopterin because chromatographic separation was performed while 7,8-BH2 was in its native oxidation state. Following chromatographic separation, 7,8-BH2 was oxidized to biopterin for fluorescence detection, but the resulting peak has a different retention time than endogenous biopterin (FIG E.4).

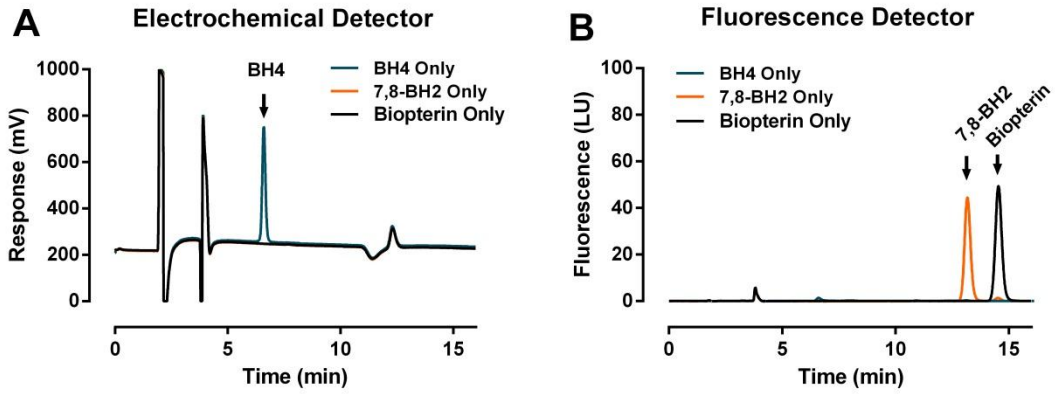


Figure E.4 | Identification of Retention times for BH4 and 7,8-BH2 standards. (**A**) BH4 was detectable as a unique peak with the electrochemical detector, but not 7,8-BH2 or biopterin. (**B**) 7,8-BH2 and biopterin were detectable as unique peaks with different retention times with the fluorescence detector. All standards were diluted to a concentration of 50 nmol/L in resuspension buffer.

Voltage Optimization

Analytical Cell Voltage

To determine the voltages required for effective detection of BH4, we repeatedly analyzed a standard containing 50 nmol/L BH4 while varying the voltage applied across the analytical cell electrodes (FIG E.5). We found that the area of the BH4 peak did not vary across electrode voltages of +75mV to 175mV. In contrast, the BH4 peak was significantly smaller if

electrode 2 was set to -300mV or -250mV (FIG E.5). Based on these findings, we selected voltages of +100mV for electrode 1 and -450mV for electrode 2 for further assay optimization.

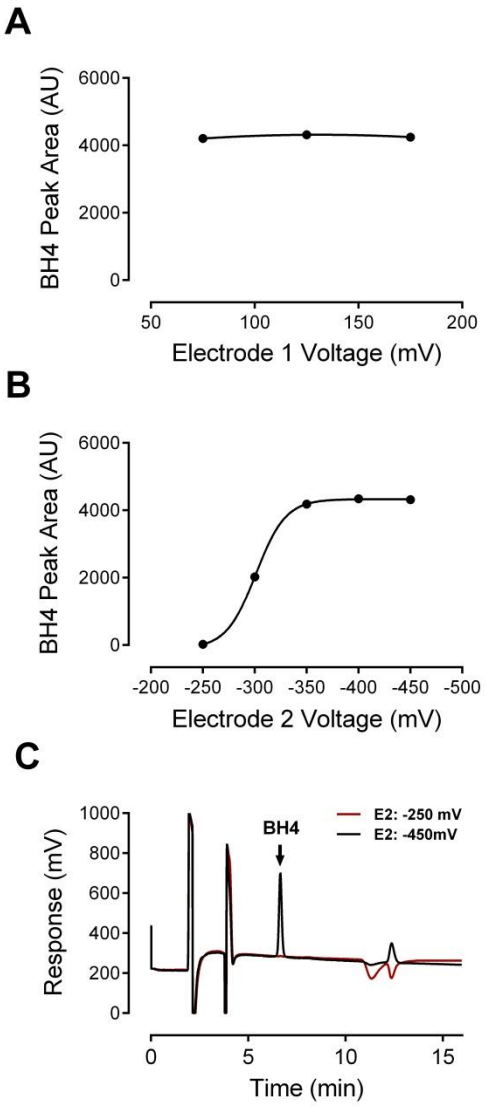


Figure E.5 | Analytical cell voltage optimization. BH4 standards were prepared at a concentration of 50 nmol/L in resuspension buffer. (**A**) The BH4 peak was quantified in arbitrary units (AU) from the electrochemical detector output as electrode 2 was held constant at -450mV while the voltage of electrode 1 was varied. (**B**) The BH4 peak was quantified as electrode 1 was held constant at +100mV while the voltage of electrode 2 was varied. (**C**) Chromatograms showing a large BH4 peak when electrode 2 is set to -450mV (black) but no BH4 peak when electrode 2 is set to -250mV (red).

Guard Cell Voltage

To determine the guard cell voltage required for effective oxidation of 7,8-BH2 for fluorescence detection, we repeatedly analyzed a standard containing 50 mol/L 7,8-BH2 and biopterin while varying the voltage applied across the guard cell electrode (FIG E.6). We found that the area of the 7,8-BH2 peak steadily increased as the guard cell electrode was raised, reaching an apparent plateau at voltages ≥ 850mV (FIG E.6). Biopterin was not affected by variation in the guard cell voltage. Based on these findings, we selected a guard cell voltage of +900mV for further assay optimization.

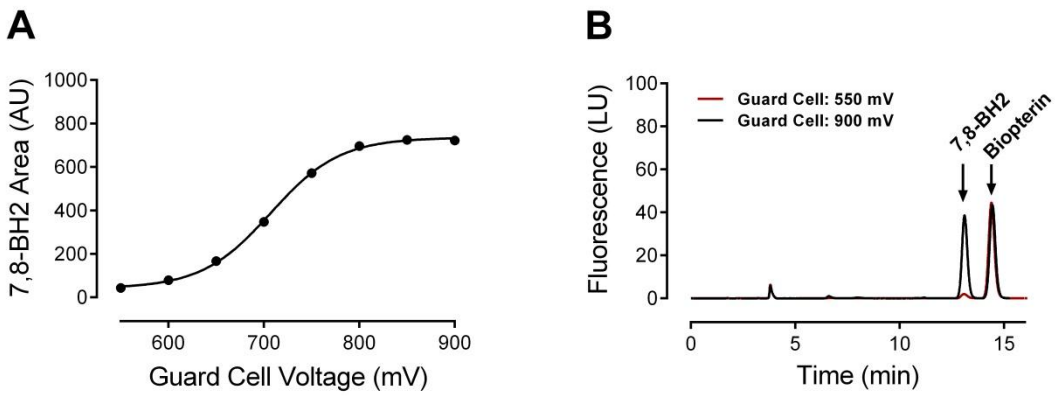


Figure E.6 | Guard cell voltage optimization. Combined 7,8-BH2 and biopterin standards were prepared at a concentration of 50 nmol/L in resuspension buffer. Analytical electrodes 1 and 2 were set to +100mV and -450mV, respectively (**A**) The 7,8-BH2 peak was quantified in arbitrary units (AU) with the fluorescence detector as the guard cell voltage was varied from +550mV to +900mV. (**B**) Fluorescence detector chromatograms showing a large 7,8-BH2 peak when the guard cell is set to +900mV (black) but a much smaller 7,8-BH2 peak when the guard cell is set to +550mV (red). Fluorescence units are arbitrary light units (LU).

Sample Processing

Plasma

Soluble protein was removed by spiking plasma samples with a solution containing trichloroacetic acid (2M) and phosphoric acid (1M). Addition of this acid solution caused soluble proteins to precipitate, allowing the protein-free supernatant to be removed following centrifugation. We tested the effects of neutralization with varying concentrations of sodium hydroxide and found that neutralization with 3.5M NaOH prevented a large peak of unknown identity from co-eluting with 7,8-BH2 in plasma samples (FIG E.7).

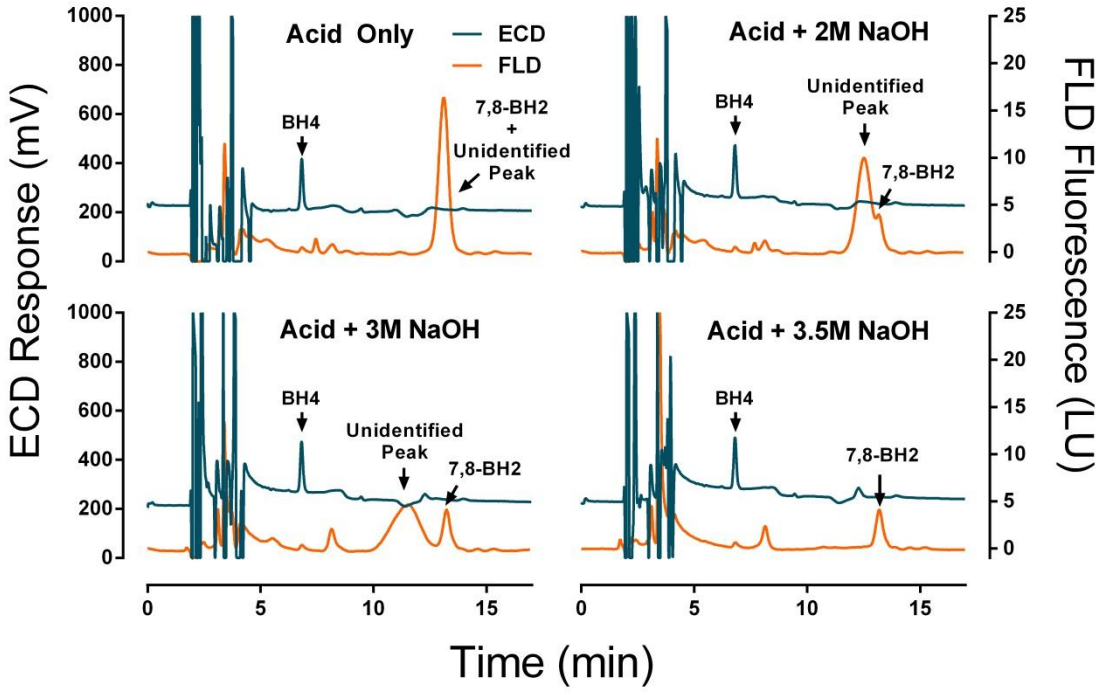


Figure E.7 | Neutralization of plasma samples. The same plasma sample was processed with precipitation acid only and with an additional neutralization step with varying concentrations of sodium hydroxide. Output from the electrochemical detector (ECD) is plotted in blue relative to the left axis. Output from the fluorescence detector (FLD) is plotted in orange relative to the right axis (units = arbitrary fluorescence light units, LU).

To determine whether neutralization interfered with detection of either BH4 or 7,8-BH2, we analyzed acidified standard solutions of BH4 and 7,8-BH2 (50 nmol/L each) with or without the additional neutralization step. We found that the peak area of the BH4 standard processed with neutralization was 97.1 ± 2.9 % of the peak obtained with acidification alone, while the peak area of the 7,8-BH2 standard processed with neutralization was 99.0 ± 7.5% of the peak obtained with acidification alone (TABLE E.1). Furthermore, the BH4 peak area in plasma processed with acidification and neutralization was 99.1 ± 3.7% of the peak area obtained when the same plasma sample was processed with acidification alone (TABLE E.1). These results demonstrate that neutralization with NaOH prevents an unknown peak from co-eluting with 7,8-BH2 without fundamentally affecting the detection of 7,8-BH2 or BH4. We therefore determined that plasma samples should be processed with acidification followed by neutralization with 3.5M NaOH.

Relative Response
(% of Precipitation Acid Only)

	Standard in Resuspension Buffer			
	Precipitation Acid Only	Precipitation Acid + 3.5M NaOH		
BH4	100	97.1	±	2.9
7,8-BH2	100	99.0	±	7.5

	Plasma			
	Precipitation Acid Only	Precipitation Acid + 3.5M NaOH		
BH4	100	99.1	±	3.7
7,8-BH2	-	-	±	-

Table E.1 | Quantitative comparison of sample processing with or without NaOH neutralization. Combined BH4 and 7,8-BH2 standards (50 nmol/L) in resuspension buffer (n=3) and plasma samples (n=3) were processed with or without NaOH neutralization. Peak areas are expressed as a mean percentage of the area obtained with acidification only ± standard deviation. The 7,8-BH2 peak could not be determined in plasma samples processed with precipitation acid only, due to interference by a peak of unknown identity.

Erythrocytes

In contrast to plasma, erythrocyte samples did not contain the same unknown peak that interfered with 7,8-BH2 in acidified plasma samples (FIG E.8). Introduction of the neutralization had no effect on BH4 in plasma samples (TABLE E.1). In the erythrocyte matrix, we found that neutralization reduced the observed BH4 peak area to 59.9 ± 3.8 % of the value observed with acidification only and increased the 7,8-BH2 peak to 158.6 ± 16.7 % of the value observed with acidification only (TABLE E.2). These finding suggests that neutralization causes oxidation of BH4 to 7,8-BH2 in the erythrocyte sample matrix, but not in plasma. We therefore determined that erythrocytes should be processed with acidification only and no neutralization step.

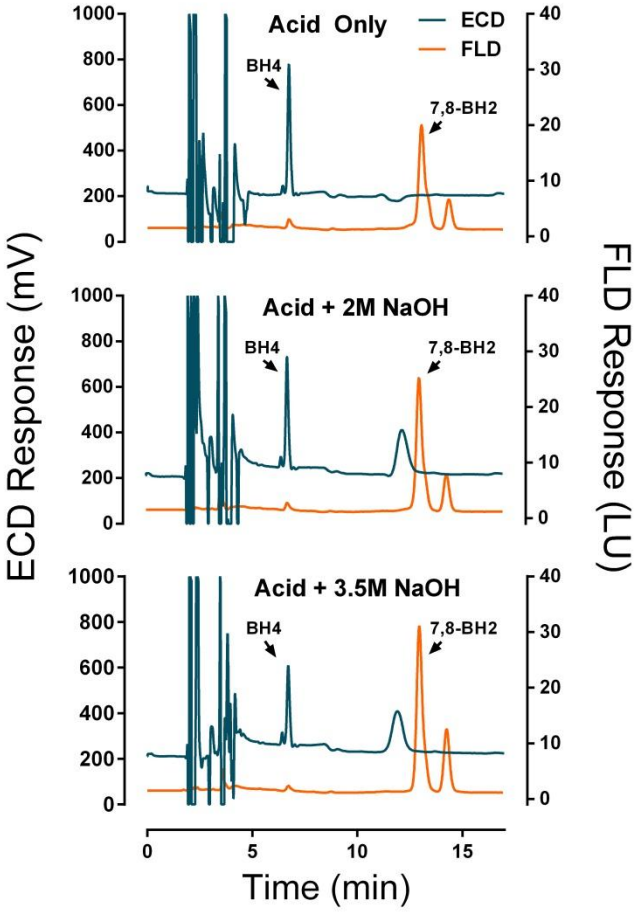


Figure E.8 | Neutralization of erythrocyte samples. The same packed erythrocyte sample was processed with precipitation acid only and with an additional neutralization step with varying concentrations of sodium hydroxide. Output from the electrochemical detector (ECD) is plotted in blue relative to the left axis. Output from the fluorescence detector (FLD) is plotted in orange relative to the right axis (units = arbitrary fluorescence light units, LU).

	Relative Response (% of Precipitation Acid Only)	
	Precipitation Acid Only	Precipitation Acid + 3.5M NaOH
BH4	100	59.9 ± 3.8
7,8-BH2	100	158.6 ± 16.7

Table E.2 | Quantitative comparison of erythrocytes processed with or without NaOH neutralization. Packed red blood cell samples (n=3) were processed with or without NaOH neutralization. Peak areas are expressed as a mean percentage of the area obtained with acidification only ± standard deviation.

Aorta

We tested the effects of neutralization with varying concentrations of sodium hydroxide in aorta samples. Similar to observations in plasma, we found that neutralization with 3.5M NaOH prevented a peak of unknown identity from co-eluting with 7,8-BH2 (FIG E.9). We therefore determined that aorta samples should be processed with acidification followed by neutralization with 3.5M NaOH.

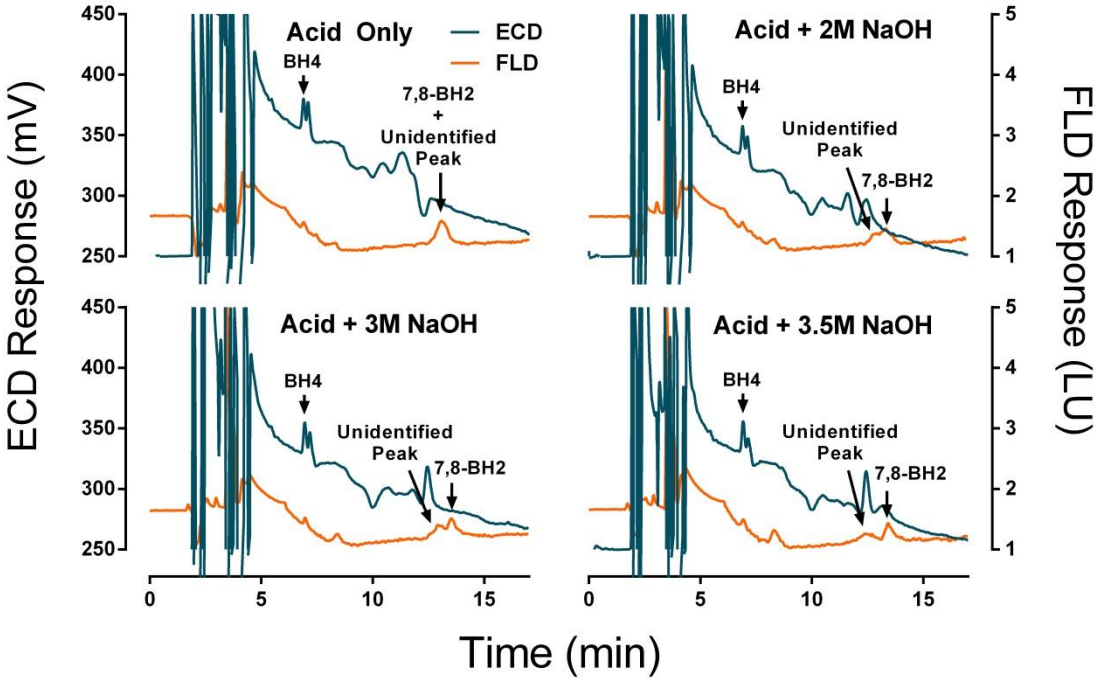


Figure E.9 | Neutralization of aorta samples. Aorta samples were processed with precipitation acid only and with an additional neutralization step with varying concentrations of sodium hydroxide. Output from the electrochemical detector (ECD) is plotted in blue relative to the left axis. Output from the fluorescence detector (FLD) is plotted in orange relative to the right axis (units = arbitrary fluorescence light units, LU).

Liver

We tested the effects of neutralization with varying concentrations of sodium hydroxide in liver samples. The effect of neutralization was less clear in liver samples than in plasma and aorta samples. In plasma and aorta samples, an unidentified peak co-eluted with 7,8-BH2 under conditions of acidification only, but eluted at an earlier time following neutralization. In liver samples, we did not find any evidence of the same unidentified peak co-eluting with 7,8-BH2 (FIG E.10). The 7,8-BH2 peak was most sharply defined in samples neutralized with 3M NaOH (FIG E.10), so this processing paradigm was selected for analysis of liver samples.

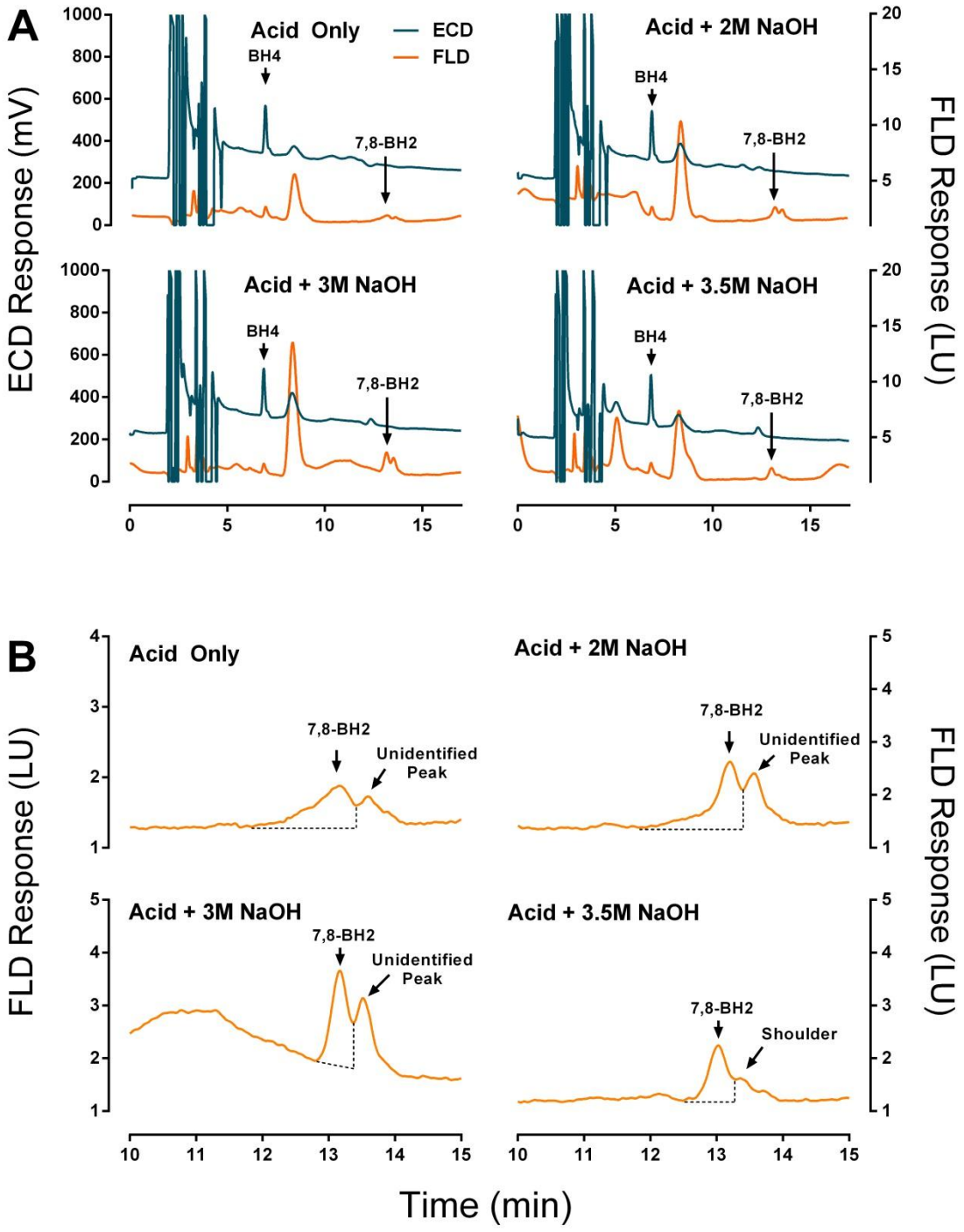


Figure E.10 | Neutralization of liver samples. (**A**) Liver samples were processed with precipitation acid only and with an additional neutralization step with varying concentrations of sodium hydroxide. Output from the electrochemical detector (ECD) is plotted in blue relative to the left axis. Output from the fluorescence detector (FLD) is plotted in orange relative to the right axis (units = arbitrary fluorescence light units, LU). (**B**) Detail of fluorescence trace from 10 to 15 minutes. Integration is shown with dotted lines.

Brain

We tested the effects of neutralization with varying concentrations of sodium hydroxide in brain samples. Similar to observations in plasma, we found that neutralization with 3.5M NaOH did not significantly alter retention times of peaks surrounding 7,8-BH2 (FIG E.11). The definition of the 7,8-BH2 peak was improved with neutralization with 3M NaOH (FIG E.11), so this processing paradigm was selected for analysis of brain samples.

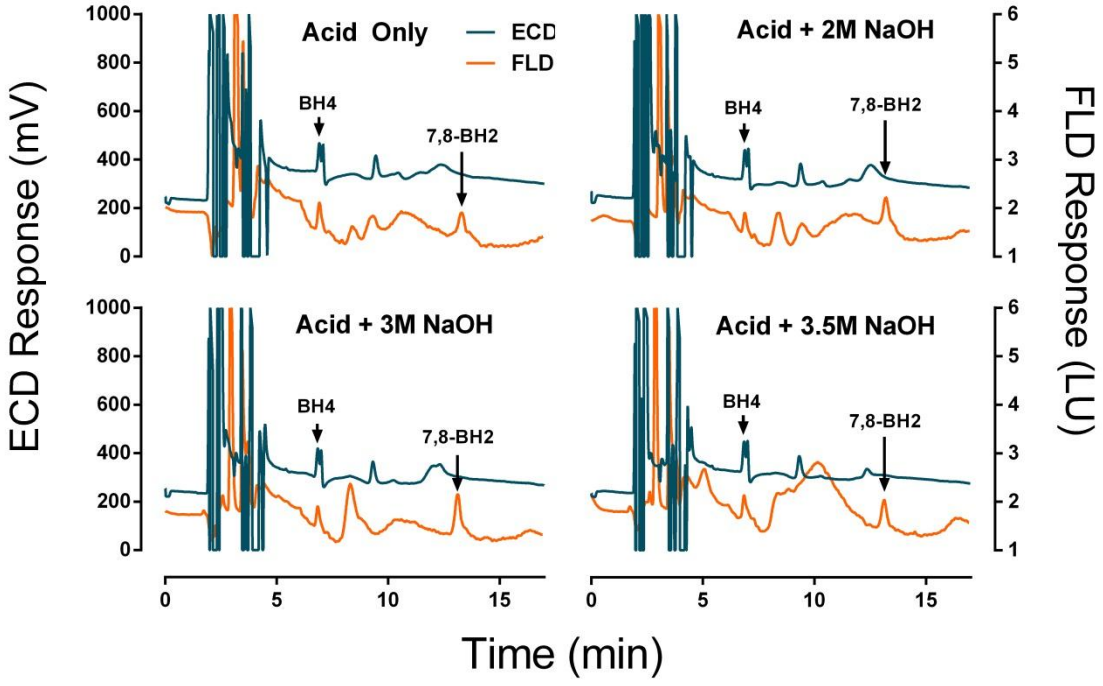


Figure E.11 | Neutralization of brain samples. Brain samples were processed with precipitation acid only and with an additional neutralization step with varying concentrations of sodium hydroxide. Output from the electrochemical detector (ECD) is plotted in blue relative to the left axis. Output from the fluorescence detector (FLD) is plotted in orange relative to the right axis (units = arbitrary fluorescence light units, LU).

Analyte Stability

We analyzed the stability of dissolved analytes maintained at 4°C in the autosampler by comparing repeat analyses of 3 combined BH4 and 7,8-BH2 standards (50 nmol/L each). We established an *a priori* threshold that samples should be processed in small enough batches to ensure <5% loss of signal due to degradation or oxidation during analysis of preceding samples. When standards were processed with precipitation acid only, the peak areas of BH4 and 7,8-BH2 remained >95% of initial through the 8th injection (TABLE E.3). From these data, we determined that erythrocyte samples could be processed in batches of up to 8 samples at a time. When standards were processed with precipitation acid followed by neutralization, the peak areas of BH4 and 7,8-BH2 remained >95% of initial through the 4th injection (TABLE E.3). From these data, we determined that plasma and tissue samples could be processed in batches of up to 4 samples at a time.

Analyte Stability + Precipitation Acid Only					Analyte Stability + Precipitation Acid Neutralized with 3.5M NaOH				
Injection (#)	Analyte	Response (% of 1st injection)			Injection (#)	Analyte	Response (% of 1st injection)		
1	BH4	100.0			1	BH4	100.0		
	7,8-BH2	100.0				7,8-BH2	100.0		
2	BH4	101.0	±	0.6	2	BH4	98.1	±	1.1
	7,8-BH2	98.8	±	1.5		7,8-BH2	100.1	±	0.8
3	BH4	101.4	±	0.5	3	BH4	96.1	±	0.9
	7,8-BH2	98.7	±	1.7		7,8-BH2	101.0	±	0.8
4	BH4	100.7	±	0.8	4	BH4	95.0	±	1.3
	7,8-BH2	98.3	±	1.2		7,8-BH2	101.5	±	1.3
5	BH4	100.9	±	0.6	5	BH4	93.7	±	1.2
	7,8-BH2	98.3	±	2.8		7,8-BH2	102.6	±	1.5
6	BH4	100.6	±	0.9	6	BH4	92.0	±	0.9
	7,8-BH2	96.9	±	0.7		7,8-BH2	102.8	±	1.6
7	BH4	101.0	±	0.7	7	BH4	90.4	±	1.2
	7,8-BH2	96.4	±	2.2		7,8-BH2	103.6	±	2.1
8	BH4	99.7	±	0.8	8	BH4	88.2	±	2.0
	7,8-BH2	95.6	±	2.0		7,8-BH2	104.7	±	2.1
9	BH4	99.8	±	0.7	9	BH4	85.3	±	2.1
	7,8-BH2	94.8	±	1.6		7,8-BH2	107.3	±	3.0
10	BH4	99.7	±	0.7	10	BH4	78.0	±	1.8
	7,8-BH2	94.4	±	1.8		7,8-BH2	110.5	±	2.9

Table E.3 | Analyte stability. Values are expressed as mean % of initial at 0hr ±SD. Data were determined from repeat assessments of three independent standards containing BH4 (50 nmol/L) and 7,8-BH2 (50 nmol/L). Standards were prepared with precipitation acid with or without additional neutralization with 3.5M NaOH.

E.5 Assay Validation

Linearity of Standard Curve

To assess linearity, a combined standard solution containing BH4 and 7,8-BH2 was diluted to yield a seven-point standard curve. Separate standard curves were either acidified with trichloroacetic acid only or acidified and neutralized with 3.5M sodium hydroxide to replicate the two sample processing paradigms established above. Under acidified or acidified/neutralized conditions, standard curves for BH4 and 7,8-BH2 were highly linear with R^2 values of 0.9998 (TABLE E.4).

	Precipitation Acid + Neutralization with 3.5M NaOH							
	Standard Concentration (nmol/L)							
Analyte	**50**	**10**	**5**	**1**	**0.5**	**0.25**	**0.1**	**R^2**
BH4	4320.3	816.1	395.9	77.4	36.9	19.5	8.5	0.9998
BH2	820.3	170.6	87.6	17.9	10.1	4.7	2.1	0.9998

	Precipitation Acid Only							
	Standard Concentration (nmol/L)							
Analyte	**50**	**10**	**5**	**1**	**0.5**	**0.25**	**0.1**	**R^2**
BH4	4479.7	883.8	447.2	90.7	49.1	33.2	9.8	0.9998
BH2	702.9	140.9	70.4	14.7	7.6	4.3	2.4	0.9998

Table E.4 | Linearity of standards assayed over a range of concentrations. Values expressed as mean integrated areas (relative light units × s) averaged from n=3 independent standard curves prepared with precipitation acid with or without additional neutralization with 3.5M NaOH.

Limit of Detection

The limit of detection (LOD) describes the lowest concentration that can be distinguished from baseline noise with a degree of confidence, generally set at 95%. The LOD was determined by assaying n=3 blanks independently prepared from resuspension buffer (1× DPBS, 0.5µM EDTA, 1mM dithioerythritol) and n=3 standard solutions containing 0.1nM BH4 and 0.1nM 7,8-BH2 (TABLE E.5). Blanks and standards were processed with precipitation acid with or without additional neutralization with sodium hydroxide as described above. The limit of detection was calculated according to the following equation (Armbruster and Pry, 2008):

$$\mathrm{LOD} = \mathrm{Mean}_{Blank} + 1.645 \times \mathrm{SD}_{Blank} + 1.645 \times \mathrm{SD}_{Low\ Standard} \qquad Eq\ E.1$$

Precipitation Acid + Neutralization with 3.5M NaOH

Analyte	LOD (nmol/L)
BH4	0.036
BH2	0.060

Precipitation Acid Only

Analyte	LOD (nmol/L)
BH4	0.056
BH2	0.045

Table E.5 | Limit of detection (LOD). Values determined from resuspension buffer blank samples (n=3) and low-concentration standards containing 0.1 nmol/L BH4 and 7,8-BH2 (n=3). LOD was determined in blank and low concentration samples processed with precipitation acid with or without additional neutralization with 3.5M NaOH.

Precision

Precision was calculated from 4 independent analyses of the same mouse plasma and erythrocyte samples analyzed on different days (inter-day precision). The coefficient of variation (CV) was calculated and expressed as a percent (%CV):

$$\%\mathrm{CV} = \frac{s}{\bar{x}} \times 100\% \qquad \textit{Eq E.2}$$

Where s is the standard deviation and $\bar{x}$ is the mean of repeated measurements.

Intra-day %CV values were <5% for BH4 and 7,8-BH2 in both plasma and erythrocyte samples (TABLE E.6).

Analyte	Mouse Plasma		Mouse RBC	
	Concentration (nmol/L)	%CV	Concentration (nmol/L)	%CV
BH4	239.9 ± 7.3	3.1	941.3 ± 25.8	2.7
BH2	137.3 ± 2.7	1.9	306.1 ± 12.2	4.0

Table E.6 | Inter-day precision. Mouse plasma and erythrocyte samples were analyzed on 4 different days. Measured concentrations are reported as mean ± SD for repeated analyses and precision was assessed by calculating the coefficient of variation as a percent (%CV).

Sample Matrix Effects

Sample matrix effects were assessed by spiking 100 nmol/L of BH4 and 7,8-BH2 standards into mouse and erythrocyte samples (TABLE E.7 & TABLE E.8). Recovery was calculated as an absolute concentration and as a percentage of the known concentration of the standard used to spike samples:

$$\%\ Recovery\ = \left(\frac{[Analyte]_{Sample+Spike} - [Analyte]_{Sample\ Alone}}{[Spike]}\right) \times 100\% \qquad Eq\ E.3$$

Mouse Plasma

Run #	Peak ID	Measured Concentration (nmol/L)		Recovery	
		Plasma Only	Plasma + 100 nmol/L Spike	Concentration (nmol/L)	Percent (%)
1	BH4	214.7	324.9	110.2	110.2
	BH2	83.3	177.0	93.7	93.7
2	BH4	191.0	296.8	105.7	105.7
	BH2	55.9	159.3	103.4	103.4
3	BH4	250.7	354.9	104.2	104.2
	BH2	61.5	169.3	107.8	107.8
Mean ± SD	**BH4**	-	-	**106.7 ± 3.1**	**106.7 ± 3.1**
	BH2	-	-	**101.6 ± 7.2**	**101.6 ± 7.2**

Table E.7 | Recovery of standards spiked into mouse plasma. Recoveries from three different spiked samples were calculated in terms of concentration (nmol/L) and percent of initial spike (%). Mean and standard deviation were calculated from these recovery values.

Mouse Red Blood Cells

Run #	Peak ID	Measured Concentration (nmol/L)		Recovery	
		Plasma Only	Plasma + 100 nmol/L Spike	Concentration (nmol/L)	Percent (%)
1	BH4	419.2	516.1	96.9	96.9
	BH2	350.5	458.6	108.0	108.0
2	BH4	561.5	659.5	98.0	98.0
	BH2	182.5	286.1	103.6	103.6
3	BH4	703.6	804.7	101.1	101.1
	BH2	223.8	322.6	98.8	98.8
Mean ± SD	**BH4**	-	-	**98.7 ± 2.2**	**98.7 ± 2.2**
	BH2	-	-	**103.5 ± 4.6**	**103.5 ± 4.6**

Table E.8 | Recovery of standards spiked into mouse red blood cell samples. Recoveries from three different spiked samples were calculated in terms of concentration (nmol/L) and percent of initial spike (%). Mean and standard deviation were calculated from these recovery values.

E.6 Conclusions

Tetrahydrobiopterin and 7,8-dihydrobiopterin are highly sensitive to oxidation-reduction reactions. Electrochemical detection takes advantage of the redox reactivity of BH4 to allow for highly sensitive quantification. This method also utilizes the natural fluorescence of biopterin for the detection of 7,8-BH2 following post-column electrochemical oxidation. Using these approaches, both BH4 and 7,8-BH2 can be quantified without pre-column derivatization or other chemical manipulation. The reactivity of BH4 and 7,8-BH2 also poses unique challenges. Both metabolites rapidly oxidize at room temperature unless a high concentration antioxidant such as dithioerythritol is present (Howells and Hyland, 1987). To counteract oxidation, we included dithioerythritol in the resuspension buffer and mobile phase to improve stability of BH4 and7,8-BH2 during sample processing and analysis. Even with this precaution, our analyte stability studies indicate that samples should be processed in small batches (4-8 samples at a time) to reduce the effect of oxidation while samples are awaiting injection.

Samples are acidified prior to analysis to remove soluble proteins that could be retained in the HPLC column matrix. We found that under these conditions, an unknown peak co-eluted with 7,8-BH2, interfering with accurate quantitation. Neutralization with sodium hydroxide effectively altered the retention time of this contaminating peak, but also decreased the stability of BH4. As a result smaller batch sizes are required to avoid excess oxidation in plasma and tissue samples processed with both acidification and neutralization steps. Further experimentation with mobile phase composition, such as adding low-concentration methanol, may allow separation of the unknown peak from 7,8-BH2 without requiring sample neutralization.

Acknowledgements

I would like to thank Keith Channon, Ashley Hale and Mark Crabtree for teaching me their BH4 HPLC method, from which this assay was adapted at the National Institutes of Health (NIH). This work was funded by the NIAID Division of Intramural Research.

References

Achan, V., M. Broadhead, M. Malaki, G. Whitley, J. Leiper, R. MacAllister, and P. Vallance. 2003. Asymmetric Dimethylarginine Causes Hypertension and Cardiac Dysfunction in Humans and Is Actively Metabolized by Dimethylarginine Dimethylaminohydrolase. *Arterioscler. Thromb. Vasc. Biol.* 23:1455–1459. doi:10.1161/01.ATV.0000081742.92006.59.

Akech, S., S. Gwer, R. Idro, G. Fegan, A.C. Eziefula, C.R.J.C. Newton, M. Levin, and K. Maitland. 2006. Volume Expansion with Albumin Compared to Gelofusine in Children with Severe Malaria: Results of a Controlled Trial. *PLoS Clin. Trials.* 1:e21. doi:10.1371/journal.pctr.0010021.

Alp, N.J., S. Mussa, J. Khoo, S. Cai, T. Guzik, A. Jefferson, N. Goh, K.A. Rockett, and K.M. Channon. 2003. Tetrahydrobiopterin-dependent preservation of nitric oxide-mediated endothelial function in diabetes by targeted transgenic GTP-cyclohydrolase I overexpression. *J Clin Invest*. 112:725–35.

Amaratunga, C., S. Sreng, S. Suon, E.S. Phelps, K. Stepniewska, P. Lim, C. Zhou, S. Mao, J.M. Anderson, N. Lindegardh, H. Jiang, J. Song, X. Su, N.J. White, A.M. Dondorp, T.J. Anderson, M.P. Fay, J. Mu, S. Duong, and R.M. Fairhurst. 2012. Artemisinin-resistant Plasmodium falciparum in Pursat province, western Cambodia: a parasite clearance rate study. *Lancet Infect. Dis.* 12:851–858. doi:10.1016/S1473-3099(12)70181-0.

Anagnostou, A., E.S. Lee, N. Kessimian, R. Levinson, and M. Steiner. 1990. Erythropoietin has a mitogenic and positive chemotactic effect on endothelial cells. *Proc Natl Acad Sci U A.* 87:5978–82.

Anagnostou, A., Z. Liu, M. Steiner, K. Chin, E.S. Lee, N. Kessimian, and C.T. Noguchi. 1994. Erythropoietin receptor mRNA expression in human endothelial cells. *Proc Natl Acad Sci U A.* 91:3974–8.

Anstey, N.M., J.B. Weinberg, M.Y. Hassanali, E.D. Mwaikambo, D. Manyenga, M.A. Misukonis, D.R. Arnelle, D. Hollis, M.I. McDonald, and D.L. Granger. 1996. Nitric oxide in Tanzanian children with malaria: inverse relationship between malaria severity and nitric oxide production/nitric oxide synthase type 2 expression. *J Exp Med*. 184:557–67.

Antoniades, C., C. Shirodaria, M. Crabtree, R. Rinze, N. Alp, C. Cunnington, J. Diesch, D. Tousoulis, C. Stefanadis, P. Leeson, C. Ratnatunga, R. Pillai, and K.M. Channon. 2007. Altered plasma versus vascular biopterins in human atherosclerosis reveal relationships between endothelial nitric oxide synthase coupling, endothelial function, and inflammation. *Circulation*. 116:2851–9.

Armbruster, D.A., and T. Pry. 2008. Limit of blank, limit of detection and limit of quantitation. *Clin Biochem Rev*. 29 Suppl 1:S49–52.

Armstrong, M., K. Jonscher, and N.A. Reisdorph. 2007. Analysis of 25 underivatized amino acids in human plasma using ion-pairing reversed-phase liquid chromatography/time-of-flight mass spectrometry. *Rapid Commun Mass Spectrom*. 21:2717–26. doi:10.1002/rcm.3124.

Ashley, E.A., C.E. Sears, S.M. Bryant, H.C. Watkins, and B. Casadei. 2002. Cardiac nitric oxide synthase 1 regulates basal and beta-adrenergic contractility in murine ventricular myocytes. *Circulation*. 105:3011–6.

Baek, K.J., B.A. Thiel, S. Lucas, and D.J. Stuehr. 1993. Macrophage nitric oxide synthase subunits. Purification, characterization, and role of prosthetic groups and substrate in regulating their association into a dimeric enzyme. *J Biol Chem*. 268:21120–9.

Bajiya, H.N., and D.K. Kochar. 1996. Incidence and outcome of neurological sequelae in survivors of cerebral malaria. *J Assoc Physicians India*. 44:679–81.

Balligand, J.L., L. Kobzik, X. Han, D.M. Kaye, L. Belhassen, D.S. O'Hara, R.A. Kelly, T.W. Smith, and T. Michel. 1995. Nitric oxide-dependent parasympathetic signaling is due to activation of constitutive endothelial (type III) nitric oxide synthase in cardiac myocytes. *J Biol Chem*. 270:14582–6.

Barcus, M.J., H. Basri, H. Picarima, C. Manyakori, Sekartuti, I. Elyazar, M.J. Bangs, J.D. Maguire, and J.K. Baird. 2007. Demographic Risk Factors for Severe and Fatal Vivax and Falciparum Malaria Among Hospital Admissions in Northeastern Indonesian Papua. *Am. J. Trop. Med. Hyg.* 77:984–991.

Barnes, K.I., D.N. Durrheim, F. Little, A. Jackson, U. Mehta, E. Allen, S.S. Dlamini, J. Tsoka, B. Bredenkamp, D.J. Mthembu, N.J. White, and B.L. Sharp. 2005. Effect of Artemether-Lumefantrine Policy and Improved Vector Control on Malaria Burden in KwaZulu–Natal, South Africa. *PLoS Med*. 2:e330. doi:10.1371/journal.pmed.0020330.

Baruch, D.I., J.A. Gormely, C. Ma, R.J. Howard, and B.L. Pasloske. 1996. Plasmodium falciparum erythrocyte membrane protein 1 is a parasitized erythrocyte receptor for adherence to CD36, thrombospondin, and intercellular adhesion molecule 1. *Proc. Natl. Acad. Sci.* 93:3497–3502.

Baruch, D.I., B.L. Pasloske, H.B. Singh, X. Bi, X.C. Ma, M. Feldman, T.F. Taraschi, and R.J. Howard. 1995. Cloning the P. falciparum gene encoding PfEMP1, a malarial variant antigen and adherence receptor on the surface of parasitized human erythrocytes. *Cell*. 82:77–87. doi:10.1016/0092-8674(95)90054-3.

Baydoun, A.R., P.W. Emery, J.D. Pearson, and G.E. Mann. 1990. Substrate-dependent regulation of intracellular amino acid concentrations in cultured bovine aortic endothelial cells. *Biochem. Biophys. Res. Commun.* 173:940–948. doi:10.1016/S0006-291X(05)80876-9.

Bazzoni, G., and E. Dejana. 2004. Endothelial cell-to-cell junctions: molecular organization and role in vascular homeostasis. *Physiol Rev*. 84:869–901.

Beare, N.A., S.P. Harding, T.E. Taylor, S. Lewallen, and M.E. Molyneux. 2009. Perfusion abnormalities in children with cerebral malaria and malarial retinopathy. *J Infect Dis*. 199:263–71.

Beare, N.A., C. Southern, C. Chalira, T.E. Taylor, M.E. Molyneux, and S.P. Harding. 2004. Prognostic significance and course of retinopathy in children with severe malaria. *Arch. Ophthalmol.* 122:1141–1147. doi:10.1001/archopht.122.8.1141.

Beare, N.A., T.E. Taylor, S.P. Harding, S. Lewallen, and M.E. Molyneux. 2006. Malarial retinopathy: a newly established diagnostic sign in severe malaria. *Am J Trop Med Hyg*. 75:790–7.

Beaumier, L., L. Castillo, A.M. Ajami, and V.R. Young. 1995. Urea cycle intermediate kinetics and nitrate excretion at normal and "therapeutic" intakes of arginine in humans. *Am J Physiol*. 269:E884–96.

Beckman, J.S., T.W. Beckman, J. Chen, P.A. Marshall, and B.A. Freeman. 1990. Apparent hydroxyl radical production by peroxynitrite: implications for endothelial injury from nitric oxide and superoxide. *Proc Natl Acad Sci U A*. 87:1620–4.

Beleslin-Cokic, B.B., V.P. Cokic, X. Yu, B.B. Weksler, A.N. Schechter, and C.T. Noguchi. 2004. Erythropoietin and hypoxia stimulate erythropoietin receptor and nitric oxide production by endothelial cells. *Blood*. 104:2073–80.

Bendall, J.K., N.J. Alp, N. Warrick, S. Cai, D. Adlam, K. Rockett, M. Yokoyama, S. Kawashima, and K.M. Channon. 2005. Stoichiometric relationships between endothelial tetrahydrobiopterin, endothelial NO synthase (eNOS) activity, and eNOS coupling in vivo: insights from transgenic mice with endothelial-targeted GTP cyclohydrolase 1 and eNOS overexpression. *Circ Res*. 97:864–71.

Bendall, J.K., R. Rinze, D. Adlam, A.L. Tatham, J. de Bono, and K.M. Channon. 2007. Endothelial Nox2 Overexpression Potentiates Vascular Oxidative Stress and Hemodynamic Response to Angiotensin II Studies in Endothelial-Targeted Nox2 Transgenic Mice. *Circ. Res.* 100:1016–1025. doi:10.1161/01.RES.0000263381.83835.7b.

Benzing, A., and K. Geiger. 1994. Inhaled nitric oxide lowers pulmonary capillary pressure and changes longitudinal distribution of pulmonary vascular resistance in patients with acute lung injury. *Acta Anaesthesiol. Scand.* 38:640–645.

Berkley, J.A., I. Mwangi, F. Mellington, S. Mwarumba, and K. Marsh. 1999. Cerebral malaria versus bacterial meningitis in children with impaired consciousness. *Qjm*. 92:151–7.

Billecke, S.S. 2006. Contribution of whole blood to the control of plasma asymmetrical dimethylarginine. *AJP Heart Circ. Physiol.* 291:H1788–H1796. doi:10.1152/ajpheart.00066.2006.

BioMarin Pharmaceutical Inc. 2007. Results From Phase 2 Clinical Study Of 6R-BH4 In Poorly Controlled Hypertension.

BioMarin Pharmaceutical Inc. 2008. BioMarin Announces Positive Results From Phase 2A Clinical Study of 6R-BH4 in Sickle Cell Disease.

BioMarin Pharmaceutical Inc. 2009. Results From Phase 2 Clinical Study of 6R-BH4 in Peripheral Arterial Disease Not Statistically Significant.

Birbeck, G.L., N. Beare, S. Lewallen, S.J. Glover, M.E. Molyneux, P.W. Kaplan, and T.E. Taylor. 2010a. Identification of malaria retinopathy improves the specificity of the clinical diagnosis of cerebral malaria: findings from a prospective cohort study. *Am J Trop Med Hyg*. 82:231–4.

Birbeck, G.L., M.E. Molyneux, P.W. Kaplan, K.B. Seydel, Y.F. Chimalizeni, K. Kawaza, and T.E. Taylor. 2010b. Blantyre Malaria Project Epilepsy Study (BMPES) of neurological outcomes in retinopathy-positive paediatric cerebral malaria survivors: a prospective cohort study. *Lancet Neurol*. 9:1173–1181. doi:10.1016/S1474-4422(10)70270-2.

Bishop, M.J., B. Crow, D. Norton, E. Paliakov, J. George, and J.A. Bralley. 2007. Direct analysis of un-derivatized asymmetric dimethylarginine (ADMA) and l-arginine from plasma using mixed-mode ion-exchange liquid chromatography–tandem mass spectrometry. *J. Chromatogr. B*. 859:164–169. doi:10.1016/j.jchromb.2007.09.024.

Bivalacqua, T.J., A.L. Burnett, W.J.G. Hellstrom, and H.C. Champion. 2007. Overexpression of arginase in the aged mouse penis impairs erectile function and decreases eNOS activity: influence of in vivo gene therapy of anti-arginase. *Am. J. Physiol. - Heart Circ. Physiol.* 292:H1340–H1351. doi:10.1152/ajpheart.00121.2005.

Blackwell, S., D.S. O'Reilly, and D.K. Talwar. 2009. HPLC analysis of asymmetric dimethylarginine (ADMA) and related arginine metabolites in human plasma using a novel non-endogenous internal standard. *Clin Chim Acta*. 401:14–9. doi:10.1016/j.cca.2008.10.032.

Bode-Böger, S.M., F. Scalera, J.T. Kielstein, J. Martens-Lobenhoffer, G. Breithardt, M. Fobker, and H. Reinecke. 2006. Symmetrical Dimethylarginine: A New Combined Parameter for Renal Function and Extent of Coronary Artery Disease. *J. Am. Soc. Nephrol.* 17:1128–1134. doi:10.1681/ASN.2005101119.

Böger, R.H., S.M. Bode-Böger, A. Szuba, P.S. Tsao, J.R. Chan, O. Tangphao, T.F. Blaschke, and J.P. Cooke. 1998. Asymmetric Dimethylarginine (ADMA): A Novel Risk Factor for Endothelial Dysfunction Its Role in Hypercholesterolemia. *Circulation*. 98:1842–1847. doi:10.1161/01.CIR.98.18.1842.

Boggild, A.K., S. Krudsood, S.N. Patel, L. Serghides, N. Tangpukdee, K. Katz, P. Wilairatana, W.C. Liles, S. Looareesuwan, and K.C. Kain. 2009. Use of peroxisome proliferator-activated receptor gamma agonists as adjunctive treatment for Plasmodium falciparum malaria: a randomized, double-blind, placebo-controlled trial. *Clin Infect Dis*. 49:841–9.

Bohmer, A., B. Beckmann, J. Sandmann, and D. Tsikas. 2012. Doubts concerning functional endothelial nitric oxide synthase in human erythrocytes. *Blood*. 119:1322–3. doi:10.1182/blood-2011-11-393124.

Boivin, M.J., P. Bangirana, J. Byarugaba, R.O. Opoka, R. Idro, A.M. Jurek, and C.C. John. 2007. Cognitive impairment after cerebral malaria in children: a prospective study. *Pediatrics*. 119:e360–6.

Brewster, D.R., D. Kwiatkowski, and N.J. White. 1990. Neurological sequelae of cerebral malaria in children. *Lancet*. 336:1039–43.

Bridges, D.J., J. Bunn, J.A. van Mourik, G. Grau, R.J. Preston, M. Molyneux, V. Combes, J.S. O'Donnell, B. de Laat, and A. Craig. 2010. Rapid activation of endothelial cells enables

Plasmodium falciparum adhesion to platelet-decorated von Willebrand factor strings. *Blood*. 115:1472–4.

Brines, M., G. Grasso, F. Fiordaliso, A. Sfacteria, P. Ghezzi, M. Fratelli, R. Latini, Q.W. Xie, J. Smart, C.J. Su-Rick, E. Pobre, D. Diaz, D. Gomez, C. Hand, T. Coleman, and A. Cerami. 2004. Erythropoietin mediates tissue protection through an erythropoietin and common beta-subunit heteroreceptor. *Proc Natl Acad Sci U A*. 101:14907–12.

Brown, H., G. Turner, S. Rogerson, M. Tembo, J. Mwenechanya, M. Molyneux, and T. Taylor. 1999a. Cytokine expression in the brain in human cerebral malaria. *J Infect Dis*. 180:1742–6.

Brown, Hien, Day, Mai, Chuong, Chau, Loc, Phu, Bethell, Farrar, Gatter, White, and Turner. 1999b. Evidence of blood–brain barrier dysfunction in human cerebral malaria. *Neuropathol. Appl. Neurobiol.* 25:331–340. doi:10.1046/j.1365-2990.1999.00188.x.

Cabrales, P., G.M. Zanini, D. Meays, J.A. Frangos, and L.J. Carvalho. 2011. Nitric oxide protection against murine cerebral malaria is associated with improved cerebral microcirculatory physiology. *J Infect Dis*. 203:1454–63.

Cabrales, P., G.M. Zanini, D. Meays, J.A. Frangos, and L.J.M. Carvalho. 2010. Murine Cerebral Malaria Is Associated with a Vasospasm-Like Microcirculatory Dysfunction, and Survival upon Rescue Treatment Is Markedly Increased by Nimodipine. *Am. J. Pathol.* 176:1306–1315. doi:10.2353/ajpath.2010.090691.

Cardounel, A.J., H. Cui, A. Samouilov, W. Johnson, P. Kearns, A.L. Tsai, V. Berka, and J.L. Zweier. 2007. Evidence for the pathophysiological role of endogenous methylarginines in regulation of endothelial NO production and vascular function. *J Biol Chem*. 282:879–87. doi:10.1074/jbc.M603606200.

Cardounel, A.J., Y. Xia, and J.L. Zweier. 2005. Endogenous methylarginines modulate superoxide as well as nitric oxide generation from neuronal nitric-oxide synthase: differences in the effects of monomethyl- and dimethylarginines in the presence and absence of tetrahydrobiopterin. *J Biol Chem*. 280:7540–9.

Cardounel, A.J., and J.L. Zweier. 2002. Endogenous Methylarginines Regulate Neuronal Nitric-oxide Synthase and Prevent Excitotoxic Injury. *J. Biol. Chem.* 277:33995–34002. doi:10.1074/jbc.M108983200.

Carroll, R.W., M.S. Wainwright, K.-Y. Kim, T. Kidambi, N.D. Gómez, T. Taylor, and K. Haldar. 2010. A Rapid Murine Coma and Behavior Scale for Quantitative Assessment of Murine Cerebral Malaria. *PLoS ONE*. 5:e13124. doi:10.1371/journal.pone.0013124.

Carter, J.A., V. Mung'ala-Odera, B.G. Neville, G. Murira, N. Mturi, C. Musumba, and C.R. Newton. 2005a. Persistent neurocognitive impairments associated with severe falciparum malaria in Kenyan children. *J Neurol Neurosurg Psychiatry*. 76:476–81.

Carter, J.A., B.G. Neville, S. White, A.J. Ross, G. Otieno, N. Mturi, C. Musumba, and C.R. Newton. 2004. Increased prevalence of epilepsy associated with severe falciparum malaria in children. *Epilepsia*. 45:978–81.

Carter, J.A., A.J. Ross, B.G. Neville, E. Obiero, K. Katana, V. Mung'ala-Odera, J.A. Lees, and C.R. Newton. 2005b. Developmental impairments following severe falciparum malaria in children. *Trop Med Int Health*. 10:3–10.

Casals-Pascual, C., R. Idro, N. Gicheru, S. Gwer, B. Kitsao, E. Gitau, R. Mwakesi, D.J. Roberts, and C.R. Newton. 2008. High levels of erythropoietin are associated with protection against neurological sequelae in African children with cerebral malaria. *Proc Natl Acad Sci U A*. 105:2634–9.

Casals-Pascual, C., O. Kai, J.O. Cheung, S. Williams, B. Lowe, M. Nyanoti, T.N. Williams, K. Maitland, M. Molyneux, C.R. Newton, N. Peshu, S.M. Watt, and D.J. Roberts. 2006. Suppression of erythropoiesis in malarial anemia is associated with hemozoin in vitro and in vivo. *Blood*. 108:2569–77.

Castillo, L., L. Beaumier, A.M. Ajami, and V.R. Young. 1996. Whole body nitric oxide synthesis in healthy men determined from [15N] arginine-to-[15N]citrulline labeling. *Proc Natl Acad Sci U A*. 93:11460–5.

Castillo, L., T.E. Chapman, M. Sanchez, Y.M. Yu, J.F. Burke, A.M. Ajami, J. Vogt, and V.R. Young. 1993. Plasma arginine and citrulline kinetics in adults given adequate and arginine-free diets. *Proc Natl Acad Sci U A*. 90:7749–53.

Castillo, L., M. Sanchez, T.E. Chapman, A. Ajami, J.F. Burke, and V.R. Young. 1994. The plasma flux and oxidation rate of ornithine adaptively decline with restricted arginine intake. *Proc Natl Acad Sci U A*. 91:6393–7.

Castillo, L., M. Sanchez, J. Vogt, T.E. Chapman, T.C. DeRojas-Walker, S.R. Tannenbaum, A.M. Ajami, and V.R. Young. 1995. Plasma arginine, citrulline, and ornithine kinetics in adults, with observations on nitric oxide synthesis. *Am J Physiol*. 268:E360–7.

De Caterina, R., P. Libby, H.B. Peng, V.J. Thannickal, T.B. Rajavashisth, M.A. Gimbrone, W.S. Shin, and J.K. Liao. 1995. Nitric oxide decreases cytokine-induced endothelial activation. Nitric oxide selectively reduces endothelial expression of adhesion molecules and proinflammatory cytokines. *J Clin Invest*. 96:60–8.

Cauwels, A., E.S. Buys, R. Thoonen, L. Geary, J. Delanghe, S. Shiva, and P. Brouckaert. 2009. Nitrite protects against morbidity and mortality associated with TNF- or LPS-induced shock in a soluble guanylate cyclase-dependent manner. *J Exp Med*. 206:2915–24. doi:10.1084/jem.20091236.

Chang, K.-H., M. Tam, and M.M. Stevenson. 2004. Inappropriately low reticulocytosis in severe malarial anemia correlates with suppression in the development of late erythroid precursors. *Blood*. 103:3727–3735. doi:10.1182/blood-2003-08-2887.

Charunwatthana, P., M. Abul Faiz, R. Ruangveerayut, R.J. Maude, M.R. Rahman, L.J. Roberts 2nd, K. Moore, E. Bin Yunus, M.G. Hoque, M.U. Hasan, S.J. Lee, S. Pukrittayakamee, P.N. Newton, N.J. White, N.P.J. Day, and A.M. Dondorp. 2009. N-acetylcysteine as adjunctive treatment in severe malaria: a randomized, double-blinded placebo-controlled clinical trial. *Crit. Care Med.* 37:516–522. doi:10.1097/CCM.0b013e3181958dfd.

Cho, H.J., Q.W. Xie, J. Calaycay, R.A. Mumford, K.M. Swiderek, T.D. Lee, and C. Nathan. 1992. Calmodulin is a subunit of nitric oxide synthase from macrophages. *J. Exp. Med.* 176:599–604. doi:10.1084/jem.176.2.599.

Chotivanich, K., J. Sritabal, R. Udomsangpetch, P. Newton, K.A. Stepniewska, R. Ruangveerayuth, S. Looareesuwan, D.J. Roberts, and N.J. White. 2004. Platelet-Induced Autoagglutination of Plasmodium falciparum-Infected Red Blood Cells and Disease Severity in Thailand. *J. Infect. Dis.* 189:1052–1055. doi:10.1086/381900.

Clark, I.A., M.M. Awburn, R.O. Whitten, C.G. Harper, N.G. Liomba, M.E. Molyneux, and T.E. Taylor. 2003. Tissue distribution of migration inhibitory factor and inducible nitric oxide synthase in falciparum malaria and sepsis in African children. *Malar. J.* 2:6. doi:10.1186/1475-2875-2-6.

Clarke, J.T., and D.M. Bier. 1982. The conversion of phenylalanine to tyrosine in man. Direct measurement by continuous intravenous tracer infusions of L-[ring-2H5]phenylalanine and L-[1-13C] tyrosine in the postabsorptive state. *Metabolism*. 31:999–1005.

Closs, E.I., F.Z. Basha, A. Habermeier, and U. Forstermann. 1997. Interference of L-arginine analogues with L-arginine transport mediated by the y+ carrier hCAT-2B. *Nitric Oxide*. 1:65–73. doi:10.1006/niox.1996.0106.

Conroy, A.L., S.J. Glover, M. Hawkes, L.K. Erdman, K.B. Seydel, T.E. Taylor, M.E. Molyneux, and K.C. Kain. 2012. Angiopoietin-2 levels are associated with retinopathy and predict mortality in Malawian children with cerebral malaria: a retrospective case-control study*. *Crit. Care Med.* 40:952–959. doi:10.1097/CCM.0b013e3182373157.

Cortese-Krott, M.M., A. Rodriguez-Mateos, R. Sansone, G.G.C. Kuhnle, S. Thasian-Sivarajah, T. Krenz, P. Horn, C. Krisp, D. Wolters, C. Heiß, K.-D. Kröncke, N. Hogg, M. Feelisch, and M. Kelm. 2012. Human red blood cells at work: identification and visualization of erythrocytic eNOS activity in health and disease. *Blood*. 120:4229–4237. doi:10.1182/blood-2012-07-442277.

Cosby, K., K.S. Partovi, J.H. Crawford, R.P. Patel, C.D. Reiter, S. Martyr, B.K. Yang, M.A. Waclawiw, G. Zalos, X. Xu, K.T. Huang, H. Shields, D.B. Kim-Shapiro, A.N. Schechter, R.O. Cannon, and M.T. Gladwin. 2003. Nitrite reduction to nitric oxide by deoxyhemoglobin vasodilates the human circulation. *Nat. Med.* 9:1498–1505. doi:10.1038/nm954.

Cosentino, F., D. Hurlimann, C. Delli Gatti, R. Chenevard, N. Blau, N.J. Alp, K.M. Channon, M. Eto, P. Lerch, F. Enseleit, F. Ruschitzka, M. Volpe, T.F. Luscher, and G. Noll. 2008. Chronic treatment with tetrahydrobiopterin reverses endothelial dysfunction and oxidative stress in hypercholesterolaemia. *Heart*. 94:487–92. doi:10.1136/hrt.2007.122184.

Cot, S., P. Ringwald, B. Mulder, P. Miailhes, J. Yap-Yap, A.K. Nussler, and W.M. Eling. 1994. Nitric oxide in cerebral malaria. *J. Infect. Dis.* 169:1417–1418.

Crabtree, M.J., C.L. Smith, G. Lam, M.S. Goligorsky, and S.S. Gross. 2008. Ratio of 5,6,7,8-tetrahydrobiopterin to 7,8-dihydrobiopterin in endothelial cells determines glucose-elicited changes in NO vs. superoxide production by eNOS. *Am J Physiol Heart Circ Physiol*. 294:H1530–40. doi:10.1152/ajpheart.00823.2007.

Crabtree, M.J., A.L. Tatham, A.B. Hale, N.J. Alp, and K.M. Channon. 2009a. Critical role for tetrahydrobiopterin recycling by dihydrofolate reductase in regulation of endothelial nitric-oxide synthase coupling: relative importance of the de novo biopterin synthesis versus salvage pathways. *J Biol Chem*. 284:28128–36.

Crabtree, M.J., A.L. Tatham, Y. Al-Wakeel, N. Warrick, A.B. Hale, S. Cai, K.M. Channon, and N.J. Alp. 2009b. Quantitative regulation of intracellular endothelial nitric-oxide synthase (eNOS) coupling by both tetrahydrobiopterin-eNOS stoichiometry and biopterin redox status: insights from cells with tet-regulated GTP cyclohydrolase I expression. *J Biol Chem*. 284:1136–44. doi:10.1074/jbc.M805403200.

Crane, B.R., A.S. Arvai, D.K. Ghosh, C. Wu, E.D. Getzoff, D.J. Stuehr, and J.A. Tainer. 1998. Structure of nitric oxide synthase oxygenase dimer with pterin and substrate. *Science*. 279:2121–6.

Crawley, J., S. Smith, F. Kirkham, P. Muthinji, C. Waruiru, and K. Marsh. 1996. Seizures and status epilepticus in childhood cerebral malaria. *Qjm*. 89:591–7.

Crawley, J., S. Smith, P. Muthinji, K. Marsh, and F. Kirkham. 2001. Electroencephalographic and clinical features of cerebral malaria. *Arch Child*. 84:247–53.

Crawley, J., C. Waruiru, S. Mithwani, I. Mwangi, W. Watkins, D. Ouma, P. Winstanley, T. Peto, and K. Marsh. 2000. Effect of phenobarbital on seizure frequency and mortality in childhood cerebral malaria: a randomised, controlled intervention study. *The Lancet*. 355:701–706. doi:10.1016/S0140-6736(99)07148-2.

Cromer, D., K.J. Evans, L. Schofield, and M.P. Davenport. 2006. Preferential invasion of reticulocytes during late-stage Plasmodium berghei infection accounts for reduced circulating reticulocyte levels. *Int. J. Parasitol.* 36:1389–1397. doi:10.1016/j.ijpara.2006.07.009.

Cunnington, C., T. Van Assche, C. Shirodaria, I. Kylintireas, A.C. Lindsay, J.M. Lee, C. Antoniades, M. Margaritis, R. Lee, R. Cerrato, M.J. Crabtree, J.M. Francis, R. Sayeed, C. Ratnatunga, R. Pillai, R.P. Choudhury, S. Neubauer, and K.M. Channon. 2012. Systemic and Vascular Oxidation Limits Efficacy of Oral Tetrahydrobiopterin Treatment in Patients with Coronary Artery Disease. *Circulation*. doi:10.1161/CIRCULATIONAHA.111.038919.

Curtius, H.C., D. Heintel, S. Ghisla, T. Kuster, W. Leimbacher, and A. Niederwieser. 1985. Tetrahydrobiopterin biosynthesis. Studies with specifically labeled (2H)NAD(P)H and 2H2O and of the enzymes involved. *Eur J Biochem*. 148:413–9.

Daff, S. 2010. NO synthase: structures and mechanisms. *Nitric Oxide*. 23:1–11. doi:10.1016/j.niox.2010.03.001.

Das, B.K., S. Mishra, P.K. Padhi, R. Manish, R. Tripathy, P.K. Sahoo, and B. Ravindran. 2003. Pentoxifylline adjunct improves prognosis of human cerebral malaria in adults. *Trop. Med. Int. Health*. 8:680–684. doi:10.1046/j.1365-3156.2003.01087.x.

Davids, M., A.J. van Hell, M. Visser, R.J. Nijveldt, P.A.M. van Leeuwen, and T. Teerlink. 2012a. Role of the human erythrocyte in generation and storage of asymmetric dimethylarginine. *AJP Heart Circ. Physiol.* 302:H1762–H1770. doi:10.1152/ajpheart.01205.2011.

Davids, M., M.C. Richir, M. Visser, B. Ellger, G. van den Berghe, P.A.M. van Leeuwen, and T. Teerlink. 2012b. Role of dimethylarginine dimethylaminohydrolase activity in regulation of tissue and plasma concentrations of asymmetric dimethylarginine in an animal model of prolonged critical illness. *Metabolism*. 61:482–490. doi:10.1016/j.metabol.2011.08.007.

Day, N.P., T.T. Hien, T. Schollaardt, P.P. Loc, L.V. Chuong, T.T. Chau, N.T. Mai, N.H. Phu, D.X. Sinh, N.J. White, and M. Ho. 1999. The prognostic and pathophysiologic role of pro- and antiinflammatory cytokines in severe malaria. *J Infect Dis*. 180:1288–97.

Day, N.P., N.H. Phu, N.T. Mai, T.T. Chau, P.P. Loc, L.V. Chuong, D.X. Sinh, P. Holloway, T.T. Hien, and N.J. White. 2000. The pathophysiologic and prognostic significance of acidosis in severe adult malaria. *Crit Care Med*. 28:1833–40.

Dayoub, H., V. Achan, S. Adimoolam, J. Jacobi, M.C. Stuehlinger, B. Wang, P.S. Tsao, M. Kimoto, P. Vallance, A.J. Patterson, and J.P. Cooke. 2003. Dimethylarginine Dimethylaminohydrolase Regulates Nitric Oxide Synthesis Genetic and Physiological Evidence. *Circulation*. 108:3042–3047. doi:10.1161/01.CIR.0000101924.04515.2E.

Dey, S., S. Bindu, M. Goyal, C. Pal, A. Alam, M.S. Iqbal, R. Kumar, S. Sarkar, and U. Bandyopadhyay. 2012. Impact of Intravascular Hemolysis in Malaria on Liver Dysfunction INVOLVEMENT OF HEPATIC FREE HEME OVERLOAD, NF-κB ACTIVATION, AND NEUTROPHIL INFILTRATION. *J. Biol. Chem.* 287:26630–26646. doi:10.1074/jbc.M112.341255.

Diehl, K.-H., R. Hull, D. Morton, R. Pfister, Y. Rabemampianina, D. Smith, J.-M. Vidal, and C.V.D. Vorstenbosch. 2001. A good practice guide to the administration of substances and removal of blood, including routes and volumes. *J. Appl. Toxicol.* 21:15–23. doi:10.1002/jat.727.

Dittrich, S., S.L. Mitchell, A.M. Blagborough, Q. Wang, P. Wang, P.F. Sims, and J.E. Hyde. 2008. An atypical orthologue of 6-pyruvoyltetrahydropterin synthase can provide the missing link in the folate biosynthesis pathway of malaria parasites. *Mol Microbiol*. 67:609–18. doi:10.1111/j.1365-2958.2007.06073.x.

Dixon, S.J., and B.R. Stockwell. 2014. The role of iron and reactive oxygen species in cell death. *Nat. Chem. Biol.* 10:9–17. doi:10.1038/nchembio.1416.

Dobbie, M., J. Crawley, C. Waruiru, K. Marsh, and R. Surtees. 2000. Cerebrospinal fluid studies in children with cerebral malaria: an excitotoxic mechanism? *Am J Trop Med Hyg*. 62:284–90.

Dondorp, A., F. Nosten, K. Stepniewska, N. Day, and N. White. 2005. Artesunate versus quinine for treatment of severe falciparum malaria: a randomised trial. *Lancet*. 366:717–25.

Dondorp, A.M., B.J. Angus, M.R. Hardeman, K.T. Chotivanich, K. Silamut, R. Ruangveerayuth, P.A. Kager, N.J. White, and J. Vreeken. 1997. Prognostic significance of reduced red blood cell deformability in severe falciparum malaria. *Am J Trop Med Hyg*. 57:507–11.

Dondorp, A.M., C.I. Fanello, I.C. Hendriksen, E. Gomes, A. Seni, K.D. Chhaganlal, K. Bojang, R. Olaosebikan, N. Anunobi, K. Maitland, E. Kivaya, T. Agbenyega, S.B. Nguah, J.

Evans, S. Gesase, C. Kahabuka, G. Mtove, B. Nadjm, J. Deen, J. Mwanga-Amumpaire, M. Nansumba, C. Karema, N. Umulisa, A. Uwimana, O.A. Mokuolu, O.T. Adedoyin, W.B. Johnson, A.K. Tshefu, M.A. Onyamboko, T. Sakulthaew, W.P. Ngum, K. Silamut, K. Stepniewska, C.J. Woodrow, D. Bethell, B. Wills, M. Oneko, T.E. Peto, L. von Seidlein, N.P. Day, and N.J. White. 2010. Artesunate versus quinine in the treatment of severe falciparum malaria in African children (AQUAMAT): an open-label, randomised trial. *Lancet*. 376:1647–57.

Dondorp, A.M., C. Ince, P. Charunwatthana, J. Hanson, A. van Kuijen, M.A. Faiz, M.R. Rahman, M. Hasan, E.B. Yunus, A. Ghose, R. Ruangveerayut, D. Limmathurotsakul, K. Mathura, N.J. White, and N.P.J. Day. 2008a. Direct In Vivo Assessment of Microcirculatory Dysfunction in Severe Falciparum Malaria. *J. Infect. Dis.* 197:79–84. doi:10.1086/523762.

Dondorp, A.M., P.A. Kager, J. Vreeken, and N.J. White. 2000. Abnormal blood flow and red blood cell deformability in severe malaria. *Parasitol Today*. 16:228–32.

Dondorp, A.M., S.J. Lee, M.A. Faiz, S. Mishra, R. Price, E. Tjitra, M. Than, Y. Htut, S. Mohanty, E.B. Yunus, R. Rahman, F. Nosten, N.M. Anstey, N.P.J. Day, and N.J. White. 2008b. The Relationship between Age and the Manifestations of and Mortality Associated with Severe Malaria. *Clin. Infect. Dis.* 47:151–157. doi:10.1086/589287.

Dondorp, A.M., F. Nosten, P. Yi, D. Das, A.P. Phyo, J. Tarning, K.M. Lwin, F. Ariey, W. Hanpithakpong, S.J. Lee, P. Ringwald, K. Silamut, M. Imwong, K. Chotivanich, P. Lim, T. Herdman, S.S. An, S. Yeung, P. Singhasivanon, N.P. Day, N. Lindegardh, D. Socheat, and N.J. White. 2009. Artemisinin resistance in Plasmodium falciparum malaria. *N Engl J Med*. 361:455–67.

Dondorp, A.M., E. Pongponratn, and N.J. White. 2004. Reduced microcirculatory flow in severe falciparum malaria: pathophysiology and electron-microscopic pathology. *Acta Trop*. 89:309–17.

Dondorp, A.M., K. Silamut, P. Charunwatthana, S. Chuasuwanchai, R. Ruangveerayut, S. Krintratun, N.J. White, M. Ho, and N.P.J. Day. 2007. Levamisole Inhibits Sequestration of Infected Red Blood Cells in Patients with Falciparum Malaria. *J. Infect. Dis.* 196:460–466. doi:10.1086/519287.

Dorovini-Zis, K., K. Schmidt, H. Huynh, W. Fu, R.O. Whitten, D. Milner, S. Kamiza, M. Molyneux, and T.E. Taylor. 2011. The neuropathology of fatal cerebral malaria in malawian children. *Am. J. Pathol.* 178:2146–2158. doi:10.1016/j.ajpath.2011.01.016.

Dowling, D.P., M. Ilies, K.L. Olszewski, S. Portugal, M.M. Mota, M. Llinas, and D.W. Christianson. 2010. Crystal structure of arginase from Plasmodium falciparum and implications for L-arginine depletion in malarial infection. *Biochemistry (Mosc.)*. 49:5600–8.

Druhan, L.J., S.P. Forbes, A.J. Pope, C.A. Chen, J.L. Zweier, and A.J. Cardounel. 2008. Regulation of eNOS-derived superoxide by endogenous methylarginines. *Biochemistry (Mosc.)*. 47:7256–63.

Du, Y.H., Y.Y. Guan, N.J. Alp, K.M. Channon, and A.F. Chen. 2008. Endothelium-specific GTP cyclohydrolase I overexpression attenuates blood pressure progression in salt-

sensitive low-renin hypertension. *Circulation*. 117:1045–54. doi:10.1161/CIRCULATIONAHA.107.748236.

Duranski, M.R., J.J. Greer, A. Dejam, S. Jaganmohan, N. Hogg, W. Langston, R.P. Patel, S.F. Yet, X. Wang, C.G. Kevil, M.T. Gladwin, and D.J. Lefer. 2005. Cytoprotective effects of nitrite during in vivo ischemia-reperfusion of the heart and liver. *J Clin Invest*. 115:1232–40. doi:10.1172/JCI22493.

El-Khoury, J., D. Bunch, E. Reineks, R. Jackson, R. Steinle, and S. Wang. 2012. A simple and fast liquid chromatography-tandem mass spectrometry method for measurement of underivatized l-arginine, symmetric dimethylarginine, and asymmetric dimethylarginine and establishment of the reference ranges. *Anal. Bioanal. Chem.* 402:771–779. doi:10.1007/s00216-011-5462-9.

Enayati, A., and J. Hemingway. 2010. Malaria Management: Past, Present, and Future. *Annu. Rev. Entomol.* 55:569–591. doi:10.1146/annurev-ento-112408-085423.

Enwonwu, C.O., B.M. Afolabi, L.A. Salako, E.O. Idigbe, H. Al-Hassan, and R.A. Rabiu. 1999. Hyperphenylalaninaemia in children with falciparum malaria. *QJM*. 92:495–503. doi:10.1093/qjmed/92.9.495.

Enwonwu, C.O., B.M. Afolabi, L.O. Salako, E.O. Idigbe, and N. Bashirelah. 2000. Increased plasma levels of histidine and histamine in falciparum malaria: relevance to severity of infection. *J Neural Transm*. 107:1273–87.

Erez, A., S.C. Nagamani, O.A. Shchelochkov, M.H. Premkumar, P.M. Campeau, Y. Chen, H.K. Garg, L. Li, A. Mian, T.K. Bertin, J.O. Black, H. Zeng, Y. Tang, A.K. Reddy, M. Summar, W.E. O'Brien, D.G. Harrison, W.E. Mitch, J.C. Marini, J.L. Aschner, N.S. Bryan, and B. Lee. 2011. Requirement of argininosuccinate lyase for systemic nitric oxide production. *Nat Med*. 17:1619–26. doi:10.1038/nm.2544.

Fan, Q., J. Miao, L. Cui, and L. Cui. 2009. Characterization of PRMT1 from Plasmodium falciparum. *Biochem J*. 421:107–18.

Feachem, R.G., A.A. Phillips, G.A. Targett, and R.W. Snow. 2010. Call to action: priorities for malaria elimination. *The Lancet*. 376:1517–1521. doi:10.1016/S0140-6736(10)61500-0.

Fiedler, U., Y. Reiss, M. Scharpfenecker, V. Grunow, S. Koidl, G. Thurston, N.W. Gale, M. Witzenrath, S. Rosseau, N. Suttorp, A. Sobke, M. Herrmann, K.T. Preissner, P. Vajkoczy, and H.G. Augustin. 2006. Angiopoietin-2 sensitizes endothelial cells to TNF-alpha and has a crucial role in the induction of inflammation. *Nat Med*. 12:235–9. doi:10.1038/nm1351.

Fiedler, U., M. Scharpfenecker, S. Koidl, A. Hegen, V. Grunow, J.M. Schmidt, W. Kriz, G. Thurston, and H.G. Augustin. 2004. The Tie-2 ligand angiopoietin-2 is stored in and rapidly released upon stimulation from endothelial cell Weibel-Palade bodies. *Blood*. 103:4150–6. doi:10.1182/blood-2003-10-3685.

Flam, B.R., P.J. Hartmann, M. Harrell-Booth, L.P. Solomonson, and D.C. Eichler. 2001. Caveolar Localization of Arginine Regeneration Enzymes, Argininosuccinate Synthase, and Lyase, with Endothelial Nitric Oxide Synthase. *Nitric Oxide*. 5:187–197. doi:10.1006/niox.2001.0340.

Förstermann, U., E.I. Closs, J.S. Pollock, M. Nakane, P. Schwarz, I. Gath, and H. Kleinert. 1994. Nitric oxide synthase isozymes. Characterization, purification, molecular cloning, and functions. *Hypertension*. 23:1121–1131. doi:10.1161/01.HYP.23.6.1121.

Francischetti, I.M.B., K.B. Seydel, R.Q. Monteiro, R.O. Whitten, C.R. Erexson, A.L.L. Noronha, G.R. Ostera, S.B. Kamiza, M.E. Molyneux, J.M. Ward, and T.E. Taylor. 2007. Plasmodium falciparum-infected erythrocytes induce tissue factor expression in endothelial cells and support the assembly of multimolecular coagulation complexes. *J. Thromb. Haemost.* 5:155–165. doi:10.1111/j.1538-7836.2006.02232.x.

Freedman, J.E., and J. Loscalzo. 2003. Nitric oxide and its relationship to thrombotic disorders. *J Thromb Haemost*. 1:1183–8.

Fukushima, T., and J.C. Nixon. 1980. Analysis of reduced forms of biopterin in biological tissues and fluids. *Anal. Biochem.* 102:176–188. doi:10.1016/0003-2697(80)90336-X.

Fulton, D., J.-P. Gratton, T.J. McCabe, J. Fontana, Y. Fujio, K. Walsh, T.F. Franke, A. Papapetropoulos, and W.C. Sessa. 1999. Regulation of endothelium-derived nitric oxide production by the protein kinase Akt. *Nature*. 399:597–601. doi:10.1038/21218.

Gamble, J.R., J. Drew, L. Trezise, A. Underwood, M. Parsons, L. Kasminkas, J. Rudge, G. Yancopoulos, and M.A. Vadas. 2000. Angiopoietin-1 Is an Antipermeability and Anti-Inflammatory Agent In Vitro and Targets Cell Junctions. *Circ. Res.* 87:603–607. doi:10.1161/01.RES.87.7.603.

Gardner, J.P., R.A. Pinches, D.J. Roberts, and C.I. Newbold. 1996. Variant antigens and endothelial receptor adhesion in Plasmodium falciparum. *Proc. Natl. Acad. Sci.* 93:3503–3508.

Gervasoni, J., F. Bonelli, C. Zuppi, B. Zappacosta, A. Mordente, R. Calvani, and S. Persichilli. 2011. Determination of asymmetric dimethyl arginine in human serum by liquid chromatography-tandem mass spectrometry: clinical application in hypertensive subjects. *Clin. Chem. Lab. Med.* 49:2109–2115. doi:10.1515/CCLM.2011.691.

Gething, P.W., A.P. Patil, D.L. Smith, C.A. Guerra, I.R. Elyazar, G.L. Johnston, A.J. Tatem, and S.I. Hay. 2011. A new world malaria map: Plasmodium falciparum endemicity in 2010. *Malar. J.* 10:378. doi:10.1186/1475-2875-10-378.

Gimenez, F., S. Barraud de Lagerie, C. Fernandez, P. Pino, and D. Mazier. 2003. Tumor necrosis factor alpha in the pathogenesis of cerebral malaria. *Cell Mol Life Sci*. 60:1623–35.

Glenister, F.K., R.L. Coppel, A.F. Cowman, N. Mohandas, and B.M. Cooke. 2002. Contribution of parasite proteins to altered mechanical properties of malaria-infected red blood cells. *Blood*. 99:1060–3.

Gomes, M., M. Faiz, J. Gyapong, M. Warsame, T. Agbenyega, A. Babiker, F. Baiden, E. Yunus, F. Binka, C. Clerk, P. Folb, R. Hassan, M. Hossain, O. Kimbute, A. Kitua, S. Krishna, C. Makasi, N. Mensah, Z. Mrango, P. Olliaro, R. Peto, T. Peto, M. Rahman, I. Ribeiro, R. Samad, and N. White. 2009. Pre-referral rectal artesunate to prevent death and disability in severe malaria: a placebo-controlled trial. *The Lancet*. 373:557–566. doi:10.1016/S0140-6736(08)61734-1.

Gordeuk, V., P. Thuma, G. Brittenham, C. McLaren, D. Parry, A. Backenstose, G. Biemba, R. Msiska, L. Holmes, E. McKinley, L. Vargas, R. Gilkeson, and A.A. Poltera. 1992. Effect of Iron Chelation Therapy on Recovery from Deep Coma in Children with Cerebral Malaria. *N. Engl. J. Med.* 327:1473–1477. doi:10.1056/NEJM199211193272101.

Gramaglia, I., P. Sobolewski, D. Meays, R. Contreras, J.P. Nolan, J.A. Frangos, M. Intaglietta, and H.C. van der Heyde. 2006. Low nitric oxide bioavailability contributes to the genesis of experimental cerebral malaria. *Nat Med*. 12:1417–22.

Grassi, B., A. Bignami, and G. Bastianelli. 1899. Ulteriore ricerche sul ciclo dei parassiti malarici umani sul corpo del zanzarone. *Atti R. Accad Lincei*. 8:21–28.

Grau, G.E., L.F. Fajardo, P.F. Piguet, B. Allet, P.H. Lambert, and P. Vassalli. 1987. Tumor necrosis factor (cachectin) as an essential mediator in murine cerebral malaria. *Science*. 237:1210–2.

Grau, G.E., C.D. Mackenzie, R.A. Carr, M. Redard, G. Pizzolato, C. Allasia, C. Cataldo, T.E. Taylor, and M.E. Molyneux. 2003. Platelet Accumulation in Brain Microvessels in Fatal Pediatric Cerebral Malaria. *J. Infect. Dis.* 187:461–466.

Grau, G.E., T.E. Taylor, M.E. Molyneux, J.J. Wirima, P. Vassalli, M. Hommel, and P.H. Lambert. 1989. Tumor necrosis factor and disease severity in children with falciparum malaria. *N Engl J Med*. 320:1586–91.

Gray, C., and A. Craig. 2002. Fibrinogen binding to intercellular adhesion molecule 1: implications for Plasmodium falciparum adhesion. *Infect Immun*. 70:3962–4.

Griffiths, M.J., F. Ndungu, K.L. Baird, D.P. Muller, K. Marsh, and C.R. Newton. 2001. Oxidative stress and erythrocyte damage in Kenyan children with severe Plasmodium falciparum malaria. *Br J Haematol*. 113:486–91.

Guidelines for the Management of Malaria. 2005. Ministry of Health and Social Welfare, Banjul, The Gambia.

Haldar, K., S.C. Murphy, D.A. Milner, and T.E. Taylor. 2007. Malaria: Mechanisms of Erythrocytic Infection and Pathological Correlates of Severe Disease. *Annu. Rev. Pathol. Mech. Dis.* 2:217–249. doi:10.1146/annurev.pathol.2.010506.091913.

Hanson, J., S.W.K. Lam, K.C. Mahanta, R. Pattnaik, S. Alam, S. Mohanty, M.U. Hasan, A. Hossain, P. Charunwatthana, K. Chotivanich, R.J. Maude, H. Kingston, N.P. Day, S. Mishra, N.J. White, and A.M. Dondorp. 2012. Relative Contributions of Macrovascular and Microvascular Dysfunction to Disease Severity in Falciparum Malaria. *J. Infect. Dis.* 206:571–579. doi:10.1093/infdis/jis400.

Hanson, J., S.J. Lee, S. Mohanty, M.A. Faiz, N.M. Anstey, P. kaew Charunwatthana, E.B. Yunus, S.K. Mishra, E. Tjitra, R.N. Price, R. Rahman, F. Nosten, Y. Htut, G. Hoque, T.T.H. Chau, N.H. Phu, T.T. Hien, N.J. White, N.P.J. Day, and A.M. Dondorp. 2010. A Simple Score to Predict the Outcome of Severe Malaria in Adults. *Clin. Infect. Dis.* 50:679–685. doi:10.1086/649928.

Hanson, J.P.M., S.W.K.M. Lam, S. Mohanty, S. Alam, R.M. Pattnaik, K.C. Mahanta, M.U. Hasan, P. Charunwatthana, S.K. Mishra, N.P.J. Day, N.J. White, and A.M. Dondorp.

2013. Fluid Resuscitation of Adults With Severe Falciparum Malaria: Effects on Acid-Base Status, Renal Function, and Extravascular Lung Water*. *Crit. Care Med. April 2013*. 41:972–981. doi:10.1097/CCM.0b013e31827466d2.

Harada, T., H. Kagamiyama, and K. Hatakeyama. 1993. Feedback regulation mechanisms for the control of GTP cyclohydrolase I activity. *Science*. 260:1507–10.

Hartwig, C.L., A.S. Rosenthal, J. D'Angelo, C.E. Griffin, G.H. Posner, and R.A. Cooper. 2009. Accumulation of artemisinin trioxane derivatives within neutral lipids of Plasmodium falciparum malaria parasites is endoperoxide-dependent. *Biochem. Pharmacol.* 77:322–336. doi:10.1016/j.bcp.2008.10.015.

Hattori, Y., S. Hattori, X. Wang, H. Satoh, N. Nakanishi, and K. Kasai. 2007. Oral administration of tetrahydrobiopterin slows the progression of atherosclerosis in apolipoprotein E-knockout mice. *Arter. Thromb Vasc Biol*. 27:865–70. doi:10.1161/01.ATV.0000258946.55438.0e.

Havlik, I., S. Looareesuwan, S. Vannaphan, P. Wilairatana, S. Krudsood, P.E. Thuma, D. Kozbor, N. Watanabe, and Y. Kaneko. 2005. Curdlan sulphate in human severe/cerebral Plasmodium falciparum malaria. *Trans. R. Soc. Trop. Med. Hyg.* 99:333–340. doi:10.1016/j.trstmh.2004.05.005.

Heitzer, T., K. Krohn, S. Albers, and T. Meinertz. 2000. Tetrahydrobiopterin improves endothelium-dependent vasodilation by increasing nitric oxide activity in patients with Type II diabetes mellitus. *Diabetologia*. 43:1435–8. doi:10.1007/s001250051551.

Van Hensbroek, M.B., E. Onyiorah, S. Jaffar, G. Schneider, A. Palmer, J. Frenkel, G. Enwere, S. Forck, A. Nusmeijer, S. Bennett, B. Greenwood, and D. Kwiatkowski. 1996a. A trial of artemether or quinine in children with cerebral malaria. *N Engl J Med*. 335:69–75.

Van Hensbroek, M.B., A. Palmer, S. Jaffar, G. Schneider, and D. Kwiatkowski. 1997. Residual neurologic sequelae after childhood cerebral malaria. *J Pediatr*. 131:125–9.

Van Hensbroek, M.B., A. Palmer, E. Onyiorah, G. Schneider, S. Jaffar, G. Dolan, H. Memming, J. Frenkel, G. Enwere, S. Bennett, D. Kwiatkowski, and B. Greenwood. 1996b. The effect of a monoclonal antibody to tumor necrosis factor on survival from childhood cerebral malaria. *J Infect Dis*. 174:1091–7.

Heresztyn, T., M.I. Worthley, and J.D. Horowitz. 2004. Determination of l-arginine and NG,NG- and NG,NG′-dimethyl-l-arginine in plasma by liquid chromatography as AccQ-Fluor™ fluorescent derivatives. *J. Chromatogr. B.* 805:325–329. doi:10.1016/j.jchromb.2004.03.020.

Higashi, Y., S. Sasaki, K. Nakagawa, Y. Fukuda, H. Matsuura, T. Oshima, and K. Chayama. 2002. Tetrahydrobiopterin enhances forearm vascular response to acetylcholine in both normotensive and hypertensive individuals. *Am J Hypertens*. 15:326–32.

Ho, M., H.L. Hoang, K.M. Lee, N. Liu, T. MacRae, L. Montes, C.L. Flatt, B.G. Yipp, B.J. Berger, S. Looareesuwan, and S.M. Robbins. 2005. Ectophosphorylation of CD36 regulates cytoadherence of Plasmodium falciparum to microvascular endothelium under flow conditions. *Infect. Immun.* 73:8179–8187. doi:10.1128/IAI.73.12.8179-8187.2005.

Hoffman, S.L., D. Rustama, N.H. Punjabi, B. Surampaet, B. Sanjaya, A.J. Dimpudus, K.T. McKee, F.P. Paleologo, J.R. Campbell, H. Marwoto, and L. Laughlin. 1988. High-Dose Dexamethasone in Quinine-Treated Patients with Cerebral Malaria: A Double-Blind, Placebo-Controlled Trial. *J. Infect. Dis.* 158:325–331. doi:10.1093/infdis/158.2.325.

Hollestelle, M.J., C. Donkor, E.A. Mantey, S.J. Chakravorty, A. Craig, A.O. Akoto, J. O'Donnell, J.A. van Mourik, and J. Bunn. 2006. von Willebrand factor propeptide in malaria: evidence of acute endothelial cell activation. *Br J Haematol*. 133:562–9.

Howells, D.W., and K. Hyland. 1987. Direct analysis of tetrahydrobiopterin in cerebrospinal fluid by high-performance liquid chromatography with redox electrochemistry: Prevention of autoxidation during storage and analysis. *Clin. Chim. Acta*. 167:23–30. doi:10.1016/0009-8981(87)90081-7.

Hu, T., M. Chouinard, A.L. Cox, P. Sipes, M. Marcelo, J. Ficorilli, S. Li, H. Gao, T.P. Ryan, M.D. Michael, and L.F. Michael. 2006. Farnesoid X Receptor Agonist Reduces Serum Asymmetric Dimethylarginine Levels through Hepatic Dimethylarginine Dimethylaminohydrolase-1 Gene Regulation. *J. Biol. Chem.* 281:39831–39838. doi:10.1074/jbc.M606779200.

Hu, X., X. Xu, G. Zhu, D. Atzler, M. Kimoto, J. Chen, E. Schwedhelm, N. Lüneburg, R.H. Böger, P. Zhang, and Y. Chen. 2009. Vascular Endothelial-Specific Dimethylarginine Dimethylaminohydrolase-1–Deficient Mice Reveal That Vascular Endothelium Plays an Important Role in Removing Asymmetric Dimethylarginine. *Circulation*. 120:2222–2229. doi:10.1161/CIRCULATIONAHA.108.819912.

Huang, Z., S. Shiva, D.B. Kim-Shapiro, R.P. Patel, L.A. Ringwood, C.E. Irby, K.T. Huang, C. Ho, N. Hogg, A.N. Schechter, and M.T. Gladwin. 2005. Enzymatic function of hemoglobin as a nitrite reductase that produces NO under allosteric control. *J Clin Invest*. 115:2099–107.

Hunt, N.H., and G.E. Grau. 2003. Cytokines: accelerators and brakes in the pathogenesis of cerebral malaria. *Trends Immunol*. 24:491–9.

Hurshman, A.R., C. Krebs, D.E. Edmondson, B.H. Huynh, and M.A. Marletta. 1999. Formation of a pterin radical in the reaction of the heme domain of inducible nitric oxide synthase with oxygen. *Biochemistry (Mosc.)*. 38:15689–96.

Hyland, K. 1985. Estimation of tetrahydro, dihydro and fully oxidised pterins by high-performance liquid chromatography using sequential electrochemical and fluorometric detection. *J. Chromatogr. B. Biomed. Sci. App.* 343:35–41. doi:10.1016/S0378-4347(00)84565-X.

Idro, R., N.E. Jenkins, and C.R. Newton. 2005. Pathogenesis, clinical features, and neurological outcome of cerebral malaria. *Lancet Neurol*. 4:827–40.

Idro, R., M. Ndiritu, B. Ogutu, S. Mithwani, K. Maitland, J. Berkley, J. Crawley, G. Fegan, E. Bauni, N. Peshu, K. Marsh, B. Neville, and C. Newton. 2007. Burden, features, and outcome of neurological involvement in acute falciparum malaria in Kenyan children. *Jama*. 297:2232–40.

Iuvone, T., F. D'Acquisto, R. Carnuccio, and M. Di Rosa. 1996. Nitric oxide inhibits LPS-induced tumor necrosis factor synthesis in vitro and in vivo. *Life Sci*. 59:PL207–11.

Jacobi, J., K. Sydow, G. von Degenfeld, Y. Zhang, H. Dayoub, B. Wang, A.J. Patterson, M. Kimoto, H.M. Blau, and J.P. Cooke. 2005. Overexpression of Dimethylarginine Dimethylaminohydrolase Reduces Tissue Asymmetric Dimethylarginine Levels and Enhances Angiogenesis. *Circulation*. 111:1431–1438. doi:10.1161/01.CIR.0000158487.80483.09.

Jain, V., A.C. Nagpal, P.K. Joel, M. Shukla, M.P. Singh, R.B. Gupta, A.P. Dash, S.K. Mishra, V. Udhayakumar, J.K. Stiles, and N. Singh. 2008. Burden of cerebral malaria in central India (2004-2007). *Am J Trop Med Hyg*. 79:636–42.

Jakeman, G.N., A. Saul, W.L. Hogarth, and W.E. Collins. 1999. Anaemia of acute malaria infections in non-immune patients primarily results from destruction of uninfected erythrocytes. *Parasitology*. 119:127–133.

Jallow, M., Y.Y. Teo, K.S. Small, K.A. Rockett, P. Deloukas, T.G. Clark, K. Kivinen, K.A. Bojang, D.J. Conway, M. Pinder, G. Sirugo, F. Sisay-Joof, S. Usen, S. Auburn, S.J. Bumpstead, S. Campino, A. Coffey, A. Dunham, A.E. Fry, A. Green, R. Gwilliam, S.E. Hunt, M. Inouye, A.E. Jeffreys, A. Mendy, A. Palotie, S. Potter, J. Ragoussis, J. Rogers, K. Rowlands, E. Somaskantharajah, P. Whittaker, C. Widden, P. Donnelly, B. Howie, J. Marchini, A. Morris, M. SanJoaquin, E.A. Achidi, T. Agbenyega, A. Allen, O. Amodu, P. Corran, A. Djimde, A. Dolo, O.K. Doumbo, C. Drakeley, S. Dunstan, J. Evans, J. Farrar, D. Fernando, T.T. Hien, R.D. Horstmann, M. Ibrahim, N. Karunaweera, G. Kokwaro, K.A. Koram, M. Lemnge, J. Makani, K. Marsh, P. Michon, D. Modiano, M.E. Molyneux, I. Mueller, M. Parker, N. Peshu, C.V. Plowe, O. Puijalon, J. Reeder, H. Reyburn, E.M. Riley, A. Sakuntabhai, P. Singhasivanon, S. Sirima, A. Tall, T.E. Taylor, M. Thera, M. Troye-Blomberg, T.N. Williams, M. Wilson, and D.P. Kwiatkowski. 2009. Genome-wide and fine-resolution association analysis of malaria in West Africa. *Nat. Genet.* 41:657–665. doi:10.1038/ng.388.

Janka, J.J., O.A. Koita, B. Traore, J.M. Traore, F. Mzayek, V. Sachdev, X. Wang, K. Sanogo, L. Sangare, L. Mendelsohn, H. Masur, G.J. Kato, M.T. Gladwin, and D.J. Krogstad. 2010. Increased pulmonary pressures and myocardial wall stress in children with severe malaria. *J Infect Dis*. 202:791–800. doi:10.1086/655225.

Janse, C.J., B. Franke-Fayard, and A.P. Waters. 2006. Selection by flow-sorting of genetically transformed, GFP-expressing blood stages of the rodent malaria parasite, Plasmodium berghei. *Nat Protoc*. 1:614–23. doi:10.1038/nprot.2006.88.

Jarvis, J.N., T. Planche, T. Bicanic, A. Dzeing-Ella, M. Kombila, S. Issifou, S. Borrmann, P.G. Kremsner, and S. Krishna. 2006. Lactic Acidosis in Gabonese Children with Severe Malaria Is Unrelated to Dehydration. *Clin. Infect. Dis.* 42:1719–1725. doi:10.1086/504329.

Jia, L., C. Bonaventura, J. Bonaventura, and J.S. Stamler. 1996. S-nitrosohaemoglobin: a dynamic activity of blood involved in vascular control. *Publ. Online 21 March 1996 Doi101038380221a0*. 380:221–226. doi:10.1038/380221a0.

John, C.C., P. Bangirana, J. Byarugaba, R.O. Opoka, R. Idro, A.M. Jurek, B. Wu, and M.J. Boivin. 2008. Cerebral malaria in children is associated with long-term cognitive impairment. *Pediatrics*. 122:e92–9.

Jones, C.E., C.J. Darcy, T. Woodberry, N.M. Anstey, and Y.R. McNeil. 2010. HPLC analysis of asymmetric dimethylarginine, symmetric dimethylarginine, homoarginine and arginine

in small plasma volumes using a Gemini-NX column at high pH. *J Chromatogr B Anal. Technol Biomed Life Sci*. 878:8–12. doi:10.1016/j.jchromb.2009.10.035.

Kaiser, K., A. Texier, J. Ferrandiz, A. Buguet, A. Meiller, C. Latour, F. Peyron, R. Cespuglio, and S. Picot. 2006. Recombinant human erythropoietin prevents the death of mice during cerebral malaria. *J Infect Dis*. 193:987–95.

Kakimoto, Y., and S. Akazawa. 1970. Isolation and Identification of Ng,Ng- and Ng,N'g-Dimethylarginine, Nε-Mono-, Di-, and Trimethyllysine, and Glucosylgalactosyl- and Galactosyl-δ-hydroxylysine from Human Urine. *J. Biol. Chem.* 245:5751–5758.

Kannan, R., D. Sahal, and V.S. Chauhan. 2002. Heme-Artemisinin Adducts Are Crucial Mediators of the Ability of Artemisinin to Inhibit Heme Polymerization. *Chem. Biol.* 9:321–332. doi:10.1016/S1074-5521(02)00117-5.

Kantele, A., and T.S. Jokiranta. 2011. Review of Cases With the Emerging Fifth Human Malaria Parasite, Plasmodium knowlesi. *Clin. Infect. Dis.* 52:1356–1362. doi:10.1093/cid/cir180.

Kassebaum, N.J., R. Jasrasaria, M. Naghavi, S.K. Wulf, N. Johns, R. Lozano, M. Regan, D. Weatherall, D.P. Chou, T.P. Eisele, S.R. Flaxman, R.L. Pullan, S.J. Brooker, and C.J.L. Murray. 2014. A systematic analysis of global anemia burden from 1990 to 2010. *Blood*. 123:615–624. doi:10.1182/blood-2013-06-508325.

Kato, G.J., Z. Wang, R.F. Machado, W.C. Blackwelder, J.G. Taylor 6th, and S.L. Hazen. 2009. Endogenous nitric oxide synthase inhibitors in sickle cell disease: abnormal levels and correlations with pulmonary hypertension, desaturation, haemolysis, organ dysfunction and death. *Br. J. Haematol.* 145:506–513. doi:10.1111/j.1365-2141.2009.07658.x.

Katusic, Z.S., A. Stelter, and S. Milstien. 1998. Cytokines stimulate GTP cyclohydrolase I gene expression in cultured human umbilical vein endothelial cells. *Arter. Thromb Vasc Biol*. 18:27–32.

Kaufman, S. 1989. An evaluation of the possible neurotoxicity of metabolites of phenylalanine. *J Pediatr*. 114:895–900.

Kerler, F., L. Hüultner, I. Ziegler, G. Katzenmaier, and A. Bacher. 1990. Analysis of the tetrahydrobiopterin synthesizing system during maturation of murine reticulocytes. *J. Cell. Physiol.* 142:268–271. doi:10.1002/jcp.1041420208.

Kielstein, J.T., and J.P. Cooke. 2007. Should We Measure Asymmetric Dimethylarginine in Patients with Coronary Artery Disease? *Clin. Chem.* 53:161–163. doi:10.1373/clinchem.2006.078881.

Kielstein, J.T., B. Impraim, S. Simmel, S.M. Bode-Böger, D. Tsikas, J.C. Frölich, M.M. Hoeper, H. Haller, and D. Fliser. 2004. Cardiovascular Effects of Systemic Nitric Oxide Synthase Inhibition With Asymmetrical Dimethylarginine in Humans. *Circulation*. 109:172–177. doi:10.1161/01.CIR.0000105764.22626.B1.

Kielstein, J.T., S.R. Salpeter, S.M. Bode-Boeger, J.P. Cooke, and D. Fliser. 2006. Symmetric dimethylarginine (SDMA) as endogenous marker of renal function—a meta-analysis. *Nephrol. Dial. Transplant.* 21:2446–2451. doi:10.1093/ndt/gfl292.

Kihara, M., J.A. Carter, and C.R. Newton. 2006. The effect of Plasmodium falciparum on cognition: a systematic review. *Trop Med Int Health*. 11:386–97.

Kirchherr, H., and W.N. Kühn-Velten. 2005. HPLC–Tandem Mass Spectrometric Method for Rapid Quantification of Dimethylarginines in Human Plasma. *Clin. Chem.* 51:249–252. doi:10.1373/clinchem.2004.042663.

Klatt, P., K. Schmidt, D. Lehner, O. Glatter, H.P. Bachinger, and B. Mayer. 1995. Structural analysis of porcine brain nitric oxide synthase reveals a role for tetrahydrobiopterin and L-arginine in the formation of an SDS-resistant dimer. *EMBO J*. 14:3687–95.

Kleinbongard, P., A. Dejam, T. Lauer, T. Rassaf, A. Schindler, O. Picker, T. Scheeren, A. Gödecke, J. Schrader, R. Schulz, G. Heusch, G.A. Schaub, N.S. Bryan, M. Feelisch, and M. Kelm. 2003. Plasma nitrite reflects constitutive nitric oxide synthase activity in mammals. *Free Radic. Biol. Med.* 35:790–796. doi:10.1016/S0891-5849(03)00406-4.

Kleinbongard, P., R. Schulz, T. Rassaf, T. Lauer, A. Dejam, T. Jax, I. Kumara, P. Gharini, S. Kabanova, B. Ozuyaman, H.G. Schnurch, A. Godecke, A.A. Weber, M. Robenek, H. Robenek, W. Bloch, P. Rosen, and M. Kelm. 2006. Red blood cells express a functional endothelial nitric oxide synthase. *Blood*. 107:2943–51.

Krause, W., M. Halminski, L. McDonald, P. Dembure, R. Salvo, D. Freides, and L. Elsas. 1985. Biochemical and neuropsychological effects of elevated plasma phenylalanine in patients with treated phenylketonuria. A model for the study of phenylalanine and brain function in man. *J. Clin. Invest.* 75:40–48. doi:10.1172/JCI111695.

Kremsner, P.G., S. Winkler, E. Wildling, J. Prada, U. Bienzle, W. Graninger, and A.K. Nüssler. 1996. High plasma levels of nitrogen oxides are associated with severe disease and correlate with rapid parasitological and clinical cure in Plasmodium falciparum malaria. *Trans. R. Soc. Trop. Med. Hyg.* 90:44–47. doi:10.1016/S0035-9203(96)90476-9.

Krishna, S., W. Supanaranond, S. Pukrittayakamee, F.T. Kuile, M. Ruprah, and N.J. White. 1996. The disposition and effects of two doses of dichloroacetate in adults with severe falciparum malaria. *Br. J. Clin. Pharmacol.* 41:29–34. doi:10.1111/j.1365-2125.1996.tb00155.x.

Krishna, S., D.W. Waller, F. ter Kuile, D. Kwiatkowski, J. Crawley, C.F. Craddock, F. Nosten, D. Chapman, D. Brewster, P.A. Holloway, and et al. 1994. Lactic acidosis and hypoglycaemia in children with severe malaria: pathophysiological and prognostic significance. *Trans R Soc Trop Med Hyg*. 88:67–73.

Krishnegowda, G., A.M. Hajjar, J. Zhu, E.J. Douglass, S. Uematsu, S. Akira, A.S. Woods, and D.C. Gowda. 2005. Induction of Proinflammatory Responses in Macrophages by the Glycosylphosphatidylinositols of Plasmodium falciparum CELL SIGNALING RECEPTORS, GLYCOSYLPHOSPHATIDYLINOSITOL (GPI) STRUCTURAL REQUIREMENT, AND REGULATION OF GPI ACTIVITY. *J. Biol. Chem.* 280:8606–8616. doi:10.1074/jbc.M413541200.

Bor-Kucukatay, M., R.B. Wenby, H.J. Meiselman, and O.K. Baskurt. 2003. Effects of nitric oxide on red blood cell deformability. *Am J Physiol Heart Circ Physiol*. 284:H1577–84.

Kurtzhals, J. a. L., O. Rodrigues, M. Addae, J.O.O. Commey, F.K. Nkrumah, and L. Hviid. 1997. Reversible suppression of bone marrow response to erythropoietin in Plasmodium

falciparum malaria. *Br. J. Haematol*. 97:169–174. doi:10.1046/j.1365-2141.1997.82654.x.

Kuzkaya, N., N. Weissmann, D.G. Harrison, and S. Dikalov. 2003. Interactions of peroxynitrite, tetrahydrobiopterin, ascorbic acid, and thiols: implications for uncoupling endothelial nitric-oxide synthase. *J Biol Chem*. 278:22546–54.

Kwiatkowski, D., I. Sambou, P. Twumasi, B.M. Greenwood, A.V.S. Hill, K.R. Manogue, A. Cerami, J. Castracane, and D.R. Brewster. 1990. TNF concentration in fatal cerebral, non-fatal cerebral, and uncomplicated Plasmodium falciparum malaria. *The Lancet*. 336:1201–1204. doi:10.1016/0140-6736(90)92827-5.

Kwiatkowski, D.P. 2005. How malaria has affected the human genome and what human genetics can teach us about malaria. *Am J Hum Genet*. 77:171–92.

Kwon, N.S., C.F. Nathan, and D.J. Stuehr. 1989. Reduced biopterin as a cofactor in the generation of nitrogen oxides by murine macrophages. *J Biol Chem*. 264:20496–501.

Landmesser, U., S. Dikalov, S.R. Price, L. McCann, T. Fukai, S.M. Holland, W.E. Mitch, and D.G. Harrison. 2003. Oxidation of tetrahydrobiopterin leads to uncoupling of endothelial cell nitric oxide synthase in hypertension. *J Clin Invest*. 111:1201–9. doi:10.1172/JCI14172.

Lee, H.W., S. Kim, and W.K. Paik. 1977. S-Adenosylmethionine:protein-arginine methyltransferase. Purification and mechanism of the enzyme. *Biochemistry (Mosc.)*. 16:78–85. doi:10.1021/bi00620a013.

Leech, J.H., J.W. Barnwell, L.H. Miller, and R.J. Howard. 1984. Identification of a strain-specific malarial antigen exposed on the surface of Plasmodium falciparum-infected erythrocytes. *J. Exp. Med.* 159:1567–1575. doi:10.1084/jem.159.6.1567.

Leiper, J., M. Nandi, B. Torondel, J. Murray-Rust, M. Malaki, B. O'Hara, S. Rossiter, S. Anthony, M. Madhani, D. Selwood, C. Smith, B. Wojciak-Stothard, A. Rudiger, R. Stidwill, N.Q. McDonald, and P. Vallance. 2007. Disruption of methylarginine metabolism impairs vascular homeostasis. *Nat. Med.* 13:198–203. doi:10.1038/nm1543.

Leiper, J.M., J. Santa Maria, A. Chubb, R.J. MacAllister, I.G. Charles, G.S. Whitley, and P. Vallance. 1999. Identification of two human dimethylarginine dimethylaminohydrolases with distinct tissue distributions and homology with microbial arginine deiminases. *Biochem. J.* 343 Pt 1:209–214.

Levy, H.L., A. Milanowski, A. Chakrapani, M. Cleary, P. Lee, F.K. Trefz, C.B. Whitley, F. Feillet, A.S. Feigenbaum, J.D. Bebchuk, H. Christ-Schmidt, and A. Dorenbaum. 2007. Efficacy of sapropterin dihydrochloride (tetrahydrobiopterin, 6R-BH4) for reduction of phenylalanine concentration in patients with phenylketonuria: a phase III randomised placebo-controlled study. *Lancet*. 370:504–10.

Looareesuwan, S., M. Ho, Y. Wattanagoon, N.J. White, D.A. Warrell, D. Bunnag, T. Harinasuta, and D.J. Wyler. 1987. Dynamic Alteration in Splenic Function during Acute falciparum Malaria. *N. Engl. J. Med.* 317:675–679. doi:10.1056/NEJM198709103171105.

Looareesuwan, S., P. Wilairatana, S. Vannaphan, V. Wanaratana, C. Wenisch, M. Aikawa, G. Brittenham, W. Graninger, and W.H. Wernsdorfer. 1998. Pentoxifylline as an ancillary treatment for severe falciparum malaria in Thailand. *Am. J. Trop. Med. Hyg.* 58:348–353.

Lopansri, B.K., N.M. Anstey, G.J. Stoddard, E.D. Mwaikambo, C.S. Boutlis, E. Tjitra, H. Maniboey, M.R. Hobbs, M.C. Levesque, J.B. Weinberg, and D.L. Granger. 2006. Elevated plasma phenylalanine in severe malaria and implications for pathophysiology of neurological complications. *Infect Immun*. 74:3355–9.

Lopansri, B.K., N.M. Anstey, J.B. Weinberg, G.J. Stoddard, M.R. Hobbs, M.C. Levesque, E.D. Mwaikambo, and D.L. Granger. 2003. Low plasma arginine concentrations in children with cerebral malaria and decreased nitric oxide production. *Lancet*. 361:676–8.

Loscalzo, J. 2001. Nitric oxide insufficiency, platelet activation, and arterial thrombosis. *Circ Res*. 88:756–62.

Lucas, R., P. Juillard, E. Decoster, M. Redard, D. Burger, Y. Donati, C. Giroud, C. Monso-Hinard, T. De Kesel, W.A. Buurman, M.W. Moore, J.-M. Dayer, W. Fiers, H. Bluethmann, and G.E. Grau. 1997. Crucial role of tumor necrosis factor (TNF) receptor 2 and membrane-bound TNF in experimental cerebral malaria. *Eur. J. Immunol.* 27:1719–1725. doi:10.1002/eji.1830270719.

Luo, Z., T. Teerlink, K. Griendling, S. Aslam, W.J. Welch, and C.S. Wilcox. 2010. Angiotensin II and NADPH Oxidase Increase ADMA in Vascular Smooth Muscle Cells. *Hypertension*. 56:498–504. doi:10.1161/HYPERTENSIONAHA.110.152959.

Mack, A.K., V.R. McGowan II, C.K. Tremonti, D. Ackah, C. Barnett, R.F. Machado, M.T. Gladwin, and G.J. Kato. 2008. Sodium nitrite promotes regional blood flow in patients with sickle cell disease: a phase I/II study. *Br. J. Haematol.* 142:971–978. doi:10.1111/j.1365-2141.2008.07259.x.

MacPherson, G.G., M.J. Warrell, N.J. White, S. Looareesuwan, and D.A. Warrell. 1985. Human cerebral malaria. A quantitative ultrastructural analysis of parasitized erythrocyte sequestration. *Am J Pathol*. 119:385–401.

Magowan, C., W. Wollish, L. Anderson, and J. Leech. 1988. Cytoadherence by Plasmodium falciparum-infected erythrocytes is correlated with the expression of a family of variable proteins on infected erythrocytes. *J. Exp. Med.* 168:1307–1320. doi:10.1084/jem.168.4.1307.

Maitland, K., S. Kiguli, R.O. Opoka, C. Engoru, P. Olupot-Olupot, S.O. Akech, R. Nyeko, G. Mtove, H. Reyburn, T. Lang, B. Brent, J.A. Evans, J.K. Tibenderana, J. Crawley, E.C. Russell, M. Levin, A.G. Babiker, and D.M. Gibb. 2011. Mortality after Fluid Bolus in African Children with Severe Infection. *N. Engl. J. Med.* 364:2483–2495. doi:10.1056/NEJMoa1101549.

Maitland, K., A. Pamba, M. English, N. Peshu, K. Marsh, C. Newton, and M. Levin. 2005. Randomized trial of volume expansion with albumin or saline in children with severe malaria: preliminary evidence of albumin benefit. *Clin Infect Dis*. 40:538–45.

Mammoto, T., S.M. Parikh, A. Mammoto, D. Gallagher, B. Chan, G. Mostoslavsky, D.E. Ingber, and V.P. Sukhatme. 2007. Angiopoietin-1 Requires p190 RhoGAP to Protect

against Vascular Leakage in Vivo. *J. Biol. Chem.* 282:23910–23918. doi:10.1074/jbc.M702169200.

Maneerat, Y., P. Viriyavejakul, B. Punpoowong, M. Jones, P. Wilairatana, E. Pongponratn, G.D.H. Turner, and R. Udomsangpetch. 2000. Inducible nitric oxide synthase expression is increased in the brain in fatal cerebral malaria. *Histopathology*. 37:269–277. doi:10.1046/j.1365-2559.2000.00989.x.

Marchiafava, E., and A. Bignami. 1892. On Summer-Autumn Malarial Fevers. *In* Two Monographs on Malaria and the Parasites of Malarial Fevers (translated from the first Italian edition by JH Thompson in 1894). New Sydenham Society, London. 1–232.

Marini, J.C. 2012. Arginine and ornithine are the main precursors for citrulline synthesis in mice. *J Nutr*. 142:572–80. doi:10.3945/jn.111.153825.

Marini, J.C., I.C. Didelija, L. Castillo, and B. Lee. 2010a. Glutamine: precursor or nitrogen donor for citrulline synthesis? *Am J Physiol Endocrinol Metab*. 299:E69–79. doi:10.1152/ajpendo.00080.2010.

Marini, J.C., I.C. Didelija, L. Castillo, and B. Lee. 2010b. Plasma arginine and ornithine are the main citrulline precursors in mice infused with arginine-free diets. *J Nutr*. 140:1432–7. doi:10.3945/jn.110.125377.

Marini, J.C., A. Erez, L. Castillo, and B. Lee. 2007. Interaction between murine spf-ash mutation and genetic background yields different metabolic phenotypes. *Am J Physiol Endocrinol Metab*. 293:E1764–71. doi:10.1152/ajpendo.00525.2007.

Marini, J.C., B. Stoll, I.C. Didelija, and D.G. Burrin. 2012. De novo synthesis is the main source of ornithine for citrulline production in neonatal pigs. *Am J Physiol Endocrinol Metab*. 303:E1348–53. doi:10.1152/ajpendo.00399.2012.

Marra, M., A.R. Bonfigli, R. Testa, I. Testa, A. Gambini, and G. Coppa. 2003. High-performance liquid chromatographic assay of asymmetric dimethylarginine, symmetric dimethylarginine, and arginine in human plasma by derivatization with naphthalene-2,3-dicarboxaldehyde. *Anal. Biochem.* 318:13–17. doi:10.1016/S0003-2697(03)00157-X.

Marsh, K., D. Forster, C. Waruiru, I. Mwangi, M. Winstanley, V. Marsh, C. Newton, P. Winstanley, P. Warn, N. Peshu, G. Pasvol, and R. Snow. 1995. Indicators of Life-Threatening Malaria in African Children. *N. Engl. J. Med.* 332:1399–1404. doi:10.1056/NEJM199505253322102.

Martens-Lobenhoffer, J., and S.M. Bode-Böger. 2003. Simultaneous detection of arginine, asymmetric dimethylarginine, symmetric dimethylarginine and citrulline in human plasma and urine applying liquid chromatography–mass spectrometry with very straightforward sample preparation. *J. Chromatogr. B.* 798:231–239. doi:10.1016/j.jchromb.2003.09.050.

Martins, Y.C., G.M. Zanini, J.A. Frangos, and L.J. Carvalho. 2012. Efficacy of Different Nitric Oxide-Based Strategies in Preventing Experimental Cerebral Malaria by Plasmodium berghei ANKA. *PLoS One*. 7:e32048. doi:10.1371/journal.pone.0032048.

Mast, Q. de, E. Groot, P.B. Asih, D. Syafruddin, M. Oosting, S. Sebastian, B. Ferwerda, M.G. Netea, P.G. de Groot, A.J.A.M. van der Ven, and R. Fijnheer. 2009. ADAMTS13 Deficiency with Elevated Levels of Ultra-Large and Active von Willebrand Factor in P. falciparum and P. vivax Malaria. *Am. J. Trop. Med. Hyg.* 80:492–498.

Masuda, S., M. Nagao, K. Takahata, Y. Konishi, F. Gallyas, T. Tabira, and R. Sasaki. 1993. Functional erythropoietin receptor of the cells with neural characteristics. Comparison with receptor properties of erythroid cells. *J Biol Chem*. 268:11208–16.

Matsushita, K., C.N. Morrell, B. Cambien, S.X. Yang, M. Yamakuchi, C. Bao, M.R. Hara, R.A. Quick, W. Cao, B. O'Rourke, J.M. Lowenstein, J. Pevsner, D.D. Wagner, and C.J. Lowenstein. 2003. Nitric oxide regulates exocytosis by S-nitrosylation of N-ethylmaleimide-sensitive factor. *Cell*. 115:139–50.

Matthews, J.R., C.H. Botting, M. Panico, H.R. Morris, and R.T. Hay. 1996. Inhibition of NF-κB DNA Binding by Nitric Oxide. *Nucleic Acids Res.* 24:2236–2242. doi:10.1093/nar/24.12.2236.

Maude, R.J., K. Silamut, K. Plewes, P. Charunwatthana, M. Ho, M.A. Faiz, R. Rahman, M.A. Hossain, M.U. Hassan, E.B. Yunus, G. Hoque, F. Islam, A. Ghose, J. Hanson, J. Schlatter, R. Lacey, A. Eastaugh, J. Tarning, S.J. Lee, N.J. White, K. Chotivanich, N.P.J. Day, and A.M. Dondorp. 2014. Randomized Controlled Trial of Levamisole Hydrochloride as Adjunctive Therapy in Severe Falciparum Malaria With High Parasitemia. *J. Infect. Dis.* 209:120–129. doi:10.1093/infdis/jit410.

McCabe, T.J., D. Fulton, L.J. Roman, and W.C. Sessa. 2000. Enhanced Electron Flux and Reduced Calmodulin Dissociation May Explain "Calcium-independent" eNOS Activation by Phosphorylation. *J. Biol. Chem.* 275:6123–6128. doi:10.1074/jbc.275.9.6123.

McDonald, K.K., S. Zharikov, E.R. Block, and M.S. Kilberg. 1997. A Caveolar Complex between the Cationic Amino Acid Transporter 1 and Endothelial Nitric-oxide Synthase May Explain the "Arginine Paradox." *J. Biol. Chem.* 272:31213–31216.

Medana, I.M., N.P. Day, T.T. Hien, N.T. Mai, D. Bethell, N.H. Phu, J. Farrar, M.M. Esiri, N.J. White, and G.D. Turner. 2002. Axonal injury in cerebral malaria. *Am J Pathol*. 160:655–66.

Medana, I.M., N.P. Day, T.T. Hien, N.J. White, and G.D. Turner. 2009. Erythropoietin and its receptors in the brainstem of adults with fatal falciparum malaria. *Malar. J.* 8:261. doi:10.1186/1475-2875-8-261.

Medana, I.M., R.B. Lindert, U. Wurster, T.T. Hien, N.P. Day, N.H. Phu, N.T. Mai, L.V. Chuong, T.T. Chau, G.D. Turner, J.J. Farrar, and N.J. White. 2005. Cerebrospinal fluid levels of markers of brain parenchymal damage in Vietnamese adults with severe malaria. *Trans R Soc Trop Med Hyg*. 99:610–7.

Meshnick, S.R., Y.Z. Yang, V. Lima, F. Kuypers, S. Kamchonwongpaisan, and Y. Yuthavong. 1993. Iron-dependent free radical generation from the antimalarial agent artemisinin (qinghaosu). *Antimicrob. Agents Chemother.* 37:1108–1114. doi:10.1128/AAC.37.5.1108.

Miller, L.H., D.I. Baruch, K. Marsh, and O.K. Doumbo. 2002. The pathogenic basis of malaria. *Nature*. 415:673–9.

Milstien, S., and Z. Katusic. 1999. Oxidation of tetrahydrobiopterin by peroxynitrite: implications for vascular endothelial function. *Biochem Biophys Res Commun*. 263:681–4.

Minneci, P.C. 2005. Hemolysis-associated endothelial dysfunction mediated by accelerated NO inactivation by decompartmentalized oxyhemoglobin. *J. Clin. Invest.* 115:3409–3417. doi:10.1172/JCI25040.

Minneci, P.C., K.J. Deans, S. Shiva, H. Zhi, S.M. Banks, S. Kern, C. Natanson, S.B. Solomon, and M.T. Gladwin. 2008. Nitrite reductase activity of hemoglobin as a systemic nitric oxide generator mechanism to detoxify plasma hemoglobin produced during hemolysis. *Am. J. Physiol. - Heart Circ. Physiol.* 295:H743–H754. doi:10.1152/ajpheart.00151.2008.

Mishra, S.K., S. Mohanty, S.K. Satpathy, and D.N. Mohapatra. 2007. Cerebral malaria in adults -- a description of 526 cases admitted to Ispat General Hospital in Rourkela, India. *Ann Trop Med Parasitol*. 101:187–93.

Mishra, S.K., and C.R. Newton. 2009. Diagnosis and management of the neurological complications of falciparum malaria. *Nat Rev Neurol*. 5:189–98.

Mitchell, J.A., M. Hecker, E.E. Ånggård, and J.R. Vane. 1990. Cultured endothelial cells maintain their L-arginine level despite the continuous release of EDRF. *Eur. J. Pharmacol.* 182:573–576. doi:10.1016/0014-2999(90)90058-E.

Mohanty, D., K. Ghosh, A.V. Pathare, and D. Karnad. 2002. Deferiprone (L1) as an adjuvant therapy for Plasmodium falciparum malaria. *Indian J. Med. Res.* 115:17–21.

Mohanty, S., S.K. Mishra, S.S. Pati, J. Pattnaik, and B.S. Das. 2003. Complications and mortality patterns due to Plasmodium falciparum malaria in hospitalized adults and children, Rourkela, Orissa, India. *Trans R Soc Trop Med Hyg*. 97:69–70.

Mohanty, S., S.K. Mishra, R. Patnaik, A.K. Dutt, S. Pradhan, B. Das, J. Patnaik, A.K. Mohanty, S.J. Lee, and A.M. Dondorp. 2011. Brain Swelling and Mannitol Therapy in Adult Cerebral Malaria: A Randomized Trial. *Clin. Infect. Dis.* 53:349–355. doi:10.1093/cid/cir405.

Molnar-Perl, I. 2001. Derivatization and chromatographic behavior of the o-phthaldialdehyde amino acid derivatives obtained with various SH-group-containing additives. *J Chromatogr A*. 913:283–302.

Molyneux, M.E., S. Looareesuwan, I.S. Menzies, S.L. Grainger, R.E. Phillips, Y. Wattanagoon, R.P.H. Thompson, and D.A. Warrell. 1989a. Reduced Hepatic Blood Flow and Intestinal Malabsorption in Severe Falciparum Malaria. *Am. J. Trop. Med. Hyg.* 40:470–476.

Molyneux, M.E., T.E. Taylor, J.J. Wirima, and A. Borgsteinj. 1989b. Clinical Features and Prognostic Indicators in Paediatric Cerebral Malaria: A Study of 131 Comatose Malawian Children. *QJM*. 71:441–459.

Mookerjee, R.P., R.N. Dalton, N.A. Davies, S.J. Hodges, C. Turner, R. Williams, and R. Jalan. 2007. Inflammation is an important determinant of levels of the endogenous nitric oxide synthase inhibitor asymmetric dimethylarginine (ADMA) in acute liver failure. *Liver Transpl.* 13:400–405. doi:10.1002/lt.21053.

Morris, C.R., G.J. Kato, M. Poljakovic, X. Wang, W.C. Blackwelder, V. Sachdev, S.L. Hazen, E.P. Vichinsky, S.M. Morris, and M.T. Gladwin. 2005. Dysregulated arginine metabolism, hemolysis-associated pulmonary hypertension, and mortality in sickle cell disease. *JAMA*. 294:81–90. doi:10.1001/jama.294.1.81.

Mpimbaza, A., G. Ndeezi, S. Staedke, P.J. Rosenthal, and J. Byarugaba. 2008. Comparison of buccal midazolam with rectal diazepam in the treatment of prolonged seizures in Ugandan children: a randomized clinical trial. *Pediatrics*. 121:e58–64.

Muchohi, S.N., G.O. Kokwaro, B.R. Ogutu, G. Edwards, S.A. Ward, and C.R. Newton. 2008. Pharmacokinetics and clinical efficacy of midazolam in children with severe malaria and convulsions. *Br J Clin Pharmacol*. 66:529–38.

Murray, C.J., L.C. Rosenfeld, S.S. Lim, K.G. Andrews, K.J. Foreman, D. Haring, N. Fullman, M. Naghavi, R. Lozano, and A.D. Lopez. 2012. Global malaria mortality between 1980 and 2010: a systematic analysis. *The Lancet*. 379:413–431. doi:10.1016/S0140-6736(12)60034-8.

Nagai, A., E. Nakagawa, H.B. Choi, K. Hatori, S. Kobayashi, and S.U. Kim. 2001. Erythropoietin and erythropoietin receptors in human CNS neurons, astrocytes, microglia, and oligodendrocytes grown in culture. *J Neuropathol Exp Neurol*. 60:386–92.

Namutangula, B., G. Ndeezi, J.S. Byarugaba, and J.K. Tumwine. 2007. Mannitol as adjunct therapy for childhood cerebral malaria in Uganda: A randomized clinical trial. *Malar. J.* 6:138. doi:10.1186/1475-2875-6-138.

Neill, A.L., and N.H. Hunt. 1995. Effects of endotoxin and dexamethasone on cerebral malaria in mice. *Parasitology*. 111 (Pt 4):443–54.

Newbold, C., P. Warn, G. Black, A. Berendt, A. Craig, B. Snow, M. Msobo, N. Peshu, and K. Marsh. 1997. Receptor-Specific Adhesion and Clinical Disease in Plasmodium falciparum. *Am. J. Trop. Med. Hyg.* 57:389–398.

Newton, C.R., N. Peshu, B. Kendall, F.J. Kirkham, A. Sowunmi, C. Waruiru, I. Mwangi, S.A. Murphy, and K. Marsh. 1994. Brain swelling and ischaemia in Kenyans with cerebral malaria. *Arch Child*. 70:281–7.

Newton, C.R.J.C., J. Crawley, A. Sowumni, C. Waruiru, I. Mwangi, M. English, S. Murphy, P.A. Winstanley, K. Marsh, and F.J. Kirkham. 1997. Intracranial hypertension in Africans with cerebral malaria. *Arch. Dis. Child.* 76:219–226. doi:10.1136/adc.76.3.219.

Newton, C.R.J.C., P.A. Winstanley, N. Peshu, K. Marsh, F.J. Kirkham, G. Pasvol, and D.A. Warrell. 1991. Intracranial pressure in African children with cerebral malaria. *The Lancet*. 337:573–576. doi:10.1016/0140-6736(91)91638-B.

Ngoungou, E.B., O. Dulac, B. Poudiougou, M. Druet-Cabanac, A. Dicko, A. Mamadou Traore, D. Coulibaly, G. Farnarier, M. Tuillas, M.M. Keita, M. Kombila, O.K. Doumbo, and P.M. Preux. 2006. Epilepsy as a consequence of cerebral malaria in area in which malaria is endemic in Mali, West Africa. *Epilepsia*. 47:873–9.

Nijveldt, R.J., T. Teerlink, M.P.C. Siroen, B. van der Hoven, H.A. Prins, M.J. Wiezer, C. Meijer, J.R.M. van der Sijp, M.A. Cuesta, S. Meijer, and P.A.M. van Leeuwen. 2004. Elevation of asymmetric dimethylarginine (ADMA) in patients developing hepatic failure after major hepatectomy. *JPEN J. Parenter. Enteral Nutr.* 28:382–387.

Nijveldt, R.J., T. Teerlink, M.P.C. Siroen, A.A. van Lambalgen, J.A. Rauwerda, and P.A.M. van Leeuwen. 2003. The liver is an important organ in the metabolism of asymmetrical dimethylarginine (ADMA). *Clin. Nutr. Edinb. Scotl.* 22:17–22.

Noedl, H., Y. Se, S. Sriwichai, K. Schaecher, P. Teja-Isavadharm, B. Smith, W. Rutvisuttinunt, D. Bethell, S. Surasri, M.M. Fukuda, D. Socheat, and L.C. Thap. 2010. Artemisinin Resistance in Cambodia: A Clinical Trial Designed to Address an Emerging Problem in Southeast Asia. *Clin. Infect. Dis.* 51:e82–e89. doi:10.1086/657120.

Nohria, A., M. Gerhard-Herman, M.A. Creager, S. Hurley, D. Mitra, and P. Ganz. 2006. Role of nitric oxide in the regulation of digital pulse volume amplitude in humans. *J. Appl. Physiol.* 101:545–548. doi:10.1152/japplphysiol.01285.2005.

Ogutu, B.R., C.R. Newton, J. Crawley, S.N. Muchohi, G.O. Otieno, G. Edwards, K. Marsh, and G.O. Kokwaro. 2002. Pharmacokinetics and anticonvulsant effects of diazepam in children with severe falciparum malaria and convulsions. *Br J Clin Pharmacol*. 53:49–57.

Ohashi, A., K. Mamada, I. Tsuboi, S. Aizawa, and H. Hasegawa. 2011. Asymmetric uptake of sepiapterin and 7,8-dihydrobiopterin as a gateway of the salvage pathway of tetrahydrobiopterin biosynthesis from the lumenal surface of rat endothelial cells. *Mol. Genet. Metab.* 104:404–406. doi:10.1016/j.ymgme.2011.06.003.

Olszewski, K.L., J.M. Morrisey, D. Wilinski, J.M. Burns, A.B. Vaidya, J.D. Rabinowitz, and M. Llinas. 2009. Host-parasite interactions revealed by Plasmodium falciparum metabolomics. *Cell Host Microbe*. 5:191–9.

Omodeo-Sale, F., L. Cortelezzi, Z. Vommaro, D. Scaccabarozzi, and A.M. Dondorp. 2010. Dysregulation of L-arginine metabolism and bioavailability associated to free plasma heme. *Am J Physiol Cell Physiol*. 299:C148–54. doi:10.1152/ajpcell.00405.2009.

Ong, P.K., B. Melchior, Y.C. Martins, A. Hofer, P. Orjuela-Sanchez, P. Cabrales, G.M. Zanini, J.A. Frangos, and L.J. Carvalho. 2013. Nitric oxide synthase dysfunction contributes to impaired cerebroarteriolar reactivity in experimental cerebral malaria. *PLoS Pathog*. 9:e1003444. doi:10.1371/journal.ppat.1003444.

Pain, A., D.J.P. Ferguson, O. Kai, B.C. Urban, B. Lowe, K. Marsh, and D.J. Roberts. 2001. Platelet-mediated clumping of Plasmodium falciparum-infected erythrocytes is a common adhesive phenotype and is associated with severe malaria. *Proc. Natl. Acad. Sci.* 98:1805–1810. doi:10.1073/pnas.98.4.1805.

Palmer, R.M., A.G. Ferrige, and S. Moncada. 1987. Nitric oxide release accounts for the biological activity of endothelium-derived relaxing factor. *Nature*. 327:524–6. doi:10.1038/327524a0.

Pamplona, A., A. Ferreira, J. Balla, V. Jeney, G. Balla, S. Epiphanio, A. Chora, C.D. Rodrigues, I.P. Gregoire, M. Cunha-Rodrigues, S. Portugal, M.P. Soares, and M.M. Mota. 2007. Heme oxygenase-1 and carbon monoxide suppress the pathogenesis of experimental cerebral malaria. *Nat Med*. 13:703–10.

Patankar, T.F., D.R. Karnad, P.G. Shetty, A.P. Desai, and S.R. Prasad. 2002. Adult cerebral malaria: prognostic importance of imaging findings and correlation with postmortem findings. *Radiology*. 224:811–6.

Patnaik, J.K., B.S. Das, S.K. Mishra, S. Mohanty, S.K. Satpathy, and D. Mohanty. 1994. Vascular clogging, mononuclear cell margination, and enhanced vascular permeability in the pathogenesis of human cerebral malaria. *Am J Trop Med Hyg*. 51:642–7.

Pearson, D.L., S. Dawling, W.F. Walsh, J.L. Haines, B.W. Christman, A. Bazyk, N. Scott, and M.L. Summar. 2001. Neonatal pulmonary hypertension--urea-cycle intermediates, nitric oxide production, and carbamoyl-phosphate synthetase function. *N Engl J Med*. 344:1832–8. doi:10.1056/NEJM200106143442404.

Penet, M.F., A. Viola, S. Confort-Gouny, Y. Le Fur, G. Duhamel, F. Kober, D. Ibarrola, M. Izquierdo, N. Coltel, B. Gharib, G.E. Grau, and P.J. Cozzone. 2005. Imaging experimental cerebral malaria in vivo: significant role of ischemic brain edema. *J Neurosci*. 25:7352–8.

Peng, H.-B., P. Libby, and J.K. Liao. 1995. Induction and Stabilization of IκBα by Nitric Oxide Mediates Inhibition of NF-κB. *J. Biol. Chem.* 270:14214–14219.

Di Perri, G., I.G. Di Perri, G.B. Monteiro, S. Bonora, C. Hennig, M. Cassatella, R. Micciolo, S. Vento, S. Dusi, D. Bassetti, and E. Concia. 1995. Pentoxifylline as a Supportive Agent in the Treatment of Cerebral Malaria in Children. *J. Infect. Dis.* 171:1317–1322.

Perticone, F., A. Sciacqua, R. Maio, M. Perticone, R. Maas, R.H. Boger, G. Tripepi, G. Sesti, and C. Zoccali. 2005. Asymmetric Dimethylarginine, L-Arginine, and Endothelial Dysfunction in Essential Hypertension. *J. Am. Coll. Cardiol.* 46:518–523. doi:10.1016/j.jacc.2005.04.040.

Pfaller, M.A., D.J. Krogstad, A.R. Parquette, and P. Nguyen-Dinh. 1982. Plasmodium falciparum: Stage-specific lactate production in synchronized cultures. *Exp. Parasitol.* 54:391–396. doi:10.1016/0014-4894(82)90048-0.

Phillips-Howard, P.A., B.L. Nahlen, M.S. Kolczak, A.W. Hightower, F.O.T. Kuile, J.A. Alaii, J.E. Gimnig, J. Arudo, J.M. Vulule, A. Odhacha, S.P. Kachur, E. Schoute, D.H. Rosen, J.D. Sexton, A.J. Oloo, and W.A. Hawley. 2003. Efficacy of Permethrin-Treated Bed Nets in the Prevention of Mortality in Young Children in an Area of High Perennial Malaria Transmission in Western Kenya. *Am. J. Trop. Med. Hyg.* 68:23–29.

Phu, N.H., T.T. Hien, N.T. Mai, T.T. Chau, L.V. Chuong, P.P. Loc, C. Winearls, J. Farrar, N. White, and N. Day. 2002. Hemofiltration and peritoneal dialysis in infection-associated acute renal failure in Vietnam. *N Engl J Med*. 347:895–902.

Phyo, A.P., S. Nkhoma, K. Stepniewska, E.A. Ashley, S. Nair, R. McGready, C. ler Moo, S. Al-Saai, A.M. Dondorp, K.M. Lwin, P. Singhasivanon, N.P. Day, N.J. White, T.J. Anderson, and F. Nosten. 2012. Emergence of artemisinin-resistant malaria on the western border of Thailand: a longitudinal study. *The Lancet*. 379:1960–1966. doi:10.1016/S0140-6736(12)60484-X.

Picot, S., A.-L. Bienvenu, S. Konate, S. Sissoko, A. Barry, E. Diarra, K. Bamba, A. Djimdé, and O.K. Doumbo. 2009. Safety of epoietin beta-quinine drug combination in children with cerebral malaria in Mali. *Malar. J.* 8:169. doi:10.1186/1475-2875-8-169.

Piraud, M., C. Vianey-Saban, K. Petritis, C. Elfakir, J.P. Steghens, and D. Bouchu. 2005. Ion-pairing reversed-phase liquid chromatography/electrospray ionization mass spectrometric analysis of 76 underivatized amino acids of biological interest: a new tool for the diagnosis of inherited disorders of amino acid metabolism. *Rapid Commun Mass Spectrom*. 19:1587–602. doi:10.1002/rcm.1957.

Planche, T., T. Agbenyega, G. Bedu-Addo, D. Ansong, A. Owusu-Ofori, F. Micah, C. Anakwa, E. Asafo-Agyei, A. Hutson, P.W. Stacpoole, and S. Krishna. 2003. A Prospective Comparison of Malaria with Other Severe Diseases in African Children: Prognosis and Optimization of Management. *Clin. Infect. Dis.* 37:890–897. doi:10.1086/377536.

Planche, T., M. Onanga, A. Schwenk, A. Dzeing, S. Borrmann, J.-F. Faucher, A. Wright, L. Bluck, L. Ward, M. Kombila, P.G. Kremsner, and S. Krishna. 2004. Assessment of Volume Depletion in Children with Malaria. *PLoS Med*. 1:e18. doi:10.1371/journal.pmed.0010018.

Pluess, B., F.C. Tanser, C. Lengeler, and B.L. Sharp. 1996. Indoor residual spraying for preventing malaria. *In* Cochrane Database of Systematic Reviews. John Wiley & Sons, Ltd.

Pongponratn, E., M. Riganti, B. Punpoowong, and M. Aikawa. 1991. Microvascular sequestration of parasitized erythrocytes in human falciparum malaria: a pathological study. *Am J Trop Med Hyg*. 44:168–75.

Pongponratn, E., G.D. Turner, N.P. Day, N.H. Phu, J.A. Simpson, K. Stepniewska, N.T. Mai, P. Viriyavejakul, S. Looareesuwan, T.T. Hien, D.J. Ferguson, and N.J. White. 2003. An ultrastructural study of the brain in fatal Plasmodium falciparum malaria. *Am J Trop Med Hyg*. 69:345–59.

Porkert, M., S. Sher, U. Reddy, F. Cheema, C. Niessner, P. Kolm, D.P. Jones, C. Hooper, W.R. Taylor, D. Harrison, and A.A. Quyyumi. 2008. Tetrahydrobiopterin: a novel antihypertensive therapy. *J Hum Hypertens*. 22:401–7. doi:10.1038/sj.jhh.1002329.

Potchen, M.J., S.D. Kampondeni, K.B. Seydel, G.L. Birbeck, C.A. Hammond, W.G. Bradley, J.K. DeMarco, S.J. Glover, J.O. Ugorji, M.T. Latourette, J.E. Siebert, M.E. Molyneux, and T.E. Taylor. 2012. Acute Brain MRI Findings in 120 Malawian Children with Cerebral Malaria: New Insights into an Ancient Disease. *Am. J. Neuroradiol.* 33:1740–1746. doi:10.3174/ajnr.A3035.

Pou, S., W.S. Pou, D.S. Bredt, S.H. Snyder, and G.M. Rosen. 1992. Generation of superoxide by purified brain nitric oxide synthase. *J Biol Chem*. 267:24173–6.

Rae, C., J.A. McQuillan, S.B. Parekh, W.A. Bubb, S. Weiser, V.J. Balcar, A.M. Hansen, H.J. Ball, and N.H. Hunt. 2004. Brain gene expression, metabolism, and bioenergetics: interrelationships in murine models of cerebral and noncerebral malaria. *Faseb J.* 18:499–510.

Rapoport, R.M., M.B. Draznin, and F. Murad. 1983. Endothelium-dependent relaxation in rat aorta may be mediated through cyclic GMP-dependent protein phosphorylation. *Nature*. 306:174–176. doi:10.1038/306174a0.

Reiter, C.D., X. Wang, J.E. Tanus-Santos, N. Hogg, R.O. Cannon, A.N. Schechter, and M.T. Gladwin. 2002. Cell-free hemoglobin limits nitric oxide bioavailability in sickle-cell disease. *Nat. Med.* 8:1383–1389. doi:10.1038/nm1202-799.

Reyburn, H., R. Mbatia, C. Drakeley, J. Bruce, I. Carneiro, R. Olomi, J. Cox, W.M. Nkya, M. Lemnge, B.M. Greenwood, and E.M. Riley. 2005. Association of transmission intensity and age with clinical manifestations and case fatality of severe Plasmodium falciparum malaria. *Jama*. 293:1461–70.

Riddle, M.S., J.L. Jackson, J.W. Sanders, and D.L. Blazes. 2002. Exchange transfusion as an adjunct therapy in severe Plasmodium falciparum malaria: a meta-analysis. *Clin Infect Dis*. 34:1192–8.

Ridnour, L.A., D.D. Thomas, D. Mancardi, M.G. Espey, K.M. Miranda, N. Paolocci, M. Feelisch, J. Fukuto, and D.A. Wink. 2004. The chemistry of nitrosative stress induced by nitric oxide and reactive nitrogen oxide species. Putting perspective on stressful biological situations. *Biol. Chem.* 385:1–10.

Roberts, C.D.J. 1992. Rapid switching to multiple antigenic and adhesive phenotypes in malaria. *Nature*. 357:689–692. doi:10.1038/357689a0.

Roberts, D.J., A. Pain, O. Kai, M. Kortok, and K. Marsh. 2000. Autoagglutination of malaria-infected red blood cells and malaria severity. *The Lancet*. 355:1427–1428. doi:10.1016/S0140-6736(00)02143-7.

Ross, R. 1897. Observations On A Condition Necessary To The Transformation Of The Malaria Crescent. *Br. Med. J.* 1:251–255.

Roviezzo, F., S. Tsigkos, A. Kotanidou, M. Bucci, V. Brancaleone, G. Cirino, and A. Papapetropoulos. 2005. Angiopoietin-2 Causes Inflammation in Vivo by Promoting Vascular Leakage. *J. Pharmacol. Exp. Ther.* 314:738–744. doi:10.1124/jpet.105.086553.

Rowe, A., J. Obeiro, C.I. Newbold, and K. Marsh. 1995. Plasmodium falciparum rosetting is associated with malaria severity in Kenya. *Infect. Immun.* 63:2323–2326.

Rowley, C.A., A.K. Ikeda, M. Seidel, T.C. Anaebere, M.D. Antalek, C. Seamon, A.K. Conrey, L. Mendelsohn, J. Nichols, A.M. Gorbach, G.J. Kato, and H. Ackerman. 2014. Microvascular oxygen consumption during sickle cell pain crisis. *Blood*. doi:10.1182/blood-2013-11-533406.

Sakanaka, M., T.C. Wen, S. Matsuda, S. Masuda, E. Morishita, M. Nagao, and R. Sasaki. 1998. In vivo evidence that erythropoietin protects neurons from ischemic damage. *Proc Natl Acad Sci U A.* 95:4635–40.

Sanni, L.A., C. Rae, A. Maitland, R. Stocker, and N.H. Hunt. 2001. Is ischemia involved in the pathogenesis of murine cerebral malaria? *Am J Pathol*. 159:1105–12.

Sawabe, K., Y. Suetake, N. Nakanishi, K.O. Wakasugi, and H. Hasegawa. 2005a. Cellular accumulation of tetrahydrobiopterin following its administration is mediated by two different processes; direct uptake and indirect uptake mediated by a methotrexate-sensitive process. *Mol. Genet. Metab.* 86, Supplement:133–138. doi:10.1016/j.ymgme.2005.06.020.

Sawabe, K., Y. Suetake, K.O. Wakasugi, and H. Hasegawa. 2005b. Accumulated BH4 in mouse liver caused by administration of either 6R- or 6SBH4 consisted solely of the 6R-diastereomer: evidence of oxidation to BH2 and enzymic reduction. *Mol. Genet. Metab.* 86 Suppl 1:S145–147. doi:10.1016/j.ymgme.2005.06.019.

Sawabe, K., K.O. Wakasugi, and H. Hasegawa. 2004. Tetrahydrobiopterin uptake in supplemental administration: elevation of tissue tetrahydrobiopterin in mice following uptake of the exogenously oxidized product 7,8-dihydrobiopterin and subsequent reduction by an anti-folate-sensitive process. *J Pharmacol Sci*. 96:124–33.

Scharpfenecker, M., U. Fiedler, Y. Reiss, and H.G. Augustin. 2005. The Tie-2 ligand Angiopoietin-2 destabilizes quiescent endothelium through an internal autocrine loop mechanism. *J. Cell Sci.* 118:771–780. doi:10.1242/jcs.01653.

Schnabel, R., S. Blankenberg, E. Lubos, K.J. Lackner, H.J. Rupprecht, C. Espinola-Klein, N. Jachmann, F. Post, D. Peetz, C. Bickel, F. Cambien, L. Tiret, and T. Münzel. 2005. Asymmetric Dimethylarginine and the Risk of Cardiovascular Events and Death in Patients With Coronary Artery Disease Results from the AtheroGene Study. *Circ. Res.* 97:e53–e59. doi:10.1161/01.RES.0000181286.44222.61.

Schnog, J.J., E.H. Jager, F.P. van der Dijs, A.J. Duits, H. Moshage, F.D. Muskiet, and F.A. Muskiet. 2004. Evidence for a metabolic shift of arginine metabolism in sickle cell disease. *Ann Hematol*. 83:371–5. doi:10.1007/s00277-004-0856-9.

Schofield, L., and G.E. Grau. 2005. Immunological processes in malaria pathogenesis. *Nat Rev Immunol*. 5:722–35.

Schofield, L., and F. Hackett. 1993. Signal transduction in host cells by a glycosylphosphatidylinositol toxin of malaria parasites. *J. Exp. Med.* 177:145–153. doi:10.1084/jem.177.1.145.

Schofield, L., S. Novakovic, P. Gerold, R.T. Schwarz, M.J. McConville, and S.D. Tachado. 1996. Glycosylphosphatidylinositol toxin of Plasmodium up-regulates intercellular adhesion molecule-1, vascular cell adhesion molecule-1, and E-selectin expression in vascular endothelial cells and increases leukocyte and parasite cytoadherence via tyrosine kinase-dependent signal transduction. *J. Immunol.* 156:1886–1896.

Schulman, S.P., L.C. Becker, D.A. Kass, H.C. Champion, M.L. Terrin, S. Forman, K.V. Ernst, M.D. Kelemen, S.N. Townsend, A. Capriotti, J.M. Hare, and G. Gerstenblith. 2006. L-arginine therapy in acute myocardial infarction: the Vascular Interaction With Age in Myocardial Infarction (VINTAGE MI) randomized clinical trial. *JAMA.* 295:58–64. doi:10.1001/jama.295.1.58.

Schwedhelm, E., R. Maas, J. Tan-Andresen, F. Schulze, U. Riederer, and R.H. Böger. 2007. High-throughput liquid chromatographic-tandem mass spectrometric determination of arginine and dimethylated arginine derivatives in human and mouse plasma. *J. Chromatogr. B.* 851:211–219. doi:10.1016/j.jchromb.2006.11.052.

Scriver, C.R., and C.L. Clow. 1980a. Phenylketonuria: epitome of human biochemical genetics (first of two parts). *N Engl J Med*. 303:1336–42.

Scriver, C.R., and C.L. Clow. 1980b. Phenylketonuria: epitome of human biochemical genetics (second of two parts). *N Engl J Med*. 303:1394–400.

Von Seidlein, L., R. Olaosebikan, I.C.E. Hendriksen, S.J. Lee, O.T. Adedoyin, T. Agbenyega, S.B. Nguah, K. Bojang, J.L. Deen, J. Evans, C.I. Fanello, E. Gomes, A.J. Pedro, C. Kahabuka, C. Karema, E. Kivaya, K. Maitland, O.A. Mokuolu, G. Mtove, J. Mwanga-Amumpaire, B. Nadjm, M. Nansumba, W.P. Ngum, M.A. Onyamboko, H. Reyburn, T. Sakulthaew, K. Silamut, A.K. Tshefu, N. Umulisa, S. Gesase, N.P.J. Day, N.J. White, and A.M. Dondorp. 2012. Predicting the Clinical Outcome of Severe Falciparum Malaria in African Children: Findings From a Large Randomized Trial. *Clin. Infect. Dis.* 54:1080–1090. doi:10.1093/cid/cis034.

Serghides, L., H. Kim, Z. Lu, D.C. Kain, C. Miller, R.C. Francis, W.C. Liles, W.M. Zapol, and K.C. Kain. 2011. Inhaled nitric oxide reduces endothelial activation and parasite accumulation in the brain, and enhances survival in experimental cerebral malaria. *PLoS One*. 6:e27714. doi:10.1371/journal.pone.0027714.

Serghides, L., S.N. Patel, K. Ayi, Z. Lu, D.C. Gowda, W.C. Liles, and K.C. Kain. 2009. Rosiglitazone Modulates the Innate Immune Response to Plasmodium falciparum Infection and Improves Outcome in Experimental Cerebral Malaria. *J. Infect. Dis.* 199:1536–1545. doi:10.1086/598222.

Serirom, S., W.H. Raharjo, K. Chotivanich, S. Loareesuwan, P. Kubes, and M. Ho. 2003. Anti-adhesive effect of nitric oxide on Plasmodium falciparum cytoadherence under flow. *Am J Pathol*. 162:1651–60.

Servillo, L., A. Giovane, N. D'Onofrio, R. Casale, D. Cautela, D. Castaldo, and M.L. Balestrieri. 2013. Determination of homoarginine, arginine, NMMA, ADMA, and SDMA in biological samples by HPLC-ESI-mass spectrometry. *Int. J. Mol. Sci.* 14:20131–20138. doi:10.3390/ijms141020131.

Seydel, K.B., D.A. Milner, S.B. Kamiza, M.E. Molyneux, and T.E. Taylor. 2006. The Distribution and Intensity of Parasite Sequestration in Comatose Malawian Children. *J. Infect. Dis.* 194:208–215. doi:10.1086/505078.

Shiman, R., T. Xia, M.A. Hill, and D.W. Gray. 1994. Regulation of rat liver phenylalanine hydroxylase. II. Substrate binding and the role of activation in the control of enzymatic activity. *J. Biol. Chem.* 269:24647–24656.

Silamut, K., N.H. Phu, C. Whitty, G.D. Turner, K. Louwrier, N.T. Mai, J.A. Simpson, T.T. Hien, and N.J. White. 1999. A quantitative analysis of the microvascular sequestration of malaria parasites in the human brain. *Am J Pathol*. 155:395–410.

Siren, A.L., M. Fratelli, M. Brines, C. Goemans, S. Casagrande, P. Lewczuk, S. Keenan, C. Gleiter, C. Pasquali, A. Capobianco, T. Mennini, R. Heumann, A. Cerami, H.

Ehrenreich, and P. Ghezzi. 2001. Erythropoietin prevents neuronal apoptosis after cerebral ischemia and metabolic stress. *Proc Natl Acad Sci U A*. 98:4044–9.

Siroen, M.P.C., J.R.M. van der Sijp, T. Teerlink, C. van Schaik, R.J. Nijveldt, and P.A.M. van Leeuwen. 2005. The human liver clears both asymmetric and symmetric dimethylarginine. *Hepatology*. 41:559–565. doi:10.1002/hep.20579.

Siroen, M.P.C., M.C. Warlé, T. Teerlink, R.J. Nijveldt, E.J. Kuipers, H.J. Metselaar, H.W. Tilanus, D.J. Kuik, J.R.M. van der Sijp, S. Meijer, B. van der Hoven, and P.A.M. van Leeuwen. 2004. The transplanted liver graft is capable of clearing asymmetric dimethylarginine. *Liver Transplant. Off. Publ. Am. Assoc. Study Liver Dis. Int. Liver Transplant. Soc.* 10:1524–1530. doi:10.1002/lt.20286.

Smith, D.C., and L.B. Sanford. 1985. Laveran's Germ: The Reception and Use of a Medical Discovery. *Am. J. Trop. Med. Hyg.* 34:2–20.

Smith, J.D., C.E. Chitnis, A.G. Craig, D.J. Roberts, D.E. Hudson-Taylor, D.S. Peterson, R. Pinches, C.I. Newbold, and L.H. Miller. 1995. Switches in expression of plasmodium falciparum var genes correlate with changes in antigenic and cytoadherent phenotypes of infected erythrocytes. *Cell*. 82:101–110. doi:10.1016/0092-8674(95)90056-X.

Snow, R.W., J.A. Omumbo, B. Lowe, C.S. Molyneux, J.O. Obiero, A. Palmer, M.W. Weber, M. Pinder, B. Nahlen, C. Obonyo, C. Newbold, S. Gupta, and K. Marsh. 1997. Relation between severe malaria morbidity in children and level of Plasmodium falciparum transmission in Africa. *Lancet*. 349:1650–4.

De Souza, J.B., J.C. Hafalla, E.M. Riley, and K.N. Couper. 2010. Cerebral malaria: why experimental murine models are required to understand the pathogenesis of disease. *Parasitology*. 137:755–72.

Spector, E.B., S.C. Rice, R.M. Kern, R. Hendrickson, and S.D. Cederbaum. 1985. Comparison of arginase activity in red blood cells of lower mammals, primates, and man: evolution to high activity in primates. *Am J Hum Genet*. 37:1138–45.

Storch, K.J., D.A. Wagner, J.F. Burke, and V.R. Young. 1988. Quantitative study in vivo of methionine cycle in humans using [methyl-2H3]- and [1-13C]methionine. *Am J Physiol*. 255:E322–31.

Stroes, E., J. Kastelein, F. Cosentino, W. Erkelens, R. Wever, H. Koomans, T. Luscher, and T. Rabelink. 1997. Tetrahydrobiopterin restores endothelial function in hypercholesterolemia. *J Clin Invest*. 99:41–6. doi:10.1172/JCI119131.

Stuehr, D.J., N.S. Kwon, C.F. Nathan, O.W. Griffith, P.L. Feldman, and J. Wiseman. 1991. N omega-hydroxy-L-arginine is an intermediate in the biosynthesis of nitric oxide from L-arginine. *J Biol Chem*. 266:6259–63.

Su, X., V.M. Heatwole, S.P. Wertheimer, F. Guinet, J.A. Herrfeldt, D.S. Peterson, J.A. Ravetch, and T.E. Wellems. 1995. The large diverse gene family var encodes proteins involved in cytoadherence and antigenic variation of plasmodium falciparum-infected erythrocytes. *Cell*. 82:89–100. doi:10.1016/0092-8674(95)90055-1.

Sugiyama, T., B.D. Levy, and T. Michel. 2009. Tetrahydrobiopterin recycling, a key determinant of endothelial nitric-oxide synthase-dependent signaling pathways in

cultured vascular endothelial cells. *J Biol Chem*. 284:12691–700. doi:10.1074/jbc.M809295200.

Tain, Y.-L., and C. Baylis. 2007. Determination of dimethylarginine dimethylaminohydrolase activity in the kidney. *Kidney Int.* 72:886–889. doi:10.1038/sj.ki.5002446.

Tanaka, K., S. Kaufman, and S. Milstien. 1989. Tetrahydrobiopterin, the cofactor for aromatic amino acid hydroxylases, is synthesized by and regulates proliferation of erythroid cells. *Proc. Natl. Acad. Sci.* 86:5864–5867.

Tang, W.H., Z. Wang, L. Cho, D.M. Brennan, and S.L. Hazen. 2009. Diminished global arginine bioavailability and increased arginine catabolism as metabolic profile of increased cardiovascular risk. *J Am Coll Cardiol*. 53:2061–7. doi:10.1016/j.jacc.2009.02.036.

Taoufiq, Z., F. Gay, J. Balvanyos, L. Ciceron, M. Tefit, P. Lechat, and D. Mazier. 2008. Rho Kinase Inhibition in Severe Malaria: Thwarting Parasite-Induced Collateral Damage to Endothelia. *J. Infect. Dis.* 197:1062–1073. doi:10.1086/528988.

Tatham, A.L., M.J. Crabtree, N. Warrick, S. Cai, N.J. Alp, and K.M. Channon. 2009. GTP cyclohydrolase I expression, protein, and activity determine intracellular tetrahydrobiopterin levels, independent of GTP cyclohydrolase feedback regulatory protein expression. *J Biol Chem*. 284:13660–8. doi:10.1074/jbc.M807959200.

Tayeh, M.A., and M.A. Marletta. 1989. Macrophage oxidation of L-arginine to nitric oxide, nitrite, and nitrate. Tetrahydrobiopterin is required as a cofactor. *J Biol Chem*. 264:19654–8.

Taylor, T.E., A. Borgstein, and M.E. Molyneux. 1993. Acid-base status in paediatric Plasmodium falciparum malaria. *Q J Med*. 86:99–109.

Taylor, T.E., W.J. Fu, R.A. Carr, R.O. Whitten, J.S. Mueller, N.G. Fosiko, S. Lewallen, N.G. Liomba, and M.E. Molyneux. 2004. Differentiating the pathologies of cerebral malaria by postmortem parasite counts. *Nat Med*. 10:143–5.

Taylor, T.E., M.E. Molyneux, J.J. WIRtMA, A. Borgstein, J.D. GOLDRtNG, and M. Hommel. 1992. Intravenous immunoglobulin in the treatment of paediatric cerebral malaria. *Clin. Exp. Immunol.* 90:357–362. doi:10.1111/j.1365-2249.1992.tb05851.x.

Teasdale, G., and B. Jennett. 1974. Asessment of Coma and Impaired Consciousness: A Practical Scale. *The Lancet*. 304:81–84. doi:10.1016/S0140-6736(74)91639-0.

Teerlink, T., R.J. Nijveldt, S. de Jong, and P.A. van Leeuwen. 2002. Determination of arginine, asymmetric dimethylarginine, and symmetric dimethylarginine in human plasma and other biological samples by high-performance liquid chromatography. *Anal Biochem*. 303:131–7.

The RTS,S Clinical Trials Partnership. 2012. A Phase 3 Trial of RTS,S/AS01 Malaria Vaccine in African Infants. *N. Engl. J. Med.* 367:2284–2295. doi:10.1056/NEJMoa1208394.

Thompson, G.N., P.J. Pacy, H. Merritt, G.C. Ford, M.A. Read, K.N. Cheng, and D. Halliday. 1989. Rapid measurement of whole body and forearm protein turnover using a [2H5]phenylalanine model. *Am J Physiol*. 256:E631–9.

Thony, B., G. Auerbach, and N. Blau. 2000. Tetrahydrobiopterin biosynthesis, regeneration and functions. *Biochem J*. 347 Pt 1:1–16.

Thuma, P.E., G.F. Mabeza, G. Biemba, G.J. Bhat, C.E. McLaren, V.M. Moyo, S. Zulu, H. Khumalo, P. Mabeza, A. M'Hango, D. Parry, A.A. Poltera, G.M. Brittenham, and V.R. Gordeuk. 1998. Effect of iron chelation therapy on mortality in Zambian children with cerebral malaria. *Trans. R. Soc. Trop. Med. Hyg.* 92:214–218. doi:10.1016/S0035-9203(98)90753-2.

Tjitra, E., N.M. Anstey, P. Sugiarto, N. Warikar, E. Kenangalem, M. Karyana, D.A. Lampah, and R.N. Price. 2008. Multidrug-Resistant Plasmodium vivax Associated with Severe and Fatal Malaria: A Prospective Study in Papua, Indonesia. *PLoS Med*. 5:e128. doi:10.1371/journal.pmed.0050128.

Tran, T.H., N.P. Day, H.P. Nguyen, T.H. Nguyen, T.H. Tran, P.L. Pham, X.S. Dinh, V.C. Ly, V. Ha, D. Waller, T.E. Peto, and N.J. White. 1996. A controlled trial of artemether or quinine in Vietnamese adults with severe falciparum malaria. *N Engl J Med*. 335:76–83.

Trang, T.T.M., N.H. Phu, H. Vinh, T.T. Hien, B.M. Cuong, T.T.H. Chau, N.T.H. Mai, D.J. Waller, and N.J. White. 1992. Acute Renal Failure in Patients with Severe Falciparum Malaria. *Clin. Infect. Dis.* 15:874–880. doi:10.1093/clind/15.5.874.

Trefz, F.K., B.K. Burton, N. Longo, M.M. Casanova, D.J. Gruskin, A. Dorenbaum, E.D. Kakkis, E.A. Crombez, D.K. Grange, P. Harmatz, M.H. Lipson, A. Milanowski, L.M. Randolph, J. Vockley, C.B. Whitley, J.A. Wolff, J. Bebchuk, H. Christ-Schmidt, and J.B. Hennermann. 2009. Efficacy of sapropterin dihydrochloride in increasing phenylalanine tolerance in children with phenylketonuria: a phase III, randomized, double-blind, placebo-controlled study. *J Pediatr*. 154:700–7.

Treutiger, C.-J., I. Hedlund, H. Helmby, J. Carlson, A. Jepson, P. Twumasi, D. Kwiatkowski, B.M. Greenwood, and M. Wahlgren. 1992. Rosette Formation in Plasmodium falciparum Isolates and Anti-Rosette Activity of Sera from Gambians with Cerebral or Uncomplicated Malaria. *Am. J. Trop. Med. Hyg.* 46:503–510.

Tripathi, A.K., D.J. Sullivan, and M.F. Stins. 2006. Plasmodium falciparum-Infected Erythrocytes Increase Intercellular Adhesion Molecule 1 Expression on Brain Endothelium through NF-κB. *Infect. Immun.* 74:3262–3270. doi:10.1128/IAI.01625-05.

Tripathi, A.K., D.J. Sullivan, and M.F. Stins. 2007. Plasmodium falciparum-infected erythrocytes decrease the integrity of human blood-brain barrier endothelial cell monolayers. *J Infect Dis*. 195:942–50.

Turner, G. 1997. Cerebral malaria. *Brain Pathol*. 7:569–82.

Turner, G.D., H. Morrison, M. Jones, T.M. Davis, S. Looareesuwan, I.D. Buley, K.C. Gatter, C.I. Newbold, S. Pukritayakamee, B. Nagachinta, and et al. 1994. An immunohistochemical study of the pathology of fatal malaria. Evidence for widespread endothelial activation and a potential role for intercellular adhesion molecule-1 in cerebral sequestration. *Am J Pathol*. 145:1057–69.

Turner, L., T. Lavstsen, S.S. Berger, C.W. Wang, J.E.V. Petersen, M. Avril, A.J. Brazier, J. Freeth, J.S. Jespersen, M.A. Nielsen, P. Magistrado, J. Lusingu, J.D. Smith, M.K.

Higgins, and T.G. Theander. 2013. Severe malaria is associated with parasite binding to endothelial protein C receptor. *Nature*. 498:502–505. doi:10.1038/nature12216.

Vallance, P., A. Leone, A. Calver, J. Collier, and S. Moncada. 1992. Accumulation of an endogenous inhibitor of nitric oxide synthesis in chronic renal failure. *Lancet*. 339:572–575.

Vander Jagt, D.L., L.A. Hunsaker, and J.E. Heidrich. 1981. Partial purification and characterization of lactate dehydrogenase from Plasmodium falciparum. *Mol. Biochem. Parasitol.* 4:255–264. doi:10.1016/0166-6851(81)90058-X.

Vasquez-Vivar, J., B. Kalyanaraman, P. Martasek, N. Hogg, B.S. Masters, H. Karoui, P. Tordo, and K.A. Pritchard. 1998. Superoxide generation by endothelial nitric oxide synthase: the influence of cofactors. *Proc Natl Acad Sci U A*. 95:9220–5.

Vasquez-Vivar, J., P. Martasek, J. Whitsett, J. Joseph, and B. Kalyanaraman. 2002. The ratio between tetrahydrobiopterin and oxidized tetrahydrobiopterin analogues controls superoxide release from endothelial nitric oxide synthase: an EPR spin trapping study. *Biochem J*. 362:733–9.

Villagra, J., S. Shiva, L.A. Hunter, R.F. Machado, M.T. Gladwin, and G.J. Kato. 2007. Platelet activation in patients with sickle disease, hemolysis-associated pulmonary hypertension, and nitric oxide scavenging by cell-free hemoglobin. *Blood*. 110:2166–2172. doi:10.1182/blood-2006-12-061697.

Vukosavljevic, N., D. Jaron, K.A. Barbee, and D.G. Buerk. 2006. Quantifying the l-arginine paradox in vivo. *Microvasc. Res.* 71:48–54. doi:10.1016/j.mvr.2005.10.006.

Waller, D., J. Crawley, F. Nosten, D. Chapman, S. Krishna, C. Craddock, D. Brewster, and N.J. White. 1991. Intracranial pressure in childhood cerebral malaria. *Trans. R. Soc. Trop. Med. Hyg.* 85:362–364. doi:10.1016/0035-9203(91)90291-6.

Waller, D., S. Krishna, J. Crawley, K. Miller, F. Nosten, D. Chapman, F.O. ter Kuile, C. Craddock, C. Berry, P.A. Holloway, and et al. 1995. Clinical features and outcome of severe malaria in Gambian children. *Clin Infect Dis*. 21:577–87.

Walther, M., D. Jeffries, O.C. Finney, M. Njie, A. Ebonyi, S. Deininger, E. Lawrence, A. Ngwa-Amambua, S. Jayasooriya, I.H. Cheeseman, N. Gomez-Escobar, J. Okebe, D.J. Conway, and E.M. Riley. 2009. Distinct roles for FOXP3 and FOXP3 CD4 T cells in regulating cellular immunity to uncomplicated and severe Plasmodium falciparum malaria. *PLoS Pathog.* 5:e1000364. doi:10.1371/journal.ppat.1000364.

Wang, D., P.S. Gill, T. Chabrashvili, M.L. Onozato, J. Raggio, M. Mendonca, K. Dennehy, M. Li, P. Modlinger, J. Leiper, P. Vallance, O. Adler, A. Leone, A. Tojo, W.J. Welch, and C.S. Wilcox. 2007. Isoform-specific regulation by N(G),N(G)-dimethylarginine dimethylaminohydrolase of rat serum asymmetric dimethylarginine and vascular endothelium-derived relaxing factor/NO. *Circ. Res.* 101:627–635. doi:10.1161/CIRCRESAHA.107.158915.

Wang, J., A.S. Sim, X.L. Wang, and D.E.L. Wilcken. 2006. L-arginine regulates asymmetric dimethylarginine metabolism by inhibiting dimethylarginine dimethylaminohydrolase activity in hepatic (HepG2) cells. *Cell. Mol. Life Sci. CMLS*. 63:2838–2846. doi:10.1007/s00018-006-6271-8.

Warrell, D.A., S. Looareesuwan, M.J. Warrell, P. Kasemsarn, R. Intaraprasert, D. Bunnag, and T. Harinasuta. 1982. Dexamethasone proves deleterious in cerebral malaria. A double-blind trial in 100 comatose patients. *N Engl J Med*. 306:313–9.

Waruiru, C.M., C.R. Newton, D. Forster, L. New, P. Winstanley, I. Mwangi, V. Marsh, M. Winstanley, R.W. Snow, and K. Marsh. 1996. Epileptic seizures and malaria in Kenyan children. *Trans R Soc Trop Med Hyg*. 90:152–5.

Watt, G., K. Jongsakul, and R. Ruangvirayuth. 2002. A pilot study of N-acetylcysteine as adjunctive therapy for severe malaria. *QJM*. 95:285–290. doi:10.1093/qjmed/95.5.285.

Wei, C.C., Z.Q. Wang, C. Hemann, R. Hille, and D.J. Stuehr. 2003. A tetrahydrobiopterin radical forms and then becomes reduced during Nomega-hydroxyarginine oxidation by nitric-oxide synthase. *J Biol Chem*. 278:46668–73. doi:10.1074/jbc.M307682200.

Wei, C.C., Z.Q. Wang, J. Tejero, Y.P. Yang, C. Hemann, R. Hille, and D.J. Stuehr. 2008. Catalytic reduction of a tetrahydrobiopterin radical within nitric-oxide synthase. *J Biol Chem*. 283:11734–42. doi:10.1074/jbc.M709250200.

Wei, C.C., Z.Q. Wang, Q. Wang, A.L. Meade, C. Hemann, R. Hille, and D.J. Stuehr. 2001. Rapid kinetic studies link tetrahydrobiopterin radical formation to heme-dioxy reduction and arginine hydroxylation in inducible nitric-oxide synthase. *J Biol Chem*. 276:315–9. doi:10.1074/jbc.M008441200.

Wei, X., Y. Li, X. Sun, X. Zhu, Y. Feng, J. Liu, Y. Jiang, H. Shang, L. Cui, and Y. Cao. 2014. Erythropoietin Protects against Murine Cerebral Malaria through Actions on Host Cellular Immunity. *Infect. Immun.* 82:165–173. doi:10.1128/IAI.00929-13.

Weinberg, J.B., T.W. Yeo, J.P. Mukemba, S.M. Florence, A.D. Volkheimer, H. Wang, Y. Chen, M. Rubach, D.L. Granger, E.D. Mwaikambo, and N.M. Anstey. 2014. Dimethylarginines: endogenous inhibitors of nitric oxide synthesis in children with falciparum malaria. *J. Infect. Dis.* jiu156. doi:10.1093/infdis/jiu156.

Weiss, G., P.E. Thuma, G. Biemba, G. Mabeza, E.R. Werner, and V.R. Gordeuk. 1998. Cerebrospinal fluid levels of biopterin, nitric oxide metabolites, and immune activation markers and the clinical course of human cerebral malaria. *J Infect Dis*. 177:1064–8.

White, N.J. 2008. Qinghaosu (Artemisinin): The Price of Success. *Science*. 320:330–334. doi:10.1126/science.1155165.

White, N.J., S. Looareesuwan, R.E. Phillips, P. Chanthavanich, and D.A. Warrell. 1988. Single dose phenobarbitone prevents convulsions in cerebral malaria. *Lancet*. 2:64–6.

White, N.J., G.D. Turner, I.M. Medana, A.M. Dondorp, and N.P. Day. 2010. The murine cerebral malaria phenomenon. *Trends Parasitol*. 26:11–5.

Wiese, L., C. Hempel, M. Penkowa, N. Kirkby, and J.A. Kurtzhals. 2008. Recombinant human erythropoietin increases survival and reduces neuronal apoptosis in a murine model of cerebral malaria. *Malar J*. 7:3.

Wijnands, K.A.P., H. Vink, J.J. Briedé, E.E. van Faassen, W.H. Lamers, W.A. Buurman, and M. Poeze. 2012. Citrulline a More Suitable Substrate than Arginine to Restore NO

Production and the Microcirculation during Endotoxemia. *PLoS ONE*. 7:e37439. doi:10.1371/journal.pone.0037439.

Wilson, A.M., R. Harada, N. Nair, N. Balasubramanian, and J.P. Cooke. 2007. L-arginine supplementation in peripheral arterial disease: no benefit and possible harm. *Circulation*. 116:188–95. doi:10.1161/CIRCULATIONAHA.106.683656.

Wojciak-Stothard, B., B. Torondel, L. Zhao, T. Renné, and J.M. Leiper. 2009. Modulation of Rac1 Activity by ADMA/DDAH Regulates Pulmonary Endothelial Barrier Function. *Mol. Biol. Cell*. 20:33–42. doi:10.1091/mbc.E08-04-0395.

Wood, K.C., M.M. Cortese-Krott, J.C. Kovacic, A. Noguchi, V.B. Liu, X. Wang, N. Raghavachari, M. Boehm, G.J. Kato, M. Kelm, and M.T. Gladwin. 2013. Circulating Blood Endothelial Nitric Oxide Synthase Contributes to the Regulation of Systemic Blood Pressure and Nitrite Homeostasis. *Arterioscler. Thromb. Vasc. Biol.* 33:1861–1871. doi:10.1161/ATVBAHA.112.301068.

World Health Organization. 2010. Guidelines for the treatment of malaria -- 2nd edition. World Health Organization, Geneva, Switzerland.

World Health Organization. 2012. World Malaria Report: 2012. World Health Organization.

World Health Organization. 2013. World Malaria Report: 2013. World Health Organization.

World Health Organization, Communicable Diseases Cluster. 2000. Severe falciparum malaria. *Trans R Soc Trop Med Hyg*. 94 Suppl 1:S1–90.

Worthmann, H., S. Chen, J. Martens-Lobenhoffer, N. Li, M. Deb, A.B. Tryc, A. Goldbecker, Q. Dong, J.T. Kielstein, S.M. Bode-Böger, and K. Weissenborn. 2011. High plasma dimethylarginine levels are associated with adverse clinical outcome after stroke. *J. Atheroscler. Thromb.* 18:753–761.

Wu, G., and C.J. Meininger. 2008. Analysis of citrulline, arginine, and methylarginines using high-performance liquid chromatography. *Methods Enzym.* 440:177–89. doi:10.1016/S0076-6879(07)00810-5.

Xia, Y., A.L. Tsai, V. Berka, and J.L. Zweier. 1998. Superoxide generation from endothelial nitric-oxide synthase. A Ca2+/calmodulin-dependent and tetrahydrobiopterin regulatory process. *J Biol Chem*. 273:25804–8.

Xu, K.Y., D.L. Huso, T.M. Dawson, D.S. Bredt, and L.C. Becker. 1999. Nitric oxide synthase in cardiac sarcoplasmic reticulum. *Proc Natl Acad Sci U A*. 96:657–62.

Yang, Y., and J. Loscalzo. 2000. Regulation of Tissue Factor Expression in Human Microvascular Endothelial Cells by Nitric Oxide. *Circulation*. 101:2144–2148. doi:10.1161/01.CIR.101.18.2144.

Yeo, T.W., D.A. Lampah, R. Gitawati, E. Tjitra, E. Kenangalem, D.L. Granger, J.B. Weinberg, B.K. Lopansri, R.N. Price, D.S. Celermajer, S.B. Duffull, and N.M. Anstey. 2008a. Safety Profile of L-Arginine Infusion in Moderately Severe Falciparum Malaria. *PLoS ONE*. 3:e2347. doi:10.1371/journal.pone.0002347.

Yeo, T.W., D.A. Lampah, R. Gitawati, E. Tjitra, E. Kenangalem, Y.R. McNeil, C.J. Darcy, D.L. Granger, J.B. Weinberg, B.K. Lopansri, R.N. Price, S.B. Duffull, D.S. Celermajer, and N.M. Anstey. 2007. Impaired nitric oxide bioavailability and L-arginine reversible endothelial dysfunction in adults with falciparum malaria. *J Exp Med*. 204:2693–704.

Yeo, T.W., D.A. Lampah, R. Gitawati, E. Tjitra, E. Kenangalem, K. Piera, R.N. Price, S.B. Duffull, D.S. Celermajer, and N.M. Anstey. 2008b. Angiopoietin-2 is associated with decreased endothelial nitric oxide and poor clinical outcome in severe falciparum malaria. *Proc Natl Acad Sci U A*. 105:17097–102.

Yeo, T.W., D.A. Lampah, I. Rooslamiati, R. Gitawati, E. Tjitra, E. Kenangalem, R.N. Price, S.B. Duffull, and N.M. Anstey. 2013. A randomized pilot study of L-arginine infusion in severe falciparum malaria: preliminary safety, efficacy and pharmacokinetics. *PLoS One*. 8:e69587. doi:10.1371/journal.pone.0069587.

Yeo, T.W., D.A. Lampah, E. Tjitra, R. Gitawati, C.J. Darcy, C. Jones, E. Kenangalem, Y.R. McNeil, D.L. Granger, B.K. Lopansri, J.B. Weinberg, R.N. Price, S.B. Duffull, D.S. Celermajer, and N.M. Anstey. 2010. Increased asymmetric dimethylarginine in severe falciparum malaria: association with impaired nitric oxide bioavailability and fatal outcome. *PLoS Pathog*. 6:e1000868.

Yeo, T.W., D.A. Lampah, E. Tjitra, R. Gitawati, E. Kenangalem, K. Piera, D.L. Granger, B.K. Lopansri, J.B. Weinberg, R.N. Price, S.B. Duffull, D.S. Celermajer, and N.M. Anstey. 2009. Relationship of cell-free hemoglobin to impaired endothelial nitric oxide bioavailability and perfusion in severe falciparum malaria. *J Infect Dis*. 200:1522–9.

Yeo, T.W., I. Rooslamiati, R. Gitawati, E. Tjitra, D.A. Lampah, E. Kenangalem, Y.R. McNeil, R.N. Price, N.M. Anstey, and S.B. Duffull. 2008c. Pharmacokinetics of l-Arginine in Adults with Moderately Severe Malaria. *Antimicrob. Agents Chemother*. 52:4381–4387. doi:10.1128/AAC.00421-08.

Zhang, W.Z., and D.M. Kaye. 2004. Simultaneous determination of arginine and seven metabolites in plasma by reversed-phase liquid chromatography with a time-controlled ortho-phthaldialdehyde precolumn derivatization. *Anal Biochem*. 326:87–92. doi:10.1016/j.ab.2003.11.006.

Zoccali, C., S. Bode-Böger, F. Mallamaci, F. Benedetto, G. Tripepi, L. Malatino, A. Cataliotti, I. Bellanuova, I. Fermo, J. Frölich, and R. Böger. 2001. Plasma concentration of asymmetrical dimethylarginine and mortality in patients with end-stage renal disease: a prospective study. *Lancet*. 358:2113–2117.

Zougbede, S., F. Miller, P. Ravassard, A. Rebollo, L. Ciceron, P.O. Couraud, D. Mazier, and A. Moreno. 2011. Metabolic acidosis induced by Plasmodium falciparum intraerythrocytic stages alters blood-brain barrier integrity. *J Cereb Blood Flow Metab*. 31:514–26.

Word Count

Word Count of Main Body Chapters

51,502

Word Count of Method Development Appendices

16,794